frontiers | Research Topics

Biomaterials and antibacterial materials for osseous-ligament system

Edited by
Yansong Qi, Alideertu Dong, Dicky Pranantyo and Liqun Xu

Published in
Frontiers in Bioengineering and Biotechnology

ISSN 1664-8714
ISBN 978-2-8325-2776-4
DOI 10.3389/978-2-8325-2776-4

About Frontiers

Frontiers is more than just an open access publisher of scholarly articles: it is a pioneering approach to the world of academia, radically improving the way scholarly research is managed. The grand vision of Frontiers is a world where all people have an equal opportunity to seek, share and generate knowledge. Frontiers provides immediate and permanent online open access to all its publications, but this alone is not enough to realize our grand goals.

Frontiers journal series

The Frontiers journal series is a multi-tier and interdisciplinary set of open-access, online journals, promising a paradigm shift from the current review, selection and dissemination processes in academic publishing. All Frontiers journals are driven by researchers for researchers; therefore, they constitute a service to the scholarly community. At the same time, the *Frontiers journal series* operates on a revolutionary invention, the tiered publishing system, initially addressing specific communities of scholars, and gradually climbing up to broader public understanding, thus serving the interests of the lay society, too.

Dedication to quality

Each Frontiers article is a landmark of the highest quality, thanks to genuinely collaborative interactions between authors and review editors, who include some of the world's best academicians. Research must be certified by peers before entering a stream of knowledge that may eventually reach the public - and shape society; therefore, Frontiers only applies the most rigorous and unbiased reviews. Frontiers revolutionizes research publishing by freely delivering the most outstanding research, evaluated with no bias from both the academic and social point of view. By applying the most advanced information technologies, Frontiers is catapulting scholarly publishing into a new generation.

What are Frontiers Research Topics?

Frontiers Research Topics are very popular trademarks of the *Frontiers journals series*: they are collections of at least ten articles, all centered on a particular subject. With their unique mix of varied contributions from Original Research to Review Articles, Frontiers Research Topics unify the most influential researchers, the latest key findings and historical advances in a hot research area.

Find out more on how to host your own Frontiers Research Topic or contribute to one as an author by contacting the Frontiers editorial office: frontiersin.org/about/contact

Biomaterials and antibacterial materials for osseous-ligament system

Topic editors

Yansong Qi — Inner Mongolia People's Hospital, China

Alideertu Dong — Inner Mongolia University, China

Dicky Pranantyo — Singapore-MIT Alliance for Research and Technology (SMART), Singapore

Liqun Xu — Southwest University, China

Citation

Qi, Y., Dong, A., Pranantyo, D., Xu, L., eds. (2023). *Biomaterials and antibacterial materials for osseous-ligament system*. Lausanne: Frontiers Media SA.

doi: 10.3389/978-2-8325-2776-4

Table of contents

frontiers | Frontiers in Bioengineering and Biotechnology

TYPE Editorial
PUBLISHED 07 June 2023
DOI 10.3389/fbioe.2023.1230500

OPEN ACCESS

EDITED AND REVIEWED BY
Hasan Uludag,
University of Alberta, Canada

*CORRESPONDENCE
Yansong Qi,
malaqinfu@126.com
Liqun Xu,
xulq@swu.edu.cn

RECEIVED 29 May 2023
ACCEPTED 01 June 2023
PUBLISHED 07 June 2023

CITATION
Pranantyo D, Dong A, Xu L and Qi Y (2023), Editorial: Biomaterials and antibacterial materials for osseous-ligament system.
Front. Bioeng. Biotechnol. 11:1230500.
doi: 10.3389/fbioe.2023.1230500

Editorial: Biomaterials and antibacterial materials for osseous-ligament system

Dicky Pranantyo[1], Alideertu Dong[2], Liqun Xu[3]* and Yansong Qi[4]*

[1]Antimicrobial Resistance Interdisciplinary Research Group, Singapore-MIT Alliance for Research and Technology, Singapore, Singapore, [2]College of Chemistry and Chemical Engineering, Inner Mongolia University, Hohhot, China, [3]Chongqing Key Laboratory for Advanced Materials and Technologies of Clean Energies, School of Materials and Energy, Southwest University, Chongqing, China, [4]Orthopedic Center (Sports Medicine Center), Inner Mongolia People's Hospital, Hohhot, China

KEYWORDS

biomaterials, synthetic materials, natural biomaterials, antimicrobial materials, osseous-ligament system, cartilage repair, biomechanics

Editorial on the Research Topic
Biomaterials and antibacterial materials for osseous-ligament system

Trauma and infection-caused osseous-ligament defects have become a constant threat to limb function and quality of life, which inflict serious health problems to millions of people worldwide and cause major economic burdens to society (Niu et al., 2022). Severe osseous-ligament defects caused by trauma occur frequently, such as comminuted fractures, torn ligaments, and injuries with open wounds. As a burgeoning branch of tissue engineering, biomaterials for osseous-ligament regeneration face a constant risk of infection despite significant advances made over the decades in cartilage, ligament, and bone repair (Shen et al., 2022). Protection against infection as well as quality and function pose a major challenge to the science of biomaterials for tissue repair. Effective biomaterials should be of suitable quality to enhance tissue growth and restore function and should not have negative hindrances on immunity and the ability to fight infection.

In this Research Topic, we introduce the recent developments of biomaterials and corresponding therapies for the osseous-ligament systems, including synthetic materials, natural biomaterials, and antimicrobial materials. We also compile the mechanism and function of biomaterials during treatment or *in vivo* studies. On the regenerative side, we present the design and fabrication of the scaffold to better stimulate the natural spatial complexity of cell types and tissue organization of bone and joints. In terms of safety and efficacy, we discuss biomaterials integration, biocompatibility and inflammation in the host, and the successful survival of the implant in the host body.

One of the key requisites for successful implants integration and tissue engineering is maintaining the infection-free condition. Various strategies have been explored to endow antibacterial functions in osseous-ligament systems, including surface modification and smart delivery of small molecules, peptides and polymers. Kurishima et al. demonstrated that TiNbSn alloy, which exhibits low Young's modulus, could be imparted with antibacterial properties by anodization with sodium tartrate electrolyte. Hao et al. reviewed the diversity, effects, and applications of antimicrobial peptides for bone tissue engineering. Wang et al. presented the recent progress of stimuli-responsive antibacterial materials for bone infection, with special attention to the advanced mechanisms of action to treat multidrug-resistant bacteria and biofilms. However, not all antibacterial materials are safe enough for biomedical applications.

Li et al. presented a systematic review of clinical studies discussing the potential side effects of antibacterial coatings in orthopaedic implants.

This Research Topic also provides critical analyses on the established treatments for ligament and bone repairs based on the clinical data obtained from patients. Wang et al. reported a clinical study on the vertebral segments of patients to discuss whether the sizing of current cervical disc arthroplasty systems match Chinese cervical anatomic dimensions. Ren et al. studied the safety, efficacy, and functional outcomes on arthroscopic fixation of posterior cruciate ligament avulsion fracture by a bio-absorbable anchor or traditional pull-out technique. Yang et al. presented a systematic review and meta-analysis on different stem fixation methods of radial head prostheses during long-term follow-up. Cui et al. summarized the efficacy and outcome of a two-staged operation for irreducible knee dislocation with a short-term follow-up. Ma et al. reported the efficacy and medium-term outcomes of ligament advanced reinforcement system compared with auto-grafts in anterior cruciate ligament reconstruction with at least 2 years follow-up. Yang et al. conducted a histological analysis and prospective clinical trial of primary repair for treating acute proximal anterior cruciate ligament tears.

Clinical evaluations on the material and morphological designs of the applied orthopaedic and osseous-ligament implants serve as the basis of future designs and direction in tissue engineering for cartilage and bone repairs. Li et al. discussed the biomechanical performance of three Ti6Al4V volar plates with the latest designs in patients with distal radius fractures using a finite element model. Wang et al. reviewed the preparation, modification, and clinical applications of porous tantalum scaffolds, discussing the emerging manufacturing technologies, surface modification techniques, and patient-oriented designs that influenced the microstructural characteristic, bioactive performance, and clinical indications of porous tantalum implants over the past two decades. Ding et al. proposed a method for designing tuberosity reconstruction baseplate for shoulder hemiarthroplasty based on morphological data, which potentially extends the applications of biomaterial carbon fibre reinforced polymer composites in orthopaedics field.

Various supplementary elements can support osseointegration and alleviate complications, which subsequently facilitate the success of orthopaedic and osseous-ligament implants. He et al. reviewed the applications of inferior vena cava filters in orthopaedics, the current status of filters, and the progress of research into biodegradable vena cava filters, coupled with possible future developments. Zheng et al. presented a systematic review to summarize the synthetic materials and specific techniques of suture tape augmentation in anterior cruciate ligament reconstruction and evaluate the clinical outcomes. Li et al. summarized the application of additive manufacturing technology in pelvic surgery, addressing the challenges in traditional pelvic surgery, such as the complex structure of the pelvis, difficulty in exposing the operative area, and poor visibility of the surgery. Guo et al. discussed the prospects of multi-layer intelligent technologies, including smart materials, variable structures, and intelligent therapeutic planning, to achieve optimal recovery of musculoskeletal injuries.

Following osseointegration, bone repair and regeneration can be propelled by modulating stem cell differentiation and chondrocyte redifferentiation. Kong et al. demonstrated that titanium dioxide nanotubes layers promote osteogenic differentiation through nuclear localization of Yap and downstream activation of Piezo1 expression. Yang et al. presented a bibliometric and visualization analysis of stem cell therapy to facilitate meniscus regeneration in the past decade. Li et al. incorporated osteogenic mesenchymal stem cells (MSC) into gelatin microcryogels to form microtissues and applied these self-assembled microtissues to induce osteogenesis for *in vivo* bone regeneration.

From the compilation of these individual contributions, the collective articles are broad in nature, ranging from initial research to clinical applications that address the challenges of antibacterial strategy and tissue engineering in bone repair. This Research Topic therefore provides references for ongoing research in natural and synthetic biomaterials (hydrogels, fibers, surfaces, coatings, polymers, peptides, and peptidomimetics) for osseous-ligament reconstruction. It encourages future directions in antibacterial functions, modulation of stem cell differentiation and chondrocyte redifferentiation, promotion of survival and integration of implants in ligaments and bone, additive manufacturing of scaffolds for tissue engineering of bone and cartilage, and translational research on tissue engineering of bone and joints.

Author contributions

DP and AD drafted the manuscript. DP, AD, LX, and YQ provided suggestions and revised the paper. All authors contributed to the article and approved the submitted version.

Conflict of interest

The authors declare that the research was conducted in the absence of any commercial or financial relationships that could be construed as a potential conflict of interest.

Publisher's note

References

Niu, X., Li, N., Du, Z., and Li, X. (2022). Integrated gradient tissue-engineered osteochondral scaffolds: Challenges, current efforts and future perspectives. *Bioact. Mater* 20, 574–597. doi:10.1016/j.bioactmat.2022.06.011

Shen, Q., Qi, Y., Kong, Y., Bao, H., Wang, Y., Dong, A., et al. (2022). Advances in copper-based biomaterials with antibacterial and osteogenic properties for bone tissue engineering. *Front. Bioeng. Biotechnol.* 9, 795425. doi:10.3389/fbioe.2021.795425

frontiers | Frontiers in Bioengineering and Biotechnology

ORIGINAL RESEARCH
published: 07 April 2022
doi: 10.3389/fbioe.2022.872088

TiO_2 Nanotubes Promote Osteogenic Differentiation Through Regulation of Yap and Piezo1

Keyu Kong†, Yongyun Chang†, Yi Hu†, Hua Qiao, Chen Zhao, Kewei Rong, Pu Zhang, Jingwei Zhang, Zanjing Zhai and Huiwu Li**

Shanghai Key Laboratory of Orthopaedic Implants, Department of Orthopaedic Surgery, Shanghai Ninth People's Hospital, Shanghai Jiaotong University School of Medicine, Shanghai, China

Surface modification of titanium has been a hot topic to promote bone integration between implants and bone tissue. Titanium dioxide nanotubes fabricated on the surface of titanium by anodic oxidation have been a mature scheme that has shown to promote osteogenesis *in vitro*. However, mechanisms behind such a phenomenon remain elusive. In this study, we verified the enhanced osteogenesis of BMSCs on nanotopographic titanium *in vitro* and proved its effect *in vivo* by constructing a bone defect model in rats. In addition, the role of the mechanosensitive molecule Yap is studied in this research by the application of the Yap inhibitor verteporfin and knockdown/overexpression of Yap in MC3T3-E1 cells. Piezo1 is a mechanosensitive ion channel discovered in recent years and found to be elemental in bone metabolism. In our study, we preliminarily figured out the regulatory relationship between Yap and Piezo1 and proved Piezo1 as a downstream effector of Yap and nanotube-stimulated osteogenesis. In conclusion, this research proved that nanotopography promoted osteogenesis by increasing nuclear localization of Yap and activating the expression of Piezo1 downstream.

Keywords: mesenchymal stem cells, osteogenic differentiation, titanium nanotubes, hippo pathway, Piezo1

OPEN ACCESS

Edited by:
Yansong Qi,
Inner Mongolia People's Hospital, China

Reviewed by:
Rui Ma,
Xi'an Jiaotong University, China
Zhengxiao Ouyang,
Central South University, China

****Correspondence:***
Zanjing Zhai
zanjing_zhai@163.com
Huiwu Li
huiwu1223@163.com

†These authors have contributed equally to this work

Specialty section:
This article was submitted to Biomaterials, a section of the journal Frontiers in Bioengineering and Biotechnology

Received: *09 February 2022*
Accepted: *08 March 2022*
Published: *07 April 2022*

Citation:
Kong K, Chang Y, Hu Y, Qiao H, Zhao C, Rong K, Zhang P, Zhang J, Zhai Z and Li H (2022) TiO_2 Nanotubes Promote Osteogenic Differentiation Through Regulation of Yap and Piezo1. Front. Bioeng. Biotechnol. 10:872088. doi: 10.3389/fbioe.2022.872088

INTRODUCTION

In recent years, the number of hip and knee arthroplasty procedures has increased rapidly (Schwartz et al., 2016). Application of artificial prosthesis has greatly improved the quality of patients' lives, but its long-term complications will make patients suffer the risk of revision. Among all the causes of revision, the most common one is aseptic loosening (Kahlenberg et al., 2019; Kelmer et al., 2021). Due to unsatisfactory interface bone integration between the prosthesis and bone tissue, there would be loosening between prosthesis and bone tissue in the long-term fretting environment. Therefore, how to enhance bone integration between prosthesis and bone tissue has always been a hot topic (Shah et al., 2019; Liu et al., 2020). At present, the most commonly used material for prostheses on the market is titanium. Therefore, many studies have focused on surface modification of titanium to enhance its osteoconduction and osteointegration (Liu et al., 2020). Among them, nanotubes fabricated on the surface of titanium by anodic oxidation etching have been reported in the

Abbreviations: ALP, alkaline phosphatase; BCA, bicinchoninic acid; BMSCs, bone marrow-derived mesenchymal stem cells; DMSO, dimethyl sulfoxide; EDS, X-ray energy dispersive analysis; FBS, fetal bovine serum; OM, osteogenic induction medium; PVDF, polyvinylidene fluoride; SEM, scanning electron microscopy; TBST, TBS + Tween; VP, verteporfin.

literature, which can significantly enhance the ability of bone marrow-derived mesenchymal stem cells to differentiate into osteoblasts (Wang et al., 2014; Zhang et al., 2016). Nanotubes can significantly enhance the adhesion and proliferation of mesenchymal stem cells (Zhang et al., 2016). At the same time, different tube diameters and lengths will exert different effects on the osteogenic differentiation ability of mesenchymal stem cells (Park et al., 2007; Wang et al., 2011). However, how stem cells perceive the difference in titanium surface topography, transform it into internal biological signals, and finally promote osteogenesis remains to be further studied.

Bone marrow-derived mesenchymal stem cells are a kind of stem cell with multidirectional differentiation ability (Chang et al., 2019; Park et al., 2019; Yong et al., 2020). Under different induction and stimulation conditions, they will differentiate into three lines: osteogenic, chondrogenic, and adipogenic cells. Studies have shown that different mechanical stimuli and different substrate stiffness will affect the differentiation of mesenchymal stem cells in different directions (Curran et al., 2006; Sun et al., 2012; Perestrelo et al., 2018). Because the stiffness of bone tissue is higher, such an environment will be more conducive to the differentiation of mesenchymal stem cells in the direction of osteogenesis. The common point of mechanical stimulation and substrate stiffness in controlling stem cell differentiation is to change the topography of cells and rearrange the cytoskeleton (Chang et al., 2019). Previous studies have proved that the uneven topography of nanotubes changes the topography of mesenchymal stem cells and promotes osteogenesis through the rearrangement of F-actin (Tong et al., 2020). However, how the physical stimulation of nanotopography changes the internal signal pathway and the final effector molecule are still unknown.

Yap is an important component of the Hippo signal pathway. When the Hippo pathway is turned on, a series of kinases upstream of Yap, such as Mst1/2 and Lats1/2, are activated to further phosphorylate Yap and Taz to prevent them from entering the nucleus and starts the regulation of downstream transcription factors. When the pathway is closed, Yap/Taz will be dephosphorylated and activated and then enters the nucleus to activate the downstream transcription factor TEAD family and start the transcription of downstream genes such as Ctgf and Cyr61 (Dupont et al., 2011; Lorthongpanich et al., 2019). The Hippo pathway has been widely proved to be involved in the process of tumor proliferation and metastasis (Fan et al., 2021; Hasegawa et al., 2021), and Yap has also been proved to be a mechanosensor, which plays an important role in osteogenesis promoted by mechanics (Dupont et al., 2011; Du et al., 2019). In addition to osteogenesis, the Hippo pathway is also involved in the differentiation and degeneration of cartilage (Deng et al., 2018) and osteoclasts (Yang et al., 2021). It plays an important role in maintaining bone homeostasis and promoting bone integration. However, what role it plays in the process of titanium nanotopography promoting osteogenesis and its mechanism are still controversial.

Piezo is a family of newly discovered mechanosensitive cation channels on the surface of the cell membrane in recent years (Sugimoto et al., 2017; Wu et al., 2017). It is divided into two subtypes: Piezo1 and Piezo2. Piezo2 is mainly distributed in sensory tissues, such as dorsal root ganglion sensory neurons and Merkel cells. Piezo1 is widely distributed in non-sensory tissues such as chondrocytes, the bladder, endothelial cells, the kidney, and red blood cells (Wu et al., 2017). Recent literature studies generally suggest that Piezo1 may be involved in the maintenance of bone homeostasis (Hao et al., 2019; Li et al., 2019; Wang et al., 2020). Asuna et al. (Sugimoto et al., 2017) found that the expression of Piezo1 increased in the process of mechanical pressure promoting osteogenesis, and the use of Yoda1, an agonist of Piezo1, can significantly promote the differentiation of stem cells into osteogenesis. Conditional knockout of the *Piezo1* gene in osteoblasts can significantly reduce bone mass and bone formation in mice. Mice with conditional Piezo1 knockout in osteoblasts and their progeny cells showed higher risks of spontaneous fracture and significantly enhanced bone resorption (Wang et al., 2020). However, the role of Piezo1 in nanotopography promoting osteogenesis and the reason behind its expression regulation and function have not been clearly determined. Hasegawa et al. found that the transcriptional activity of Piezo1 was regulated by the Yap-TEAD compound in oral squamous cell carcinoma cells and whether such regulation plays a role in osteogenesis remains to be explored (Hasegawa et al., 2021).

In this study, we found that the nanotopography of the titanium surface can significantly promote the osteogenic differentiation of bone marrow-derived mesenchymal stem cells *in vivo* and *in vitro*. By adoption of the Yap inhibitor verteporfin and knockdown and overexpression of Yap, it is proved that Yap is involved in the process of mesenchymal stem cells sensing the changes of physical topography and transforming them into biological signals. It is proposed and preliminarily proved that Piezo1, which has been widely studied in the orthopedic field in recent years, is a downstream key molecule for nanotopography to promote osteogenesis through Yap.

MATERIALS AND METHODS

Fabrication of TiO_2 Nanotubes

Our method of fabricating nanotubes on titanium surfaces has been explained in detail in our previous work (Tong et al., 2020). In brief, pure titanium slices were polished and then washed sequentially with anhydrous alcohol and deionized water in an ultrasonic cleaning machine. Titanium was fixed as the anode and a platinum piece as the cathode in a solution of 0.15 M NH_4F and 90% glycol for 1 h under 50 V.

Surface Characterization

Samples fabricated at 50 V were washed with deionized water and dried at room temperature. Scanning electron microscopy (SEM450, FEI Nova Nano SEM; Thermo Fisher Scientific, Waltham, MA, United States) was employed to scan and analyze the structure of nanotubes, including their inner diameters. In addition, X-ray energy dispersive analysis (EDS,

Xplore30, Oxford Instrument, Oxford, United Kingdom) was performed to analyze the elemental composition of nanotubes.

Cell Lines and Reagents

The osteoblast-like cell line MC3T3-E1 was purchased from the Cell Bank of the Chinese Academy of Sciences (Shanghai, China) and was cultured in α-minimal essential medium (*α*-MEM; Gibco, Thermo Fisher Scientific, Waltham, MA, United States) with 10% fetal bovine serum (FBS) and 1% penicillin-streptomycin (Gibco, Thermo Fisher Scientific, Waltham, MA, United States) solution. Verteporfin was purchased from MCE (New Jersey, United States) and dissolved in DMSO. To avoid the cytotoxicity of DMSO, the final concentration of DMSO in the culture medium was less than 0.1%.

BMSC's Isolation and Cell Culture

Four-week-old male Sprague–Dawley (SD) rats were purchased from the experimental animal center of Shanghai Ninth People's Hospital (Shanghai, China). Rat femurs and tibias were separated aseptically, and bone marrow-derived mesenchymal stem cells (BMSCs) were collected by rinsing the medullary cavity with culture medium. BMSCs were further cultured in α-minimal essential medium with 10% fetal bovine serum (FBS) and 1% penicillin-streptomycin (Gibco, Thermo Fisher Scientific, Waltham, MA, United States) solution. BMSCs were incubated at 37°C in a humidified atmosphere consisting of 95% air and 5% CO_2. Only cells between passages three and seven were used for experiments. Osteogenic induction medium (Cyagen, United States) was composed of growth medium supplemented with 100 nM dexamethasone, 10 mM *ß*-glycerophosphate, and 50 μM ascorbic acid.

Cell Proliferation

A total of 24-well-size smooth titanium slices and titanium slices for nanotopography were placed in a 24-well cell culture plate. BMSCs were cultured at a density of 3×10^4 cells per well. Cell viability and proliferation were assessed using Cell Counting Kit-8 (CCK8) (Dojindo, Kumamoto, Japan) at 24, 48, and 72 h after seeding. At the end of each experimental period, cells were incubated with 50 μl of the CCK-8 reagent and 500 μl *α*-MEM for 2 h at 37°C. Optical density values were recorded on a spectrophotometer at 450 nm on an Infinite M200 PRO multimode microplate reader (Tecan Life Sciences, Mänedorf, Switzerland).

Construction of Stable Knockdown/Overexpression Cell Line

Knockdown/overexpression lentiviruses of Yap labeled with GFP and puromycin resistance were purchased from OBIO, Shanghai. First, MC3T3-E1 cells were seeded on a six-well plate at a density of 1.5×10^5 per well. After cells adhered to the wall, a corresponding amount of virus was added to the culture medium according to an optimal multiplicity of infection (MOI) of 20. To promote the entry of virus into the cells, polybrene was added in a ratio of 1:200. After 48 h of infection, the fluorescence intensity was observed under the fluorescence microscope to help determine the infection efficiency. Puromycin was added to screen the resistant cells. After 24 h, the fresh medium was replaced to obtain a stable Yap knockdown/overexpression MC3T3-E1 cell line.

Alkaline Phosphatase Staining and ALP Activity Analysis

BMSCs and MC3T3-E1 cells were seeded onto smooth titanium slices, nanotube titanium slices, or 24-well plates at a density of 3×10^4 per well and cultured with osteogenic medium. After 7 days of incubation, cells were washed three times with PBS for 5 minutes each, fixed with 4% paraformaldehyde for 10 minutes, and washed with PBS three times again. Finally, cells were incubated in the BCIP/NBT alkaline phosphatase color development kit, according to the manufacturer's instructions (Beyotime Institute of Biotechnology, Jiangsu, China).

For alp activity analysis, cells were first lysed with RIPA buffer without protease and phosphatase inhibitors, and then, the centrifuged lysates were assayed using an ALP Assay Kit (Beyotime Institute of Biotechnology, Jiangsu, China) following the protocol provided.

Alizarin Red S Staining

Cells were cultured in 24-well plates at a density of 1×10^5 cells per well and cultured in osteogenic medium for at least 21 days. During the late period of osteogenic differentiation, calcium deposition in the osteoblast was examined by alizarin red S staining. In brief, we used PBS to clean the cultured cells three times, fixed the cells for 10 min in 4% PFA, and stained them with 1% alizarin red S solution (Cyagen, United States) for 10 min. To remove non-specific staining, we used 50% ethanol to clean the stained cells thoroughly. Calcium deposits were represented by positive red staining, and representative images were taken.

Immunocytochemistry

For immunofluorescence, cells were seeded on smooth and nano-topographic titanium slices at a density of 1×10^5 cells per well for two days. After washing with PBS, 4% PFA was used to fix the BMSCs for 10 min, and 0.3% Triton X-100 was used to permeabilize the cell membrane for 5 min after washing three times with PBS. After blocking with 10% goat serum (Solarbio, Beijing, China) for 1h, the cells were incubated with a primary antibody for YAP (diluted 1:200, purchased from Proteintech, United States) overnight at 4°C. After 1 day, the cells were washed three times with PBS for 5 mins. Then, they were incubated with an Alexa Fluor 555 conjugate secondary antibody (anti-rabbit, 1: 200; Abcam, United Kingdom) for 2 h and subsequently incubated with DAPI (Beyotime Institute of Biotechnology, Jiangsu, China) for 5 min. Finally, after PBS wash again, fluorescence images were captured with a confocal microscope (Olympus, Inc., Tokyo, Japan).

Protein Extraction and Western Blotting

After appropriate treatment, cells were rinsed with PBS and lysed with RIPA (Beyotime Institute of Biotechnology, Jiangsu, China) added with protease and phosphatase inhibitors (Thermo Fisher

TABLE 1 | Primers used in the qRT-PCR assay.

Gene	Organism	Forward (5–3′)	Reverse (5–3′)
Gapdh	*Rattus norvegicus*	GGCAAGTTCAACGGCACAG	CGCCAGTAGACTCCACGACAT
Col1a1	*Rattus norvegicus*	TGATGGACCTGCTGGCTCTC	GACCACGTTCACCACTTGCT
Osx	*Rattus norvegicus*	CCAATGACTACCCACCCTTTCC	ATGGATGCCCGCCTTGTA
Ocn	*Rattus norvegicus*	GGACCCTCTCTCTGCTCACTCTG	ACCTTACTGCCCTCCTGCTTGG
Opn	*Rattus norvegicus*	TGATGACGACGACGATGACGAC	TGTGCTGGCAGTGAAGGACTC
Alpl	*Rattus norvegicus*	GACAATGAGATGCCGCCAGAG	CATCCAGTTCATATTCCACATCAGTTC
Gapdh	*Mus musculus*	GGCAAGTTCAACGGCACAG	CGCCAGTAGACTCCACGACAT
Runx2	*Mus musculus*	AGACCAGCAGCACTCCATATCTCT	CGTCAGCGTCAACACCATCATTCT
Osx	*Mus musculus*	AAGTTCACCTGCCTGCTCTGTTC	GGCGGCTGATTGGCTTCTTCTT
Ocn	*Mus musculus*	AAGCAGGAGGGCAATAAGGTAGTG	TCTTCAAGCCATACTGGTCTGATAGC
Opn	*Mus musculus*	GACGATGATGATGACGATGGAGACC	CTGTAGGGACGATTGGAGTGAAAGTG
Alpl	*Mus musculus*	TCACGGCGTCCATGAGCAGAA	TACAGGCAAGGCAGATAGCGAACT
Ctgf	*Mus musculus*	ACACCGCACAGAACCACCACTC	TAATGGCAGGCACAGGTCTTGATGAAC
Cyr61	*Mus musculus*	ATACTGCGGCTCCTGCGTAG	CCTGAACTTGTGGATGTCATTGAATAG
Axl	*Mus musculus*	CTTGTGTCCATTCAACTGTGCTACG	TTCCATCCTCTTGCCGCTCAG
Yap	*Mus musculus*	GCCTACACTGGAGCAGGATGGA	GATAGGTGCCACTGTTAAGAAAGGGAT
Piezo1	*Mus musculus*	AGTATCTGCTTCTTCTTCCTGCTCTTG	GACTTCTCCTCAATCTGGCGATGG

Scientific, Waltham, MA, United States) for 10 min on ice. Protein was collected as the supernatant after a centrifugation of 12,000×*g* for 15 min. Isolation of nuclear and cytoplasmic proteins was achieved with a kit from Beyotime (P0028). Protein concentration was measured by using a BCA kit, and total protein underwent denaturation after being boiled at 99°C for 10 min with a loading buffer. An equal amount of protein was loaded onto a 4–20% SDS- PAGE gel, and proteins with different molecular weights were separated by electrophoresis and then electroblotted onto a PVDF membrane. TBST with 5% bovine serum albumin was used to block unspecific antigen on the membrane for 1 h at RT, and the membrane was incubated with the primary antibody at 4°C overnight. After being washed with TBST, the membrane was incubated with the secondary antibody for 2 h at RT, and protein immunoreactivity was detected on a LI-COR Odyssey fluorescence imaging system (Odyssey, LI-COR Biosciences, Lincoln, NE, United States). Primary antibodies used in this study included Piezo1 (15939-1-AP, Proteintech), *ß*-actin (ab8227, Abcam), Runx2 (12556S, Cell Signaling Technology), osteopontin (ab8448, Cell Signaling Technology), and anti-Yap (13584-1-AP, Proteintech). Secondary antibodies were anti-rabbit IgG (H + L; DyLight™ 800 4× PEG conjugate; Abcam).

Quantitative Real-Time PCR

Quantitative Real-time PCR was performed after cells were treated for the appropriate number of days, according to the conditions required for each experiment. Total RNA was extracted from cells using a total RNA Kit (R6812-01HP, Omega Bio-Tek Inc., Norcross, GA, United States). The concentration of RNA samples was determined by optical density at 260 nm wavelength. RNA samples were reverse-transcribed into cDNA with a cDNA synthesis kit (Takara, Shiga, Japan), according to the manufacturer's instructions. Quantitative Real-time PCR was performed with QuantStudio six Flex real-time PCR system (Life Technologies) with a SYBR Green kit (Bimake) for quantitative real-time PCR of Ctgf, Cyr61, Piezo1, Runx2, Opn, Osx, Ocn, Col1a1 and Alpl. The final volume is 10μl, including 1 μl cDNA, 5 μl SYBR Green Mix, 0.4 μl upstream and 0.4 μl downstream primers, and 3.2 μl dH2O. *Gapdh* was used as an internal reference, and the expressions of different genes were analyzed with the 2-ΔΔCt method and expressed as fold changes compared to the expression of *Gapdh*. The experiment was repeated three times independently. Primers for each gene were designed by Primer Premier 6.0 software. The sequences of the primers used are listed in **Table 1**.

Surgical Procedure

Animal experiments and surgery were conducted in the animal laboratory of Shanghai Ninth People's Hospital affiliated with Shanghai Jiaotong University. National Laboratory Animal Care and Use guidelines were followed. The animal experiment plan was approved by the ethics committee of Shanghai Ninth People's Hospital. The preparation of nanotopography titanium nails is the same as the method described before. Twelve 6-week-old male SD rats were randomly divided into two groups: 1) the smooth titanium nail group and 2) nanotopography titanium nail group. During the operation, the rats were anesthetized by an intraperitoneal injection of 4% chloral hydrate; the skin was prepared and disinfected with iodophor. After cutting the knee joint skin, the distal femur was exposed and a hole with a diameter of 2 mm and a depth of 4 mm was drilled at the lateral epicondyle of the femur from medial to lateral with a surgical drill. A sterilized titanium rod was implanted into the hole. After implantation, the muscle tissue and skin were sutured at different levels. The rats were sacrificed 2 months after the operation, and the femurs were collected and fixed in 4% PFA for subsequent analysis.

Micro-CT and Histological Evaluation

We used a high-resolution Micro-CT scanner (skyscan 1072; Skyscan, Aartselaar, Belgium) to scan the amount of new bone around the implant. 0.5 μm thickness of bone around the implant was defined as the new bone and analyzed. We measured the microstructure index of trabecular bone mineral density (BV/

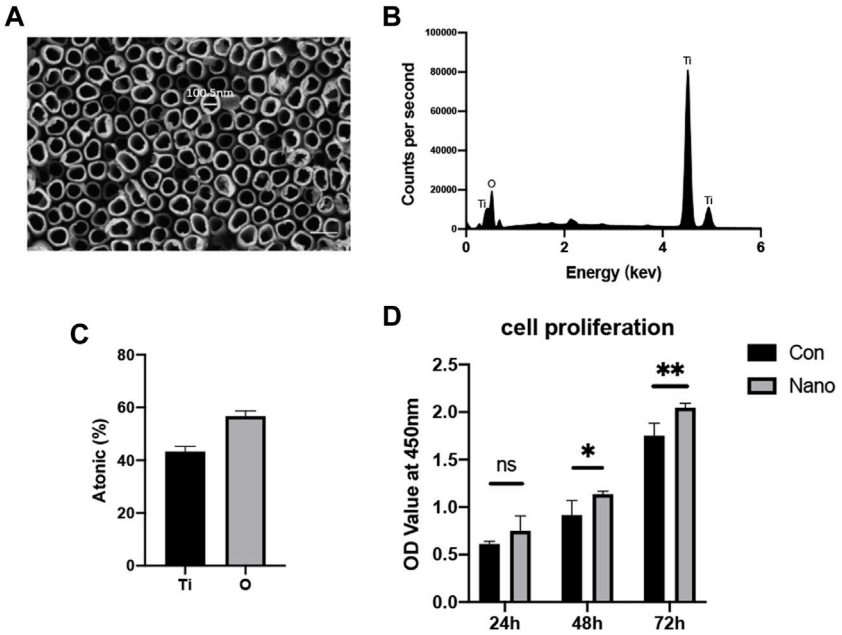

FIGURE 1 | Nanotopography surface characteristics and biocompatibility. **(A)** Lumen structure of nanotubes observed by SEM with a diameter of approximately 100 nm. Scale bar: 200 nm. **(B)** EDS analysis of the chemical element composition of nanotubes. **(C)** Ti and O element ratio on nanotopography. **(D)** CCK8 test of BMSCs seeded on nanotubes and smooth titanium. *$p < 0.05$, **$p < 0.01$.

TV), trabecular thickness (TB. Th), trabecular number (TB. N), and trabecular spacing (TB. SP). For histological evaluation, pre-fixed femoral specimens were decalcified in 10% ethylenediaminetetraacetic acid (EDTA). After decalcification, the implant was gently removed and embedded into paraffin to perform tissue section (5 μm). For histological evaluation, tissue sections were stained with hematoxylin and eosin (H&E). To evaluate immunohistochemistry, tissue sections were dewaxed in xylene and standard alcohol gradients and then washed with PBS. Then, nonspecific binding sites were blocked with 10% goat serum. The sections were incubated with primary antibodies (anti-OCN, anti-Piezo1, and anti-Yap purchased from Proteintech) at 4°C overnight. The next day, sections were washed with PBS and incubated with the appropriate HRP-labeled secondary antibody (Abcam) at RT for 1 h and then further developed with diaminobenzidine solution.

Statistical Analysis

SPSS 18.0 software was used for all statistical analysis. All data are representative of at least three independent experiments unless otherwise indicated. Data are expressed in the form of mean ± standard deviation. Differences between three or more groups were evaluated by one-way analysis of variance followed by the Student–Newman–Keuls *post hoc* test, and differences between two groups were analyzed by Student's t test. Graphpad 8.0 was used to draw all relevant figures. p values < 0.05 were considered statistically significant. All quantitative data were distributed normally.

RESULTS

Nanotubes Fabricated by Anodic Oxidation Show Satisfactory Lumen Structure and Biocompatibility

SEM results show that nanotubes fabricated at 50 V constant pressures are evenly distributed on the surface of titanium. The inner diameter of a nanotube is approximately 100 nm, and there are no residual impurities on the nanotube surface after ultrasonic vibration washing (**Figure 1A**). The results of energy spectrum scanning also show that titanium and oxygen account for the highest proportion in the element composition, and the element proportion is about 1:2, indicating that the main component of nanotubes is titanium dioxide (**Figures 1B,C**). The CCK8 results of 24, 48, and 72 h showed that compared with a smooth surface, titanium with nanotopography had no adverse effect on the proliferation of mesenchymal stem cells in short-term or long-term culture (**Figure 1D**). The aforementioned results show that nanotubes have satisfactory biocompatibility and will not produce obvious toxicity to cells.

Nanotopography Can Promote Osteogenesis *In Vivo* and *In Vitro*

It is reported that nanotopography with different diameters will affect the osteogenic ability of BMSCs. Our results showed that nanotubes with an inner diameter of 100 nm could significantly increase the mRNA expression of osteogenic genes such as *Col1a1*,

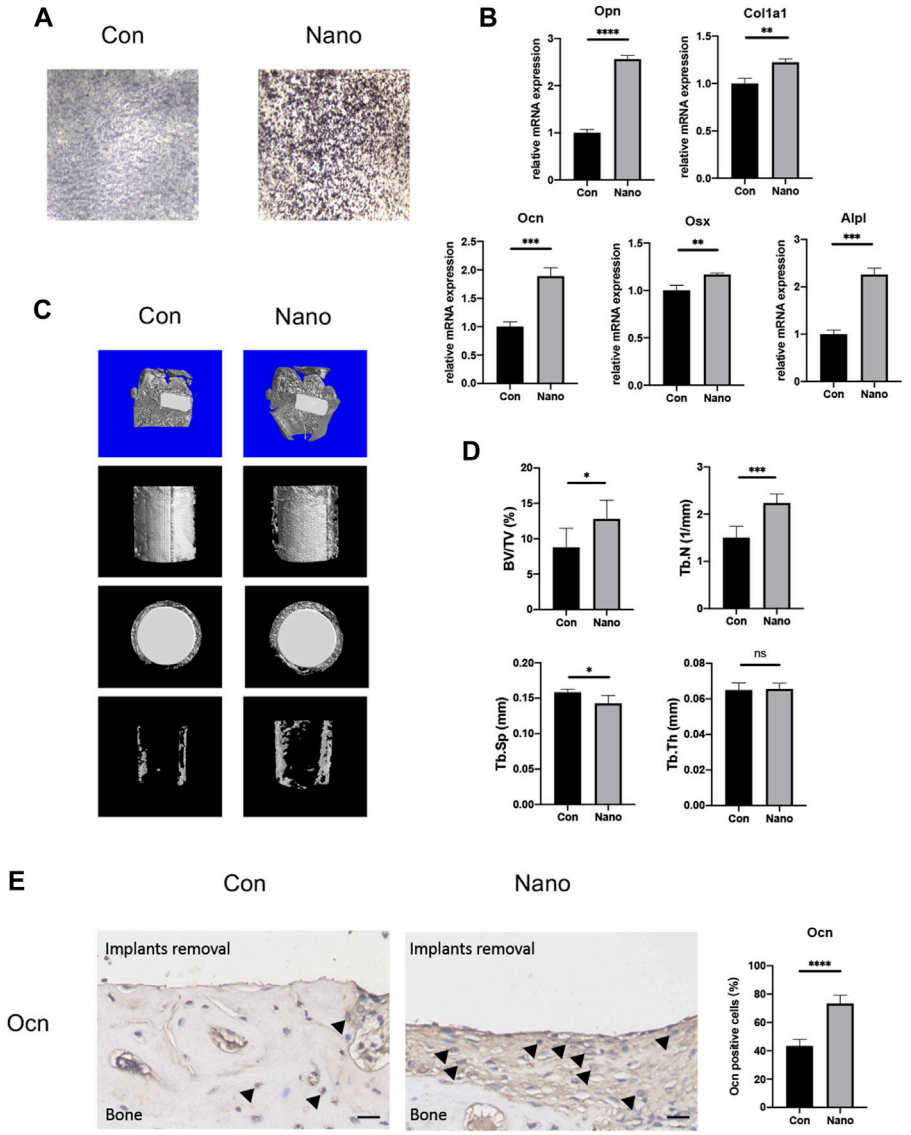

FIGURE 2 | Nanotopography promotes osteogenic differentiation of BMSCs both *in vivo* and *in vitro*. **(A)** ALP staining of BMSCs on different topographies. **(B)** Gene expression of osteogenic differentiation markers of BMSCs seeded on various topographies. **(C)** Micro-CT scans of the distal femur and presentative reconstruction of the new bone around implants from different views. **(D)** Analysis of BV/TV, Tb. N, Tb. Sp, and Tb. Th for new bones around implants with different topographies. **(E)** Immunohistochemistry staining and quantitative analysis of Ocn in new bones around implants. Scale bar: 10 μm $^{*}p < 0.05$, $^{**}p < 0.01$, $^{***}p < 0.001$, $^{****}p < 0.0001$.

Alpl, *Runx2*, *Ocn*, *Opn*, and *Osx in vitro*. ALP staining also showed that nanotubes could significantly increase the expression of alkaline phosphatase, which is one of the markers of osteogenesis (**Figures 2A,B**). At the same time, we implanted titanium rods with different topographies in the distal femur condyles of rats to verify the osteogenic effect of nanotopography *in vivo*. The results of micro-CT showed that the BV/TV value of new bone trabeculae around the implant in the nanotopography group was higher. The number of bone trabeculae was significantly greater than that in the control group (**Figures 2C, D**). After removing the titanium rod, immunohistochemistry of Ocn also showed that the new bone around the implant in the nano topography group was significantly more than that in the control group (**Figure 2E**). Our results show that nano topography can significantly promote differentiation and osteogenesis of BMSCs *in vivo* and *in vitro*.

Yap is Involved in Nano Topography Osteogenesis

BMSCs were seeded on smooth and nanotopography titanium slices, respectively, for cell immunofluorescence staining of Yap. It was found that the distribution of Yap was more concentrated in the nucleus in the nano topography group (**Figure 3A**). Yap activation promotes the expression of downstream genes by entering the

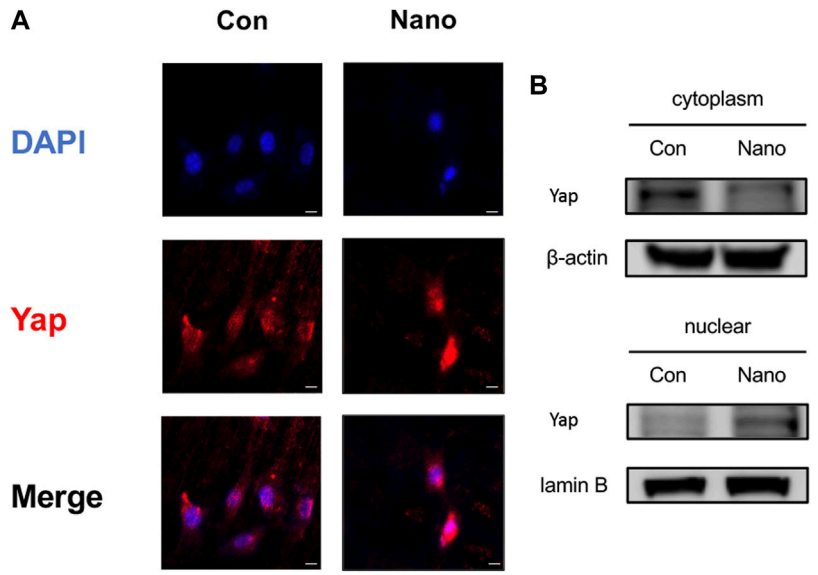

FIGURE 3 | Yap entering the nucleus plays an important role in nanotopography-related osteogenesis. **(A)** Immunofluorescence staining of Yap proved the accumulation of Yap in the nucleus under stimulation of nanotubes. Scale bar: 10 μm. **(B)** Western Blot of Yap in the nucleus and cytoplasm proved its accumulation in the nucleus when seeded on nanotubes.

nucleus. Therefore, the results show that Yap activation in the nucleus may be involved in the process of nanotopography promoting osteogenesis. In addition, when we separated the cytoplasmic and nuclear proteins, we found that the distribution of Yap in the nucleus was significantly higher in the nanotopography group than that in the control group (**Figure 3B**).

Inhibition of Yap or Knockdown/ Overexpression of Yap Can Affect the Osteogenesis of MC3T3-E1 Cells

To stably manipulate the expression of Yap, we chose the MC3T3-E1 cell line for further research. In order to verify the effect of Yap on osteogenesis and its role in nano topography osteogenesis, we selected verteporfin, an inhibitor of Yap, for experiments. First, when VP with different concentration gradients treated cells, the expression of Yap downstream genes such as Ctgf and Cyr61 were significantly inhibited (**Figure 4A**). When BMSCs seeded on titanium nanotubes were treated with 0.5 and 1 μM verteporfin for 7 days, it was found that the expression of osteogenic genes such as *Alpl*, *Runx2*, *Ocn*, *Opn*, and *Osx* decreased significantly (**Figure 4B**), and the results of ALP staining and AR staining of osteogenesis showed that verteporfin could significantly inhibit osteogenesis whether MC3T3-E1 cells were seeded on titanium or not (**Figures 4C,E**). Then, we constructed a Yap knockdown/overexpression cell line to further explain the role of Yap in osteogenesis (**Figure 5A**). The results of real-time quantitative PCR and ALP staining showed that the osteogenesis on nanotubes was inhibited when Yap was knockdown, while osteogenesis was significantly enhanced when Yap was overexpressed (**Figures 5B–D**). Finally, in order to further confirm the conclusion of this research, we carried out the rescue experiment. Western blot results showed that the overexpression of Yap could significantly rescue the inhibitory effect of VP on osteogenesis of BMSCs on nanotubes (**Figure 5E**). Results show that Yap is involved in the process of osteogenesis and plays an important role in the promotion of osteogenesis by nano topography.

Yap Can Regulate the Expression of Piezo1

It has been reported that Yap may regulate the expression and function of Piezo1 in tumor cells to regulate its proliferation and migration (Hasegawa et al., 2021). This study also preliminarily explored the possible downstream mechanism of Yap regulating nanotopography osteogenesis by regulating the expression of the Piezo1 gene. First, we used the Yap inhibitor VP with different concentration gradients to treat cells. It was found that the mRNA expression of Piezo1 decreased significantly with the increase of VP concentration (**Figure 6A**). Then, we detected the mRNA and protein expression of Piezo1 in Yap knockdown/ overexpression cell lines constructed as earlier. The results of real-time quantitative PCR and Western blot showed that the expression of Piezo1 decreased when Yap was knocked down, while the expression of Piezo1 increased when Yap was overexpressed (**Figures 6B,C**). This suggests that Piezo1 may be one of the downstream mechanisms of Yap regulating nanotopography osteogenesis. In addition, in sections of

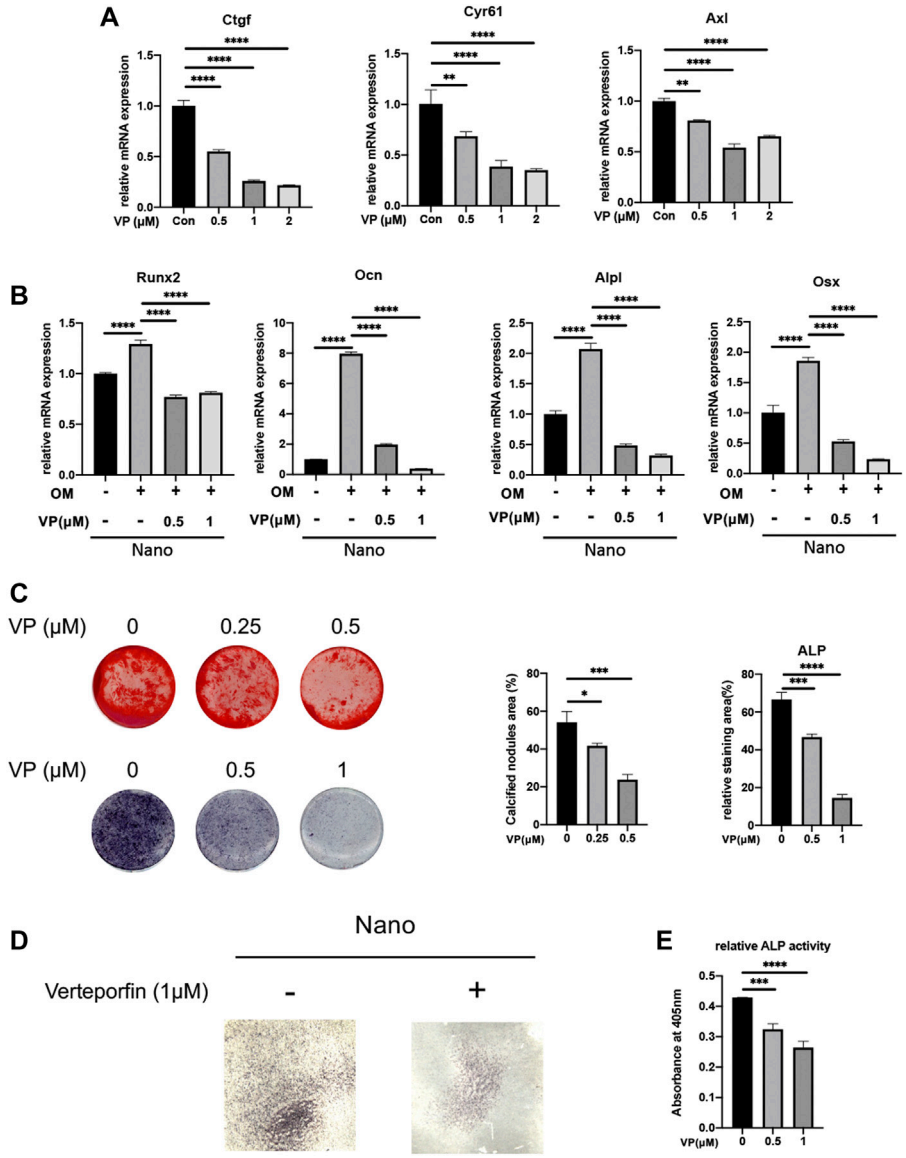

FIGURE 4 | Yap inhibitor, verteporfin, inhibits osteogenic differentiation of MC3T3-E1 cells seeded on nanotubes or 24-well plates. **(A)** Gene expression of Yap downstream genes Ctgf, Cyr61, and Axl under different concentrations of verteporfin. **(B)** Expression of osteogenic genes of MC3T3-E1 cells seeded on nanotubes. OM: osteogenic induction medium. **(C)** Alizarin Red S staining and ALP staining of MC3T3-E1 cells seeded on 24-well plates and quantitative analysis of calcified nodules areas and relative ALP staining areas. **(D)** ALP staining of MC3T3-E1 cells seeded on nanotubes with verteporfin. **(E)** Relative ALP activities of MC3T3-E1 cells on nanotubes treated with verteporfin. $^{*}p < 0.05$, $^{**}p < 0.01$, $^{***}p < 0.001$, and $^{****}p < 0.0001$.

immunohistochemistry, the expression of Piezo1 in newborn bones in the nanotopography group is evidently higher than that in the control group (**Figure 6D**). A diagram of this research is illustrated in **Figure 7**.

DISCUSSION

This study confirmed that fabrication of nanotubes on titanium surfaces by anodic oxidation can promote the osteogenic differentiation of mesenchymal stem cells both *in vivo* and *in vitro* and verified that Yap plays an important role in this process. In addition, we also verified the possible downstream regulatory gene *Piezo1* of Yap regulating osteogenesis, which provides an effective intervention target for promoting bone integration between orthopaedic plants and bone tissue *in vivo* in the future.

In the process of fracture healing and implant osteointegration, the most critical step is the adhesion and aggregation of bone marrow-derived mesenchymal stem cells locally and their differentiation into osteoblasts (Shah et al., 2019). After nanotubes are fabricated on a titanium surface, there will be a

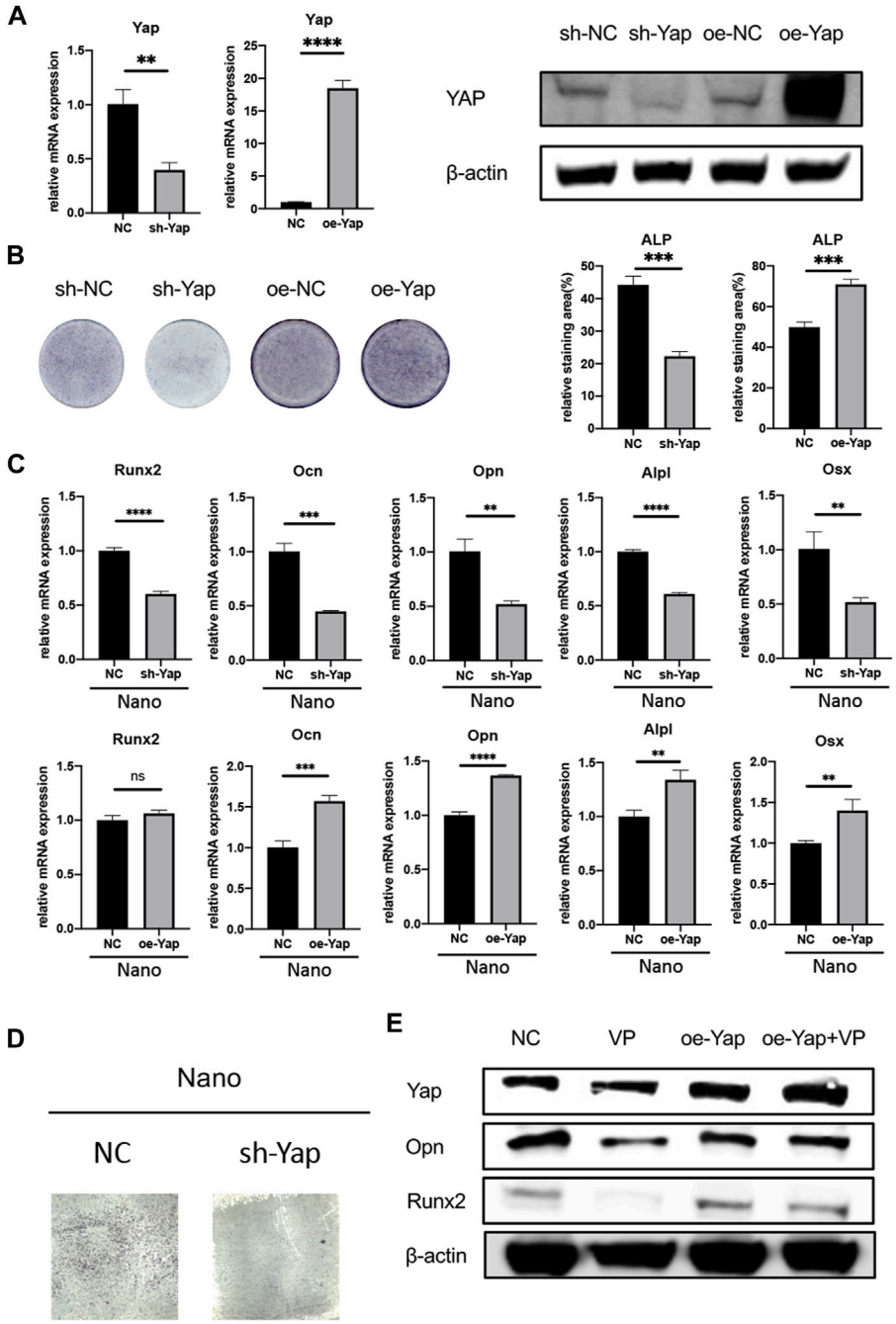

FIGURE 5 | Knockdown/overexpression of Yap regulates osteogenesis. **(A)** Verification of knockdown and overexpression of Yap through rt-qPCR and Western Blot. oe, overexpression. **(B)** ALP staining of sh-Yap and oe-Yap and quantitative analysis of the relative staining area. **(C)** Expression of osteogenic genes of sh-Yap and oe-Yap on nanotopography. **(D)** ALP staining of sh-Yap cells on nanotubes. **(E)** Overexpression of Yap could rescue anti-osteogenic effect of verteporfin. $^{*}p < 0.05$, $^{**}p < 0.01$, $^{***}p < 0.001$, and $^{****}p < 0.0001$.

gap with a diameter of about 100 nm between the nanotubes and the center of the nanotubes, which can accommodate the synapses of cells so as to promote the adhesion and proliferation of stem cells (Reznikov et al., 2018). Our CCK8 data also showed that a titanium sheet with nano topography could significantly enhance the proliferation of cells compared with the control group. In terms of differentiation, many literature studies have reported that both mechanical signals such as tensile force and physical signals such as material surface topography and stiffness can promote BMSC's osteogenesis once appropriate stimulation frequency and time are

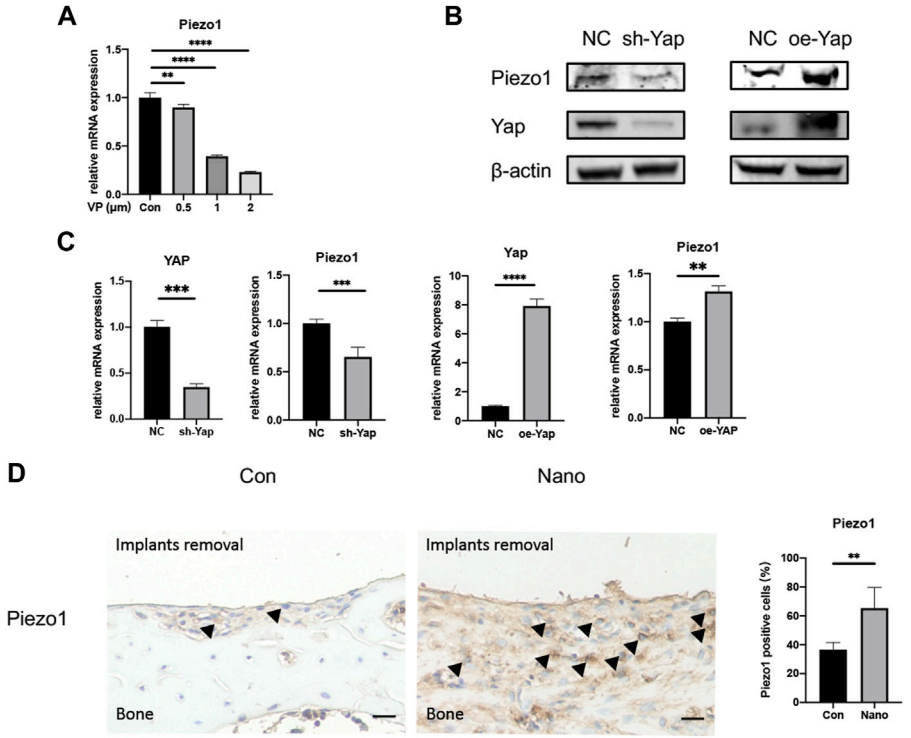

FIGURE 6 | Yap could regulate the expression of Piezo1. **(A)** Verteporfin inhibits expression of Piezo1 in a dose-dependent manner. **(B)** Knockdown or overexpression of Yap could regulate the protein expression of Piezo1. oe, overexpression. **(C)** Knockdown or overexpression of Yap could regulate the mRNA expression of Piezo1. **(D)** Expression of Piezo1 was elevated in bones around defects by immunohistochemistry and quantitative analysis. Scale bar: 10 μm $^{*}p < 0.05$, $^{**}p < 0.01$, $^{***}p < 0.001$, and $^{****}p < 0.0001$.

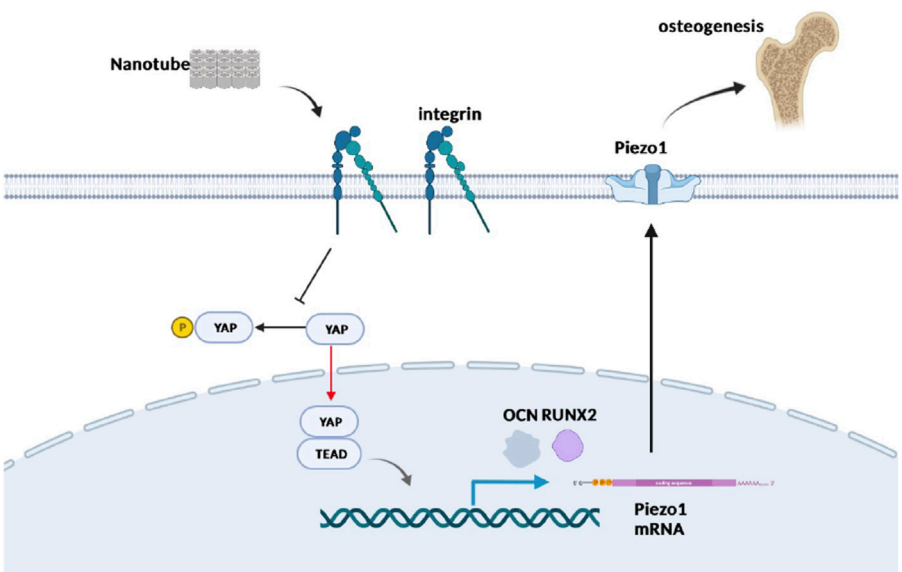

FIGURE 7 | Schematic plot to illustrate the role of Yap and Piezo1 in promoting nanotube-related osteogenesis. Nanotopography is recognized by mechanosensors such as integrins residing in the cell membrane, which suppresses the Hippo pathway and promotes nuclear entry of Yap. Furthermore, Yap activates TEADs and enhances the expression of Piezo1, which has been proved to be significant in osteogenesis. Created in BioRender.com.

applied (Arnsdorf et al., 2009; Shi et al., 2011; Shi et al., 2012). Arnsdorf et al. (Arnsdorf et al., 2009) reported that 1 hour of oscillatory fluid flow with a peak shear stress of 1.0 Pa evidently increases the expression of Runx2. In contrast, Shi et al.(Shi et al., 2012) found that 3% continuous cyclic mechanical tension inhibited osteogenic differentiation of MSCs, which emphasized the importance of stimulation frequency. Data in this study also prove that nanotubes fabricated at a 50 V constant pressure can promote the expression of osteogenic genes and the formation of new bone both *in vivo* and *in vitro*. The mechanism of this kind of physical signal promoting osteogenesis has also been widely discussed. At present, the recognized mechanism is that the physical signal of external force and material stimulates the mechanical receptors on the cell surface by changing the morphology of the cell and then further changing the F-actin cytoskeleton in the cell so as to activate the downstream pathway (Arnsdorf et al., 2009; Tong et al., 2020). However, it is still unclear how mechanical signals activate the downstream signal pathway in osteogenesis.

At present, there are two kinds of mechanical receptors widely studied. One is integrin, which mediates the interaction between cells and the extracellular matrix and is composed of two subunits, α and β. Subunit α has 18 subtypes while β has eight subtypes; the main integrin type in mesenchymal stem cells is $\alpha5\beta1$. It has been reported in the literature that $\alpha5$ (Cha et al., 2020; Zhang et al., 2021), αV (Lopes et al., 2019), $\alpha11$ (Shen et al., 2019), and other subunits are involved in the process of osteogenic differentiation. Lopes et al. (Lopes et al., 2019) knocked down integrin αV in MC3T3-E1 cells, and the expression of osteogenic markers significantly decreased. Integrin and downstream RhoA, FAK, and vinculin form an adhesive plaque complex and connect with F-actin. By changing the polymerization of F-actin and the proportion of monomers, the activation state of the downstream pathway can be changed (Arnsdorf et al., 2009; Tong et al., 2020). The second kind of mechanoreceptor molecules is a variety of ion channels found on the cell surface. Piezo1 is a newly discovered mechanoreceptor cation channel in recent years. It has been reported that Piezo1 is closely related to osteogenic differentiation. Since our team has discussed the role of F-actin in the differentiation of BMSCs in previous work (Tong et al., 2020), the relevant contents are not involved in this study.

The Yap/Taz pathway is a widely recognized mechanical response pathway. After receiving a mechanical signal, Yap and Taz will dephosphorylate and enter the nucleus to activate the downstream TEAD transcription factors and promote the transcription of related genes. Aragona et al. (Aragona et al., 2013) found that actin depolymerization-related molecule cofilin can regulate Yap/Taz pathway, suggesting the significance of the Yap/Taz pathway in the process of actin transmitting mechanical signal. At the same time, Tong et al. (Tong et al., 2020) also showed that the Yap/Taz pathway was a possible downstream signal pathway of F-actin. Therefore, this study focuses on the role of Yap in nanotube-stimulated osteogenesis. Contradictions exist in the previous literature study. In the research by Zhang et al.(Zhang et al., 2016), the authors believe that the activation of Yap is inhibited in the process of nanotube-promoting osteogenesis. In our study, Yap inhibitors and Yap knockdown/overexpression cell lines were used to prove that Yap activation plays a promoting role in both nanotube-stimulated osteogenesis and normal osteogenesis. However, the specific effector molecules downstream of Yap remain to be revealed. Verteporfin is a photosensitizer used in photodynamic therapy to eliminate abnormal intraocular blood vessels associated with age-related macular degeneration and other diseases (Brown et al., 2006). It can inhibit the combination of Yap and TEAD. Our data show that it can significantly inhibit the osteogenic differentiation of stem cells.

As mentioned earlier, Piezo1 has received extensive attention in recent years (Sugimoto et al., 2017). In recent years, many literature studies have reported its role in mechanical signal transduction and bone metabolism (Wang et al., 2020; Lee et al., 2021). Li et al. (Li et al., 2019) found administration of a Piezo1 agonist could increase bone mass, which mimicked the effect of physical exercise. In addition, conditional knockout of Piezo1 in osteoblasts and osteocytes greatly reduced bone strength in mice. Sugimoto et al. (Sugimoto et al., 2017) studied the role of Piezo1 in differentiation and proved its promoting effect on osteogenic differentiation. These studies all revealed the importance of Piezo1 in mechano-related osteogenesis. Studies by Japanese scholars (Hasegawa et al., 2021) have shown that Yap can regulate the expression of Piezo1 in oral squamous cell carcinoma cells and further regulate the proliferation and metastasis of squamous cell carcinoma. Our data shows that inhibiting Yap or knockdown and overexpression of Yap in osteoblasts will affect the expression of Piezo1 mRNA and protein. Therefore, our study preliminarily proved the possible downstream effector molecule, Piezo1, of Yap. However, whether such regulation is at the protein level or transcriptional level and how to regulate the expression of Piezo1 still need further research.

In conclusion, this study not only confirmed the important role of Yap in the process of nanotopography-promoting osteogenesis but also creatively proposed and verified its downstream effector molecule, Piezo1, a mechanosensitive cation channel.

DATA AVAILABILITY STATEMENT

The original contributions presented in the study are included in the article/**Supplementary Material**; further inquiries can be directed to the corresponding authors.

ETHICS STATEMENT

The animal study was reviewed and approved by the ethics committee of Shanghai Ninth People's Hospital.

AUTHOR CONTRIBUTIONS

KK, YC, and YH carried out most of the *in vitro* and *in vivo* experiments and drafted the manuscript. HQ, CZ, KR, PZ, and JZ

analyzed data and participated in most *in vivo* experiments. ZZ and HL designed the whole project and revised the manuscript. All authors have read and approved the manuscript.

FUNDING

This study was supported by the National Natural Science Foundation of China (Grant Nos. 81672181 and 82072397), the Shanghai Municipal Education Commission Two-hundred Talent, the National Key R&D Program of China (Grant No. 2017YFC0110704), and the Project of Biobank (YBKA201911) from Shanghai Ninth People's Hospital.

SUPPLEMENTARY MATERIAL

The Supplementary Material for this article can be found online at: https://www.frontiersin.org/articles/10.3389/fbioe.2022.872088/full#supplementary-material

REFERENCES

Aragona, M., Panciera, T., Manfrin, A., Giulitti, S., Michielin, F., Elvassore, N., et al. (2013). A Mechanical Checkpoint Controls Multicellular Growth through YAP/TAZ Regulation by Actin-Processing Factors. *Cell* 154 (5), 1047–1059. doi:10.1016/j.cell.2013.07.042

Arnsdorf, E. J., Tummala, P., Kwon, R. Y., and Jacobs, C. R. (2009). Mechanically Induced Osteogenic Differentiation - the Role of RhoA, ROCKII and Cytoskeletal Dynamics. *J. Cel. Sci.* 122 (Pt 4), 546–553. doi:10.1242/jcs.036293

Brown, D. M., Kaiser, P. K., Michels, M., Soubrane, G., Heier, J. S., Kim, R. Y., et al. (2006). Ranibizumab versus Verteporfin for Neovascular Age-Related Macular Degeneration. *N. Engl. J. Med.* 355 (14), 1432–1444. doi:10.1056/NEJMoa062655

Cha, B. H., Kim, J. S., Bello, A., Lee, G. H., Kim, D. H., Kim, B. J., et al. (2020). Efficient Isolation and Enrichment of Mesenchymal Stem Cells from Human Embryonic Stem Cells by Utilizing the Interaction between Integrin α 5 β 1 and Fibronectin. *Adv. Sci.* 7 (17), 2001365. doi:10.1002/advs.202001365

Chang, Y., Shao, Y., Liu, Y., Xia, R., Tong, Z., Zhang, J., et al. (2019). Mechanical Strain Promotes Osteogenic Differentiation of Mesenchymal Stem Cells on TiO2 Nanotubes Substrate. *Biochem. Biophys. Res. Commun.* 511 (4), 840–846. doi:10.1016/j.bbrc.2019.02.145

Curran, J. M., Chen, R., and Hunt, J. A. (2006). The Guidance of Human Mesenchymal Stem Cell Differentiation *In Vitro* by Controlled Modifications to the Cell Substrate. *Biomaterials* 27 (27), 4783–4793. doi:10.1016/j.biomaterials.2006.05.001

Deng, Y., Lu, J., Li, W., Wu, A., Zhang, X., Tong, W., et al. (2018). Reciprocal Inhibition of YAP/TAZ and NF-κB Regulates Osteoarthritic Cartilage Degradation. *Nat. Commun.* 9 (1), 4564. doi:10.1038/s41467-018-07022-2

Du, Y., Montoya, C., Orrego, S., Wei, X., Ling, J., Lelkes, P. I., et al. (2019). Topographic Cues of a Novel Bilayered Scaffold Modulate Dental Pulp Stem Cells Differentiation by Regulating YAP Signalling through Cytoskeleton Adjustments. *Cell Prolif.* 52 (6), e12676. doi:10.1111/cpr.12676

Dupont, S., Morsut, L., Aragona, M., Enzo, E., Giulitti, S., Cordenonsi, M., et al. (2011). Role of YAP/TAZ in Mechanotransduction. *Nature* 474 (7350), 179–183. doi:10.1038/nature10137

Fan, Y., Du, Z., Ding, Q., Zhang, J., Op Den Winkel, M., Gerbes, A., et al. (2021). SEPT6 Drives Hepatocellular Carcinoma Cell Proliferation, Migration and Invasion via the Hippo/YAP Signaling Pathway. *Int. J. Oncol.* 58 (6), 25. doi:10.3892/ijo.2021.5205

Hao, L., Li, L., Wang, P., Wang, Z., Shi, X., Guo, M., et al. (2019). Synergistic Osteogenesis Promoted by Magnetically Actuated Nano-Mechanical Stimuli. *Nanoscale* 11, 23423–23437. doi:10.1039/c9nr07170a

Hasegawa, K., Fujii, S., Matsumoto, S., Tajiri, Y., Kikuchi, A., and Kiyoshima, T. (2021). YAP Signaling Induces PIEZO1 to Promote Oral Squamous Cell Carcinoma Cell Proliferation. *J. Pathol.* 253 (1), 80–93. doi:10.1002/path.5553

Kahlenberg, C. A., Swarup, I., Krell, E. C., Heinz, N., and Figgie, M. P. (2019). Causes of Revision in Young Patients Undergoing Total Hip Arthroplasty. *J. Arthroplasty* 34 (7), 1435–1440. doi:10.1016/j.arth.2019.03.014

Kelmer, G., Stone, A. H., Turcotte, J., and King, P. J. (2021). Reasons for Revision: Primary Total Hip Arthroplasty Mechanisms of Failure. *J. Am. Acad. Orthop. Surg.* 29 (2), 78–87. doi:10.5435/jaaos-d-19-00860

Lee, W., Nims, R. J., Savadipour, A., Zhang, Q., Leddy, H. A., Liu, F., et al. (2021). Inflammatory Signaling Sensitizes Piezo1 Mechanotransduction in Articular Chondrocytes as a Pathogenic Feed-Forward Mechanism in Osteoarthritis. *Proc. Natl. Acad. Sci. U.S.A.* 118 (13), e2001611118. doi:10.1073/pnas.2001611118

Li, X., Han, L., Nookaew, I., Mannen, E., Silva, M. J., Almeida, M., et al. (2019). Stimulation of Piezo1 by Mechanical Signals Promotes Bone Anabolism. *Elife* 8, e49631. doi:10.7554/eLife.49631

Liu, Y., Rath, B., Tingart, M., and Eschweiler, J. (2020). Role of Implants Surface Modification in Osseointegration: A Systematic Review. *J. Biomed. Mater. Res.* 108 (3), 470–484. doi:10.1002/jbm.a.36829

Lopes, H. B., Freitas, G. P., Fantacini, D. M. C., Picanço-Castro, V., Covas, D. T., Rosa, A. L., et al. (2019). Titanium with Nanotopography Induces Osteoblast Differentiation through Regulation of Integrin αV. *J. Cel. Biochem.* 120 (10), 16723–16732. doi:10.1002/jcb.28930

Lorthongpanich, C., Thumanu, K., Tangkiettrakul, K., Jiamvoraphong, N., Laowtammathron, C., Damkham, N., and U-pratya, Y. (2019). YAP as a Key Regulator of Adipo-Osteogenic Differentiation in Human MSCs. *Stem Cel Res Ther.* 10 (1), 402. doi:10.1186/s13287-019-1494-4

Park, J., Bauer, S., von der Mark, K., and Schmuki, P. (2007). Nanosize and Vitality: TiO2 Nanotube Diameter Directs Cell Fate. *Nano Lett.* 7 (6), 1686–1691. doi:10.1021/nl070678d

Park, J. S., Kim, M., Song, N.-J., Kim, J.-H., Seo, D., Lee, J.-H., et al. (2019). A Reciprocal Role of the Smad4-Taz Axis in Osteogenesis and Adipogenesis of Mesenchymal Stem Cells. *Stem Cells* 37 (3), 368–381. doi:10.1002/stem.2949

Perestrelo, T., Correia, M., Ramalho-Santos, J., and Wirtz, D. (2018). Metabolic and Mechanical Cues Regulating Pluripotent Stem Cell Fate. *Trends Cel. Biol.* 28 (12), 1014–1029. doi:10.1016/j.tcb.2018.09.005

Reznikov, N., Bilton, M., Lari, L., Stevens, M. M., and Kröger, R. (2018). Fractal-like Hierarchical Organization of Bone Begins at the Nanoscale. *Science* 360 (6388), eaao2189. doi:10.1126/science.aao2189

Schwartz, B. E., Piponov, H. I., Helder, C. W., Mayers, W. F., and Gonzalez, M. H. (2016). Revision Total Hip Arthroplasty in the United States: National Trends and In-Hospital Outcomes. *Int. Orthop. (Sicot)* 40 (9), 1793–1802. doi:10.1007/s00264-016-3121-7

Shah, F. A., Thomsen, P., and Palmquist, A. (2019). Osseointegration and Current Interpretations of the Bone-Implant Interface. *Acta Biomater.* 84, 1–15. doi:10.1016/j.actbio.2018.11.018

Shen, B., Vardy, K., Hughes, P., Tasdogan, A., Zhao, Z., Yue, R., et al. (2019). Integrin Alpha11 Is an Osteolectin Receptor and Is Required for the Maintenance of Adult Skeletal Bone Mass. *Elife* 8, e42274. doi:10.7554/eLife.42274

Shi, Y., Li, H., Zhang, X., Fu, Y., Huang, Y., Lui, P. P. Y., et al. (2011). Continuous Cyclic Mechanical Tension Inhibited Runx2 Expression in Mesenchymal Stem Cells through RhoA-ERK1/2 Pathway. *J. Cel. Physiol.* 226 (8), 2159–2169. doi:10.1002/jcp.22551

Shi, Y., Fu, Y., Tong, W., Geng, Y., Lui, P. P. Y., Tang, T., et al. (2012). Uniaxial Mechanical Tension Promoted Osteogenic Differentiation of Rat Tendon-Derived Stem Cells (rTDSCs) via the Wnt5a-RhoA Pathway. *J. Cel. Biochem.* 113 (10), 3133–3142. doi:10.1002/jcb.24190

Sugimoto, A., Miyazaki, A., Kawarabayashi, K., Shono, M., Akazawa, Y., Hasegawa, T., et al. (2017). Piezo Type Mechanosensitive Ion Channel Component 1

Functions as a Regulator of the Cell Fate Determination of Mesenchymal Stem Cells. *Sci. Rep.* 7 (1), 17696. doi:10.1038/s41598-017-18089-0

Sun, Y., Villa-Diaz, L. G., Lam, R. H. W., Chen, W., Krebsbach, P. H., and Fu, J. (2012). Mechanics Regulates Fate Decisions of Human Embryonic Stem Cells. *PLoS One* 7 (5), e37178. doi:10.1371/journal.pone.0037178

Tong, Z., Liu, Y., Xia, R., Chang, Y., Hu, Y., Liu, P., et al. (2020). F-actin Regulates Osteoblastic Differentiation of Mesenchymal Stem Cells on TiO2 Nanotubes through MKL1 and YAP/TAZ. *Nanoscale Res. Lett.* 15 (1), 183. doi:10.1186/s11671-020-03415-9

Wang, N., Li, H., Lü, W., Li, J., Wang, J., Zhang, Z., et al. (2011). Effects of TiO2 Nanotubes with Different Diameters on Gene Expression and Osseointegration of Implants in Minipigs. *Biomaterials* 32 (29), 6900–6911. doi:10.1016/j.biomaterials.2011.06.023

Wang, W., Liu, Q., Zhang, Y., and Zhao, L. (2014). Involvement of ILK/ERK1/2 and ILK/p38 Pathways in Mediating the Enhanced Osteoblast Differentiation by Micro/nanotopography. *Acta Biomater.* 10 (8), 3705–3715. doi:10.1016/j.actbio.2014.04.019

Wang, L., You, X., Lotinun, S., Zhang, L., Wu, N., and Zou, W. (2020). Mechanical Sensing Protein PIEZO1 Regulates Bone Homeostasis via Osteoblast-Osteoclast Crosstalk. *Nat. Commun.* 11 (1), 282. doi:10.1038/s41467-019-14146-6

Wu, J., Lewis, A. H., and Grandl, J. (2017). Touch, Tension, and Transduction - the Function and Regulation of Piezo Ion Channels. *Trends Biochem. Sci.* 42 (1), 57–71. doi:10.1016/j.tibs.2016.09.004

Yang, W., Lu, X., Zhang, T., Han, W., Li, J., He, W., et al. (2021). TAZ Inhibits Osteoclastogenesis by Attenuating TAK1/NF-κB Signaling. *Bone Res.* 9 (1), 33. Article 33. doi:10.1038/s41413-021-00151-3

Yong, K. W., Choi, J. R., Choi, J. Y., and Cowie, A. C. (2020). Recent Advances in Mechanically Loaded Human Mesenchymal Stem Cells for Bone Tissue Engineering. *Ijms* 21 (16), 5816. doi:10.3390/ijms21165816

Zhang, H., Cooper, L. F., Zhang, X., Zhang, Y., Deng, F., Song, J., et al. (2016). Titanium Nanotubes Induce Osteogenic Differentiation through the FAK/RhoA/YAP cascade. *RSC Adv.* 6 (50), 44062–44069. doi:10.1039/c6ra04002k

Zhang, D., Ni, N., Wang, Y., Tang, Z., Gao, H., Ju, Y., et al. (2021). CircRNA-vgll3 Promotes Osteogenic Differentiation of Adipose-Derived Mesenchymal Stem Cells via Modulating miRNA-dependent Integrin α5 Expression. *Cell Death Differ.* 28 (1), 283–302. doi:10.1038/s41418-020-0600-6

Conflict of Interest: The authors declare that the research was conducted in the absence of any commercial or financial relationships that could be construed as a potential conflict of interest.

Publisher's Note: All claims expressed in this article are solely those of the authors and do not necessarily represent those of their affiliated organizations, or those of the publisher, the editors, and the reviewers. Any product that may be evaluated in this article, or claim that may be made by its manufacturer, is not guaranteed or endorsed by the publisher.

frontiers | Frontiers in Bioengineering and Biotechnology

ORIGINAL RESEARCH
published: 11 April 2022
doi: 10.3389/fbioe.2022.883335

Antibacterial Activity of an Anodized TiNbSn Alloy Prepared in Sodium Tartrate Electrolyte

Hiroaki Kurishima[1], Yu Mori[1], Keiko Ishii[2], Hiroyuki Inoue[3], Takayuki Mokudai[4], Satoko Fujimori[1], Eiji Itoi[1], Shuji Hanada[4], Naoya Masahashi[4] and Toshimi Aizawa[1]*

[1]Department of Orthopedic Surgery, Tohoku University Graduate School of Medicine, Sendai, Japan, [2]Department of Medical Microbiology, Mycology and Immunology, Tohoku University Graduate School of Medicine, Sendai, Japan, [3]Department of Materials Science, Graduate School of Engineering, Osaka Prefecture University, Sakai, Japan, [4]Institute for Materials Research, Tohoku University, Sendai, Japan

In this study, we anodized a TiNbSn alloy with low Young's modulus in an electrolyte of sodium tartrate with and without hydrogen peroxide (H_2O_2). The photo-induced characteristics of the anodized alloy were analyzed for crystallinity and electrochemical conditions with comparisons to the effect with the addition of H_2O_2. The antibacterial activity was evaluated using methicillin-resistant *Staphylococcus aureus* and other pathogenic bacteria according to ISO 27447, and time decay antibacterial tests were also conducted. The anodized oxide had a porous microstructure with anatase- and rutile-structured titanium dioxide (TiO_2). In contrast, the peaks of rutile-structured TiO_2 were accelerated in the anodized TiNbSn alloy with H_2O_2. The formation of hydroxyl radicals and methylene blue breaching performance under ultraviolet irradiation was confirmed in the anodic oxide on TiNbSn alloy with and without H_2O_2. The anodic oxide on TiNbSn alloy had a robust antibacterial activity, and no significant difference was detected with or without H_2O_2. We conclude that anodized TiNbSn alloy with sodium tartrate electrolyte may be a functional biomaterial with a low Young's modulus and an antibacterial function.

Keywords: antibacterial activity, anodic oxide, photocatalyst (TiO_2), sodium tartrate, TiNbSn alloys

OPEN ACCESS

Edited by:
Liqun Xu,
Southwest University, China

Reviewed by:
Xuefeng Hu,
Sichuan University, China
Rong Wang,
Ningbo Institute of Materials Technology and Engineering (CAS), China

****Correspondence:***
Yu Mori
yu-mori@med.tohoku.ac.jp

Specialty section:
This article was submitted to Biomaterials, a section of the journal Frontiers in Bioengineering and Biotechnology

Received: *24 February 2022*
Accepted: *18 March 2022*
Published: *11 April 2022*

Citation:
Kurishima H, Mori Y, Ishii K, Inoue H, Mokudai T, Fujimori S, Itoi E, Hanada S, Masahashi N and Aizawa T (2022) Antibacterial Activity of an Anodized TiNbSn Alloy Prepared in Sodium Tartrate Electrolyte. Front. Bioeng. Biotechnol. 10:883335. doi: 10.3389/fbioe.2022.883335

INTRODUCTION

The development of antibacterial metals has been in use with antibacterial metal ions such as silver and copper, or antibacterial agents such as iodine and vancomycin (Ando et al., 2010; Shirai et al., 2011; Han et al., 2017; Wang et al., 2019). However, there is a risk that these added toxic substances have the potential to leak into the bloodstream and result in subsequent side effects (Punjataewakupt et al., 2019). Titanium dioxide (TiO_2) has previously been reported as a photocatalytic material and is used for air and water purification due to decomposition of the redox species by photogenerated carriers upon illumination corresponding to bandgap energy (Fujishima and Honda, 1972). In the

Abbreviations: ANOVA, Analysis of variance; DMPO, 5,5-dimethel-a-pyrroline-N-oxide; E. coli, *Escherichia coli;* ESR, Electron spin resonance; H_2O_2, Hydrogen peroxide; ISO, International organization for standardization; JIS, Japanese Industrial Standards; MB, Methylene blue; MRSA, Methicillin-resistant *Staphylococcus aureus;* MSSA, Methicillin-sensitive *Staphylococcus aureus;* ●OH, Hydroxyl radicals; ROS, Reactive oxygen radicals; SCDLP, Soybean-casein digest broth with lectin and polysorbate; SEM, Scanning electron microscopy; TiO_2, Titanium dioxide; UV, Ultraviolet; XPS, X-ray photoelectron spectroscopy; XRD, X-ray diffraction.

medical field, there are reports that TiO_2 also has an antibacterial activity (Ohko et al., 2001; Yao et al., 2008) and an antitumor effect (Cai et al., 1992; Kubota et al., 1994). The irradiation of water on TiO_2 by ultraviolet (UV) light results in its decomposition by the photocatalytic effect to produce reactive oxygen radicals (ROS) such as hydroxyl radicals (•OH), superoxide anions, and hydrogen peroxide (H_2O_2) (Fujishima and Honda, 1972). The ROS has been reported to have antibacterial and antitumor effects by destructing the structure of bacteria and tumor cells (Watts et al., 1995; Maness et al., 1999; Liou and Chang, 2012). In contrast, TiO_2 is considered a stable and safe substance that is used as an additive in food and drugs (Ophus et al., 1979; Skocaj et al., 2011). TiO_2 coating on biocompatible alloy has the potential to be an ideal technology due to its antibacterial performance by UV irradiation, as well as inherent safety and stability.

Ti6Al4V alloy is a biocompatible material that is resistant to corrosion, therefore it is widely used in orthopaedic implants (Head et al., 1995). However, the elasticity modulus of Ti6Al4V (Young's modulus: 110 GPa) is higher in comparison to human cortical bone (10–30 GPa) (Long and Rack, 1998). In medical practice, differences of Young's modulus between femoral implants used in total hip arthroplasty and that of human cortical bone may cause disproportionate stress distribution and lead to pain in the thigh (Glassman et al., 2006). For the resolution of these problems, β-type TiNbSn alloy which has a lower Young's modulus <50 GPa was developed to reduce the possibility of stress shielding and thigh pain (Miura et al., 2011). β-structured TiNbSn alloy increases its stiffness and Young's modulus when the alloy is annealed at temperatures above 673 K (Hanada et al., 2014). The results of a clinical trial of a TiNbSn alloy hip prosthesis have been reported, showing that the TiNbSn alloy hip prosthesis was effective in deterring thigh pain and bone atrophy due to stress shielding 3 years after surgery (Chiba et al., 2021). Previous reports have also described that tibial fracture healing in mice and rabbits was enhanced using intramedullary nails made with TiNbSn alloy in comparison to using Ti6Al4V alloy and stainless steel (Fujisawa et al., 2018; Kogure et al., 2019; Mori et al., 2021). To improve the biocompatibility of TiNbSn alloy, it underwent anodic oxidation with acetic acid and sulfuric acid which demonstrated improved osseointegration with hydroxyapatite formation in experimental models (Tanaka et al., 2016; Masahashi et al., 2017; Kunii et al., 2019; Masahashi et al., 2019). Sodium tartrate has been reported to inhibit the surface cracking of anodic oxides. Since high voltage is applied, there is a high possibility of embrittlement of the oxide film, but sodium tartrate is effective in suppressing such embrittlement (Masahashi et al., 2021). A study of anodic oxidation of TiNbSn alloy with sodium tartrate has reported no change in Young's modulus after anodic oxidation (Hatakeyama et al., 2021). Thus, TiNbSn alloy is a promising biomaterial in the field of orthopaedic prosthesis. Furthermore, anodic oxidation of TiNbSn alloy with sodium tartrate indicated photocatalytic activity with UV irradiation (Masahashi et al., 2021). We conceived the idea that photocatalytic activity could be applied to antibacterial activity.

To date, there are few reports of the antibacterial ability of TiO_2 by anodic oxidation (Miura et al., 2015). Furthermore, there are no reports on the effect of anodic oxidation with sodium tartrate on the improvement of surface quality and antibacterial activity of β-type titanium alloy with low Young's modulus. Therefore, the present study aimed to evaluate the antibacterial effect of UV irradiation of anodized TiNbSn alloy prepared in the sodium tartrate electrolyte. Furthermore, we investigated the effect of H_2O_2 addition to the electrolyte on antibacterial and photocatalytic activities of anodized TiNbSn alloy for the purpose of accelerating the formation of well-crystallized TiO_2 and increasing the antibacterial ability.

MATERIALS AND METHODS

Preparation of Anodized TiNbSn Alloy

The composition of TiNbSn alloy used in the present study was Ti-21Nb-2Sn (at%), and was fabricated by thermo-mechanical treatment using extrusion and swaging. The detailed procedure was as previously published (Hanada et al., 2013). TiNbSn alloy plates with dimensions of 25 × 25 × 1 mm, 10 × 20 × 1 mm and 10 × 10 × 1 mm were polished with emery paper (1,500 grit), rinsed in ethanol using an ultrasonic cleaner, and prepared as the anode electrode. Anodic oxidation was performed on the TiNbSn alloy plates for 30 min in 50 mM-sodium tartrate containing 0.7 M-H_2O_2 galvanostatically at a constant current density of 50 mA/cm^2 up to a maximum of 380 V using a DC power supply (PRK 500-3.2, Matsusada Precision, Japan), as previously described (Masahashi et al., 2021). TiNbSn alloy plates anodized with only the 50 mM-sodium tartrate were also prepared to assess the effect of H_2O_2 addition. The anodized electrode was rinsed with distilled water, dried at 293 K, and subsequently annealed for 5 h at 723 K in the atmosphere. The anodized TiNbSn alloy with dimensions of 10 × 10 × 1 mm and 10 × 20 × 1 mm were used for the electron spin resonance (ESR) tests and methylene blue (MB) bleaching tests, respectively. The anodized alloy with dimensions of 25 × 25 × 1 mm were used for surface analyses and antibacterial tests.

Surface Analyses

Surface analyses of the anodized alloy were performed as previously described (Masahashi et al., 2017, 2019; Masahashi et al., 2021). The microstructure of the samples was observed using scanning electron microscopy (SEM; VE-8900, Keyence, Japan), laser microscopy (VK-X 150, Keyence, Japan), and analyses by X-ray Diffraction (XRD; X'Pert diffractometer, PANalytical, Netherlands) with a thin-film geometry arrangement using a 0.5° glancing angle, and a rotating detector was also performed. The upper surface of the samples was analyzed by X-ray photoelectron spectroscopy (XPS) equipped with an electron spectrometer (Kratos AXIS-Ultra DLD, Shimadzu, Japan) with monochromated Al Kα radiation at a base pressure of 3.0 × 10^{-7} Pa. The full width at half maximum intensity of the Ag 3d5/2 peak was 0.73 eV, and the base pressure of the spectrometer was 6.5 × 10^{-8} Pa. The analysis

of absorption spectrum was performed using a UV-vis spectrophotometer (V-550, Jasco, Japan).

Photocatalytic Assessment

For the evaluation of the photocatalytic activity under UV light irradiation (SLUV-4, As-one corporation, Japan), the amount of •OH production was measured by X-band ESR spectrometer (JES-FA-100, JEOL, Japan) using the spin-trapping agent 5,5-dimethel-a-pyrroline-N-oxide (DMPO, Labotech, Japan) as previously described (Iwatsu et al., 2020). UV light irradiation was performed with a wavelength of 365 nm and intensity of 1.0 mW/cm^2. The photocatalytic activity was also evaluated using MB bleaching tests according to the evaluation method of Japanese Industrial Standards, JIS R 1703-2:2014. The anodized oxide was placed in an optical quartz cell containing 2 ml of 25 mg/L MB aqueous solution until the concentration of MB became constant, as to avoid the effect of MB adsorption on the photocatalytic activity. A UV lamp was used to supply the UV light at a wavelength of 365 nm, and the intensity of the irradiated light was 1.0 mW/cm^2 at the surface (Masahashi et al., 2009).

Antibacterial Assays

Two different antibacterial tests were performed in the present study. The first antibacterial test was performed according to the evaluation methods of the International organization for standardization, ISO 27447:2019 (Japanese Industrial Standards, JIS R 1702:2012). For the Gram-positive coccus assays, methicillin-sensitive *Staphylococcus aureus* (MSSA; NBRC12732) and methicillin-resistant *Staphylococcus aureus* (MRSA; ATCC43300) were evaluated for their antibacterial activities. For the Gram-negative *bacillus*, *Escherichia coli* (*E. coli*; NBRC3972) was used for the antibacterial assays. Each bacterium was cultured on nutrient agar (Difco nutrient agar, Becton Dickinson, NJ, United States) medium at 35°C for 36–43.5 h. The cultured bacteria were prepared on a 1/500 density of nutrient broth (Nutrient broth, Eiken Chemical, Japan) medium to obtain a bacterial count of 5.3×10^6 cells/mL. This solution was utilized for the antibacterial test. Before antibacterial testing of anodized TiNbSn alloy samples, the antibacterial performance of untreated TiNbSn alloys was explored in comparison with that of glass. Antibacterial tests of MSSA and *E. coli* under low-intensity UV light irradiation demonstrated no antibacterial performance in either untreated TiNbSn alloy or glass (**Figure A1**). Based on the above results, a glass plate was set as the control for the antibacterial test in this study. Three plates of anodized TiNbSn alloy and three plates of glass as the negative control were used in ISO27447 antibacterial test. Each TiNbSn alloy plate or glass was placed on a plastic net and placed on paper containing 6 ml of sterile water to retain moisture in each Petri dish. The anodized TiNbSn alloy plates and glasses were inoculated with 37.5 µL (2×10^5 cells) of the test bacterial solution, and both the solution and samples adhered with a sterile polyethylene film (VF-10, Kokuyo, Japan). To prevent drying, a 1.1 mm thick glass plate (TEMPAX, Schott, Germany) was placed on top of the Petri dish. The intensity of UV light transmitted through the film and glass plate was 0.21 mW/cm^2, and the bacteria were incubated with UV light irradiation at a wavelength of 352 nm (FL 20S Bl-B 20W, Nippon Electric Company, Japan) for 8 h at 25°C. For the control group, the bacteria on each sample were cultured in the dark for 8 h at 25°C. After UV irradiation, the samples and film were placed in a plastic bottle containing 20 ml of soybean-casein digest broth with lectin and polysorbate (SCDLP) medium (SCDLP broth, Eiken chemical, Japan), and the test bacterial solution was removed through washing. A volume of 100 µL of the bacterial washout SCDLP medium solution was diluted in 900 µL of saline solution, resulting in a 1/10 dilution of bacterial washout solution. To the nutrient agar medium, 100 µL of bacterial washout solution and 1/10 diluted solution were added and subsequently incubated. The number of viable bacteria was determined by measuring the number of colonies formed with incubation at 35°C after 40–48 h on nutrient agar. The antibacterial activity value (R_L) of TiNbSn alloy and the effect of UV light irradiation ($\triangle$R) had been calculated from the following equation:

$$R_L = \log 10 (G_L/T_L)$$
$$\Delta R = \log 10 (G_L/T_L) - \log 10 (G_D/T_D)$$

T_L: The average number of viable bacteria on three pieces of TiNbSn alloy plates after 8 h of UV irradiation.

G_L: The average number of viable bacteria on three pieces of glass after 8 h of UV irradiation.

T_D: The average number of viable bacteria on three pieces of TiNbSn alloy plates after 8 h of storage in the dark.

G_D: The average number of viable bacteria on three pieces of glass after 8 h of storage in the dark.

For both cases, the antibacterial activity was defined to be more than 2.0 in following ISO 27447 (JIS R 1702). Where no viable bacteria were observed in the anodized TiNbSn alloy, the viable bacteria count (T_L) was recorded as 10.

A time decay antibacterial assay was conducted for MRSA which is considered as one of the most problematic bacteria clinically. This was conducted by partially modifying ISO27447 by increasing the UV intensity to 1.0 mW/cm^2 and shortening the irradiation time from 8 h to less than 3 h. The logarithmic decrease in the number of viable bacteria remaining on anodized TiNbSn alloy prepared in the electrolyte with or without H_2O_2, and on glass at 1, 2, and 3 h from time point zero was compared.

Statistical Analyses

Statistical analyses were performed using JMP, Version 15 (SAS, NC, United States). Statistical significance between the values of •OH in the ESR method was determined using one-way analysis of variance (ANOVA) and post hoc analysis using Tukey-Kramer test. The correlation between time and the production of •OH was evaluated using Spearman's rank correlation test. For the time decay antibacterial tests, significant differences in logarithmic decrease in the number of viable bacteria at each time point were determined using one-way ANOVA and post hoc analysis using Steel-Dwass test. Values of <0.05 were considered statistically significant.

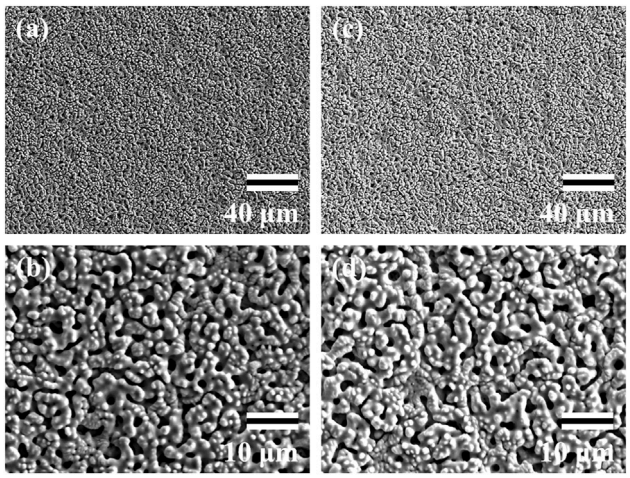

FIGURE 1 | SEM images of the anodic oxides prepared in a sodium tartrate electrolyte. a and b indicate anodic oxides with H_2O_2, c and d indicate anodic oxides without H_2O_2. Three independent experiments were conducted. Representative results are shown. Scale bar is 40.0 μm in the lower magnification images **(A,C)** and 10.0 μm in the higher magnification images **(B,D)**. SEM: Scanning electron microscope.

RESULTS

Surface Analyses

The SEM data for surface analyses of the anodized TiNbSn alloy are shown in **Figure 1**. The anodized alloy had uniform porous microstructures with fine micropores. There was no difference in the formation of porous microstructure between anodized oxide prepared in the electrolyte with and without H_2O_2. The laser microscopy analyses (n = 3) are shown in **Figure 2**. The mean values for surface roughness of the anodized alloy with and without H_2O_2 were 0.495 and 0.470 μm, respectively. The measurements of the surface area ratio, which are the ratios of the measured surface area to the projected area were 2.8 and 2.8%, respectively. There were no differences in the surface roughness and surface area ratio regardless of the electrolyte composition.

Figure 3 shows the XRD profiles of the anodic oxide of TiNbSn alloy prepared in the electrolyte with and without H_2O_2. Anatase- and rutile-structured TiO_2 were detected in both anodized TiNbSn alloy, however, the peaks of rutile-structured TiO_2 were accelerated in the anodized TiNbSn alloy prepared in the electrolyte with H_2O_2. The XPS spectra of the anodic oxides had peaks for the Ti, Nb, Sn, O, S, and C, and a weak N peak. Peaks corresponding to C and N originated from contamination during sample preparation and air exposure. The anodic oxide on TiNbSn alloy was composed of TiO_2, Nb_2O_5, and SnO or SnO_2, as was previously described (Tanaka et al., 2016; Kunii et al., 2019). The Ti 2p revealed that the surface was completely composed of titanium oxide for the oxides prepared in the electrolyte prepared in the electrolyte with and without H_2O_2. The symmetrical shape of the Ti 2p spectrum suggested that reduced Ti^{3+} ions were not present in the oxides. The O 1s peak at approximately 529.9 eV was ascribed to oxygen in TiO_2, and shoulder peaks at a higher binding energy side than the main peak was originated from H_2O. The Ti 2p3/2, Nb 3d5/2, and Sn 3d5/2 spectra had a peak corresponding to the binding energy of approximately 458.8, 207.3, and 486.6 eV, respectively, and they could be assigned as TiO_2, Nb_2O_5, and SnO or SnO_2 from the literature (**Figure 4**) (Charstain, 1992). Semi-quantitative analysis utilizing the XPS spectra concluded that any distinct difference between the oxides prepared in the electrolyte with and without H_2O_2 was not observed (**Figure 5**). Assuming that the oxides were composed of TiO_2, Nb_2O_5, and SnO_2, the fraction of oxides was calculated from the atomic fraction of the metal. The fraction of constituent oxides was estimated as 62 and 65% of TiO_2, 37 and 34% of Nb_2O_5, and 1.1 and 0.6% of SnO_2, for the anodic oxide prepared in the electrolyte with and without H_2O_2, respectively. It was concluded that both the chemical composition and constituent oxide fraction was almost similar among both oxides. The absorption spectra of the anodized TiNbSn alloy, which were prepared in a sodium tartrate electrolyte (a) with and (b) without H_2O_2 was evaluated (**Figure 6**). Absorbances of the anodic oxides decrease with increasing wavelength, which is a typical spectrum of semiconductors. The sharp decrease in absorbance with increasing wavelength was a little more pronounced in (a) than in (b), but there was no significant difference between the spectra of (a) and (b). These results suggest that crystallized TiO_2 was formed on TiNbSn alloy and H_2O_2 addition to the electrolyte did not accelerate the maturation of the crystallized structure of TiO_2.

Photocatalytic Assessment

The •OH spectrum on anodized TiNbSn alloy prepared in the electrolyte with and without H_2O_2 by ESR method is shown in **Figure 7** (n = 3). The quantitative assessment of the amounts of •OH is shown in **Figure 8**. There was no significant difference in the amounts of •OH between the anodized TiO_2 prepared in the electrolyte with or without H_2O_2 at both the 5 and 15 min in time point (p = 0.817 and p = 0.369, respectively). There was a strong correlation between the amount of •OH and UV irradiation time in both the anodized TiO_2 prepared in the electrolyte with and without H_2O_2 (r = 0.878, p = 0.021 with the addition of H_2O_2; and r = 0.891, p = 0.017 without the addition of H_2O_2). The reduction ratio of the MB bleaching test is plotted in **Figure 9** and there was no difference in the reduction ratio between the anodic oxides prepared in the electrolyte with or without H_2O_2.

Antibacterial Test

An antibacterial test was conducted in duplicate for each bacterial species according to the ISO27447 antibacterial test. The antibacterial activity values of the anodized TiNbSn alloy plates with 0.21 mW/cm^2 of UV light irradiation are detailed in **Table 1**. The antibacterial activity values with the UV light irradiation were more than 2.0 for all the bacterial species regardless of the addition of H_2O_2 to the electrolyte. These results demonstrate that the photocatalytic activity of the anodized TiNbSn alloy under UV irradiation had a robust antibacterial effect. The logarithmic reduction values obtained in the antibacterial test were calculated using glass, anodized

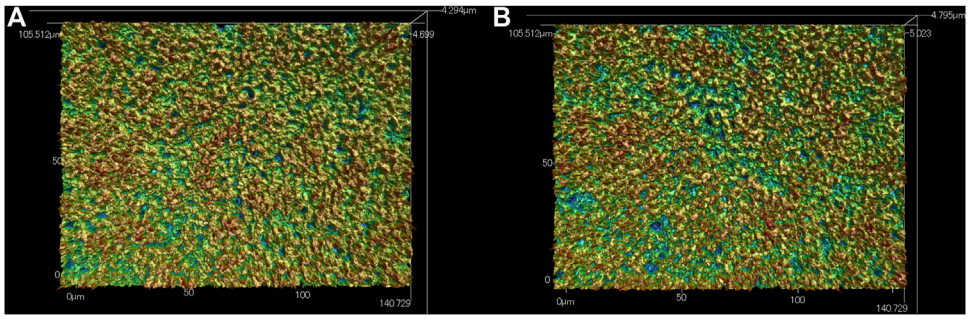

FIGURE 2 | Laser Microscopic images of the anodic oxides prepared in a sodium tartrate electrolyte. **(A)** indicates anodic oxides with H_2O_2, **(B)** indicates anodic oxides without H_2O_2. Three independent experiments were conducted. Representative results are shown.

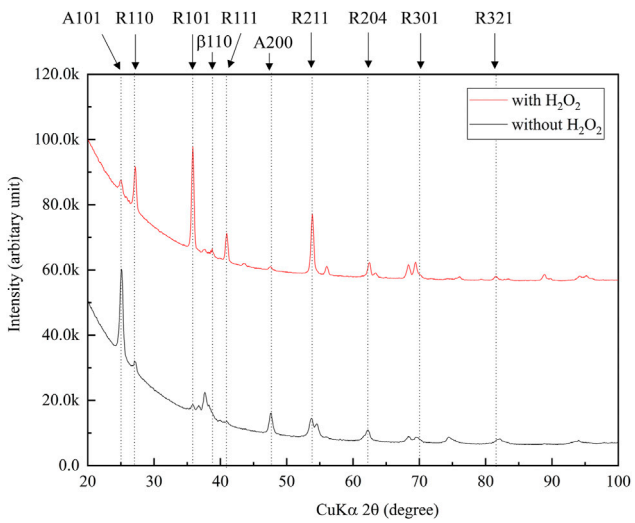

FIGURE 3 | XRD narrow scan profiles of the anodic oxides prepared in the sodium tartrate electrolyte with and without H_2O_2. The peaks of rutile-structured TiO_2 were accelerated in anodic oxide with H_2O_2. The sample size is $n = 1$ in each group. XRD: X-ray Diffraction.

TiNbSn alloy prepared in the electrolyte with or without H_2O_2 under 1.0 mW/cm^2 of UV light irradiation ($n = 5$ (**Figure 10**). The logarithmic reduction values of the anodized TiNbSn alloy were significantly larger than those of glass at 1 and 2 h. The logarithmic reduction values of MRSA after 1-h with UV light irradiation were significantly increased in both anodized TiNbSn alloy prepared in the electrolyte with and without H_2O_2, in comparison to the glass ($p = 0.033$ and $p = 0.033$ with and without addition of H_2O_2 respectively). Similarly, after 2-h of UV light irradiation, the logarithmic reduction values were significantly increased in both anodized TiNbSn alloys compared to those of the glasses ($p = 0.033$ and $p = 0.033$ with and without addition of H_2O_2 to the electrolyte, respectively). In contrast, there was no significant differences after 3-h of UV light irradiation between all the groups. Comparing the logarithmic reduction values between the anodized TiNbSn alloys prepared in the electrolyte with and without H_2O_2, there were no significant differences in the two groups after 1- and 2-h UV light irradiation.

DISCUSSION

Overview

In this study, the antibacterial activity of anodized TiNbSn alloy, prepared in a sodium tartrate electrolyte with and without H_2O_2, was demonstrated. The addition of H_2O_2 to the electrolyte did not alter the porous microstructures and the absorption transition of the anodic oxide prepared in the H_2O_2 free electrolyte. Furthermore, it did not change the photocatalytic activity and the amount of generated •OH. Although it is inferred that the addition of H_2O_2 accelerated the formation of well-crystallized TiO_2, there was no significant difference in the photocatalytic and antibacterial performances between the two anodic oxides prepared in the electrolyte with and without H_2O_2.

Achievement of TiO_2 With the Formation of Highly Crystallized and Porous Oxides Regardless of H_2O_2 Addition

In the present study, SEM and laser microscopy demonstrated that anodic oxide on TiNbSn alloy prepared in a sodium tartrate electrolyte had a fine porous microstructure regardless of H_2O_2 addition to the electrolyte. Previous studies have reported that dielectric breakdown leads to porous microstructure formation on the anodic oxide prepared in an electrolyte of sulfuric acid aqueous solution (Diamanti and Pedeferri, 2007; Park et al., 2007). In a recent study, anodic oxide prepared in the electrolyte of sodium tartrate with applying a constant voltage of 500 V developed a porous microstructure regardless of the addition of H_2O_2 to the electrolyte (Masahashi et al., 2021). Those results were consistent with the results of the present study. The authors considered that the higher the anodic oxidation voltage is applied, the more frequent breakdown occurs, resulting in the formation of highly crystallized and porous oxides. Since H_2O_2 is a strong oxidizing agent, we added H_2O_2 to sodium tartrate, a weak acid, in the expectation that it would accelerate the

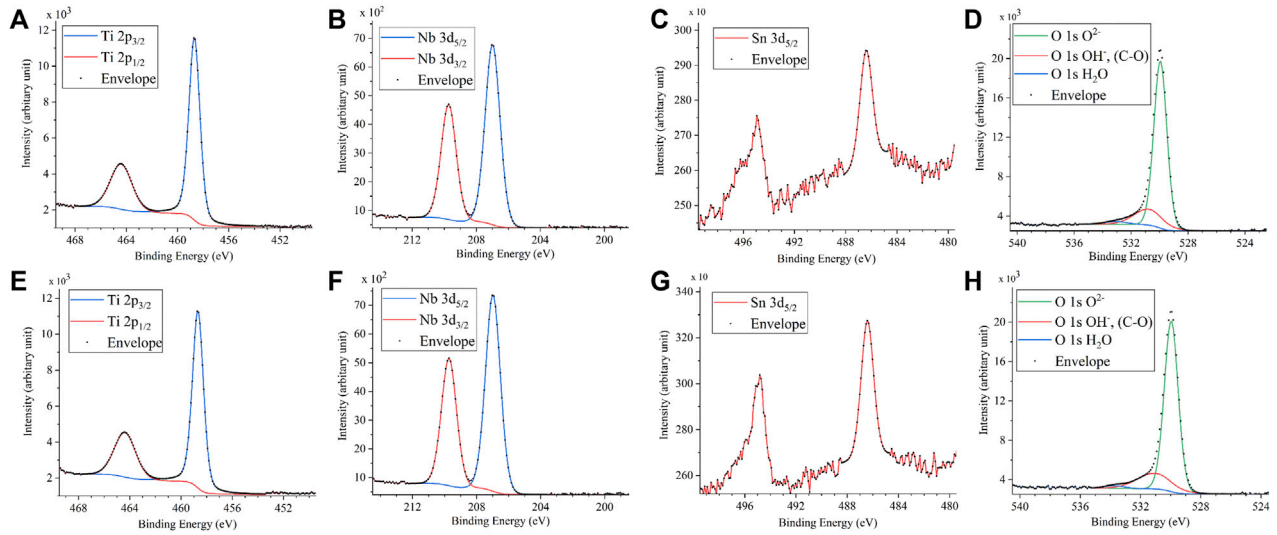

FIGURE 4 | XPS spectra of **(A)** Ti 2p, **(B)** Nb, **(C)** Sn, and **(D)** O 1s on the anodic oxide with and **(E)** Ti 2p, **(F)** Nb, **(G)** Sn and **(H)** O 1s on the anodic oxide without H_2O_2. The sample size is n = 1 in each group. XPS: X-ray photoelectron spectroscopy.

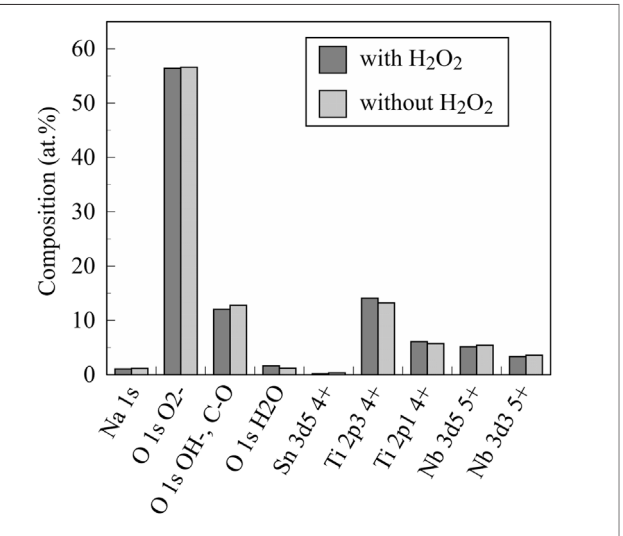

FIGURE 5 | The chemical composition of investigated anodic oxides on the TiNbSn alloy calculated by semi-quantitative analysis using the XPS spectra. The sample size is n = 1 in each group. XPS: X-ray photoelectron spectroscopy.

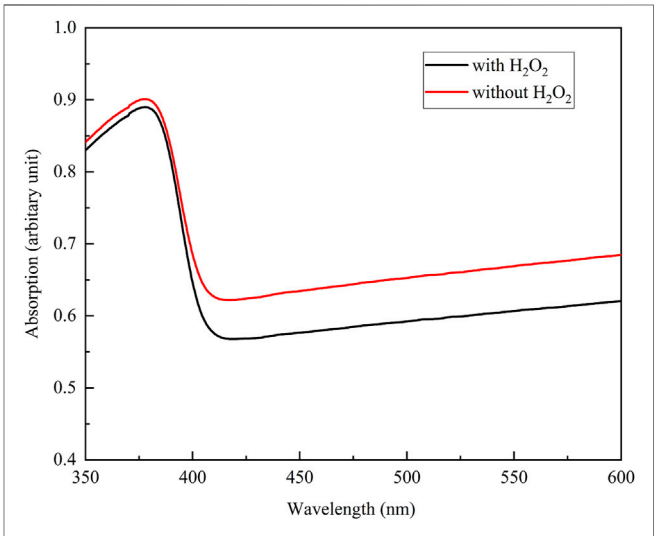

FIGURE 6 | The absorption spectra of the anodic oxide prepared in the sodium tartrate electrolyte with and without H_2O_2. The sample size is n = 1 in each group.

anodic oxidation reaction. We consider that the promotion of anodic oxidation reactions leads to an increase in the crystallinity of TiO_2. Actually, the addition of H_2O_2 to the electrolyte accelerated anodic oxidation reaction, which is verified by the galvanostatically controlled duration during anodization (**Figure A2**). In the present set-up for anodization, the galvanostatic controlling mode changes to the potentiostatic controlling mode when the electrode voltage arrived at the set voltage of 380 V. This electrochemical behavior was monitored by the electrolysis curve, and the curve revealed that the addition of H_2O_2 reduced the galvanostatically controlled duration (**Figure A2**). High voltage induces dielectric breakdown accompanied by spark discharge at the surface of the TiNbSn electrode, which promotes crystallization of anodic oxide owing to self-heating (Masahashi et al., 2021). The galvanostatic period is shorter with the addition of H_2O_2 than without the addition of H_2O_2. Voltage also increases in the short term, and self-heating also progresses earlier, which is presumed to be advantageous for the maturation of the anodic oxide. In contrast, reduction of the galvanostatically controlled duration retards the crystallization of anodic oxide, which

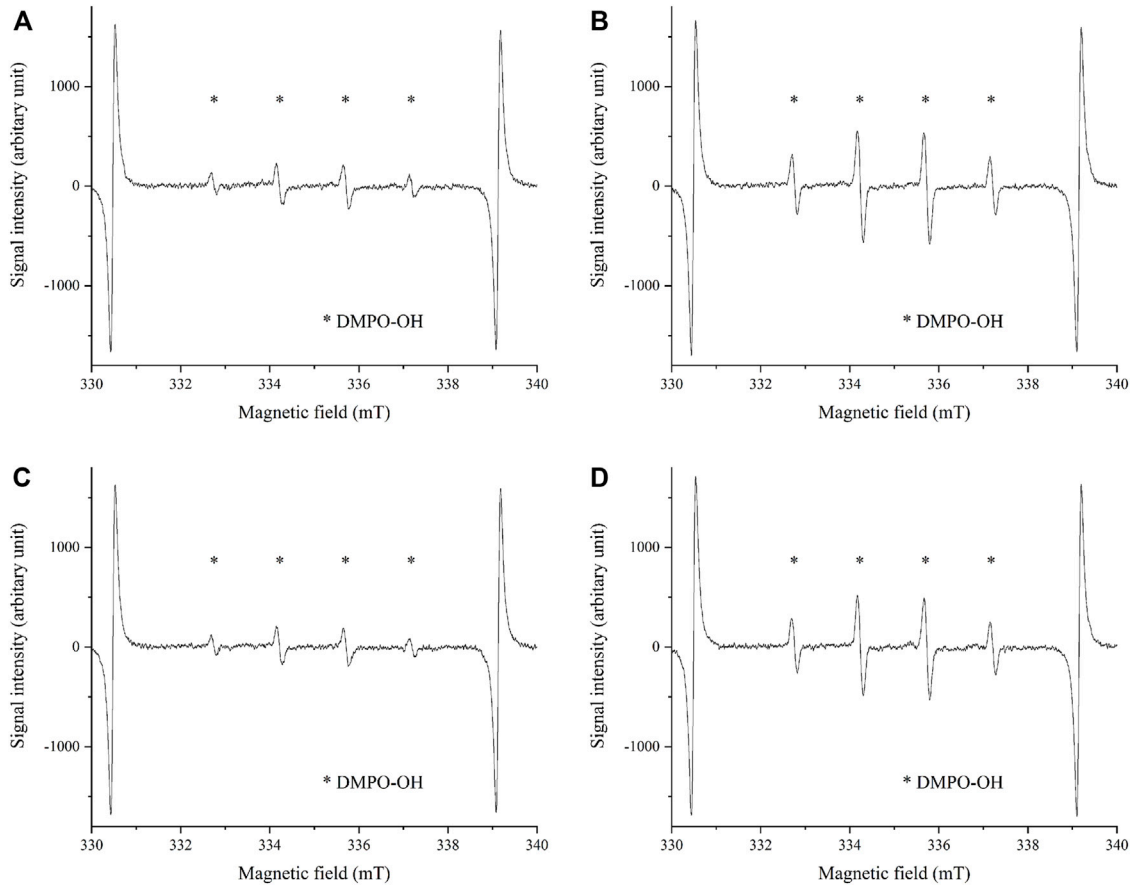

FIGURE 7 | The •OH spectrum by ESR method on anodic oxides prepared in the sodium tartrate electrolyte with and without H_2O_2. The peaks of •OH are shown in both anodic oxides by ESR methods using DMPO. The sample size is $n = 3$ in each group. **(A)** UV irradiation on anodic oxide with H_2O_2 for 5 min **(B)** UV irradiation on anodic oxide with H_2O_2 for 15 min **(C)** UV irradiation on anodic oxide without H_2O_2 for 5 min **(D)** UV irradiation on anodic oxide without H_2O_2 for 15 min. ESR: Electron spin Resonance, DMPO: 5,5-dimethel-a-pyrroline-N-oxide.

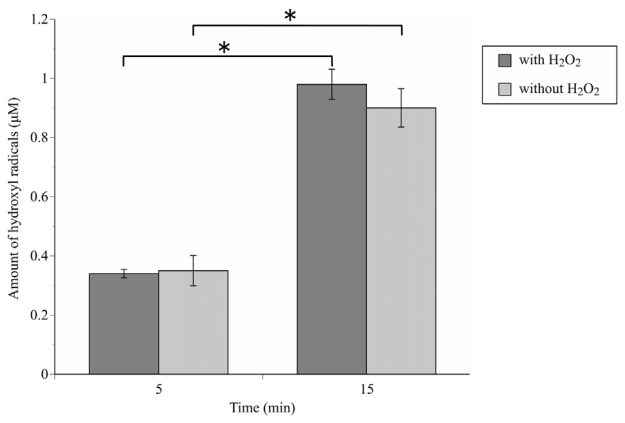

FIGURE 8 | The comparison of the amount of generated •OH radicals by ESR methods between anodic oxides in the sodium tartrate electrolyte with and without H_2O_2. The sample size is $n = 3$ in each group. The one-way ANOVA post hoc by Tukey-Kramer test was used for statistical evaluation. *: $p < 0.05$ ESR: Electron spin Resonance, ANOVA: analysis of variance.

deteriorates the photocatalytic activity due to the high density of lattice defects. Low crystallinity increases the recombination probability of photogenerated charges, resulting in low photocatalytic activity. It is considered that the effect of H_2O_2 addition to the electrolyte on photocatalytic activities was weakened by the above two contradictory effects.

Increased Ratio of Rutile-Structured TiO_2 by H_2O_2 Addition did Not Affect Photocatalytic Activity

The XRD analysis demonstrated that the addition of H_2O_2 to the electrolyte increased the ratio of rutile-structured TiO_2. It has been reported that anatase-structured TiO_2 had higher bandgap energy than rutile-structured TiO_2, and ROS generated from the anatase structure had a longer lifetime than rutile (Xu et al., 2011; Zhang et al., 2014; Hu et al., 2018). Therefore, anatase-structured TiO_2 has been reported to have higher photocatalytic activity than rutile-structured TiO_2. From those previous studies, anatase-structured TiO_2 exhibits an advantage in photocatalytic activity and antibacterial performance, however,

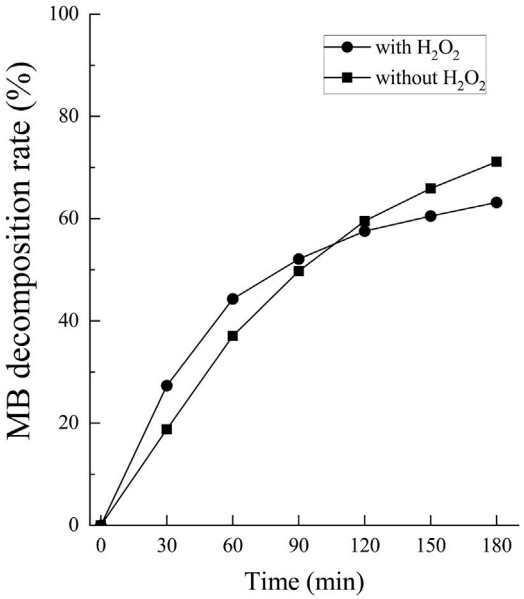

FIGURE 9 | The comparison of the degradation rate of MB between anodic oxides in the sodium tartrate electrolyte with and without H_2O_2. The sample size is n = 1 in each group. MB: Methylene blue.

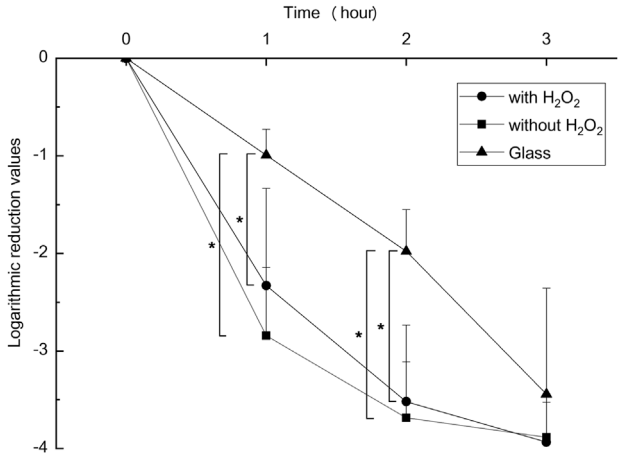

FIGURE 10 | The comparison of logarithmic reduction values in each specimen. The sample size is n = 5 in each group. The one-way ANOVA post hoc by Steel-Dwass test was used for statistical evaluation. *: $p < 0.05$ ANOVA: analysis of variance.

TABLE 1 | The assessment of antibacterial values and effects of photocatalysis according to the ISO 27447 test.

	Bacteria	Antibacterial Values	Effect of photocatalysis
With H_2O_2	MSSA	3.90, 3.82	3.21, 3.64
	MRSA	2.53, 3.69	2.14, 2.63
	E. coli	2.99, 4.20	3.01, 4.29
Without H_2O_2	MSSA	3.90, 3.82	3.41, 2.98
	MRSA	3.35, 3.69	3.03, 2.74
	E. coli	4.21, 4.20	3.58, 4.33

The assessment was performed in duplicate per assay and repeated in triplicate. Representative data is shown.
MSSA, methicillin-sensitive Staphylococcus Aureus; MRSA, methicillin-resistant Staphylococcus Aureus; E. coli, Escherichia coli.

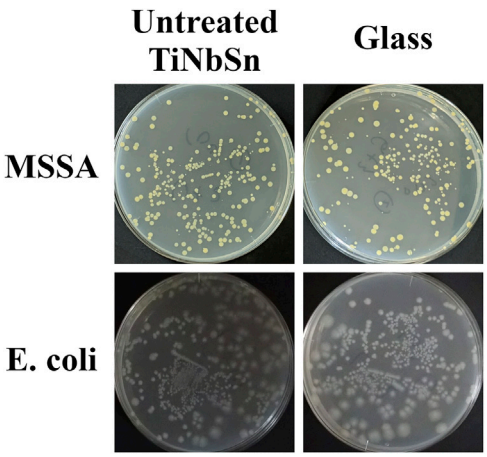

FIGURE A1 | Bacterial culture tests on untreated TiNbSn alloy and glass plate. The photographs show the results of the culture of MSSA and *E. coli* washout solution after antibacterial tests with untreated TiNbSn alloy and glass plate under low-intensity UV light irradiation (0.21 mW/cm^2) for 8 h. Three independent experiments were conducted. Representative results are shown. *E. coli: Escherichia coli,* MSSA: Methicillin-resistant *Staphylococcus aureus*.

there were no significant differences between anodic oxides prepared in the electrolyte with and without H_2O_2. Thus, there was no difference in photocatalytic activity and antibacterial performance between TiO_2 after anodic oxidation with rutile and anatase structures. The authors considered this is ascribed to the density of lattice defects acting as recombination sites, and further studies are required to elucidate.

The previous study reported that the addition of H_2O_2 treatment demonstrated no apparent improvements in the evaluation of radical production by ESR examination (Masahashi et al., 2021). Those results were consistent with the present study, and ESR examination demonstrated that the amounts of •OH significantly increased depending on the duration of the UV irradiation regardless of H_2O_2 addition. The degradation rate of MB also increased depending on the duration of the UV irradiation regardless of H_2O_2 addition to the electrolyte, suggesting that the photocatalytic activity varied with illumination time.

TiNbSn Alloy With Anodic Oxidation in a Sodium Tartrate had the Antibacterial Activity With or Without H_2O_2 Addition

The ISO27447 antibacterial test demonstrated that the anodic oxide on TiNbSn alloy prepared in a sodium tartrate with and without H_2O_2, had antibacterial activity against MSSA, MRSA, and *E. coli,* under the low intensity of UV irradiation. These

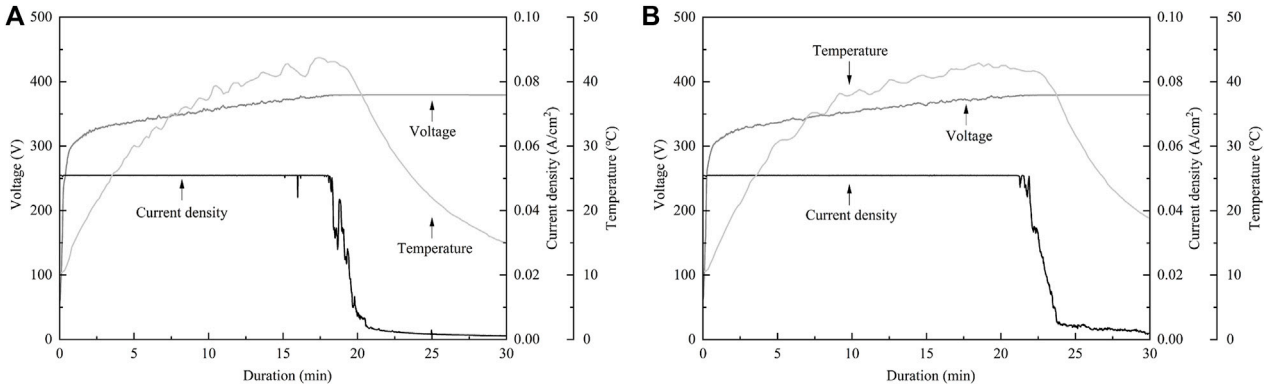

FIGURE A2 | The electrochemical behavior monitored by the electrolysis Curve. **(A)** The electrolysis curve in anodic oxide with H_2O_2, **(B)** The electrolysis curve in anodic oxide without H_2O_2. The sample size is $n = 1$ in each group.

results suggest that the photocatalytic performance of anodic oxide on TiNbSn alloy was suitable for the sterilization of pathological bacteria, regardless of drug resistance, and that this antibacterial performance may be suitable for the clinical setting. The authors considered that this anodic oxidation technique could potentially contribute to the problem of refractory bacterial infection including vancomycin-resistant bacteria (Wright, 2007). While there are side effects to antibacterial drugs, the TiO_2 surface is considered safe due to the anodic oxide strongly adhesive on the substrate, and TiO_2 being biologically inert (Ophus et al., 1979; Punjataewakupt et al., 2019). The antibacterial effect of anodic oxide was considered suitable in the terms of safety.

The time decay antibacterial test was performed to identify whether the antibacterial activity could be achieved in a shorter time using higher intensity UV irradiation than that within the ISO27447 test. The anodic oxide on TiNbSn alloy prepared in the electrolyte with and without H_2O_2 significantly reduced MRSA. The authors considered that three-hour UV irradiation directly killed MRSA, however irradiation below 2 hours demonstrated antibacterial activity by photocatalysis of anodic oxide on TiNbSn alloy. It has already been previously reported that anodic oxide has antibacterial activity (Yeniyol et al., 2015), however, results in our study showed much higher antibacterial activity compared to the previous report. In the results of ESR tests, •OH radicals were generated in 5 min of UV irradiation, suggesting a possible antibacterial effect in a short-time of UV irradiation. Increased intensity of UV irradiation and larger surface of anodized samples can be expected to increase the amount of •OH radicals generated even with short-time UV irradiation. We would like to examine whether stable anodic oxidation is possible for large specimens in future research. This study is the first step toward imparting antibacterial performance by anodic oxidation for titanium alloys in biological applications. In the application of TiNbSn alloy to hip and knee prosthesis, UV irradiation on hip and knee prosthesis anodized with sodium tartrate during surgery for surgical site infection may be useful for killing multidrug-resistant bacteria, thus contributing to infection control and prosthesis preservation. With the development of the technique of anodic oxidation on TiNbSn alloy, the development of biomedical materials that exhibit antibacterial activity by UV irradiation is expected.

CONCLUSION

The photocatalytic activity of the anodic oxide of TiNbSn alloy prepared in a sodium tartrate with or without H_2O_2 was demonstrated. The anodized oxide exhibited a porous microstructure, and well crystallized anatase and rutile-structured TiO_2 regardless of H_2O_2 addition to the electrolyte. The abundant generation of •OH and photocatalytic activity under UV irradiation was confirmed in the anodic oxide on TiNbSn alloy prepared in the electrolyte with and without H_2O_2, and there was no difference between the two types of anodic oxides. In the antibacterial test, no significant difference was detected between anodic oxide on TiNbSn alloy with and without H_2O_2, and both anodic oxides on TiNbSn alloy indicated a robust antibacterial activity. Anodic oxide on TiNbSn alloy may be a promising biomaterial with low Young's modulus and antibacterial performance.

DATA AVAILABILITY STATEMENT

The original contributions presented in the study are included in the article/Supplementary Material, further inquiries can be directed to the corresponding author.

AUTHOR CONTRIBUTIONS

HK: Conceptualization, Methodology, Investigation, Writing–review, and editing. YM: Methodology, Investigation, Writing–review, and

editing. KI: Methodology, Investigation. HI: Methodology, Investigation, Software. TM: Investigation, Software. SF: Investigation. EI: Supervision. SH: Supervision. NM: Methodology, Investigation, Writing–review, and editing. TA: Supervision.

FUNDING

This study was financially supported by the JSPS KAKENHI to YM (18K09052) and NM (20H02458).

REFERENCES

Ando, Y., Miyamoto, H., Noda, I., Sakurai, N., Akiyama, T., Yonekura, Y., et al. (2010). Calcium Phosphate Coating Containing Silver Shows High Antibacterial Activity and Low Cytotoxicity and Inhibits Bacterial Adhesion. *Mater. Sci. Eng. C* 30 (1), 175–180. doi:10.1016/j.msec.2009.09.015

Cai, R., Kubota, Y., Shuin, T., Sakai, H., Hashimoto, K., and Fujishima, A. (1992). Induction of Cytotoxicity by Photoexcited Tio2 Particles. *Cancer Res.* 52 (8), 2346–2348.

Charstain, J. (1992). *Hand Book of Photoelctron Spectroscopy*. Waltham, Massachusetts, United States: Perkin-Elmer.

Chiba, D., Yamada, N., Mori, Y., Oyama, M., Ohtsu, S., Kuwahara, Y., et al. (2021). Mid-term Results of a New Femoral Prosthesis Using Ti-Nb-Sn alloy with Low Young's Modulus. *BMC Musculoskelet. Disord.* 22 (1), 987. doi:10.1186/s12891-021-04879-1

Diamanti, M. V., and Pedeferri, M. P. (2007). Effect of Anodic Oxidation Parameters on the Titanium Oxides Formation. *Corrosion Sci.* 49 (2), 939–948. doi:10.1016/j.corsci.2006.04.002

Fujisawa, H., Mori, Y., Kogure, A., Tanaka, H., Kamimura, M., Masahashi, N., et al. (2018). Effects of Intramedullary Nails Composed of a New β-type Ti-Nb-Sn alloy with Low Young's Modulus on Fracture Healing in Mouse Tibiae. *J. Biomed. Mater. Res.* 106 (8), 2841–2848. doi:10.1002/jbm.b.34064

Fujishima, A., and Honda, K. (1972). Electrochemical Photolysis of Water at a Semiconductor Electrode. *Nature* 238 (5358), 37–38. doi:10.1038/238037a0

Glassman, A. H., Bobyn, J. D., and Tanzer, M. (2006). New Femoral Designs. *Clin. Orthopaedics Relat. Res.* 453 (453), 64–74. doi:10.1097/01.blo.0000246541.41951.20

Han, J., Yang, Y., Lu, J., Wang, C., Xie, Y., Zheng, X., et al. (2017). Sustained Release Vancomycin-Coated Titanium alloy Using a Novel Electrostatic Dry Powder Coating Technique May Be a Potential Strategy to Reduce Implant-Related Infection. *Bst* 11 (3), 346–354. doi:10.5582/bst.2017.01061

Hanada, S., Masahashi, N., and Jung, T. K. (2013). Effect of Stress-Induced α″ Martensite on Young's Modulus of β Ti-33.6Nb-4Sn alloy. *Mater. Sci. Eng. A* 588, 403–410. doi:10.1016/j.msea.2013.09.053

Hanada, S., Masahashi, N., Jung, T. K., Miyake, M., Sato, Y. S., and Kokawa, H. (2014). Effect of Swaging on Young′s Modulus of β Ti-33.6Nb-4Sn alloy. *J. Mech. Behav. Biomed. Mater.* 32, 310–320. doi:10.1016/j.jmbbm.2013.10.027

Hatakeyama, M., Masahashi, N., Michiyama, Y., Inoue, H., and Hanada, S. (2021). Mechanical Properties of Anodized TiNbSn alloy for Biomedical Applications. *Mater. Sci. Eng. A* 825, 141898. doi:10.1016/j.msea.2021.141898

Head, W. C., Bauk, D. J., and Emerson, R. H. (1995). Titanium as the Material of Choice for Cementless Femoral Components in Total Hip Arthroplasty. *Clin. Orthop. Relat. Res.* 311, 85–90.

Hu, L., Xu, C., Peng, L., Gu, F. L., and Yang, W. (2018). Photocatalytic Activity and the Radiative Lifetimes of Excitons via an Ab Initio Approach. *J. Mater. Chem. A.* 6 (31), 15027–15032. doi:10.1039/c8ta04140g

Iwatsu, M., Kanetaka, H., Mokudai, T., Ogawa, T., Kawashita, M., and Sasaki, K. (2020). Visible Light-induced Photocatalytic and Antibacterial Activity of N-doped TiO 2. *J. Biomed. Mater. Res.* 108 (2), 451–459. doi:10.1002/jbm.b.34401

Kogure, A., Mori, Y., Tanaka, H., Kamimura, M., Masahashi, N., Hanada, S., et al. (2019). Effects of Elastic Intramedullary Nails Composed of Low Young's Modulus Ti-Nb-Sn alloy on Healing of Tibial Osteotomies in Rabbits. *J. Biomed. Mater. Res.* 107 (3), 700–707. doi:10.1002/jbm.b.34163

Kubota, Y., Shuin, T., Kawasaki, C., Hosaka, M., Kitamura, H., Cai, R., et al. (1994). Photokilling of T-24 Human Bladder Cancer Cells with Titanium Dioxide. *Br. J. Cancer* 70 (6), 1107–1111. doi:10.1038/bjc.1994.456

Kunii, T., Mori, Y., Tanaka, H., Kogure, A., Kamimura, M., Mori, N., et al. (2019). Improved Osseointegration of a TiNbSn Alloy with a Low Young's Modulus Treated with Anodic Oxidation. *Sci. Rep.* 9 (1), 13985. doi:10.1038/s41598-019-50581-7

Liou, J.-W., and Chang, H.-H. (2012). Bactericidal Effects and Mechanisms of Visible Light-Responsive Titanium Dioxide Photocatalysts on Pathogenic Bacteria. *Arch. Immunol. Ther. Exp.* 60 (4), 267–275. doi:10.1007/s00005-012-0178-x

Long, M., and Rack, H. J. (1998). Titanium Alloys in Total Joint Replacement-A Materials Science Perspective. *Biomaterials* 19 (18), 1621–1639. doi:10.1016/s0142-9612(97)00146-4

Maness, P.-C., Smolinski, S., Blake, D. M., Huang, Z., Wolfrum, E. J., and Jacoby, W. A. (1999). Bactericidal Activity of Photocatalytic TiO 2 Reaction: toward an Understanding of its Killing Mechanism. *Appl. Environ. Microbiol.* 65 (9), 4094–4098. doi:10.1128/aem.65.9.4094-4098.1999

Masahashi, N., Mizukoshi, Y., Semboshi, S., and Ohtsu, N. (2009). Enhanced Photocatalytic Activity of Rutile TiO2 Prepared by Anodic Oxidation in a High Concentration Sulfuric Acid Electrolyte. *Appl. Catal. B: Environ.* 90 (1-2), 255–261. doi:10.1016/j.apcatb.2009.03.011

Masahashi, N., Mori, Y., Kurishima, H., Inoue, H., Mokudai, T., Semboshi, S., et al. (2021). Photoactivity of an Anodized Biocompatible TiNbSn alloy Prepared in Sodium Tartrate/hydrogen Peroxide Aqueous Solution. *Appl. Surf. Sci.* 543, 148829. doi:10.1016/j.apsusc.2020.148829

Masahashi, N., Mori, Y., Tanaka, H., Kogure, A., Inoue, H., Ohmura, K., et al. (2019). Bioactive TiNbSn alloy Prepared by Anodization in Sulfuric Acid Electrolytes. *Mater. Sci. Eng. C* 98, 753–763. doi:10.1016/j.msec.2019.01.033

Masahashi, N., Mori, Y., Tanaka, H., Kogure, A., Inoue, H., Ohmura, K., et al. (2017). Study of Bioactivity on a TiNbSn alloy Surface. *Thin Solid Films* 639, 22–28. doi:10.1016/j.tsf.2017.08.023

Miura, K., Yamada, N., Hanada, S., Jung, T.-K., and Itoi, E. (2011). The Bone Tissue Compatibility of a New Ti-Nb-Sn alloy with a Low Young's Modulus. *Acta Biomater.* 7 (5), 2320–2326. doi:10.1016/j.actbio.2011.02.008

Miura, Y., Fujii, Y., Miyao, Y., Mizukoshi, Y., and Masahashi, N. (2015). Fabrication of Antibacterial Photocatalytic Titanium Foil by Anodic Oxidation. *Chem. Lett.* 44 (3), 277–278. doi:10.1246/cl.140976

Mori, Y., Fujisawa, H., Kamimura, M., Kogure, A., Tanaka, H., Mori, N., et al. (2021). Acceleration of Fracture Healing in Mouse Tibiae Using Intramedullary Nails Composed of β-Type TiNbSn Alloy with Low Young's Modulus. *Tohoku J. Exp. Med.* 255 (2), 135–142. doi:10.1620/tjem.255.135

Ohko, Y., Utsumi, Y., Niwa, C., Tatsuma, T., Kobayakawa, K., Satoh, Y., et al. (2001). Self-sterilizing and Self-Cleaning of Silicone Catheters Coated with TiO2 Photocatalyst Thin Films: A Preclinical Work. *J. Biomed. Mater. Res.* 58 (1), 97–101. doi:10.1002/1097-4636(2001)58:1<97::aid-jbm140>3.0.co;2-8

Ophus, E. M., Rode, L., Gylseth, B., Nicholson, D. G., and Saeed, K. (1979). Analysis of Titanium Pigments in Human Lung Tissue. *Scand. J. Work Environ. Health* 5 (3), 290–296. doi:10.5271/sjweh.3104

Park, Y.-J., Shin, K.-H., and Song, H.-J. (2007). Effects of Anodizing Conditions on Bond Strength of Anodically Oxidized Film to Titanium Substrate. *Appl. Surf. Sci.* 253 (14), 6013–6018. doi:10.1016/j.apsusc.2006.12.112

Punjataewakupt, A., Napavichayanun, S., and Aramwit, P. (2019). The Downside of Antimicrobial Agents for Wound Healing. *Eur. J. Clin. Microbiol. Infect. Dis.* 38 (1), 39–54. doi:10.1007/s10096-018-3393-5

Shirai, T., Shimizu, T., Ohtani, K., Zen, Y., Takaya, M., and Tsuchiya, H. (2011). Antibacterial Iodine-Supported Titanium Implants. *Acta Biomater.* 7 (4), 1928–1933. doi:10.1016/j.actbio.2010.11.036

Skocaj, M., Filipic, M., Petkovic, J., and Novak, S. (2011). Titanium Dioxide in Our Everyday Life; Is it Safe? *Radiol. Oncol.* 45 (4), 227–247. doi:10.2478/v10019-011-0037-0

Tanaka, H., Mori, Y., Noro, A., Kogure, A., Kamimura, M., Yamada, N., et al. (2016). Apatite Formation and Biocompatibility of a Low Young's Modulus Ti-Nb-Sn Alloy Treated with Anodic Oxidation and Hot Water. *PLoS One* 11 (2), e0150081. doi:10.1371/journal.pone.0150081

Wang, X., Dong, H., Liu, J., Qin, G., Chen, D., and Zhang, E. (2019). *In Vivo* antibacterial Property of Ti-Cu Sintered alloy Implant. *Mater. Sci. Eng. C* 100, 38–47. doi:10.1016/j.msec.2019.02.084

Watts, R. J., Kong, S., Orr, M. P., Miller, G. C., and Henry, B. E. (1995). Photocatalytic Inactivation of Coliform Bacteria and Viruses in Secondary Wastewater Effluent. *Water Res.* 29 (1), 95–100. doi:10.1016/0043-1354(94)E0122-M

Wright, G. D. (2007). The Antibiotic Resistome: the Nexus of Chemical and Genetic Diversity. *Nat. Rev. Microbiol.* 5 (3), 175–186. doi:10.1038/nrmicro1614

Xu, M., Gao, Y., Moreno, E. M., Kunst, M., Muhler, M., Wang, Y., et al. (2011). Photocatalytic Activity of Bulk TiO2 Anatase and Rutile Single Crystals Using Infrared Absorption Spectroscopy. *Phys. Rev. Lett.* 106 (13), 138302. doi:10.1103/PhysRevLett.106.138302

Yao, Y., Ohko, Y., Sekiguchi, Y., Fujishima, A., and Kubota, Y. (2008). Self-sterilization Using Silicone Catheters Coated with Ag and TiO2 Nanocomposite Thin Film. *J. Biomed. Mater. Res.* 85b (2), 453–460. doi:10.1002/jbm.b.30965

Yeniyol, S., Mutlu, I., He, Z. M., Yuksel, B., Boylan, R. J., Urgen, M., et al. (2015). Photocatalytical Antibacterial Activity of Mixed-phase TiO2 Nanocomposite Thin Films against Aggregatibacter Actinomycetemcomitans. *Biomed. Res. Int.* 2015, 705871. doi:10.1155/2015/705871

Zhang, J., Zhou, P., Liu, J., and Yu, J. (2014). New Understanding of the Difference of Photocatalytic Activity Among Anatase, Rutile and Brookite TiO2. *Phys. Chem. Chem. Phys.* 16 (38), 20382–20386. doi:10.1039/c4cp02201g

Conflict of Interest: The authors declare that the research was conducted in the absence of any commercial or financial relationships that could be construed as a potential conflict of interest.

frontiers | Frontiers in Bioengineering and Biotechnology

ORIGINAL RESEARCH
published: 25 April 2022
doi: 10.3389/fbioe.2022.861788

The Efficacy and Outcome of a Two-Staged Operation for Irreducible Knee Dislocation: A Prospective Short-Term Follow-Up

Shengyu Cui[1,2†], *Hong Yi*[1,2†], *Xinhui Zhu*[1,2], *Jianbo Fan*[1,2], *Yi Ding*[3] *and Wei Liu*[1,2*]

[1]*Department of Orthopedic Surgery, The Second Affiliated Hospital of Nantong University, Nantong, China,* [2]*Nantong First Peoples Hospital, Nantong, China,* [3]*Rehabilitation Hospital Affiliated to National Research Center for Rehabilitation Technical Aids, Beijing, China*

OPEN ACCESS

Edited by:
Yansong Qi,
Inner Mongolia People's Hospital, China

Reviewed by:
Xi Gong,
Peking University Third Hospital, China
Bin Wang,
Second Hospital of Shanxi Medical University, China

***Correspondence:**
Wei Liu
mdliuwei@163.com

[†]*These authors have contributed equally to this work*

Specialty section:
This article was submitted to Biomaterials, a section of the journal Frontiers in Bioengineering and Biotechnology

Received: *25 January 2022*
Accepted: *22 March 2022*
Published: *25 April 2022*

Citation:
Cui S, Yi H, Zhu X, Fan J, Ding Y and Liu W (2022) The Efficacy and Outcome of a Two-Staged Operation for Irreducible Knee Dislocation: A Prospective Short-Term Follow-Up. Front. Bioeng. Biotechnol. 10:861788. doi: 10.3389/fbioe.2022.861788

Background: Irreducible knee dislocation (IKD) is a very rare but serious type of knee dislocation; it can lead to soft tissue necrosis due to incarceration of the medial structures and faces great difficulty in the postoperative rehabilitation, too. IKD needs careful pre-operative planning. There is no universal agreement about the appropriate surgical strategy for IKD. The purpose of this study was to investigate the clinical efficacy, safety, and outcome of the two-staged operation in treatment of IKD.

Methods: IKD patients were included from June 1, 2016 to May 31, 2020. In the stage-1 surgery, acute reduction and extra-articular structure repair were performed. Following an intermediate rehabilitation, delayed cruciate ligament reconstructions were performed in stage-2. Physical examination, CT, MRI, and X-ray were performed during the pre-operative period. Knee function, joint stability, ligament laxity, knee range of motion (ROM), and alignment were accessed at follow-ups. The minimum and maximum follow-up times were 0.5 years and 1 year, respectively.

Results: In total, 17 IKD patients were included. There were three subjects (17.65%) missing at the 1 year follow-up and the average follow-up was 11.18 ± 2.53 months. After stage-1, normal alignment and superior valgus/varus stability were restored in most subjects; however, a notable anterior–posterior instability still existed in most patients. The intermediate rehabilitation processed smoothly (6.94 ± 1.20 weeks), and all patients achieved knee ROM of 0–120° finally. At 0.5 years and 1 year follow-up after stage-2, all subjects had achieved normal knee stability, ROM, and satisfying joint function. No infection or DVT was observed.

Conclusions: The two-staged operation for IKD has superior efficacy on knee stability and function, and it can facilitate the rehabilitation and achieve satisfactory short-term outcome.

Keywords: irreducible knee dislocation, knee stability, staged-surgery, medial collateral ligament, cruciate ligament, rehabilitation

INTRODUCTION

Irreducible knee dislocation (IKD) is a rare but serious type of knee injury (Malik and Macdonald, 2019), constituting up to 4% of all knee dislocation (KD) (Robertson et al., 2006; Schaefer et al., 2018). IKD is considered irreducible because of the soft tissue incarceration during closed reduction, for example, the capsuloretinacular structure, medial collateral ligament (MCL), vastus medialis muscle, or the gastrocnemius muscle are likely to trap in the medial compartment (Chen et al., 2011; Price et al., 2019). The "pucker sign" or "dimple sign" is considered as the diagnostic characteristic of IKD, which is due to invagination of the soft tissue into joint space (Jeevannavar and Shettar, 2013).

IKDs belong to the KD-IIIM (Solarino et al., 2015), according to Schenck's (Jr, 1994) classification. IKD is a great challenge for orthopedists and needs very careful preoperative planning. First, IKD should be treated urgently in case of some severe complications, such as knee flexion contracture (KFC) and soft tissue necrosis (Hill and Rana, 1981). Second, multiple ligament injury always faces difficulties in rehabilitation. It has been reported that knee functional prognosis can be seriously compromised in IKD patients (Hill and Rana, 1981).

Recently, literature has favored the two-staged surgery with intermediate rehabilitation. The stage-1 surgery consists of acute reduction with extra-articular structure repair (Solarino et al., 2015), followed by an intermediate aggressive rehabilitation, and the stage-2 surgery consists of delayed ACL and PCL reconstruction (Levy et al., 2009; Howells et al., 2011; Burrus et al., 2016). Several case reports have indicated that the two-staged surgery combined with intermediate rehabilitation facilitated the recovery of ROM and knee function (Levy et al., 2009; Howells et al., 2011; Burrus et al., 2016) or resulted in a better outcome of the joint stability and function (Mook et al., 2009; Jang et al., 2014). However, as the IKD case is very limited, only several case reports exist (Malik and Macdonald, 2019), lacking systematic clinical and follow-up studies. At present, there is no universal agreement about the appropriate operating time or stage for treating IKD (Malik and Macdonald, 2019). The purpose of this study was to investigate the clinical efficacy, safety, and outcome of the two-staged operation in treatment of IKD.

MATERIALS AND METHODS

Patient Involvement

IKD patients were included between June 1, 2016, and May 31, 2020, in our department. The inclusion criteria were as follows: 1) age: 18–60 years old, BMI≤31; 2) KD-IIIM (multiligament knee injury with ACL, PCL, and MCL ruptured) (Solarino et al., 2015; Jr, 1994) (**Figures 1A, B**); 3) irreducible (the closed reduction could not be performed); 4) the two-staged surgery was performed; 5) the stage-1 surgery was performed in 1 week post injury. The exclusion criteria were as follows: 1) KD-IIIL (multiligament knee injury with ACL, PCL, and LCL + PLC rupture) (Jr, 1994; Solarino et al., 2015); 2) history of lower extremity fracture, ligament rupture, and operations; 3) rheumatoid arthritis, ankylosing spondylitis, Parkinson's disease, or other nervous system diseases.

The protocols and procedures for the protection of human subjects were approved by the Ethics Committee in our hospital (IRB ethical approval: KY-2016-OB08), and all of the methods were conducted in accordance with the approved guidelines.

The Two-Staged Surgery and Intermediate Rehabilitation

In the beginning, vascular and nerve injury assessment was performed on the patients. The two-staged operation was performed by the same senior surgeon. Knee X-ray and CT were performed before the operation.

The stage-1 operation consisted of urgent open reduction and extra-articular structure (MCL, medial retinaculum, and capsule) repair. With a pneumatic tourniquet inflated on the thigh, a 5-cm longitudinal incision was made proximally from the medial femoral epicondyle, distally to the lower border of pes anserinus. This reverted the skin and subcutaneous fat flap posteriorly and exposed the damaged medial structures (**Figure 2A**), which were incarcerated into the condylar notch (**Figure 2B**). The torn MCL, medial retinaculum, and capsule were replaced and meticulously sutured with interrupted #1 absorbable braided sutures. The ruptured MCL and medial gastrocnemius muscle from the bony attachment were reinserted at its origin with a suture anchor (**Figure 2C**). Finally, the dislocated joint restored normal alignment after stage-1 (**Figure 2D**).

The intermediate rehabilitation lasted for 6–8 weeks (Ng et al., 2020). An above-the-knee plaster was applied with the joint flexed to about 20°. The patients were asked to follow the instructions for non–weight bearing for 2 weeks. Then, partly weight bearing was allowed and a rehabilitation program was started to restore the joint range of motion (ROM) of 0–120° and muscle strength (3rd–6th week). Full weight bearing was allowed in the 6th–8th week. The MRI, clinical assessment, and self-administered questionnaire (Lysholm and International Knee Documentation Committee (IKDC) score (Ranger et al., 2011)) were assessed after the rehabilitation.

The stage-2 operation was begun when the rehabilitation was accomplished with an ROM of 0–120°. All patients underwent the arthroscopic reconstruction of ACL and PCL (**Figure 2H**). Unilateral semitendinous and gracilis tendons were used as auto-graft. The femoral side was fixed using EndoButton CL (Smith and Nephew, Memphis, TN, United States), and the tibial side was fixed using the poly-L-lactic acid biodegradable interference screw.

Follow-Up

The follow-up was started when stage-2 surgery was completed. The end was re-dislocation/death/missing, whichever occurred first. The minimum follow-up was 0.5 years, and the maximum was 1 year. General parameters included age, gender, body mass index (BMI), occupation, trauma level, MCL injury type, time between injury and stage-1, time between stage-1 and stage-2, follow-up time, and complications. Knee X-ray photographs,

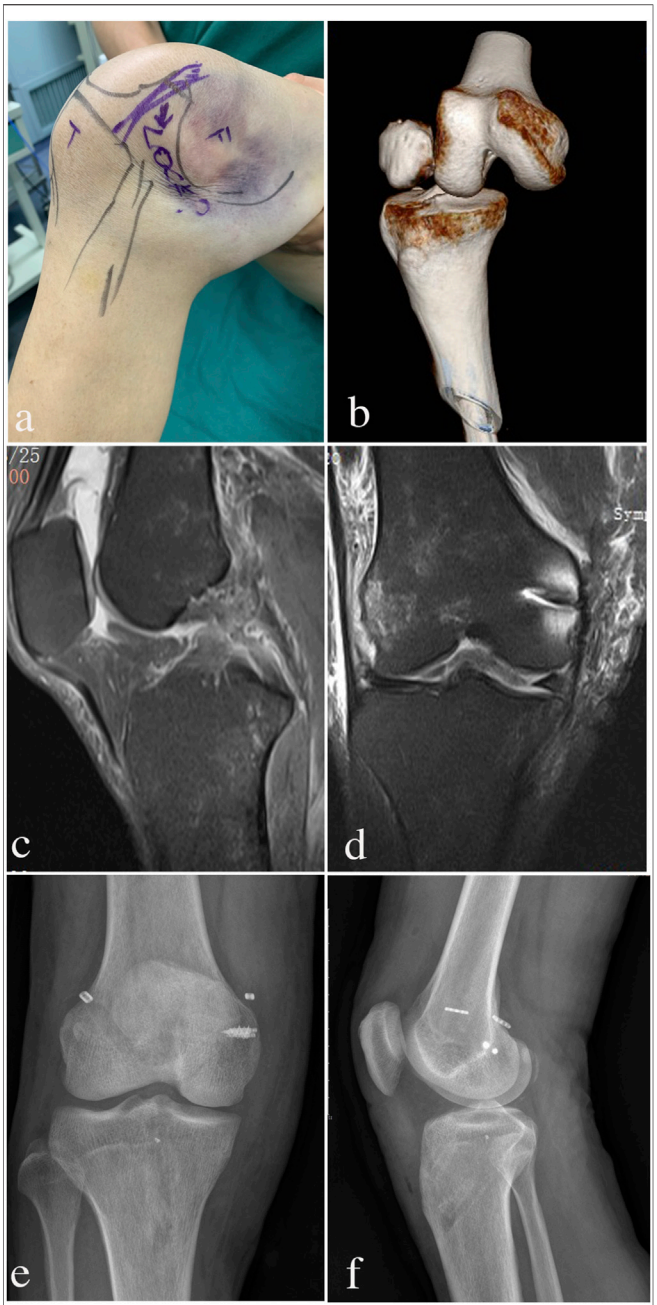

FIGURE 1 | Evolution process of IKD patient appearance and imaging examinations from injury to postoperative follow-up. **(A)** "Dimple sign" and severe ecchymosis with invagination of skin and soft tissue can be observed on the medical side; **(B)** before the stage-1 operation, CT showed the knee posterolateral dislocation; **(C)**: before stage-2 operation, MRI showed that the MCL structure had been repaired; d: before stage-2 operation, MRI showed the ACL and PCL rupture; **(E,F)**: X-ray showed normal knee alignments at 0.5 years and 1 year follow-up.

clinical assessments, and self-administered questionnaires (Lysholm and International Knee Documentation Committee (IKDC) score (Ranger et al., 2011)) were performed at 0.5 years and 1 year follow-up. All of the subject data were checked and entered into the database by two researchers, and double entry was used to carry out quality control.

IKD Clinical Assessments

The physical examination for assessing joint stability of IKD included the Lachman test, posterior drawer test, pivot shift, and varus and valgus stress test (Ranger et al., 2011).

Ligament laxity was measured using KT-1000: the forward shift is tested when the knee is flexed at 30°, and the backward shift is tested when the knee is flexed at 70°. According to IKDC standards, laxity is evaluated by comparing to the healthy side: a difference of less than 3 mm is normal, 3–5 mm is close to normal, 6–10 mm is abnormal, and more than 10 mm is severe.

The ROM was measured using a standardized goniometry technique. The knee flexion contracture (KFC) was assessed by passive physical examination. KFC is defined as the gap value of extension loss compared to the normal side, and more than 5° was considered KFC according to the Knee Society Score (KSS) system (Insall et al., 1989).

Statistical Analysis

The sample size was pre-calculated by using the following formula: $n = (\mu_\alpha + \mu_\beta)^2\ \sigma^2/\delta^2$, a was set at 0.05, β was set at 0.01, and the power was 90% (1-β). The comparisons of the count data were processed by the chi-square test or Fisher's exact test, and continuous data were processed by independent sample t-tests and Levene's variance homogeneity tests. The level of significance was set at 0.05. All of the statistical analyses were performed using SPSS 20.0.0 (SPSS Inc., 2009; Chicago, IL, United States).

RESULTS

Basic Characteristics

The calculated sample size was 14 (power: 90%). Finally, there were 17 IKD patients included in this study (**Table 1**). Most of the IKD patients were injured by low-energy trauma (n = 14): three subjects suffered a sprain of knee when jogging or other exercising; four sprained the knee by themselves during farming; two sprained themselves by accidents during indoor daily life; five were caused by motor vehicle accident. The others were caused by high-energy traffic accident (n = 2) or fall (n = 1). All of the patients were transferred by ambulance to the Emergency department, and urgent reduction (stage-1 surgery) was performed in 0–3 days (**Table 1**). The knee was fixed in a slight flexion and valgus posture with severe ecchymosis on the medial side, and sometimes the "dimple sign" can be observed (**Figure 1A**). CT showed posterolateral knee dislocation (**Figure 1B**). None of the patients had vascular (both the posterior tibial artery and dorsalis pedis artery) or peripheral nerve (both the sensory and motor) injury.

The Two-Staged Surgery and Intermediate Rehabilitation

The stage-1 surgery was performed in 0.76 ± 0.90 days after injury (**Table 1**). Two patients had reversible joint stiffness after the

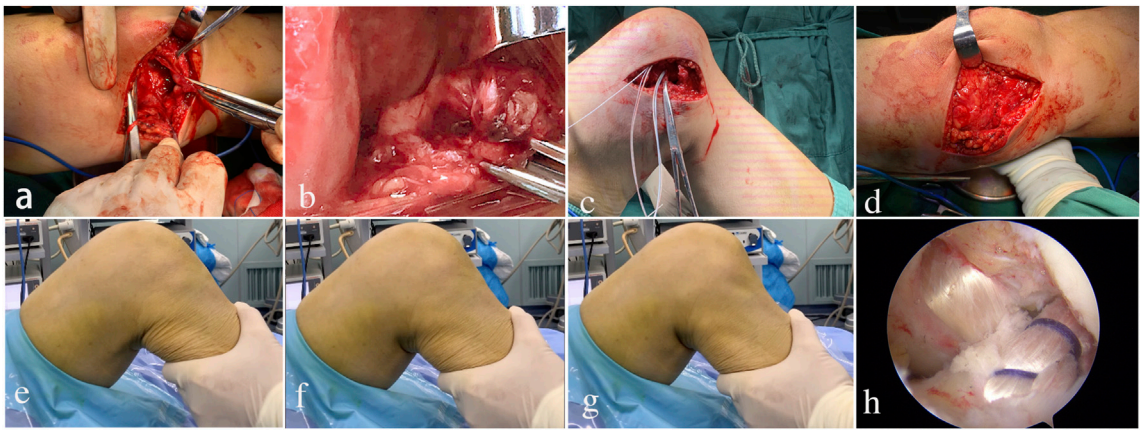

FIGURE 2 | Two-staged operation procedures. **(A,B)**: in stage-1, the damaged MCL and other medial structures were exposed, which were found interposed into the condylar notch; **(C,D)**: the torn MCL and medial retinaculum were replaced and repaired, and the dislocated knee was back to normal alignment following the suture of the medial joint capsule; **(E–G)**: before stage-2 began, the drawer tests found notable anterior-posterior instability, that is, the anterior drawer test, **(F)**, neutral position, **(G)**, the posterior drawer test; **(H)**: the ACL and PCL reconstruction in stage-2.

TABLE 1 | Basic characteristics and clinical conditions at baseline of the follow-up.

Baseline Indicators	Details
Enrolled subjects	17
Age	42.47 ± 8.90 (range: 29–60)
Sex (male/female)	11/6
BMI	25.89 ± 2.14 (range: 22.00–29.10)
Trauma	Self-injured: nine cases
	Low-velocity motor vehicle accident: five cases
	High-velocity traffic accident: two cases
	Fall: one case
Occupation	Farmer: eight
	Manual worker: five
	Office worker: two
	Retired: two
Time to stage-1* surgery (day)	0.76 ± 0.90 (range: 0–3)
Duration from stage-1 to 2 (week)	6.94 ± 1.20 (range: 6–10)
Type of MCL injury	Femoral attachment: 6
	Tibial attachment: 4
	Mid-substance: 6
	Peel-off: 1
Follow-up time (month)	11.18 ± 2.53 (range: 6–14)
Subject number in 0.5 years	17
Subject number in 1 year	14 (missed 3)
Total missing	3/17
Complications	Stage-1: stiffness (2/17)
	Stage-2: hemarthrosis (3/17), fever (3/17)
	0.5 years: KFC (5/17)
	1 year: KFC (3/14)

*Note: * stage-1, surgery was performed together with the urgent reduction.*
BMI (body mass index).

stage-1 surgery (**Table 1**), and they were intervened by physics therapy with extended rehabilitation for 1–2 weeks until an ROM of 0–120° was restored. No infection or DVT was observed.

After the intermediate rehabilitation, all patients had obtained normal knee alignment (**Figure 1D**), ROM (0–120°), and valgus/varus stability in the pre-stage-2 period (**Table 2**). MRI showed ACL and PCL ruptures in all patients (**Figure 1C**). Lachman and posterior drawer test also found notable anterior–posterior instability in most patients (**Figures 2E–G**).

The duration from stage-1 to stage-2 surgery was 6.94 ± 1.20 weeks (**Table 1**). Three subjects had hemarthrosis (10–20 ml) with transiently absorptive fever (<38.0°C)

TABLE 2 | Clinical assessments of knee stability before stage-2 operation and during the follow-ups.

Physical Examination/Measurement		A: pre-Stage-2* (*n* = 17)	B: 0.5 years (*n* = 17)	C: 1 year (*n* = 14)	$P_{A\text{-}C}$ / χ^2	$P_{A\text{-}B}$ / χ^2
Lachman test	–	0	17	14	<0.001	<0.001
	±	1	0	0	$\chi^2 = 34.000$	$\chi^2 = 31.000$
	+	16	0	0	$\upsilon = 2$	$\upsilon = 2$
Posterior draw	–	0	17	14	<0.001	<0.001
	±	2	0	0	$\chi^2 = 34.000$	$\chi^2 = 31.000$
	+	15	0	0	$\upsilon = 2$	$\upsilon = 2$
Pivot shift	–	0	17	14	<0.001	<0.001
	±	4	0	0	$\chi^2 = 34.000$	$\chi^2 = 31.000$
	+	13	0	0	$\upsilon = 2$	$\upsilon = 2$
Valgus stress	–	13	16	14	0.146	0.052
	±	4	1	0	$\chi^2 = 2.110$	$\chi^2 = 3.782$
	+	0	0	0	$\upsilon = 1$	$\upsilon = 1$
Varus stress	–	15	16	13	0.545	0.665
	±	2	1	1	$\chi^2 = 0.366$	$\chi^2 = 0.188$
	+	0	0	0	$\upsilon = 1$	$\upsilon = 1$
30° forward shift	<3 mm	0	14	12	<0.001	<0.001
	3–5 mm	0	3	0	$\chi^2 = 34.000$	$\chi^2 = 31.000$
	5–10 mm	2	0	0	$\upsilon = 3$	$\upsilon = 3$
	>10 mm	15	0	2		
70° backward shift	<3 mm	0	15	11	<0.001	<0.001
	3–5 mm	0	2	3	$\chi^2 = 34.000$	$\chi^2 = 31.000$
	5–10 mm	1	0	0	$\upsilon = 3$	$\upsilon = 2$
	>10 mm	16	0	0		

*Note: *pre-stage-2: just before the stage-2, operation began, when the stage-1 operation and rehabilitation of 6–8 weeks had been accomplished; the 30° forward shift and 70° backward shift were performed by KT-1000; there was no difference between 0.5 years and 1 year follow-up.*

(**Table 1**), but those implications disappeared spontaneously in 1–2 days. Finally, all patients underwent the arthroscopic reconstruction of ACL and PCL with unilateral semitendinous and gracilis tendons as auto-grafts (**Figure 2H**).

Follow-Ups

The average follow-up time was 11.18 ± 2.53 months (**Table 1**). There were three subjects missing at 1 year follow-up, who cannot be contacted through phone call/e-mail or claimed that they cannot participate anymore, and the total missing rate was 17.65% (**Table 1**). There were five and three subjects who had mild KFC at 0.5 years and 1 year follow-up, respectively (**Table 1**).No infection or DVT was observed during the follow-ups.

Most of the subjects had achieved normal joint stability during follow-ups (**Table 2**). The positive rates of Lachman, posterior drawer, pivot shift test, and forward and backward shift decreased significantly at 0.5 years and 1 year follow-up than those at the pre-stage-2 period, and no difference was found between 0.5 years and 1 year follow-up (**Table 2**). The valgus/varus instability rate showed no statistical difference among the three periods (**Table 2**).

Every subject had achieved a normal knee ROM at both follow-ups (**Table 3**). The knee extension angle at 0.5 years follow-up had an increasing trend compared to that in pre-stage-2, and there was no difference between 0.5 years and 1 year follow-up (**Table 3**). At 1 year follow-up, the knee extension angle showed a significant increase compared to that in pre-stage-2 (**Table 3**) (**Figure 3**). The knee flexion angle at 0.5 year follow-up showed a significant increase than that at pre-stage-2, and this angle was further increased at the 1 year follow-up (**Table 3**). The flexion angle at the 1 year follow-up was much bigger than that at pre-stage-2 (**Table 3**) (**Figure 3**). Lysholm and IKDC scores increased significantly at 0.5 years follow-up than those at pre-stage-2, and those parameters were further increased at the 1 year follow-up (**Table 3**). The normal knee alignment was observed at 0.5 years and 1 year follow-up (**Figures 1E, F**).

DISCUSSION

As IKD is a rare type of knee dislocation, most of the present studies were case reports or case series studies (Malik and Macdonald, 2019). In this study, the patients were enrolled from a province (local population: 84.8 million) in eastern China, where the climate is very rainy and locates on multiple interprovincial highways. The results found that most patients were farmers (8/17) and manual workers (5/17), and we considered that it can be attributed to the high risky environment characteristics for IKD. It has been reported that most IKDs are caused by low-energy trauma (Hussin et al., 2016; Hohmann et al., 2017; Schaefer et al., 2018), and the results showed that 82% IKD cases were caused by low-energy trauma (14/17), including sports traumas, self-spraining, and low-velocity motor vehicle accident.

IKD always needs very careful preoperative planning. Previous study has found that one-staged surgery may achieve high rates of arthrofibrosis and knee stiffness (Levy et al., 2009; Howells et al., 2011; Wu et al., 2014; Burrus et al., 2016) and postoperative instability and re-dislocation (Gu et al., 2004; Wu et al., 2014). It is

TABLE 3 | Knee range of motion and joint function at the pre-stage-2 period and follow-ups.

Parameters	A: pre-Stage-2* (*n* = 17)	B: 0.5 years (*n* = 17)	C: 1 year (*n* = 14)	$P_{A\text{-}B}$ *t*,*υ*<	$P_{A\text{-}C}$ *t*,*υ*	$P_{B\text{-}C}$ *t*,*υ*
Knee extension	−1.29 ± 1.26	−2.53 ± 2.27	−3.07 ± 2.46	0.058 *t* = 1.963 *υ* = 32	0.025 *t* = 2.447 *υ* = 18.531	0.529 *t* = 0.637 *υ* = 29
Knee flexion	123.41 ± 4.08	128.88 ± 6.90	138.07 ± 8.89	0.008 *t* = -2.814 *υ* = 32	<0.001 *t* = -5.697 *υ* = 17.472	0.003 *t* = -3.242 *υ* = 29
Lysholm	46.06 ± 6.43	77.12 ± 4.68	84.50 ± 4.50	<0.001 *t* = -16.112 *υ* = 32	<0.001 *t* = -18.865 *υ* = 29	<0.001 *t* = -4.448 *υ* = 29
IKDC	11.22 ± 2.23	74.52 ± 3.06	79.00 ± 5.71	<0.001 *t* = -16.112 *υ* = 32	<0.001 *t* = -14.402 *υ* = 29	0.003 *t* = -3.187 *υ* = 29

*Note: *pre-stage-2: just before the stage-2, operation began, when the stage-1 operation and rehabilitation of 6–8 weeks had been accomplished; IKDC: International Knee Documentation Committee.*

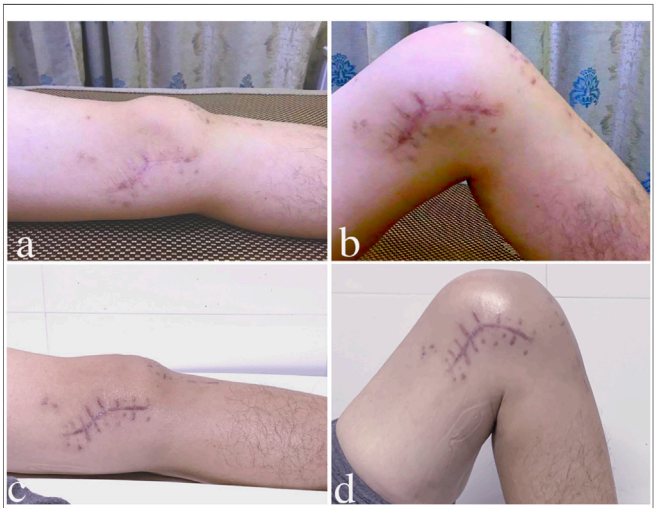

FIGURE 3 | Knee ROM at the intermediate rehabilitation and 1-year follow-up. **(A,B)**: subject achieved a normal knee extension and flexion angle after the intermediate rehabilitation; **(C,D)**: at 1 year follow-up, the same patient's knee extension and flexion angle showed a further increase.

supposed that the two-staged surgery combined with intermediate rehabilitation can obtain good efficacy and result in satisfying functional outcome (Levy et al., 2009; Mook et al., 2009; Howells et al., 2011; Jang et al., 2014; Burrus et al., 2016).

In this study, stage-1 surgery was performed within 3 weeks after injury because it is considered to be the critical time frame to repair the soft tissue without significant scarring (Ng et al., 2020). Our results showed that repairing of MCL and other extra-articular structures in stage-1 can provide sufficient anti-valgus stability, and it was maintained very well during the follow-ups. Soft tissue incarceration is the key feature of IKD: valgus stress separates the medial tibial plateau from the condyle, which increases the capsular volume and generates a negative pressure, trapping the medial structures into the condylar notch; as a result, the medial condyle dislocates the joint with soft tissue invagination (the 'pucker sign') (Jeevannavar and Shettar, 2013). Hence, the results indicated that urgent surgery is needed in order to minimize the risk of soft tissue necrosis. The MCL is the most powerful medial structure of the knee. Our results indicated that the MCL should be anatomically repaired in the stage-1 surgery of IKD as well in order to achieve superior healing capability (Kovachevich et al., 2009; Xu et al., 2017).

The intermediate aggressive rehabilitation facilitated the recovery of ROM and knee function. Once the normal ROM was restored, the stage-2 surgery (delayed reconstruction of ACL and PCL) was begun (Levy et al., 2009; Howells et al., 2011; Burrus et al., 2016). In this study, the stage-2 surgery of ACL and PCL reconstruction was performed based on normal ROM, knee alignment, and medial stability contributed by intermediate rehabilitation. We considered that both ACL and PCL reconstruction were essential for the IKD patients because of the results found.

A notable anterior/posterior instability and rotational instability existed commonly after the stage-1 surgery. Similar to our findings, Solarino et al. also reported that the IKD patients may experience a feeling of joint instability without ACL or PCL reconstruction even for elderly subjects (Solarino et al., 2015). However, Bistolfi et al. declaimed that cruciate ligament reconstruction can be avoided in elderly patients or subjects who were not professionally engaged in a high-level sport (Bistolfi et al., 2011). Our results found that a superior anterior–posterior stability and rotational stability can be achieved and maintained at least 1 year after the stage-2. It has been reported that the delayed cruciate ligament reconstruction (>3 weeks) offers better ROM and rehabilitation (Levy et al., 2009; Howells et al., 2011; Burrus et al., 2016). Our results indicate that both ACL and PCL should be reconstructed in the stage-2 surgery of IKD, contributing to joint stability and functional outcome.

On the other side, IKD always affects the pes anserinus tendon. The hamstring is one of the most commonly utilized auto-grafts for ligament reconstruction (Mahmoud et al., 2014), and the graft quality is of great significance in clinical efficacy and outcome (Moghamis et al., 2019). Hence, ligament reconstruction should be delayed in stage-2 (Solarino et al., 2015). The present study found that the intermediate rehabilitation (6–8 weeks) progressed very well after the stage-1, and only two cases of stiffness occurred, but they can be successfully reversed by physics therapy. Finally, all subjects started the stage-2 surgery with

normal ROM and knee alignment. Our results suggest that the intermediate duration of 6–8 weeks is sufficient for the pes anserinus to restore, and unilateral auto-graft can provide sufficient tendon strength for both reconstructions.

Our results showed that all subjects had achieved a full ROM, superior joint stability, and continuously increased IKDC and Lysholm scores at follow-ups. Similarly, systematic reviews demonstrated that the two-staged surgery resulted in a good outcome on the joint stability and function in KD-III injuries, which was better than acute or delayed surgery (Mook et al., 2009; Jang et al., 2014). Our results indicated that the two-staged surgery with intermediate rehabilitation can have a satisfactory functional outcome.

Our study presents several limitations. First, as the incidence of IKD is very low, our sample size was small. Second, the follow-up time was not very long. A further longitudinal study with more samples and longer follow-up and different cohort studies are required to determine the long-term outcome of the two-staged operation.

CONCLUSION

The two-staged surgery on treatment of IKD has superior efficacy on knee stability and function, and it can facilitate the rehabilitation and achieve a satisfactory short-term outcome.

DATA AVAILABILITY STATEMENT

The data analyzed in this study is subject to the following licenses/restrictions: All of the data have been showed in this study. There are no additional unpublished data from this study. Requests to access these datasets should be directed to polocsy@163.com (SC).

ETHICS STATEMENT

The studies involving human participants were reviewed and approved by. Ethical approval was obtained prior to start of each study (IRB ethical approval: KY-2016-OB08) for the protection of human subjects by the Ethical committee of the Second Affiliated Hospital of Nantong University. The patients/participants provided their written informed consent to participate in this study.

AUTHOR CONTRIBUTIONS

Conceptualization: SC and WL; data curation: HY, XZ, and JF; formal analysis: HY, XZ, and YD; investigation: SC, HY, and JF; writing—original draft: SC; writing—review and editing: XZ and WL.

FUNDING

The study was funded by the National Natural Science Foundation of China (Grant No. 81501866) (WL), the Science and Technology Bureau of Nantong (Grant Nos. MA2019005 and MB2019001) (WL), the Science & Technology Bureau of Nantong (Grant No.jcz21019) (SC), and the Jiangsu Provincial Young Medical Talent Foundation (Grant No. QNRC2016411) (HY).

REFERENCES

Bistolfi, A., Massazza, G., Rosso, F., Ventura, S., Cenna, E., Drocco, L., et al. (2011). Non-reducible Knee Dislocation with Interposition of the Vastus Medialis Muscle. *J. Orthopaed Traumatol.* 12 (2), 115–118. doi:10.1007/s10195-011-0134-2

Burrus, M. T., Werner, B. C., and Griffin, J. W. (2016). Diagnostic and Management Strategies for Multiligament Knee Injuries: A Critical Analysis Review. *JBJS Rev.* 4 (2), e1. doi:10.2106/jbjs.rvw.o.00020

Chen, W., Zhang, Y.-z., Su, Y.-l., and Pan, J.-s. (2011). Irreducible Lateral Knee Dislocation with Incarceration of the Lateral Femoral Condyle in the Posterolateral Capsuloligamentary Structures: a Case Report and Literature Review. *Orthopaedic Surg.* 3 (2), 138–142. doi:10.1111/j.1757-7861.2011.00126.x

Gu, M. Q., Deng, L., and Liu, Y. (2004). Posterolateral Dislocation of the Knee Joints: Analysis of 9 Cases. *Chin. J. Traumatol.* 7 (4), 210–216.

Hill, J. A., and Rana, N. A. (1981). Complications of Posterolateral Dislocation of the Knee: Case Report and Literature Review. *Clin. Orthopaedics Relat. Res.* 154 (154), 212. doi:10.1097/00003086-198101000-00032

Hohmann, E., Glatt, V., and Tetsworth, K. (2017). Early or Delayed Reconstruction in Multi-Ligament Knee Injuries: A Systematic Review and Meta-Analysis. *The Knee* 24 (5), 909–916. doi:10.1016/j.knee.2017.06.011

Howells, N. R., Brunton, L. R., Robinson, J., Porteus, A. J., Eldridge, J. D., and Murray, J. R. (2011). Acute Knee Dislocation: An Evidence Based Approach to the Management of the Multiligament Injured Knee. *Injury* 42 (11), 1198–1204. doi:10.1016/j.injury.2010.11.018

Hussin, P., Mawardi, M., and Halim, A. A. (2016). A Rare Variant of Knee Dislocation. *Gchir* 37 (2), 71–73. doi:10.11138/gchir/2016.37.2.071

Insall, J. N., Dorr, L. D., Scott, R. D., and Norman, W. (1989). Rationale, of the Knee Society Clinical Rating System. *Clin. Orthopaedics Relat. Res.* 248, 13–14. doi:10.1097/00003086-198911000-00004

Jang, K.-M., Lee, H.-S., and Wang, J. H. (2014). Open Reduction of Irreducible Posterolateral Rotary Knee Dislocation without Sectioning of Incarcerated Vastus Medialis: A Case Report with Video Illustration. *The Knee* 21 (2), 582–585. doi:10.1016/j.knee.2012.09.018

Jeevannavar, S. S., and Shettar, C. M. (2013). 'Pucker Sign' an Indicator of Irreducible Knee Dislocation. *BMJ Case Rep.* 2013 (oct04), bcr2013201279. doi:10.1136/bcr-2013-201279

Jr, S. R. (1994). The Dislocated Knee. *Instr. Course Lect* 43, 127–136.

Kovachevich, R., Shah, J. P., Arens, A. M., Stuart, M. J., Dahm, D. L., and Levy, B. A. (2009). Operative Management of the Medial Collateral Ligament in the Multi-Ligament Injured Knee: an Evidence-Based Systematic Review. *Knee Surg. Sports Traumatol. Arthrosc.* 17 (7), 823–829. doi:10.1007/s00167-009-0810-4

Levy, B. A., Dajani, K. A., Whelan, D. B., Stannard, J. P., Fanelli, G. C., Stuart, M. J., et al. (2009). Decision Making in the Multiligament-Injured Knee: an Evidence-Based Systematic Review. *Arthrosc. J. Arthroscopic Relat. Surg.* 25 (4), 430–438. doi:10.1016/j.arthro.2009.01.008

Mahmoud, S. S. S., Odak, S., Coogan, S., and McNicholas, M. J. (2014). A Prospective Study to Assess the Outcomes of Revision Anterior Cruciate Ligament Reconstruction. *Int. Orthopaedics (Sicot)* 38 (7), 1489–1494. doi:10.1007/s00264-014-2324-z

Malik, S. S., and Macdonald, P. B. (2019). Erratum to: The Irreducible Knee Dislocation. *J. Knee Surg.* 33 (4), e1. doi:10.1055/s-0039-3402743

Moghamis, I., Abuodeh, Y., Darwiche, A., Ibrahim, T., Al Ateeq Al Dosari, M., and Ahmed, G. (2019). Anthropometric Correlation with Hamstring Graft Size in Anterior Cruciate Ligament Reconstruction Among Males. *Int. Orthopaedics (Sicot)* 44 (3), 577–584. doi:10.1007/s00264-019-04452-5

Mook, W. R., Miller, M. D., Diduch, D. R., Hertel, J., Boachie-Adjei, Y., and Hart, J. M. (2009). Multiple-ligament Knee Injuries: a Systematic Review of the Timing of Operative Intervention and Postoperative Rehabilitation. *The J. Bone Jt. Surgery-American Volume* 91 (12), 2946–2957. doi:10.2106/jbjs.h.01328

Ng, J. W. G., Myint, Y., and Ali, F. M. (2020). Management of Multiligament Knee Injuries. *EFORT Open Rev.* 5 (3), 145–155. doi:10.1302/2058-5241.5.190012

Price, R. C., Christopher, S., and Richter, D. L. (2019). Irreducible Knee Dislocation Associated with a Tertiary Gastrocnemius Head: A Case Report. *JBJS case connector* 9 (4), e0476. doi:10.2106/jbjs.cc.18.00476

Ranger, P., Renaud, A., Phan, P., Dahan, P., De Oliveira, E., and Delisle, J. (2011). Evaluation of Reconstructive Surgery Using Artificial Ligaments in 71 Acute Knee Dislocations. *Int. Orthopaedics (Sicot)* 35 (10), 1477–1482. doi:10.1007/s00264-010-1154-x

Robertson, A., Nutton, R. W., and Keating, J. F. (2006). Dislocation of the Knee. *J. Bone Jt. Surg Br* 88 (2), 706–711. doi:10.1302/0301-620X.88B6.17448

Schaefer, M., Weber, J., and Faller, P. (2018). One-Stage Arthroscopic Reduction Combined with Multiligament Reconstruction or Repair for Irreducible Posterolateral Knee Dislocation: A Retrospective Case Series with Minimum 2-Year Follow-Up. *J. Knee Surg.* 31 (10), 1015–1021. doi:10.1055/s-0038-1632394

Solarino, G., Notarnicola, A., Maccagnano, G., Piazzolla, A., and Moretti, B. (2015). Irreducible Posterolateral Dislocation of the Knee: a Case Report. *Joints* 03 (02), 91–96. doi:10.11138/jts/2015.3.2.091

Wu, J., Yao, J., and Yuan, H. (2014). The Timing of Surgical Treatment of Knee Dislocations: a Systematic Review. *Knee Surg. Sports Traumatol. Arthrosc.* 23 (10), 3108–3113. doi:10.1007/s00167-014-3435-1

Xu, H., Tu, J., Xu, B., and Guo, R. (2017). Initial Assessment and Implications for Surgery: The Missed Diagnosis of Irreducible Knee Dislocation. *J. Knee Surg.* 31 (03), 254–263. doi:10.1055/s-0037-1602135

Conflict of Interest: The authors declare that the research was conducted in the absence of any commercial or financial relationships that could be construed as a potential conflict of interest.

frontiers | Frontiers in Bioengineering and Biotechnology

ORIGINAL RESEARCH
published: 27 May 2022
doi: 10.3389/fbioe.2022.913900

Primary Repair for Treating Acute Proximal Anterior Cruciate Ligament Tears: A Histological Analysis and Prospective Clinical Trial

*Yue Yang[1], Zhuangzhuang Jin[2], Jianghua Luo[3], Delong Zhang[1], Peng Shen[1], Dianbin Zheng[1], Donghao Liu[1] and Lunhao Bai[1]**

[1]Department of Orthopaedic Surgery, Shengjing Hospital of China Medical University, Shenyang, China, [2]Department of Emergency Medicine, Shengjing Hospital of China Medical University, Shenyang, China, [3]Department of Orthopedic Surgery, Zhongshan Hospital Affiliated to Xiamen University, Xiamen, China

OPEN ACCESS

Edited by:
Yansong Qi,
Inner Mongolia People's Hospital, China

Reviewed by:
Yinghui Hua,
Huashan Hospital Affiliated to Fudan University, China
Jie Li,
Tianjin Medical University, China
Chen Huang,
Peking University Third Hospital, China

***Correspondence:**
Lunhao Bai
bailh211@163.com

Specialty section:
This article was submitted to Biomaterials, a section of the journal Frontiers in Bioengineering and Biotechnology

Received: 06 April 2022
Accepted: 17 May 2022
Published: 27 May 2022

Citation:
Yang Y, Jin Z, Luo J, Zhang D, Shen P, Zheng D, Liu D and Bai L (2022) Primary Repair for Treating Acute Proximal Anterior Cruciate Ligament Tears: A Histological Analysis and Prospective Clinical Trial. Front. Bioeng. Biotechnol. 10:913900. doi: 10.3389/fbioe.2022.913900

Reconstruction surgery for acute proximal anterior cruciate ligament (ACL) tears remains controversial. Recently, ACL primary repair has received increasing attention in ACL treatment. This study aimed to explore the histological characteristics of ACL healing in primary repair and compare its therapeutic and prognostic results with the reconstruction of acute proximal ACL tears. Histological experiments using rabbits and a prospective clinical trial were conducted. We established a rabbit model of ACL primary repair, and histological changes were observed using haematoxylin and eosin (HE) and toluidine blue staining. We performed immunohistochemical analysis of CD34 and S-100 and measured the expression of collagen I and II using qRT-PCR, Western blotting, and immunohistochemistry. The prospective clinical trial involved performing ACL primary repair and reconstruction in patients with acute proximal ACL tears to detect proprioception and evaluate the function of joints. We discovered that primary repair promoted cell proliferation in the tendon-bone transition and ligament portions, reduced osteoarthritis-like pathological changes, and maintained blood vessels and proprioceptors within the ACL. In the clinical trial, primary repair achieved similar therapeutic outcomes, including recovery of knee function and proprioception, in the follow-up period as ACL reconstruction. However, the primary repair had a significantly shorter operative time and lower cost than reconstruction. Therefore, doctors should consider the benefit of primary repair in treating acute proximal ACL tears.

Keywords: anterior cruciate ligament, acute proximal tears, primary repair, reconstruction surgery, histological study, prospective clinical trial

Abbreviations: FFCP, forefoot contact phase; FFP, foot flat phase; FFPOP, forefoot push-off phase; ICP, initial contact phase; JPR, joint position reproduction; TDPM, threshold to detect passive motion.

1 INTRODUCTION

The anterior cruciate ligament (ACL) is most vulnerable to sports injuries (Yang et al., 2019). Compared to the limited effect of conservative treatment in the healing of torn ACLs, the surgical intervention aims to restore knee stability and reduce degeneration changes found in ACL-deficient knees. The management of ACL remnant tissue is essential for clinical outcomes and prognosis. The blood vessels covered by the synovium of the ACL provide a microenvironment for synovial cell proliferation (Takahashi et al., 2016). Furthermore, the proprioceptors in the remnant tissue participate in adjusting muscle movements around the knee joint, thereby accelerating the rehabilitation of knee function (Lee et al., 2015). However, improper handling of the remnant tissue could result in excessive graft volume compared with the space of the intercondylar fossa, resulting in an increased incidence of problematic postoperative loss of extension (Tanabe et al., 2016). Thus, the preservation technique of the remnant tissue deserves proper application in ACL surgery.

Primary repair and reconstruction are representative therapeutic strategies (Achtnich et al., 2016). ACL reconstruction is widely performed and has shown excellent outcomes. However, not all patients experience satisfactory recovery after ACL reconstruction (Kazusa et al., 2013). Therefore, many surgeons have switched their attention to ACL primary repair because of its less invasive nature and potential for self-healing (van der List and DiFelice, 2017; Ahmad et al., 2019; Schneider et al., 2020). Several inherent advantages exist in ACL primary repair, including fewer graft-related complications and maintenance of the original anatomical structures and proprioceptors (Kiapour et al., 2017). Furthermore, recent studies have reported that ACL primary repair is a safe procedure with acceptable overall failure rates among adult patients (Heusdens et al., 2019; Douoguih et al., 2020). However, the clinical efficacy and underlying mechanisms of ACL healing with these two strategies remain controversial.

Although clinical research on ACL primary repair with remnant tissue preservation cannot be neglected, histological research can provide a solid theoretical foundation for further studies. Tendon-bone healing in the transition area and tendon-tendon healing in the ligament portion are essential processes for ACL healing (Maniar et al., 2015). Recent studies have reported that growth factors or stem cells can potentially be administered to accelerate the healing response (Dallo et al., 2017; Xu et al., 2021). Microfracture in ACL primary repair produces a persistent microenvironment for cell proliferation (Achtnich et al., 2016). Both the clinical efficacy and histological characteristics of ACL primary repair should be investigated. However, existing studies have not combined these two aspects.

We hypothesised that primary repair would have similar clinical efficacy as ACL reconstruction, and histological results would provide a foundation for future mechanistic studies. The purpose of this study was to analyse the outcomes of primary repair with remnant tissue preservation in treating acute proximal ACL tears by combining the evaluation of the histological characteristics and clinical efficacy. This study used rabbits to fill the research gaps in ACL primary repair, considering the limitations of conducting histological research using humans. Clinical efficacy was investigated in a prospective clinical trial in patients diagnosed with acute proximal ACL tears with intact remnants, and ACL reconstruction was used as the gold standard.

2 MATERIALS AND METHODS

2.1 Histological Experiments

2.1.1 Experimental Animals

Male New Zealand white rabbits aged 6 months and weighing 3.0–3.5 kg were purchased from the Maohua Company (Shenyang, China). Four rabbits were kept in one cage and lived in a controlled environment (22 ± 2°C, 50 ± 10% humidity, and 12 h/12 h light-dark cycle with the light period from 6 a.m. to 6 p.m.). All the rabbits had access to adequate drinking water and were fed ad libitum for 2 weeks to acclimatise them to laboratory conditions. The study followed the 3R rules for animal testing and was approved by the Ethics Committee of Shengjing Hospital.

2.1.2 ACL Primary Repair on Rabbits

There were three groups in the animal experiments: the control group (CG), ACL cutting-off (ACLC) group, and ACL primary repair (ACLP) group. Every 12 rabbits were attributed to each group. Each rabbit was anaesthetised *via* inhalation of a 3% isoflurane-air mixture, and the respiratory rate, heart rate, and body temperature were monitored. The rabbits were then fixed in the supine position, and the skin of both lower limbs was disinfected with iodophor. The articular structures of rabbit knees were exposed by separating the skin and subcutaneous tissues layer-by-layer. The ACL was cut off from the femoral insertion site in the ACLC group. A suture was passed through the ACL bundle several times, and a femoral tunnel was drilled from the femoral footprint, with the knee flexed at 90°. The suture pulled the stump of the ACL through the femoral tunnel, and a cortical bone screw was used to fix the suture to the lateral condyle. The tissue fragments and blood clots in joint cavity was irrigated with normal saline. After the surgery, the animals were returned to their original cages without limitation. The procedure on CG was performed only to expose the knee cavity, which was then closed layer-by-layer. The procedure on ACLC was similary to ACLP, but without repairing the ACL (**Supplementary Figure S1**).

2.1.3 Sample Collection and Histological Evaluation

The rabbits were sacrificed by overdose anaesthesia 12 weeks after the operation. First, any structures outside the knee joint capsule were removed, maintaining the femoral ligament-tibial complex. The samples were fixed in 4% paraformaldehyde solution for 48 h. Next, the samples were soaked in 10% ethylenediaminetetraacetic acid (EDTA) solution for decalcification for the following 1 month. The EDTA solution was refreshed every 2, 3 days. After decalcification, the samples were dehydrated in a series of ethanol solutions and embedded in

TABLE 1 | Primers used in the study.

Primers	5′ to 3′	3′ to 5′
Collagen I	GCCATCAAGGTCTTCTGCG	GAACTGGAAGCCATCGGTC
Collagen II	ACACTGCCAACGTCCAGATG	GTGATGTTCTGGGAGCCCTC
GAPDH	GGGAAGCTGGTCATCAACGG	GTACTCGGCACCAGCATCAC

paraffin for further experiments. The paraffin-embedded tissues were cut into 5-μM thick sections and stained with haematoxylin and eosin (HE) or toluidine blue stain for evaluation. Finally, the modified Mankin scoring system was used to analyse osteoarthritis (OA)-like changes in the knee joints of the rabbits (Lin et al., 2021).

2.1.4 Immunohistochemistry

After deparaffinisation, rehydration, and washing, enzymatic antigen retrieval of each tissue section was performed at 37°C for 30 min. The sections were treated with 3% H_2O_2 in methanol for 10 min to quench endogenous peroxidase activity, and goat serum (5%) was used to block non-specific binding sites. Next, the sections were incubated overnight at 4°C with the following primary antibodies: mouse monoclonal anti-CD34 (1:2,000; 60180-1-Ig, Proteintech, Shenyang, China), mouse monoclonal anti-S100 (1:100; BM0120, BOSTER, Shanghai, China), mouse monoclonal anti-collagen I (1:100; 66761-1-Ig, Proteintech), and mouse monoclonal anti-collagen II (1:300; ab185430, Abcam, Shanghai, China). After washing with phosphate-buffered saline (PBS) on the following day, the sections were incubated with the appropriate biotin-conjugated secondary antibodies at 22 ± 2°C for 30 min. The sections were then incubated with horseradish peroxidase-conjugated streptavidin at 22 ± 2°C for 1 h. Finally, the sections were stained with diaminobenzidine (DAB) and counterstained with haematoxylin. Image Pro Plus version 6.0 software (Media Cybernetics, Rockville, MD, United States) was used to calculate the mean optical density.

2.1.5 Quantitative Reverse Transcription-PCR

Briefly, total RNA was collected from the tendon-bone transition area and articular cartilage using TRIzol® reagent (Thermo Fisher Scientific, Waltham, MA, United States). A PrimeScript RT Reagent Kit with gDNA Eraser (Takara, Shiga, Japan) was used to synthesise complementary DNA, and Quantitative Reverse Transcription-PCR (qRT-PCR) was performed using an ABI Prism 7500 Fast Real-Time PCR System (Thermo Fisher Scientific) and SYBR Premix Ex Taq II (Takara). The $2^{-\Delta\Delta CT}$ method was used to evaluate the relative expression of *GAPDH* as the reference. Primers were designed and synthesised by Sangon Biotech (Shanghai, China) (**Table 1**).

2.1.6 Western Blotting

Briefly, proteins were collected from the tendon-bone transition area and articular cartilage using radioimmunoprecipitation assay (RIPA) lysis buffer (P0013C, Beyotime, Shenyang, China) supplemented with 1% phenylmethylsulfonyl fluoride (PMSF; ST506, Beyotime). A BCA protein assay kit (P0010; Beyotime) was used to quantify the proteins, and 30 μg protein per sample was subjected to polyacrylamide gel electrophoresis. Next, the proteins were transferred onto polyvinylidene difluoride (PVDF) membranes using wet blotting. The membranes were incubated overnight at 4°C with the following primary antibodies after blocking non-specific binding sites: mouse monoclonal anti-collagen I (1:3,000; 66761-1-Ig, Proteintech), mouse monoclonal anti-collagen II (1:3,000; ab185430, Abcam, United States), and mouse monoclonal GAPDH (1:1,000; 60004-1-Ig; Proteintech). The membranes were then incubated with horseradish peroxidase-conjugated secondary antibodies at 22 ± 2°C for 2 h. Enhanced chemiluminescence reagent was used to detect immunoreactivity. Finally, Image Pro Plus version 6.0 software (Media Cybernetics) was used to calculate the band intensities.

2.2 Clinical Trial

2.2.1 Patient Information and Inclusion and Exclusion Criteria

Our study followed the latest Strengthening the Reporting of Cohort Studies in Surgery guidelines (Agha et al., 2019). Furthermore, the study protocol was approved by the ethics committee and prospectively registered in the Chinese Clinical Trial Registry (https://www.chictr.org.cn/showproj.aspx?proj=124186, ChiCTR2100045145). Informed consent was obtained from all patients. Baseline information, including clinical history, surgical date, nursing, and imaging data, was collected from the hospital information system.

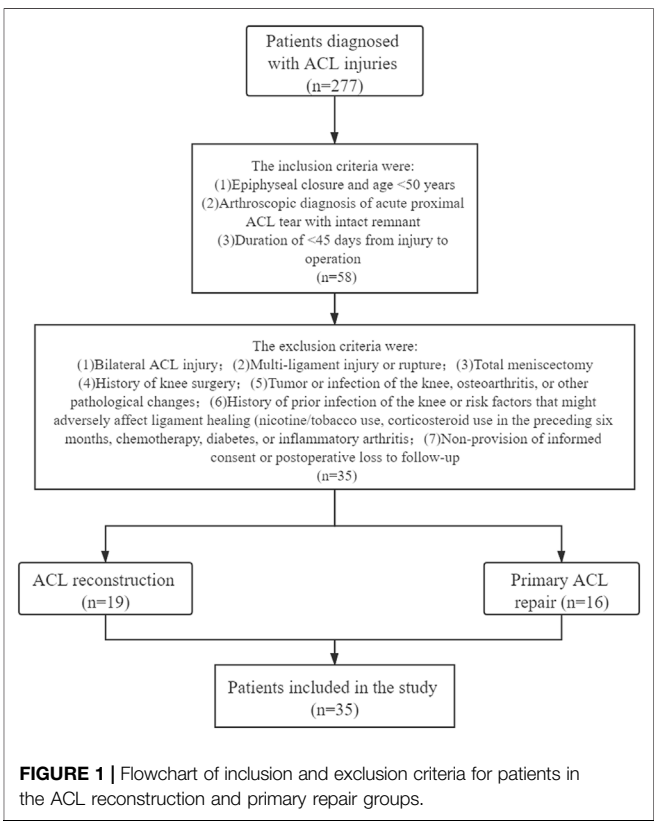

FIGURE 1 | Flowchart of inclusion and exclusion criteria for patients in the ACL reconstruction and primary repair groups.

The inclusion criteria were epiphyseal closure, age <50 years, arthroscopic diagnosis of acute proximal ACL tear with an high quality remnant, and an interval of 45 days between the injury and surgery. The exclusion criteria were: 1) bilateral ACL injury; 2) multi-ligament injury or rupture; 3) total meniscectomy; 4) history of knee surgery; 5) tumour or infection of the knee, OA, or other pathological changes; 6) history of prior infection of the knee or risk factors that might adversely affect ligament healing (nicotine/tobacco use, corticosteroid therapy in the preceding 6 months, chemotherapy, diabetes, or inflammatory arthritis); and 7) non-provision of informed consent or postoperative loss to follow-up. The inclusion and exclusion criteria and flow chart of the clinical trial are shown in **Figure 1**.

To fully respect the patient's right to informed consent, we explained the advantages and disadvantages of ACL primary repair and ACL reconstruction to each patient and obtained their authorisation and consent preoperatively. Each patient decided on the surgical plan and signed a surgical consent form before the operation.

2.2.2 Surgical Technique

All ACL primary repairs (Group P) and ACL reconstructions (Group R) were performed by the same senior surgeon. After successful induction of anaesthesia, the patient was placed in the supine position on the operation table. The affected knee was prepared and draped for arthroscopy. Equipment and implants in the standard knee arthroscopy set were used. A scalpel was used to make a 0.4 cm longitudinal incision, and anterolateral and anteromedial portals were created. A probe was used to explore the joint cavities sequentially. Finally, the proximal ACL tear was diagnosed. The ACL remnant tissue quality was evaluated by sherman scoring system before surgery and Takeshi scoring system during ACL surgery (Sherman et al., 1991; Muneta et al., 2016).

2.2.2.1 ACL Primary Repair Procedure

The ACL primary repair procedure is shown in the **Supplementary Video S1**. Briefly, the degree of ACL damage was assessed *via* arthroscopy. Next, an AR-7200 suture (Smith & Nephew, London, UK) was passed through the ACL bundle *via* a Scorpion Suture Passer (Smith & Nephew). The ACL bundle was retracted to expose the ACL footprint on the lateral femoral condyle. A planer was used to trim the damaged joint surfaces, and a microfracture device (Smith & Nephew) was used to drill a hole to freshen the femoral footprint area and promote the healing of the ACL bundle.

A femoral tunnel was drilled from the femoral footprint, with the knee flexed at 90°. Next, the AR-7200 sutures were retrieved through the medial portal and passed through the core hole of the PushLock anchor (Smith & Nephew). The PushLock anchor was deployed into the femoral tunnel, with the knee flexed at 90°.

The free end of the AR-7200 suture was cut using an open-ended suture cutter (Smith & Nephew), and a probe was used to assess tension in the ACL bundle. ACL impingement should not be observed on arthroscopy. Next, an intraoperative Lachman test was performed to confirm minimal anteroposterior translation after primary repair. Intra-articular electrocautery was used to achieve haemostasis. The tissue fragments and blood clots in joint cavity was irrigated with normal saline. Finally, the arthroscopic equipment was removed, and the surgical portal was closed layer-by-layer (**Supplementary Figure S2**).

2.2.2.2 ACL Reconstruction Procedure

The semimembranosus and semitendinosus were harvested from patients. These ligaments were folded, quadrupled, and stitched using an AR-7200 suture (Smith & Nephew) following a Bunnell-type pattern and immersed in gentamicin saline for further use. After installing the tibial guide frame, the arthroscope was used to determine the inner port of the tibial tunnel 7 mm from the anterior edge of the posterior cruciate ligament and 3 mm behind the midpoint of the ACL implantation point. The outer port of the tibial tunnel was located 1.5 cm posterior to the tibial tubercle and 1 cm above the pes anserinus. The tibial tunnel was created based on the diameter of the graft ligaments. The anteromedial auxiliary portal was established to drill the femoral tunnel at the femoral footprint of the ACL. The femoral tunnel was created 1 mm from the posterior femoral cortex and was 3 cm deep.

Another suture was placed at the proximal end of the remnant with a suture hook (Smith & Nephew). The free ends of the sutures were retrieved through the anteromedial portals. The remnant tissue of the ACL bundle was preserved and protected using sutures during ACL reconstruction. A pulling suture was used to insert the graft into the tibial and femoral tunnels. An EndoButton loop steel plate (Smith & Nephew) was used to fix and tighten the looped graft ligament. A squeezing screw was used to fix the tibial end of the graft with the knee at a 20° extension.

The proximal ACL remnant and the articular portion of the graft were sutured using an AR-7200 suture when the tibia was completely fixed. The free end of the AR-7200 suture on the ACL remnant bundle was passed through the core hole of the PushLock anchor (Smith & Nephew). The PushLock anchor was deployed into the femoral tunnel with the knee at 90° flexion. The free end of the AR-7200 suture was cut using an open-ended suture cutter (Smith & Nephew).

Mobility of the affected knee was tested from 0° to 130°. Graft impingement should not be observed under arthroscopy, and the change in graft length should be <2 mm. A probe was used to assess tension in the ACL bundle, and an intraoperative Lachman test was performed to confirm the minimal anteroposterior translation. Intra-articular electrocautery was used to achieve haemostasis. The tissue fragments and blood clots in joint cavity was irrigated with normal saline. Finally, the arthroscopic equipment was removed, and the surgical portal was closed layer-by-layer (**Supplementary Figure S3**).

2.2.3 Postoperative Management

Postoperatively, all patients underwent magnetic resonance imaging and were guided to undergo rehabilitation exercises (**Supplementary Figure S4**). The patients wore limb braces, and drainage tubes were removed after approximately 24 h. The brace was fixed at 0–30° within 1 week after the operation. After 1 month, the range of motion of the knee joint was expected

to reach 90–110° and allow for a gradual transition to total weight-bearing.

2.2.4 Clinical Efficacy Assessment

The Lysholm score and International Knee Documentation Committee (IKDC) score were used to evaluate the basic function of the knee joint subjectively (Chai at al., 2019; Mouarbes et al., 2019), and the knee joint passive relaxation test (Kneelax) was used to evaluate the stability of the knee joint objectively. The threshold to detect passive motion (TDPM) test, joint position reproduction (JPR) test, and foot pressure analysis were used to evaluate proprioception.

2.2.4.1 Knee-Joint Assessment Using Kneelax 3

Kneelax 3 (Shanghai Huanxi Medical Instrument Co., Ltd., Shanghai, China) was used to evaluate the stability of the knee joint. The distance of the anterior tibial displacement per millimetre under 132 N tension was recorded for statistical analysis.

2.2.4.2 TDPM

The TDPM was evaluated using a continuous passive motion (CPM) machine. The patient was placed in a recumbent position with earmuffs and eyeshades to isolate the visual and auditory sensations. The lower limbs were placed in the CPM machine. The machine started to drive at 15° and an angular speed of 0.5°/s. When the patient perceived lower-limb movement, the machine was stopped. Simultaneously, the patient indicated the direction of the movement. This test was repeated three times, and the average time was recorded as the TDPM value.

2.2.4.3 JPR

JPR tests were performed under the same conditions as mentioned in **Section 2.2.4.2**. The limbs were placed at various measurement angles (30°, 60°, and 90°) and rested for 10 s. The CPM machine was stopped when the patient perceived the measurement angle. The test was repeated three times to obtain the average difference between the perceived and measurement angles. Finally, the JPR value was obtained by calculating the average difference for each angle.

2.2.4.4 Foot Pressure Analysis of Gait

A foot pressure analysis system was used to collect data on the walking parameters of patients. It analysed the proportion of each stage of the walking support phase and evaluated the stability of the centre of weight distribution of patients. The gait system divides the single-foot support phase into four phases: the initial contact phase (ICP), forefoot contact phase (FFCP), foot flat phase (FFP), and forefoot push-off phase (FFPOP) (**Supplementary Figure S5**).

2.3 Statistical Analysis

The Shapiro–Wilk test was used to evaluate the normality, and the Levene test was used to evaluate the homogeneity of variance before assessing the differences between groups. The Student's *t*-test was used to analyse normally distributed data with homogeneity of variance, and the results were expressed as the mean ± standard deviation. Otherwise, the Wilcoxon rank-sum test was used, and the results were expressed as medians with interquartile ranges. Categorical data were analysed using the chi-square test. Statistical analyses were performed using SPSS version 21.0 (IBM Corp., Armonk, NY, United States). $p < 0.05$ was considered statistically significant.

3 RESULTS

3.1 Primary Repair Promotes Cell Proliferation in Tendon-Bone Transition and Ligament Portions

As shown in **Figure 2A**, the normal ACL has a smooth surface and is covered by synovial tissue with tiny blood vessels. The ligament tissue of the ACLC group was almost completely absorbed at postoperative week 12. Synovial-like tissue could be seen on the ligament surface in the ACLP group without apparent scar formation at the healing site. At postoperative week 12, the tendon-bone junction was tighter, the tide line was wide, and more tissue interpenetration could be seen in the ACLP group. Increased nucleus density was observed in the ligament portion of the ACLP group at postoperative week 12. The cell counts of the ACLP group were significantly increased at postoperative week 12 ($p < 0.05$), whereas 0 cell count was observed in the ACLC group (**Figure 2B**). Additionally, no healing response was observed in the tendon-bone transition area of the ACLC group.

3.2 Primary Repair Reduces OA-like Pathological Changes

OA-like changes are long-term pathological features worthy of attention after ACL healing. **Figure 3A** showed the H&E and toluidine blue staining of the rabbit knee surface, respectively. After cutting the ligament in the ACLC group, OA-like changes such as local cartilage damage, empty cartilage lacunae, and light staining of the extracellular matrix could be observed. However, the ACLP group had a relatively smooth cartilage surface, a higher density of chondrocytes. ACLP had an significant decreased Mankin scores compared to ACLC (**Figure 3C**, $p < 0.05$). The relative expressions of collagen I in the transition area and collagen II in articular cartilage were evaluated using immunohistochemistry (**Figure 3B**), Western blotting (**Figure 3D**) and qPCR (**Figure 3E**). Increased expression of collagen I and II was observed in the ACLP group ($p < 0.05$). This may suggest that the stability restored by primary repair reduced the process of knee joint degeneration.

3.3 Primary Repair Protects Blood Vessels and Proprioceptors Within the ACL

CD34 is a protein characteristic of the vascular structure. The expression of CD34 in the ACLP group was significantly higher than that in the ACLC group. The statistical value of microvessel density (MVD) was used as the evaluation standard for ligament

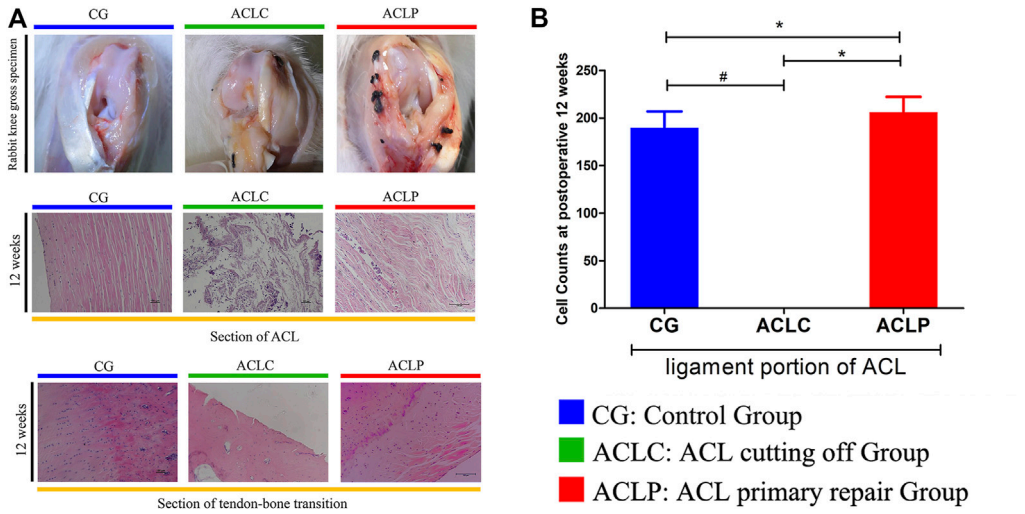

FIGURE 2 | (A) The gross specimen of the rabbit knee and HE staining of the ACL portion and tendon-bone transition area at postoperative week 12. **(B)** Cell Counts of ACL portion. #: $p < 0.05$ versus ACLC group; *: $p < 0.05$ versus ACLP group. $n = 12$ in each group. Data are expressed as mean ± SD.

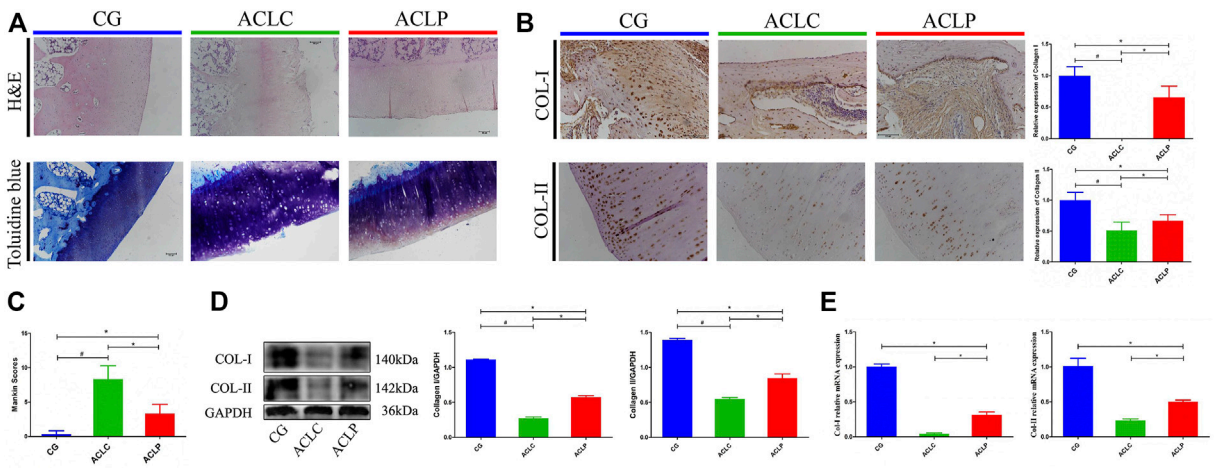

FIGURE 3 | (A) HE and toluidine blue staining of articular cartilage in the rabbit knee. **(B)** Immunohistochemistry of collagen I and II in articular cartilage. **(C)** Mankin scores of each group. **(D)** Western blotting of collagen I and II in articular cartilage. **(E)** Relative mRNA expression of collagen I and II in articular cartilage. #: $p < 0.05$ versus ACLC group; *: $p < 0.05$ versus ACLP group. $n = 12$ in each group. Data are expressed as mean ± SD.

blood supply (Nayak et al., 2020). The MVD of the ACLP group was significantly higher than that of the ACLC group (**Figures 4A,B**, $p < 0.05$). S-100 protein is a marker of proprioceptors in the ligaments. The expression of S-100 in the ACLP group was significantly higher than that in the ACLC group (**Figures 4C,D**, $p < 0.05$).

3.4 No Difference Exists in Preoperative Baseline Information

Group P contained 16 patients, and Group R had 19 patients. No significant differences were observed in the preoperative distributions of sex, age, affected knee, ASA grade, and comorbidities between the two patient groups (**Table 2**). It means that the these groups were at the same baseline before surgery and postoperative outcomes were comparable. We also created a visual representation of the data from **Table 2** (**Figure 5**).

3.5 ACL Primary Repair Substantially Decreased the Operation Time and Costs

Surgery-related data are presented in **Table 3**. There were no significant differences in the time from injury to operation, anaesthesia method, time to partial or total standing, postoperative length of stay, and complications. However,

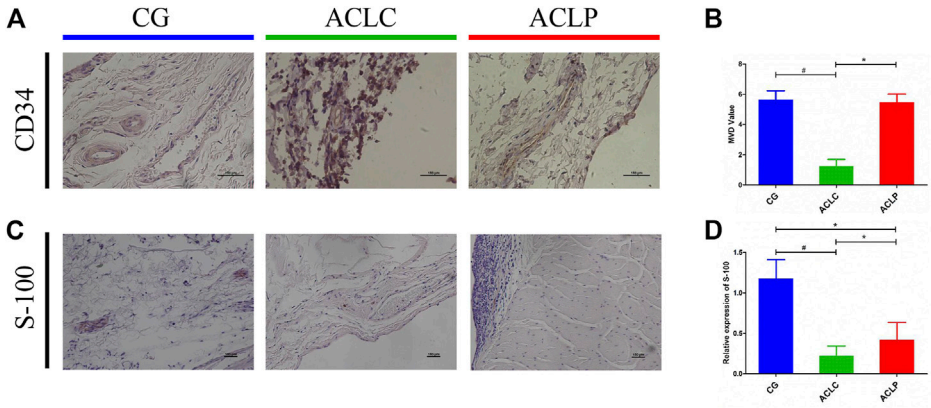

FIGURE 4 | (A) Immunohistochemistry of CD34. **(B)** MVD value of each group according to immunohistochemistry results of CD34. **(C)** Immunohistochemistry of S-100 protein. **(D)** Statistical analysis of S-100 protein. #: $p < 0.05$ versus ACLC group; *: $p < 0.05$ versus ACLP group. $n = 12$ in each group. Data are expressed as mean ± SD.

TABLE 2 | Baseline characteristics of patients.

Baseline characteristics		Group P (n = 16)	Group R (n = 19)	p value
Gender	Male	11 (68.75%)	11 (57.89%)	0.508
	Female	5 (31.25%)	8 (42.11%)	
Mean age at injury (years)		37.00 ± 9.66	39.53 ± 12.81	0.521
Laterality of injury	Left	8 (50.00%)	11 (57.89%)	0.640
	Right	8 (50.00%)	8 (42.11%)	
ASA grade	I	11	13	0.983
	II	5	6	
	III	0	0	
	IV	0	0	
Comorbidities	Cardiovascular system disease	3	4	0.865
	Respiratory system disease	1	1	0.900
	Urological system disease	1	0	0.269
	Thrombogenesis	1	1	0.900
	Metabolic disorder	1	1	0.900

ASA, american society of anaesthesiologists.

Group P had less operative time and costs than Group R ($p < 0.05$).

3.6 Group P Patients Have Similar Knee Function as Group R

The follow-up period for the 35 patients was 12 months. The preoperative and postoperative Lysholm and IKDC scores of the knee joints in the two groups are shown in **Table 4**. The postoperative Lysholm and IKDC scores increased significantly compared with the corresponding baseline preoperative scores in both groups ($p < 0.05$). There were no significant differences in the function of the knee joint preoperatively and at 3 and 12 months postoperatively between both groups (**Table 4**). The preoperative and postoperative distances of anterior tibial displacement assessed using Kneelax in both groups are shown in **Table 4**. There were no significant differences in the anterior tibial displacement between the groups at 3 and 12 months postoperatively, and adequate anterior and posterior stability was achieved (**Table 4**). **Figure 6** is a visual display of the data in **Table 4**.

3.7 Group P Obtained Similar Proprioception Scores as Group R

A comparison of proprioceptive assessments between the two groups is shown in **Table 5** and **Figure 7**. **Table 5** is for comparison between groups (Group P verus Group R). While **Figure 7** is a visual display of the same data for intra-group comparison (Affected side versus Healthy side). Group P obtained similar proprioception function as Group R at 3 and 12 months postoperatively, which was reflected by TDPM, JPR, ICP, FFCP, FFP, and FFPOP (**Table 5**). What stands out in the **Figure 7** is an significant increased JPR and TDPM preoperative value in Affected side of each group, compared to the Healthy side (JPR: **Figure 7A**; TDPM: **Figure 7B**, *$p < 0.05$). However, no

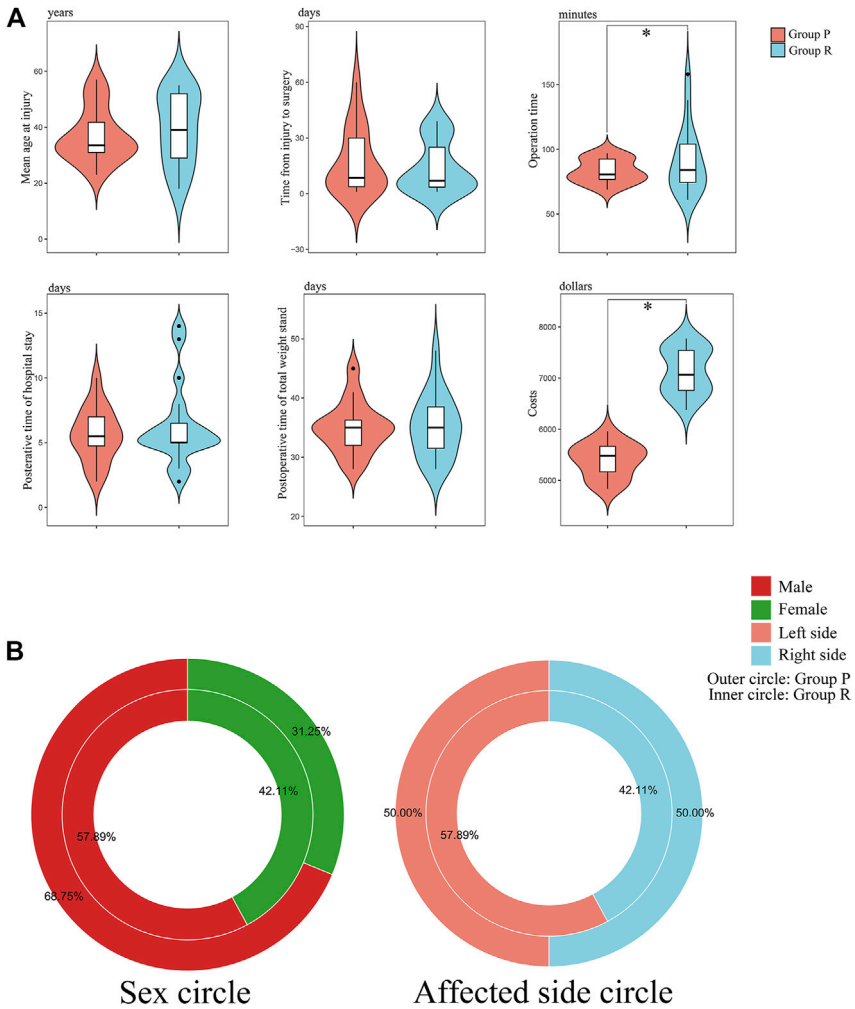

FIGURE 5 | Visual chart of baseline characteristics and surgical data of patients. **(A)** Violin plots of key data: age at injury; time from injury to surgery; operation time; postoperative time of hospital stay; postoperative time of total weight stand; and costs. *: $p < 0.05$ versus Group P. **(B)** Donut diagram of sex and affected side distribution.

TABLE 3 | Surgical data.

Parameters		Group P (n = 16)	Group R (n = 19)	p value
Time from injury to operation (days)		16.5 (9–35.75)	15 (9–35)	0.829
Method of anaesthesia	General anaesthesia	6	6	0.713
	CSEA	10	13	
Operation time (min)		73.8 (68.9–78.6)	85.2 (78.4–91.9)	0.007
Median time to partial standing (days)		2 (2–3)	2 (2–3)	>0.999
Median time to total standing (days)		34.94 ± 4.31	35.11 ± 5.28	0.920
Postoperative length of stay (days)		5.63 ± 2.09	6.26 ± 3.11	0.490
Postoperative complications		0	0	
Cost (thousand dollars)		5.39 ± 0.33	7.14 ± 0.45	<0.001

difference in JPR and TDPM value could be obsevered between Affected and Healthy side at postoperative 12 months. Further, **Figure 7C** illustrated no statistical difference existed in total time, ICP, FFCP, FFP, and FFPOP (Affected side versus Healthy side).

4 DISCUSSION

ACL primary repair is a surgical technique used to treat acute proximal ACL tears and is currently being refined. In this study,

TABLE 4 | Follow-up and function measurements.

Parameters		Group P (*n* = 16)	Group R (*n* = 19)	*p* value
Age at the latest follow-up (years)		34.5 (32–44.25)	40 (30–54)	0.446
Lysholm score	Preoperatively	44.87 ± 9.66	43.89 ± 8.05	0.745
	3 months postoperatively	75.38 ± 4.33	73.31 ± 3.71	0.139
	12 months postoperatively	91.06 ± 2.91	90.89 ± 2.94	0.867
IKDC score	Preoperatively	40.25 ± 9.90	39.47 ± 9.38	0.813
	3 months postoperatively	76.88 ± 5.24	75.05 ± 6.73	0.385
	12 months postoperatively	90.95 ± 2.62	90.99 ± 2.21	0.963
Kneelax value (mm)	Preoperatively	6.52 ± 1.09	7.00 ± 1.01	0.185
	3 months postoperatively	2.38 ± 0.49	2.45 ± 0.43	0.671
	12 months postoperatively	2.39 ± 0.47	2.48 ± 0.42	0.548

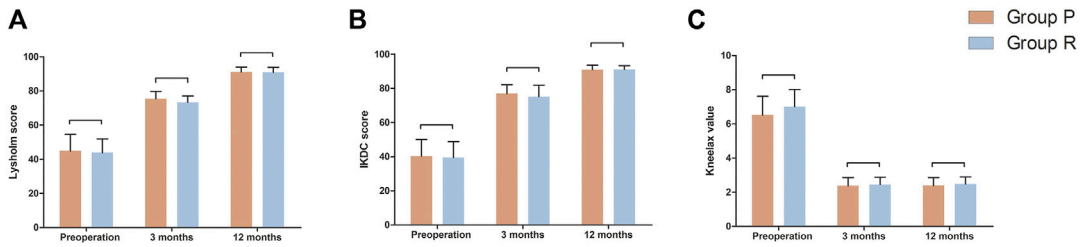

FIGURE 6 | Function measurements of affected knee joint in Group P and Group R. **(A)** Lysholm score. **(B)** IKDC score. **(C)** Kneelax value. Data are expressed as mean ± SD.

TABLE 5 | Distribution of proprioceptive parameters of the knee.

Parameters		Group P (*n* = 16)	Group R (*n* = 19)	*p* value
TDPM value of affected side	Preoperatively	2.79 ± 0.52	2.72 ± 0.46	0.701
	3 months postoperatively	2.01 ± 0.16	2.04 ± 0.51	0.769
	12 months postoperatively	1.39 ± 0.21	1.36 ± 0.19	0.652
TDPM value of healthy side	Preoperatively	1.34 ± 0.12	1.34 ± 0.11	0.920
	3 months postoperatively	1.31 ± 0.14	1.27 ± 0.09	0.330
	12 months postoperatively	1.30 ± 0.08	1.32 ± 0.10	0.488
JPR value of affected side	Preoperatively	5.18 ± 0.88	4.92 ± 0.74	0.359
	3 months postoperatively	3.67 ± 0.55	3.84 ± 0.81	0.467
	12 months postoperatively	2.46 ± 0.39	2.64 ± 0.34	0.155
JPR value of healthy side	Preoperatively	2.46 ± 0.22	2.42 ± 0.26	0.468
	3 months postoperatively	2.50 ± 0.21	2.47 ± 0.13	0.646
	12 months postoperatively	2.46 ± 0.30	2.42 ± 0.16	0.606
Total time (ms)	Affected side	707.56 ± 92.61	729.89 ± 75.48	0.437
	Healthy side	741.06 ± 84.18	759.42 ± 72.59	0.493
ICP	Affected side	36.56 ± 8.61	37.53 ± 7.95	0.733
	Healthy side	38.19 ± 7.39	39.32 ± 7.89	0.667
FFCP	Affected side	69.75 ± 23.32	73.84 ± 20.70	0.586
	Healthy side	72.88 ± 20.46	76.53 ± 19.44	0.592
FFP	Affected side	325.69 ± 76.85	343.42 ± 74.00	0.493
	Healthy side	344.75 ± 70.32	360.63 ± 70.12	0.510
FFPOP	Affected side	275.56 ± 45.02	275.58 ± 44.04	0.999
	Healthy side	285.25 ± 42.18	282.95 ± 42.53	0.874

we performed a series of basic experiments and a prospective clinical trial on ACL primary repair. The basic experiments revealed the advantage of primary repair in promoting healing in the tendon-bone transition area and ligament portion. The clinical trial suggested that primary repair could obtain a similar postoperative prognosis as ACL reconstruction in treating acute proximal ACL tears.

The ACL healing process starts with an inflammatory response, followed by cell and extracellular matrix proliferation in several weeks (Nyland et al., 2020). The

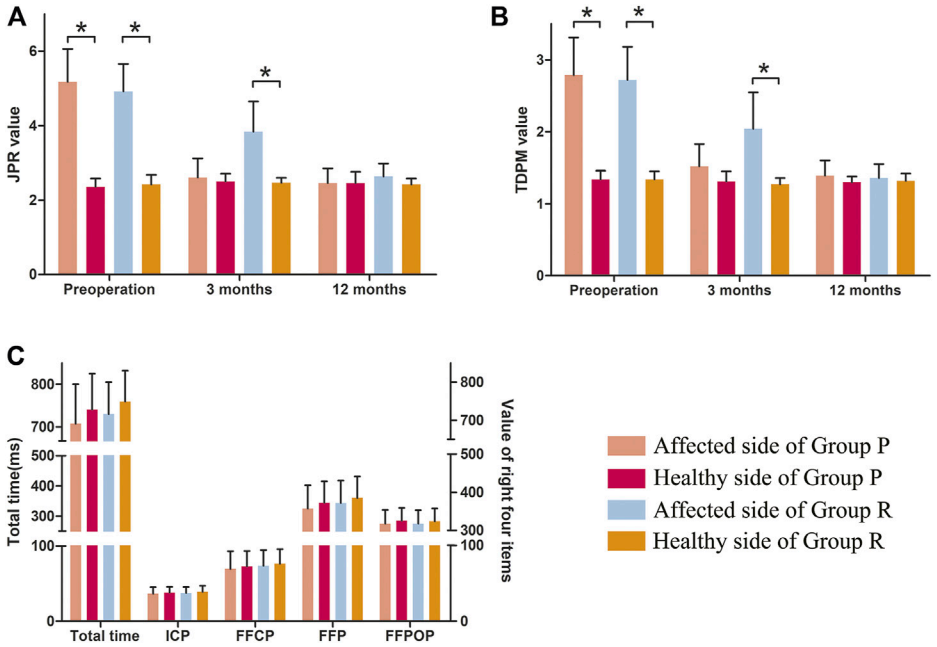

FIGURE 7 | Proprioception of the knee in Group P and Group R. **(A)** JPR value. **(B)** TDPM value. **(C)** Total time, ICP, FFCP, FFP, and FFPOP. *: $p < 0.05$ versus healthy side in each group. Data are expressed as mean ± SD.

healing response in the tendon-bone transition area and ligament portion directly influences the stability of the repaired ACL (Woodall et al., 2018). Therefore, remnant tissue preservation and microfracture are applied in ACL primary repair to provide a microenvironment for tissue cell proliferation (Ouanezar et al., 2018). Interestingly, our results illustrated that primary repair achieved a good degree of healing in the tendon-bone transition area and ligament portion in an animal model, which was the foundation of the therapeutic effects achieved in the clinical trial.

The microvessels provide sufficient blood supply for the generation of tissue cells, and proprioceptors regulate deep sensations and muscle strength of the knee joint, which are also histological indices of ACL healing evaluation (Takahashi et al., 2016). CD34 is the most sensitive marker of blood vessels in various organs (Jiang et al., 2021). In this study, cutting the ACL resulted in the disintegration and absorption of ACL remnants, thereby reducing the microvessels. However, typical vascular structures, including many red blood cells, were observed in the ACLP group. This shows that the primary repair effectively preserves the vascular structure in the stump and has a significant effect on tissue healing. S-100 is a proprioceptor marker protein in ligaments (Zhang et al., 2016). Immunohistochemical staining confirmed that neural structures were mainly present in the synovial tissue surrounding the ligament. This indicates that proprioceptive receptors in the ACL can be retained after the primary repair. Therefore, we evaluated the proprioceptive function of primary repair compared with that of reconstruction in the clinical trial. Primary repair achieved similar results as reconstruction in proprioceptive function tests, including TDPM, JPG, ICP, FFCP, FFP, and FFPOP. The results for the microvessels and proprioceptors support each other.

ACL ruptures are strongly associated with an increased risk of post-traumatic OA (Jungmann et al., 2016). On the one hand, the OA-like pathological change was detected. On the other hand, knee function tests were performed during the follow-up period of clinical trials, and a contrasting trend of OA-like pathological changes was observed between the ACLC and ACLP groups. The high Mankin scores and the increased collagen I and II levels in qPCR, Western blotting, and immunohistochemistry indicated that primary repair prevented OA characteristic occuring in the animal model. Furthermore, upward trends existed in the Lysholm score, IKDC score, and Kneelax value with increasing follow-up time. Therefore, ACL primary repair could restore knee stability.

Indications are worth considering before ACL primary repair. Our results show three key indications: the acute phase of history (no more than 2 months), proximal tears, and intact remnant tissue. If these indications are not met, they will eventually be reflected in the quality of the remnant, such as excessive absorption or insufficient tension to support primary repair (Haviv et al., 2019). Although primary repair has a narrow range of indications, it can still bring considerable benefits to target patients compared with ACL reconstruction. First, it achieved a similar prognosis in the follow-up period as ACL reconstruction. Second, primary repair has the advantages of a shorter operation time, operation-related trauma, and costs. Third, patients have an opportunity to undergo reconstruction surgery rather than more difficult revision surgery if primary repair failure occurs. These advantages of primary repair were reflected in the clinical trial of our study.

Our study has some limitations. First, the potential molecular mechanism of the healing response in the tendon-bone transition area and ligament portion was not investigated. Second, randomisation was not performed to respect patients' right to informed consent. Third, the exclusion criteria may have introduced selection bias in our results. Due to financial and technical constraints, we have not been able to achieve ACL reconstruction in an animal model. Future research can improve this defect to obtain more in-depth research conclusion. Furthermore, we will continue to follow up the selected patients and pay attention to the occurrence of long-term complications, such as graft fracture, occurrence of secondary injury, etc.

In conclusion, we investigated the role and prognosis of ACL primary repair in treating acute proximal ACL tears using histological studies and a clinical trial. ACL primary repair promoted the healing response in the tendon-bone transition area and ligament portion, with increased blood vessels and proprioceptors. The histological results served as the foundation of the clinical trial in our study. The trial revealed that ACL primary repair achieved similar levels of therapeutic performance as ACL reconstruction, including recovery of function, stability, and proprioception in the knee joint. Therefore, we believe that ACL primary repair could be a clinical alternative to the current reconstruction technique to treat acute proximal ACL tears.

DATA AVAILABILITY STATEMENT

The original contributions presented in the study are included in the article/**Supplementary Material**, further inquiries can be directed to the corresponding author.

ETHICS STATEMENT

The studies involving human participants were reviewed and approved by the Shengjing Hospital of China Medical University. The patients/participants provided their written informed consent to participate in this study. The animal study was reviewed and approved by the Shengjing Hospital of China Medical University. Written informed consent was obtained from the individual(s) for the publication of any potentially identifiable images or data included in this article.

AUTHOR CONTRIBUTIONS

YY: conceptualisation, methodology, data analysis, writing the original draft, review and editing, funding acquisition. ZJ: data analysis, writing original draft, review and editing. JL: data analysis, review and editing. DeZ: methodology of basic experiments, data analysis, review and editing. PS, DiZ, and DL: methodology of clinical trials, review and editing. LB: conceptualisation, methodology, data analysis, funding acquisition, resources, review, and editing.

FUNDING

This study was funded by the National Natural Science Foundation of China (82102613 and 82172479) and the Fundamental Research Project of Liaoning Provincial Department of Education (LJKQZ2021028).

ACKNOWLEDGMENTS

We would like to thank the Fourth Orthopaedics Department and the Emergency Medicine Department of Shengjing Hospital for their cooperation.

SUPPLEMENTARY MATERIAL

The Supplementary Material for this article can be found online at: https://www.frontiersin.org/articles/10.3389/fbioe.2022.913900/full#supplementary-material

Supplementary Figure S1 | The surgery procedures of primary repair performed on the rabbit.

Supplementary Figure S2 | Operative procedure of ACL primary repair. **(A)** The ruptured ACL must be acute and proximal, and the remnant must not have been absorbed to apply this technique. **(B)** The proximal end of the ACL was treated with a microfracture to provide adequate blood supply for primary repair. **(C)** AR-7200 was used to suture the ACL approximately 2 cm from the broken end. **(D)** A PushLock anchor was used to fix the ACL remnant at the attachment imprint.

Supplementary Figure S3 | Operative procedure for ACL reconstruction. **(A)** The ACL rupture must be an acute proximal ACL tear and the remnant must not have been absorbed to apply this technique. **(B)** After installing the tibial guide frame, the arthroscope was used to determine the inner port of the tibial tunnel at 7 mm from the anterior edge of the posterior cruciate ligament and 3 mm behind the midpoint of the ACL implantation point. **(C)** The femoral tunnel was created 1 mm from the posterior femoral cortex and 3 cm deep. **(D)** Another suture was placed at the proximal end of the remnant with a suture hook. **(E)** A PushLock anchor was used to fix the remnant of the ACL at the attachment imprint.

Supplementary Figure S4 | Preoperative and postoperative magnetic resonance and arthroscopic images.

Supplementary Figure S5 | (A) CPM machine. **(B–D)** Schematic diagram of the gait plantar pressure analysis system.

REFERENCES

Achtnich, A., Herbst, E., Forkel, P., Metzlaff, S., Sprenker, F., Imhoff, A. B., et al. (2016). Acute Proximal Anterior Cruciate Ligament Tears: Outcomes after Arthroscopic Suture Anchor Repair versus Anatomic Single-Bundle Reconstruction. *Arthroscopy* 32, 2562–2569. doi:10.1016/j.arthro.2016.04.031

Agha, R., Abdall-Razak, A., Crossley, E., Dowlut, N., Iosifidis, C., Mathew, G., et al. (2019). STROCSS 2019 Guideline: Strengthening the Reporting of Cohort Studies in Surgery. *Int. J. Surg.* 72, 156–165. doi:10.1016/j.ijsu.2019.11.002

Ahmad, S. S., Difelice, G. S., van der List, J. P., Ateschrang, A., and Hirschmann, M. T. (2019). Primary Repair of the Anterior Cruciate Ligament: Real Innovation or Reinvention of the Wheel? *Knee Surg. Sports Traumatol. Arthrosc.* 27, 1–2. doi:10.1007/s00167-018-5312-9

Chai, F., Wan, F., Jiang, J., and Chen, S. (2019). Micro-scale Assessment of the Postoperative Effect of Anterior Cruciate Ligament Reconstruction Preclinical Study Using a 7.1T Micro-magnetic Resonance Imaging. *Exp. Ther. Med.* 17, 214–220. doi:10.3892/etm.2018.6080

Dallo, I., Chahla, J., Mitchell, J. J., Pascual-Garrido, C., Feagin, J. A., and LaPrade, R. F. (2017). Biologic Approaches for the Treatment of Partial Tears of the Anterior Cruciate Ligament: A Current Concepts Review. *Orthop. J. Sports Med.* 5, 232596711668172. doi:10.1177/2325967116681724

Douoguih, W. A., Zade, R. T., Bodendorfer, B. M., Siddiqui, Y., and Lincoln, A. E. (2020). Anterior Cruciate Ligament Repair with Suture Augmentation for Proximal Avulsion Injuries. *Arthrosc. Sports Med. Rehabil.* 2, e475–e480. doi:10.1016/j.asmr.2020.05.003

Haviv, B., Kittani, M., Yaari, L., Rath, E., Heller, S., Shemesh, S., et al. (2019). The Detached Stump of the Torn Anterior Cruciate Ligament Adheres to the Femoral Notch Wall and Then to the Posterior Cruciate Ligament Within 6 Months From Injury. *Knee Surg. Sports Traumatol. Arthrosc.* 27, 2653–2658. doi:10.1007/s00167-018-5293-8

Heusdens, C. H. W., Hopper, G. P., Dossche, L., Roelant, E., and Mackay, G. M. (2019). Anterior Cruciate Ligament Repair with Independent Suture Tape Reinforcement: a Case Series with 2-year Follow-Up. *Knee Surg. Sports Traumatol. Arthrosc.* 27, 60–67. doi:10.1007/s00167-018-5239-1

Hh, M., Aa, T., M, S., and Ds, H. (2015). The Current Role of Stem Cells in Orthopaedic Surgery. *Malays Orthop J.* 9 (3), 1–7. doi:10.5704/MOJ.1511.016

Jiang, L., Chen, T., Sun, S., Wang, R., Deng, J., Lyu, L., et al. (2021). Nonbone Marrow CD34 + Cells Are Crucial for Endothelial Repair of Injured Artery. *Circ. Res.* 129, e146–e165. doi:10.1161/CIRCRESAHA.121.319494

Jungmann, P. M., Baum, T., Nevitt, M. C., Nardo, L., Gersing, A. S., Lane, N. E., et al. (2016). Degeneration in ACL Injured Knees with and without Reconstruction in Relation to Muscle Size and Fat Content-Data from the Osteoarthritis Initiative. *PLoS One* 11, e0166865. doi:10.1371/journal.pone.0166865

Kazusa, H., Nakamae, A., and Ochi, M. (2013). Augmentation Technique for Anterior Cruciate Ligament Injury. *Clin. Sports Med.* 32, 127–140. doi:10.1016/j.csm.2012.08.012

Kiapour, A. M., Fleming, B. C., and Murray, M. M. (2017). Structural and Anatomic Restoration of the Anterior Cruciate Ligament Is Associated with Less Cartilage Damage 1 Year after Surgery: Healing Ligament Properties Affect Cartilage Damage. *Orthop. J. Sports Med.* 5, 232596711772388. doi:10.1177/2325967117723886

Lee, D.-H., Lee, J.-H., Ahn, S.-E., and Park, M.-J. (2015). Effect of Time after Anterior Cruciate Ligament Tears on Proprioception and Postural Stability. *PLoS One* 10, e0139038. doi:10.1371/journal.pone.0139038

Lin, Z., Miao, J., Zhang, T., He, M., Wang, Z., Feng, X., et al. (2021). JUNB-FBXO21-ERK axis Promotes Cartilage Degeneration in Osteoarthritis by Inhibiting Autophagy. *Aging Cell* 20, e13306. doi:10.1111/acel.13306

Mouarbes, D., Menetrey, J., Marot, V., Courtot, L., Berard, E., and Cavaignac, E. (2019). Anterior Cruciate Ligament Reconstruction: A Systematic Review and Meta-Analysis of Outcomes for Quadriceps Tendon Autograft versus Bone-Patellar Tendon-Bone and Hamstring-Tendon Autografts. *Am. J. Sports Med.* 47, 3531–3540. doi:10.1177/0363546518825340

Muneta, T., Koga, H., Nakamura, T., Horie, M., Watanabe, T., and Sekiya, I. (2016). Behind-remnant Arthroscopic Observation and Scoring of Femoral Attachment of Injured Anterior Cruciate Ligament. *Knee Surg. Sports Traumatol. Arthrosc.* 24, 2906–2914. doi:10.1007/s00167-015-3574-z

Nayak, M., Nag, H. L., Nag, T. C., Digge, V., and Yadav, R. (2020). Ultrastructural and Histological Changes in Tibial Remnant of Ruptured Anterior Cruciate Ligament Stumps: a Transmission Electron Microscopy and Immunochemistry-Based Observational Study. *Musculoskelet. Surg.* 104, 67–74. doi:10.1007/s12306-019-00599-x

Nyland, J., Huffstutler, A., Faridi, J., Sachdeva, S., Nyland, M., and Caborn, D. (2020). Cruciate Ligament Healing and Injury Prevention in the Age of Regenerative Medicine and Technostress: Homeostasis Revisited. *Knee Surg. Sports Traumatol. Arthrosc.* 28, 777–789. doi:10.1007/s00167-019-05458-7

Ouanezar, H., Blakeney, W. G., Fernandes, L. R., Borade, A., Latrobe, C., Temponi, E. F., et al. (2018). Clinical Outcomes of Single Anteromedial Bundle Biologic Augmentation Technique for Anterior Cruciate Ligament Reconstruction with Consideration of Tibial Remnant Size. *Arthrosc. J. Arthrosc. Relat. Surg.* 34, 714–722. doi:10.1016/j.arthro.2017.08.309

Schneider, K. N., Schliemann, B., Gosheger, G., Theil, C., Weller, J., Buddhdev, P. K., et al. (2020). Good to Excellent Functional Short-Term Outcome and Low Revision Rates Following Primary Anterior Cruciate Ligament Repair Using Suture Augmentation. *J. Clin. Med.* 9, 3068. doi:10.3390/jcm9103068

Sherman, M. F., Lieber, L., Bonamo, J. R., Podesta, L., and Reiter, I. (1991). The Long-Term Followup of Primary Anterior Cruciate Ligament Repair. *Am. J. Sports Med.* 19, 243–255. doi:10.1177/036354659101900307

Takahashi, T., Kondo, E., Yasuda, K., Miyatake, S., Kawaguchi, Y., Onodera, J., et al. (2016). Effects of Remnant Tissue Preservation on the Tendon Graft in Anterior Cruciate Ligament Reconstruction. *Am. J. Sports Med.* 44, 1708–1716. doi:10.1177/0363546516643809

Tanabe, Y., Yasuda, K., Kondo, E., and Kitamura, N. (2016). Clinical Results of Anterior Cruciate Ligament Reconstruction with Ligament Remnant Tissue Preservation: A Systematic Review. *Asia Pac J. Sports Med. Arthrosc. Rehabil. Technol.* 4, 1–8. doi:10.1016/j.asmart.2016.04.001

van der List, J. P., and DiFelice, G. S. (2017). Primary Repair of the Anterior Cruciate Ligament: A Paradigm Shift. *Surg.* 15, 161–168. doi:10.1016/j.surge.2016.09.006

Woodall, B. M., Elena, N., Gamboa, J. T., Shin, E. C., Pathare, N., McGahan, P. J., et al. (2018). Anterior Cruciate Ligament Reconstruction with Amnion Biological Augmentation. *Arthrosc. Tech.* 7, e355–e360. doi:10.1016/j.eats.2017.10.002

Xu, Y., Zhang, W.-X., Wang, L.-N., Ming, Y.-Q., Li, Y.-L., and Ni, G.-X. (2021). Stem Cell Therapies in Tendon-Bone Healing. *World J. Stem Cells* 13 (7), 753–775. doi:10.4252/wjsc.v13.i7.753

Yang, J., Dong, Y., Wang, J., Chen, C., Zhu, Y., Wu, Y., et al. (2019). Hydroxypropylcellulose Coating to Improve Graft-To-Bone Healing for Anterior Cruciate Ligament Reconstruction. *ACS Biomater. Sci. Eng.* 5, 1793–1803. doi:10.1021/acsbiomaterials.8b01145

Zhang, L., Jiang, K., Chai, H., Zhou, M., and Bai, J. (2016). A Comparative Animal Study of Tendon Grafts Healing after Remnant-Preserving versus Conventional Anterior Cruciate Ligament Reconstruction. *Med. Sci. Monit.* 22, 3426–3437. doi:10.12659/msm.900265

Conflict of Interest: The authors declare that the research was conducted in the absence of any commercial or financial relationships that could be construed as a potential conflict of interest.

Publisher's Note: All claims expressed in this article are solely those of the authors and do not necessarily represent those of their affiliated organizations, or those of the publisher, the editors and the reviewers. Any product that may be evaluated in this article, or claim that may be made by its manufacturer, is not guaranteed or endorsed by the publisher.

frontiers | Frontiers in Bioengineering and Biotechnology

TYPE Original Research
PUBLISHED 02 September 2022
DOI 10.3389/fbioe.2022.960075

OPEN ACCESS

EDITED BY
Alideertu Dong,
Inner Mongolia University, China

REVIEWED BY
Hai-jun Wang,
Peking University Third Hospital, China
Yi Ding,
Capital Medical University, China
Yunfei Hou,
Peking University People's Hospital, China

*CORRESPONDENCE
Yongsheng Xu,
xys_sportsmedicine@126.com

SPECIALTY SECTION
This article was submitted to Biomaterials, a section of the journal Frontiers in Bioengineering and Biotechnology

RECEIVED 02 June 2022
ACCEPTED 05 August 2022
PUBLISHED 02 September 2022

CITATION
Ma B, Wang Y and Xu Y (2022), The efficacy and medium-term outcomes of ligament advanced reinforcement system compared with auto-grafts in anterior cruciate ligament reconstruction: At least 2 years follow-up.
Front. Bioeng. Biotechnol. 10:960075.
doi: 10.3389/fbioe.2022.960075

The efficacy and medium-term outcomes of ligament advanced reinforcement system compared with auto-grafts in anterior cruciate ligament reconstruction: At least 2years follow-up

Bingxian Ma, Yongxiang Wang and Yongsheng Xu*

Department of Orthopedics, Inner Mongolia People's Hospital, Hohhot, China

Background: Graft choice is an important step in the pre-operative plan of anterior cruciate ligament reconstruction (ACLR). The four-strand hamstring tendon (4SHT) is the most widely used auto-graft, while the Ligament Advanced Reinforcement System (LARS) is the newest typical biomaterial for ACLR. The physical activity level (PAL) before injury can affect the efficacy and outcomes of ACLR. This study aims to compare the efficacy and functional outcomes between ACLR using LARS and 4SHT in patients different PALs.

Methods: This was a prospective paired case-control study. ACL rupture patients included from 1 January 2017 to 31 December 2019 were subsequently divided into the high and plain PAL groups, according to their baseline PAL before injury. Clinical assessments included: Lachman test, pivot shift test, ligament laxity, Lysholm and International Knee Documentation Committee (IKDC) scores, and rate of returning to sports. The minimum follow-up was 2 years (y).

Results: A total of 58 patients had accomplished the 2 y follow-up (missing rate: 6.5%). In the high PAL group (n = 22), the positive rate of A–P laxity of the LARS subgroup was lower than the 4SHG subgroup (p = 0.138), while the Lysholm score (p = 0.002), IKDC score (p = 0.043), and rate of returning to sports (p = 0.010) of the LARS were higher than the 4SHG at 1 year follow-up; the positive rates of A–P laxity (p = 0.009) and pivot test (p = 0.027) were lower in the LARS than the 4SHG at 2 y follow-up. In the plain PAL group (n = 36), the positive rate of A–P laxity in the LARS subgroup was lower than the 4SHG at 1 year follow-up (p = 0.017); the positive rates of A–P laxity (p = 0.001), Lachman (p = 0.034), and pivot tests (p = 0.034) in the LARS were also lower than the 4SHG at 2 y follow-up, but the IKDC score (p = 0.038) and rate of returning to sports (p = 0.019) in the 4SHG were higher than the LARS.

Conclusion: In patients with high PAL, LARS can acquire better knee stability, sooner functional recovery, and returning to sports than 4SHG, while in patients

without high PAL, 4SHG acquires better functional outcomes and a higher rate of returning to sports.

KEYWORDS

anterior cruciate ligament reconstruction (ACLR), ligament advanced reinforcement system (LARS), artificial ligament, biomaterials, biomechanical property, knee stability

Introduction

Anterior cruciate ligament (ACL) injury is a very common disease in sports medicine, and it occurs both in athletes and common people. In order to restore knee function and sports ability, arthroscopic ACL reconstruction (ACLR) is performed in ACL rupture patients in most cases. ACLR always needs careful pre-operative planning, according to the differences in patients' background, including the career, baseline physical activity level (PAL), age, and returning to sports. The graft choice is a very important step of the operation strategy because the graft quality and characteristics are directly associated with the clinical efficacy and outcome of ACLR (Moghamis et al., 2019).

The present clinically used grafts for ACLR include auto-grafts, artificial grafts, and allogeneic tendon grafts, each one has its unique characteristics and advantages (Yang et al., 2020). Double-bundle four-strand hamstring tendon (4SHT) is the most commonly used auto-grafts for ACLR (Gifstad et al., 2013), and evidence have suggested that it can provide better anterior–posterior (A–P) stability and functional outcomes (Yang et al., 2020). Ligament Advanced Reinforcement System (LARS) is a typical scaffold-type biomaterial for ligament reconstruction, produced by the newest synthetic technique (Jia et al., 2017). The LARS ligament is manufactured by polyethylene terephthalate and consists of two different parts (Parchi et al., 2013): ① the intra-osseous part is made of longitudinal fibers, bound together by a transverse knitted structure; ② the intra-articular part comprises only longitudinal parallel fibers, which are pre-twisted at 90°. The stretching resistance force of LARS is much stronger than an intact ACL. It has been reported that LARS can accelerate the rehabilitation and fasten the early return to sports, attributed by the refined biomaterial quality (Krupa et al., 2016; Bugell et al., 2017).

Until now, there is still controversy about which kind of graft is the best choice for ACLR (Su et al., 2020). We consider that the patient's baseline physical activity may have impacts on the efficacy and outcomes of ACLR, consequently affecting the result of a graft choice. Although several clinical studies have compared the efficacy of ACLR using 4SHT with using LARS, few has focused on the differences in the patients' physical exercise background or career, lacking of systematic comparisons performed in the subgroups of different activity levels. We hypothesized that ACLR using 4SHT or LARS may have the different results of efficacy and functional outcomes in patients with different PALs.

Materials and methods

Patient involvement

Patients diagnosed with ACL rupture were included between 1 January 2017 and 31 December 2019, in our department. The inclusion criteria were: ① age: 20–50 years old, BMI≤31; ② acute ACL rupture less than 3 months; ③ single knee; ④ agree to participate in this study after signing the informed consent; ⑤ agree to the arrangement of the subgrouping (graft choice). The exclusion criteria were: ① multi-ligament injury; ② ACL re-rupture; ③ history of lower extremity fracture, ligament rupture, and operations; ④ knee osteoarthritis with the Kellgren–Lawrence grade>2, rheumatoid arthritis, and gouty arthritis; ⑤ nerve system diseases such as Parkinson's disease.

The protocols and procedures for the protection of human subjects reviewed and approved by the Ethics Committee of Inner Mongolia People's Hospital.

PAL levels and grouping

In order to evaluate patients' PAL before the injury (in the past 6 months), they were asked for their weekly physical exercise intensity and duration, and the International Physical Activity Questionnaire (IPAQ) was used to assess the PAL (Ethnic et al., 2009). IPAQ has been used for assessing the pre-operative PAL in the field of surgery (Angenete et al., 2016), it was developed as a common questionnaire to measure multiple domains of physical activity in all countries, including the leisure time, work, transportation, and house-hold tasks (Ethnic et al., 2009), which is particularly important in the developing and transitional countries because where assessment confined to leisure time activity may miss substantial daily physical activity undertaken for the purpose of work or travel (Bull et al., 2004). High PAL includes professional athletes, sports enthusiasts, and common people who meet either of the two criteria of high level from the International Physical Activity Questionnaire (IPAQ) (Ethnic et al., 2009): ① 40 min of vigorous-intensity activity such as jogging, lap swimming, and playing tennis >3 days/week; ② 60 min of moderate-intensity activity such as brisk walking, casual bicycling, and gardening >5 days a week.

This was a prospective paired cohort study. Patients with high PAL were equally divided into the 4HSG and LARS subgroups after matching their sex and age, and patients with plain PAL were also divided into the two subgroups after matching.

Arthroscopic ACLR with different grafts

Routine arthroscopy and anatomic ACLR were performed on all patients by the same senior surgeon, and any meniscal and/or cartilaginous injuries were treated before ACLR.

In the 4SHG subgroup, both the semitendinosus tendon and gracilis tendon were harvested and disconnected, folded into four strands, and sutured to each other. The tibial drill guide was adjusted to a sagittal angle of 55°, and the intra-articular guide tip was placed in the center of the ACL stump, which was preserved as much as possible. The femoral tunnel guide tip was located at the ACL femoral insertion site. The femoral tunnel diameter ranged from 7.5 to 8.0 mm, according to the diameter of the auto-graft. The femoral side was fixed with an Endobutton (Smith & Nephew, Memphis, TN, United States), and the tibial side was fixed with a bio-absorbable (poly-L-lactic acid) interference screw (Biosure HA; Smith & Nephew).

In the LARS (LARS; Surgical Implants and Devices, Arc-sur-Tille, France) subgroup, the intra-articular guiding of ACL tibial and femoral insertion site was the same, and the ACL stump was also preserved as much as possible. Diameters of the tibial and femoral bone tunnel were set at 7.5 or 8.0 mm, which matched with the chosen graft, respectively. If the patients' weight was over 80 kg, we chose the AC50DB (8.0 mm, 100- gauge fiber), otherwise the AC40DB (7.5 mm, 80-gauge fiber). LARS ligament was introduced into the joint from the tibial tunnel by a guidewire. The tension was adjusted by a full range of motion (ROM) of the knee, and no impingement was found. Both the tibial and femoral fixations were performed with the titanium interference-fit screws (Surgical Implants and Devices; LARS).

Rehabilitation

Both groups underwent the same rehabilitation scheme. The isometric contraction of the quadriceps was started as soon as possible after surgery. A lockable functional brace was used for a whole day in the first 2 weeks, and it was only used during walking for the next 2 weeks. A ROM of 90° could be achieved in the first week, and 120° in 8 weeks. For muscle strength, patients were requested to do the leg-raising exercises with the brace at least 200 times/day, during the first month after surgery. Full weight-bearing (walking without crutches) was allowed at least 1 month after surgery.

Follow-ups

The follow-up was started when ACLR was completed. The end was re-rupture/death/missing, whichever occurred first. The minimum follow-up was 1 year (y), and the maximum was 2 y. General clinical parameters included: the injury time before operation, meniscus tear (yes/no), diameter of the graft, follow-up time, and complications. The clinical assessments of the efficacy and functional outcomes of ACLR included: the physical examination, ligament laxity (KT-2000), and knee ROM, as well as the subjective scoring systems of knee function. Knee X-ray photographs were also performed at 1 and 2 y follow-ups to evaluate the internal fixation location of the reconstructed ACL.

All of the follow-up data were checked and entered into a database by two researchers, and a double-entry is carried out for the quality control.

Clinical assessments

Lachman test and pivot shift test are two physical examinations that can determine ACL rupture, which can be used to determine the stability recovery after ACLR (Yang et al., 2020). Lachman test was used to assess the A–P joint stability, and pivot shift test was used to assess the rotational stability (Cui et al., 2022). Lachman test was classified as: hard end-point (-), doubtable laxity (±), and soft end-point (+). Pivot shift was classified as (Bull et al., 2004): normal (-), glide (±), and clunk or gross (+).

Ligament laxity was measured by: the forward shift is tested when the knee is flexed at 30°. A–P laxity is evaluated by comparing to the healthy side, and it is classified as (Ranger et al., 2011): normal, grade 1 (difference between 1 and 5 mm), grade 2 (between 5 and 10 mm), and grade 3 (>10 mm).

The knee flexion contracture (KFC) angle was assessed by passive physical examination of ROM. KFC is defined as the gap value of extension loss compared to the normal side, and more than 5° was considered as KFC, according to the Knee Society Score (KSS) system (Insall et al., 1989; Yi et al., 2020). KFC degree is classified as normal (<5°), grade 1 (mild, KFC between 5° and 15°), grade 2 (moderate, between 15° and 30°), and grade 3 (severe, KFC >30°) (Insall et al., 1989; Yi et al., 2020).

Subjective assessments of knee function

To evaluate the functional outcomes of living quality and motor function, the Lysholm knee scoring scale (Wang et al., 2016) and International Knee Documentation Committee (IKDC) score (Fu and Chan, 2011) were accessed by self-questionnaires at follow-ups. The rate of returning to sports was used to evaluate the outcome of physical activity.

Clinical failure

At 2 y follow-up, cases who met any of the following results were regarded as clinical failure (Su et al., 2020): ① an overall IKDC score of C (60–70 score) or D (<60–70 score); ② Lachman

TABLE 1 Basic characteristics of the 4SHG and LARS subgroups in patients with different PALs.

Characteristics	High PAL (n = 22)			Plain PAL (n = 36)		
	4SHG	LARS	*p*-value	4SHG	LARS	*p*-value
Enrolled subjects (n)	11	11	--	18	18	--
Sex (male/female)	7/4	8/3	$\chi^2 = 0.210$ $p = 0.647$	11/7	9/9	$\chi^2 = 0.450$ $p = 0.502$
Age (year)	25.4 ± 7.2	25.8 ± 6.5	$t = -0.125$ $p = 0.902$	33.4 ± 8.9	33.5 ± 7.8	$t = -0.040$ $p = 0.968$
BMI	22.05 ± 1.16	22.83 ± 1.54	$t = -1.345$ $p = 0.194$	24.21 ± 1.86	24.00 ± 1.63	$t = 0.361$ $p = 0.720$
Time before ACLR (week)	3.7 ± 4.4	2.4 ± 3.4	$t = 0.812$ $p = 0.426$	3.6 ± 4.1	4.0 ± 4.7	$t = -0.282$ $p = 0.780$
Meniscus injury (with/without)	3/8	2/10	$\chi^2 = 0.259$ $p = 0.611$	5/13	5/13	--
Graft diameter (mm)	7.86 ± 0.23	7.82 ± 0.25	$t = 0.439$ $p = 0.666$	7.86 ± 0.23	7.86 ± 0.23	--

PAL (physical activity level), BMI (body mass index), ACLR (anterior cruciate ligament reconstruction).

test (+); ③ pivot shift test (+); ④ A–P laxity of grade 2 or 3; ⑤ KFC; and ⑥ re-rupture. The clinical failure rates were calculated.

Statistical analysis

Continuous data were expressed as mean ± SD, and comparisons of the continuous data were processed by the independent samples t-tests and Levene variance homogeneity tests between subgroups. Count data were expressed as number (n) and rate (/), and comparisons of the count data were processed by the Chi-square test or Fisher's exact test. The level of significance was set at 0.05. All of the statistical analyses were performed using SPSS 20.0 (SPSS Inc, 2009; Chicago, IL, United States).

Results

Basic characteristics

Finally, 58 patients had accomplished the 2 y follow-up. The high PAL group (n = 22) consisted of 11 professional athletes, six college students, two military soldiers, one manual worker, and two sports teachers/coaches. The plain PAL group (n = 36) consisted of 23 office workers, seven college students, three high school students, and three freelancers/housewives. The patients of the two groups were divided equally into the 4SHG and LARS subgroups after matching their sex and age. Most of the patients were injured by sports (n = 52): 35 subjects suffered a sprain of the knee when doing competitive sports, 17 sprained the knee by themselves when skiing or skating; four slipped and sprained the knee by themselves during farming, and two were caused by motor vehicle accident (n = 6). The basic characteristics, as well as baseline medical characteristics of the 4SHG and LARS subgroups, did not have significance in the two groups (Table 1).

Follow-ups

At the beginning of this study, there were 62 patients included in this study, and the initial sample size of the high PAL group and plain PAL group were 22 and 40, respectively. The patients of the two groups were divided equally into the 4SHG and LARS subgroups after matching their sex and age. One patient of the plain PAL group (4SHG subgroup) was missing at the 1 year follow-up, and another three patients of the plain PAL group (1 in 4SHG subgroup, two in LARS subgroup) were missing at the 2 y follow-up. The four missing patients cannot be contacted through phone call/e-mail or declaimed that he/she cannot participate anymore. The total missing rate was 6.5% (4/62). Those missing subjects were excluded from the database, in order to control the bias.

Comparisons of 4SHG and LARS in patients with high PAL

In the high PAL group, the positive rates of Lachman and pivot shift test, as well as KFC did not have significance between the 4SHG subgroup and LARS subgroup at 1 year follow-up. However, the positive rate of A–P shift in the 4SHG subgroup was higher than in the LARS subgroup, and the Lysholm score, IKDC score, as well as the rate of returning to sports in the 4SHG subgroup was lower than

TABLE 2 Comparisons of efficacy, safety, and functional outcomes between the 4SHG and LARS subgroups in high PAL patients.

Parameter		1 y follow-up (n = 22)			2 y follow-up (n = 22)		
		4SHG	LARS	*p*-value	4SHG	LARS	*p*-value
Lachman	-	11	11	--	8	11	$\chi^2 = 3.474$
	±	0	0		3	0	$p = 0.062$
	+	0	0		0	0	
Pivot shift	-	9	11	$\chi^2 = 2.200$	7	11	$\chi^2 = 4.899$
	±	2	0	$p = 0.138$	4	0	$p = 0.027^*$
	+	0	0		0	0	
A–P laxity	Normal	4	10	$\chi^2 = 7.071$	2	9	$\chi^2 = 9.455$
	Grade 1	7	1	$p = 0.008^{**}$	6	2	$p = 0.009^*$
	Grade 2	0	0		3	0	
	Grade 3	0	0		0	0	
KFC	Normal	11	11	--	11	11	--
	Grade 1	0	0		0	0	
	Grade 2	0	0		0	0	
	Grade 3	0	0		0	0	
Lysholm		76.00 ± 4.70	82.64 ± 4.12	$t = -3.513$	87.27 ± 5.18	89.27 ± 4.52	$t = -0.965$
				$p = 0.002^{**}$			$p = 0.346$
IKDC		74.18 ± 5.31	79.09 ± 5.36	$t = -2.159$	81.91 ± 5.11	83.45 ± 3.14	$t = -0.855$
				$p = 0.043^*$			$p = 0.403$
Failure rate	Yes	--	--	--	3	0	$\chi^2 = 3.474$
	No				8	11	$p = 0.062$
Returning to sports	Yes	3	9	$\chi^2 = 6.600$	11	11	--
	No	8	2	$p = 0.010^*$	0	0	

PAL (physical activity level), A–P (anterior–posterior), KFC (knee flexion contracture); Lachman test was classified as: hard end-point (-), doubtable laxity (±), soft end-point (+); pivot shift was classified as: normal (-), glide (±), clunk or gross (+); A–P laxity was performed by KT-2000, at 30° flexion and classified as: normal, grade 1 (1–5 mm), grade 2 (5–10 mm), and grade 3 (>10 mm); KFC is classified as normal (<5°), grade 1 (5°–15°), grade 2 (15°–30°), and grade 3 (KFC >30°).

*, $p < 0.05$.

**, $p < 0.01$.

the LARS subgroup at 1 year follow-up (Table 2). At 2 y follow-up, the positive rates of Lachman and KFC still did not have significance between the subgroups, but the positive rates of pivot shift and A–P shift in the 4SHG subgroup were higher than those in the LARS subgroup; however, the Lysholm score, IKDC score, and rate of returning to sports did not show a significant difference between the two subgroups (Table 2). At 2 y follow-up, only three clinical failure cases with the A–P laxity of grade 2 were found in the 4SHG subgroup; however, the failure rate did not show a significant difference between subgroups (Table 2).

Comparisons of 4SHG and LARS in patients with plain PAL

At 1 year follow-up, the positive rates of Lachman test, pivot shift and KFC, and the Lysholm and IKDC scores, as well as the rate of returning to sports did not have significance between the 4SHG subgroup and LARS subgroup in patients without high PAL (Table 3). The positive rate of A–P shift in the 4SHG subgroup was lower than that in the LARS subgroup at 1 year follow-up (Table 3). At 2 y follow-up, the positive rates of Lachman, pivot shift, and A–P shift in the 4SHG subgroup were higher than those in the LARS subgroup; however, the rate of returning to sports and IKDC score in the LARS subgroup were lower than that in the 4SHG subgroup (Table 3). The KFC rate and Lysholm score did not have a significant difference between the two subgroups at 2 y follow-up (Table 3). At 2 y follow-up, there were four clinical failure cases with the A–P laxity of grade 2 in the 4SHG subgroup, and one clinical failure case with KFC in the LARS subgroup, and the failure rate did not show a significant difference between subgroups (Table 3).

Discussion

Recently, 4SHT and LARS have become the most commonly used auto-graft and biomaterial artificial graft

TABLE 3 Comparisons of efficacy, safety, and functional outcomes between the 4SHG and LARS subgroups in plain PAL patients.

Parameter		1 y follow-up (n = 36)			2 y follow-up (n = 36)		
		4SHG	LARS	*p*-value	4SHG	LARS	*p*-value
Lachman	-	17	18	χ^2 = 1.029	14	18	χ^2 = 4.500
	±	1	0	*p* = 0.310	4	0	*p* = 0.034*
	+	0	0		0	0	
Pivot shift	-	16	18	χ^2 = 2.118	14	18	χ^2 = 4.500
	±	2	0	*p* = 0.146	4	0	*p* = 0.034*
	+	0	0		0	0	
A–P shift	Normal	8	16	χ^2 = 8.121	4	15	χ^2 = 14.138
	Grade 1	9	2	*p* = 0.017*	10	3	*p* = 0.001*
	Grade 2	1	0		4	0	
	Grade 3	0	0		0	0	
KFC	Normal	18	16	χ^2 = 2.118	18	17	χ^2 = 1.029
	Grade 1	0	2	*p* = 0.146	0	1	*p* = 0.310
	Grade 2	0	0		0	0	
	Grade 3	0	0		0	0	
Lysholm		76.33 ± 4.58	77.39 ± 4.79	*t* = -0.676	85.56 ± 4.15	82.72 ± 4.44	*t* = 1.978
				p = 0.504			*p* = 0.056
IKDC		75.67 ± 3.65	78.22 ± 3.62	*t* = -1.842	86.56 ± 3.94	84.00 ± 3.09	*t* = 2.165
				p = 0.074			*p* = 0.038*
Failure rate	Yes	--	--	--	4	1	χ^2 = 2.090
	No				14	17	*p* = 0.148
Returning to sport	Yes	2	4	χ^2 = 0.800	12	5	χ^2 = 5.461
	No	16	14	*p* = 0.371	6	13	*p* = 0.019*

PAL (physical activity level), A–P (anterior–posterior), KFC (knee flexion contracture); Lachman test was classified as: hard end-point (-), doubtable laxity (±), soft end-point (+); pivot shift was classified as: normal (-), glide (±), clunk or gross (+); A–P laxity was performed by KT-2000, at 30° flexion and classified as: normal, grade 1 (1–5 mm), grade 2 (5–10 mm), and grade 3 (>10 mm); KFC is classified as normal (<5°), grade 1 (5°–15°), grade 2 (15°–30°), and grade 3 (KFC >30°).
*, $p < 0.05$.

for ACLR (Gifstad et al., 2013; Yang et al., 2020) (Liu et al., 2010; Su et al., 2020), respectively. Because of their different origins, 4SHT and LARS have unique characteristics and advantages (Yang et al., 2020), which was why we considered that 4SHT and LARS may have different application populations. ACL often occurs in athletes, or in common people who are doing improper exercise or fitness. The patient's baseline PAL in pre-injury is one of the most powerful factors affecting the efficacy and outcomes of ACLR. It has been well known that athletes/sports enthusiasts who had high PAL can obtain distinct results of efficacy and outcomes, compared to the common people without high PAL. In this article, we systematically compared the ACLR using 4SHT with using LARS in two different patients with or without high PAL. The results showed that the efficacy and functional outcomes of 4SHT and LARS were not consistent in patients with different PALs, which verified the previous hypothesis.

LARS resulted in better efficacy and outcomes in high PAL patients

In high PAL patients, ACLR with LARS can obtain better knee stability, sooner functional recovery and returning to sports than the 4SHG subgroup. The results found that the A–P stability of LARS was higher than that of 4SHG at 1 year follow-up, and the A–P stability and rotation stability were found at 2 y follow-up. LARS is a newly developed artificial ligament, unlike the earlier synthetic ligaments, it consists of two distinct segments (Parchi et al., 2013): ① the intra-osseous part, which is made of longitudinal fibers, bound together by a transverse knitted structure; ② the intra-articular part, which comprises only longitudinal parallel fibers (free fibers), pre-twisted at 90°. The architecture of LARS allows it to mimic the natural ACL and produce sufficient joint stability in short-term. Three reasons may contribute to the superior joint stability of LARS, which was found at the short-term follow-up (1 year). First, LARS is much

stronger than the natural ACL or 4SHG auto-graft due to its biomechanical properties, the ultimate tensile strength of 7.5 and 8.0 mm LARS is 3,600 and 4,600 N, respectively (Bourlos et al., 2016). Second, the orientation of intra-articular free fibers helps to reduce the shearing forces. Literally, LARS can produce sufficient joint stability immediately after ACLR, correcting the dislocation as soon as possible (Ye et al., 2013). Third, LARS also works as a scaffold, which induced the fibroblastic ingrowth between the fibers (Yuanliang et al., 2020). Hence, the ACL stumps were preserved as much as we can to encourage the fibro-vascular ingrowth. *In vivo* study found that the fibroblastic ingrowth begins immediately after ACLR, which can form a sheath wrapping the intra-articular segment at 1 month post-operatively, afterward the re-growth of LARS was found at 6 months post-operatively, which presented as a completely covered ligament with regenerated collagen, synovial tissue, and vascular network, similar to the normal ACL (Yu et al., 2014). Hence, the re-growth time of LARS is shorter than that of the 4SHG auto-graft, and the latter usually costs 1 year for the vascular formation. Moreover, the ingrowth of soft tissue between the LARS fibers acts as a viscoelastic element, protecting the reconstructed ligament against the friction in bone tunnel (Vaquette et al., 2013). Those aforementioned mechanisms can explain the phenomenon of why a better joint stability can be found in the LARS subgroup at 1 year post-operatively.

The results also showed that the Lysholm score, IKDC score, and the rate of returning to sports in the LARS subgroup were higher than the 4SHG at 1 year follow-up; however, those parameters were comparable between two subgroups at 2 y follow-up. It indicated that although LARS and 4SHG resulted in similar functional outcomes eventually, ACLR using LARS can obtain a sooner recovery of knee function and returning to sports than 4SHG. It has been reported that LARS may acquire earlier symptom relief and function restoration than hamstring auto-grafts (Chen et al., 2017), and Newman et al. (2013) pointed out that the medium-term outcomes of LARS and auto-graft were comparable. The sooner recovery of LARS can be attributed by its superior efficacy of knee stability in the short-term post-operatively. As ACL is the first stabilizer of knee, ACLR using LARS results in better functional recovery in short-term. It has been reported that LARS can accelerate the rehabilitation and fasten the early return to sports, which is attributed by the refined biomaterial quality (Krupa et al., 2016; Bugell et al., 2017). Hence, LARS is very suitable for patients with high PAL, such as athletes and sports enthusiasts, who required a sooner recovery and returning to sports. LARS ligaments have been approved by CFDA since 2004 and been used for ACL reconstruction over 30,000 cases in China (Chen et al., 2019). Due to the early return to sports and impressive clinical effects, LARS has gradually become the most widely accepted biomaterial for athlete patients in China (Krupa et al., 2016; Bugell et al., 2017).

4SHG resulted in better functional outcomes in common patients

The results in the plain PAL patients were not consistent with the high PAL patients. The present results found that the 4SHG subgroup resulted in a higher IKDC score, as well as a higher rate of returning to sports at 2 y follow-up, comparing to the LARS. It indicated that ACLR using 4SHG could be more suitable than the LARS for common people. 4SHG consists of the auto semitendinosus tendon and gracilis tendon, and this double-bundle four-strand auto-graft can reconstruct the anteromedial and posterolateral bundle of ACL, respectively (Eck et al., 2010; Jon, 2011). Thus, 4SHG can restore the anatomical structure of natural ACL as much as possible, with fewer complications (Xie et al., 2015). LARS may not be suitable for common people. A long-term follow-up study has reported that the unsatisfied patients were over 40% after ACLR with LARS, and 27.8% of patients sustained a re-rupture, with an averaged IKDC of 76.60 ± 18.18 (Tiefenböck et al., 2015). A meta-analysis of long-term (>2 years) follow-ups also showed that the rank of Lysholm score and IKDC score in 4SHG were higher than artificial grafts including LARS, and the authors concluded that 4SHG may be a better choice for the patients who underwent ACLR (Yang et al., 2020); however, this meta-analysis did not perform the comparisons in different populations, many included study did not present the baseline PAL data, only several studies declaimed that they had included the athletes/recreational players.

In the present study, the only complication was KFC, and other complications such as infection, fever, re-rupture, or hemarthrosis were not found during follow-ups. In the LARS subgroup of plain PAL patients, two KFC cases were found at 1 y follow-up, and one case's KFC symptom still existed at 2 y follow-up. We considered the reversible KFC case may be caused by synovitis, and the other case may be caused by a foreign body reaction. It has been reported that ACL can cause a rare foreign body reaction with granuloma (Henry et al., 2018), which blocks knee flexion by passive physical examination, causing the KFC.

Our results found that although the LARS subgroup had a higher joint stability than the 4SHG, the former resulted in a lower IKDC score and a lower rate of returning to sports at the medium-term follow-up, eventually. However, this inconsistency between knee stability and function did not happen in the high PAL patients. The differences in the patients' baseline PAL and proprioceptive sensation may be one of the main reasons. It has been known that the proprioceptive sensation and static postural control are impaired after the injury and operation (Relph and Herrington, 2016; Kim et al., 2017) because the loss of mechanical receptors can decrease the neuromuscular control of knee stability. Patients with high PAL, such as athletes/sports enthusiasts, are prone to have a highly developed neuromuscular system and proprioceptive sensation system, which contributes to the sooner functional recovery and returning to sports after ACLR with LARS. On the contrary, in patients without high PAL, the neuromuscular system and proprioceptive sensation are

very weak to adapt to the artificial ligament (LARS) during the post-operative recovery period, which leads to worse functional outcomes. It has been concluded that the non-suitable patients' selection was one of the main failure reasons of LARS in ACLR (Chen et al., 2019). The present results suggest that the pre-injury PAL may be an indicator for the patients' selection for ACLR using LARS.

Limitations

Our study still has several limitations. First, the sample size of each subgroup was small. Literally, more potential affecting factors like lifestyle, job, and family commitments also needed to be matched. However, the sample size of this prospective study was no sufficient to do those matching, and we can only choose to match the main factors (sex and age) in order to control the bias. Second, the follow-up has lasted 2 y, which only presents the medium-term outcomes. Third, the present study cannot avoid the recall bias generated from self-reported IPAQ of pre-injury. Furthermore, multi-center longitudinal studies with more samples and long-term follow-ups are required to compare and determine the long-term functional outcomes of LARS and auto-grafts in patients with different PALs.

Conclusion

The efficacy and functional outcomes of ACLR using LARS and 4SHG were not consistent in patients with different pre-injury PALs. In patients with high PAL, LARS can obtain better knee stability, sooner functional recovery and returning to sports than 4SHG, while in patients without high PAL, 4SHG acquires better functional outcomes and higher rate of returning to sports.

Data availability statement

The original contributions presented in the study are included in the article/Supplementary Material; further inquiries can be directed to the corresponding author.

Ethics statement

The studies involving human participants were reviewed and approved by the Ethics Committee of Inner Mongolia People's Hospital. The patients/participants provided their written informed consent to participate in this study.

Author contributions

BM wrote the manuscript. YW participated in critical revision of the manuscript for intellectual content and sorted out and screened the relevant literatures. YX designed the outline and revised the manuscript. All authors have read and approved the final version of this manuscript.

Funding

This study was supported by the National Natural Science Foundation of China (grant numbers: 81560374, 82172444), the Science and Technology Plan Project of Inner Mongolia (grant numbers: 201802154, 2021GG0127), the Natural Science Foundation of Inner Mongolia (grant number: 2017MS08136), and the Hospital Fund Project of Inner Mongolia People's Hospital (grant number: 2020YN24).

Acknowledgments

The authors would like to thank Liyuan Tao (Ph.D., Associate Professor) from the Research Center of Clinical Epidemiology in Peking University Third Hospital for the statistics support.

Conflict of interest

The authors declare that the research was conducted in the absence of any commercial or financial relationships that could be construed as a potential conflict of interest.

Publisher's note

References

Angenete, E., Angera˚s, S. U., Börjesson, M., Ekelund, J., Gellerstedt, M., Thorsteinsdottir, T., et al. (2016). Physical activity before radical prostatectomy reduces sick leave after surgery - results froma prospective, non-randomized controlled clinical trial (LAPPRO). *BMC Urol.* 16 (1), 50. doi:10.1186/s12894-016-0168-0

Bourlos, D. N., Mastrokalos, D. S., Chronopoulos, E., and Babis, G. C. (2016). LARS artificial ligament versus ABC purely polyester ligament for anterior cruciate ligament reconstruction. *Orthop. J. Sports Med.* 4 (6), 232596711665335. doi:10.1177/2325967116653359(2016-6-15)

Bugell, G., Dell'Osso, G., and Ascione, F. (2018). LARS in ACL reconstruction: Evaluation of 60 cases with 5-year minimum follow-up. *Musculoskeletal Surgery* 102 (1), 57–62. doi:10.1007/s12306-017-0499-3

Bull, F., Armstrong, T., and Dixon, T. (2004). Comparative quantification of health risks global and regional burden of disease attributable to selected major risk factors. Physical inactivity. Geneva: World Health Organization, 729–881.

Chen, S., Chen, T., and Wan, F. (2019). The experience of ACL reconstruction with synthetics ligament: Where are we now? *Orthop. J. Sports Med.* 7 (11), 2325967119S0045. doi:10.1177/2325967119s00455

Chen, T., Zhang, P., Chen, J., Hua, Y., and Chen, S. (2017). Long-term outcomes of anterior cruciate ligament reconstruction using either synthetics with remnant preservation or hamstring autografts: A 10-year longitudinal study. *Am. J. Sports Med.* 45, 2739–2750. doi:10.1177/0363546517721692

Cui, S., Yi, H., Zhu, X., Fan, J., Ding, Y., and Liu, W. (2022). The efficacy and outcome of a two-staged operation for irreducible knee dislocation: A prospective short-term follow-up. *Front. Bioeng. Biotechnol.* 10, 861788. doi:10.3389/fbioe.2022.861788

Eck, C., Lesniak, B. P., Schreiber, V. M., and Fu, F. H. (2010). Anatomic single- and double-bundle anterior cruciate ligament reconstruction flowchart. *Arthrosc. J. Arthrosc. Relat. Surg.* 26 (2), 258–268. doi:10.1016/j.arthro.2009.07.027

Ethnic, C., Dutch, B., and Singh, A. S. (2009). *International journal of behavioral nutrition and physical activity BioMed central correction*. Switzerland: Springer.

Fu, S. N., and Chan, Y. H. (2011). Translation and validation of Chinese version of international knee documentation committee subjective knee form. *Disabil. Rehabil.* 33 (13-14), 1186–1189. doi:10.3109/09638288.2010.524274

Gifstad, T., Sole, A., Strand, T., Uppheim, G., Grontvedt, T., and Drogset, J. O. (2013). Long-term follow-up of patellar tendon grafts or hamstring tendon grafts in endoscopic ACL reconstructions. *Knee Surg. Sports Traumatol. Arthrosc.* 21 (3), 576–583. doi:10.1007/s00167-012-1947-0

Henry, J., Konarski, A. J., Joseph, L., and Pillai, A. (2018). Foreign body reaction with granuloma following Achilles tendon reconstruction with the LARS ligament. *J. Surg. Case Rep.* 2018 (1), rjx258. doi:10.1093/jscr/rjx258

Insall, J., Dorr, L. D., Scott, R. D., and Norman, W. (1989). Rationale of the Knee Society clinical rating system. *Clin. Orthop. Relat. Res.* 11 (248), 13–14. doi:10.1097/00003086-198911000-00004

Jia, Z., Xue, C., Wang, W., Liu, T., Huang, X., and Xu, W. (2017). Clinical outcomes of anterior cruciate ligament reconstruction using LARS artificial graft with an at least 7-year follow-up. *Medicine* 96 (14), e6568. doi:10.1097/md.0000000000006568

Jon, K. (2011). James. Anatomic single- and double-bundle anterior cruciate ligament reconstruction, Part 2. *Am. J. Sports Med.* 39 (9), 1789.

Kim, H. J., Lee, J. H., and Lee, D. H. (2017). Proprioception in patients with anterior cruciate ligament tears: A meta-analysis comparing injured and uninjured limbs. *Am. J. Sports Med.* 45 (12), 2916–2922. doi:10.1177/0363546516682231

Krupa, S., Królikowska, A., and Reichert, P. (2016). Postoperative knee joint stability following anterior cruciate ligament reconstruction using the ligament advanced reinforcement system. *Polim. Med.* 46 (2), 155–161. doi:10.17219/pim/68646

Liu, Z. T., Zhang, X. L., Jiang, Y., and Zeng, B. F. (2010). Four-strand hamstring tendon autograft versus LARS artificial ligament for anterior cruciate ligament reconstruction. *Int. Orthop.* 34 (1), 45–49. doi:10.1007/s00264-009-0768-3

Moghamis, I., Abuodeh, Y., Darwiche, A., Ibrahim, T., Al Ateeq Al Dosari, M., and Ahmed, G. (2019). Anthropometric correlation with hamstring graft size in anterior cruciate ligament reconstruction among males. *Int. Orthop.* 44 (3), 577–584. doi:10.1007/s00264-019-04452-5

Newman, S., Atkinson, H., and Willis-Owen, C. A. (2013). Anterior cruciate ligament reconstruction with the ligament augmentation and reconstruction system: A systematic review. *Int. Orthop.* 37 (2), 321–326. doi:10.1007/s00264-012-1654-y

Parchi, P. D., Gianluca, C., Dolfi, L., Baluganti, A., Nicola, P., Chiellini, F., et al. (2013). Anterior cruciate ligament reconstruction with LARS artificial ligament results at a mean follow-up of eightyears. *Int. Orthop.* 37 (8), 1567–1574. doi:10.1007/s00264-013-1917-2

Ranger, P., Renaud, A., Phan, P., Dahan, P., De Oliveira, E., and Delisle, J. (2011). Evaluation of reconstructive surgery using artificial ligaments in 71 acute knee dislocations. *Int. Orthop.* 35 (10), 1477–1482. doi:10.1007/s00264-010-1154-x

Relph, N., and Herrington, L. (2016). The effect of conservatively treated acl injury on knee joint position sense. *Int. J. Sports Phys. Ther.* 11 (4), 536–543.

Su, M., Jia, X., Zhang, Z., Jin, Z., Li, Y., Dong, Q., et al. (2020). Medium-term (least 5 Years) comparative outcomes in anterior cruciate ligament reconstruction using 4SHG, allograft, and LARS ligament. *Clin. J. Sport Med.* 1, e101–e110. publish ahead of print. doi:10.1097/jsm.0000000000000730

Tiefenböck, T. M., Thurmaier, E., Schmid, H., Tiefenbock, M., Winnisch, M., Jostl, J., et al. (2015). Clinical and functional outcome after anterior cruciate ligament reconstruction with the LARS™ system with a minimum follow-up of 10 years. *Sports Orthop. Traumatology Sport-Orthopadie - Sport-Traumatologie* 31 (2), 169. doi:10.1016/j.orthtr.2015.03.024

Vaquette, C., Viateau, V., Guérard, S., Anagnostou, F., Manassero, M., Castner, D. G., et al. (2013). The effect of polystyrene sodium sulfonate grafting on polyethylene terephthalate artificial ligaments on *in vitro* mineralisation and *in vivo* bone tissue integration. *Biomaterials* 34 (29), 7048–7063. doi:10.1016/j.biomaterials.2013.05.058

Wang, W., Liu, L., Chang, X., Jia, Z. Y., Zhao, J. Z., and Xu, W. D. (2016). Cross-cultural translation of the Lysholm knee score in Chinese and its validation in patients with anterior cruciate ligament injury. *BMC Musculoskelet. Disord.* 17 (1), 436. doi:10.1186/s12891-016-1283-5

Xie, X., Liu, X., Chen, Z., Yu, Y., Peng, S., and Li, Q. (2015). A meta-analysis of bone–patellar tendon–bone autograft versus four-strand hamstring tendon autograft for anterior cruciate ligament reconstruction. *Knee* 22 (2), 100–110. doi:10.1016/j.knee.2014.11.014

Yang, W., Huang, X., and Wang, S. (2020). The long-term outcome of different grafts in anterior cruciate ligament reconstruction: A network meta-analysis of randomised controlled trials. *J. Orthop. Transl.* 26, 16–30. doi:10.1016/j.jot.2020.03.008

Ye, J. X., Shen, G. S., Zhou, H. B., Xu, W., Xie, Z. G., Dong, Q. R., et al. (2013). Arthroscopic reconstruction of the anterior cruciate ligament with the LARS artificial ligament: Thirty-six to fifty-two months follow-up study. *Eur. Rev. Med. Pharmacol. Sci.* 17 (11), 1438–1446.

Yi, D., Baoge, L., Hui, Q., Yin, L., He, W., Si, F., et al. (2020). Can knee flexion contracture affect cervical alignment and neck tension? A prospective self-controlled pilot study. *Spine J.* 20 (2), 251–260. doi:10.1016/j.spinee.2019.09.008

Yu, S. B., Yang, R. H., Zuo, Z. N., and Dong, Q. R. (2014). Histological characteristics and ultrastructure of polyethylene terephthalate LARS ligament after the reconstruction of anterior cruciate ligament in rabbits. *Int. J. Clin. Exp. Med.* 7 (9), 2511–2518.

Yuanliang, D., Haifeng, D., Zhihui, W., Wu, D., Shi, C., Xiao, T., et al. (2020). A case report of traumatic osteoarthritis associated with LARS artificial ligament use in anterior cruciate ligament reconstruction. *BMC Musculoskelet. Disord.* 21 (1), 745. doi:10.1186/s12891-020-03764-7

frontiers | Frontiers in Bioengineering and Biotechnology

TYPE Review
PUBLISHED 30 September 2022
DOI 10.3389/fbioe.2022.1016598

OPEN ACCESS

EDITED BY
Yansong Qi,
Inner Mongolia People's Hospital, China

REVIEWED BY
Qichang Mei,
Ningbo University, China
Long Cui,
Chinese Academy of Sciences (CAS), China
Liyuan Tao,
Peking University Third Hospital, China

*CORRESPONDENCE
Fuchun Sun,
fcsun@mail.tsinghua.edu.cn

SPECIALTY SECTION
This article was submitted to Biomaterials, a section of the journal Frontiers in Bioengineering and Biotechnology

RECEIVED 11 August 2022
ACCEPTED 14 September 2022
PUBLISHED 30 September 2022

CITATION
Guo N, Tian J, Wang L, Sun K, Mi L, Ming H, Zhe Z and Sun F (2022), Discussion on the possibility of multi-layer intelligent technologies to achieve the best recover of musculoskeletal injuries: Smart materials, variable structures, and intelligent therapeutic planning.
Front. Bioeng. Biotechnol. 10:1016598.
doi: 10.3389/fbioe.2022.1016598

Discussion on the possibility of multi-layer intelligent technologies to achieve the best recover of musculoskeletal injuries: Smart materials, variable structures, and intelligent therapeutic planning

Na Guo[1,2], Jiawen Tian[1,2], Litao Wang[3], Kai Sun[4], Lixin Mi[5], Hao Ming[6], Zhao Zhe[4] and Fuchun Sun[1,2]*

[1]Department of Computer Science and Technology, Tsinghua University, Beijing, China, [2]Institute of Precision Medicine, Tsinghua University, Beijing, China, [3]College of Engineering, China Agricultural University, Beijing, China, [4]Department of Biomedical Engineering, Tsinghua University, Beijing, China, [5]Musculoskeletal Department, Beijing Rehabilitation Hospital, Beijing, China, [6]Orthopaedics, Chinese PLA General Hospital, Beijing, China

Although intelligent technologies has facilitated the development of precise orthopaedic, simple internal fixation, ligament reconstruction or arthroplasty can only relieve pain of patients in short-term. To achieve the best recover of musculoskeletal injuries, three bottlenecks must be broken through, which includes scientific path planning, bioactive implants and personalized surgical channels building. As scientific surgical path can be planned and built by through AI technology, 4D printing technology can make more bioactive implants be manufactured, and variable structures can establish personalized channels precisely, it is possible to achieve satisfied and effective musculoskeletal injury recovery with the progress of multi-layer intelligent technologies (MLIT).

KEYWORDS

smart materials, variable structures, intelligent therapeutic planning, best recover of musculoskeletal, multi-layer intelligent technologies

1 Introduction

In the past 30 years, intelligent technologies has facilitated the development of precise orthopaedic, an important direction in orthopedics/sports medicine, in the following three areas (Figure 1):

1) Digital orthopedics technologies have promoted the appreciation of digital anatomy (Pei and Yan, 2014) and biomechanics (Bhandarkar and Dhatrak, 2022). The three-dimensional models of bones reconstructed by digital orthopedics technologies, provide a means to establish the spatial relationship between anatomical structures. Shape statistical analysis allows that Elaborate anatomical analysis of bone can be performed. F. Chen Chen et al. (2018a) proposed a method to automatically identify three subtypes of femur cavities by k-means clustering analysis algorithm, on the basis of measuring the angle between the coronal plane and the radius of the femoral curvature (RFC) plane digitally. This method can provide a possible solution for the scientific design of Intramedullary (IM) nails, which will potentially facilitate IM nail implantation and reduce complications. Ghezlbash al. Ghezelbash et al. (2020) reviews the relevant findings of *in vitro* and finite element model studies on load-sharing in healthy, aged, degenerate and damaged human lumbar motion segments. They believed finite element model studies could improve understandings of functional biomechanics of human lumbar spine in normal and perturbed conditions.
2) 3D printing is an innovative technology for personalized treatment. Y. Liu et al. Liu et al. (2020) have prepared 3D printed polycaprolactone-hydroxyapatite (PCL-HA) porous scaffolds with loaded heparan sulfate (HS). This PCL-HA-HS scaffolds can accelerate the repairing of biological bone defects with sound compression resistance and good biocompatibility, which may be an effective biomaterial for bone defect repair. The study of B. Liu et al. Liu et al. (2021) showed that 3D printing technology can realize prosthesis stabilization and new bone regeneration in treating bone defects of limbs, to make patients achieve satisfactory limb function recovery. For total knee arthroplasty surgery, 3D printing navigation templates could predict prosthesis size accurately and provide an effective and precise guidance of osteotomy (Ding et al., 2017). 3D printing technology allowed

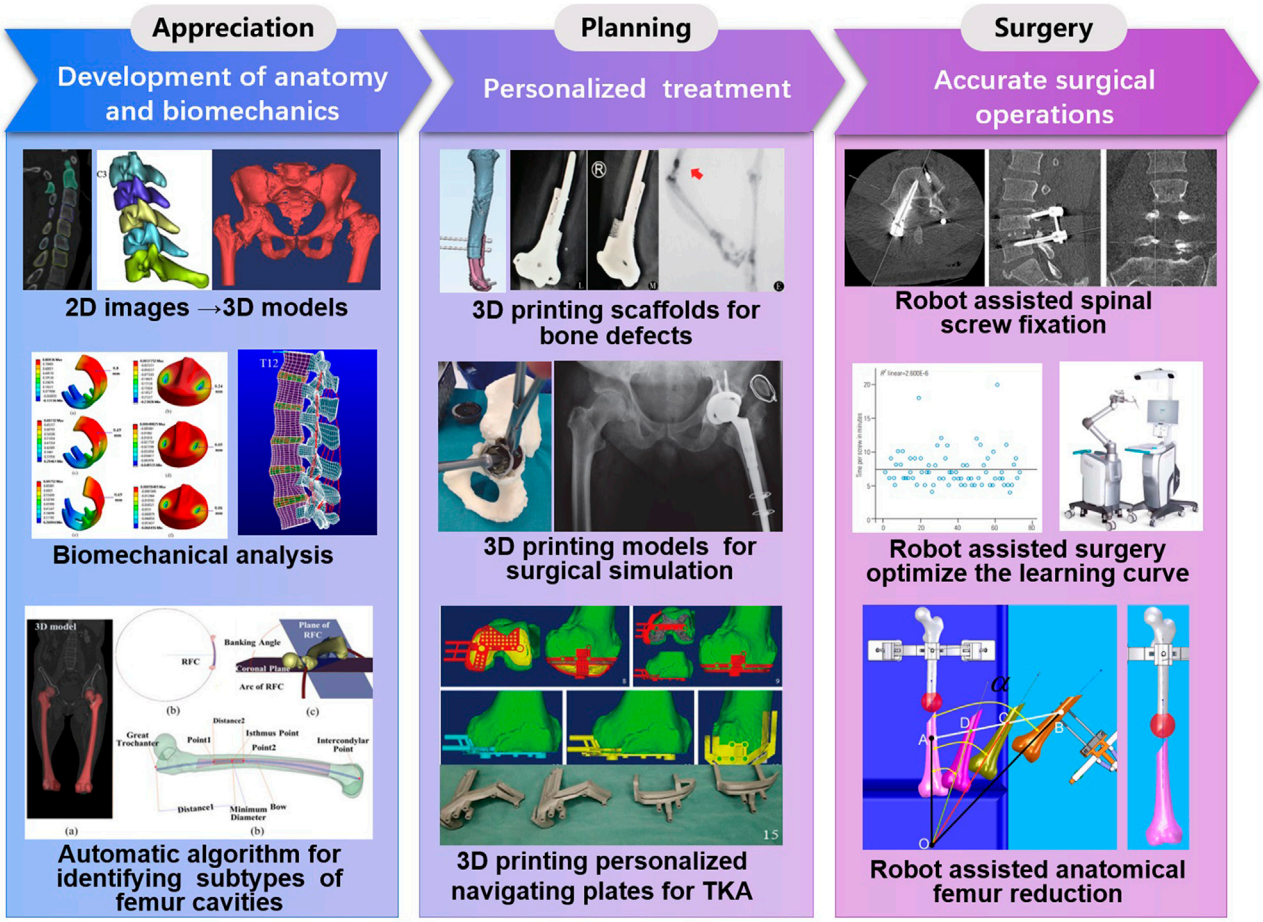

FIGURE 1
Intelligent technologies for precise orthopaedic.

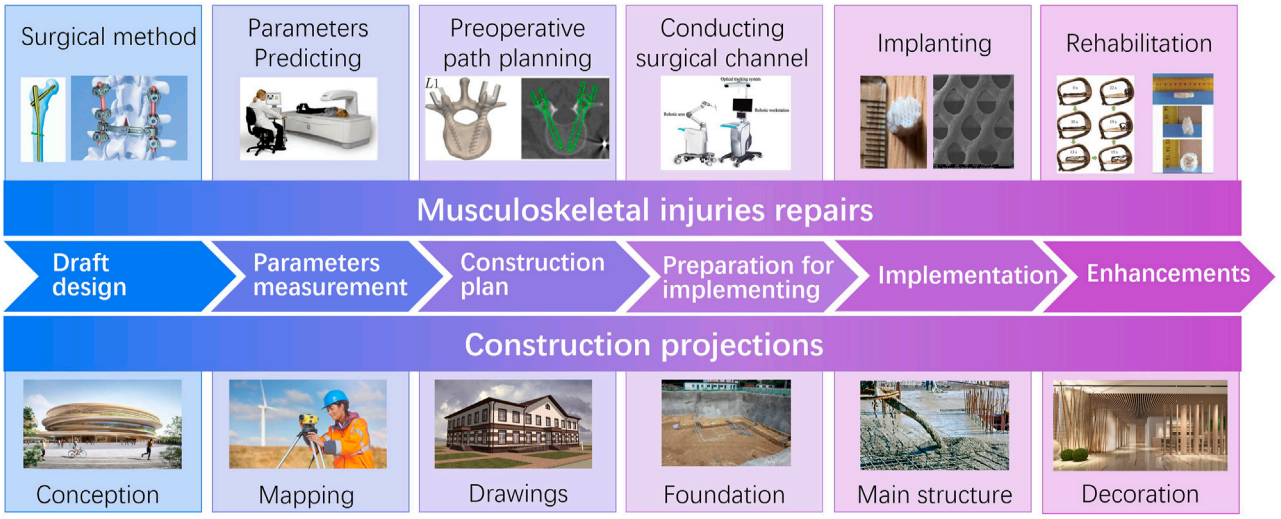

FIGURE 2
Comparison between construction projections and musculoskeletal injury repairs.

TABLE 1 Comparison between construction projections and musculoskeletal injury repairs.

Stage		Construction projections	Musculoskeletal injuries repairs
Scheme design	Draft design	Conception: Draw draft on basis of user requirements	Surgical plan: Select surgical method according to the patient's condition, such as screw fixation, vertebroplasty, etc.
	Parameters measurement	Geographical mapping: Conduct field location-survey to get engineering mapping, including geotechnical, hydrology, etc.	Physical parameters prediction: Predict physical parameters of anatomical tissues, including bone mineral density, bone size, anatomical angle, etc.
	Construction plan	Construction drawings: Develop detailed construction plan according to the drafts and the mapping, including processes, materials, tools, etc.	Pre-operation path planning: Calculate surgical path on basis of predicted physical parameters and 3D reconstruction models, such as the position of the screw, the osteotomy plane, etc.
Scheme implementation	Preparation for implementing	Foundation building: Lay the foundation of the new building	Surgical channel establishment: Establish surgical channels with the use of a surgical robot
	Implementation	Construction of the main structure: Conducting the main structure on basis of construction plan, like reinforced concrete structures, etc.	Surgical procedure: Implant bone tissue engineering scaffolds
Enhancements		Decoration: Decorated the building according to the functional needs of users	Rehabilitation: Achieve satisfied recovery by staged stimulus action

accurate surgical simulation using life-size models, to valuate complex pelvic deformities precisely. This technology can improve anatomical appreciation and make personalized preoperative planning (Hughes et al., 2017), leading to reduce the risk of neurovascular injury.

3) Accurate surgical operations are carried out by robotics. In the past 5 years, the number of publications on orthopedic robotics has increased from 2500 to 6500 (Bernardo and Edoardo, 2021). Robot-assisted orthopedics surgeries can not only improve the accuracy of the operations (Jamwal et al., 2021), reduce operation time, radiation dose, and complications (Ye and Chen, 2009), but also optimize the learning curve (Nicolas et al., 2016; Kam et al., 2019; Tian et al., 2019).

However, simple internal fixation, ligament reconstruction or arthroplasty can only relieve pain of patients in short-term, because of the complexity of the musculoskeletal system (Neumann, 2010). The following problems limit the long-term therapeutic efficacy of precise orthopaedic:

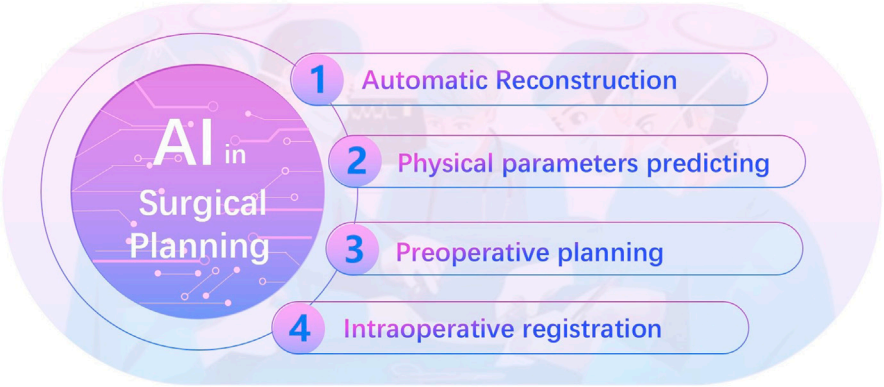

FIGURE 3
AI in surgical planning.

1) Current surgical planning paths are the optimal geometric paths, but not the optimal bio-mechanical paths, which may not result in the optimal functional recovery of patients. The osseous tissue is not a uniform organization, which is mainly made up of two types of structural tissues, namely cancellous (trabecular) and cortical bone (Wubneh et al., 2018). The geometric center and the density center of the femoral head are different. Moreover, the density of different parts varies each other (Ahrend et al., 2021). Johns Hopkins University's Vijayan R. Vijayan et al. (2019) reported an algorithm for automatic spinal pedicle screw planning using Active Shape Model (ASM) registration. But the manual path drawn by doctor is different with the automatic path calculated by the ASM algorithm. The fact that the clinical experiences, like predictions of bone mineral densities of different parts, may be considered into the manual preoperative planning by surgeons can result in the differences.
2) The fact that traditional bone grafts and bone substitute materials cannot provide signals for endogenous repair (Loebel and Burdick, 2018), can cause failure to induce bone formation or promote angiogenesis. Therefore, traditional orthopedics treatments may provide unsatisfied musculoskeletal rehabilitations. Bone grafts with shape memory effect, stimuli responsiveness, can maximize the new bones forming and the neovascularization, which are of great significance for improving the recovery of patients.

As shown in Figure 2, similarly to the construction process of a building, MLIT for musculoskeletal injuries consists of three stages: scheme design, scheme implementation, and enhancements (Table 1).

Therefore, the multi-layer intelligent technologies (MLIT), including smart materials, variable structures, and intelligent therapeutic planning, which are on basis of the musculoskeletal biomechanical characteristics and the rehabilitation model of stimulus implants, will be the main trend of precise orthopaedic. Specifically, three bottlenecks must be broken through to achieve satisfied recovery: scientific path should be planned and built by AI algorithms, bioactive implants should be manufactured with smart materials, and personalized channels should be established by variable structures. This article will discuss the feasibility of satisfied and effective musculoskeletal injury recovery in the following aspects:

1) Scientific surgical path can be planned and built by through AI technology
2) Responsive bioactive implants made through 3D printing technology can provide signals for endogenous repair
3) Personalized surgical channels can be established through intelligent robotics precisely

2 Status of multi-layer intelligent technologies

2.1 Scientific surgical path can be planned and built by through AI technology

Surgical placement and appropriate implant fixation had equal importance as the inherent implant characteristics in maintaining long-term implant stability (Li et al., 2019). Biomechanical surgical path must be planned on basis of the pathogenesis of musculoskeletal diseases, to reach the satisfied musculoskeletal injury recovery. This requires physical parameters to be predicted precisely, to establish build kinesiology models of musculoskeletal system. In the past decade, AI technologies has made dramatic advances on

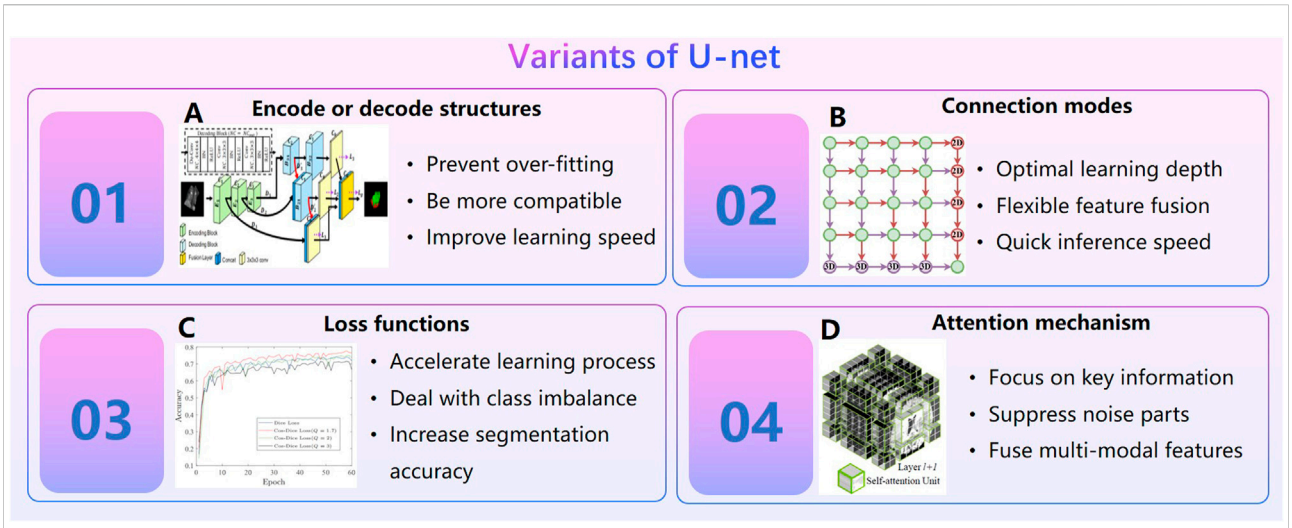

FIGURE 4
Variants of U-net. **(A)**. Cascade decoder: A Universal Decoding Method for Biomedical Image Segmentation (Liang et al., 2019). **(B)**. MNet: Rethinking 2D/3D Networks for Anisotropic Medical Image Segmentation (Dong et al., 2022). **(C)**. A Novel Focal Tversky loss function with improved Attention U-Net for lesion segmentation (Abraham and Khan, 2018). **(D)**. Swin UNETR: Swin Transformers for Semantic Segmentation of Brain Tumors in MRI Images.

Orthopaedic in the following four aspects (Zhou et al., 2020a; Lopez et al., 2021a) (Figure 3): automatic reconstruction, physical parameters predicting, preoperative planning and intraoperative images registration.

2.1.1 Automatic reconstruction algorithm

In the early study, threshold segmentation or seed growth combined with manual repair are often used to segment medical images like CT, MRI etc. This semi-automatic method is very inefficient. AI technology, especially the U-net (Li et al., 2017; Falk et al., 2019), has promoted the rapid development of medical image segmentation. In general, variants of the U-net can be divided into four categories (Figure 4): ① Design encoder or decode structures. Cascade decoder conducted more effective decoding of hierarchically encoded features (Liang et al., 2019). The encoder of TernausNet removed the fully connected layers and replace them with a single convolutional layer of 512 channels that serves as a bottleneck central part of the network, and the decoder of TernausNet transposed convolutions layers that doubles thesize of a feature map (Iglovikov and Shvets, 2018). TernausNet was helpful to prevent over-fitting. ②Optimize connection modes of encoding module and decoding module. MNet proposed a skip connection method to balance the spatial representation inter axes *via* learning (Dong et al., 2022); UNet++ redesigned skip connections to exploit multiscale features in image segmentation (Zhou et al., 2020b).③ Set new loss function. Loss function is a method to measure the quality of model prediction, which is of course important to an AI model. Dice loss is a common loss function for medical image segmentation. However, it may cause oscillation during training when the prediction is close to ground truth (Chen et al., 2018b). Cos-Dice loss function was used in W-net to make the network more stable (Chen et al., 2018b). The adjustable penalty weights of the misclassified voxels were used in dice coefficient to adapt to unbalanced class frequency (Huang et al., 2018). Loss functions based on the Tversky index (Salehi et al., 2017; Abraham and Khan, 2018; Huang et al., 2018; Das and Zhang, 2020)were used to address the issue of data imbalance. ④Import attention mechanism. Swin Unet was a semantic segmentation of brain tumors in MRI Images using a swin transformer encoder which can extract features at five different resolutions by utilizing shifted windows for computing self-attention (Hatamizadeh et al., 2021). RA-UNet proposed a 3D hybrid residual attention-aware segmentation method to precisely extract the liver volume of interests (VOI) and segment tumors from the liver VOI (Jin et al., 2018). TransUNet was a variant of U-net using a transformer encodes which tokenized image patches from a convolution neural network (CNN) feature map as the input sequence for extracting global contexts (Chen et al., 2021). UNEt TRansformers (UNETR) utilized a transformer as the encoder to learn sequence representations of the input volume and effectively capture the global multi-scale information (Hatamizadeh et al., 2022). Particularly in 2021, the nn-Unet proposed by Isensee F. et al. Isensee et al. (2021) at Heidelberg University in Germany surpasses most existing approaches on 23 public datasets used in international biomedical segmentation competitions. Variants of the U-net or other deep learning algorithms are widely used in segmentations for pelvic, spine, femur, knee arthroscopy and other orthopedics fields (Zeng et al.,

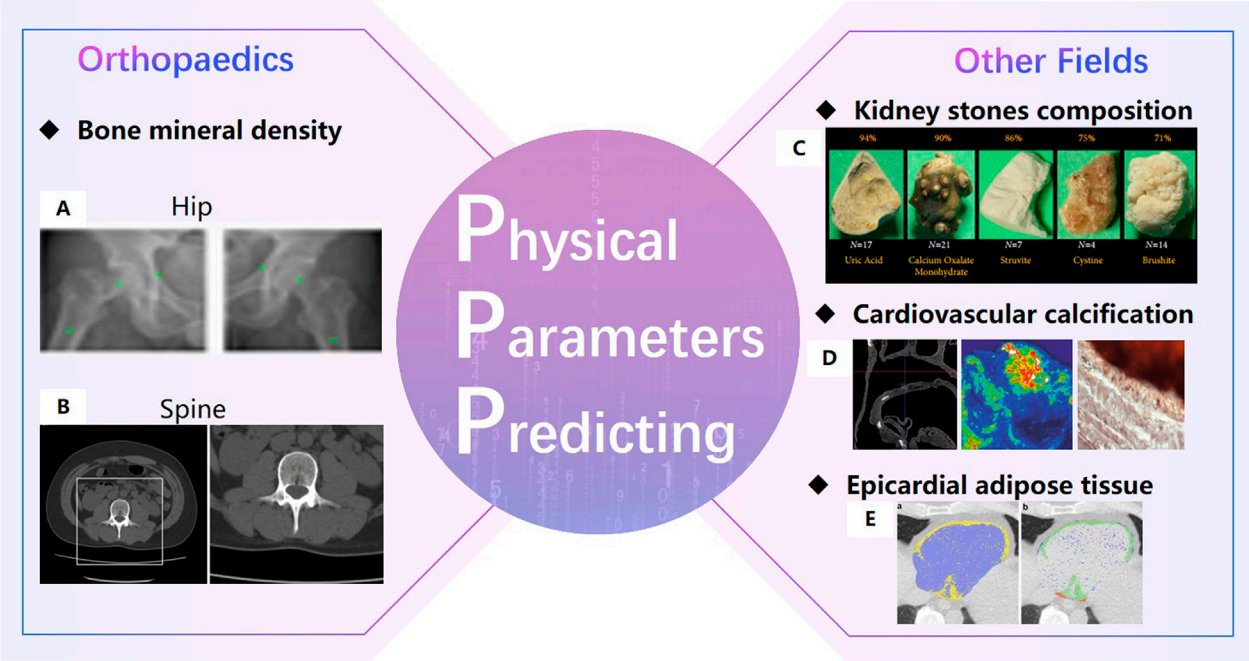

FIGURE 5
Physical Parameters Predicting (Hsieh et al., 2021). **(A)**. Bone mineral density prediction of hip (Yasaka et al., 2020). **(B)**. Bone mineral density prediction of lumbar spine. **(C)** automatically detect kidney stones composition (Black et al., 2020). **(D)**. cardiovascular calcification (Dhivya et al., 2015).**(E)**. Epicardial adipose tissue prediction (Molnar et al., 2021).

2017; Balagopal et al., 2018; Kolařík et al., 2019; Isensee et al., 2021).

2.1.2 Physical parameters predicting method

Extraordinarily important is that AI technology perform well in predicting physical parameters of organizations. In 2019, a review by Rogers M.A. Rogers and Aikawa (2019) of Harvard University in the United States showed that AI technology can analyze the cardiovascular calcification on quantitatively large data sets. In 2020, Black K.M. et al. Black et al. (2020) of the University of Michigan automatically detected kidney stones composition from digital photographs of stones by ResNet-10, and precisions for each stone type were above 75%. In 2021, the study of Lopez F. et al. Lopez et al. (2021b) showed that the DCCN approach is the best method with a precision of 98% for four kidney stones classification with *in-vivo* endoscopic images. In 2021, Molnar D. Molnar et al. (2021) et al. of Gothenburg in Sweden proposed a Crop-Net for fat prediction, with a precision of 99.4%.

In the field of orthopedics, AI technology can predict bone density accurately (Figure 5). Hsieh C.I. from Chang Gung Hospital in Taiwan (Hsieh et al., 2021) proposed the Dual-energy X-ray A bsorptiometry (DXA)to predict bone mineral density and fracture risk, and the accuracy of hip osteoporosis prediction reached 95%. In 2020, the BMDCNN is applied to predict the bone mineral density (BMD) of the lumbar spine by Yasaka K. Yasaka et al. (2020) from the University of Tokyo, and the internal and external AUC of osteoporosis AUC 0.965 and 0.970.

2.1.3 Preoperative planning

Preoperative planning is an essential part of Clinical Decision Support System(CDSS). Screw placement position (Cai et al., 2019), implants size (Dong et al., 2021; Polce et al., 2021), osteotomy morphology are three common preoperative planning needs in Orthopaedic surgery (Figure 6). Target reconstructions, landmark/anatomical components recognization (Cai et al., 2019; Siemionow et al., 2021), physical parameters (bone mineral density (Caprara et al., 2021), morphological parameters (Soodmand et al., 2019)), finite element analysis (Zheng et al., 2018a; Caprara, 2021), personal information and other risk constraints may be possible inputs for preoperative planning. AI technologies can play a role in the processing of planning inputs. AI applications in bone reconstructions and physical parameters predictions have been discussed in Section 2.1.1 and 2.1.2. It is well-attended to predict how bone adapts to different loads in surgical planning (Jordi et al., 2022). FE is commonly performed in biomechanics analysis. It is necessary to build statistical shape models (SSM) based on a set of landmark

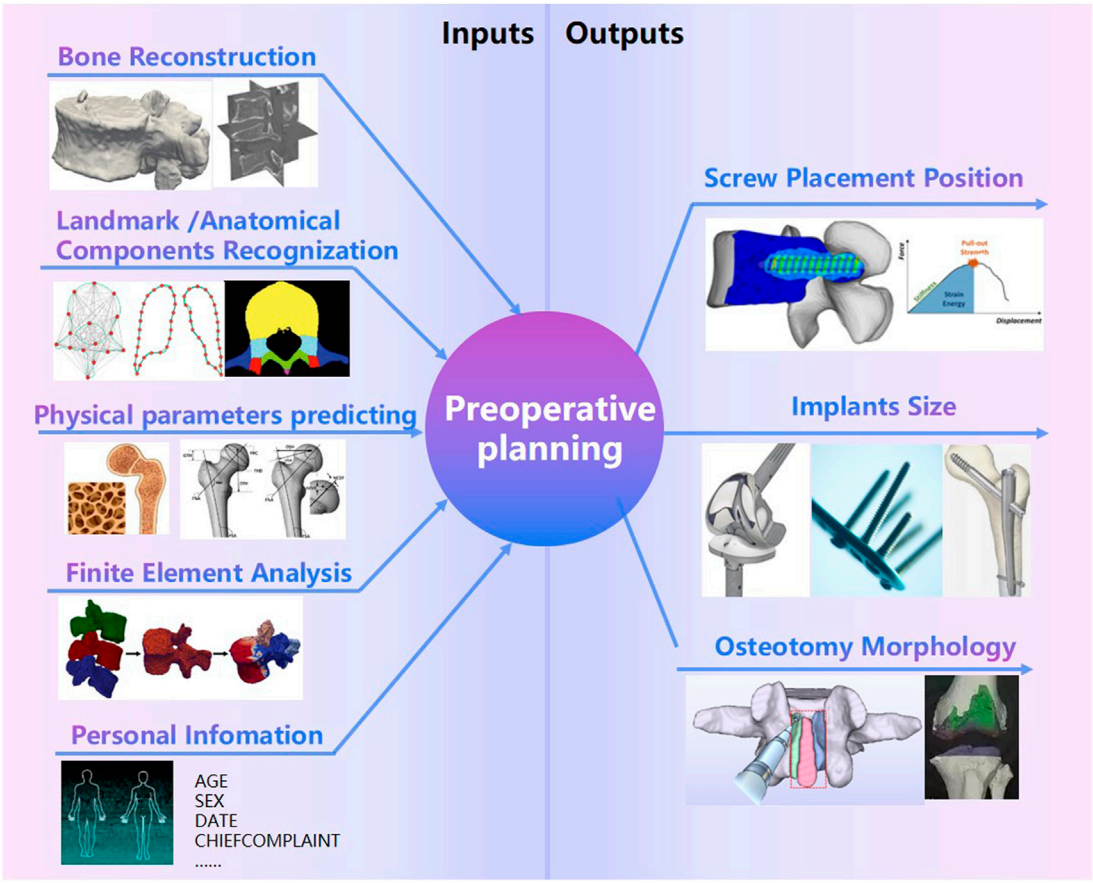

FIGURE 6
Preoperative planning.

points (Zheng and Yu, 2017) for FE analysis. An SSM built by the training dataset is a set of annotated images (Zheng and Yu, 2017). AI technologies make the landmarks/anatomical components recognization automatically (Siemionow et al., 2021). Nathan proposed a deep learning method based on the PointNet++ architecture for biomechanical modeling of facial tissue deformation in orthognathic surgical planning (Lampen et al., 2022). Xiao Xiao et al. (2021) proposed an estimating Reference Bony Shape Models for Orthognathic surgical planning using 3D point-cloud deep learning. Due to the incompleteness of information and uncertainty of healing prediction, preoperative planning dose not have a rapid development like reconstruction technologies.

2.1.4 Intraoperative registration

The accuracy of robotic assisted surgery mainly depends on the space registration. The 2D-3D registration is commonly used in spinal surgery or pelvic surgery and the 3D-3D registration is commonly used in TKA (total knee arthroplasty) surgery. There are always tow workflows of 2D-3D registration (Figure 7): 1) Projection based 2D-3D registration. Digitally reconstructed radiographs (DRR) are generated from CT images, and then mutual information, normalized cross correlation, sum of square differences or other similarity measurements are used to calculate the relationship between X-ray images and DRRs (Guo et al., 2019). 2) Reconstruction based 2D-3D registration. 3D point clouds are reconstructed from 2D x-ray or ultrasonic images. Transformation matrix are calculated through tow 3D point clouds (Wang et al., 2018). The intraoperative point clouds of knee are commonly collected by probes with markers in TKA surgery. The preoperative and intraoperative point clouds are matched through ICP or CPD algorithms.

Due to the sparsity inconsistency of point clouds between preoperative images and intraoperative images, deformation differences caused by different parameters of different imaging devices, the accuracy of surgical registration methods has been paid a great attention, but not yet been well solved. Registration methods based on deep-learning (Lu et al., 2021) have shown be capable of addressing the

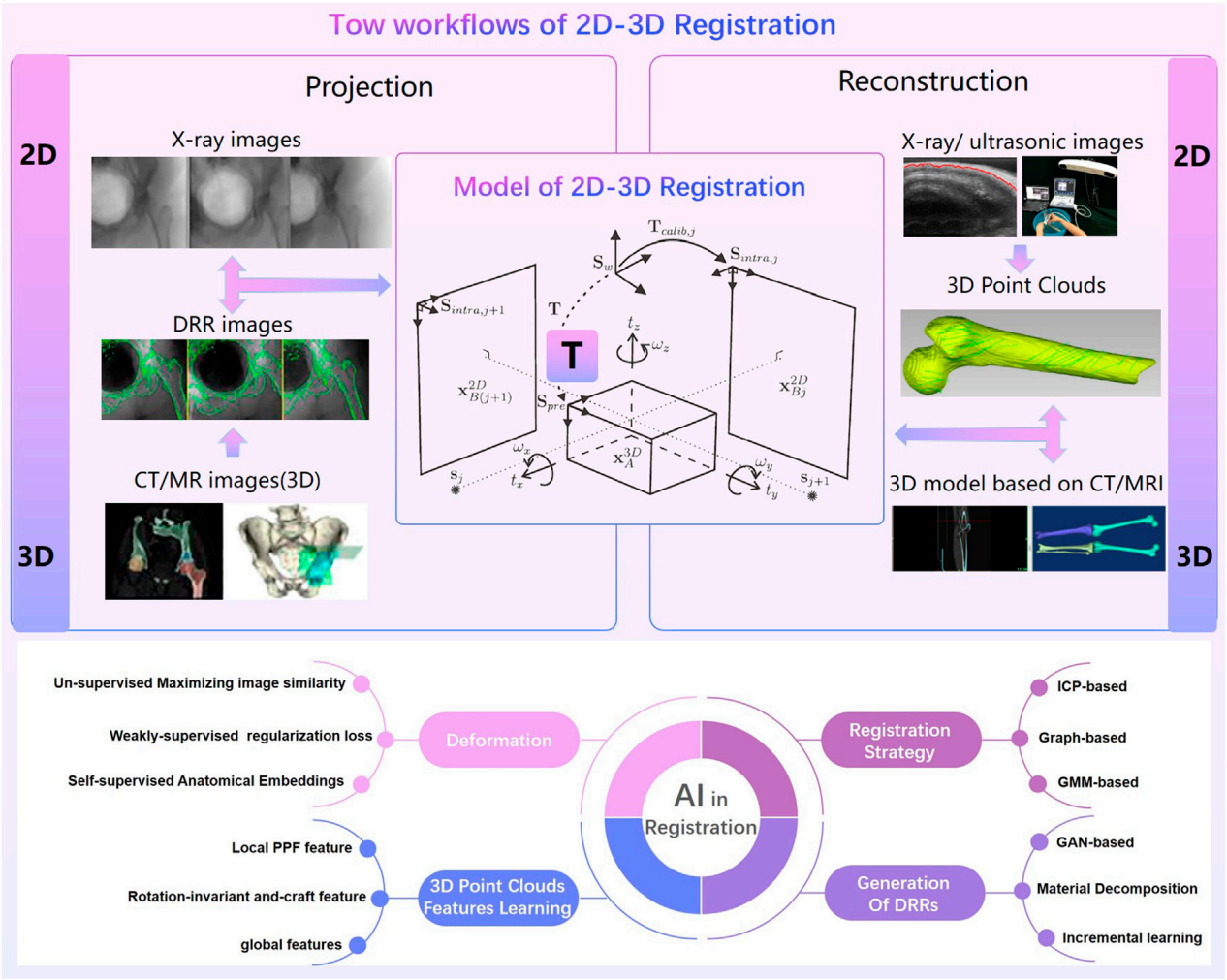

FIGURE 7
Tow workflows of 2D-3D Registration and AI in Registration.

limitations of conventional registration methods (Figure 7), as they have a better performance in predicting deformations, learning 3D point clouds features, generating DRRs and optimizing registration strategy. Unsupervised learning (Chen et al., 2022) estimate voxel-to-voxel deformable transformation by maximizing image similarity (Fan et al., 2019). Weakly-supervised regularization loss is able to map thecomplex appearance to a common space (Blendowski et al., 2021). Self-supervised anatomical embedding (SAM) (Yan et al., 2022) is capable of computing dense anatomical/semantic correspondences between two images at the pixel level. Feature learning methods use the deep neural network to learn a robust feature correspondence search (Huang et al., 2021a), which includes a local PPF feature using the distribution of neighbour points (Deng et al., 2018), a rotation-invariant hand-craft feature (Gojcic et al., 2019), a global features (Qi et al., 2017) etc. There are three registration strategies using AI (Huang et al., 2021a): ICP-based variations, graph-based, GMM-based and semi-definite registration methods. Deep Closest Point(DCP) uses deep features to estimate correspondences to avoid spurious local optima of most ICP algorithms (Wang and Solomon, 2019). The surface registration are solved effectively by transforming the registration problem into a graph matching problem (Le-Huu and Paragios, 2017). For Gaussian mixture models (GMM), DeepGMR (Yuan et al., 2020) uses a neural network to learn pose-invariant point-to-distribution parameter correspondences. DRRs are simulated by algorithm which may differ from the real X-ray images. To improve the quality of DRRs, GAN-based training, material decomposition, and incremental learning are proposed. A GAN-based disentanglement learning framework (Han et al.,

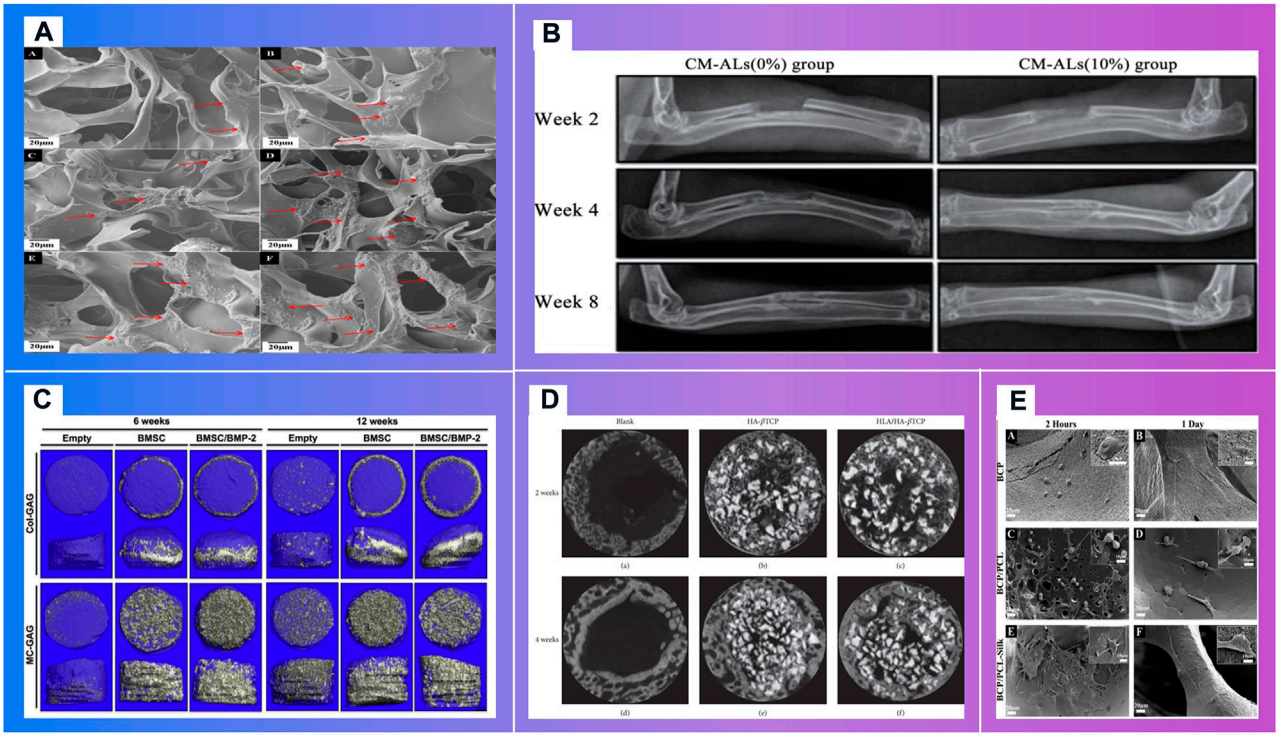

FIGURE 8
Bioactive materials demonstrating the osteoblast migrations. **(A)**. *In vitro* mineralization on mCT scanning of BMSCs cultured on Col-GAG and MC-GAG scaffolds in the absence and presence of BMP-2 (Makvandi et al., 2020) **(B)**. *In vitro* mineralization on mCT scanning of BMSCs cultured on Col-GAG and MC-GAG scaffolds in the absence and presence of BMP-2 (Ren et al., 2016) **(C)**. X-ray analysis of new bone formation in CM-ALs (0%) and CM-ALs (10%) implanted groups (Wu et al., 2017). **(D)**. Micro-CT images of the artificial defects at weeks 2 and 4. (Chang et al., 2016) **(E)**. Morphology of cultured HOB on **(A,B)** BCP, **(C,D)** BCP/PCL and **(E,F)** BCP/PCL–silk scaffolds after 2 and 24 h (Roohani-Esfahani et al., 2012)

2021) can transfer the rib structural priors from DRRs. DeepDRR is a framework for DRRs embedding material decomposition and scatter estimation in 3D and 2D, combined with analytic forward projection and noise injection (Unberath et al., 2018). Incremental learning can improve continuously acquire new knowledge by continuously acquiring new knowledge (Jiang et al., 2021).

2.2 Responsive bioactive implants made through 3D printing technology can provide signals for endogenous repair

Autograft, allografts and metal-based material scaffolds are commonly used in the clinical treatment of bone defects. However, chronic inflammation, immune rejection or stress shield and inflammation have hindered their clinical application. New bioactive responsive implants made through 3D printing technology and adaptively expanded, which can provide signals for endogenous repair, is highly necessary to promote bone regeneration (Figure 8). Bioactive materials, especially bioactive polymers high osteoinduction, excellent angiogenesis, biocompatibility and unlimited size, can interact with proteins, cells or tissues *in vivo* and cause biological reactions.

2.2.1 Responsive bioactive materials can promote the reconstruction of organizations

Bioactive materials can guide bone regeneration (Mistry et al., 2015) (Figure 9). Dhivya S.et al. Dhivya et al. (2015) explored a nanoparticulate mineralized collagen glycosaminoglycan scaffold that induces healing of critical-sized rabbit cranial defects. These inorganic nano materials delivery of bioactive agents. However, their widespread employment may be reduced due to the possible toxicity and the lack of biodegradability (Makvandi et al., 2020).

Polymer materials consisting of inorganic nanomaterials and organic polymer materials, with high ductility, biocompatibility and biodegradability, are widely used in bone repair scaffolds (Figure 11). Their specific structure and surface properties can be specifically recognized and interact with target biomolecules. Makvandi P.et al. Makvandi et al. (2020) developed a graphene oxide (GO)–Chitosan (CS)–Hyaluronic acid (HA) based bioactive composite scaffold containing an osteogenesis-inducing drug simvastatin (SV). The elongated morphology of the cells after

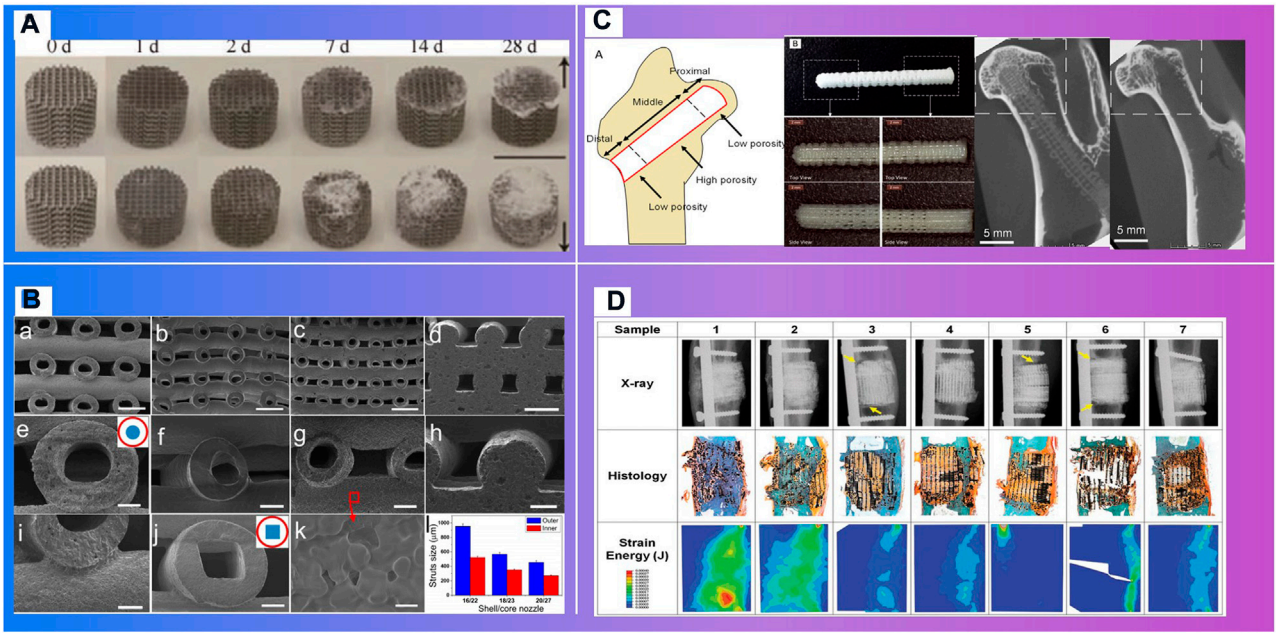

FIGURE 9
Materials with biodegradability. **(A)**. Degradation process (Li et al., 2020). **(B)**. SEM images of printed HSP bioceramic scaffolds *via* core/shell nozzle of 16/22 18/23 and 20/27 and printed SSP bioceramic scaffolds as the control (Luo et al., 2015). **(C)**. A functionally graded scaffold (Kawai et al., 2018). **(D)**. Mathematical modeling of total strain energy for defects implanted with the Sr-HT-Gahnite scaffold at 12 months postimplantation (Li et al., 2019).

48 h incubation has demonstrated the osteoblast migration using the SV loaded GO–CS–HA scaffolds. A collagen–hydroxyapatite(HA) scaffold (Unnithan et al., 2017) with a degree of interconnectivity of 99%, can not only deliver biological factors, promote stem cell differentiation and ossification (Thitiset et al., 2013; Villa et al., 2015), but also theoretically be applied in a load bearing application when combined with mechanical fixation (Zhang et al., 2018). Mouse BMSCs isolated from the femur and tibia of CD1 wild type animals, were seeded dropwise on to the top of either the Col–HA scaffold. Cells well were attached on the scaffolds after 12 h of seeding. In the study of *in vivo* bone formation in a mouse calvaria defect, scaffolds were implanted. After 3 weeks of implantation, calvaria containing critical size defects filled with BMSCs combined with either the Col–HA scaffold in X-ray images (Unnithan et al., 2017). The research of Ren X. et al. Ren et al. (2016) demonstrated that a nanoparticulate mineralized collagen glycosaminoglycan scaffold showed more efficient mineralization of MC-GAG scaffolds than non-mineralized Col-GAG scaffolds in either the histologic analyses or mCT scanning images. Wu H. et al. Wu et al. (2017) has fabricated a chitosan-based microsphere delivery system to controlled release of alendronate (AL), which can release AL for up to 30 days. CM-ALs (10%) scaffolds showed better performance in large-sized bone defects repairs than CM-ALs (0%). The new bone increasing ratio (NBIR) of HLA/HA-βTCP samples was 1.78 times higher than the blank group at week 2 (Chang et al., 2016). The study of Roohaniesfahani S.I. et al. Roohani-Esfahani et al. (2012) showed that, BCP/PCL scaffolds with silk layer is more favorable than BCP/PCL scaffolds with collagen layer in mechanical properties and biological properties.

More importantly, responsive bioactive materials, especially shape memory polymers (SMP) (Figure 10), can remember the temporary shape and return to the original shape under the condition of the external stimuli, like heat, pH, electricity, magnetic field, etc (Zhang et al., 2012; Rezwan et al., 2006; Zheng et al., 2018b). This specific shape memory could simplify complex transplant procedures, with excellent chemical stability, biocompatibility and biodegradability, which can stimulate specific cellular responses. Deng Z.et al. Deng et al. (2016) designed and synthesized a series of shape memory copolymers with electroactivity, super stretchability and tunable recovery temperature based on poly(e-caprolactone) (PCL) with different molecular weight and conductive amino capped aniline trimer. They proved that they can enhance myogenic differentiation from C2C12 myoblast cells. Xie R.et al. Xie et al. (2017) prepared a novel polyurethane or hydroxyapatite based SMP porous foam for the treatment of load-bearing bone defects by gas foaming. The foam can match the trabecular bone, possess the feasibility of minimally invasive delivery. And it can also overcome the disadvantages of traditional polymer foams in terms of insufficient mechanical properties, inadequate pore structures, low

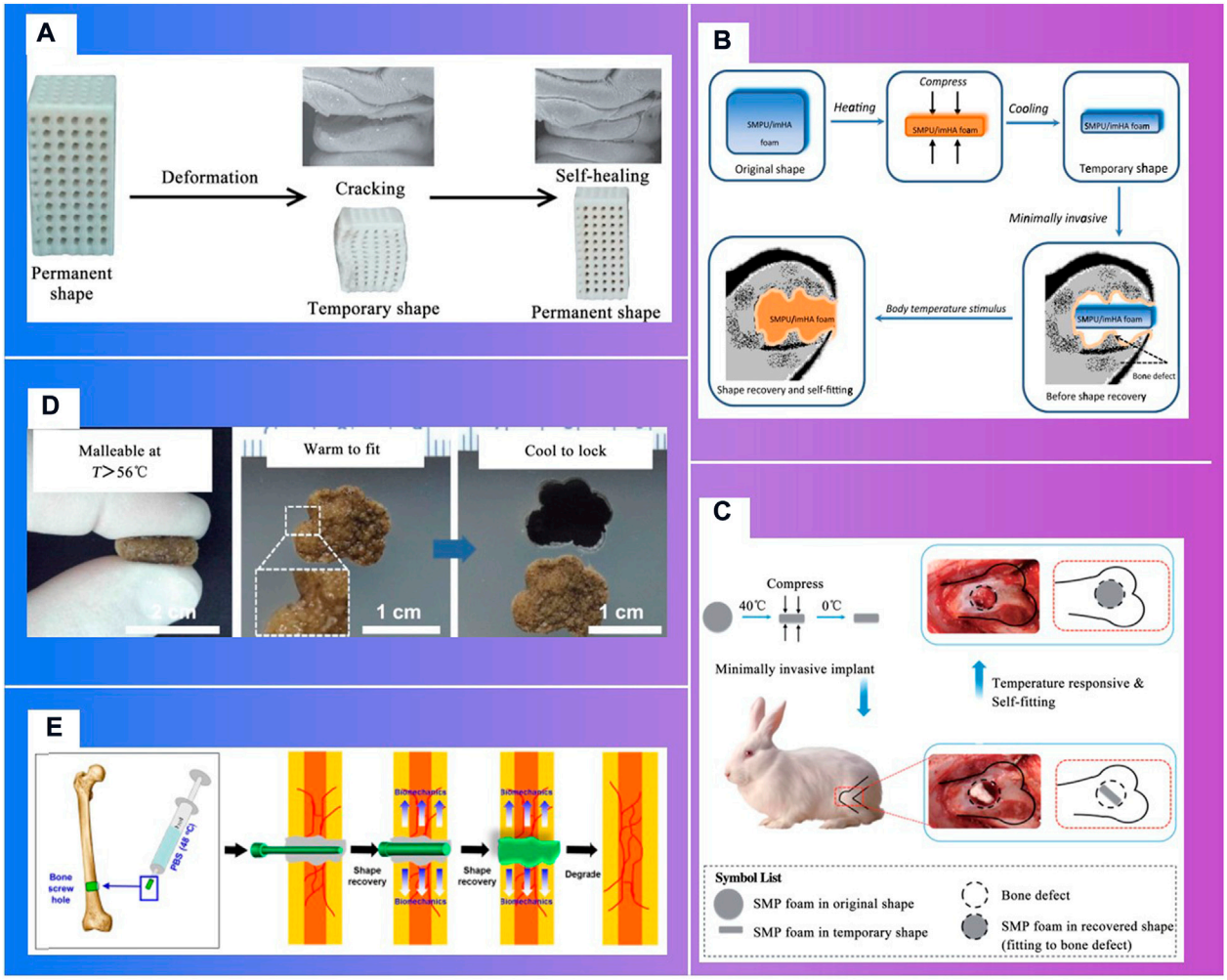

FIGURE 10
Shape memory polymers in bone tissue engineering. **(A)** t Fixing of a temporary shape of a 3D-printed PLA/HA scaffold through compression (Senatov et al., 2016) (Xie et al., 2017). **(B)**. Schematic of body-temperature responsive SMPU/imHA foam for minimally invasive delivery in application of bone regeneration (Xie et al., 2017). **(C)**. Schematic of self-adaptive SMP foam as a bone scaffold for bone regeneration (Xie et al., 2018). **(D)**. Self-adaptive process of polydopamine-coated shape memory porous PCL scaffolds (Zhang et al., 2014). **(E)**. Schematic illustration showing the application of shape-memory-capable scaffold of the Hap/PLMC naofibers (Xie et al., 2018).

biocompatibility and inconvenience in operation. The rabbit femoral defect model (Xie et al., 2018) demonstrated that a SMP foam bone scaffold could play an important role in promoting neovascularization and bone remodeling. A shape memory PCL porous scaffold was made from photocrosslinking (ε-caprolactone) (PCL) polydiacrylate through SCPL method (Zhang et al., 2014), and it evidently promoted the adhesion and proliferation of osteoblasts. SMP scaffolds show strong self adaptability, as evidenced by the following facts. One of these is that smaller SMP scaffolds than bone defect size can match bone defect boundary after shape expansion (Zhang et al., 2012; Xie et al., 2017), the other is that larger SMP scaffolds can promote the inward growth of bone, due to the binding force with bone tissue (Zhang et al., 2014; Bao et al., 2016).

2.2.2 3D bioprinting technology can personalize implants

Three-dimensional printing technologies that can fabricate the microstructure of materials precisely, have shown distinct advantages to personalize implants in bone tissue engineering (Luo et al., 2015). In clinical medicine, 3D printing technologies can be divided into two stages (Figure 11): one is conventional 3D printing objects without cellular information exchange, like surgical guiding paltes (Butscher et al., 2013), prosthesis (Xu et al., 2013; Turnbull et al., 2018); the other is bioactive 3D printing objects can provide signals for endogenous repair, which particularly is of great significance to bone regeneration and vascular reconstruction, such as degradable scaffolds (Xu et al., 2019a), living cell printing (Kolesky et al., 2014), and stimuli-

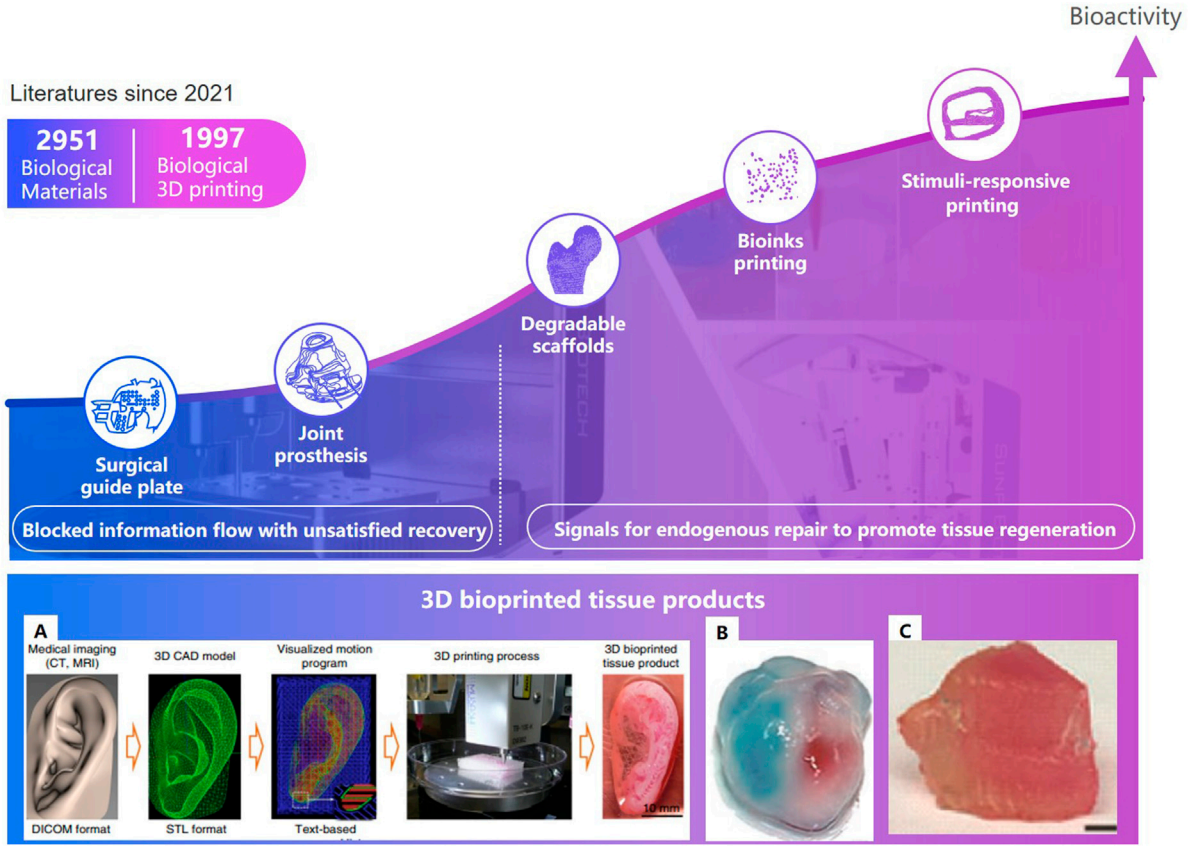

FIGURE 11
Development of tissue engineering and 3D bioprinted tissue product. **(A)**. The ITOP system (Groll et al., 2018).**(B)**. Ventricles (Zhang et al., 2016). **(C)**. Thyroid cartilage (Van Belleghem et al., 2020).

responsive printing materials with programmable behavior (Gladman et al., 2016) (Qi et al., 2014).

Degradable 3D printing scaffolds can gradually release the occupied space with the recovery of the damaged part (Figure 7.C) (Li et al., 2020). Kawai T. et al. Kawai et al. (2018) of Stanford University designed and 3D printed a functionally graded scaffold (FGS) made of polycaprolactone (PCL) and b-tricalcium phosphate (b-TCP) to treat Osteonecrosis of the femoral head. The *in vivo* degradation rate and the bone ingrowth ratio of the scaffold is significantly higher than the empty-tunnel group. Li et al. Li et al. (2019) at University of Sydney developed a 3D-printed Sr-HT-Gahnite scaffolds implanted into critical-sized segmental defects in sheep tibia. Compared with bone autografts, the scaffolds possessing both osteoconductive and osteoinductive properties, can induce substantial bone formation and defect bridging. Spiral fractures were observed in the study. The fractures may have a negative effect on the recovery. Thus, implants should be fixed at appropriate position.

2.2.3 Bio implants through bio-inks can migrate in planned direction

Bioinks is a formulation of cells suitable for processing by an automated biofabrication technology that may also contain biologically active components and biomaterials (Groll et al., 2018). Biomaterials may consist of cells, collagen, and other bioactive ingredients; Auxiliary biomaterials, such as gelatin, alginate hydrogel, carbomer glue, etc, can be used to improve mechanical strength of implants, maintain the shape of the printed object, and ensure the adhesion and survival rate of cells. In 2015, Kang H.W. et al. Kang et al. (2016) of the Wake Forest Institute for Regenerative Medicine developed a system that deposits cell-laden hydrogels together with synthetic biodegradable polymers that impart mechanical strength. The printed mandible, skull, cartilage and skeletal muscle can incorporate multiple cell types at precise locations to recapitulate native structure and function. In 2016, Zhang Y. S. Zhang et al. (2016) of Harvard Medical School proposed a novel hybrid strategy based on 3D bioprinting to fabricate endothelializedmyocardium. Endothelial cells controlled anisotropy, can gradually migrate towards the peripheries of the microfibers.

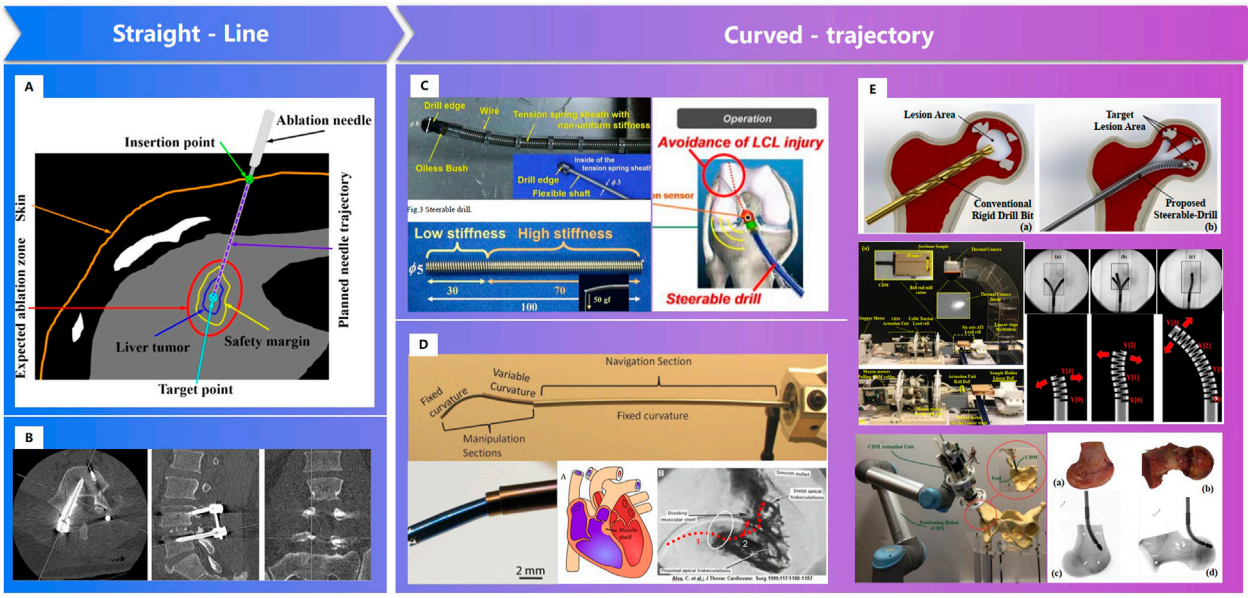

FIGURE 12
Surgical channels constructed by robot. **(A)**. Straight needle trajectory planning for radiofrequency ablation and microwave ablation of liver tumors (Zhang et al., 2019). **(B)**. Linear surgical channel for spinal screw internal fixation (Nicolas et al., 2016). **(C)**. A "Steerable Drill" for ACL Reconstruction to Create the Arbitrary Trajectory of a Bone Tunnel (DePhillipo et al., 2018). **(D)**. Endoscopic Add-on Stiffness Probe (Gilbert et al., 2014). **(E)**. A less-invasive surgical workstation to treat osteolytic lesions behind a well-fixed acetabular implant (Bakhtiarinejad et al., 2020)-(Alambeigi et al., 2014).

With the continuous upgrading of material technology, biological 3D printing strategy is constantly updated. In 2019, Van Belleghem S.et al. Van Belleghem et al. (2020), from the University of Maryland College Park, proposed a 3D printing strategy for dual bioinks. The graft consisting of both degradable and nondegradable parts, providing long term mechanical integrity and shape retention. A pre-programmed responsive bioactive materials can be used in various application where the human intervention is not possible. This technology may lead to satisfied repair. The materials which responds to external stimuli is called 4D printing (Tibbits, 2014). A porous PLA/HAP scaffolds can stand up to three compression-heating-compression cycles without delamination. The scaffolds can narrow the cracks during heating, which may resulted in 'self-healing'. The significant changes of post implantation have higher requirements to ensure the stability during deformation process of the implants, and that the deformation not cause additional damage to the surrounding tissues.

2.3 Personalized surgical channels can be established through intelligent robotics precisely

In clinical, there are linear channels established, due to the limitation of the structure of instruments (Nicolas et al., 2016; Zhang et al., 2019). Fracture or scoliosis treatments are great different between children and the elderly, because children have better self-healing in growth. Linear channels may be not meet the biomechanics needs, especially for the elderly. As smart materials and variable structures developed, such as memory alloys, concentric tube structures, etc., curved-trajectory, with less trauma and better therapeutic effect, attracts the researchers' great attention (Figure 12). Moreover, intelligent sensing technology and intelligent operation technology also make the surgery more efficiency.

2.3.1 Personalized surgical channels can be established through variable structures

Personalized surgical channels are linear channels, curved-channels or linear- curved mixed channels based on the status of patients. In 2011, Watanabe H. Watanabe et al. (2011) et al. developed a steerable drill for ACL reconstruction to construct an arbitrary trajectory of a bone tunnel. Gilbert H. Gilbert et al. (2014) adopted a needle-sized tentacle-like robot that require access through constrained paths in transnasal skull base surgery. In 2012, Gosline, A. H. et al. Gosline et al. (2012) manufactured a steerable curved concentric tube robot that can enter the heart through the vasculature, using a unique metal MEMS process.

Since 2014, Alambeigi F. of Johns Hopkins University et al. Alambeigi et al. (2014), Alambeigi et al. (2016a), Alambeigi et al. (2016b); Wilkening et al., 2017; Bakhtiarinejad et al., 2020) has researched the novel steerable drill using a continuum dexterous

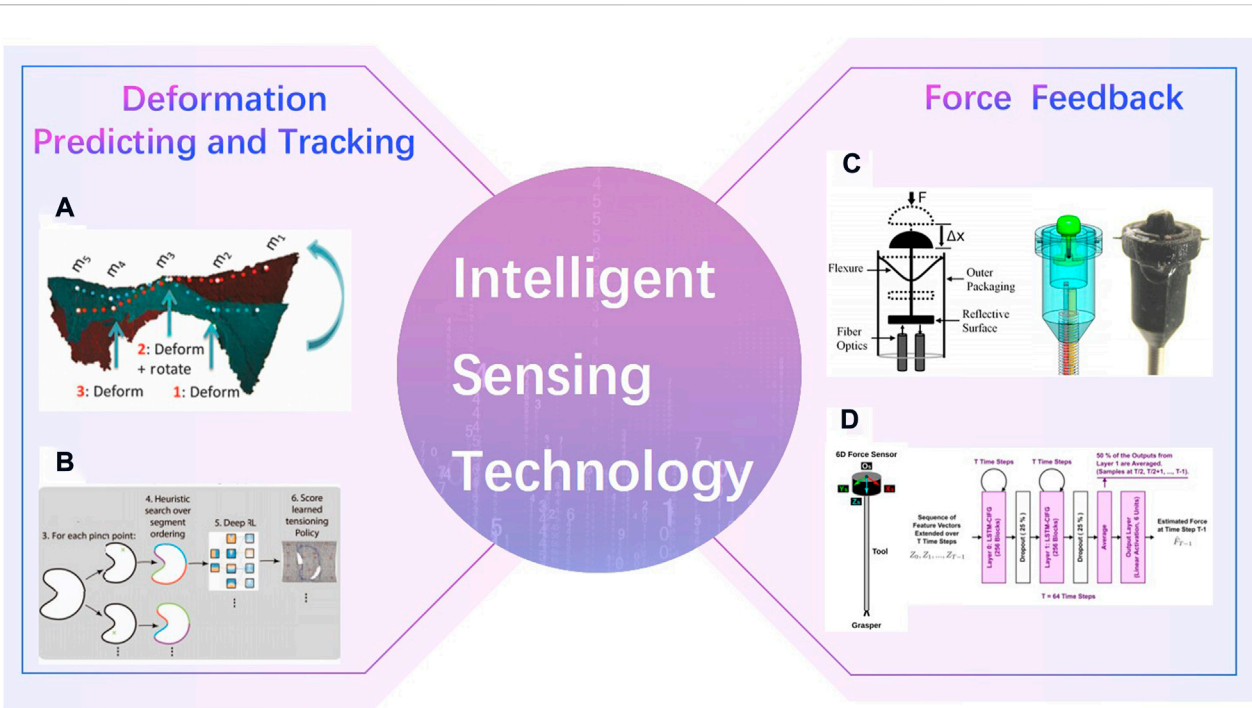

FIGURE 13
Intelligent Sensing Technology. **(A)** *in vivo* supervised autonomous soft tissue surgery (Shademan et al., 2016) **(B)**. Deep reinforcement learning policies were used in Pattern Cutting task (Thananjeyan et al., 2017). **(C)**. Force sensors in robotic surgery (Kesner and Howe, 2011) **(D)**. Semi-Supervised Deep Neural Network Model (Marban et al., 2018).

manipulator (CDM), and carried out experiments on both simulated and human cadaveric bones. Bakhtiarinejad M. Bakhtiarinejad et al. (2020) studied the use of curved drilling technique for treatment of osteonecrosis of femoral head. The biomechanical study demonstrated that a novel robot-assisted curved core decompression (CCD) technique is introduced to provide surgeons with direct access to the lesions causing minimal damage to the healthy bone. The progress of bistable structure, shape memory polymer and intelligent variable structure promoted the adaptability of surgical robot, which enable the biomechanical channels for orthopaedics.

2.3.2 Intelligent sensing technology can lead to precise trajectory in complex environment

Unlike industrial scene, the intraoperative environments are always complex. The robot cannot perceive, explain and understand the surrounding environment as well as surgeons is one of the key factors that the robotics ca not perform surgery automatically. Deformation predicting and tracking, and haptic feedback are tow common intelligent sensing technologies in surgical robotics (Figure 13). Shademan Shademan et al. (2016) demonstrated *in vivo* supervised autonomous soft tissue surgery which can suture a wound automatically. Deep reinforcement learning policies were used in Pattern Cutting task to induce tension in the material as cutting proceeds (Thananjeyan et al., 2017). Force sensors were developed to estimate interaction forces in robotic surgery (Kesner and Howe, 2011; Marban et al., 2018). And a Semi-Supervised Deep Neural Network Model was applied to understand the operation pattern (Marban et al., 2018).

2.3.3 Robotic skill learning can improve the automation level of surgical robotics

The surgical robotics in clinical are commonly semi-automatic. They can perform intraoperative actions based on the double closed-loop control of force position mixing in puncture (Wells et al., 2016), cochlear implant (Wang et al., 2020), fracture reduction (Lei et al., 2019) or other surgeries. However, it is impossible to dynamically adjust the task strategy according to the actual situation (Graham et al., 2008; Zhang, 2018). Skill learning (Silver et al., 2016; Mahler et al., 2019) make robots execute task which difficult by traditional control methods (Levine et al., 2016; Sun et al., 2017; Mandlekar et al., 2018), like pouring water and screwing screws, automatically.

3 Future research directions for satisfied repair of musculoskeletal injuries

The multi-layer intelligent technologies (MLIT) offer possibilities to achieve satisfied repair of musculoskeletal

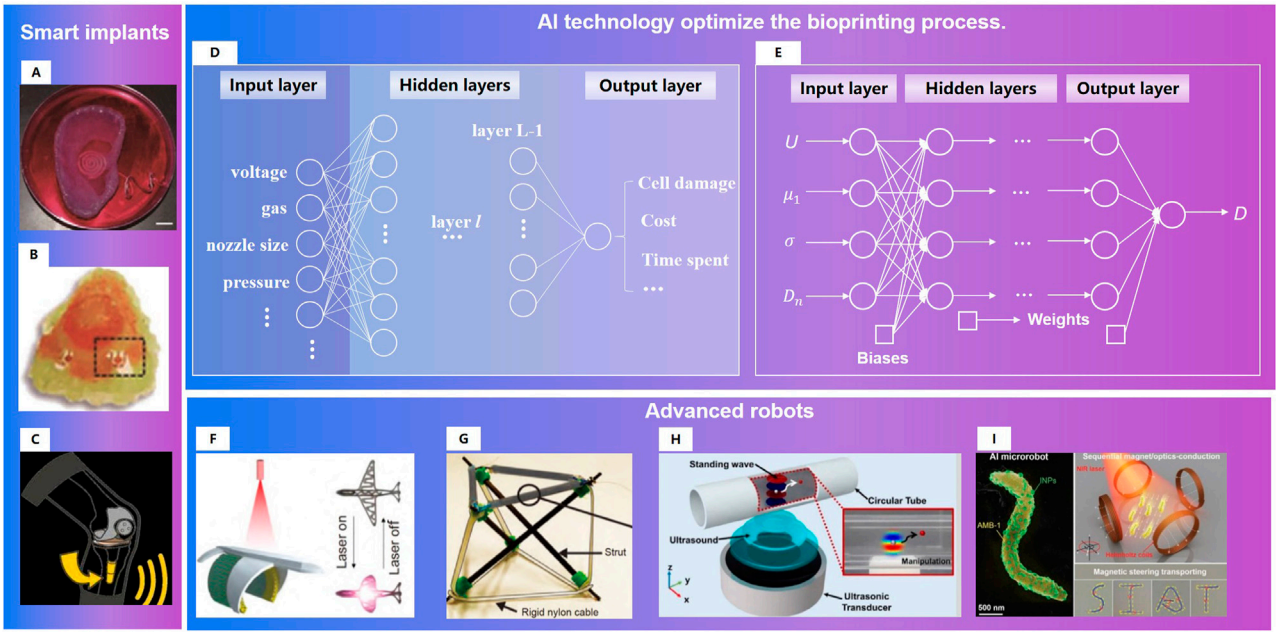

FIGURE 14
Research directions for satisfied repair of musculoskeletal injuries: 1) Smart implants. **(A)**A bionic ear (Mannoor et al., 2013). **(B)**. An odor-perceptive nose-like hybrid (Jodat et al., 2020). **(C)**. Smart prosthesis (Zimmerbiomet, 2021) 2)AI technology optimize the bioprinting process. **(D)**. Example neural network for process optimization in three-dimensional bioprinting (Ruberu et al., 2021). **(E)**. FCNNs for multi-objective optimization of drop-on-demand (DOD) bioprinting (Shi et al., 2019). 3)Advanced robots. **(F)**. Tissue engineering robot with light activated deformable wing (Xu et al., 2019b). **(G)**. Variable-stiffness tensegrity structures (Zappetti et al., 2020). **(H)**. An ultrasound-controlled actuator for targeted drug delivery (Lee et al., 2020). **(I)**. Acoustic powering and magnetic steering for actuating and navigating microrobots (Aghakhani et al., 2020).

injuries. However, there are still no wide range of clinical applications, because of the following reasons: 1) the pathogenesis like the femoral head necrosis or the spinal tumor, the healing process like the ligament or the bone repair, and the biomechanical or kinematics models are not clarified in detail. 2) the real environment is hard to simulate. As there are differences between the simulation environment and the real environment, further verification of some research results should be implemented. 3) some theoretical designed surgical plan cannot be realized as expected. Further research will be needed for satisfied repair of musculoskeletal injuries:

3.1 The research on the pathogenesis or the healing process can be more effective through new AI technologies

3.1.1 Biomechanical models based on multi-physical parameter prediction will be built

Current biomechanical models are always based on 3D reconstructed models. However, morphology and parameters of the ligament, meniscus (Antico et al., 2020) and other tissue are always artificially devised (Viris et al., 2016), and the same density of different bone tissues like cortical bone, cancellous bone and trabecular bone structures are commonly set in biomechanical analysis. It is said that kinematics simulations are greatly different from real scene (Bell et al., 1996). To build real biomechanical models, physical parameter such as the bone density, ligament elastic modulus, must be predicted precisely.

Although some physical parameters predicting methods are proposed, which are discussed in Section2.1.2, lots of parameters still cannot be predicted for the lack of data with high-quality labels. Standard labeling procedure, and cross check of data labels are necessary.

3.1.2 Causal relationship between symptoms and physiological factors will be discovered by causal discovery

R Ganz (Siebenrock et al., 2010) proposed a surgical plan which can retain the vascular supply of the femoral head, to guarantee the oxygen and nutritional supply to the cells (Kramer et al., 2009). However, excessive vascular supply may be not conducive to recovery. Further research on the pathogenesis or the healing process for femoral head necrosis, especially the causality, but not only the correlation between the symptoms and physiological factors should be deserved. Now causal discovery, which can promote the research of disease mechanism, has been applied in hippocampal function analysis (Mannoor et al., 2013; Sanchez-Romero et al., 2018).

Causal discovery can be a useful theory for the research on the pathogenesis or the healing process.

3.2 Intelligent technologies will make add the functionality of implants and make the implants manufacture process more efficiently

3.2.1 Implant with intelligent sense will provide real recovery status

Implants bioprinting combined with intelligent sense is also a research hotspot (Figure 14). In 2013, Mannoor M.S.et al. Mannoor et al. (2013) generated a bionic ear *via* additive manufacturing of biological cells with structural and nanoparticle derived electronic elements. In 2019, Jodat, Y.A. et al. Jodat et al. (2020) designed an odor-perceptive nose-like hybrid, with 3D cartilage-like tissue constructs. It is composed of a mechanically robust cartilage-like construct and a biocompatible biosensing platform. Patients can not recover only by surgery without rehabilitation training as the human body systems has changed after operations. Doctors can obtain the patient's status through regular follow-up. These data were often temporary and fragmented, and could not truly reflect the patient's postoperative status. The smart prosthesis persona IQ of Zimmer Biomet has passed FDA certification (Zimmerbiomet, 2021). Persona IQ can not only implant in patients like the traditional prosthesis, but also record the range, speed and other index of gait, for assessing postoperative recovery progress. Implant with intelligent sense will provide real recovery status for changing rehabilitation plans.

3.2.2 Intelligent models 3D/4D printing process will optimize the manufacturing process

The performance of 3d/4d printed matter is not only related to its own physical, mechanical and biological properties, but also affected by the process parameters of the printing process (Naghieh et al., 2020). Study of Zheng W. et al. Zheng et al. (2021) showed the following facts: ① Higher pressures caused instability of extruded biomaterial, and subsequently, poor printability; ②Fell under or above the range of nozzle speeds caused poor strand printability; ③ The more viscous the biomaterial, the more appropriate printability could be achieved. Due to the complex conditions, it is hard to build an accurate mathematical printing model. Data driven AI technology (Shi et al., 2019; Yu and Jiang, 2020; Ruberu et al., 2021) has obvious advantages in the multi-objective optimization of biological printing process (Figure 14).

3.3 Advanced materials and variable structures will improve the treatment performance of robotics

As the physiological state of patients are different and changing (Ionov, 2018), such as temperature, pH (Ca2+ concentration), to achieve satisfied repair in long-term therapy, personalized surgical channels should be conducted (Xu et al., 2019b; Zappetti et al., 2020; Wang et al., 2022) or the endogenous repairs should be guided by the micro nano robots (Aghakhani et al., 2020; Lee et al., 2020). Combining the improvement of intraoperative operation skills and the providing signals for postoperative repair, the treatment effect can be improved through robots.

4 Conclusion

Satisfied recovery, a key goal of precise orthopaedics, has became possible, as AI technology in orthopaedics has progressed in the following apsects: physical parameters can be predicted precisely through AI technology, bioactive implants made through 3D printing technology can provide signals for endogenous repair, and personalized surgical channels can be established through intelligent robotic technology. However, the multi-layer intelligent technologies (MLIT) has not been used widely. With further study on biomechanical models for multi-physical parameter prediction, stimulus response mechanism of bioactive implants, smart implants, intelligent modeling of 3D/4D printing process and variable structure in long-term therapy (Senatov et al., 2016; Lin et al., 2019; Su et al., 2019), satisfied repair may be achieved by the multi-layer intelligent technologies (MLIT).

Author contributions

NG: Conceptualization, investigation, writing–review, and editing. JT: Investigation, review. LW: Investigation, writing and editing. KS: Investigation. LM: Methodology, Supervision. HM: Investigation and supervision. ZZ: Methodology, and supervision. FS: Supervision.

Funding

The study was funded by the National Natural Science Foundation of China Youth Fund (Grant No.62103224), and Special support from China Postdoctoral Foundation (Grant No.2020TQ0168).

Conflict of interest

The authors declare that the research was conducted in the absence of any commercial or financial relationships that could be construed as a potential conflict of interest.

Publisher's note

References

Abraham, N., and Khan, N. M. A Novel Focal Tversky loss function with improved Attention U-Net for lesion segmentation. Preprint, 2018.

Aghakhani, A., Yasa, O., Wrede, P., and Sitti, M. (2020). Acoustically powered surface-slipping mobile microrobots. *Proc. Natl. Acad. Sci. U. S. A.* 117 (7), 3469–3477. doi:10.1073/pnas.1920099117

Ahrend, M. D., Teunis, T., Noser, H., Schmidutz, F., Richards, G., Gueorguiev, B., et al. (2021). 3D computational anatomy of the scaphoid and its waist for use in fracture treatment. *J. Orthop. Surg. Res.* 16 (1), 216. doi:10.1186/s13018-021-02330-8

Alambeigi, F., Murphy, R. J., Basafa, E., Taylor, R. H., and Armand, M. (2014). Control of the coupled motion of a 6 DoF robotic arm and a continuum manipulator for the treatment of pelvis osteolysis. *Annu. Int. Conf. IEEE Eng. Med. Biol. Soc.* 36, 6521–6525. doi:10.1109/EMBC.2014.6945122

Alambeigi, F., Wang, Y., Murphy, R. J., Iordachita, I., and Armand, M. (2016). Toward robot-assisted hard osteolytic lesion treatment using a continuum manipulator. *Annu. Int. Conf. IEEE Eng. Med. Biol. Soc.* 2016, 5103–5106. doi:10.1109/EMBC.2016.7591875

Alambeigi, F., Sefati, S., Murphy, R. J., Iordachita, I., and Armand, M. Design and characterization of a debriding tool in robot-assisted treatment of osteolysis. Proceedings of the IEEE International Conference on Robotics and Automation (ICRA), Stockholm, Sweden, 2016, pp. 5664–5669. doi:10.1109/ICRA.2016.7487787

Antico, M., Sasazawa, F., Dunnhofer, M., Camps, S., Jaiprakash, A., Pandey, A., et al. (2020). Deep learning-based femoral cartilage automatic segmentation in ultrasound imaging for guidance in robotic knee arthroscopy. *Ultrasound Med. Biol.* 46 (2), 422–435. doi:10.1016/j.ultrasmedbio.2019.10.015

Bakhtiarinejad, M., Alambeigi, F., Chamani, A., Unberath, M., Khanuja, H., and Armand, M. "A biomechanical study on the use of curved drilling technique for treatment of osteonecrosis of femoral head," in Proceedings of the Medical Image Computing and Computer-Assisted Intervention, 2020, Cham (Springer).

Balagopal, A., Kazemifar, S., Dan, N., Lin, M. H., Hannan, R., Owrangi, A., et al. (2018). Fully automated organ segmentation in male pelvic CT images. *Phys. Med. Biol.* 63 (24), 245015. doi:10.1088/1361-6560/aaf11c

Bao, M., Wang, X., Yuan, H., Lou, X., Zhao, Q., and Zhang, Y. (2016). HAp incorporated ultrafine polymeric fibers with shape memory effect for potential use in bone screw hole healing. *J. Mat. Chem. B* 4 (31), 5308–5320. doi:10.1039/C6TB01305h

Bell, K. L., Garrahan, N., Kneissel, M., Loveridge, N., Grau, E., Stanton, M., et al. (1996). Cortical and cancellous bone in the human femoral neck: Evaluation of an interactive image analysis system. *Bone* 19 (5), 541–548. doi:10.1016/S8756-3282(96)00245-1

Bernardo, I., and Edoardo, B. (2021). Robotics in orthopaedic surgery: Why, what and how? *Archives Orthop. Trauma Surg.* 141 (12), 2035–2042.

Bhandarkar, S., and Dhatrak, P. (2022). Optimization of a knee implant with different biomaterials using finite element analysis. *Mater. Today Proc.* 59 (1), 459–467. doi:10.1016/j.matpr.2021.11.466

Black, K. M., Law, H., Aldoukhi, A., Deng, J., and Ghani, K. R. (2020). Deep learning computer vision algorithm for detecting kidney stone composition. *BJU Int.* 125 (6), 920–924. doi:10.1111/bju.15035

Blendowski, M., Hansen, L., and Heinrich, M. P . (2021). Weakly-supervised learning of multi-modal features for regularised iterative descent in 3D image registration. *Med. Image Anal.* 67, 101822. doi:10.1016/j.media.2020.101822

Butscher, A., Bohner, M., Doebelin, N., Hofmann, S., and Müller, R. (2013). New depowdering-friendly designs for three-dimensional printing of calcium phosphate bone substitutes. *Acta biomater.* 9 (11), 9149–9158. doi:10.1016/j.actbio.2013.07.019

Cai, D., Wang, Z., and Liu, Y., Automatic path planning for navigated pedicle screw surgery based on deep neural network, Proceedings of the 2019 WRC Symposium on Advanced Robotics and Automation (WRC SARA). 2019.

Caprara, S., Fasser, M. R., and Spirig, J. M., (2021). Bone density optimized pedicle screw instrumentation improves screw pull-out force in lumbar vertebrae. *Comput. Methods Biomechanics Biomed. Eng.* 203, 1–11. doi:10.1080/10255842.2021.1959558

Caprara, S. (2021). *Towards the integration of computational methods in spinal surgical planning: A combination of deep learning, statistical, and finite element methods.* Switzerland: ETH Zurich Research Collection. doi:10.3929/ethz-b-000475269

Chang, Y. L., Lo, Y. J., Feng, S. W., Huang, Y. C., Tsai, H. Y., Lin, C. T., et al. (2016). Bone healing improvements using hyaluronic acid and hydroxyapatite/beta-tricalcium phosphate in combination: An animal study. *Biomed Res. Int.* 2016, 1–8. doi:10.1155/2016/8301624

Chen, F., Zhao, Z., Gao, C., Liu, J., Su, X., Zhao, J., et al. (2018). Clustering of morphological features for identifying femur cavity subtypes with difficulties of intramedullary nail implantation. *IEEE J. Biomed. Health Inf.* 22 (4), 1209–1217. doi:10.1109/JBHI.2017.2761980

Chen, W., Zhang, Y., He, J., Qiao, Y., Chen, Y., Shi, H., et al. W-net: Bridged U-net for 2D medical image segmentation. 2018, preprint.

Chen, J., Lu, Y., and Yu, Q., (2021). TransUNet: Transformers make strong encoders for medical image segmentation. *Comput. Vis. Pattern Recognit.* doi:10.48550/arXiv.2102.04306

Chen, Z., Wei, J., and Li, R., (2022). "Unsupervised multi-modal medical image registration via discriminator-free image-to-image translation," in Proceedings of the International Joint Conference on Artificial Intelligence, Vienna, Austria.

Das, K., and Zhang, Q. . Convolutional recurrent residual U-net embedded with attention mechanism and focal Tversky loss function for cancerous nuclei detection. Preprint, 2020.

Deng, Z., Guo, Y., Zhao, X., Li, L., Dong, R., Guo, B., et al. (2016). Stretchable degradable and electroactive shape memory copolymers with tunable recovery temperature enhance myogenic differentiation. *Acta Biomater.* 46, 234–244. doi:10.1016/j.actbio.2016.09.019

Deng, H., Birdal, T., and Ilic, S. (2018). "Ppfnet: Global context aware local features for robust 3d point matching," in Proceedings of the IEEE Conference on Computer Vision and Pattern Recognition, 18-23 June 2018, Salt Lake City, UT, USA, 195–205.

DePhillipo, N. N., Moatshe, G., Brady, A., Chahla, J., Aman, Z. S., Dornan, G. J., et al. (2018). Effect of meniscocapsular and meniscotibial lesions in ACL-deficient and ACL-reconstructed knees: A biomechanical study. *Am. J. Sports Med.* 46 (10), 2422–2431. doi:10.1177/0363546518774315

Dhivya, S., Ajita, J., and Selvamurugan, N. (2015). Metallic nanomaterials for bone tissue engineering. *J. Biomed. Nanotechnol.* 11 (10), 1675–1700. doi:10.1166/jbn.2015.2115

Ding, H., Miao, Q., Liu, H., Wang, H., Tu, Q., Chen, J., et al. (2017). Preoperative design and clinical application of TKA assisted by CAD combined with 3D printing navigation templates. *Chin. Orthop. J. Clin. Basic Res.* 9 (5), 261–268. doi:10.3969/j.issn.1674-666X.2017.05.001

Dong, Q., Huang, Z., and Sun, Y., Prediction of accuracy and screw size by pedicle anatomic parameters and screws in idiopathic scoliosis with freehand screw placement based on machine learning. Preprint, 2021.

Dong, Z., He, Y., and Qi, X., "MNet: Rethinking 2D/3D networks for anisotropic medical image segmentation," in Proceedings of the International Joint Conference on Artificial Intelligence, Vienna, Austria, 10 May 2022.

Falk, T., Mai, D., Bensch, R., Çiçek, Ö., Abdulkadir, A., and Marrakchi, Y. (2019). U-net: Deep learning for cell counting, detection, and morphometry. *Nat. Methods* 16 (1), 67–70. doi:10.1038/s41592-018-0261-2

Fan, J., Cao, X., Wang, Q., Yap, P., and Shen, D. (2019). Adversarial learning for mono- or multi-modal registration. *Med. image Anal.* 58, 101545. doi:10.1016/j.media.2019.101545

Ghezelbash, F., Schmidt, H., Shirazi-Adl, A., and El-Rich, M. (2020). Internal load-sharing in the human passive lumbar spine: Review of *in vitro* and finite element model studies. *J. Biomech.* 102, 109441. doi:10.1016/j.jbiomech.2019.109441

Gilbert, H., Hendrick, R., Remirez, A., and Webster, R., III (2014). A robot for transnasal surgery featuring needle-sized tentacle-like arms. *Expert Rev. Med. devices* 11 (1), 5–7. doi:10.1586/17434440.2013.854702

Gladman, A. S., Matsumoto, E. A., Nuzzo, R. G., Mahadevan, L., and Lewis, J. A. (2016). Biomimetic 4D printing. *Nat. Mat.* 15 (4), 413–418. doi:10.1038/nmat4544

Gojcic, Z., Zhou, C., Wegner, J. D., and Wieser, A. (2019). "The perfect match: 3d point cloud matching with smoothed densities," in Proceedings of the IEEE Conference on Computer Vision and Pattern Recognition, Long Beach, CA, June 15–20, 2019, 5545–5554.

Gosline, A. H., Vasilyev, N. V., Veeramani, A., Wu, M., Schmitz, G., Chen, R., et al. (2012). Metal MEMS tools for beating-heart tissue removal. IEEE Int. Conf. Robot. Autom, Saint Paul, MN, May 14–18, 2012, 1921–1926. doi:10.1109/ICRA.2012.6225210

Graham, A. E., Xie, S. Q., Aw, K. C., Mukherjee, A. S., and Xu, W. L. (2008). Bone–muscle interaction of the fractured femur. *J. Orthop. Res.* 26 (8), 1159–1165. doi:10.1002/jor.20611

Groll, J., Burdick, J. A., Cho, D. W., Derby, B., Gelinsky, M., Heilshorn, S. C., et al. (2018). A definition of bioinks and their distinction from biomaterial inks. *Biofabrication* 11 (1), 013001. doi:10.1088/1758-5090/aaec52

Guo, N., Yang, B., Ji, X., Wang, Y., Hu, L., and Wang, T. (2019). Intensity-based 2D-3D registration for an ACL reconstruction navigation system. *Int. J. Med. Robot.* 15, e2008. doi:10.1002/rcs.2008

Han, L., Lyu, Y., and Peng, C., GAN-based disentanglement learning for chest X-ray rib suppression. Preprint, 2021.

Hatamizadeh, A., Nath, V., Tang, Y., Yang, D., Roth, H. R., and Xu, D. (2021). Swin UNETR: Swin transformers for semantic segmentation of brain tumors in MRI images. *Brainlesion Glioma, Multiple Scler. Stroke Trauma. Brain Inj. BrainLes* 2021, 272–284. doi:10.1007/978-3-031-08999-2_22

Hatamizadeh, A., Yang, D., and Roth, H., (2022). "Unetr: Transformers for 3D medical image segmentation," in 2022 IEEE/CVF Winter Conference on Applications of Computer Vision (WACV), Waikoloa, HI, 15 February 2022. doi:10.1109/WACV51458.2022.00181

Hsieh, C. I., Zheng, K., Lin, C., Mei, L., Lu, L., Li, W., et al. (2021). Automated bone mineral density prediction and fracture risk assessment using plain radiographs via deep learning. *Nat. Commun.* 12, 5472. doi:10.1038/s41467-021-25779-x

Huang, Q., Sun, J., Hui, D., Wang, X., and Wang, G. (2018). Robust liver vessel extraction using 3D U-Net with variant dice loss function. *Comput. Biol. Med.* 101, 153–162. doi:10.1016/j.compbiomed.2018.08.018

Huang, X., Mei, G., and Zhang, J., A comprehensive survey on point cloud registration. Preprint, 2021.

Huang, B., Cao, B., Zhang, J., Feng, Y., Wang, L., Chen, X., et al. (2021). Induction of ferroptosis in human nasopharyngeal cancer cells by cucurbitacin B: Molecular mechanism and therapeutic potential. *Cell Death Dis.* 1, 237–267. doi:10.1038/s41419-021-03516-y

Hughes, A. J., DeBuitleir, C., Soden, P., O'Donnchadha, B., Tansey, A., Abdulkarim, A., et al. (2017). 3D printing aids acetabular reconstruction in complex revision hip arthroplasty. *Adv. Orthop.* 2017, 1–7. doi:10.1155/2017/8925050

Iglovikov, V., and Shvets, A. TernausNet: U-net with VGG11 encoder pre-trained on ImageNet for image segmentation, Preprint, 2018.

Ionov, L. (2018). 4D biofabrication: Materials, methods, and applications. *Adv. Healthc. Mat.* 7 (17), e1800412. doi:10.1002/adhm.201800412

Isensee, F., Jaeger, P. F., Kohl, S. A. A., Petersen, J., and Maier-Hein, K. (2021). nnU-Net: a self-configuring method for deep learning-based biomedical image segmentation. *Nat. Methods* 18 (2), 203–211. doi:10.1038/s41592-020-01008-z

Jamwal, P. K., Hussain, S., and Ghayesh, M. H. (2021). Intrinsically compliant parallel robot for fractured femur reduction: Mechanism optimization and control. *Robotics Aut. Syst.* 141, 103787. doi:10.1016/j.robot.2021.103787

Jiang, J., Cetin, E., and Celiktutan, O. (2021). "IB-DRR: Incremental learning with information-back discrete representation replay," in Proceedings of the 2021 IEEE/CVF Conference on Computer Vision and Pattern Recognition Workshops (CVPRW), Nashville, TN, USA, 19-25 June 2021.

Jin, Q., Meng, Z., Sun, C., and Leyi, W. (2018). Ran SRA-UNet: A hybrid deep attention-aware network to extract liver and tumor in CT scans. *J. latex Cl. files octber*. doi:10.3389/fbioe.2020.605132

Jodat, Y. A., Kiaee, K., Jarquin, D. V., Hernández, R., Wang, T., Joshi, S., et al. (2020). A 3D-printed hybrid nasal cartilage with functional electronic olfaction. *Adv. Sci. (Weinh).* 7 (5), 1901878. doi:10.1002/advs.201901878

Jordi, M., Anne, E., Maureen, v. E., Ruben, P., Tymour, F., Kees, J. B., et al. (2022). A review on the application of deep learning for CT reconstruction, bone segmentation and surgical planning in oral and maxillofacial surgery. *Dentomaxillofacial Radiol.* 51, 20210437. doi:10.1259/dmfr.20210437

Kam, J., Gan, C., Dimou, S., Awad, M., Kavar, B., Nair, G., et al. (2019). Learning curve for robot-assisted percutaneous pedicle screw placement in thoracolumbar surgery. *Asian Spine J.* 13 (6), 920–927. doi:10.31616/asj.2019.0033

Kang, H. W., Lee, S. J., Ko, I. K., Kengla, C., Yoo, J. J., and Atala, A. (2016). A 3D bioprinting system to produce human-scale tissue constructs with structural integrity. *Nat. Biotechnol.* 34 (3), 312–319. doi:10.1038/nbt.3413

Kawai, T., Shanjani, Y., Fazeli, S., Behn, A. W., Okuzu, Y., Goodman, S. B., et al. (2018). Customized, degradable, functionally graded scaffold for potential treatment of early stage osteonecrosis of the femoral head. *J. Orthop. Res.* 36 (3), 1002–1011. doi:10.1002/jor.23673

Kesner, S. B., and Howe, R. D. (2011). "Force control of flexible catheter robots for beating heart surgery," *IEEE Int Conf Robot Autom.*, 2011, 1589–1594. doi:10.1109/ICRA.2011.5979690

Kolařík, M., Burget, R., Uher, V., Říha, K., and Dutta, M. K. (2019). Optimized high resolution 3D dense-U-net network for brain and spine segmentation. *Appl. Sci. (Basel).* 9, 404. doi:10.3390/app9030404

Kolesky, D. B., Truby, R. L., Gladman, A. S., Busbee, T. A., Homan, K. A., and Lewis, J. A. (2014). 3D bioprinting of vascularized, heterogeneous cell-laden tissue constructs. *Adv. Mat.* 26 (19), 3124–3130. doi:10.1002/adma.201305506

Kramer, J., Scheurecker, G., Scheurecker, A., et al. (2009). *Femoral head necrosis*. Dordrecht, Netherlands: Springer Netherlands.

Lampen, N., Kim, D., Fang, X., Xu, X., Kuang, T., Deng, H. H., et al. (2022). Deep learning for biomechanical modeling of facial tissue deformation in orthognathic surgical planning. *Int. J. Comput. Assist. Radiol. Surg.* 17, 945–952. doi:10.1007/s11548-022-02596-1

Lee, H. S., Go, G., Choi, E., Kang, B., Park, J. O., and Kim, C. S. (2020). Medical microrobot - wireless manipulation of a drug delivery carrier through an external ultrasonic actuation: Preliminary results. *Int. J. Control Autom. Syst.* 18 (1), 175–185. doi:10.1007/s12555-019-0239-6

Le-Huu, D. K., and Paragios, N. (2017). "Alternating direction graph matching," in Proceedings of the 2017 IEEE Conference on Computer Vision and Pattern Recognition (CVPR), Hawaii, United States, July 2017, (IEEE), 4914–4922. doi:10.1109/CVPR.2017.522

Lei, J., Zheng, G., and Hu, L., (2019). "Force/position control simulation of robot-assisted fracture reduction," in Proceedings of the 2019 WRC Symposium on Advanced Robotics and Automation (WRC SARA) (IEEE), 21-22 August 2019, Beiging, China.

Levine, S., Finn, C., Darrell, T., and Abbeel, P. (2016). End-to-End training of deep visuomotor policies. *J. Mach. Learn. Res.* 17 (1), 1334–1373. doi:10.1016/j.dam.2015.09.011

Li, X., Hao, C., Qi, X., Qi, D., Fu, C. W., and HengH-DenseUNet, P. A. (2017). H-DenseUNet: Hybrid densely connected UNet for liver and tumor segmentation from CT volumes. *IEEE Trans. Med. Imaging* 37 (12), 2663–2674. doi:10.1109/TMI.2018.2845918

Li, J., Dunstan, C. R., Entezari, A., Li, Q., Steck, R., Saifzadeh, S., et al. (2019). A novel bone substitute with high bioactivity, strength, and porosity for repairing large and load-bearing bone defects. *Adv. Healthc. Mat.* 8 (8), 1801298. doi:10.1002/adhm.201801298

Li, Y., Pavanram, P., Zhou, J., Lietaert, K., Taheri, P., Li, W., et al. (2020). Additively manufactured biodegradable porous zinc. *Acta Biomater.* 101, 609–623. doi:10.1016/j.actbio.2019.10.034

Liang, P., Chen, J., and Zheng, H., (2019). "Cascade decoder: A universal decoding method for biomedical image segmentation," in Proceedings of the 2019 IEEE 16th International Symposium on Biomedical Imaging (ISBI 2019), Venice, Italy, April 8–11, 2019 (IEEE), pp. 339–342. doi:10.1109/ISBI.2019.8759430

Lin, C., Lv, J., Li, Y., Zhang, F., and Liu, Y., (2019). 4D-Printed biodegradable and remotely controllable shape memory occlusion devices. *Adv. Funct. Mat.* 29 (51), 1906569. doi:10.1002/adfm.201906569

Liu, Y., Wang, R., Chen, S., Xu, Z., Wang, Q., Yuan, P., et al. (2020). Heparan sulfate loaded polycaprolactone-hydroxyapatite scaffolds with 3D printing for bone defect repair. *Int. J. Biol. Macromol.* 148, 153–162. doi:10.1016/j.ijbiomac.2020.01.109

Liu, B., Sun, C., Hou, G., Yang, Z., Liu, Z., Tian, G., et al. (2021). Clinical application of 3D printing technology: Bone defect reconstruction of limbs based on 'precision orthopaedics'. *Chin. J. Minim. Invasive Surg.* 21 (4), 303–308. doi:10.3969/j.issn.1009-6604.2021.04.004

Loebel, C., and Burdick, J. A. (2018). Engineering stem and stromal cell therapies for musculoskeletal tissue repair. *Cell Stem Cell* 22 (3), 325–339. doi:10.1016/j.stem.2018.01.014

Lopez, C., Gazgalis, A., Boddapati, V., Shah, R. P., Cooper, H. J., and Geller, J. A. (2021). Artificial learning and machine learning decision guidance applications in

total hip and knee arthroplasty: A systematic review. *Arthroplast. Today* 11, 103–112. doi:10.1016/j.artd.2021.07.012

Lopez, F., Varela, A., Hinojosa, O., Mendez, M., Trinh, D. H., ElBeze, Y., et al. Assessing deep learning methods for the identification of kidney stones in endoscopic images. Proceedings of the 2021 43rd Annual International Conference of the IEEE Engineering in Medicine & Biology Society (EMBC), Mexico, 2021: 2778–2781. doi:10.1109/EMBC46164.2021.9630211

Lu, J., Ofverstedt, J., Lindblad, J., and Sladoje, N. Is image-to-image translation the panacea for multimodal image registration? A comparative study. 2021, ArXiv, 2021 abs/2103.16262.

Luo, Y., Zhai, D., Huan, Z., Zhu, H., Xia, L., Chang, J., et al. (2015). Three-dimensional printing of hollow-struts-packed bioceramic scaffolds for bone regeneration. *ACS Appl. Mat. Interfaces* 7 (43), 24377–24383. doi:10.1021/acsami.5b08911

Mahler, J., Matl, M., Satish, V., Danielczuk, M., DeRose, B., McKinley, S., et al. (2019). Learning ambidextrous robot grasping policies. *Sci. Robot.* 4 (26), eaau4984. doi:10.1126/scirobotics.aau4984

Makvandi, P., Wang, C., Zare, E. N., Borzacchiello, A., Niu, L., and Tay, F. R. (2020). Metal-based nanomaterials in biomedical applications: Antimicrobial activity and cytotoxicity aspects. *Adv. Funct. Mat.* 30 (22), 1910021. doi:10.1002/adfm.201910021

Mandlekar, A., Zhu, Y., and Garg, A., Robo Turk: A crowdsourcing platform for robotic skill learning through imitation. Proceedings of the International Conference on Robot Learning, Zürich, Switzerland, 2018:1–15.

Mannoor, M. S., Jiang, Z., James, T., Kong, Y., Malatesta, K. A., Soboyejo, W. O., et al. (2013). 3D printed bionic ears. *Nano Lett.* 13 (6), 2634–2639. doi:10.1021/nl4007744

Marban, A., Srinivasan, V., and Samek, W., (2018). "Estimation of interaction forces in robotic surgery using a semi-supervised deep neural network model," in Proceedings of the 2018 IEEE/RSJ International Conference on Intelligent Robots and Systems (IROS) (IEEE), 01-05 Oct. 2018, Madrid, Spain.

Mistry, S., Kundu, D., Datta, S., and Basu, D. (2015). Comparison of bioactive glass coated and hydroxyapatite coated titanium dental implants in the human jaw bone. *Aust. Dent. J.* 56 (1), 68–75. doi:10.1111/j.1834-7819.2010.01305.x

Molnar, D., Enqvist, O., Ulén, J., Larsson, M., Brandberg, J., Johnsson, A. A., et al. (2021). Artificial intelligence based automatic quantification of epicardial adipose tissue suitable for large scale population studies. *Sci. Rep.* 11 (1), 23905. doi:10.1038/s41598-021-03150-w

Naghieh, S., Sarker, M. D., Sharma, N. K., Barhoumi, Z., and Chen, X. (2020). Printability of 3D printed hydrogel scaffolds: Influence of hydrogel composition and printing parameters. *Appl. Sci. (Basel).* 10 (1), 292. doi:10.3390/app10010292

Neumann, D. A. (2010). *Kinesiology of the musculoskeletal system*. Maryland Heights, Missouri, United States: Mosby, Elsevier.

Nicolas, N., Emilie, C. S., Vincent, C., Benoit, B., Matthieu, V., and Julien, B. (2016). Robot-assisted spine surgery: Feasibility study through a prospective case-matched analysis. *Eur. Spine J.* 25 (3), 947–955. doi:10.1007/s00586-015-3758-8

Pei, G. X., and Yan, Y. B. (2014). Current status and progress of digital orthopaedics in China. *J. Orthop. Transl.* 2 (3), 107–117. doi:10.1016/j.jot.2014.05.001

Polce, E. M., Kunze, K. N., and Paul, K. M. (2021). Machine learning predicts femoral and tibial implant size mismatch for total knee arthroplasty. *Arthroplasty Today* 8 (11), 268–277. doi:10.1016/j.artd.2021.01.006

Qi, G., Dunn, C. K., Qi, H. J., and Dunn, M. L. (2014). Active origami by 4D printing. *Smart Mater. Struct.* 23 (9), 094007. doi:10.1088/0964-1726/23/9/094007

Qi, C. R., Su, H., Mo, K., and Guibas, L. J. (2017). "Pointnet: Deep learning on point sets for 3d classification and segmentation," in Proceedings of the IEEE Conference on Computer Vision and Pattern Recognition, Hawaii, United States, July 2017, pp. 77–85. doi:10.1109/CVPR.2017.16

Raviv, D., Zhao, W., Mcknelly, C., Papadopoulou, A., Kadambi, A., Shi, B., et al. (2014). Active printed materials for complex self-evolving DeformationsActive printed materials for complex self-evolving deformations. *Sci. Rep.* 4, 7422. doi:10.1038/srep07422

Ren, X., Tu, V., Bischoff, D., Weisgerber, D. W., Lewis, M. S., Yamaguchi, D. T., et al. (2016). Nanoparticulate mineralized collagen scaffolds induce *in vivo* bone regeneration independent of progenitor cell loading or exogenous growth factor stimulation. *Biomaterials* 89, 67–78. doi:10.1016/j.biomaterials.2016.02.020

Rezwan, K., Chen, Q. Z., Blaker, J. J., and Boccaccini, A. R. (2006). Biodegradable and bioactive porous polymer/inorganic composite scaffolds for bone tissue engineering. *Biomaterials* 27 (18), 3413–3431. doi:10.1016/j.biomaterials.2006.01.039

Rogers, M. A., and Aikawa, E. (2019). Cardiovascular calcification: Artificial intelligence and big data accelerate mechanistic discovery. *Nat. Rev. Cardiol.* 16 (5), 261–274. doi:10.1038/s41569-018-0123-8

Roohani-Esfahani, S. I., Lu, Z. F., Li, J. J., Ellis-Behnke, R., Kaplan, D. L., and Zreiqat, H. (2012). Effect of self-assembled nanofibrous silk/polycaprolactone layer on the osteoconductivity and mechanical properties of biphasic calcium phosphate scaffolds. *Acta biomater.* 8 (1), 302–312. doi:10.1016/j.actbio.2011.10.009

Ruberu, K., Senadeera, M., Rana, S., Gupta, S., Chung, J., Yue, Z., et al. (2021). Coupling machine learning with 3D bioprinting to fast track optimisation of extrusion printing. *Appl. Mater. Today* 22, 100914. doi:10.1016/j.apmt.2020.100914

Salehi, S. S. M., Erdogmus, D., and Gholipour, A. "Tversky loss function for image segmentation using 3D fully convolutional deep networks," in Proceedings of the Machine Learning in Medical Imaging, Quebec City, QC, September 2017 (Springer). doi:10.1007/978-3-319-67389-9_44

Sanchez-Romero, R., Ramsey, J. D., and Zhang, K., Causal discovery of feedback networks with functional magnetic resonance imaging, Preprint, 2018.

Senatov, F. S., Niaza, K. V., Zadorozhnyy, M. Y., Maksimkin, A. V., Kaloshkin, S. D., and Estrin, Y. Z., (2016). Mechanical properties and shape memory effect of 3D-printed PLA-based porous scaffolds. *J. Mech. Behav. Biomed. Mater.* 57, 139–148. doi:10.1016/j.jmbbm.2015.11.036

Shademan, A., Decker, R. S., Opfermann, J. D., Leonard, S., Krieger, A., and Kim, P. C. W. (2016). Supervised autonomous robotic soft tissue surgery. *Sci. Transl. Med.* 8 (337), 337ra64. 337ra64-337ra64. doi:10.1126/scitranslmed.aad9398

Shi, J., Song, J., Song, B., and Lu, W. (2019). Multi-objective optimization design through machine learning for drop-on-demand bioprinting. *Engineering* 5 (3), 586–593. doi:10.1016/j.eng.2018.12.009

Siebenrock, K. A., Powell, J. N., and Ganz, R. (2010). Osteochondritis dissecans of the femoral head. *HIP Int.* 20 (4), 489–496. doi:10.1177/112070001002000412

Siemionow, K. B., Forsthoefel, C. W., Foy, M. P., Gawel, D., and Luciano, C. J. (2021). Autonomous lumbar spine pedicle screw planning using machine learning: A validation study. *J. Craniovertebral Junction Spine* 12 (3), 223–227.

Silver, D., Huang, A., Maddison, C. J., Guez, A., Sifre, L., van den Driessche, G., et al. (2016). Mastering the game of Go with deep neural networks and tree search. *Nature* 529 (7587), 484–489. doi:10.1038/nature16961

Soodmand, E., Zheng, G., Steens, W., Bader, R., Nolte, L., and Kluess, D. (2019). Surgically relevant morphological parameters of proximal human femur: A statistical analysis based on 3D reconstruction of CT data. *Orthop. Surg.* 11, 135–142. doi:10.1111/os.12416

Su, J. W., Gao, W., Trinh, K., Kendere, S. M., Pulatsu, E. T., Zhang, C., et al. (2019). 4D printing of polyurethane paint-based composites. *Int. J. Smart Nano Mater.* (29), 1–12. doi:10.1080/19475411.2019.1618409

Sun, F., Liu, C., and Huang, W., (2017). Object classification and grasp planning using visual and tactile sensing. *IEEE Trans. Syst. Man Cybern. Syst.* 46 (7), 969–979. doi:10.1109/TSMC.2016.2524059

Thananjeyan, B., Garg, A., and Krishnan, S., (2017). "Multilateral surgical pattern cutting in 2D orthotropic gauze with deep reinforcement learning policies for tensioning," in Proceedings of the 2017 IEEE International Conference on Robotics and Automation (ICRA) (IEEE). 29 May 2017-03 June 2017, Singapore.

Thitiset, T., Damrongsakkul, S., Bunaprasert, T., Leeanansaksiri, W., and Honsawek, S. (2013). Development of collagen/demineralized bone powder scaffolds and periosteum-derived cells for bone tissue engineering application. *Int. J. Mol. Sci.* 14 (1), 2056–2071. doi:10.3390/ijms14012056

Tian, W., Liu, Y., Liu, B., He, D., Wu, J., Han, X., et al. (2019). Guideline for thoracolumbar pedicle screw placement assisted by orthopaedic surgical robot. *Orthop. Surg.* 11 (2), 153–159. doi:10.1111/os.12453

Tibbits, S. (2014). 4D printing: Multi-material shape change. *Archit. Des.* 84 (1), 116–121. doi:10.1002/ad.1710

Turnbull, G., Clarke, J., Picard, F., Riches, P., Jia, L., Han, F., et al. (2018). 3D bioactive composite scaffolds for bone tissue engineering. *Bioact. Mater.* 3 (3), 278–314. doi:10.1016/j.bioactmat.2017.10.001

Unberath, M., Zaech, A.-N., and Lee, S. C., (2018). "DeepDRR – a catalyst for machine learning in fluoroscopy-guided procedures," in *Medical image computing and computer assisted intervention – MICCAI 2018. MICCAI 2018. Lecture notes in computer science*. Editors A. Frangi, J. Schnabel, C. Davatzikos, C. Alberola-López, and G. Fichtinger (Cham: Springer), 11073. doi:10.1007/978-3-030-00937-3_12

Unnithan, A. R., Sasikala, A. R. K., Park, C. H., and Kim, C. S. (2017). A unique scaffold for bone tissue engineering: An osteogenic combination of graphene oxide–hyaluronic acid–chitosan with simvastatin. *J. Industrial Eng. Chem.* 46, 182–191. doi:10.1016/j.jiec.2016.10.029

Van Belleghem, S., Torres, L., Santoro, M., Mahadik, B., Wolfand, A., Kofinas, P., et al. (2020). Hybrid 3D printing of synthetic and cell-laden bioinks for shape retaining soft tissue grafts. *Adv. Funct. Mat.* 30 (3), 1907145. doi:10.1002/adfm.201907145

Vijayan, R., Silva, T. D., Han, R., Zhang, X., Uneri, A., Doerr, S., et al. (2019). Automatic pedicle screw planning using atlas-based registration of anatomy and

reference trajectories. *Phys. Med. Biol.* 64 (16), 165020. doi:10.1088/1361-6560/ab2d66

Villa, M. M., Wang, L., Huang, J., Rowe, D. W., and Wei, M. (2015). Bone tissue engineering with a collagen-hydroxyapatite scaffold and culture expanded bone marrow stromal cells. *J. Biomed. Mat. Res.* 103 (2), 243–253. doi:10.1002/jbm.b.33225

Viris, A., Stefanoudakis, G., Petousis, M., Vidakis, N., Tsainis, A. M., and Kandyla, B. (2016). Evaluation of an intact, an ACL-deficient, and a reconstructed human knee joint finite element model. *Comput. Methods Biomech. Biomed. Engin.* 19 (3), 263–270. doi:10.1080/10255842.2015.1015526

Wang, Y., and Solomon, J. M. . Deep closest point: Learning representations for point cloud registration. Preprint, 2019.

Wang, T., Wang, L., and Tang, P., (2018). Automatic bone segmentation and ultrasound—CT registration for robotic assisted femoral shaft fracture reduction. *J. Med. Imaging Health Inf.* 8 (1), 151–156(6). doi:10.1166/jmihi.2018.2249

Wang, J., Liu, H., Ke, J., Hu, L., Zhang, S., Yang, B., et al. (2020). Image-guided cochlear access by non-invasive registration: A cadaveric feasibility study. *Sci. Rep.* 10, 18318. doi:10.1038/s41598-020-75530-7

Wang, S., Xie, Z., Yuan, F., Li, L., Liu, Y., Wang, T., et al. (2022). Bio-inspired physical intelligence for soft robotics. *Chin. Sci. Bull.* 67 (10), 959–975. doi:10.1360/TB-2021-1217

Watanabe, H., Kanou, K., Kobayashi, Y., and Fujie, M. G. (2011). "Development of a "steerable drill" for ACL reconstruction to create the arbitrary trajectory of a bone tunnel[C]," in IEEE/RSJ International Conference on Intelligent Robots and Systems, IROS 2011, San Francisco, CA, September 25–30, 2011 (IEEE).

Wells, T. S., Yang, S., Maclachlan, R. A., Lobes, L. A., Martel, J. N., and Riviere, C. N. (2016). Hybrid position/force control of an active handheld micromanipulator for membrane peeling. *Int. J. Med. Robot. Comput. Assist. Surg.* 12 (1), 85–95. doi:10.1002/rcs.1659

Wilkening, P., Alambeigi, F., Murphy, R. J., Taylor, R. H., and Armand, M. (2017). Development and experimental evaluation of concurrent control of a robotic arm and continuum manipulator for osteolytic lesion treatment. *IEEE Robot. Autom. Lett.* 2 (3), 1625–1631. doi:10.1109/LRA.2017.2678543

Wu, H., Lei, P., Liu, G., Zhang, Y. S., Yang, J., Zhang, L., et al. (2017). Reconstruction of large-scale defects with a novel hybrid scaffold made from poly(L-lactic acid)/Nanohydroxyapatite/Alendronate-loaded chitosan microsphere: *In vitro* and *in vivo* studies. *Sci. Rep.* 7 (1), 359. doi:10.1038/s41598-017-00506-z

Wubneh, A., Tsekoura, E. K., Ayranci, C., and Uludağ, H. (2018). Current state of fabrication technologies and materials for bone tissue engineering. *Acta Biomater.* 80, 1–30. doi:10.1016/j.actbio.2018.09.031

Xiao, D., Lian, C., Deng, H., Kuang, T., Liu, Q., Ma, L., et al. (2021). Estimating reference Bony shape models for orthognathic surgical planning using 3D point-cloud deep learning. *IEEE J. Biomed. Health Inf.* 25 (8), 2958–2966. Epub 2021 Aug 5. PMID: 33497345; PMCID: PMC8310896. doi:10.1109/JBHI.2021.3054494

Xie, R., Hu, J., Ng, F., Tan, L., Qin, T., Zhang, M., et al. (2017). High performance shape memory foams with isocyanate-modified hydroxyapatite nanoparticles for minimally invasive bone regeneration. *Ceram. Int.* 43 (6), 4794–4802. doi:10.1016/j.ceramint.2016.11.216

Xie, R., Hu, J., Hoffmann, O., Zhang, Y., Ng, F., Qin, T., et al. (2018). Self-fitting shape memory polymer foam inducing bone regeneration: A rabbit femoral defect study. *Biochimica Biophysica Acta - General Subj.* 1862 (4), 936–945. doi:10.1016/j.bbagen.2018.01.013

Xu, T., Binder, K. W., Albanna, M. Z., Dice, D., Zhao, W., Yoo, J. J., et al. (2013). Hybrid printing of mechanically and biologically improved constructs for cartilage tissue engineering applications. *Biofabrication* 5 (1), 015001. doi:10.1088/1758-5082/5/1/015001

Xu, X., Tao, J., Wang, S., Yang, L., Zhang, J., Zhang, J., et al. (2019). 3D printing of nerve conduits with nanoparticle-encapsulated RGFP966. *Appl. Mater. Today* 16, 247–256. doi:10.1016/j.apmt.2019.05.014

Xu, B., Han, X., Hu, Y., Lou, Y., Chen, C., Chen, Z., et al. (2019). A remotely controlled transformable soft robot based on engineered cardiac tissue construct. *Small* 15 (18), e1900006. doi:10.1002/smll.201900006

Yan, K., Cai, J., Jin, D., Miao, S., Guo, D., Harrison, A. P., et al. (2022). Sam: Self-Supervised learning of pixel-wise anatomical embeddings in radiological images. *IEEE Trans. Med. Imaging*, 1. doi:10.1109/TMI.2022.3169003

Yasaka, K., Akai, H., Kunimatsu, A., Kiryu, S., and Abe, O. (2020). Prediction of bone mineral density from computed tomography: Application of deep learning with a convolutional neural network. *Eur. Radiol.* 30 (6), 3549–3557. PMID: 32060712. doi:10.1007/s00330-020-06677-0

Ye, R., and Chen, Y. (2009). "Path planning for robot assisted femur shaft fracture reduction: A preliminary investigation," in Proceedings of the 2009 IEEE International Conference on Virtual Environments, Human-Computer Interfaces and Measurements Systems (IEEE), 11-13 May 2009, Hong Kong, China, 113–117. doi:10.1109/VECIMS.2009.5068876

Yu, C., and Jiang, J. (2020). A perspective on using machine learning in 3D bioprinting. *Int. J. Bioprint.* 6 (1), 253. doi:10.18063/ijb.v6i1.253

Yuan, W., Eckart, B., Kim, K., Jampani, V., Fox, D., and Kautz, J. (2020). "DeepGMR: Learning Latent Gaussian Mixture Models for Registration," in Computer Vision – ECCV 2020. ECCV 2020. Lecture Notes in Computer Science, October 29, 2020. Editors A. Vedaldi, H. Bischof, T. Brox, and J. M. Frahm (Springer, Cham) vol 12350. doi:10.1007/978-3-030-58558-7_43

Zappetti, D., Jeong, S. H., Shintake, J., and Floreano, D. (2020). Phase changing materials-based variable-stiffness tensegrity structures. *Soft Robot.* 7 (3), 362–369. doi:10.1089/soro.2019.0091

Zeng, G., Yang, X., and Li, J., (2017). "3D U-net with multi-level deep supervision: Fully automatic segmentation of proximal femur in 3D MR images," in Proceedings of the International Workshop on Machine Learning in Medical Imaging, Cham (Springer).

Zhang, D., Burkes, W. L., Schoener, C. A., and Grunlan, M. A. (2012). Porous inorganic–organic shape memory polymers. *Polymer* 53 (14), 2935–2941. doi:10.1016/j.polymer.2012.04.053

Zhang, D., George, O. J., Petersen, K. M., Jimenez-Vergara, A. C., Hahn, M. S., and Grunlan, M. A. (2014). A bioactive "self-fitting" shape memory polymer scaffold with potential to treat cranio-maxillo facial bone defects. *Acta biomater.* 10 (11), 4597–4605. doi:10.1016/j.actbio.2014.07.020

Zhang, Y. S., Andrea, A., Simone, B., Su-Ryon, S., Kai, Z., Zahra, G. M., et al. (2016). Bioprinting 3D microfibrous scaffolds for engineering endothelialized myocardium and heart-on-a-chip. *Biomaterials* 110, 45–59. doi:10.1016/j.biomaterials.2016.09.003

Zhang, Z., Ma, Z., Zhang, Y., Chen, F., Zhou, Y., and An, Q. (2018). Dehydrothermally crosslinked collagen/hydroxyapatite composite for enhanced *in vivo* bone repair. *Colloids Surfaces B Biointerfaces* 163, 394–401. doi:10.1016/j.colsurfb.2018.01.011

Zhang, R., Wu, S., Wu, W., Gao, H., and Zhou, Z. (2019). Computer-assisted needle trajectory planning and mathematical modeling for liver tumor thermal ablation: A review. *Math. Biosci. Eng.* 16 (5), 4846–4872. PMID: 31499693. doi:10.3934/mbe.2019244

Zhang, Y. (2018). *Springer, Singapore. Jointly published with People's Medical Publishing House, Beijing, China* (eBook). doi:10.1007/978-981-10-6044-1

Zheng, G., and Yu, W. (2017). Statistical shape and deformation models based 2D–3D reconstruction. *Stat. Shape Deformation Analysis*, 329–349. doi:10.1016/b978-0-12-810493-4.00015-8

Zheng, G., Tian, W., and Zhuang, X. (2018). "Biomechanical optimization-based planning of periacetabular osteotomy: Artificial intelligence and smart image-guided technology for orthopaedics," in *Intelligent orthopaedics* 1093, 157–168. doi:10.1007/978-981-13-1396-7_13

Zheng, W., Wang, Y., Zhang, F., Li, C., Liu, Y., and Leng, J. (2018). Development of shape memory polymers micro/nanofiber membranes in biomedical applications. *Sci. Sin. -Tech.* 48 (8), 811–826. doi:10.1360/n092018-00126

Zheng, W., Dong, X., He, Y., Liu, Y., and Leng, J. (2021). Development of bioactive polymers and their composite materials in bone tissue engineering. *J. Harbin Inst. Technol.* 53 (8), 1. doi:10.11918/202007079

Zhou, X. Y., Guo, Y., Shen, M., and Yang, G. Z. (2020). Application of artificial intelligence in surgery. *Front. Med.* 14 (4), 417–430. doi:10.1007/s11684-020-0770-0

Zhou, Z., Siddiquee, M., Tajbakhsh, N., and Liang, J. (2020). UNet++: Redesigning skip connections to exploit multiscale features in image segmentation. *IEEE Trans. Med. Imaging* 39 (6), 1856–1867. doi:10.1109/tmi.2019.2959609

Zimmerbiomet The Smart Knee® by combining the power of Persona® the Personalized Knee® with CANARY caturio te with CHIRP system, Persona IQ is smart, connected and simple. Available at: https://www.zimmerbiomet.com/en/products-and-solutions/specialties/knee/persona-iq.html [Accessed August 20,2021]

frontiers | Frontiers in Bioengineering and Biotechnology

TYPE Review
PUBLISHED 06 October 2022
DOI 10.3389/fbioe.2022.1030162

OPEN ACCESS

EDITED BY
Dicky Pranantyo,
Singapore-MIT Alliance for Research and Technology (SMART), Singapore

REVIEWED BY
Xuefeng Hu,
Sichuan University, China
Chao Zhou,
Changzhou University, China
Rong Wang,
Ningbo Institute of Materials Technology and Engineering (CAS), China

*CORRESPONDENCE
Jingfeng Li,
jingfengli@whu.edu.cn

†These authors have contributed equally to this work

SPECIALTY SECTION
This article was submitted to Biomaterials, a section of the journal Frontiers in Bioengineering and Biotechnology

RECEIVED 28 August 2022
ACCEPTED 20 September 2022
PUBLISHED 06 October 2022

CITATION
Hao Z, Chen R, Chai C, Wang Y, Chen T, Li H, Hu Y, Feng Q and Li J (2022), Antimicrobial peptides for bone tissue engineering: Diversity, effects and applications.
Front. Bioeng. Biotechnol. 10:1030162.
doi: 10.3389/fbioe.2022.1030162

Antimicrobial peptides for bone tissue engineering: Diversity, effects and applications

Zhuowen Hao[1†], Renxin Chen[1†], Chen Chai[2†], Yi Wang[1], Tianhong Chen[1], Hanke Li[1], Yingkun Hu[1], Qinyu Feng[1] and Jingfeng Li[1*]

[1]Department of Orthopedics, Zhongnan Hospital of Wuhan University, Wuhan, China, [2]Emergency Center, Hubei Clinical Research Center for Emergency and Resuscitation, Zhongnan Hospital of Wuhan University, Wuhan, China

Bone tissue engineering has been becoming a promising strategy for surgical bone repair, but the risk of infection during trauma repair remains a problematic health concern worldwide, especially for fracture and infection-caused bone defects. Conventional antibiotics fail to effectively prevent or treat bone infections during bone defect repair because of drug-resistance and recurrence, so novel antibacterial agents with limited resistance are highly needed for bone tissue engineering. Antimicrobial peptides (AMPs) characterized by cationic, hydrophobic and amphipathic properties show great promise to be used as next-generation antibiotics which rarely induce resistance and show potent antibacterial efficacy. In this review, four common structures of AMPs (helix-based, sheet-based, coil-based and composite) and related modifications are presented to identify AMPs and design novel analogs. Then, potential effects of AMPs for bone infection during bone repair are explored, including bactericidal activity, anti-biofilm, immunomodulation and regenerative properties. Moreover, we present distinctive applications of AMPs for topical bone repair, which can be either used by delivery system (surface immobilization, nanoparticles and hydrogels) or used in gene therapy. Finally, future prospects and ongoing challenges are discussed.

KEYWORDS

antimicrobial peptides, bone regeneration, topical applications, delivery system, gene therapy

1 Introduction

Bone shows self-healing properties after trauma, but the repair of critical bone defects typically needs surgical therapies such as autogenous bone grafts, allogenous bone grafts and exogenous bone grafts (Zhai et al., 2020). In recent decades, bone tissue engineering shows great promise to become emerging strategy for surgical bone repair, which is mainly composed of four pillars including biomaterial scaffolds, bioactive factors, repair stem cells and biophysical stimuli (Hao et al., 2021). While great advances have been made in bone tissue engineering, the risk of infection during trauma repair remains a

problematic health concern worldwide, especially for fracture and infection caused bone defects. It has been reported that the incidence of fracture-associated bone infections varies from 1.8% to 27% determined by the grade/type of fracture and fracture site (Birt et al., 2017). And bone defects caused by infections are generally correlated to pathogen recurrence. Once infection occurs during bone repair, pathogens may disturb bone regeneration and bone remodeling, resulting in further bone loss and causing enormous economic burden to the patient and society.

Bone infections may be mainly caused by three different mechanisms including contiguous contamination, hematogenous spread, and vascular or neurologic insufficiency (Birt et al., 2017). And common pathogens for bone infections are staphylococci such as *Staphylococcus aureus (S. aureus)* and streptococci. Other microbes such as anaerobes and Gram-negative anaerobic bacilli may also cause bone infections (Chen Y et al., 2021). Current antimicrobial strategies for bone defect infections are mainly based on systematic or topical administration of antibiotics. But antibiotic treatments are currently corrected with antimicrobial resistance because of improper over-reliance and over-prescription, which may cause infection recurrent, prolonged hospitalization and increased medical costs (Browne et al., 2020). Therefore, new generation of antimicrobial agents with limited resistance nature are highly needed in clinical practice.

Antimicrobial peptides (AMPs), also known as cationic host defense peptides (CHDPs), are emerging agents for infection treatments because of broad-spectrum antibacterial properties, controllable biocompatibility, diverse structures and categories. Compared with traditional antibiotics, AMPs rarely induce antimicrobial resistance by virtue of multiple antibacterial modes of action and their attacks to low-affinity targets such as bacterial membranes rather than a highly specific molecule (Zhang Q et al., 2021). Some AMPs, besides, also show immunomodulation capacities and regenerative effects such as cell proliferation and migration as well as angiogenesis. Considering that systemic application of AMPs is impeded by several shortcomings such as easily degradation in blood and rapid withdrawal by liver and kidney, topical administration of AMPs is highly recommended for trauma and infection repair.

Currently, AMPs have been locally used for soft tissue repair such as diabetic foot ulcers, skin infections and burn wounds in clinic traits (Browne et al., 2020; Mahlapuu et al., 2020), and several researches have reviewed their topical application in wound healing (Dart et al., 2019; Nguyen et al., 2020; Thapa et al., 2020). Herein, we first reviewed the topical application of AMPs for bone repair (Figure 1). In this review, diverse structures of AMPs are initially summarized and additional focuses are laid on those in clinic traits. Then potential effects of AMPs for bone tissue engineering are presented, which include bactericidal activity, immunomodulation and regenerative effects. And we also summarize topical strategies to immobilize or deliver AMPs for bone repair. The motivation of this review is to successfully promote the clinical translation of AMPs for bone tissue engineering.

2 Diverse antimicrobial peptides with distinctive structures

AMPs are a series of oligopeptides with 5–100 amino acids, charactered by a cationic character with net charge from +2 to +13, hydrophobicity with generally 50% hydrophobic resides, and amphipathicity which regulate the balance between hydrophilic residues and hydrophobic resides (Kumar et al., 2018). They can be obtained from virtually all organisms including bacteriophages, bacteria, fungus, plants and animals (Bin Hafeez et al., 2021). Depending on their major secondary structures, AMPs can be mainly divided to four groups: helical AMPs, sheet-based AMPs, extended AMPs, and composite AMPs (Figure 2). And some AMPs may further show cyclic structures in head-to-tail, side chain-to-tail, head-to-side chain or side chain-to-side chain models (Chow et al., 2019).

2.1 Helix-based antimicrobial peptides

Many kinds of helical structures exist in nature, such as α-helix, collagen triple helix and β-spinal helix. Most of helical AMPs are based on α-helix which generally has 3.6 amnio acids per turn. The α-helical structure is formed by hydrogen bonds, which are attributed to the interaction between the N-H group of the *n*th residues and the C=O group of $(n-4)^{th}$ residues (Zou et al., 2020). And those redisues that rarely induce steric interference are typically used to construct α-helix, so α-helicalAMPs are rich in Leu, Ala, Gly, and Lys (Bin Hafeez et al., 2021). Common α-helical AMPs mainly include LL-37, magainin, melittin, cecropin, pleurocidin, moricin, aurein1-2, brevinin 1, maculatins, citropin, and buforin (Zou et al., 2020; Bin Hafeez et al., 2021). And some analogs derived from them have been tested in clinical trials.

LL-37 (LLGDFFRKSKEKIGKEFKRIVQRIKDFLRNLVPRTES) is an α-helical AMP with 37 amino acids obtained by proteolytic cleavage from the C-terminal of a human cathelicidin antimicrobial protein named hCAP18, it and its derivatives have been used in clinical trials. Showing +6 net charge under physiological pH, LL-37 has multiple functions for tissue repair including antibacterial and antibiofilm properties, immunomodulation, and angiogenesis. In a phase 2 clinical trial, LL-37 has been topically loaded to cream for the treatment of diabetic foot ulcer (NCT04098562). Another phase 2 clinical trial also explored its therapeutic effects in hard-to-heal venous leg ulcers (EudraCT 2018-000536-10). However, there are mainly three disadvantages corresponding

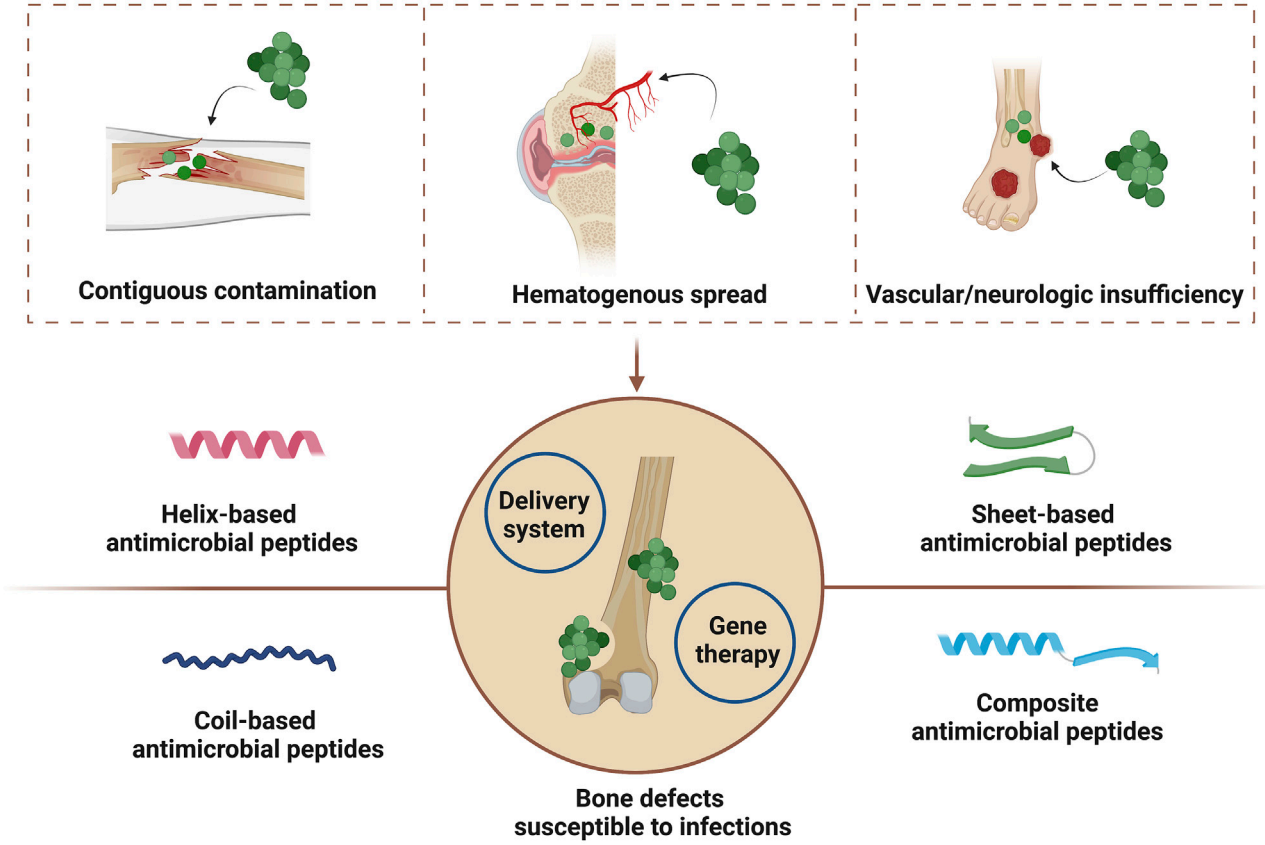

FIGURE 1
Mechanisms of bone infections and antimicrobial peptide-based strategies for the healing of bone defects susceptible to infections. Created with BioRender.com.

to LL-37: high cost for synthesis because of long sequence, rapid protease degradation and existing cytotoxicity and hemolysis (Ridyard and Overhage, 2021). So dozens of LL-37 derivatives have been developed, among which OP-145 (IGKEFKRIVERIKRFLRELVRPLR) has been used to treat chronic suppurative otitis media in clinic trail (ISRCTN12149720).

Pexiganan (GIGKFLKKAKKFGKAFVKILKK) is a synthetic analog derived from magainin (GIGKFLHSAGKFGKAFVGEIMKS), an α-helical AMP with 23 residues in length which is identified from the African clawed frog (*Xenopus laevis*) (Goldstein et al., 2017). The AMP has been tested in several clinical trials. Lipsky et al. compared the treatment efficacy for infection between topical pexiganan cream and systemic oral ofloxacin in patients with mildly infected diabetic foot ulcer, and found that topical pexiganan showed equivalently effective results with oral ofloxacin of clinical improvement rates, microbiological eradication, and wound healing, but without apparent bacterial resistance (NCT00563394 and NCT00563433) (Lipsky et al., 2008). Besides, another group further compare the antimicrobial treatment for mild infections of diabetic foot ulcers between topical pexiganan cream and placebo cream in two phase 3 clinic trails (NCT01590758 and NCT01594762).

Showing an optimized amphiphilic αhelical structure, PLG0206 (RRWVRRVRRWVRRVVRVVRRWVRR) which was firstly named as WLBU2 is another synthetic AMP derived from lentivirus lytic peptide 1, which contains a hydrophilic surface composed of arginine residues and a hydrophobic surface containing valine and tryptophan residues (Deslouches et al., 2005). The AMP has been confirmed to highly target to bacteria with limited toxicity, to reduce biofilm burdens, and to show broad-spectrum antimicrobial activity (Huang et al., 2021). In a phase 1 clinical trial, it has been revealed that the AMP is safe and well tolerated by healthy research objects when it is intravenously infused with doses from 0.05 to 1 mg/kg (Huang et al., 2022). In another clinical trial, PLG0206 have been intravenously tested at 3 mg/kg for microbial infections. (ACTRN12618001920280).

In addition to α helix, other helical structures may also exist in AMPs. For example, PR-39 (RRRPRPPYLPRPRPPPFFPPRLPPRIPPGFPPRFPPRFR) is a proline rich AMP with proline residue accounting for almost half of the amino acid sequence. Although proline residue disturb the formation of α-helix, it was shown that the peptide contains collagen like type II poly-l-proline helix conformation (Holani et al., 2016).

2.2 Sheet-based antimicrobial peptides

Multiple sheet-based structures exist in nature, including parallel β-sheet, anti-parallel β-sheet, and β-hairpin. Most of sheet-based AMPs adopt a β-hairpin like conformation, which contain conserved cysteine residues to form disulfide bonds (Bin Hafeez et al., 2021). Common sheet-based AMPs include protegrins, bactenecin, defensins, tachyplesins, and polyphemusin, and some of their analogs have been used in clinical trials.

Most β-hairpin AMPs and derivatives are isolated or modified from natural AMPs. Protegrin-1 (RGGRLCYCRRRFCVCVGR) isolated form porcine leukocytes is one of β-hairpin like antimicrobial peptides with broad-spectrum antimicrobial activity (Steinberg et al., 1997). Derived from protegrin-1, iseganan and murepavadin have been used in clinal trials. Iseganan, also named as IB-367, has been topically used in oral solution to prevent oral infections after chemotherapy or radiotherapy (Giles et al., 2003; Trotti et al., 2004) Elad et al. (2012). Found that topical application of iseganan in patients suffered from chemotherapy could dramatically lower the loads of oral aerobic bacterial, streptococcal, and yeast. Murepavadin (POL7080) is another protegrin-1 analog, which shows potent antimicrobial activity to extensively drug resistant (XDR) *Pseudomonas aeruginosa* isolated from clinic patients (Sader et al., 2018). Intravenous murepavadin has been tested in clinic trials for the treatment of hospital-acquired bacterial pneumonia (HABP) and ventilator-associated bacterial pneumonia (VABP) caused by *Pseudomonas aeruginosa* (Martin-Loeches et al., 2018). And it has been shown that intravenous murepavadin was well tolerated in healthy subjects and subjects with renal function impairment (Dale et al., 2018; Wach et al., 2018). Bactenecin (RLCRIVVIRVCR) is also a sheet-based AMP showing β-hairpin conformation with a disulfide bond, which shows broad antimicrobial activities (Lee et al., 2008). Sun et al. used strategies of amino acid substitutions to improve net cationic charge and lower hydrophobicity, thus designing six derivatives of bactenecin: RRFRIVVIRWLR, RRWRIVVIRWRR, RKWRIVVIRVRR, RWRRIVVIRVRR, RWKRIVVIRKRR, and RKRRIVVIRRKR. And they found that these derivatives, especially RKWRIVVIRVRR and RWRRIVVIRVRR, showed increased antimicrobial activities and reduced cytotoxicity when compared with bactenecin.

Some β-hairpin like AMPs can be rationally designed depending on the design principles of β-hairpin supramolecular peptides, which could assemble to form nanofiber matrices and show antimicrobial activities. Based on the design principle of β-hairpin supramolecular peptides, Veiga et al. (2012). Designed an arginine-rich AMP named PEP8R (VRVRVRVRV^{D}PPTRVRVRVRV), and they found that hydrogels assembled by PEP6R at 1.5% or higher concentrations show potent antibacterial activities towards *Staphylococcus aureus (S. aureus), Escherichia coli (E. coli)* but with great cytocompatibility. And the difference between β-hairpin like AMPs with both antimicrobial properties as well as assembling properties and those without assembling properties lies in the former follow the structure feature that hydrophobic residues and hydrophilic residues are regularly spaced except some residues to form β-turn structures.

In addition to those AMPs adopting β-hairpin conformation, there are also some iterative β-sheet AMPs. D-IK8 (IRIKIRIK) is an iterative ion-complementary β-sheet AMP composed of D-amino acids, which show enhanced protein stability, increased antimicrobial activities and unchanged hermetic properties when compared with its L-enantiomer (Ong et al., 2014). And it has been revealed that D-IK8 show strong activities against methicillin-resistant *Staphylococcus aureus* (MRSA) (Mohamed et al., 2016). Besides, Jiang et al. (2015). Designed a series of multidomain peptides assembling in β-sheet conformations: $K_2W(QL)_6K_2$, $WK_2(QL)_6K_2$, and $K_3W(QL)_6K_2$, and found that the solution of $K_3W(QL)_6K_2$ showed the best antimicrobial activities with MIC of 20 μM. But when these peptides assembled into nanofiber hydrogels at 2 wt% concentration, $K_3W(QL)_6K_2$ hydrogels with worst mechanical properties demonstrated the lowest antimicrobial properties while $K_2W(QL)_6K_2$ with highest storage modules showed the best bactericidal effect. These results revealed that the antimicrobial effects of hydrogels formed by sheet-based AMPs are determined by surface chemistry and mechanical properties of nanofiber hydrogels.

2.3 Coil-based antimicrobial peptides

Coil-based AMPs present unique structures devoid of both α-helical and β-sheet structures. And these peptides are generally rich in tryptophan, proline, and glycine (Bin Hafeez et al., 2021). Indolicidin (ILPWKWPWWPWRR), which belongs to the cathelicidin family, is one coil-based AMP rich in tryptophan and proline, and the AMP shows high potency against various microorganisms including bacteria, fungi and viruses (Batista Araujo et al., 2022). To improve bioactivity and reduce cytotoxicity, multiple derivatives have been developed, among which omiganan (ILRWPWWPWRRK) has been topically tested in clinic studies. In a randomized controlled trial, topical omiganan gel has been verified to reduce papillomavirus load

in patients with external anogenital warts (Rijsbergen et al., 2020). Two clinic research GL13K explored the effects of topical omiganan gel for atomic dermatitis patients, and the results revealed that the AMP could reduce *Staphylococcus* genus and improve microbial diversity (Niemeyer-van der Kolk et al., 2020; Niemeyer-van der Kolk et al., 2022). And omifanan was also tested in other clinic diseases such as atheter infections (NCT00231153) and acne vulgaris (NCT02571998) (Mahlapuu et al., 2020). Besides, KAMP-19 (RAIGGGLSSVGGGSSTIKY) derived from keratin is another coil-based AMP, which has been verified to adopt a random coil structure in the presence of membrane mimicking sodium dodecyl sulfate micelles or lipopolysaccharides/1,2-dielaidoyl-sn-glycero-3-phosphoethanolamine liposomes. And it was also shown that the peptide could exert bactericidal effects by inducing pore forming and destruct bacterial cell membrane (Lee et al., 2016).

2.4 Composite antimicrobial peptides

While abovementioned AMPs mainly show a single secondary structure, there are a plethora of AMPs presenting multiple structures, which can be assumed as composite AMPs. Some natural AMPs contains multiple structures. For example, human β-defensin3 (HBD-3), GIINTLQKYYCRVRGGRCAVLSCLPKEEQIGK CSTRGRKCCRRKK, is a canonic example which presents αβββ conformations (Dhople et al., 2006). Cystatin (SEDRSRLLGAPVPVDENDEGLQRALQFAMAEYNRASND KYSSRVVRVISAKRQLVSGIKYILQVEIGRTTCPKSSG DLQXCEFHDEPEMAKYTTCTFVVYSIPWLNQIKLLESKCQ) is also a naturally existing AMP containing both α-helix and β-sheet structures. Moreover, multiple structures can be also endowed to AMPs by artificially splicing distinctive peptide pieces from different agents. Melimine (TLISWIKNKRKQRPRVSRRRRRRGGRRRR) is a synthetic AMP which combines functional regions of mellitin (an α-helical AMP with 26 residues obtained from the venom of European honey bee) and protamine, which shows broad spectrum antibacterial properties (Yasir et al., 2020). Dutta et al. covalently coated melamine to contact lenses which were used in a 1-day clinical trial, and found that the melamine-immobilized lenses shows high antimicrobial activity but without cytotoxicity. And it has been orally administrated for the treatment of keratitis in another clinical trial (ACTRN12613000369729). Furthermore, Mel4 (KNKRKRRRRRRGGRRRR) is a clipped AMP derived from melamine, which was also covalently loaded to contact lenses for extended wear in a clinical trial (Kalaiselvan et al., 2022). The results showed that Mel4 coated lenses failed to change the conjunctival microbiota compared with control lenses (Kalaiselvan et al., 2022). But it may retain antibacterial activity during the initial wearing since the long wearing time.

3 Potential effects of antimicrobial peptides for bone tissue engineering

While most AMPs are used for soft tissue repair in clinic trials, they also show great promise for bone tissue engineering. They may exert their effects for bone repair by bactericidal activity, anti-biofilm formation, immunomodulation, and regenerative functions (Figure 3).

3.1 Bactericidal activity

One of critical effects of AMPs is bactericidal activity, and the antimicrobial mode of actions can be classified to two types: on the one hand, the integrity of bacterial structures such as cell membrane and cell wall may be directly disrupted by AMPs; on the other hand, AMPs could directly induce cell process inhibition by binding to specific molecules.

3.1.1 Cell structure targeting

The integrity of cell membrane is critical for the bacterial homeostasis, and most AMPs exert their antimicrobial effects by destabilizing bacterial membrane which is negatively charged because of anionic lipids such as lipopolysaccharides for Gram-negative bacteria or teichoic acids for Gram-positive bacteria. Animal cell membrane, in contrast, is composed of zwitterionic phospholipids such as phosphatidylcholine and sphingomyelin. So initial electrostatic interaction is generally initiated between anionic bacterial membrane and cationic AMPs. When AMPs aggregate on the surface of bacterial membrane to form stable conformation, two broad modes of action have been proposed to interpret antimicrobial mechanisms: transmembrane pore models and non-membrane pore models (Figure 4A) (Luo and Song, 2021).

Transmembrane pore models refer to that pores can be induced by AMPs within bacterial membrane. Barrel stave model is one of critical transmembrane pore models. When AMPs gather upon bacterial membrane above critical concentration, they cause membrane thinning and lipid shift after conformational changes, which then insert vertically to membrane bilayer with their hydrophobic regions towards hydrophobic regions of membrane liquids and their hydrophilic regions inside to form a channel lumen (Luo and Song, 2021). And the lateral interaction of barrel stave channels is enhanced by peptide-peptide interactions. Different form barrel stave model, toroidal pore model is another important transmembrane pore model. When AMPs aggregate at specific concentration, they mediate local curvature of membrane phospholipid, which cause the rearrangement of membrane bilayer. And AMPs interact with lipids to form toroidal pore channels but without lateral peptide-peptide interactions. Namely, the membrane layer is curved but not shifted which allows to form channels partly by AMPs and partly by

phospholipid head group. Furthermore, there are also other transmembrane pore models such as disordered toroidal pore model and aggregate model (Nguyen et al., 2011).

Non-membrane pore models are termed that AMPs fail to induce pore formation but promote the formation of micelles. Carpet/detergent-like model is one of canonic non-membrane pore models. Initially, AMPs aggregate parallelly on the outer surface of bacterial membrane and interact with anionic phospholipids to form carpet structures. When the local concentration of AMPs reaches over a threshold concentration, bacterial membrane interacted with carpet can be further disintegrated to form micelles, which is known as a detergent-like effect (Nguyen et al., 2011). Agglutination model, besides, is also anther non-membrane pore model, and micelles are induced by the interaction between AMPs and cell wall components on the outer surface of bacterial membrane (Sinha et al., 2017). Moreover, other non-membrane pore models include but not limit to membrane thinning/thickening model and non-bilayer intermediate model.

While most AMPs show their antimicrobial activity by membrane lysis, some AMPs exert their antibacterial activity by influencing cell wall synthesis to destroy cell wall integrity (Figure 4B). Lipid II is an important precursor for cell wall synthesis, and some AMPs such as α-defensin Human Neutrophil Peptide 1 (HNP-1) show high affinity to this molecule and affect cell wall synthesis, which then undermines cell wall integrity (de Leeuw et al., 2010). Besides, Wenzel et al. (2014). Reported that a short AMP, RWRWRW-NH2, could insert into Gram-positive membrane and delocalize peripheral membrane proteins which are critical for cell wall synthesis, which then disturb cell wall integrity. Furthermore, cell wall synthesis can be also affected by the genetic modulating of AMPs. For example, it has been found that LL-37 could regulate *Sfp1* gene to affect cell wall synthesis, thus destabilizing cell wall intensity (Hsu et al., 2021). Another group also reported that cell wall intensity was damaged by a AMP, combined with upregulated cell wall synthesis-related gene and downregulated cell membrane ergosterol synthesis-related genes (Ma et al., 2020). Similar results were observed by a novel AMP named sparamosin26–54 (Chen Z et al., 2021). Therefore, cell wall integrity can be disturbed by influencing cell wall synthesis, and related mode of actions can be grouped to binding to cell wall precursor, modulating cell wall s1ynthesis proteins, and regulating cell wall synthesis related genes. And detailed modes of action are highly needed to interpret.

In addition to targeting membrane and cell wall, some AMPs may also target intracellular organelles (Figure 4C) Graf and Wilson (2019). Showed that proline-rich AMPs target ribosome and then inhibit protein synthesis to induce bacterial death. Besides, it has been also reported that an AMP named myristoyl-CM4 could target mitochondria of cancer cells and cause mitochondrial dysfunction, which then induce cancer cell death (Li C et al., 2018). But whether AMPs could target microbial mitochondria remains unknown, which need further researches.

3.1.2 Intracellular molecule targeting

While most AMPs show their antimicrobial activity by destructing cell structures, especially membrane lysis, some AMPs also target intracellular molecules to kill microbes after translocation. Nucleic acid is one of common molecular targets for AMPs. Buforin II is one AMP showing broad spectrum antimicrobial properties, which mainly binds to DNA and RNA to disturb cell functions but without membrane lysis (Park et al., 1998). In addition to direct binding, an AMP named TO17 have been reported to induce the degradation of genomic DNA and total RNA (He et al., 2018a). Proteins, besides, are also important intracellular targets for AMPs. As an example, Chung et al. revealed that LL-37 could translocate bacterial membrane and bind to *Francisella* cytoplasmic acyl carrier protein (AcpP), which then changed the profiles of fatty acid (Chung et al., 2015). Moreover, AMPs could also target intracellular enzyme to exert anti-microbial functions. One study from Braffmana's group revealed that AMPs microcin J25 (MccJ25) and capistruin (Cap) could bind to the second channel of RNA polymerase and inhibit its bioactivity (Braffman et al., 2019).

3.2 Anti-biofilm properties

Biofilms are sessile microbial communities which are attached to a biotic/abiotic surface or embedded in a matrix as aggregates (Roy et al., 2018). The surface of biomaterials is vulnerable to support the formation of biofilm when bone repair materials are implanted to bone defects. And biofilms are generally correlated to chronic bone infection, which are difficult to treat because of bacterial resistance (Vallet-Regí et al., 2020). So anti-film properties are highly needed for bone tissue engineering. And recent studies showed that some AMPs show potent anti-film properties (Figure 5).

Some AMPs could inhibit biofilm formation and development. Four stages are generally needed for biofilm formation and development: microorganism aggregation or attachment, microbial adhesion, biofilm development and maturity, and biofilm aging (Di Somma et al., 2020; Luo and Song, 2021). Inhibiting initial attachment is one of important mode of action for AMPs to obstacle biofilm formation. For example, LL-37 have been reported to bind to the main cell wall component (mannan) of *Candida albicans* to inhibit initial adhesion, which may help to inhibit biofilm formation (Tsai et al., 2011). Another research also showed that a short AMP 1037 with nine residues could obstacle initial attachment by suppressing swimming and swarming motilities (de la Fuente-Núñez et al., 2012). Besides, AMPs could exert anti-biofilm

functions by modulating guanosine 5′-diphosphate 3′-diphosphate (ppGpp) and guanosine 5′-triphosphate 3′-diphosphate (pppGpp) which are two critical molecules for biofilm formation and development in alarm system to encounter stress environments. As an example, an AMP 1018 has been reported to target enzymes RelA and SpoT to block the synthesis of ppGpp and pppGpp, thus showing potent anti-biofilm properties (de la Fuente-Núñez et al., 2014). Furthermore, AMPs also induce genic regulation to inhibit biofilm formation and development. The AMP 1037 has been reported to downregulate or upregulate some gene expressions to inhibit biofilm formation and development (de la Fuente-Núñez et al., 2012). Besides, it was also reported that AMPs could promote biofilm aging and dispersion, which promote AMPs to kill bacteria (Hancock et al., 2021).

Some AMPs could destruct established biofilms, and two main modes of actions have been proposed. On the one hand, some AMPs could directly induce the degradation of biofilm matrix. Libardo et al. reported that an AMP piscidin three from fish could interact with Cu^{2+} to activate nuclease activity to clear extracellular DNA, thus damaging pre-formed biofilms (Libardo et al., 2017). On the other hand, some AMPs could infiltrate biofilms and destroy bacterial membrane in biofilms. One study showed that an AMP sculentin (1–21) could disturb membrane of *pseudomonas aeruginosa* in biofilms, thus induce biofilm disruption (Luca et al., 2013).

3.3 Immunomodulation

In addition to direct anti-microbial and anti-biofilm properties, AMPs could modulate immune system to enhance microbe clearing and control diverse inflammation. Both innate and adaptive immune system can be influenced by AMPs, the actions of which mainly include recruitment of multiple immune cells (such as macrophages, neutrophils, mast cells, dendritic cells, and lymphocytes), modulation of neutrophil functions, initiation of antigen-presenting cells, and activation of T cell/B cell responses (Mookherjee et al., 2020). And AMP-related immunomodulation mechanisms can be attributed to their interaction with membrane receptors (such as CXCR2 and FPR2) and intracellular receptors (such as SQSTM1 and GAPDH) of immune cells (Hilchie et al., 2013). Besides, AMPs could also control diverse inflammation by inhibiting pro-inflammatory cytokines and promoting anti-inflammatory cytokines, and related mechanisms mainly include intercepting inflammatory inducers to target to related sensors and suppressing inflammation-related signaling pathways and transcription factor expression (van der Does et al., 2019).

AMPs may promote bone tissue regeneration by immunomodulation, which mainly depends on macrophage polarization. Moderate macrophage polarization from M1 phenotype to M2 phenotype helps to bone tissue regeneration (Hao et al., 2022). And some AMPs have been verified to promote macrophage polarization. For example, Chen et al. (2018). Reported that an AMP cathelicidin-WA could effective promote M1 macrophages induced by *E. coli* K88 to switch to M2 macrophages. Another group also showed that an AMP, innate defense regulator-1018, could effectively transfer M1 state to M2-M1 state, which shows both anti-inflammatory and pro-inflammatory properties (Pena et al., 2013).

3.4 Regenerative functions

In recent years, AMPs have been verified to exert regenerative functions for bone tissue engineering by promoting angiogenesis and osteogenesis as well as inhibiting osteoclastogenesis. Angiogenesis is an important process during bone regeneration, which support the delivery of nutrients and oxygen. Some AMPs could induce angiogenesis. Histatin-1 is an AMP with 38 amino which is rich in human saliva, and the peptide have been shown to enhance angiogenesis, as confirmed by tube formation assay and the chick chorioallantoic membrane model (Torres et al., 2017). Besides, some AMPs could promote osteogenesis by modulate stem cell behaviors. LL-37 is a promising AMP to promote the proliferation, migration, and osteogenic differentiation of MSCs (Liu H et al., 2018). And human β defensin 3 has also been reported to promote MSC osteogenesis (Wang B et al., 2022). Furthermore, some AMPs could also inhibit osteoclastogenesis. Zhou et al. immobilized a AMP named GL13K (GKIIKLKASLKLL) to titanium surface, which was then used to culture RAW 264.7 cells, and they found that GL13K modified implant induced less osteoclast number than pristine implant (Zhou et al., 2021). Liu et al. also reported that LL-37 could reduce LPS-induce osteoclastogenesis (Liu Z et al., 2018).

4 Topical applications of antimicrobial peptides for bone tissue engineering

Severe bone defects caused by trauma, infection and tumor formation often require surgical reconstruction using artificial implants (Panayotov et al., 2016). After the implantation procedure, pathogens tend to accumulate on the surface of the implant material, forming a biofilm that protects them from the host's defenses (Ghigo 2001). Conventional implant materials are prone to induce biomaterial-associated infections (BAI) because they lack antimicrobial properties (Campoccia et al., 2013a). Once BAI occurs, it can lead to serious consequences, including surgical failure, sepsis, disability and even death (Campoccia et al., 2013b). In addition to ensuring as much asepsis as possible during the procedure, the prevailing clinical practice is the postoperative systemic prophylactic application of antibiotics

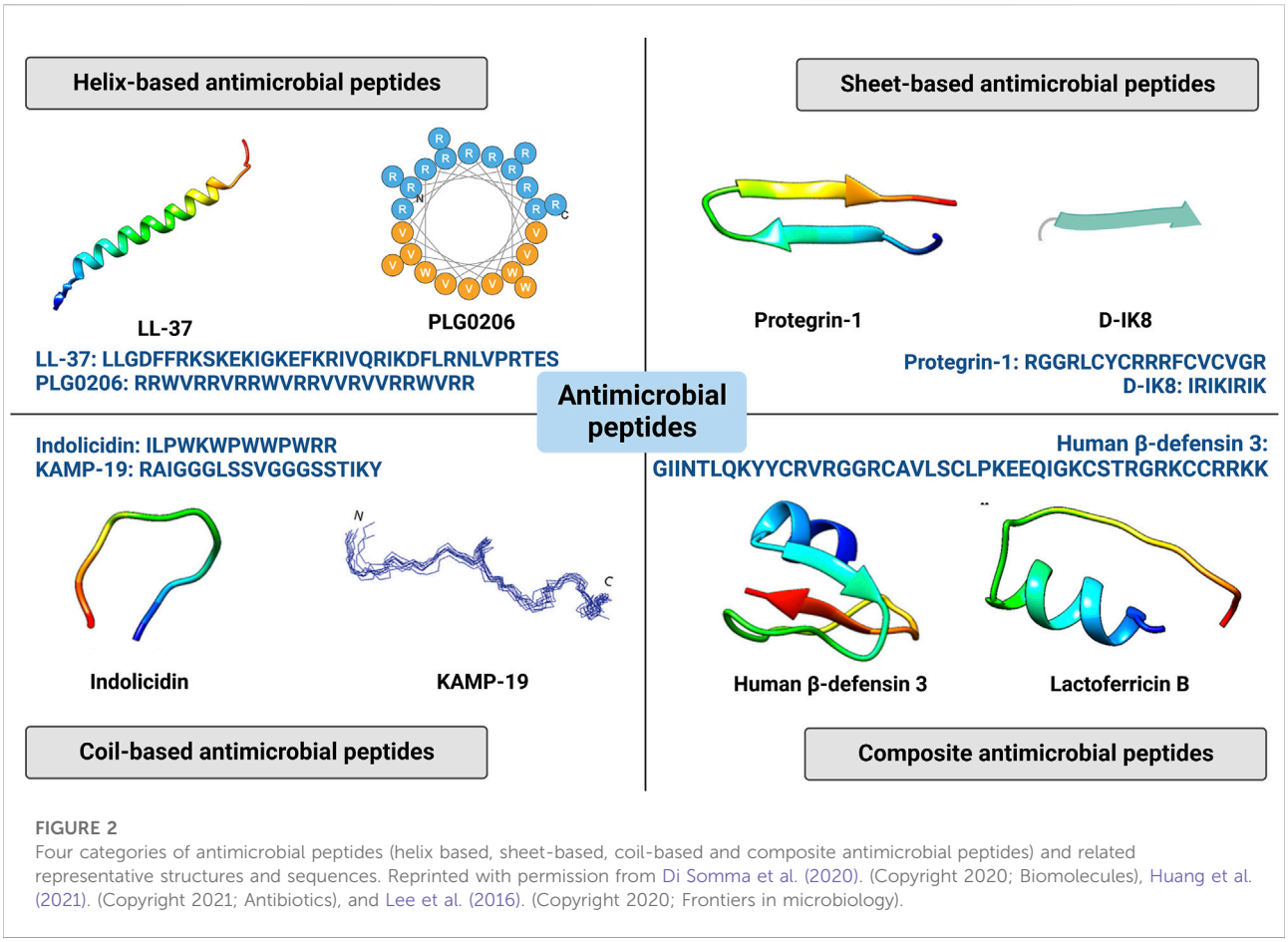

FIGURE 2
Four categories of antimicrobial peptides (helix based, sheet-based, coil-based and composite antimicrobial peptides) and related representative structures and sequences. Reprinted with permission from Di Somma et al. (2020). (Copyright 2020; Biomolecules), Huang et al. (2021). (Copyright 2021; Antibiotics), and Lee et al. (2016). (Copyright 2020; Frontiers in microbiology).

for this nasty situation. However, systemic administration has problems such as low efficiency, local tissue toxicity, and the development of drug resistance (Dik et al., 2018). Therefore local application of antimicrobial agents is considered to be a more effective strategy for the prevention of BAI. AMPs have a unique bactericidal mechanism that significantly reduces the possibility of bacterial resistance (Wang et al., 2019). Thus AMPs are gradually replacing antibiotics as the active factor in such antimicrobial strategies. In this part, we summarize AMPs delivery strategies that may be applied to bone tissue engineering for subsequent investigators to develop more effective bone tissue engineering scaffolds (Table 1), and we also focus on potential value of AMPs to be used in gene therapy (Figure 6).

4.1 Delivery system for antimicrobial peptides

4.1.1 Surface immobilization

Implant surface immobilization is an essential strategy in the field of antimicrobial delivery system, whereby coatings containing AMPs are loaded on the surface of the implant material to prevent biofilm formation at the tissue-material interface. Previous studies have developed a wide variety of AMP coatings. However, there are two main challenges in developing ideal AMP coatings: first, to immobilize them on the surface while ensuring their biological activity; and second, to load them at the right dose and release them at the right time. According to the position or order of the AMPs in the loading process, we classify the surface immobilization strategies of AMPs into three major categories: direct immobilization, immobilization after modification and indirect immobilization.

Direct immobilization means that the coating process does not involve any special treatment of the implant surface or the AMPs, and the peptide sequence is directly coated and immobilized on the surface of the implant material using a primary coating method. This is one of the simplest AMPs immobilization strategies. It directly co-incubates the AMPs solution with the implanted material, allowing the AMPs to physically adhere to the material surface. For example, Su et al. applied Mel4 solution directly to titanium scaffolds for investigating the effectiveness of AMPs in preventing infection after internal fixation of open fractures (Zhang S et al., 2021). They inoculated rabbits with *Staphylococcus aureus* and

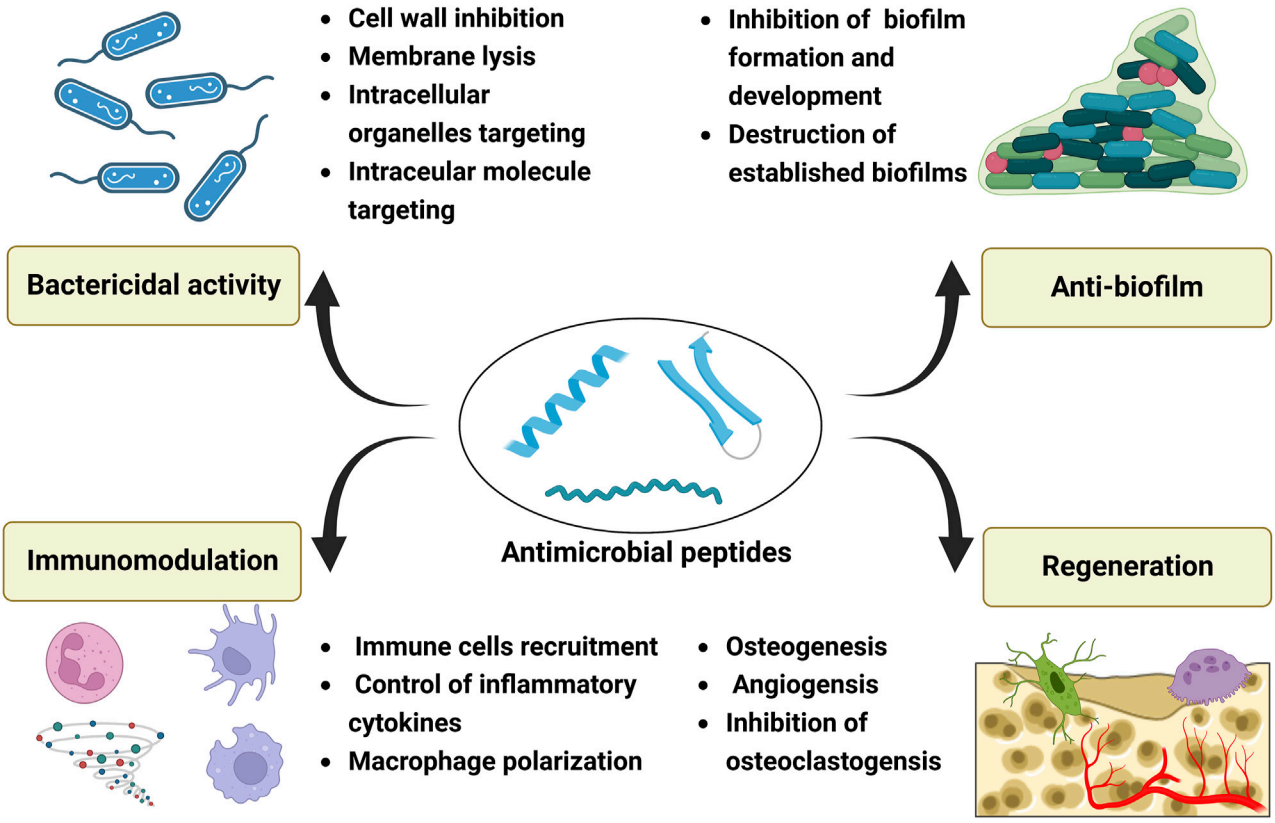

FIGURE 3
Potential effects of antimicrobial peptides for bone tissue engineering, and these effects can be mainly divided into four groups: bactericidal activity, anti-biofilm properties, immunomodulation and regenerative functions. Created with BioRender.com.

Pseudomonas aeruginosa, the common causative agents of open fractures, and implanted a titanium scaffold loaded with Mel4 into the rabbit femur to observe its therapeutic effect on postoperative infection. This simple titanium surface coating demonstrated significant antimicrobial efficacy, which provides a promising strategy for controlling infections after open fracture internal fixation. In addition, Li et al. immobilized the bifunctional chimeric peptide P15-CSP on the surface of tissue culture (TC) plastic by dry-coating, designing a bifunctional surface that is both antibacterial and osteogenic (Li et al., 2015). This chimeric peptide is a combination of the antimicrobial peptide P15 and the capacity-stimulating peptide (CSP) *via* the linker peptide A (EAAAK)nA, and both peptides are cationic peptides. In contrast, TC plastics have a special anionic surface, so they immobilize P15-CSP on the material surface by inter-ionic forces. Despite the initial success of these direct immobilization strategies for AMPs loading, two problems may be faced by simple physical adsorption alone: non-uniform loading of AMPs and poor immobilization to achieve long-term antimicrobial effects.

Immobilization after modification refers to the treatment of the implant surface or processing of the AMPs prior to immobilization. Common implant surface treatment measures include sulfonation, silylation, surface modification with polydopamine, and electrolytic deposition techniques. In addition, the pre-processing of AMPs mainly consists of linking metal-binding sequences or specific anchoring sequences. Compared to direct immobilization, modification followed by immobilization provides a uniform and stable fixation of the AMPs on the surface of the implant material. For example, Yuan et al. immobilized mouse beta-defensin-14 (MBD-14) on the surface of a polyetheretherketone (PEEK) bone scaffold to improve the antimicrobial activity and osseointegration of the scaffold (Yuan et al., 2019). Long-term drug delivery of MBD-14 is difficult to achieve by direct coating immobilization alone. Previous studies have shown that porous surfaces facilitate drug loading and delivery (Andrew et al., 2010; Lee et al., 2019). To increase the AMPs loading, they treated the PEEK surface by a sulfonation technique before immobilizing the AMPs. The PEEK surface was etched with concentrated sulfuric acid to create a three-dimensional porous structure, after which

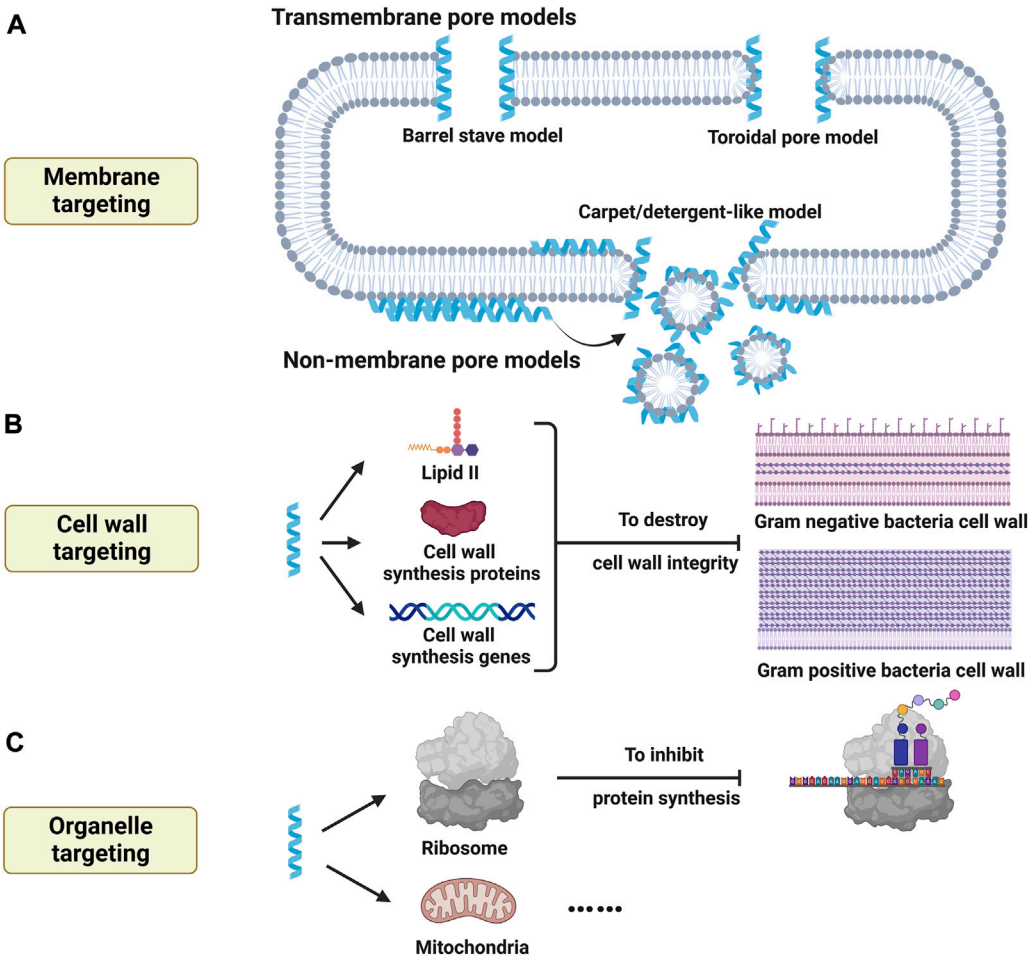

FIGURE 4
Bactericidal activity of antimicrobial peptides by targeting cell structures. **(A)** Antimicrobial peptides target to cell membrane to induce membrane lysis by transmembrane pore models (barrel stave model, toroidal pore model, *etc.*) and non-membrane pore models (Carpet/detergent-like model, *etc.*). **(B)** Antimicrobial peptides target cell wall synthesis and influence cell wall integrity by binding to lipid II, modulating cell wall synthesis related proteins and genes. **(C)** Antimicrobial peptides target organelles to influence physiological activities of microorganisms, thus exerting bactericidal effects. Created with BioRender.com.

the AMPs was freeze-dried and immobilized on its surface. This MBD-14-loaded PEEK scaffold inhibited *Staphylococcus aureus* and *Pseudomonas aeruginosa* for up to 28 days in an *in vitro* antimicrobial assay. This excellent slow release effect resulted from the high AMPs loading due to the porous structure and the covalent binding of MBD-14 to the residual sulfonic acid groups on the surface of the sulfonated material. In addition, Kazemzadeh-Narbat et al. treated titanium plates by using electrolytic deposition technique to form microporous calcium phosphate coatings on their surfaces (Kazemzadeh-Narbat et al., 2010). It creates a larger surface area for the peptide to interact with the material surface. And the cationic antimicrobial peptides can be electrostatically attracted to the negatively charged phosphate groups in the calcium phosphate coating, enhancing the retentive effect while increasing the loading. In addition, the calcium phosphate coating has been shown to have osteoconductive properties that promote bone formation around the implant (Kazemzadeh-Narbat et al., 2010). This multi-effect scaffold is a desired characteristic for the ideal orthopedic implant.

Another popular material surface treatment strategy is silanization. Silanization is the process of surface treatment of metallic or non-metallic materials with an aqueous solution of organosilane to functionalize the surface. This method is commonly used to modify hydroxyl-rich materials, such as titanium or other metal oxides. Silylation enables the introduction of reactive groups, such as amino or carboxyl groups, making it possible to chemically graft AMPs on the surface of biologically inert materials. Due to the effectiveness and low cost of silylation technology, a large number of studies in

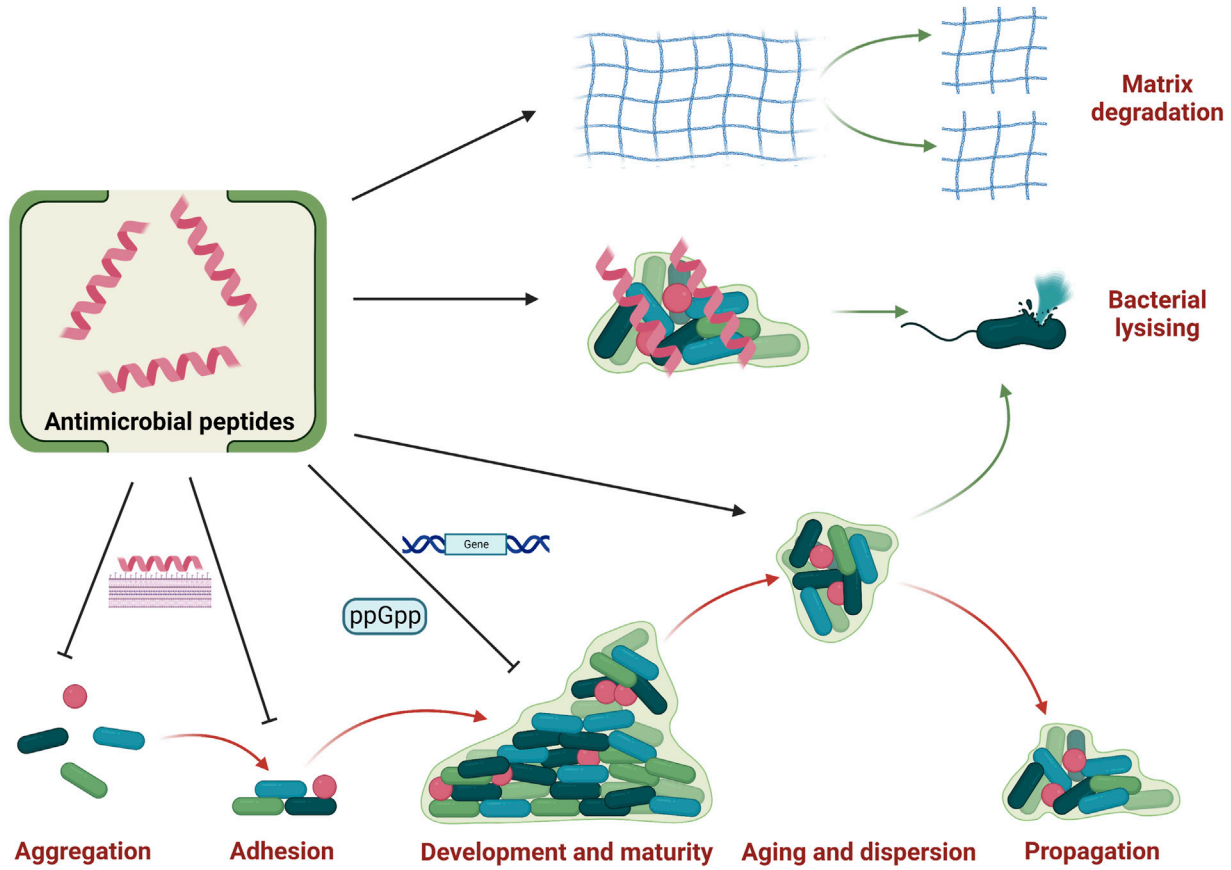

FIGURE 5
Anti-biofilm properties of antimicrobial peptides. Antimicrobial peptides could influence the biofilm cycle by inhibiting aggregation and adhesion as well as restraining the development and maturity. They also promote biofilm aging and dispersion, thus exposing bacteria to antimicrobial peptides to induce bacterial lysis. Besides, some antimicrobial peptides could also promote the matrix degradation of established biofilm. And there are also some antimicrobial peptides could penetrated established biofilm and interact with bacteria to exert bactericidal activity. Created with BioRender.com.

the field of AMPs delivery have converged (Hoyos-Nogués et al., 2017; Chen J et al., 2020; Fischer et al., 2021). For example, Chen et al. immobilized the antimicrobial peptide GL13K on a titanium implant scaffold by silanizing the titanium surface with a CPTES solution (Chen X et al., 2020). Specifically, the free amine (nucleophile) of the peptide underwent a direct nucleophilic substitution reaction with the chlorine atom (leaving group) of the organic functional group of CPTES, resulting in the immobilization of AMPs by forming a covalent bond with the silanized surface (Fischer et al., 2021). The lysine terminus of GL13K is a potential anchor site, and previous studies have demonstrated that this anchor site does not affect its antimicrobial activity. Based on this, they safely and effectively loaded GL13K onto titanium-based scaffolds and demonstrated that the modified titanium implants inhibited peri-implantitis through immunomodulatory effects. Our previous literature has shown the important role of immune regulation in osteogenesis (Chen et al., 2022). Therefore, surface-functionalized scaffold materials with immunomodulatory properties are highly promising strategies in orthopedic repair. In addition, AMPs immobilized on the surface of the implant material inhibit the adhesion of bacteria on the surface of the material along with the adhesion of osteoblasts. This is certainly unfriendly to peri-implant osseointegration. For this reason, Hoyos-Nogués et al. coupled the antimicrobial peptide LF1-11 to the RGD peptide, a cell adhesion sequence, *via* a solid-phase synthesis platform and covalently grafted it onto the surface of titanium implants with the help of silylation techniques (Hoyos-Nogués et al., 2017). The equimolar coupling of two peptide sequences with different activities ensured uniform cell adhesion and antimicrobial potential. Antibacterial tests and osteogenic series showed that this modified titanium plate demonstrated good antibacterial properties along with improved osteoblast adhesion, proliferation and mineralization. This is an advantage over classical monofunctional bone scaffolds. In additional, some optimization strategies for oral implants

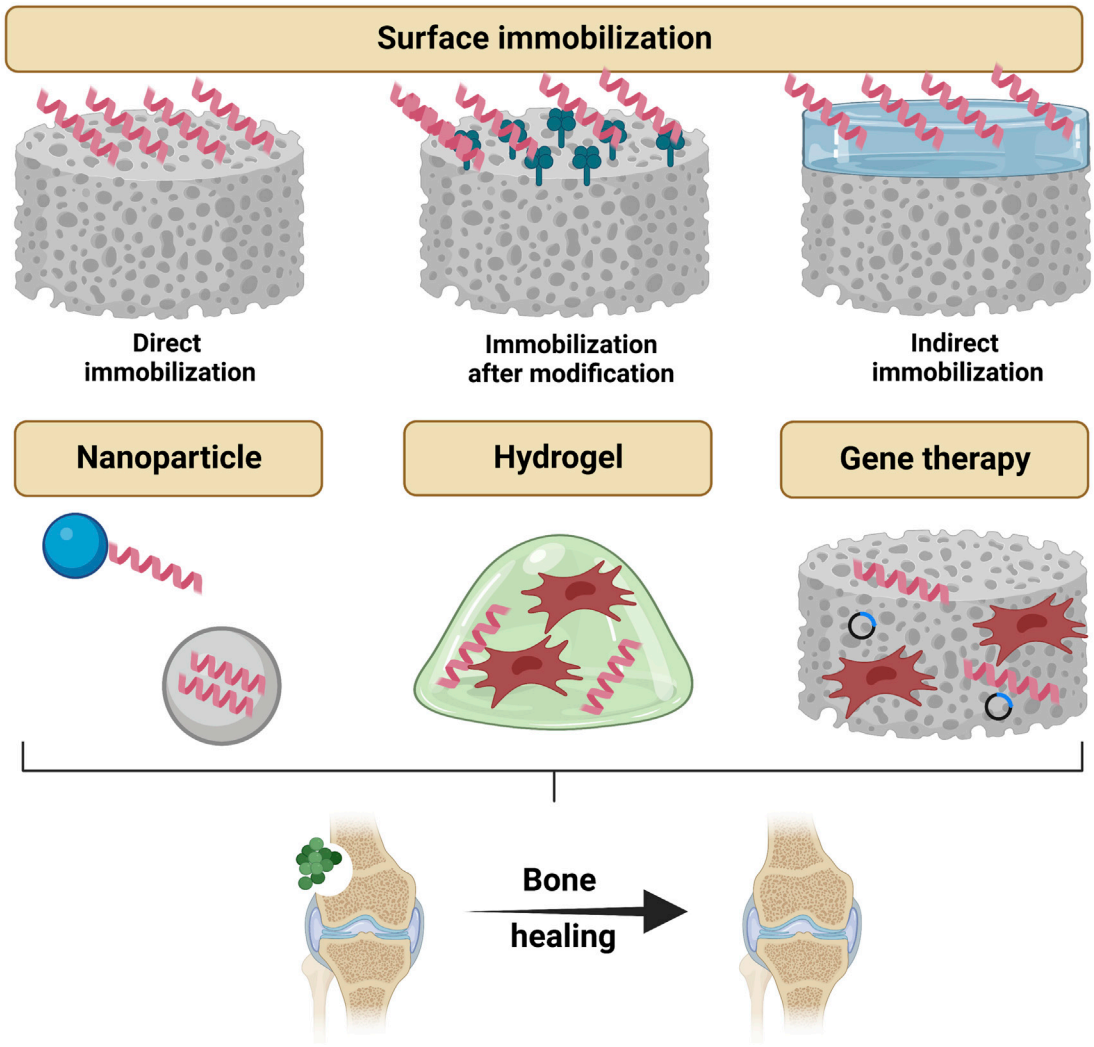

FIGURE 6
Topical strategies to administrate antimicrobial peptides for bone tissue engineering, which include delivery by surface immobilization (direct immobilization, immobilization after modification and indirect immobilization), delivery by nanoparticles, delivery by hydrogels and gene therapies. Created with BioRender.com.

using silanization technology to load AMPs are very novel. Since the challenges faced by oral implants and orthopedic implants are similar: antimicrobial and osseointegration, we believe that some loading strategies in the oral field can provide a reference for orthopedic implants. For example, Fischer's team has produced a titanium surface coating with dual bone-enabling and antibacterial functions through silanization and peptide co-fixation. The coating is characterized by its bioreactivity. The scaffold is loaded with GL13K, which provides antimicrobial activity, and matrix metalloprotease 9 (MMP-9) cleavable peptide (MMP9-CP), which provides bone-enabling effects. Among them, MMP9-CP is an enzyme-mediated cleavable peptide that promotes the release of MMP9 in the presence of osteoclast-released MMP9. MMPs are known to play an important role in bone repair and bone remodeling (Sternlicht and Werb, 2001). Therefore, future bone tissue engineering scaffolds can learn from this multifunctional coating strategy with bioresponsiveness to play a precise role in the corresponding bone repair process. Although the chemical immobilization of AMPs on the surface by silane coupling agents has been very effective, the complex and time-consuming pre-treatment of the material and the potential cytotoxicity of the complex chemical process are issues that need to be considered when utilizing this immobilization strategy in the future (He et al., 2018b).

In addition, over the past decade or so, scientists have benefited from the revelation of mussel foot adhesion proteins to develop polydopamine-based coating strategies (Ryu et al., 2018). Specifically, because the quinine and catechol groups of

TABLE 1 Comparison of antimicrobial peptide properties and related applications.

AMPs	Structures	Delivery system	Antibacterial properties	Other properties	Applications	Ref
LL37	Helix-based	Surface immobilization, nanoparticles	*Staphylococcus aureus, methicillin-resistant Staphylococcus aureus (MRSA)*	Osteogenesis, Osteoclastogenesis inhibition, immunomodulation	Rat femoral defect model, rat infected bone defect model	He S et al. (2018) He et al. (2019) Shen et al. (2019)
LF1-11	Helix-based	Surface immobilization	*Streptococcus sanguinis, Staphylococcus aureus*	-	Antimicrobial and osteogenic assays *In vitro*	Hoyos-Nogués et al. (2017)
KR-12	Helix-based	Surface immobilization	*Pseudomonas aeruginosa, Staphylococcus aureus, Escherichia coli*	Osteogenesis	Rat femoral defect model	Meng et al. (2020) Trzcińska et al. (2020)
GL13K	Sheet-based	Surface immobilization	*Pseudomonas aeruginosa, Escherichia coli, Fusobacterium nucleatum, Porphyromonas gingivalis*	Osteoclastogenesis inhibition, immunomodulation	Rabbit femoral defect model	Chen J et al. (2020) Cheng et al. (2017) Fischer et al. (2021) Li et al. (2017)
HHC-36	Sheet-based	Surface immobilization, hydrogels	*Staphylococcus aureus, Staphylococcus epidermidis, Escherichia coli, Pseudomonas aeruginosa、MASA*	Osteogenesis	Rabbit tibial osteomyelitis model	Chen X et al. (2020) Cheng et al. (2017) Wang L et al. (2022)
Tet213	Coil-based	Surface immobilization, hydrogels	*Staphylococcus aureus, Pseudomonas aeruginosa*	-	Rabbit tibial osteomyelitis model	Kazemzadeh-Narbat et al. (2010) Yang et al. (2018)
Pac-525	Coil-based	nanoparticles	*Staphylococcus aureus, Escherichia coli, Porphyromonas gingivalis, Fusobacterium nucleatum, Streptococcus sanguis*	-	Antimicrobial and osteogenic assays *In vitro*	He et al. (2018a) He et al. (2020)
PSI 10	Coil-based	Surface immobilization, nanoparticles	*Escherichia coli, Staphylococcus aureus, MRSA*	-	Rat femoral defect model	Tian et al. (2015) Zhongxing et al. (2021)
HBD-3	Composite	Surface immobilization	*Staphylococcus aureus, Escherichia coli*	Osteogenesis	Antimicrobial and osteogenic assays *In vitro*	Liu H et al. (2018) Wang B et al. (2022)
MBD-14	Composite	Surface immobilization	*Staphylococcus aureus, Escherichia coli*	Osteogenesis	Rat femoral osteomyelitis model	Yuan et al. (2019)
Mel4	Composite	Surface immobilization	*Staphylococcus aureus, Pseudomonas aeruginosa*	-	Rabbit infected bone defect model	Zhang Q et al. (2021)

polydopamine can create a chelated structure with the material through a series of chemical reactions, it has broad adhesion properties and can adhere to almost any surface. The mechanism by which polydopamine coatings can be used to load bioactive factors such as AMPs lies in the fact that such amine-containing nucleophilic reagents can be coupled to pDAs *via* Schiff base reactions or Michael addition reactions of benzoquinone groups under weak alkaline conditions, leading to secondary modification (Trzcińska et al., 2020). The advantages of the polydopamine coating strategy are low cost, ease of handling, wide application and optimized biocompatibility. So this strategy is also widely used in AMPs delivery system (He S et al., 2018; Meng et al., 2020; Trzcińska et al., 2020). For example, Trzcińska et al. (2020). Introduced an autonomously synthesized KR-12 analogue on the surface of titanium implants *via* a polydopamine coating. In detail, the treated titanium plates were first co-incubated with dopamine in alkaline Tris buffer to form a polydopamine coating on the titanium surface, providing an active platform for subsequent secondary modification of AMPs. AMPs solutions were then prepared at the MIC value of this peptide and co-incubated with pDA-coated titanium plates to obtain AMPs-loaded titanium implants (Trzcińska et al., 2020).5 (6)-FAM fluorescent labeling showed successful loading of AMP on the coating surface. In addition to the initial 6 h burst release, 50%–60% of the peptide remained unreleased after 30 days, indicating a very stable and reliable attachment of the lysine residue of the peptide to the dopamine surface and a reliable way to load AMPs on future orthopedic implant materials with slow local release. In addition, Meng et al. introduced KR-12 on the surface of PEEK bone implants using pDA as a linking layer and applied it to the repair of femoral defects in rats (Meng et al., 2020). The secondary modified PEEK-pDA-KR-12 scaffolds showed significant improvement in physical properties such as hydrophilicity as well as surface roughness. Furthermore, they

immersed the prepared active scaffolds in *S. aureus* solution and implanted them into rat femurs after 24 h. The experiments showed that the scaffolds loaded with KR-12 had remarkable antibacterial activity (Meng et al., 2020). In addition, *in vivo* studies in mice demonstrated that the scaffold significantly promoted osteogenic differentiation of MSCs and peri-implant bone formation, which is consistent with previous reports. Previous reports have demonstrated that KR-12 promotes osteogenic differentiation of MSCs through the bone morphogenetic protein (BMP)/Smad signaling pathway without cytotoxicity (Li H et al., 2018). In conclusion, the loading of KR-12 through the PDA junction layer can improve the defect of low osseointegration ability of PEEK scaffolds and confer good antimicrobial activity. This approach can be applied to many other types of bone regeneration materials in the future.

In addition to treating the surface of the material, treating the AMPs themselves is a popular and effective loading strategy. Binding sequences are peptide sequences that are able to bind to specific surfaces or functional groups. Modifying AMPs sequences with specific binding sequences to give them a stronger binding ability to the surface is also a mainstream approach to immobilize AMPs on the surface of implant materials (Zhang et al., 2018; Wisdom et al., 2020; Zhongxing et al., 2021). The advantage of this loading strategy is that it does not change the surface of the material, thus avoiding the destruction of its original properties. Yazici et al. designed bifunctional peptides with titanium surface affinity and antimicrobial activity, TiBP1-GGG-AMP and TiBP2-GGG-AMP, based on titanium-binding sequences (Haynie et al., 1995; Yazici et al., 2016). This type of peptide is composed of a solid-binding peptide and an AMP motif (E14LKK) by standard solid-phase synthesis technique to chimerize. They use a triple glycine (GGG) flexible linker to couple the two peptides to ensure that the activity of both parts is not affected. It was shown that the two designed peptides have stronger affinity than simply direct immobilization. And *in vitro* experiments, the titanium plates coated with the chimeric peptides exhibited significant anti-biofilm properties against both Gram-positive and Gram-negative bacteria (Yazici et al., 2016). Wisdom et al. also used the peptide binding sequence to modify AMP and highlighted that the chimeric peptide could achieve 100% coverage of the titanium sample surface within minutes (Wisdom et al., 2020). This result further supports the advantages of solid binding peptides in the field of AMPs immobilization. Liu et al. used hydroxyapatite binding domain (HABD) coupled to bone morphogenetic protein two mimetic peptide (BMP2-MP) and antimicrobial peptide PSI10 (RRWPWWPWRR), respectively, to enhance their binding to HA bone scaffolds (Zhongxing et al., 2021). They fabricated HA bone repair scaffolds using 3D printing technology and compared the binding ability of chimeric peptides and common peptides to the surface of the material. The results showed that the chimeric peptide containing HABD adsorbed 9–11 times more than the unmodified peptide on the surface of the HA scaffold. So, HABD is a "bridge" between AMPs and the material surface, which can increase the drug loading and achieve the slow release of AMPs at the same time (Bansal et al., 2019). The antimicrobial assay suggested that HABD labeling did not affect the activity of the peptide. Although Liu did not integrate the osteogenic and antimicrobial active units into the same bone scaffold, this loading strategy provides clarity for the subsequent fabrication of osteogenic scaffolds. In addition to modification using the specific binding sequences mentioned above, non-specific binding sequences, such as DOPA sequences, have also been applied for peptide pretreatment. Li et al. chimerized DOPA sequences with AMP so that AMP could be anchored to the PEEK bone scaffold (Li et al., 2021). They constructed a rabbit infectious osteomyelitis model and implanted AMP-loaded PEEK scaffolds into rabbit femurs. The results showed that the scaffold had a long-term stable antimicrobial effect as well as optimized osseointegration ability. In conclusion, the key to AMPs by combining sequence modifications lies in how to ensure the function of each functional domain to the maximum extent possible. To cope with this problem, researchers usually utilize a variety of spacer units (rigid linkers, flexible linkers, *etc.*) as bridges for coupling (Yazici et al., 2016; Wisdom et al., 2020). As to which protection measures are the most effective remains to be further explored.

Indirect immobilization refers to the physical separation of the AMPs from the material surface by means of a matrix while immobilization. This type of matrix is called "container". Compared to the first two immobilization methods, the main difference is that there is no direct physical contact between the AMPs and the material surface, and the "container" can provide more diverse release modes for the AMPs (Li et al., 2017; Liu H et al., 2018; Chen J et al., 2020). For example, Liu et al. prepared a nano-hydroxyapatite coating on the surface of a titanium plate by impregnation coating (Liu Z et al., 2018). The bifunctional titanium material was then developed by the physical properties of nano-hydroxyapatite particles to adsorb HBD-3 and BMP-2. The slow and simultaneous release of HBD-3 and BMP-2 conferred the scaffold with long-term resistance to biofilm and the ability to promote osteogenic differentiation. Adsorption of AMPs using nano-hydroxyapatite coating can avoid complex chemical processes and the effect of catalyst residues on peptide activity. In addition, titanium dioxide nanotubes are widely used in the study of surface loading of AMPs on titanium implants because of their excellent biocompatibility as carriers of biofactors and their ability to provide local slow release function (Chen X et al., 2020; Wang L et al., 2022). Wang et al. used anodic oxidation and hydrothermal synthesis to prepare uniformly distributed and well-arranged TNTs structures on the surface of titanium plates (Wang B et al., 2022). The fabricated TNTs were hollow tube-like structures, which provided the structural basis for subsequent

high loading of AMPs. Then, they applied the vacuum-assisted physisorption method to load the fused peptide (HHC36-RGD) into the TNTs. Further studies demonstrated that the titanium implants constructed by Liu were effective in preventing bacterial infection and promoting early osseointegration, reconciling the conflict between traditional antimicrobial materials and osteogenic surfaces, and were a promising material for anti-infection bone repair. However, the release pattern exhibited by TNTs - "abrupt release, slow release, near linear release" - is only theoretically consistent with the conventional antimicrobial process. To this end, Chen et al. developed a titanium dioxide nanotube structure with PH-controlled release, enabling smart drug delivery on demand (Chen J et al., 2020). Specifically, after loading HHC36 inside the TNTs, they closed the outer mouth of the nanotubes with a pH-responsive molecular gate, polymethylmethacrylate (PMAA). pMAA swelled in pH ≈ 7.4 (physiological environment without bacterial infection), preventing the abrupt release of AMPs and thus mitigating cytotoxicity; in contrast, PMAA in pH ≤ 6.0 (acidic microenvironment produced by bacterial infection) disintegrates and rapidly releases AMPs showing powerful bactericidal activity (Chen X et al., 2020). A rabbit tibial infection model confirmed the biocompatibility, responsiveness and sterilization activity of this Pandora's box-like controlled release system. This upgrade from slow release to controlled release is certainly a goal to be pursued for future drug delivery system. Moreover, it has been suggested that titanium nanopores (NPs) structures have stronger bonding strength to titanium plates compared to nanotubes (NTs) and have better biocompatibility and osteogenesis induction. Shen et al. fabricated NPs and NTs on the surface of titanium plates by varying the process parameters and loaded the antimicrobial peptide LL37 onto them, respectively (Shen et al., 2019). By comparison, they verified that the NPs coating is more stable than the NTs coating and seems to be more suitable for the preparation of AMP-loaded combination titanium implants for bone injury treatment.

4.1.2 Nanoparticles

Nanoparticles are an effective tool for local delivery of drugs and have been widely used in recent years for topical application of bioactive factors. Delivery of AMPs with nanoparticles has also gradually become a research hotspot to assist in the repair of infected bone defects. Commonly used nanoparticles for drug delivery system include polymeric microspheres and inorganic particles (He et al., 2018a; He et al., 2020; Honda et al., 2020). Honda et al. noticed that the amine group of fish sperm protein arginine adsorbed with the phosphate group and hydroxyl group of HAp through electrostatic interactions, so they loaded fish sperm protein onto HAp by intermittent adsorption and compressed it into bone implants (Honda et al., 2020). It has the osteogenic properties expected of a bone scaffold and the antimicrobial activity conferred by AMPs. In addition, this team found that HAp-adsorbed fisetin is released by ion exchange, so the salt concentration in the local environment can modulate the release of AMPs from the nanoparticles (Honda et al., 2020). Another team used negatively charged filamentous protein particles (SFNPs) to adsorb positively charged LL37 and crosslink it to the surface of the titanium scaffold (He et al., 2019). LL37 was able to recruit MSCs and macrophages and induce M2 polarization, which significantly promoted bone formation around the titanium scaffold. Since positive charge is one of the characteristics of AMPs, negatively charged SFNPs are a universal platform for loading AMPs.

Relying solely on physical adsorption tends to produce high levels of synaptic release, which shows some cytotoxicity. However, encapsulation of AMPs with degradable polymeric microspheres to degrade and release it per microsphere unit can reduce the sudden release due to binding instability. He et al. prepared PLGA microspheres encapsulated with Pac-525 and KSL-W using electrospray technology, and the encapsulation rate of PLGA microspheres up to more than 90% was observed by electron microscopy, which confirmed the drug loading performance of PLGA microspheres (He et al., 2020). With the degradation of microspheres, AMPs was slowly released in small dose units, and studies showed that its long-term antimicrobial effect was very promising (>35 days). In addition, AMP-loaded PLGA microspheres mounted on porous mineralized collagen scaffolds exhibited excellent antibacterial and osteogenic activities (He et al., 2020). In addition, AMP-loaded nanoparticles can be attached to other forms of implants to accomplish drug delivery, such as metal scaffolds, fibrous membrane scaffolds, *etc.* For example, He's team also used the aforementioned PLGA microspheres for the osteogenic layer in a layer-by-layer fibrous membrane scaffold to produce a guided bone regeneration (GBR) membrane with antimicrobial properties (He et al., 2018b). Tian et al. coated HA particles loaded with AMPs analogs on the surface of a magnesium alloy scaffold, which improved the corrosion resistance of the magnesium alloy while providing anti-biofilm properties (Tian et al., 2015). The modified magnesium alloy scaffold perfectly repaired the femoral condylar injury in rabbits. Clearly, the protection, delivery and slow release of AMPs with degradable polymeric microspheres offer a promising future for the treatment of infected bone defects.

4.1.3 Hydrogels

In the field of tissue engineering, hydrogels are considered to be ideal scaffolds for delivery of active factors. In recent years, researchers have been gradually using hydrogel scaffolds to deliver AMPs for infectious tissue repair. Yang et al. successfully combined RADA16 and Tet213 to make a self-assembled hydrogel scaffold for the treatment of osteomyelitis (Yang et al., 2018). It is known that RADA16 peptide hydrogel consists of a high mass ratio of water, can self-assemble under physiological conditions, and it has the potential to induce new

bone production. Yang et al. loaded AMPs into RADA16 without changing its appearance and properties. The novel hydrogels were produced with a dense nanofiber network structure, which on the one hand has antibacterial ability and on the other hand can provide a suitable growth environment for bone marrow mesenchymal stem cells and promote the proliferation of osteoblasts (Yang et al., 2018). The production process of AMPs delivery by means of hydrogels is simple and the resulting novel hydrogels can be applied by local injection. This also exposes the shortcomings of its osteoconductivity. Therefore, the use of hydrogel-loaded drugs alone for bone defect repair is currently rare. To this end, Cheng et al. made a coating of AMP-loaded methacrylate-based hydrogel (GelMA), with titanium providing the necessary mechanical properties and osteoconductivity of the bone scaffold (Cheng et al., 2017). This novel hydrogel coating consists of silicate nanoparticles to provide bone-enabling activity, antimicrobial peptide HHC36 to provide antimicrobial activity, and catechol moieties to provide adhesion. In addition, AMP is released from the hydrogel in a diffusive manner due to the absence of chemical coupling between HHC36 and the hydrogel backbone, which may lead to a rapid release of AMPs. To achieve long-term release, Cheng enhanced the binding strength of AMP by photo-crosslinking (Cheng et al., 2017). The resulting novel hydrogel coating exhibited stable antibacterial ability. In conclusion, hydrogels are good scaffolds for *in vivo* protection and delivery of AMPs, but AMPs release kinetics and its application to bone tissue engineering scaffolds need to be further investigated.

4.2 Gene therapy by antimicrobial peptides

In recent years, gene therapy involves strategies to transfer nucleic acids encoding target proteins or peptides to repair cells such as MSCs, thus promoting cell differentiation and tissue regeneration (Atasoy-Zeybek and Kose, 2018). And gene therapy could fulfill long-term expressions of target factors and avoid shortcomings about direct applications of protein or peptides, such as burst release and protease degradation. So transferring genes which encode AMPs to stem cells is a potential technique to treat infection diseases. Zhou et al. has transferred LL-37 gene to distal airway stem cells which were then transplanted to infected lung foci, and found that these engineered cells could express LL-37 and prevent bioengineered artificial lung from infection (Zhou et al., 2020). Therefore, using engineered stem cells which express AMPs is a promising strategy to repair infection bone defects, which needs further attention.

Depending on the vector types, gene therapy strategies can be grouped into viral gene therapy and non-viral gene therapy. And non-viral strategies are better than viral techniques on account of high biosafety and low cost. But one apparent obstacle is low level of transfection efficiency. AMPs could help to improve transfection capacity in gene therapy by enhancing cellular and nucleus entry. Peng et al. used AMP conjugated gold nanoparticles to delivery plasmid DNA (pDNA) to MSC, and found that the transfection efficiency was dramatically improved by AMP (Peng et al., 2016). And another research group verifies that an AMP, θ-defensin, can also effectively used to load and carry miRNA to MSCs, with higher efficiency than common polyethylenimine and Lipofectamine 3,000 (Yu et al., 2017). Although some AMPs potent ability to induce pDNA to stem cells, they have not been used to induce pDNA encoding osteoinductive proteins or peptides to be transferred into stem cells for tissue engineering, especially for bone regeneration. Besides, it remains unknown whether the antimicrobial properties combined with ability to improve transfection efficiency will be simultaneously maintained *in vivo*. And gene-activated matrix incorporated scaffolds, repair cells, interest genes and AMPs are also highly needed established for bone tissue engineering.

5 Discussion

One major challenge is the emergence of multi-resistant bacteria, so traditional antibiotics gradually fail to meet current requirements in clinic practice. And bone infection during bone repair such as the repair of fracture or infection-caused bone defects is devasting to patients and the society. Antimicrobial peptides are emerging bactericidal agents to replace traditional antibiotics because of broad spectrum antimicrobial activities and limited resistance. And there are many kinds ofAMPs, which be categorized to helix-based AMPs, sheet-based AMPs, coil-based AMPs and composite AMPs depending on their distinctive structures. These AMPs show great promise for the prevention and treatment of bone infections during bone repair, as they can exert plenty of effects which include bactericidal activity, anti-biofilm properties, immunomodulation. And AMPs could also promote bone regeneration by immunomodulation to regulate immune-microenvironment. Besides, AMPs could promote angiogenesis and modulate MSC behaviors. Regarding the application of AMPs, not only can they be immobilized on the surface of bone implant biomaterials, but also they can be incorporated into biomaterials, and related controlled release techniques have been developed. Furthermore, AMPs can be used in gene therapy to help nucleic acid delivery.

Although the application of antimicrobial peptides *in situ* for bone tissue engineering has great prospects, the number of antimicrobial peptides is so huge that it is highly needed to screen. And some parent AMPs also need be modified to design related derivatives. The overall purposes of screening and modification are to improve antibiological activity, reduce cytotoxicity and hemolysis, and enhance enzyme resistance. Besides, concise mechanisms about modes of action of AMPs

remain unclear, especially anti-biofilm and immunomodulate mechanisms. In addition, AMPs are facing many challenges in bone tissue engineering applications. First, how to ensure the activity of AMPs during the delivery process. Simplifying the loading process and reducing the use of chemical reagents is the key to solving this problem. Although there are many strategies for delivering AMPs in bone tissue engineering, most of them are cumbersome in terms of steps, which not only consume human and material resources, but also are very detrimental to ensure the activity of AMPs. Therefore, there is an urgent need to develop simple and effective load strategies. Secondly, how to avoid the initial burst release of AMPs as well as to ensure a suitable local long-term peptide concentration. Excessive concentrations can lead to cytotoxicity, while insufficient concentrations make it difficult to achieve the desired effect, so a balance between cytotoxicity and effectiveness needs to be obtained. Increasing the drug loading and imparting slow-release properties or even controlled release properties seems to be the key factors to solve this problem. Although some teams have explored AMPs-related controlled release materials, there are few relevant studies in the field of bone tissue engineering. Breakthroughs in smart release studies could lead to better utilization of AMPs for bone tissue engineering in the future. Finally, how to ensure the osteogenesis-related properties of the material itself while providing biofilm resistance. This is an area that current researchers are working to address, but not doing enough. The dominant approach currently is to synthesize multifunctional chimeric peptides using solid-phase synthesis techniques, where peptide sequences with osteogenic activity are chimerized with AMPs. The limitations of this scheme are the high cost and the difficulty to ensure the function of multiple peptide sequences simultaneously. In fact, there are some AMPs, such as LL37, which themselves have osteogenic, immunomodulatory or angiogenic properties. Further exploration and discovery of more AMPs with osteogenic activity or the use of their osteogenic mechanisms to synthesize more effective AMPs could solve this problem. Therefore, researchers are needed in the future to explore the molecular mechanisms of osteogenesis of AMPs in greater depth and lay the foundation for the application of AMPs in bone tissue engineering. In conclusion, AMPs with limited resistance show great promise to be used as alternatives to traditional antibiotics for bone defects susceptible to infections, which may open a brilliant prospect for bone tissue engineering to treat clinic bone defects.

Author contributions

ZH, RC, and CC contributed equally to this work. ZH analyzed the literature, prepared and wrote the manuscript, and drew the figures. RC and CC researched and analyzed the literature, prepared the manuscript. YW and HL revised and modified the manuscript. YH and QF modified the manuscript and figures. JL supervised, administrated and edited the work. All authors have approved for the publication.

Funding

We thanks to the funds to support the work, which include the National Natural Science Foundation of China (No: 81871752), the Key Research and Development Program of Hubei Province (No: 2022BCA052), Hubei Provincial Natural Science Foundation (No: 2020CFB551), Zhongnan Hospital of Wuhan University Science, Technology and Innovation Seed Fund (No: cxpy2019074), and Translational Medicine and Interdisciplinary Research Joint Fund of Zhongnan Hospital of Wuhan University (No. ZNJC202014).

Conflict of interest

The authors declare that the research was conducted in the absence of any commercial or financial relationships that could be construed as a potential conflict of interest.

Publisher's note

All claims expressed in this article are solely those of the authors and do not necessarily represent those of their affiliated organizations, or those of the publisher, the editors and the reviewers. Any product that may be evaluated in this article, or claim that may be made by its manufacturer, is not guaranteed or endorsed by the publisher.

References

Andrew, J. S., Anglin, E. J., Wu, E. C., Chen, M. Y., Cheng, L., Freeman, W. R., et al. (2010). Sustained release of a monoclonal antibody from electrochemically prepared mesoporous silicon oxide. *Adv. Funct. Mat.* 20, 4168–4174. doi:10.1002/adfm.201000907

Atasoy-Zeybek, A., and Kose, G. T. (2018). Gene therapy strategies in bone tissue engineering and current clinical applications. *Adv. Exp. Med. Biol.* 1119, 85–101. doi:10.1007/5584_2018_253

Bansal, R., Care, A., Lord, M. S., Walsh, T. R., and Sunna, A. (2019). Experimental and theoretical tools to elucidate the binding mechanisms of solid-binding peptides. *N. Biotechnol.* 52, 9–18. doi:10.1016/j.nbt.2019.04.001

Batista Araujo, J., Sastre de Souza, G., and Lorenzon, E. N. (2022). Indolicidin revisited: Biological activity, potential applications and perspectives of an antimicrobial peptide not yet fully explored. *World J. Microbiol. Biotechnol.* 38, 39. doi:10.1007/s11274-022-03227-2

Bin Hafeez, A., Jiang, X., Bergen, P. J., and Zhu, Y. (2021). Antimicrobial peptides: An update on classifications and databases. *Int. J. Mol. Sci.* 22, 11691. doi:10.3390/ijms222111691

Birt, M. C., Anderson, D. W., Bruce Toby, E., and Wang, J. (2017). Osteomyelitis: Recent advances in pathophysiology and therapeutic strategies. *J. Orthop.* 14, 45–52. doi:10.1016/j.jor.2016.10.004

Braffman, N. R., Piscotta, F. J., Hauver, J., Campbell, E. A., Link, A. J., and Darst, S. A. (2019). Structural mechanism of transcription inhibition by lasso peptides microcin j25 and capistruin. *Proc. Natl. Acad. Sci. U. S. A.* 116, 1273–1278. doi:10.1073/pnas.1817352116

Browne, K., Chakraborty, S., Chen, R., Willcox, M. D., Black, D. S., Walsh, W. R., et al. (2020). A new era of antibiotics: The clinical potential of antimicrobial peptides. *Int. J. Mol. Sci.* 21, 7047. doi:10.3390/ijms21197047

Campoccia, D., Montanaro, L., and Arciola, C. R. (2013a). A review of the biomaterials technologies for infection-resistant surfaces. *Biomaterials* 34, 8533–8554. doi:10.1016/j.biomaterials.2013.07.089

Campoccia, D., Montanaro, L., and Arciola, C. R. (2013b). A review of the clinical implications of anti-infective biomaterials and infection-resistant surfaces. *Biomaterials* 34, 8018–8029. doi:10.1016/j.biomaterials.2013.07.048

Chen, J., Shi, X., Zhu, Y., Chen, Y., Gao, M., Gao, H., et al. (2020). On-demand storage and release of antimicrobial peptides using pandora's box-like nanotubes gated with a bacterial infection-responsive polymer. *Theranostics* 10, 109–122. doi:10.7150/thno.38388

Chen, R., Hao, Z., Wang, Y., Zhu, H., Hu, Y., Chen, T., et al. (2022). Mesenchymal stem cell-immune cell interaction and related modulations for bone tissue engineering. *Stem Cells Int.* 2022, 1–19. doi:10.1155/2022/7153584

Chen, S., Lu, Z., Wang, F., and Wang, Y. (2018). Cathelicidin-wa polarizes e. Coli k88-induced m1 macrophage to m2-like macrophage in raw264.7 cells. *Int. Immunopharmacol.* 54, 52–59. doi:10.1016/j.intimp.2017.10.013

Chen, X., Zhou, L., Wu, D., Huang, W., Lin, Y., Zhou, B., et al. (2020). The effects of titanium surfaces modified with an antimicrobial peptide gl13k by silanization on polarization, anti-inflammatory, and proinflammatory properties of macrophages. *BioMed Res. Int.* 2020, 1–9. doi:10.1155/2020/2327034

Chen, Y. C., Yang, Y., Zhang, C., Chen, H. Y., Chen, F., and Wang, K. J. (2021). A novel antimicrobial peptide sparamosin(26-54) from the mud crab scylla paramamosain showing potent antifungal activity against cryptococcus neoformans. *Front. Microbiol.* 12, 746006. doi:10.3389/fmicb.2021.746006

Chen, Z. Y., Gao, S., Zhang, Y. W., Zhou, R. B., and Zhou, F. (2021). Antibacterial biomaterials in bone tissue engineering. *J. Mat. Chem. B* 9, 2594–2612. doi:10.1039/d0tb02983a

Cheng, H., Yue, K., Kazemzadeh-Narbat, M., Liu, Y., Khalilpour, A., Li, B., et al. (2017). Mussel-inspired multifunctional hydrogel coating for prevention of infections and enhanced osteogenesis. *ACS Appl. Mat. Interfaces* 9, 11428–11439. doi:10.1021/acsami.6b16779

Chow, H. Y., Zhang, Y., Matheson, E., and Li, X. (2019). Ligation technologies for the synthesis of cyclic peptides. *Chem. Rev.* 119, 9971–10001. doi:10.1021/acs.chemrev.8b00657

Chung, M. C., Dean, S. N., and van Hoek, M. L. (2015). Acyl carrier protein is a bacterial cytoplasmic target of cationic antimicrobial peptide ll-37. *Biochem. J.* 470, 243–253. doi:10.1042/bj20150432

Dale, G. E., Halabi, A., Petersen-Sylla, M., Wach, A., and Zwingelstein, C. (2018). Pharmacokinetics, tolerability, and safety of murepavadin, a novel antipseudomonal antibiotic, in subjects with mild, moderate, or severe renal function impairment. *Antimicrob. Agents Chemother.* 62, e00490–18. doi:10.1128/aac.00490-18

Dart, A., Bhave, M., and Kingshott, P. (2019). Antimicrobial peptide-based electrospun fibers for wound healing applications. *Macromol. Biosci.* 19, e1800488. doi:10.1002/mabi.201800488

de la Fuente-Núñez, C., Korolik, V., Bains, M., Nguyen, U., Breidenstein, E. B., Horsman, S., et al. (2012). Inhibition of bacterial biofilm formation and swarming motility by a small synthetic cationic peptide. *Antimicrob. Agents Chemother.* 56, 2696–2704. doi:10.1128/aac.00064-12

de la Fuente-Núñez, C., Reffuveille, F., Haney, E. F., Straus, S. K., and Hancock, R. E. (2014). Broad-spectrum anti-biofilm peptide that targets a cellular stress response. *PLoS Pathog.* 10, e1004152. doi:10.1371/journal.ppat.1004152

de Leeuw, E., Li, C., Zeng, P., Li, C., Diepeveen-de Buin, M., Lu, W. Y., et al. (2010). Functional interaction of human neutrophil peptide-1 with the cell wall precursor lipid ii. *FEBS Lett.* 584, 1543–1548. doi:10.1016/j.febslet.2010.03.004

Deslouches, B., Phadke, S. M., Lazarevic, V., Cascio, M., Islam, K., Montelaro, R. C., et al. (2005). De novo generation of cationic antimicrobial peptides: Influence of length and tryptophan substitution on antimicrobial activity. *Antimicrob. Agents Chemother.* 49, 316–322. doi:10.1128/aac.49.1.316-322.2005

Dhople, V., Krukemeyer, A., and Ramamoorthy, A. (2006). The human beta-defensin-3, an antibacterial peptide with multiple biological functions. *Biochimica Biophysica Acta - Biomembr.* 1758, 1499–1512. doi:10.1016/j.bbamem.2006.07.007

Di Somma, A., Moretta, A., Canè, C., Cirillo, A., and Duilio, A. (2020). Antimicrobial and antibiofilm peptides. *Biomolecules* 10, 652. doi:10.3390/biom10040652

Dik, D. A., Fisher, J. F., and Mobashery, S. (2018). Cell-wall recycling of the gram-negative bacteria and the nexus to antibiotic resistance. *Chem. Rev.* 118, 5952–5984. doi:10.1021/acs.chemrev.8b00277

Elad, S., Epstein, J. B., Raber-Durlacher, J., Donnelly, P., and Strahilevitz, J. (2012). The antimicrobial effect of iseganan hcl oral solution in patients receiving stomatotoxic chemotherapy: Analysis from a multicenter, double-blind, placebo-controlled, randomized, phase iii clinical trial. *J. Oral Pathol. Med.* 41, 229–234. doi:10.1111/j.1600-0714.2011.01094.x

Fischer, N. G., Chen, X., Astleford-Hopper, K., He, J., Mullikin, A. F., Mansky, K. C., et al. (2021). Antimicrobial and enzyme-responsive multi-peptide surfaces for bone-anchored devices. *Mater. Sci. Eng. C* 125, 112108. doi:10.1016/j.msec.2021.112108

Ghigo, J. M. (2001). Natural conjugative plasmids induce bacterial biofilm development. *Nature* 412, 442–445. doi:10.1038/35086581

Giles, F. J., Miller, C. B., Hurd, D. D., Wingard, J. R., Fleming, T. R., Sonis, S. T., et al. (2003). A phase iii, randomized, double-blind, placebo-controlled, multinational trial of iseganan for the prevention of oral mucositis in patients receiving stomatotoxic chemotherapy (prompt-ct trial). *Leukemia lymphoma* 44, 1165–1172. doi:10.1080/1042819031000079159

Goldstein, E. J. C., Citron, D. M., Tyrrell, K. L., and Leoncio, E. S. (2017). *In vitro* activity of pexiganan and 10 comparator antimicrobials against 234 isolates, including 93 pasteurella species and 50 anaerobic bacterial isolates recovered from animal bite wounds. *Antimicrob. agents Chemother.* 61, e00246–17. doi:10.1128/aac.00246-17

Graf, M., and Wilson, D. N. (2019). Intracellular antimicrobial peptides targeting the protein synthesis machinery. *Adv. Exp. Med. Biol.* 1117, 73–89. doi:10.1007/978-981-13-3588-4_6

Hancock, R. E. W., Alford, M. A., and Haney, E. F. (2021). Antibiofilm activity of host defence peptides: Complexity provides opportunities. *Nat. Rev. Microbiol.* 19, 786–797. doi:10.1038/s41579-021-00585-w

Hao, Z., Li, H., Wang, Y., Hu, Y., Chen, T., Zhang, S., et al. (2022). Supramolecular peptide nanofiber hydrogels for bone tissue engineering: From multihierarchical fabrications to comprehensive applications. *Adv. Sci. (Weinheim, Baden-Wurttemberg, Ger.* 9, e2103820. doi:10.1002/advs.202103820

Hao, Z., Xu, Z., Wang, X., Wang, Y., Li, H., Chen, T., et al. (2021). Biophysical stimuli as the fourth pillar of bone tissue engineering. *Front. Cell Dev. Biol.* 9, 790050. doi:10.3389/fcell.2021.790050

Haynie, S. L., Crum, G. A., and Doele, B. A. (1995). Antimicrobial activities of amphiphilic peptides covalently bonded to a water-insoluble resin. *Antimicrob. Agents Chemother.* 39, 301–307. doi:10.1128/aac.39.2.301

He, S. W., Wang, G. H., Yue, B., Zhou, S., and Zhang, M. (2018). To17: A teleost antimicrobial peptide that induces degradation of bacterial nucleic acids and inhibits bacterial infection in red drum, sciaenops ocellatus. *Fish shellfish Immunol.* 72, 639–645. doi:10.1016/j.fsi.2017.11.038

He, Y., Jin, Y., Wang, X., Yao, S., Li, Y., Wu, Q., et al. (2018a). An antimicrobial peptide-loaded gelatin/chitosan nanofibrous membrane fabricated by sequential layer-by-layer electrospinning and electrospraying techniques. *Nanomater. (Basel, Switz.* 8, 327. doi:10.3390/nano8050327

He, Y., Jin, Y., Ying, X., Wu, Q., Yao, S., Li, Y., et al. (2020). Development of an antimicrobial peptide-loaded mineralized collagen bone scaffold for infective bone defect repair. *Regen. Biomater.* 7, 515–525. doi:10.1093/rb/rbaa015

He, Y., Mu, C., Shen, X., Yuan, Z., Liu, J., Chen, W., et al. (2018b). Peptide ll-37 coating on micro-structured titanium implants to facilitate bone formation *in vivo* via mesenchymal stem cell recruitment. *Acta biomater.* 80, 412–424. doi:10.1016/j.actbio.2018.09.036

He, Y., Yang, X., Yuan, Z., Shen, X., Xu, K., Lin, C., et al. (2019). Regulation of msc and macrophage functions in bone healing by peptide ll-37-loaded silk fibroin nanoparticles on a titanium surface. *Biomater. Sci.* 7, 5492–5505. doi:10.1039/c9bm01158g

Hilchie, A. L., Wuerth, K., and Hancock, R. E. (2013). Immune modulation by multifaceted cationic host defense (antimicrobial) peptides. *Nat. Chem. Biol.* 9, 761–768. doi:10.1038/nchembio.1393

Holani, R., Shah, C., Haji, Q., Inglis, G. D., Uwiera, R. R. E., and Cobo, E. R. (2016). Proline-arginine rich (pr-39) cathelicidin: Structure, expression and functional implication in intestinal health. *Comp. Immunol. Microbiol. Infect. Dis.* 49, 95–101. doi:10.1016/j.cimid.2016.10.004

Honda, M., Matsumoto, M., and Aizawa, M. (2020). Potential application of protamine for antimicrobial biomaterials in bone tissue engineering. *Int. J. Mol. Sci.* 21, 4368. doi:10.3390/ijms21124368

Hoyos-Nogués, M., Velasco, F., Ginebra, M. P., Manero, J. M., Gil, F. J., and Mas-Moruno, C. (2017). Regenerating bone via multifunctional coatings: The blending of cell integration and bacterial inhibition properties on the surface of biomaterials. *ACS Appl. Mat. Interfaces* 9, 21618–21630. doi:10.1021/acsami.7b03127

Hsu, C. M., Liao, Y. L., Chang, C. K., and Lan, C. Y. (2021). Candida albicans sfp1 is involved in the cell wall and endoplasmic reticulum stress responses induced by human antimicrobial peptide ll-37. *Int. J. Mol. Sci.* 22, 10633. doi:10.3390/ijms221910633

Huang, D., Dobbins, D., Ghahramani, P., Friedland, I., and Steckbeck, J. (2022). A phase 1 study of the safety, tolerability, and pharmacokinetics of single ascending doses of a first-in-human engineered cationic peptide, plg0206, intravenously administered in healthy subjects. *Antimicrob. Agents Chemother.* 66, e0144121. doi:10.1128/aac.01441-21

Huang, D., Pachuda, N., Sauer, J. M., Dobbins, D., and Steckbeck, J. (2021). The engineered antibiotic peptide plg0206 eliminates biofilms and is a potential treatment for periprosthetic joint infections. *Antibiot. (Basel, Switz.* 11, 41. doi:10.3390/antibiotics11010041

Jiang, L., Xu, D., Sellati, T. J., and Dong, H. (2015). Self-assembly of cationic multidomain peptide hydrogels: Supramolecular nanostructure and rheological properties dictate antimicrobial activity. *Nanoscale* 7, 19160–19169. doi:10.1039/c5nr05233e

Kalaiselvan, P., Dutta, D., Bhombal, F., Konda, N., Vaddavalli, P. K., Sharma, S., et al. (2022). Ocular microbiota and lens contamination following mel4 peptide-coated antimicrobial contact lens (macl) extended wear. *Cont. Lens Anterior Eye* 45, 101431. doi:10.1016/j.clae.2021.02.017

Kazemzadeh-Narbat, M., Kindrachuk, J., Duan, K., Jenssen, H., Hancock, R. E., and Wang, R. (2010). Antimicrobial peptides on calcium phosphate-coated titanium for the prevention of implant-associated infections. *Biomaterials* 31, 9519–9526. doi:10.1016/j.biomaterials.2010.08.035

Kumar, P., Kizhakkedathu, J. N., and Straus, S. K. (2018). Antimicrobial peptides: Diversity, mechanism of action and strategies to improve the activity and biocompatibility *in vivo*. *Biomolecules* 8, 4. doi:10.3390/biom8010004

Lee, J. T., Wang, G., Tam, Y. T., and Tam, C. (2016). Membrane-active epithelial keratin 6a fragments (kamps) are unique human antimicrobial peptides with a non-αβ structure. *Front. Microbiol.* 7, 1799. doi:10.3389/fmicb.2016.01799

Lee, J. Y., Yang, S. T., Lee, S. K., Jung, H. H., Shin, S. Y., Hahm, K. S., et al. (2008). Salt-resistant homodimeric bactenecin, a cathelicidin-derived antimicrobial peptide. *FEBS J.* 275, 3911–3920. doi:10.1111/j.1742-4658.2008.06536.x

Lee, S. W. L., Paoletti, C., Campisi, M., Osaki, T., Adriani, G., Kamm, R. D., et al. (2019). Microrna delivery through nanoparticles. *J. Control. Release* 313, 80–95. doi:10.1016/j.jconrel.2019.10.007

Li, C., Liu, H., Yang, Y., Xu, X., Lv, T., Zhang, H., et al. (2018). N-myristoylation of antimicrobial peptide cm4 enhances its anticancer activity by interacting with cell membrane and targeting mitochondria in breast cancer cells. *Front. Pharmacol.* 9, 1297. doi:10.3389/fphar.2018.01297

Li, H., Zhang, S., Nie, B., Du, Z., Long, T., and Yue, B. (2018). The antimicrobial peptide kr-12 promotes the osteogenic differentiation of human bone marrow stem cells by stimulating bmp/smad signaling. *RSC Adv.* 8, 15547–15557. doi:10.1039/c8ra00750k

Li, N., Bai, J., Wang, W., Liang, X., Zhang, W., Li, W., et al. (2021). Facile and versatile surface functional polyetheretherketone with enhanced bacteriostasis and osseointegrative capability for implant application. *ACS Appl. Mat. Interfaces* 13, 59731–59746. doi:10.1021/acsami.1c19834

Li, T., Wang, N., Chen, S., Lu, R., Li, H., and Zhang, Z. (2017). Antibacterial activity and cytocompatibility of an implant coating consisting of TiO_2 nanotubes combined with a GL13K antimicrobial peptide. *Int. J. Nanomedicine* 12, 2995–3007. doi:10.2147/ijn.S128775

Li, X., Contreras-Garcia, A., LoVetri, K., Yakandawala, N., Wertheimer, M. R., De Crescenzo, G., et al. (2015). Fusion peptide p15-csp shows antibiofilm activity and pro-osteogenic activity when deposited as a coating on hydrophilic but not hydrophobic surfaces. *J. Biomed. Mat. Res. A* 103, 3736–3746. doi:10.1002/jbm.a.35511

Libardo, M. D. J., Bahar, A. A., Ma, B., Fu, R., McCormick, L. E., Zhao, J., et al. (2017). Nuclease activity gives an edge to host-defense peptide piscidin 3 over piscidin 1, rendering it more effective against persisters and biofilms. *FEBS J.* 284, 3662–3683. doi:10.1111/febs.14263

Lipsky, B. A., Holroyd, K. J., and Zasloff, M. (2008). Topical versus systemic antimicrobial therapy for treating mildly infected diabetic foot ulcers: A randomized, controlled, double-blinded, multicenter trial of pexiganan cream. *Clin. Infect. Dis. official Publ. Infect. Dis. Soc. Am.* 47, 1537–1545. doi:10.1086/593185

Liu, H. W., Wei, D. X., Deng, J. Z., Zhu, J. J., Xu, K., Hu, W. H., et al. (2018). Combined antibacterial and osteogenic *in situ* effects of a bifunctional titanium alloy with nanoscale hydroxyapatite coating. *Artif. Cells Nanomed. Biotechnol.* 46, S460–s470. doi:10.1080/21691401.2018.1499662

Liu, Z., Yuan, X., Liu, M., Fernandes, G., Zhang, Y., Yang, S., et al. (2018). Antimicrobial peptide combined with bmp2-modified mesenchymal stem cells promotes calvarial repair in an osteolytic model. *Mol. Ther.* 26, 199–207. doi:10.1016/j.ymthe.2017.09.011

Luca, V., Stringaro, A., Colone, M., Pini, A., and Mangoni, M. L. (2013). Esculentin(1-21), an amphibian skin membrane-active peptide with potent activity on both planktonic and biofilm cells of the bacterial pathogen pseudomonas aeruginosa. *Cell. Mol. Life Sci.* 70, 2773–2786. doi:10.1007/s00018-013-1291-7

Luo, Y., and Song, Y. (2021). Mechanism of antimicrobial peptides: Antimicrobial, anti-inflammatory and antibiofilm activities. *Int. J. Mol. Sci.* 22, 11401. doi:10.3390/ijms222111401

Ma, H., Zhao, X., Yang, L., Su, P., Fu, P., Peng, J., et al. (2020). Antimicrobial peptide AMP-17 affects Candida albicans by disrupting its cell wall and cell membrane integrity. *Infect. Drug Resist.* 13, 2509–2520. doi:10.2147/idr.S250278

Mahlapuu, M., Björn, C., and Ekblom, J. (2020). Antimicrobial peptides as therapeutic agents: Opportunities and challenges. *Crit. Rev. Biotechnol.* 40, 978–992. doi:10.1080/07388551.2020.1796576

Martin-Loeches, I., Dale, G. E., and Torres, A. (2018). Murepavadin: A new antibiotic class in the pipeline. *Expert Rev. anti-infective Ther.* 16, 259–268. doi:10.1080/14787210.2018.1441024

Meng, X., Zhang, J., Chen, J., Nie, B., Yue, B., Zhang, W., et al. (2020). Kr-12 coating of polyetheretherketone (peek) surface via polydopamine improves osteointegration and antibacterial activity *in vivo*. *J. Mat. Chem. B* 8, 10190–10204. doi:10.1039/d0tb01899f

Mohamed, M. F., Abdelkhalek, A., and Seleem, M. N. (2016). Evaluation of short synthetic antimicrobial peptides for treatment of drug-resistant and intracellular staphylococcus aureus. *Sci. Rep.* 6, 29707. doi:10.1038/srep29707

Mookherjee, N., Anderson, M. A., Haagsman, H. P., and Davidson, D. J. (2020). Antimicrobial host defence peptides: Functions and clinical potential. *Nat. Rev. Drug Discov.* 19, 311–332. doi:10.1038/s41573-019-0058-8

Nguyen, H. L. T., Trujillo-Paez, J. V., Umehara, Y., Yue, H., Peng, G., Kiatsurayanon, C., et al. (2020). Role of antimicrobial peptides in skin barrier repair in individuals with atopic dermatitis. *Int. J. Mol. Sci.* 21, 7607. doi:10.3390/ijms21207607

Nguyen, L. T., Haney, E. F., and Vogel, H. J. (2011). The expanding scope of antimicrobial peptide structures and their modes of action. *Trends Biotechnol.* 29, 464–472. doi:10.1016/j.tibtech.2011.05.001

Niemeyer-van der Kolk, T., Buters, T. P., Krouwels, L., Boltjes, J., de Kam, M. L., van der Wall, H., et al. (2022). Topical antimicrobial peptide omiganan recovers cutaneous dysbiosis but does not improve clinical symptoms in patients with mild to moderate atopic dermatitis in a phase 2 randomized controlled trial. *J. Am. Acad. Dermatology* 86, 854–862. doi:10.1016/j.jaad.2020.08.132

Niemeyer-van der Kolk, T., van der Wall, H., Hogendoorn, G. K., Rijneveld, R., Luijten, S., van Alewijk, D., et al. (2020). Pharmacodynamic effects of topical omiganan in patients with mild to moderate atopic dermatitis in a randomized, placebo-controlled, phase ii trial. *Clin. Transl. Sci.* 13, 994–1003. doi:10.1111/cts.12792

Ong, Z. Y., Cheng, J., Huang, Y., Xu, K., Ji, Z., Fan, W., et al. (2014). Effect of stereochemistry, chain length and sequence pattern on antimicrobial properties of short synthetic β-sheet forming peptide amphiphiles. *Biomaterials* 35, 1315–1325. doi:10.1016/j.biomaterials.2013.10.053

Panayotov, I. V., Orti, V., Cuisinier, F., and Yachouh, J. (2016). Polyetheretherketone (peek) for medical applications. *J. Mat. Sci. Mat. Med.* 27, 118. doi:10.1007/s10856-016-5731-4

Park, C. B., Kim, H. S., and Kim, S. C. (1998). Mechanism of action of the antimicrobial peptide buforin ii: Buforin ii kills microorganisms by penetrating the cell membrane and inhibiting cellular functions. *Biochem. biophysical Res. Commun.* 244, 253–257. doi:10.1006/bbrc.1998.8159

Pena, O. M., Afacan, N., Pistolic, J., Chen, C., Madera, L., Falsafi, R., et al. (2013). Synthetic cationic peptide idr-1018 modulates human macrophage differentiation. *PloS one* 8, e52449. doi:10.1371/journal.pone.0052449

Peng, L. H., Huang, Y. F., Zhang, C. Z., Niu, J., Chen, Y., Chu, Y., et al. (2016). Integration of antimicrobial peptides with gold nanoparticles as unique non-viral vectors for gene delivery to mesenchymal stem cells with antibacterial activity. *Biomaterials* 103, 137–149. doi:10.1016/j.biomaterials.2016.06.057

Ridyard, K. E., and Overhage, J. (2021). The potential of human peptide ll-37 as an antimicrobial and anti-biofilm agent. *Antibiot. (Basel, Switz.* 10, 650. doi:10.3390/antibiotics10060650

Rijsbergen, M., Rijneveld, R., Todd, M., Feiss, G. L., Kouwenhoven, S. T. P., Quint, K. D., et al. (2020). Results of phase 2 trials exploring the safety and efficacy of omiganan in patients with human papillomavirus-induced genital lesions. *Br. J. Clin. Pharmacol.* 86, 2133–2143. doi:10.1111/bcp.14181

Roy, R., Tiwari, M., Donelli, G., and Tiwari, V. (2018). Strategies for combating bacterial biofilms: A focus on anti-biofilm agents and their mechanisms of action. *Virulence* 9, 522–554. doi:10.1080/21505594.2017.1313372

Ryu, J. H., Messersmith, P. B., and Lee, H. (2018). Polydopamine surface chemistry: A decade of discovery. *ACS Appl. Mat. Interfaces* 10, 7523–7540. doi:10.1021/acsami.7b19865

Sader, H. S., Flamm, R. K., Dale, G. E., Rhomberg, P. R., and Castanheira, M. (2018). Murepavadin activity tested against contemporary (2016-17) clinical isolates of xdr pseudomonas aeruginosa. *J. Antimicrob. Chemother.* 73, 2400–2404. doi:10.1093/jac/dky227

Shen, X., Al-Baadani, M. A., He, H., Cai, L., Wu, Z., Yao, L., et al. (2019). Antibacterial and osteogenesis performances of ll37-loaded titania nanopores *in vitro* and *in vivo*. *Int. J. Nanomedicine* 14, 3043–3054. doi:10.2147/ijn.S198583

Sinha, S., Zheng, L., Mu, Y., Ng, W. J., and Bhattacharjya, S. (2017). Structure and interactions of a host defense antimicrobial peptide thanatin in lipopolysaccharide micelles reveal mechanism of bacterial cell agglutination. *Sci. Rep.* 7, 17795. doi:10.1038/s41598-017-18102-6

Steinberg, D. A., Hurst, M. A., Fujii, C. A., Kung, A. H., Ho, J. F., Cheng, F. C., et al. (1997). Protegrin-1: A broad-spectrum, rapidly microbicidal peptide with *in vivo* activity. *Antimicrob. Agents Chemother.* 41, 1738–1742. doi:10.1128/aac.41.8.1738

Sternlicht, M. D., and Werb, Z. (2001). How matrix metalloproteinases regulate cell behavior. *Annu. Rev. Cell Dev. Biol.* 17, 463–516. doi:10.1146/annurev.cellbio.17.1.463

Thapa, R. K., Diep, D. B., and Tønnesen, H. H. (2020). Topical antimicrobial peptide formulations for wound healing: Current developments and future prospects. *Acta biomater.* 103, 52–67. doi:10.1016/j.actbio.2019.12.025

Tian, J., Shen, S., Zhou, C., Dang, X., Jiao, Y., Li, L., et al. (2015). Investigation of the antimicrobial activity and biocompatibility of magnesium alloy coated with ha and antimicrobial peptide. *J. Mat. Sci. Mat. Med.* 26, 66. doi:10.1007/s10856-015-5389-3

Torres, P., Díaz, J., Arce, M., Silva, P., Mendoza, P., Lois, P., et al. (2017). The salivary peptide histatin-1 promotes endothelial cell adhesion, migration, and angiogenesis. *FASEB J.* 31, 4946–4958. doi:10.1096/fj.201700085R

Trotti, A., Garden, A., Warde, P., Symonds, P., Langer, C., Redman, R., et al. (2004). A multinational, randomized phase iii trial of iseganan hcl oral solution for reducing the severity of oral mucositis in patients receiving radiotherapy for head-and-neck malignancy. *Int. J. Radiat. Oncology*Biology*Physics* 58, 674–681. doi:10.1016/s0360-3016(03)01627-4

Trzcińska, Z., Bruggeman, M., Ijakipour, H., Hodges, N. J., Bowen, J., and Stamboulis, A. (2020). Polydopamine linking substrate for amps: Characterisation and stability on ti6al4v. *Mater. (Basel)* 13, 3714. doi:10.3390/ma13173714

Tsai, P. W., Yang, C. Y., Chang, H. T., and Lan, C. Y. (2011). Human antimicrobial peptide ll-37 inhibits adhesion of candida albicans by interacting with yeast cell-wall carbohydrates. *PloS one* 6, e17755. doi:10.1371/journal.pone.0017755

Vallet-Regí, M., Lozano, D., González, B., and Izquierdo-Barba, I. (2020). Biomaterials against bone infection. *Adv. Healthc. Mat.* 9, e2000310. doi:10.1002/adhm.202000310

van der Does, A. M., Hiemstra, P. S., and Mookherjee, N. (2019). Antimicrobial host defence peptides: Immunomodulatory functions and translational prospects. *Adv. Exp. Med. Biol.* 1117, 149–171. doi:10.1007/978-981-13-3588-4_10

Veiga, A. S., Sinthuvanich, C., Gaspar, D., Franquelim, H. G., Castanho, M. A., and Schneider, J. P. (2012). Arginine-rich self-assembling peptides as potent antibacterial gels. *Biomaterials* 33, 8907–8916. doi:10.1016/j.biomaterials.2012.08.046

Wach, A., Dembowsky, K., and Dale, G. E. (2018). Pharmacokinetics and safety of intravenous murepavadin infusion in healthy adult subjects administered single and multiple ascending doses. *Antimicrob. Agents Chemother.* 62, e02355–17. doi:10.1128/aac.02355-17

Wang, B., Bian, A., Jia, F., Lan, J., Yang, H., Yan, K., et al. (2022). "Dual-functional" strontium titanate nanotubes designed based on fusion peptides simultaneously enhancing anti-infection and osseointegration. *Biomater. Adv.* 133, 112650. doi:10.1016/j.msec.2022.112650

Wang, J., Dou, X., Song, J., Lyu, Y., Zhu, X., Xu, L., et al. (2019). Antimicrobial peptides: Promising alternatives in the post feeding antibiotic era. *Med. Res. Rev.* 39, 831–859. doi:10.1002/med.21542

Wang, L., Wei, X., Duan, C., Yang, J., Xiao, S., Liu, H., et al. (2022). Bone marrow mesenchymal stem cell sheets with high expression of hbd3 and ctgf promote periodontal regeneration. *Biomater. Adv.* 133, 112657. doi:10.1016/j.msec.2022.112657

Wenzel, M., Chiriac, A. I., Otto, A., Zweytick, D., May, C., Schumacher, C., et al. (2014). Small cationic antimicrobial peptides delocalize peripheral membrane proteins. *Proc. Natl. Acad. Sci. U. S. A.* 111, E1409–E1418. doi:10.1073/pnas.1319900111

Wisdom, E. C., Zhou, Y., Chen, C., Tamerler, C., and Snead, M. L. (2020). Mitigation of peri-implantitis by rational design of bifunctional peptides with antimicrobial properties. *ACS Biomater. Sci. Eng.* 6, 2682–2695. doi:10.1021/acsbiomaterials.9b01213

Yang, G., Huang, T., Wang, Y., Wang, H., Li, Y., Yu, K., et al. (2018). Sustained release of antimicrobial peptide from self-assembling hydrogel enhanced osteogenesis. *J. biomaterials Sci. Polym. Ed.* 29, 1812–1824. doi:10.1080/09205063.2018.1504191

Yasir, M., Dutta, D., Kumar, N., and Willcox, M. D. P. (2020). Interaction of the surface bound antimicrobial peptides melimine and mel4 with staphylococcus aureus. *Biofouling* 36, 1019–1030. doi:10.1080/08927014.2020.1843638

Yazici, H., O'Neill, M. B., Kacar, T., Wilson, B. R., Oren, E. E., Sarikaya, M., et al. (2016). Engineered chimeric peptides as antimicrobial surface coating agents toward infection-free implants. *ACS Appl. Mat. Interfaces* 8, 5070–5081. doi:10.1021/acsami.5b03697

Yu, M., Yan, J., He, W., Li, C., Ma, P. X., and Lei, B. (2017). Synthetic θ-defensin antibacterial peptide as a highly efficient nonviral vector for redox-responsive mirna delivery. *Adv. Biosyst.* 1, e1700001. doi:10.1002/adbi.201700001

Yuan, X., Ouyang, L., Luo, Y., Sun, Z., Yang, C., Wang, J., et al. (2019). Multifunctional sulfonated polyetheretherketone coating with beta-defensin-14 for yielding durable and broad-spectrum antibacterial activity and osseointegration. *Acta Biomater.* 86, 323–337. doi:10.1016/j.actbio.2019.01.016

Zhai, M., Zhu, Y., Yang, M., and Mao, C. (2020). Human mesenchymal stem cell derived exosomes enhance cell-free bone regeneration by altering their mirnas profiles. *Adv. Sci. (Weinheim, Baden-Wurttemberg, Ger.* 7, 2001334. doi:10.1002/advs.202001334

Zhang, Q. Y., Yan, Z. B., Meng, Y. M., Hong, X. Y., Shao, G., Ma, J. J., et al. (2021). Antimicrobial peptides: Mechanism of action, activity and clinical potential. *Mil. Med. Res.* 8, 48. doi:10.1186/s40779-021-00343-2

Zhang, S., Zhou, X., Liu, T., Huang, Y., and Li, J. (2021). The effects of peptide mel4-coated titanium plates on infection rabbits after internal fixation of open fractures. *Arch. Orthop. Trauma Surg.* 142, 729–734. doi:10.1007/s00402-020-03694-y

Zhang, X., Geng, H., Gong, L., Zhang, Q., Li, H., Zhang, X., et al. (2018). Modification of the surface of titanium with multifunctional chimeric peptides to prevent biofilm formation via inhibition of initial colonizers. *Int. J. Nanomedicine* 13, 5361–5375. doi:10.2147/ijn.S170819

Zhongxing, L., Shaohong, W., Jinlong, L., Limin, Z., Yuanzheng, W., Haipeng, G., et al. (2021). Three-dimensional printed hydroxyapatite bone tissue engineering scaffold with antibacterial and osteogenic ability. *J. Biol. Eng.* 15, 21. doi:10.1186/s13036-021-00273-6

Zhou, L., Han, Y., Ding, J., Chen, X., Huang, S., Xing, X., et al. (2021). Regulation of an antimicrobial peptide gl13k-modified titanium surface on osteogenesis, osteoclastogenesis, and angiogenesis base on osteoimmunology. *ACS Biomater. Sci. Eng.* 7, 4569–4580. doi:10.1021/acsbiomaterials.1c00639

Zhou, Y. Q., Shi, Y., Yang, L., Sun, Y. F., Han, Y. F., Zhao, Z. X., et al. (2020). Genetically engineered distal airway stem cell transplantation protects mice from pulmonary infection. *EMBO Mol. Med.* 12, e10233. doi:10.15252/emmm.201810233

Zou, P., Chen, W. T., Sun, T., Gao, Y., Li, L. L., and Wang, H. (2020). Recent advances: Peptides and self-assembled peptide-nanosystems for antimicrobial therapy and diagnosis. *Biomater. Sci.* 8, 4975–4996. doi:10.1039/d0bm00789g

frontiers | Frontiers in Bioengineering and Biotechnology

TYPE Original Research
PUBLISHED 25 October 2022
DOI 10.3389/fbioe.2022.1036223

OPEN ACCESS

EDITED BY
Yansong Qi,
Inner Mongolia People's Hospital, China

REVIEWED BY
Jia Shao,
Henan Provincial People's Hospital, China
Yongxiong He,
Second Affiliated Hospital of Hainan Medical University, China
Bin Zhu,
Capital Medical University, China

*CORRESPONDENCE
Ai-Bing Huang,
hab165@163.com

†These authors have contributed equally to this work

SPECIALTY SECTION
This article was submitted to Biomaterials, a section of the journal Frontiers in Bioengineering and Biotechnology

RECEIVED 04 September 2022
ACCEPTED 13 October 2022
PUBLISHED 25 October 2022

CITATION
Wang L, Bai M, Li X-B, Wang Z-R, Wang B and Huang A-B (2022), Does the sizing of current cervical disc arthroplasty systems match Chinese cervical anatomic dimensions?
Front. Bioeng. Biotechnol. 10:1036223. doi: 10.3389/fbioe.2022.1036223

Does the sizing of current cervical disc arthroplasty systems match Chinese cervical anatomic dimensions?

Lu Wang[1,2†], Meng Bai[3†], Xing-Bin Li[1,2†], Zhao-Rui Wang[1,2], Bang Wang[1,2] and Ai-Bing Huang[1,2*]

[1]Postgraduate School, Dalian Medical University, Dalian, Liaoning, China, [2]Department of Orthopedics, Taizhou People's Hospital Affiliated to Nanjing Medical University, Taizhou, Jiangsu, China, [3]Department of Orthopedics, Xi'an People's Hospital, Xi'an, Shaanxi, China

Objective: The objectives of this study were to analyze the computed tomography (CT) scan imaging data of the cervical spine from healthy volunteers and to correlate the measurements to the dimensions of current cervical disc arthroplasty systems.

Methods: A total of 130 participants (78 males and 52 females) with a mean age of 41.0 years (range 18.0–66.0 years) who had undergone computed tomography scans of the cervical spine were included. The linear parameters of the C3 to C7 levels, including anterior-posterior diameter (AP), middle disc height (DH), anterior disc height (ADH), posterior disc height (PDH) and center mediolateral diameter (ML), were measured. The analysis was conducted comparing different cervical levels, sexes, and age groups. Known dimensions from eight cervical disc arthroplasty systems were compared with the morphologic data.

Results: A total of 520 vertebral segments were measured. The mean values for the measured parameters were as follows: anterior-posterior diameter 16.08 ± 1.84 mm, mediolateral diameter 16.13 ± 1.99 mm, anterior disc height 3.88 ± 1.11 mm, disc height 5.73 ± 1.00 mm, posterior disc height 2.83 ± 0.94 mm, and mediolateral diameter/anterior-posterior diameter 1.01 ± 0.13. All parameters except for posterior disc height were significantly different across the different cervical levels ($p < 0.05$). There were also significant sex differences in terms of the linear parameters. No differences were found in the majority of parameters among the different age groups ($p > 0.05$), except for anterior-posterior diameter at the C6/7 level. A comparison of the bone dimensions from the study data and the dimensions of the implants indicated the presence of a size mismatch in the currently available cervical disc prostheses.

Abbreviations: CT, computed tomography; AP, anterior-posterior diameter; DH, middle disc height; ADH, anterior disc height; PDH, posterior disc height; ML, mediolateral diameter; ACDF, anterior cervical decompression and fusion; CDR, cervical disc replacement; PACS, picture archiving and communication system; HO, heterotopic ossification; FDA, Food and Drug Administration.

Conclusion: There is a large discrepancy between the cervical anatomical data of Chinese patients and the sizes of currently available prostheses. The dimensions collected in this study could be used to design and develop appropriate disc prostheses for Chinese patients.

KEYWORDS

anatomical measurement, cervical disc replacement, prosthesis, match, cervical disc arthroplasty

Introduction

Cervical spondylosis is a degenerative condition of the intervertebral discs and vertebral bodies, in which compression of the cervical nerve root or spinal cord leads to several motor and sensory dysfunctions. Essential surgical treatments may be indicated for patients with persistent radicular pain after conservative treatment and profound or progressive motor weakness. Anterior cervical decompression and fusion (ACDF) was first described by Smith and Robinson in the 1950s, and since then, it has been widely performed for the treatment of degenerative disc disease associated with radiculopathy or myelopathy (Smith and Robinson, 1958). However, ACDF sacrifices segmental mobility, and the fusion of one or more segments in this procedure may increase stress and motion at the adjacent unfused segments, accelerating adjacent segment degeneration (ASD) and spondylotic changes (Donk et al., 2018; Vleggeert-Lankamp et al., 2019).

Over the past several years, cervical disc replacement (CDR) has been extensively introduced to restore mobility at the operated segment and decrease the aforementioned stress, which in turn should prevent the development of ASD due to ACDF (4). Despite the good prospects for this technique, some adverse complications have been reported, namely, heterotopic ossification (HO), prosthesis migration and subsidence, bone loss, and segmental kyphosis (Li et al., 2019; Virk et al., 2021). While the reasons for the development of these conditions are undoubtedly complex, some reports have revealed that many of these factors are associated with the mismatch between the dimensions of the cervical endplates and the footprints of the prostheses (Thaler et al., 2013; Guo et al., 2020). Although differences in cervical endplate size among different races was previously confirmed (Yao et al., 2018), few artificial discs are designed specifically to satisfy the demand of the Chinese population. At present, an increasing number of types of artificial cervical disc prostheses have received approval from the U.S. Food and Drug Administration (FDA). Regionally, do the sizes of current prostheses exactly meet the anatomical characteristics of the cervical spine in East Chinese adults? Supportive anthropometric evidence for answering this question is lacking.

Consequently, the purpose of the present study was to compare the parameters of cervical vertebrae in the Chinese population with the sizes of eight artificial cervical disc prostheses approved by the FDA and to provide reference data for the design of future cervical devices.

Materials and methods

This is a retrospective study. After approval of our ethics committee, we collected data from 130 participants (78 males and 52 females) with a mean age of 41 years (range 18–66 years) who underwent CT scans of the cervical spine between January 2015 and December 2018. Age was categorized into three groups for analysis: Group A (<35 years), Group B (35–49 years), and Group C (≥50 years) (Table 1).

All participants were recruited, and those without signs of anatomical anomalies and no obvious degenerative conditions of the cervical spine (e.g., cervical disc herniation, osteophyte formation and ossification of the anterior or posterior longitudinal ligament) in the CT examination were included in the study, while patients with congenital dysplasia, tumor, bone fracture, infection, and prior cervical spine surgery were excluded.

CT scans were performed for all patients with 64-slice multidetector row CT scanners. All images were transferred to a picture archiving and communication system (PACS) and were measured directly using the built-in tools of the PACS workstations.

For better determine the dimension, the measurement was taken from the mid-sagittal plane and the mid-coronal plane. The linear parameters of each intervertebral segment (C3/4, C4/5, C5/6, and C6/7) were measured as follows: (Food and Drug Administration, 2007a) the anterior-posterior (AP) diameter, measured as the mean value of the AP diameters of the superior endplate (AP1), middle intervertebral space (AP2) and inferior endplate (AP3) in sagittal CT scans to

TABLE 1 Study population categorized by sex and age.

Groups	Age	n (130)	
		Male	Female
Group A	<35	24	16
Group B	35–49	31	18
Group C	≥50	23	18

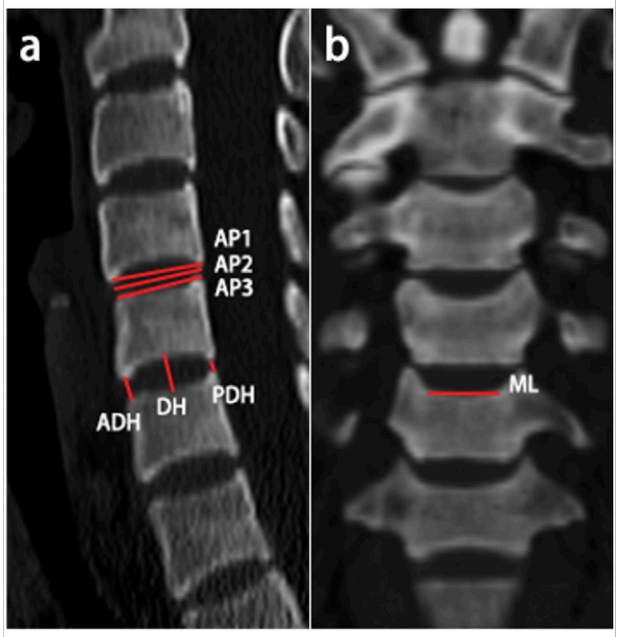

FIGURE 1
Schematic representation of the measured linear parameters. **(A)** The anterior-posterior diameter and anterior/middle/posterior disc height were measured in sagittal CT scans; **(B)** The center mediolateral diameter of the superior vertebral endplates was measured in coronal CT scans.

minimize measurement errors (Figure 1A); (Vleggeert-Lankamp et al., 2019) the disc height of the anterior (ADH), middle (DH) and posterior (PDH) disc space (Figure 1A); and (Donk et al., 2018) the center mediolateral (ML) diameter of the superior endplates in coronal CT scans (Figure 1B). The above measurements were taken by two of the authors. Mean data was obtained for final analysis.

For the matching performance evaluation, cervical measurements were compared with the sizes of eight current, FDA-approved brands of artificial cervical disc prostheses: Prestige ST (Medtronic), Bryan (Medtronic), ProDisc-C (Synthes), PCM (NuVasive), Prestige LP (Medtronic), Secure-C (Globus), Mobi-C (LDR) and M6-C (Spinal Kinetics). The sizes of each prosthesis are listed in Figure 2).

Statistical analysis was performed using Excel (Microsoft Excel 2019), SPSS (IBM SPSS Statistics 26), and Prism software (GraphPad Prism 8). Based on Skewness and Kurtosis, the data showed normal distribution. The measurement data are expressed as the mean ± standard deviation ($\bar{x} \pm s$). Differences between groups were compared by independent sample t tests or one-way analysis of variance. p values less than 0.05 ($p < 0.05$) were considered statistically significant.

Results

A total of 130 patients with 520 vertebral segments were included in the analyses. The mean values for each measurement were as follows: AP 16.08 ± 1.84 mm, ML 16.13 ± 1.99 mm, ADH 3.88 ± 1.11 mm, DH 5.73 ± 1.00 mm, and PDH 2.83 ± 0.94 mm. Morphological CT scan data are presented in Table 2. All measurements except PDH were significantly different among cervical segments.

The analysis results for males and females are shown in Table 3. The majority of comparisons were statistically significant ($p < 0.05$). Nevertheless, there was a marginally significant difference in the ML at the C4/C5 segment (15.63 ± 1.47 mm vs. 15.18 ± 1.28 mm, $p = 0.07$). There was no significant difference in ADH at either C3/4 (3.46 ± 1.02 mm vs. 3.22 ± 0.87 mm, P=0.18) or C5/6 [4.16 ± 1. (Food and Drug Administration, 2012a) mm vs. 3.76 ± 1.20 mm, P=0.06]. The DH at the C5/6 segment was 5.72 ± 1.04 mm in males and 5.44 ±

Device								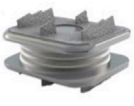
Trade Name	Prestige ST	Bryan	ProDisc-C	PCM	Prestige LP	Secure-C	Mobi-C	M6-C
Manufacturer	Medtronic	Medtronic	Synthes	NuVasive	Medtronic	Globus	LDR	Spinal Kinetics
AP Dimensions (mm)	12, 14, 16, 18	14, 15, 16, 17, 18	12, 14, 16, 18	14, 16, 17	12, 14, 16, 18	11, 13, 14	13, 14, 15	12.5, 14, 15, 16
ML Dimensions (mm)	17.8	14, 15, 16, 17, 18	15, 17, 19	17, 20	15, 17.8	12, 14, 16	15, 17, 19	15, 17
Disc Heights (mm)	6, 7, 8	6	5, 6, 7	6.5, 7.2, 8	5, 6, 7, 8	7, 8, 9, 10, 11, 12	5, 6, 7	6, 7

FIGURE 2
Prosthesis information: Prestige ST (10), Bryan (Food and Drug Administration, 2009), ProDisc-C (12), PCM(13), Prestige LP (14, 15), Secure-C (16), Mobi-C (17, 18), M6-C (19).

TABLE 2 Dimensions of Linear Parameters ($\bar{X} \pm S$, mm).

Dimensions	C3/4	C4/5	C5/6	C6/7	Total
AP	15.42 ± 1.64	15.78 ± 1.81	16.42 ± 1.88	16.72 ± 1.76	16.08 ± 1.84
ML	14.58 ± 1.45	15.45 ± 1.41	16.59 ± 1.59	17.91 ± 1.72	16.13 ± 1.99
ADH	3.37 ± 0.97	3.74 ± 1.03	3.74 ± 1.17	4.42 ± 1.00	3.88 ± 1.11
DH	5.51 ± 0.99	5.59 ± 0.92	5.59 ± 0.96	6.21 ± 0.99	5.73 ± 1.00
PDH	2.96 ± 0.92	2.94 ± 0.97	2.94 ± 0.94	2.72 ± 0.92	2.83 ± 0.94

0.82 mm in females, showing no statistically significant difference ($p = 0.10$). The DH at the C6/7 segment was 6.31 ± 1.02 mm in males and 6.06 ± 0.92 mm in females, showing no statistically significant difference ($p = 0.16$). Additionally, there was no significant difference in the PDH at C4/5 (3.05 ± 1.01 mm vs. 2.76 ± 0.89 mm, $p = 0.09$), C5/6 (2.74 ± 0.97 mm vs. 2.66 ± 0.89 mm, $p = 0.61$) or C6/7 (2.62 ± 0.94 mm vs. 2.79 ± 0.91 mm, $p = 0.30$).

The AP in group B was significantly larger than that in group A at the C5/C6 and C6/C7 segments ($p = 0.04$ and $p = 0.02$). There were no other differences in the parameters between the age groups (Figure 3).

The width of the ML increased with increasing AP. Figure 4 shows the surprising differences between the footprints of the cervical disc prostheses and the cervical measurement distribution. A notable proportion of mediolateral prosthesis diameters were larger than the ML when the anterior-posterior diameters of the prostheses matched the AP distribution at the C3/4 segment (Figure 4A). At the C4/5 segment, the matching degree between the mediolateral diameters of the prostheses and the ML was better than that at the C3/4 segment, but the mediolateral diameters of the prostheses were mismatched for smaller values of the ML. The matching degree between the anterior-posterior diameters of the prostheses and the AP was lower than that at the C3/4 segment, and the anterior-posterior diameters of the prostheses were mismatched for larger values of the AP (Figure 4B). The highest matching degree between the mediolateral diameters of the prostheses and the ML was observed at the C5/6 segment, but the anterior-posterior diameters of the prostheses were mismatched for large values of the AP (Figure 4C). At the C6/7 segment, all implant devices were too small to match the measured ML and AP values (Figure 4D). In general, the matching degree between the AP and ML and the sizes of the different types of prostheses were unsatisfactory.

Moreover, a negative correlation was observed between ML/AP and AP, and the slopes for women were steeper than those for men with increasing AP between cervical segments. Again, the width-to-depth ratio of most designs, which represents the degree of endplate asymmetry, did not follow similar trends well, particularly for the Bryan device (Figure 5).

TABLE 3 Sex differences in Linear Parameters ($\bar{X} \pm S$).

Dimensions	Group	C3/4	C4/5	C5/6	C6/7	Total
AP (mm)	Male	16.29 ± 1.39	16.63 ± 1.57	17.27 ± 1.82	17.57 ± 1.59	16.94 ± 1.67
	Female	14.10 ± 0.98	14.49 ± 1.33	15.14 ± 1.11	15.44 ± 1.14	14.80 ± 1.25
	p value	0.00	0.00	0.00	0.00	0.00
ML (mm)	Male	14.92 ± 1.33	15.63 ± 1.47	16.90 ± 1.59	18.45 ± 1.62	16.47 ± 2.01
	Female	14.09 ± 1.49	15.18 ± 1.28	16.11 ± 1.50	17.12 ± 1.58	15.62 ± 1.84
	p value	0.00	0.07	0.01	0.00	0.00
ADH (mm)	Male	3.46 ± 1.02	3.98 ± 1.05	4.16 ± 1.13	4.64 ± 0.95	4.06 ± 1.12
	Female	3.22 ± 0.87	3.38 ± 0.89	3.76 ± 1.20	4.09 ± 0.98	3.61 ± 1.04
	p value	0.18	0.00	0.06	0.00	0.00
DH (mm)	Male	5.86 ± 0.94	5.91 ± 0.84	5.72 ± 1.04	6.31 ± 1.02	5.95 ± 0.98
	Female	4.98 ± 0.82	5.13 ± 0.84	5.44 ± 0.82	6.06 ± 0.92	5.4 ± 0.94
	p value	0.00	0.00	0.10	0.16	0.00
PDH (mm)	Male	3.16 ± 0.96	3.05 ± 1.01	2.74 ± 0.97	2.62 ± 0.94	2.94 ± 0.97
	Female	2.67 ± 0.79	2.76 ± 0.89	2.66 ± 0.89	2.79 ± 0.91	2.68 ± 0.87
	p value	0.00	0.09	0.61	0.30	0.00

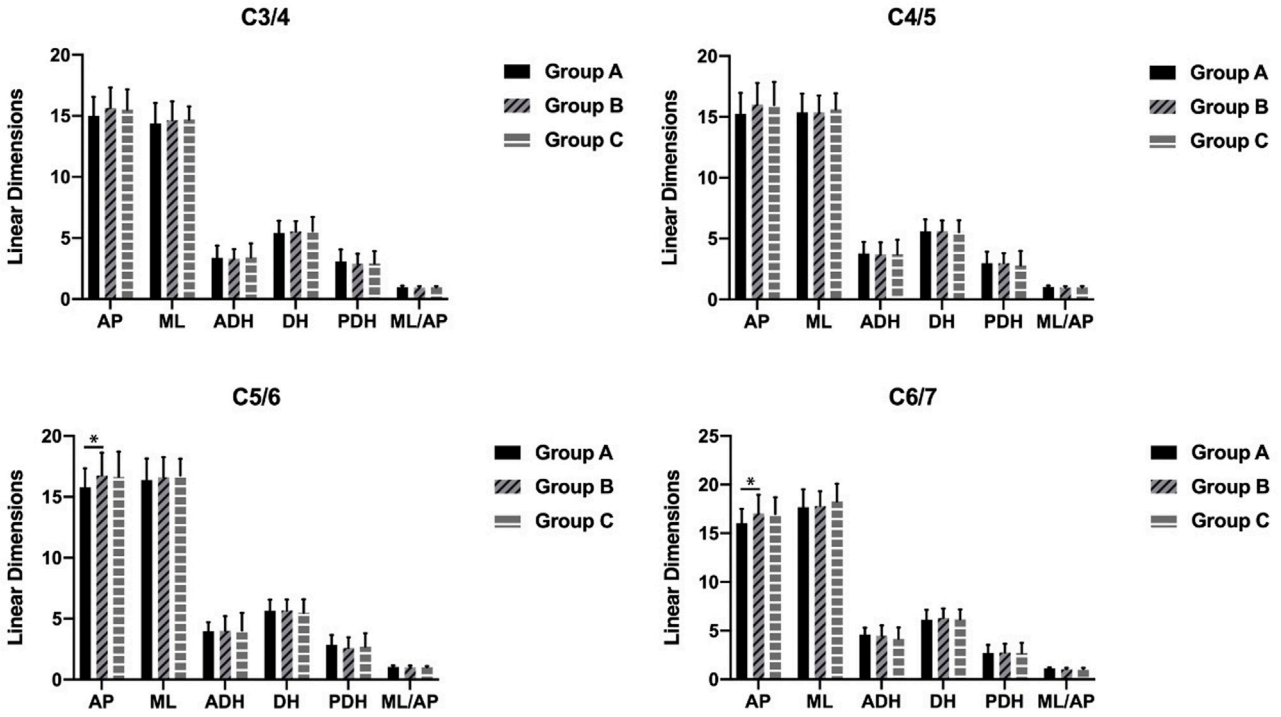

FIGURE 3
Differences among different age groups (*$p < 0.05$).

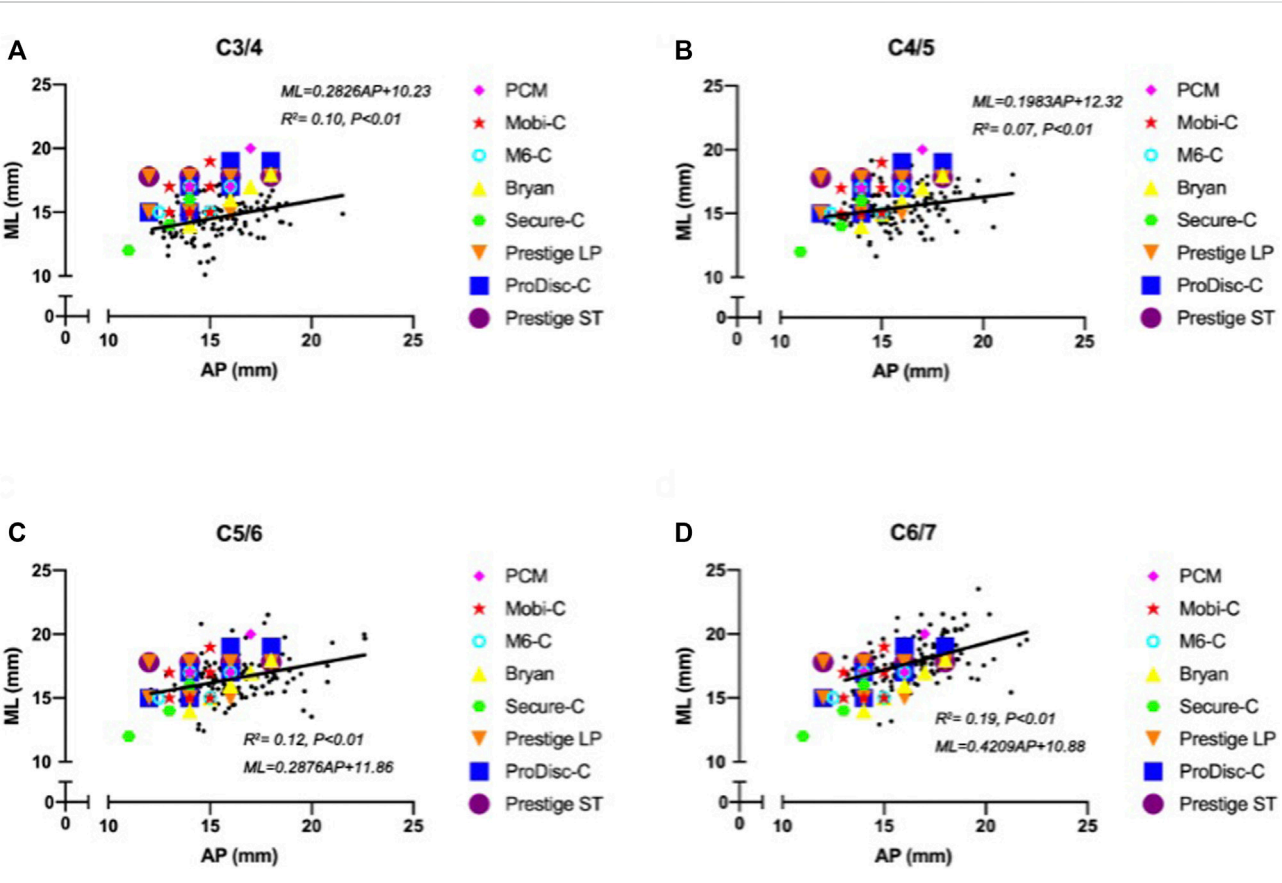

FIGURE 4
Mismatch between cervical anatomical data and the sizes of prostheses.

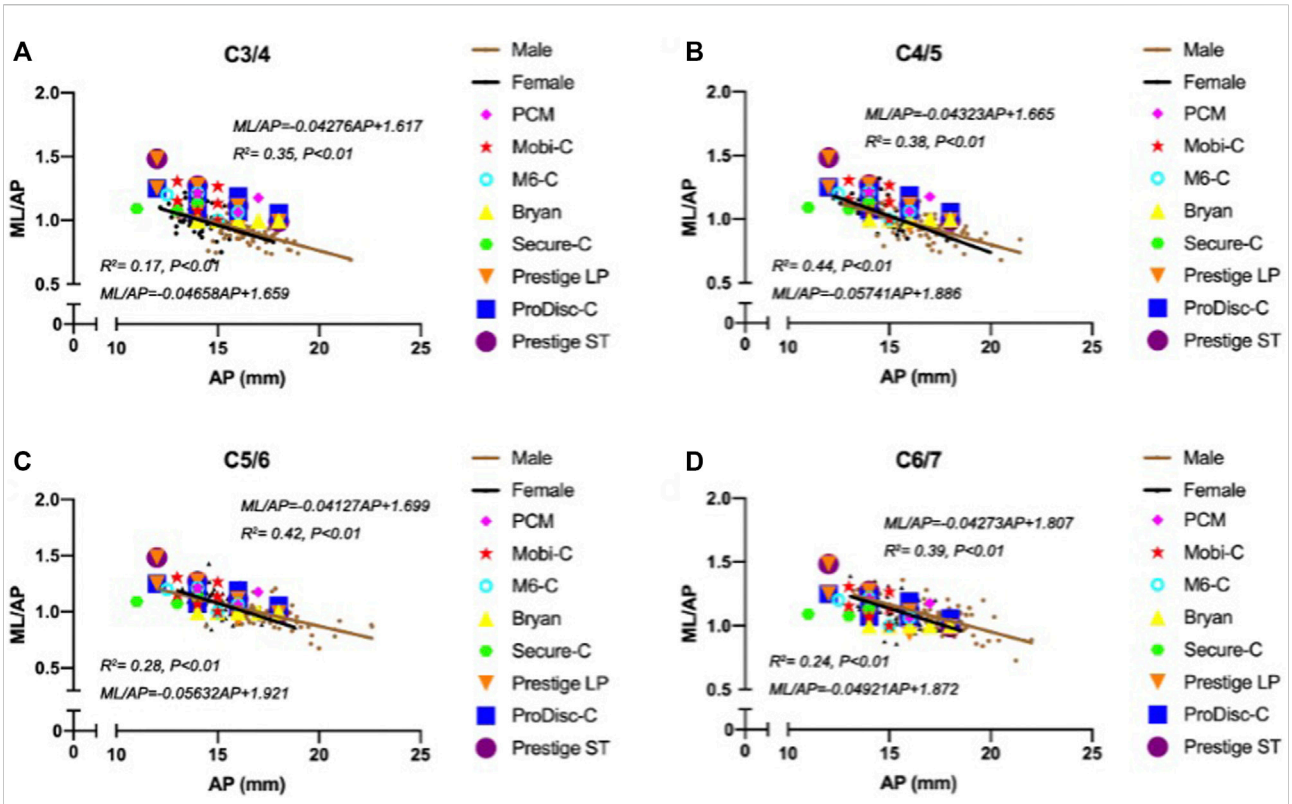

FIGURE 5
Mismatch of the width-to-depth ratio between cervical anatomical data and prostheses.

Many studies have reported on the measurement of cervical spine endplates (Kim et al., 1976; Panjabi et al., 1976; Tan et al., 2004; Feng et al., 2017). The results in the present study are shown compared with previous measurements from different parts of the world in Figure 6.

The minimum height of the prostheses was 5 mm (Mobi-C, ProDisc-C, Prestige LP), and the maximum prosthetic height was (Food and Drug Administration, 2007b) mm (Secure-C). The DH measurements ranged from 2.07 to 8.98 mm among the 130 patients. A considerable proportion of DH measurements were smaller than the minimum height of the available prostheses, as shown in Figure 7. Up to 34 patients had smaller DH values at C3/4 (26.15%), 31 patients had smaller values at C4/5 (23.85%), 33 patients had smaller values at C5/6 (25.38%) and 13 patients had smaller values at C6/7 (10%).

Discussion

Over the past few decades, ACDF has become the standard procedure for the effective treatment of degenerative cervical spondylosis. Excessive compensatory activity, however, may lead to ASD, and some complications, including bone graft nonunion, implant migration, subsidence and bone donor site pain, have been observed during long-term follow-up (Yan et al., 2017). In contrast, as a nonfusion decompression method, CDR has become a more favored strategy in terms of preserving the motion of index segments and natural cervical kinematics (Findlay et al., 2018). Many biomechanical and clinical studies have shown that as an alternative to ACDF, CDR not only achieves similar outcomes but also reduces the incidence of ASD through motion preservation (Zou et al., 2017; Zhao and Yuan, 2019). In addition, CDR has been undergoing constant improvements and evidence-based redesigns to reduce prosthesis-related complications, such as implant dislocation, subsidence, migration, device wear and HO, which are often-mentioned side-effects (Lin et al., 1976), although the majority of them are usually asymptomatic in the short term and can be mitigated to a certain degree by proper patient selection and attention to the surgical technique (Salari and McAfee, 2012).

In our study, there was a large discrepancy between the cervical anatomical data of Chinese individuals and the footprints of currently available prostheses. The footprint

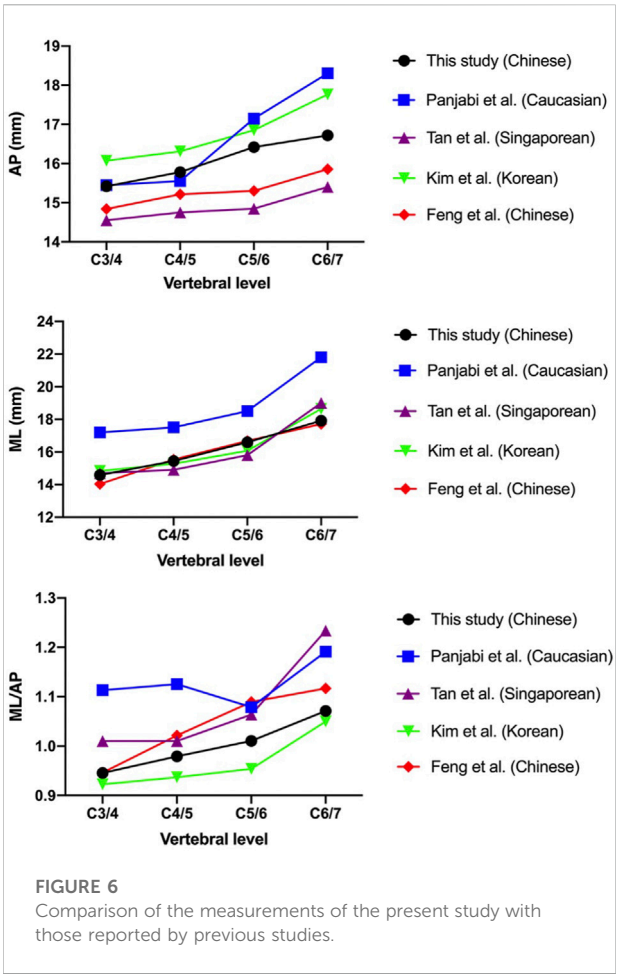

FIGURE 6
Comparison of the measurements of the present study with those reported by previous studies.

is the part of the disk prosthesis designed to cover the endplate of the vertebra. Size matching between the prosthesis and cervical vertebra can not only provide a greater contact area between the prosthesis and cervical endplate but can also cover the peripheral marginal zones of the cervical endplate, which provides much stronger support than the central areas. Our results are consistent with other studies demonstrating the presence and prevalence of serious footprint mismatch. Thaler et al. (Thaler et al., 2013) measured the dimensions of cervical vertebrae from the CT scans of 24 patients and assessed the accuracy of matches achieved with common cervical disc prostheses (Bryan, Prestige LP, Discover, ProDisc-C). Overall, they found that compared with the cervical endplate diameters, 53.5% of the largest device footprints were smaller in their anterior-posterior diameter, and 51.1% were smaller in the mediolateral diameter. In the same manner, Dong et al. (Dong et al., 2015) reported that the mismatch in the available dimensions of prostheses and the anatomic data of cervical endplates ranged from 17.03% to 57.61% in the anterior-posterior diameter and 35.51%–94.93% in the mediolateral diameter. In fact, given that there is a one-to-one correspondence between the measurements of cervical vertebrae and the sizes of cervical disc prostheses in a practical clinical setting rather than a size comparison of the frequency distribution, the true mismatching degree of prostheses might have been underestimated.

Footprint mismatch has been implicated as a major contributor to the development of prosthesis-related complications such as implant subsidence, migration and HO [(Food and Drug Administration, 2019), (Tu et al., 2012)]. An oversized implant may protrude and thus compress the nerves and soft tissues, which can further cause clinical issues and diseases. Undersized footprints could potentially cause subsidence and dislocation because of inadequate load distribution (Lin et al., 1976; Thaler et al., 2013). Guo et al. (Guo et al., 2020) reported that the mean footprint matching degree was 0.877 ± 0.068 in the sagittal plane and 0.852 ± 0.092 in the coronal plane. The mean overall footprint matching degree was 0.699 ± 0.102, and HO occurrence was significantly related to footprint mismatch. In multivariable analysis, Yang et al. (Yang et al., 2019) showed that patients with residual exposed endplates larger than 2 mm 4.5 times more likely to develop high-grade HO ($p = 0.02$) than patients with residual exposed endplates less than or equal to 2 mm. Therefore, maximizing the implant-endplate interface may help to reduce high-grade HO and preserve motion. Following data analysis, the ML/AP among different segments and sexes showed a statistically significant difference in our study. From the C3/4 to C6/7 discs, the vertebral endplate gradually becomes more elliptical (Feng et al., 2017). Although many prosthesis models are currently available for CDR, our findings indicated that the width-to-depth ratio of most designs did not follow similar trends well. Considering the above, it is important to design an artificial disc that imitates the shape of the endplates adjacent to a natural disc in all three dimensions.

The height of the artificial cervical disc prosthesis is mainly designed according to the middle disc height. Our study found that a considerable proportion of disc height measurements were less than the minimums height of available implants. An appropriate artificial disc height can achieve near-normal biomechanical properties. The increased disc height could result in decreased overlap of the facet joint articulation, reducing the restriction of flexion-extension motion, which would facilitate cervical rotation in the sagittal plane. A few studies (Peng et al., 2009; Kang et al., 2010) have suggested that the postoperative intersegmental range of motion is affected by disc height or disc height increment. Prostheses with heights ≥2 mm greater than normal can lead to marked changes in the abovementioned cervical biomechanics and bone-implant interface stress, which may induce ASD and subsidence (Yuan et al., 2018). Thus, when selecting an appropriate cervical implant, surgeons should consider patient height as well as estimated normal disc height.

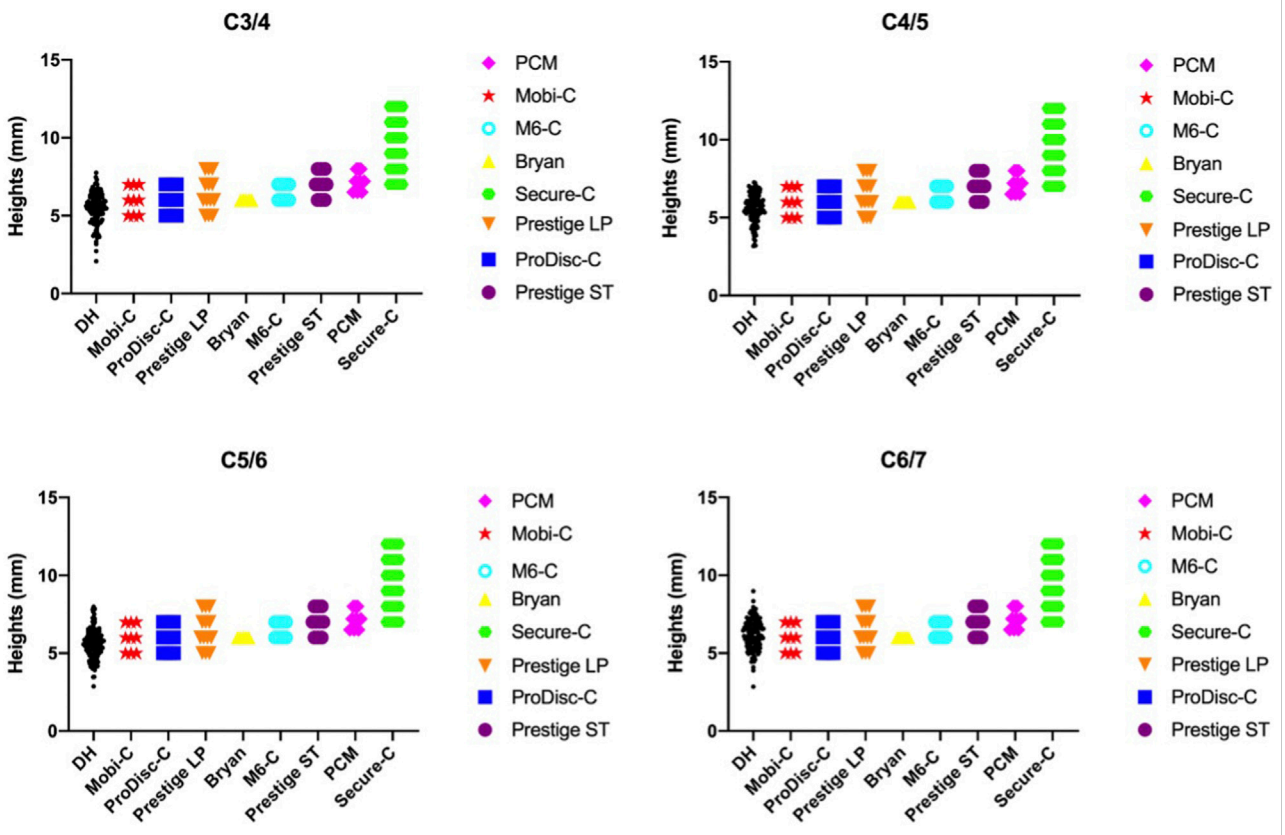

FIGURE 7
Mismatch between cervical anatomical data and the sizes of prostheses.

Possible reasons for footprint mismatch include the following: first, the footprint dimensions of currently available disk prostheses were derived from early white cadaver data, and anatomic studies illustrated a large discrepancy between the footprint dimensions and anatomic data (Thaler et al., 2013; Karaca et al., 2016). Second, the available prostheses only provide limited choices in the contour footprint dimensions that cannot match various anatomic dimensions. Our findings are aligned with those of previous studies showing that the linear parameters of the cervical endplates vary among different ethnicities (Kim et al., 1976; Panjabi et al., 1976; Tan et al., 2004; Feng et al., 2017). In particular, the MLs in Caucasian cervical vertebrae are considerably larger than those reported in Asian subjects, as are the ML/AP values at the C3/4 and C4/5 segments. As the field of medicine continues to adopt 3D printing technologies, the use of 3D printing materials may provide a better quantitative understanding of anatomical implant design and help decrease postoperative complications.

The current study nevertheless had several limitations. One is the relatively small number of recruited subjects. Data from 130 Chinese subjects were collected retrospectively. Although geographical discrepancy was avoided in this analysis as much as possible, more patients should probably be included in future studies, which could minimize the problem with statistical bias. In addition, several other types and brands of cervical disc devices unapproved by the FDA for the treatment of cervical spondylosis and discogenic disease were not included in the present study. Lastly, we must acknowledge that the design characteristics of artificial disc was not only based on these anatomy parameters. There are several factors that provided challenges when trying to design a new generation disc. Although the aforementioned morphometric evaluation of cervical vertebrae is not a new subject, we will collect more data and extract more features to provide useful guidance and reference for the design of Chinese artificial discs with higher accuracy in future studies.

Conclusion

Following data analysis, cervical measurements showed significant differences among different segments and sexes.

There was a large discrepancy between the cervical anatomical data of Chinese individuals and the sizes of currently available prostheses. This study may provide useful guidance and a reference for the design of artificial discs for Chinese populations.

Data availability statement

The original contributions presented in the study are included in the article/supplementary material, further inquiries can be directed to the corresponding author.

Author contributions

LW, MB and AH conceived the study and design. They were involved in drafting and revising the manuscript. XL, ZW and BW provided critical revision of the manuscript. All authors read and approved the final manuscript.

Acknowledgments

We thank Hong-Qi Sun from Third Affiliated Hospital of Southern Medical University for participating in this study.

Conflict of interest

The authors declare that the research was conducted in the absence of any commercial or financial relationships that could be construed as a potential conflict of interest.

Publisher's note

All claims expressed in this article are solely those of the authors and do not necessarily represent those of their affiliated organizations, or those of the publisher, the editors and the reviewers. Any product that may be evaluated in this article, or claim that may be made by its manufacturer, is not guaranteed or endorsed by the publisher.

References

Chang, C. C., Huang, W. C., Wu, J. C., and Mummaneni, P. V. (2018). The option of motion preservation in cervical spondylosis: Cervical disc arthroplasty update. *Neurospine* 15 (4), 296–305. doi:10.14245/ns.1836186.093

Dong, L., Tan, M. S., Yan, Q. H., Yi, P., Yang, F., Tang, X. S., et al. (2015). Footprint mismatch of cervical disc prostheses with Chinese cervical anatomic dimensions. *Chin. Med. J. Engl.* 128 (2), 197–202. doi:10.4103/0366-6999.149200

Donk, R. D., Verhagen, W. I. M., Hosman, A. J. F., Verbeek, A., and Bartels, R. H. M. A. (2018). Symptomatic adjacent segment disease after anterior cervical discectomy for single-level degenerative disk disease. *Clin. Spine Surg.* 31 (1), E50–E54. doi:10.1097/BSD.0000000000000551

Feng, H., Fang, X. Y., Huang, D. G., Yu, C. C., Li, H. K., Zhao, S. C., et al. (2017). A morphometric study of the middle and lower cervical vertebral endplates and their components. *Med. Baltim.* 96 (10), e6296. doi:10.1097/MD.0000000000006296

Findlay, C., Ayis, S., and Demetriades, A. K. (2018). Total disc replacement versus anterior cervical discectomy and fusion: A systematic review with meta-analysis of data from a total of 3160 patients across 14 randomized controlled trials with both short- and medium- to long-term outcomes. *Bone Jt. J.* 100-B (8), 991–1001. doi:10.1302/0301-620X.100B8.BJJ-2018-0120.R1

Food and Drug Administration (2009). Data from: BRYAN® cervical disc. Summary of safety and effectiveness data (SSED). Available at: https://fda.report/PMA/P060023/6/P060023B.pdf.

Food and Drug Administration (2019). Data from: M6-CTM artificial cervical disc. Summary of safety and effectiveness data (SSED). Available at: https://www.accessdata.fda.gov/cdrh_docs/pdf17/P170036B.pdf.

Food and Drug Administration (2013). Data from: Mobi-C® cervical disc prosthesis one-level. Summary of safety and effectiveness data (SSED). Available at: https://www.accessdata.fda.gov/cdrh_docs/pdf11/P110002B.pdf.

Food and Drug Administration (2013). Data from: Mobi-C® cervical disc prosthesis two-level. Summary of safety and effectiveness data (SSED). Available at: https://www.accessdata.fda.gov/cdrh_docs/pdf11/P110009B.pdf.

Food and Drug Administration (2012). Data from: PCM® cervical disc. Summary of safety and effectiveness data (SSED). Available from: https://www.accessdata.fda.gov/cdrh_docs/pdf10/P100012B.pdf.

Food and Drug Administration (2016). Data from: PRESTIGE LP™ cervical disc. Summary of safety and effectiveness data (SSED). Available at: https://www.accessdata.fda.gov/cdrh_docs/pdf9/P090029S003B.pdf.

Food and Drug Administration (2007). Data from: PRESTIGE® cervical disc system. Summary of safety and effectiveness data (SSED). Available at https://www.accessdata.fda.gov/cdrh_docs/pdf6/P060018B.pdf.

Food and Drug Administration (2014). Data from: PRESTIGE® LP cervical disc. Summary of safety and effectiveness data (SSED). Available at: https://www.accessdata.fda.gov/cdrh_docs/pdf9/P090029B.pdf.

Food and Drug Administration (2007). Data from: ProDisc™-C total disc replacement. Summary of safety and effectiveness data (SSED). Available at: http://www.accessdata.fda.gov/cdrh_docs/pdf7/P070001b.pdf.

Food and Drug Administration (2012). Data from: SECURE®-C cervical artificial disc. Summary of safety and effectiveness data (SSED). Available at: https://www.accessdata.fda.gov/cdrh_docs/pdf10/P100003B.pdf.

Guo, Q., Fang, Z., Guan, H., Xiong, W., and Li, F. (2020). The effect of footprint mismatch on heterotopic ossification after cervical disk replacement. *Clin. Spine Surg.* 33 (6), E241–E250. doi:10.1097/BSD.0000000000000943

Kang, K. C., Lee, C. S., Han, J. H., and Chung, S. S. (2010). The factors that influence the postoperative segmental range of motion after cervical artificial disc replacement. *Spine J.* 10 (8), 689–696. doi:10.1016/j.spinee.2010.04.016

Karaca, S., Akpolat, A. O., Oztermeli, A., Erdem, M. N., and Aydogan, M. (2016). Discrepancy between cervical disc prostheses and anatomical cervical dimensions. *Acta Orthop. Traumatol. Turc.* 50 (5), 544–547. doi:10.1016/j.aott.2016.03.003

Kim, M. K., Kwak, D. S., Park, C. K., Park, S. H., Oh, S. M., Lee, S. W., et al. (1976). Quantitative anatomy of the endplate of the middle and lower cervical vertebrae in Koreans. *Spine* 32 (14), E376–E381. doi:10.1097/BRS.0b013e318067e384

Li, G., Wang, Q., Liu, H., and Yang, Y. (2019). Postoperative heterotopic ossification after cervical disc replacement is likely a reflection of the degeneration process. *World Neurosurg. x.* 125, e1063–e1068. doi:10.1016/j.wneu.2019.01.244

Lin, C. Y., Kang, H., Rouleau, J. P., Hollister, S. J., and Marca, F. L. (1976). Stress analysis of the interface between cervical vertebrae end plates and the bryan, Prestige LP, and ProDisc-C cervical disc prostheses: An *in vivo* image-based finite element study. *Spine* 34 (15), 1554–1560. doi:10.1097/BRS.0b013e3181aa643b

Panjabi, M. M., Duranceau, J., Goel, V., Oxland, T., and Takata, K. (1976). Cervical human vertebrae. Quantitative three-dimensional anatomy of the middle and lower regions. *Spine (Phila Pa* 16 (8), 861–869. doi:10.1097/00007632-199108000-00001

Peng, C. W. B., Quirno, M., Quirnoa, M., Bendo, J. A., Spivak, J. M., and Goldstein, J. A. (2009). Effect of intervertebral disc height on postoperative motion and clinical outcomes after Prodisc-C cervical disc replacement. *Spine J.* 9 (7), 551–555. doi:10.1016/j.spinee.2009.03.008

Salari, B., and McAfee, P. C. (2012). Cervical total disk replacement: Complications and avoidance. *Orthop. Clin. North Am.* 43 (1), 97–107. doi:10.1016/j.ocl.2011.08.006

Smith, G. W., and Robinson, R. A. (1958). The treatment of certain cervical-spine disorders by anterior removal of the intervertebral disc and interbody fusion. *J. Bone Jt. Surg.* 40A (3), 607–624. doi:10.2106/00004623-195840030-00009

Tan, S. H., Teo, E. C., and Chua, H. C. (2004). Quantitative three-dimensional anatomy of cervical, thoracic and lumbar vertebrae of Chinese Singaporeans. *Eur. Spine J.* 13 (2), 137–146. doi:10.1007/s00586-003-0586-z

Thaler, M., Hartmann, S., Gstöttner, M., Lechner, R., Gabl, M., and Bach, C. (2013). Footprint mismatch in total cervical disc arthroplasty. *Eur. Spine J.* 22 (4), 759–765. doi:10.1007/s00586-012-2594-3

Tu, T. H., Wu, J. C., Huang, W. C., Wu, C. L., Ko, C. C., and Cheng, H. (2012). The effects of carpentry on heterotopic ossification and mobility in cervical arthroplasty: Determination by computed tomography with a minimum 2-year follow-up: Clinical article. *J. Neurosurg. Spine* 16 (6), 601–609. doi:10.3171/2012.3.SPINE11436

Virk, S., Phillips, F., Khan, S., and Qureshi, S. (2021). A cross-sectional analysis of 1347 complications for cervical disc replacements from medical device reports maintained by the United States Food and Drug Administration. *Spine J.* 21 (2), 265–272. doi:10.1016/j.spinee.2020.09.005

Vleggeert-Lankamp, C. L. A., Janssen, T. M. H., van Zwet, E., Goedmakers, C. M. W., Bosscher, L., Peul, W., et al. (2019). The NECK trial: Effectiveness of anterior cervical discectomy with or without interbody fusion and arthroplasty in the treatment of cervical disc herniation; a double-blinded randomized controlled trial. *Spine J.* 19 (6), 965–975. doi:10.1016/j.spinee.2018.12.013

Yan, S. Z., Di, J., and Shen, Y. (2017). Adjacent segment degeneration following anterior cervical discectomy and fusion versus the bryan cervical disc arthroplasty. *Med. Sci. Monit.* 23, 2692–2700. doi:10.12659/msm.905178

Yang, M. M. H., Ryu, W. H. A., Casha, S., DuPlessis, S., Jacobs, W. B., and Hurlbert, R. J. (2019). Heterotopic ossification and radiographic adjacent-segment disease after cervical disc arthroplasty. *J. Neurosurg.* 31, 660–669. doi:10.3171/2019.5.SPINE19257

Yao, Q., Yin, P., Khan, K., Tsai, T. Y., Li, J. S., Hai, Y., et al. (2018). Differences of the morphology of subaxial cervical spine endplates between Chinese and white men and women. *Biomed. Res. Int.* 2018, 1–8. doi:10.1155/2018/2854175

Yuan, W., Zhang, H., Zhou, X., Wu, W., and Zhu, Y. (2018). The influence of artificial cervical disc prosthesis height on the cervical biomechanics: A finite element study. *World Neurosurg.* 113, e490–e498. doi:10.1016/j.wneu.2018.02.062

Zhao, X., and Yuan, W. (2019). Biomechanical analysis of cervical range of motion and facet contact force after a novel artificial cervical disc replacement. *Am. J. Transl. Res.* 11 (5), 3109–3115.

Zou, S., Gao, J., Xu, B., Lu, X., Han, Y., and Meng, H. (2017). Anterior cervical discectomy and fusion (ACDF) versus cervical disc arthroplasty (CDA) for two contiguous levels cervical disc degenerative disease: A meta-analysis of randomized controlled trials. *Eur. Spine J.* 26 (4), 985–997. doi:10.1007/s00586-016-4655-5

frontiers | Frontiers in Bioengineering and Biotechnology

TYPE Original Research
PUBLISHED 28 October 2022
DOI 10.3389/fbioe.2022.1047187

OPEN ACCESS

EDITED BY
Yansong Qi,
Inner Mongolia People's Hospital, China

REVIEWED BY
Zhenxing Shao,
Peking University Third Hospital, China
Chengyu Zhuang,
Shanghai Jiao Tong University, China

*CORRESPONDENCE
Jianhai Chen,
shoulderchen@126.com

†These authors have contributed equally to this work

SPECIALTY SECTION
This article was submitted to Biomaterials, a section of the journal Frontiers in Bioengineering and Biotechnology

RECEIVED 17 September 2022
ACCEPTED 17 October 2022
PUBLISHED 28 October 2022

CITATION
Ding Z, Ju J, Ma M, Zhang Y and Chen J (2022), Tuberosity reconstruction baseplate for shoulder hemiarthroplasty: Morphological design and biomaterial application. *Front. Bioeng. Biotechnol.* 10:1047187. doi: 10.3389/fbioe.2022.1047187

Tuberosity reconstruction baseplate for shoulder hemiarthroplasty: Morphological design and biomaterial application

Zhentao Ding[1,2,3†], Jiabao Ju[1,2,3†], Mingtai Ma[1,2,3], Yichong Zhang[1,2,3] and Jianhai Chen[1,2,3*]

[1]Department of Orthopedics and Trauma, Peking University People's Hospital, Beijing, China, [2]National Center for Trauma Medicine, Peking University People's Hospital, Beijing, China, [3]Key Laboratory of Trauma and Neural Regeneration (Peking University), Ministry of Education, Beijing, China

Background: Shoulder hemiarthroplasty is prone to tuberosity malposition and migration, reducing the rate of tuberosity healing. We proposed to design a tuberosity reconstruction baseplate to assist in tuberosity integration and to evaluate the mechanical properties of baseplate made from the novel biomaterial carbon fiber reinforced polymer (CFRP) composites.

Methods: The three-dimensional model of native proximal humerus was constructed by computed tomography (CT) data. The morphological design of baseplate was based on the tuberosity contour and rotator cuff footprint. Finite element models were created for different thicknesses of CFRP composites, poly (ether-ether-ketone) (PEEK) and titanium-nickel (TiNi) alloy. The permissible load and suture hole displacements were applied to evaluate the mechanical properties.

Results: The structurally optimized model made of CFRP composites provided superior strength and deformability, compared to the PEEK material and TiNi alloy. Its permissible load was above 200 N and the suture hole displacement was between 0.9 and 1.4 mm.

Conclusion: This study proposed a method for designing tuberosity reconstruction baseplate based on morphological data and extended the application of biomaterial CFRP composites in orthopedics field. The optimized model made of CFRP composites allowed a certain extent of elastic deformation and showed the possibility for dynamic compression of tuberosity bone blocks.

KEYWORDS

tuberosity reconstruction baseplate, shoulder hemiarthroplasty, tuberosity healing, carbon fiber reinforced polymer, finite element analysis, structure optimization

Introduction

Proximal humeral fractures are the third most common type of osteoporotic fracture in elderly patients (Launonen et al., 2015). Older patients often present with comminuted Neer 3- and 4-part fractures and are vulnerable to complications after plate fixation (Stone and Namdari, 2019). Nowadays, shoulder hemiarthroplasty is an effective treatment option for non-reconstructable proximal humeral fractures. However, recent clinical follow-up studies have demonstrated that the recovery of mobility and function after hemiarthroplasty is not satisfactory (Yahuaca et al., 2020; Amundsen et al., 2021). Nonunion and malunion of tuberosities are risk factors for postoperative joint function (Tanner and Cofield, 1983; Kralinger et al., 2004). Therefore, the focus of hemiarthroplasty is on restoring anatomical structure of the proximal humerus.

Tuberosity malposition is associated substantially with the implant design and fixation technique. After implantation of the humeral prosthetic stem, the tuberosity fracture fragments are repositioned by suture traction, and then the greater and lesser tuberosity are reattached to the stem by cerclage (Neer, 1970). However, the cerclage suture is prone to inferior migration of tuberosities, which leads to malreduction (Boileau et al., 2002). Furthermore, due to the secondary migration following rotator cuff contraction, the cerclage suture is difficult to achieve effective tuberosity reconstruction (Grubhofer et al., 2021). In the setting of bony comminution and local osteoporosis, there is also lack of anatomical landmark for tuberosity reduction (Frankle et al., 2001).

In the light of these issues, we propose to design a tuberosity reconstruction baseplate placed between the prosthetic humeral head and stem to assist in tuberosity reduction and fixation. The contour of greater and lesser tuberosity designed on this baseplate serves as a landmark for anatomical reduction. Prefabricated suture holes corresponding to the rotator cuff insertions are available to determine relative position of the prosthetic humeral head and tuberosities. In addition, the baseplate is expected to have a certain elastic deformability. With continuous traction of the rotator cuff, the baseplate is able to provide dynamic compression between the tuberosity bone blocks by tension band effect. In this study, the materials for baseplate were screened by finite element analysis, including the novel biomaterial carbon fiber reinforced polymer (CFRP) composites [CF/epoxy laminates, Toray Company Ltd., material code T800/3900 (Ahmad et al., 2019)] and two other conventional orthopedic implant materials. Subsequently, the strength and deformability of baseplate were improved through structural optimization.

Materials and methods

Tuberosity reconstruction baseplate design

The geometry of tuberosity reconstruction baseplate consists of the greater and lesser tuberosity and intertubercular groove that provides a landmark for the anatomical reduction in hemiarthroplasty procedure. The morphological design requires a suitable section to depict the humeral shape of anatomical neck and its distal region. The anatomical neck section is approximately circular and does not allow for a distinct tuberosity contour. Therefore, the baseplate design should be based on the distal section of anatomical neck.

A 47-year-old male volunteer (Ethics Committee of Peking University People's Hospital, 2020PHB072-01, Beijing, China) with no severe trauma history or obvious anatomical abnormality was recruited. Computed tomography (CT) data of the proximal humerus were imported into Mimics 19.0 (Materialise, Leuven, Belgium) in DICOM format. Automatic threshold-based segmentation extracted bone tissue from the CT data to construct a 3D model of the native proximal humerus (Figure 1A). In this model, the contour of anatomical neck could be clearly identified. The osteotomy level was set at a 45-degree angle to the humeral stem, and the humeral head was virtually resected along the anatomical neck to obtain the anatomical neck section (Figure 1B). The virtual osteotomy level was translated distally to obtain sections 1–5 mm from anatomical neck (Figure 1C). Among these, section 5 mm from anatomical neck showed a clear contour of the greater and lesser tuberosity as well as intertubercular groove. Therefore, this section was chosen for the morphological design (Figure 1D). According to the anatomical landmarks of proximal humerus, the rotator cuff footprint was depicted on the 3D model (Figure 1E) (Curtis et al., 2006; Mochizuki et al., 2008). Prefabricated suture holes were determined at the corresponding locations on baseplate. The suture holes were set at 2 mm in diameter and 2 mm from the edge. Each suture hole was spaced more than 1 cm apart.

The blueprint of tuberosity reconstruction baseplate was shown in Figure 2. Two prominences corresponded to the greater and lesser tuberosity. Five suture holes adjacent to the tuberosities corresponded to superior and inferior subscapularis, supraspinatus, infraspinatus, and teres minor, respectively, for knotting and fixing the baseplate to rotator cuff. Two additional holes were provided at 6 o'clock position for vertical knotting. The baseplate thicknesses were set to 1, 1.5, 2, 2.5, and 3 mm, and the diameter was set to 40 mm to create five finite element models.

Finite element analysis

The finite element models were automatically meshed in Hypermesh 12.0 (Altair Engineering GmbH, Böblingen, Germany). The mesh type was a 4-node linear tetrahedral element (C3D4) with the mesh size of 0.4 mm. Preprocessing and linear static analysis were performed in Ansys 19.0 (ANSYS, Inc., Canonsburg, PA, United States). The baseplates were manufactured from three of the most widely used orthopedic implant materials, including poly

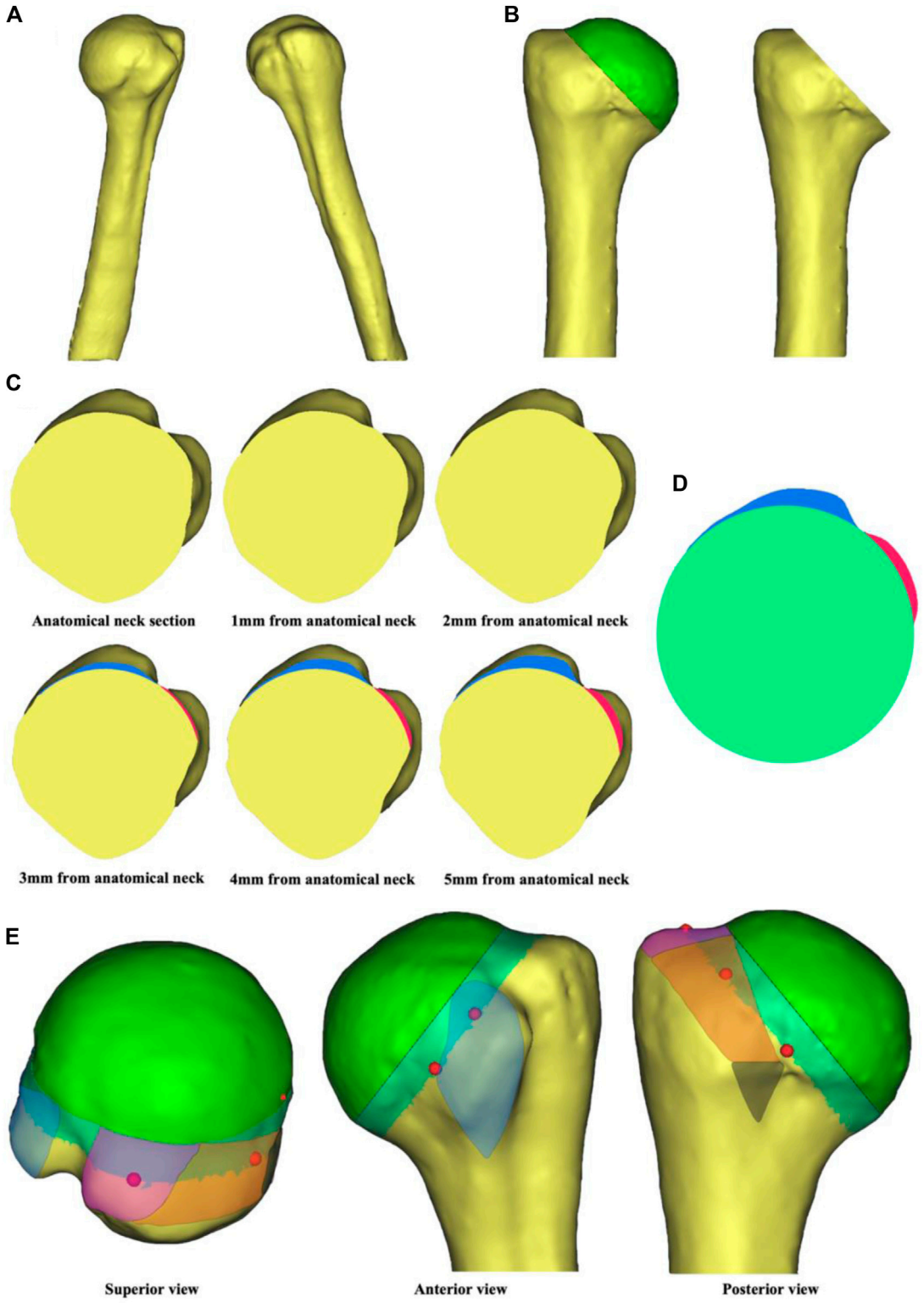

FIGURE 1
Steps in tuberosity reconstruction baseplate design. **(A)** Construction of a 3D native proximal humerus model. **(B)** Virtual osteotomy along the anatomical neck. **(C)** Anatomical neck section and sections 1–5 mm from anatomical neck. The blue region represents contour of the greater tuberosity and the red region represents contour of the lesser tuberosity. **(D)** Morphological design of the baseplate. **(E)** Location of the suture holes based on rotator cuff footprint. The blue region is for subscapularis, the purple region is for supraspinatus, the orange region is for infraspinatus, and the black region is for teres minor. The red dots are reference points for the location of suture holes.

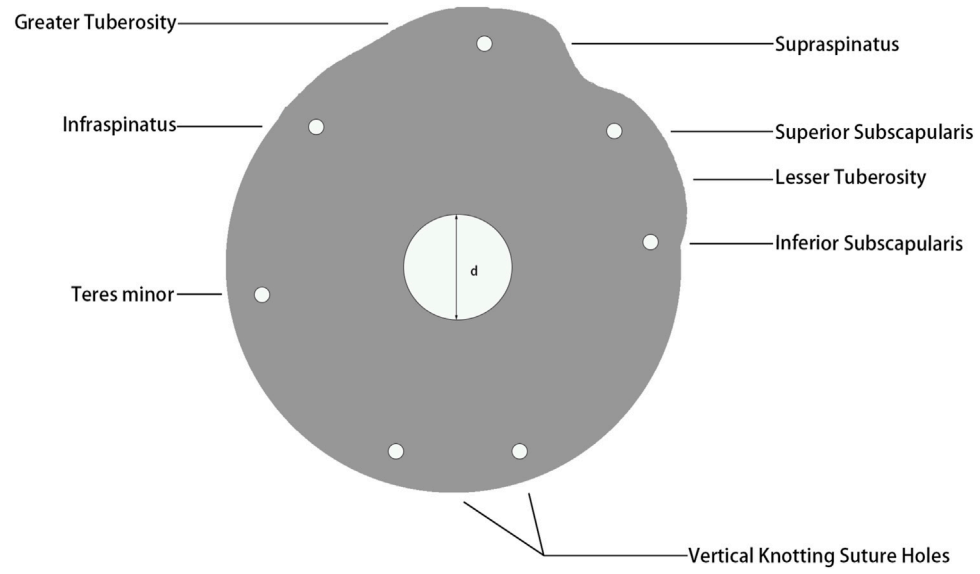

FIGURE 2
Blueprint of tuberosity reconstruction baseplate.

TABLE 1 Mechanical properties of baseplate materials.

Material	Young's modulus (MPa)	Poisson's ratio	Density (kg/m^3)	Yield strength (MPa)
PEEK	3,450	0.40	1,300	95
TiNi	83,000	0.33	6,450	443
CFRP	E_1 = 100,000	μ_1 = 0.40	1,550	1,000
	E_2 = 5,000	μ_2 = 0.30		

(ether-ether-ketone) (PEEK), titanium-nickel (TiNi) alloy and the novel biomaterial CFRP composites. The PEEK and TiNi alloy were set to be homogeneous and isotropic. The CFRP composites consisted of multiple layers stacked in different directions with quasi-isotropic properties. Each of the layers was 0.1875 mm thick and the stacking sequence was $[45/0/-45/90]_s$. The Young's modulus, Poisson's ratio, density and yield strength of three baseplate materials were presented in Table 1 (Song et al., 2000; Ahmad et al., 2018; Vogel et al., 2018). In addition, the shear modulus of CFRP composites was set at 3,000 MPa. None of these baseplates exceeded the yield strength and were therefore modelled as linear elastic.

Due to the complex actual loading conditions of rotator cuff, loads of the same magnitude were applied vertically at seven suture holes to simulate extreme situations. The central hole was constrained. Firstly, a 1N load was applied at each suture hole to obtain the maximum von Mises stress by finite element analysis. And then the permissible load was calculated from the yield strength of materials. With the permissible load applied, the displacements of five suture holes corresponding to rotator cuff in each finite element model were compared.

In vivo, the maximum force of a single rotator cuff muscle does not exceed 200 N (Meyer et al., 2018). Also, many of the high-strength sutures available for rotator cuff repair have a failure strength above 200 N (Borbas et al., 2021). Therefore, when the permissible load exceeds 200 N, the baseplate only produces elastic deformation in practice and does not yield. In addition, if a certain extent of displacement occurs in the suture holes corresponding to rotator cuff, it is possible for the baseplate to perform as a tension band to achieve dynamic compression between tuberosities.

Structure optimization

Based on the finite element analysis of three baseplate materials, the model with higher permissible load and larger suture hole displacement could be selected for further structure optimization. During the optimization process, thicker materials or more layers were designed

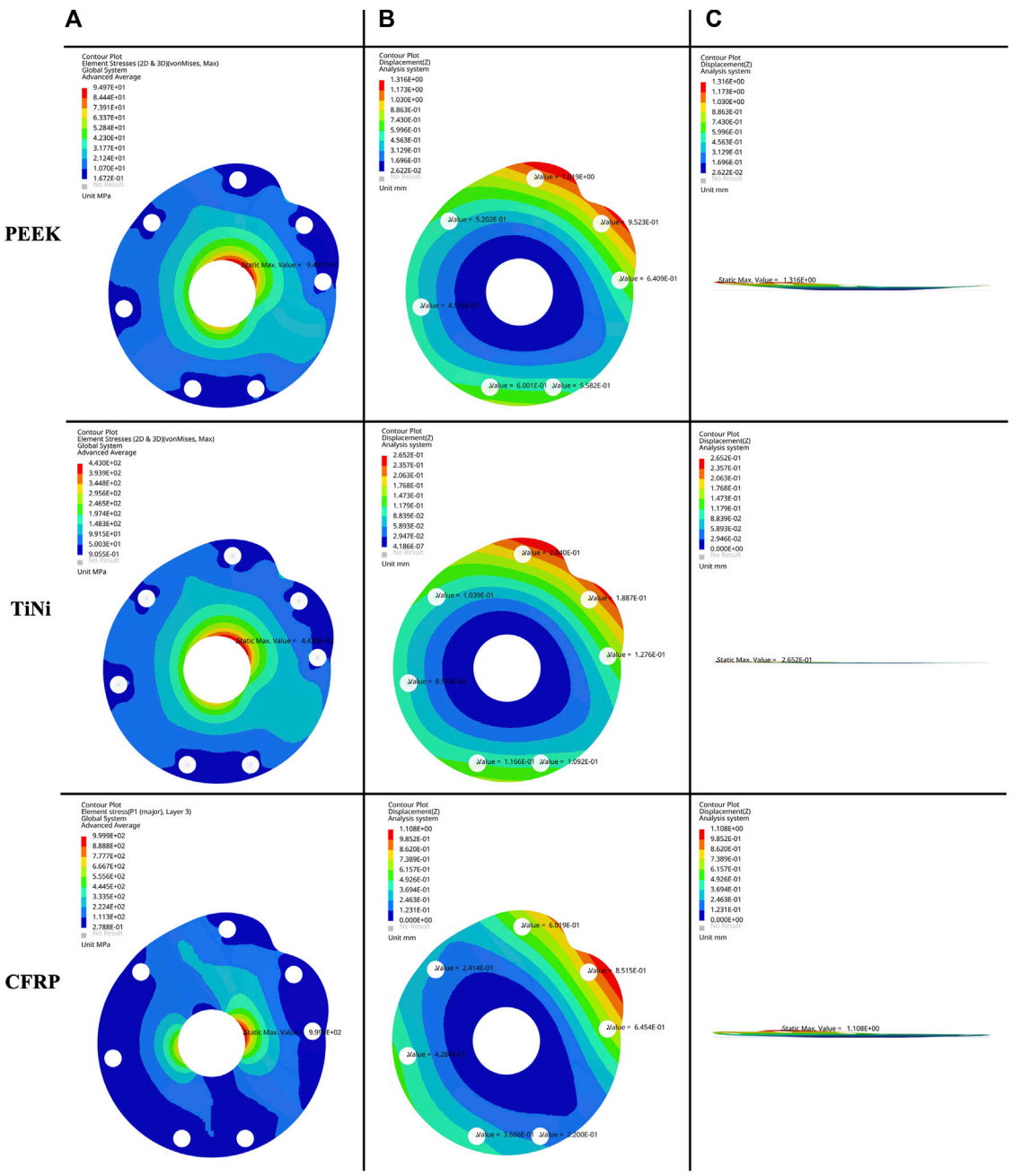

FIGURE 3
(A) Frontal view of von Mises stress nephogram, **(B)** frontal view and **(C)** lateral view of displacement nephogram for a 2 mm thick baseplate model under permissible load.

at the von Mises stress concentrations to increase the permissible load, while thinner materials or fewer layers were designed in other regions to enhance the deformability. A stress of 200N was loaded vertically on each suture hole of the hybrid design model. The maximum von Mises stress and suture hole displacements were recorded.

Results

Stress distribution and displacement

The von Mises stress nephogram (Figure 3A) and displacement nephogram (Figure 3B,C) for three baseplate materials with a thickness of 2 mm showed similar distribution pattern. The von

TABLE 2 Permissible load and suture hole displacement of finite element models.

Material	Thickness (mm)	Permissible load (MPa)	Suture hole displacement (mm)
PEEK	1.0	9.3	0.8–1.9
	1.5	21.0	0.6–1.3
	2.0	37.4	0.5–1.0
	2.5	58.8	0.3–0.8
	3.0	85.0	0.3–0.7
TiNi	1.0	43.0	0.2–0.4
	1.5	96.9	0.1–0.3
	2.0	172.7	0.1–0.2
	2.5	270.8	0.1
	3.0	391.3	0.1
CFRP	1.0	67.8	0.8–1.4
	1.5	103.2	0.7–1.4
	2.0	211.4	0.4–0.9
	2.5	396.7	0.4–0.8
	3.0	407.3	0.2–0.8

Mises stress was concentrated around the central hole, with the highest stress from 12 o' to 3 o'clock position, followed by 6 o'–9 o'clock. The displacement was largest at the suture holes corresponding to supraspinatus and superior subscapularis.

The permissible loads and suture hole displacements for three baseplate materials with five thicknesses were demonstrated in Table 2. As the baseplate thickened, the permissible load increased and the suture hole displacement decreased. For the same thickness, the baseplate made of PEEK had a lower permissible load and a higher suture hole displacement. The baseplate made of TiNi alloy had a higher permissible load and a lower suture hole displacement. The baseplate made of CFRP composites had the highest permissible load and a similar displacement to the PEEK material.

Structure optimization

The CFRP baseplates with thicknesses of 1.5 and 2 mm provided displacements up to 0.7–1.4 and 0.4–0.9 mm respectively, which could serve as base models for structure optimization (Table 2). In the optimized model with hybrid design, two different stacking methods with different thicknesses were designed (Figure 4A), each with six layers (Figure 4B). Stack 1 was located in the peripheral region with a thickness of 1.3125 mm. Stack two was located around the central hole, mainly from 12 o'clock to 3 o'clock and from 6 o'clock to 9 o'clock. Stack 2 had a thickness of 1.875 mm.

The maximum von Mises stress of the structurally optimized model was 988 MPa when 200 N load was applied at each suture hole, which was lower than the yield strength of CFRP composite material (Figure 5A). At the greater tuberosity, the suture hole displacements were 1.1, 0.9 and 1.0 mm for the supraspinatus, infraspinatus and teres minor, respectively (Figure 5B). At the lesser tuberosity, the suture hole displacements were 1.4 and 1.2 mm for the superior and inferior subscapularis, respectively (Figure 5B). In comparison, the optimized model presented higher displacements for suture holes. The overall deformation of baseplate was visualized through the lateral view of displacement nephogram (Figure 5C).

Discussion

This study presented a feasible method to design a tuberosity reconstruction baseplate based on CT data of the native proximal humerus for application in shoulder hemiarthroplasty. Three commonly used orthopedic implant materials and five thicknesses were screened through finite element analysis. Among these, an optimized model with hybrid design made of CFRP composites demonstrated higher permissible load and larger suture hole displacements, with the potential to achieve anatomical reduction and dynamic compression of tuberosities.

The function of shoulder joint after hemiarthroplasty is highly dependent on the tuberosity healing and therefore the tuberosity reconstruction has received a lot of attention (Simovitch et al., 2019). Doursounian et al. (2019) passed two high-strength sutures through the subscapularis and infraspinatus insertions and knotted them to achieve horizontal fixation of tuberosities, then passed two more sutures sequentially through drilled holes on the humeral shaft and the supraspinatus insertion to achieve vertical fixation with a figure-of-eight tension band. Onggo et al. (2021) found that fracture stems significantly improved the healing rate of greater tuberosity compared to nonfracture stems, possibly due to the lateral fin providing a platform for

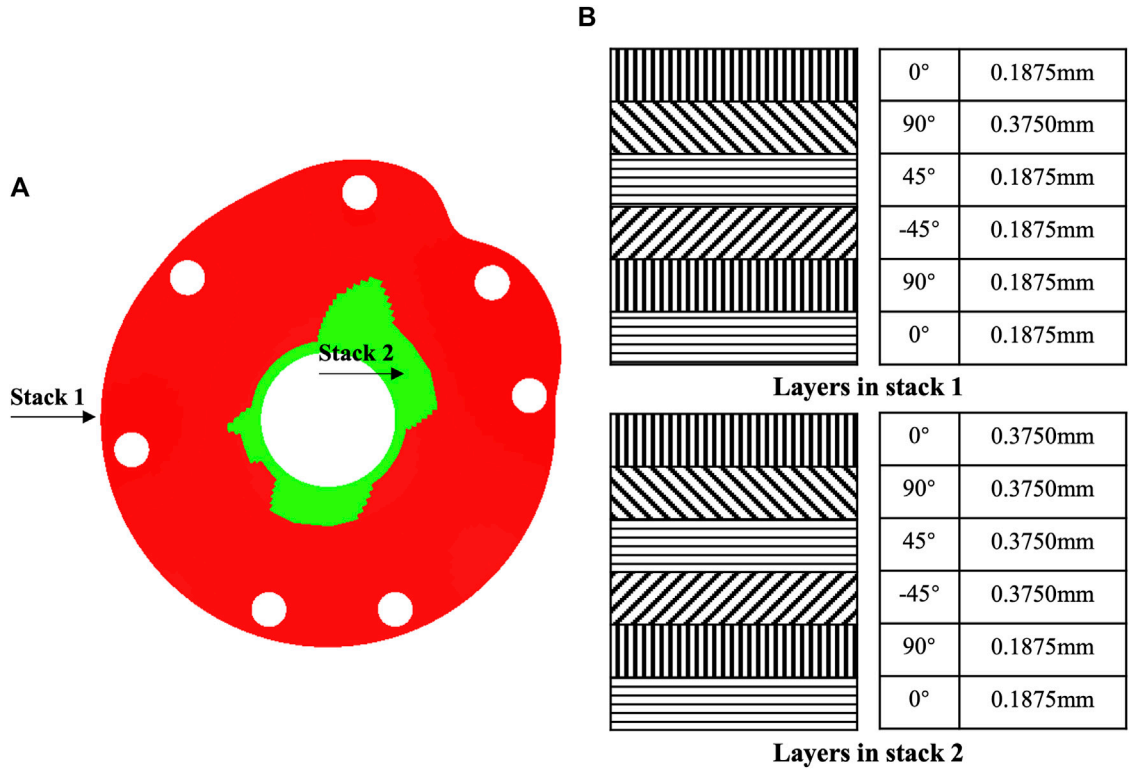

FIGURE 4
Structure optimization of tuberosity reconstruction baseplate. **(A)** Hybrid structural design and **(B)** stack design.

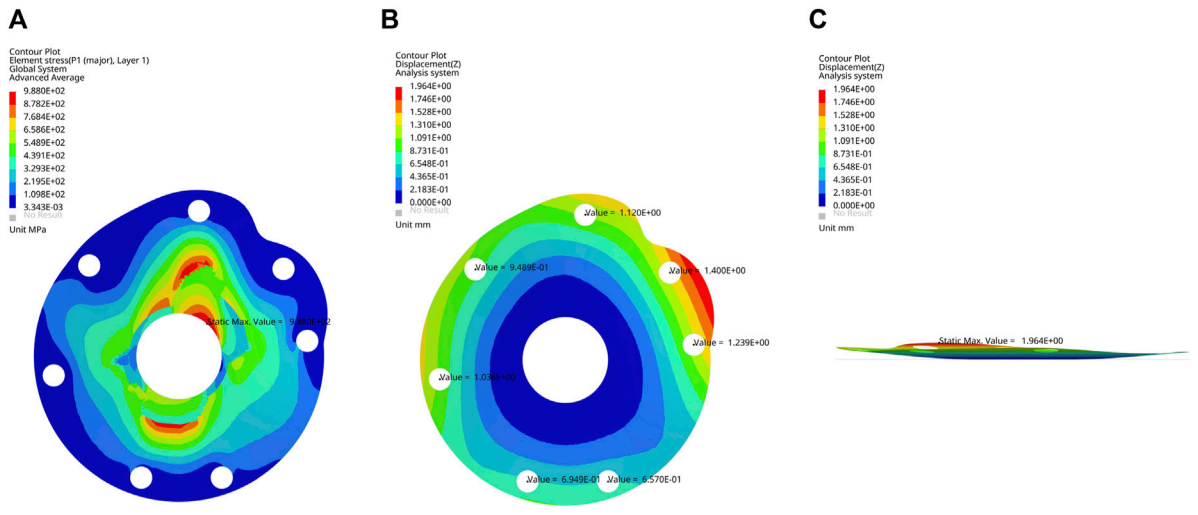

FIGURE 5
(A) Frontal view of von Mises stress nephogram, **(B)** frontal view and **(C)** lateral view of displacement nephogram for the optimized baseplate model under 200 N load.

tuberosity reconstruction. Krause et al. (2007) used steel cable cerclage to enhance fixation stability and significantly reduced the incidence of tuberosity migration and resorption. However, these methods did not overcome the inherent shortcomings of cerclage. Cerclage suture tends to result in low tuberosity reduction and there is no continuous compressive stress between the fracture fragments (Cadet and Ahmad, 2012). As the edema resolves, the fracture fragments separate under the traction of rotator cuff, eventually appearing as scar formation rather than bony healing (Grubhofer et al., 2021).

Due to the unpredictability of tuberosity healing in hemiarthroplasty, more surgeons prefer to reverse total shoulder arthroplasty (RTSA) for complex proximal humeral fractures (Panagopoulos et al., 2022). However, the revision of RTSA is still a challenge, so the hemiarthroplasty remains an irreplaceable treatment option at present (Schultz et al., 2021). The main features of tuberosity reconstruction baseplate include the provision of landmarks and suture holes for anatomical reduction and a potential tension band effect based on elastic deformability. Therefore, the baseplate offers a promising alternative technique to tuberosity suture augmentation.

The results of this study showed that the PEEK material had lower strength but superior deformability. The TiNi alloy had higher strength but inferior deformability. The CFRP composite material, in contrast, provided the highest strength with similar deformability to the PEEK material. The CFRP composites are commonly applied in the automotive and aerospace industries as a high strength-to-weight ratio material. In recent years, CFRP composites has been applied increasingly in orthopedics field, gradually replacing traditional metal-based implants (Merolli, 2019; Lin et al., 2020). In the CF/epoxy composites chosen for baseplate, the carbon fibers with moderate elastic modulus and high tensile strength are reinforced with epoxy resin (Ahmad et al., 2019). The presence of epoxy resin adversely affects the shear modulus, but the increased deformability meets the mechanical requirements of baseplate (Mahboob et al., 2021). Moreover, hybrid design is a popular technique for structural optimization (Ghosh et al., 2022). This technique maximizes the deformability of baseplate while maintaining its mechanical strength.

In vitro biomechanical experiments found that the maximum contraction force of supraspinatus muscle was approximately 302 N (Burkhart, 2000). Meyer et al. (2018) performed high voltage electrical stimulation on the suprascapular nerve during rotator cuff repair surgery and discovered that the maximum contraction force of single rotator cuff muscle did not exceed 200 N. The loading conditions of rotator cuff in daily activities is complicated and many patients are unable to achieve the theoretical maximum contraction. Furthermore, the strength of rotator cuff muscles varies in different positions (Tsuruike et al., 2021). Thus, in this study we only used simplified loading configurations to screen baseplate materials and thicknesses by simulating extreme conditions. This may lead to an overestimation of baseplate deformability.

There are other limitations to this study. There are variations in tuberosity geometry in different populations, but only data from a single volunteer were utilized as the design basis. In addition, there is no definite evidence to suggest whether a displacement of 0.9–1.4 mm in the optimized model enables the dynamic compression effect. The next step is to validate the mechanical properties of baseplate in cadaveric and mechanical experiments.

Conclusion

This study proposed the concept of tuberosity reconstruction baseplate and provided a design procedure based on CT data of the native proximal humerus. A structurally optimized model made of CFRP composites presented the potential to realize anatomical reduction and dynamic compression of tuberosities. As a novel biomaterial, the mechanical properties and clinical efficacy of CFRP composites need further evaluation.

Data availability statement

The raw data supporting the conclusion of this article will be made available by the authors, without undue reservation.

Ethics statement

The studies involving human participants were reviewed and approved by The Ethics Committee of Peking University People's Hospital. The patients/participants provided their written informed consent to participate in this study. Written informed consent was obtained from the individual(s) for the publication of any potentially identifiable images or data included in this article.

Author contributions

JC contributed to conception and design of the study. JJ performed the finite element analysis and statistical analysis. ZD wrote the first draft of the manuscript. MM and YZ wrote sections of the manuscript. All authors contributed to manuscript revision, read, and approved the submitted version.

Funding

This work was financially supported by the Peking University People's Hospital Scientific Research Development Funds (RDL 2021-08).

Conflict of interest

The authors declare that the research was conducted in the absence of any commercial or financial relationships that could be construed as a potential conflict of interest.

The reviewer ZS declared a shared parent affiliation with the authors to the handling editor at the time of review.

Publisher's note

References

Ahmad, F., Abbassi, F., Park, M. K., and Hong, J.-W. (2019). Numerical investigation to evaluate effect of fiber orientation on penetration-resistance of an aircraft composite material. *Mech. Adv. Mater. Struct.* 26 (19), 1613–1621. doi:10.1080/15376494.2018.1444226

Ahmad, F., Abbassi, F., Park, M. K., Jung, J.-W., and Hong, J.-W. (2018). Finite element analysis for the evaluation of the low-velocity impact response of a composite plate. *Adv. Compos. Mater.* 28, 271–285. doi:10.1080/09243046.2018.1510589

Amundsen, A., Brorson, S., Olsen, B. S., and Rasmussen, J. V. (2021). Ten-year follow-up of stemmed hemiarthroplasty for acute proximal humeral fractures. *Bone & Jt. J.* 103 (6), 1063–1069. doi:10.1302/0301-620x.103b6.bjj-2020-1753.r1

Boileau, P., Krishnan, S., Tinsi, L., Walch, G., Coste, J., and Molé, D. (2002). Tuberosity malposition and migration: Reasons for poor outcomes after hemiarthroplasty for displaced fractures of the proximal humerus. *J. shoulder Elb. Surg.* 11 (5), 401–412. doi:10.1067/mse.2002.124527

Borbas, P., Fischer, L., Ernstbrunner, L., Hoch, A., Bachmann, E., Bouaicha, S., et al. (2021). High-strength suture tapes are biomechanically stronger than high-strength sutures used in rotator cuff repair. *Arthrosc. Sports Med. Rehabilitation* 3 (3), e873–e880. doi:10.1016/j.asmr.2021.01.029

Burkhart, S. S. (2000). A stepwise approach to arthroscopic rotator cuff repair based on biomechanical principles. *Arthrosc. J. Arthrosc. Relat. Surg.* 16 (1), 82–90. doi:10.1016/s0749-8063(00)90133-6

Cadet, E. R., and Ahmad, C. S. (2012). Hemiarthroplasty for three- and four-part proximal humerus fractures. *Am. Acad. Orthop. Surg.* 20 (1), 17–27. doi:10.5435/JAAOS-20-01-017

Curtis, A. S., Burbank, K. M., Tierney, J. J., Scheller, A. D., and Curran, A. R. (2006). The insertional footprint of the rotator cuff: An anatomic study. *Arthrosc. J. Arthrosc. Relat. Surg.* 22 (6), 603–609. doi:10.1016/j.arthro.2006.04.001

Doursounian, L., Gaillard, J., Cambon-Binder, A., Zbili, D., and Sautet, A. (2019). Hemiarthroplasty for proximal humerus fractures with conservation of the whole humeral head as autograft: Does it improve greater tuberosity healing? *Int. Orthop.* 43 (5), 1155–1164. doi:10.1007/s00264-018-3995-7

Frankle, M. A., Greenwald, D. P., Markee, B. A., Ondrovic, L. E., and Lee, W. E., 3rd (2001). Biomechanical effects of malposition of tuberosity fragments on the humeral prosthetic reconstruction for four-part proximal humerus fractures. *J. Shoulder Elb. Surg.* 10 (4), 321–326. doi:10.1067/mse.2001.113962

Ghosh, R., Chanda, S., and Chakraborty, D. (2022). Application of finite element analysis to tissue differentiation and bone remodelling approaches and their use in design optimization of orthopaedic implants: A review. *Int. J. Numer. Method. Biomed. Eng.* 38, e3637. doi:10.1002/cnm.3637

Grubhofer, F., Ernstbrunner, L., Bachmann, E., Wieser, K., Borbas, P., Bouaicha, S., et al. (2021). Cow-hitch fixation in fracture hemiarthroplasty. *JSES Int.* 5 (6), 1027–1033. doi:10.1016/j.jseint.2021.07.011

Kralinger, F., Schwaiger, R., Wambacher, M., Farrell, E., Menth-Chiari, W., Lajtai, G., et al. (2004). Outcome after primary hemiarthroplasty for fracture of the head of the humerus: A retrospective multicentre study of 167 patients. *J. Bone Jt. Surg. Br. volume* 86 (2), 217–219. doi:10.1302/0301-620x.86b2.14553

Krause, F. G., Huebschle, L., and Hertel, R. (2007). Reattachment of the tuberosities with cable wires and bone graft in hemiarthroplasties done for proximal humeral fractures with cable wire and bone graft: 58 patients with a 22-month minimum follow-up. *J. Orthop. trauma* 21 (10), 682–686. doi:10.1097/bot.0b013e31815917e0

Launonen, A. P., Lepola, V., Saranko, A., Flinkkilä, T., Laitinen, M., and Mattila, V. M. (2015). Epidemiology of proximal humerus fractures. *Arch. Osteoporos.* 10 (1), 2–5. doi:10.1007/s11657-015-0209-4

Lin, C.-Y. J., Kang, H., and Hollister, S. J. (2020). "Biomechanics of osteo-synthetics," in *Frontiers in orthopaedic biomechanics* (Berlin, Germany: Springer), 397–425.

Mahboob, A., Gil, L., Bernat-Maso, E., and Eskenati, A. R. (2021). Experimental and numerical study of shear interface response of hybrid thin CFRP–Concrete slabs. *Materials* 14 (18), 5184. doi:10.3390/ma14185184

Merolli, A. (2019). Bone repair biomaterials in orthopedic surgery. *Bone Repair Biomater.* 2019, 301–327. doi:10.1016/B978-0-08-102451-5.00011-1

Meyer, D., Hoppeler, H., and Gerber, C. (2018). "Structure and contractile force of the supraspinatus muscle is correlated with the results of rotator cuff reconstruction," in Orthopaedic proceedings: *The British editorial society of bone & joint surgery*. London: Bone & Joint Publishing, 293.

Mochizuki, T., Sugaya, H., Uomizu, M., Maeda, K., Matsuki, K., Sekiya, I., et al. (2008). Humeral insertion of the supraspinatus and infraspinatus. New anatomical findings regarding the footprint of the rotator cuff. *J. Bone Jt. Surgery-American Volume* 90 (5), 962–969. doi:10.2106/JBJS.G.00427

Neer, C. S., 2nd (1970). Displaced proximal humeral fractures. *J. Bone Jt. Surg.* 52 (6), 1090–1103. doi:10.2106/00004623-197052060-00002

Onggo, J. R., Nambiar, M., Onggo, J. D., Hau, R., Pennington, R., and Wang, K. K. (2021). Improved functional outcome and tuberosity healing in patients treated with fracture stems than nonfracture stems during shoulder arthroplasty for proximal humeral fracture: A meta-analysis and systematic review. *J. Shoulder Elb. Surg.* 30 (3), 695–705. doi:10.1016/j.jse.2020.09.044

Panagopoulos, G. N., Pugliese, M., Leonidou, A., Butt, F., Jaibaji, M., Megaloikonomos, P. D., et al. (2022). Acute versus delayed reverse total shoulder arthroplasty for proximal humeral fractures: A consecutive cohort study. *J. Shoulder Elb. Surg.* 31 (2), 276–285. doi:10.1016/j.jse.2021.07.003

Schultz, B. J., Lowe, D. T., Egol, K. A., and Zuckerman, J. D. (2021). Shoulder hemiarthroplasty for proximal humerus fracture. *J. Orthop. Trauma* 35, S3–S4. doi:10.1097/bot.0000000000002158

Simovitch, R. W., Roche, C. P., Jones, R. B., Routman, H. D., Marczuk, Y., Wright, T. W., et al. (2019). Effect of tuberosity healing on clinical outcomes in elderly patients treated with a reverse shoulder arthroplasty for 3-and 4-part proximal humerus fractures. *J. Orthop. Trauma* 33 (2), e39–e45. doi:10.1097/bot.0000000000001348

Song, G., Lam, P., Srivatsan, T., Kelly, B., and Agrawa, B. (2000). Application of shape memory alloy wire actuator for precision position control of a composite beam. *J. Mater. Eng. Perform.* 9 (3), 330–333. doi:10.1361/105994900770346006

Stone, M. A., and Namdari, S. (2019). Surgical considerations in the treatment of osteoporotic proximal humerus fractures. *Orthop. Clin. North Am.* 50 (2), 223–231. doi:10.1016/j.ocl.2018.10.005

Tanner, M. W., and Cofield, R. H. (1983). Prosthetic arthroplasty for fractures and fracture-dislocations of the proximal humerus. *Clin. Orthop. Relat. Res.* 179 (179), 116–128. doi:10.1097/00003086-198310000-00017

Tsuruike, M., Ellenbecker, T. S., and Lauffenburger, C. (2021). Electromyography activity of the teres minor muscle with varying positions of horizontal abduction in the quadruped position. *JSES Int.* 5 (3), 480–485. doi:10.1016/j.jseint.2020.12.014

Vogel, D., Schulze, C., Dempwolf, H., Kluess, D., and Bader, R. (2018). Biomechanical behavior of modular acetabular cups made of poly-ether-ether-ketone: A finite element study. *Proc. Inst. Mech. Eng. H.* 232 (10), 1030–1038. doi:10.1177/0954411918797600

Yahuaca, B. I., Simon, P., Christmas, K. N., Patel, S., Gorman, R. A., II, Mighell, M. A., et al. (2020). Acute surgical management of proximal humerus fractures: ORIF vs. hemiarthroplasty vs. reverse shoulder arthroplasty. *J. Shoulder Elb. Surg.* 29 (7), e161–S40. doi:10.1016/j.jse.2020.01.046

frontiers | Frontiers in Bioengineering and Biotechnology

TYPE Systematic Review
PUBLISHED 01 November 2022
DOI 10.3389/fbioe.2022.1041531

OPEN ACCESS

EDITED BY
Yansong Qi,
Inner Mongolia People's Hospital, China

REVIEWED BY
Jianhai Chen,
Peking University People's Hospital, China
Ming Xiang,
Sichuan Provincial Orthopedics Hospital, China
Bei Liu,
University of Rochester Medical Center, United States

*CORRESPONDENCE
Yi Lu,
luyi_sports@126.com

SPECIALTY SECTION
This article was submitted to Biomaterials, a section of the journal Frontiers in Bioengineering and Biotechnology

RECEIVED 11 September 2022
ACCEPTED 21 October 2022
PUBLISHED 01 November 2022

CITATION
Yang G, Li S, Zhang H and Lu Y (2022), A systematic review and meta-analysis on different stem fixation methods of radial head prostheses during long-term follow-up.
Front. Bioeng. Biotechnol. 10:1041531.
doi: 10.3389/fbioe.2022.1041531

A systematic review and meta-analysis on different stem fixation methods of radial head prostheses during long-term follow-up

Guang Yang, Shangzhe Li, Hailong Zhang and Yi Lu*

Department of Sports Medicine, Beijing Ji Shui Tan Hospital, School of Medicine, Peking University, Beijing, China

Background: Radial head arthroplasty (RHA) is typically performed for non-reconstructible radial head fractures with or without valgus stability. The fixation methods can be divided into cemented rigid fixation, such as screw fixation, and uncemented micromovement fixation, including smooth stem, press-fit, expanded device, in-growth stem, and grit-blasted stem fixations. Different fixation methods may impact long-term clinical outcomes and cause complications. This study aimed to compare the long-term follow-up outcomes of cemented and uncemented radial head prostheses.

Methods: A computerized literature search was performed in the PubMed/MEDLINE, Embase, Cochrane Library, and Web of Science databases for studies on radial head prostheses, replacement, and arthroplasty published from inception to April 2022. The prostheses fixation method was divided into cemented and uncemented fixation groups. The outcomes of interest included the participant characteristics, prostheses types, clinical outcomes, reoperation rates, and complication rates during long-term follow-up.

Results: A total of 57 studies involving 2050 patients who underwent RHA were included in our analysis. Cemented fixation was used in 23 of these studies, uncemented fixation in 35 studies, and both cemented and uncemented fixations in one study. Both fixation groups showed significantly improved clinical outcomes after treatment. In particular, both the reoperation and complication rates were lower in the uncemented fixation group (12% and 22%, respectively) than that in the cemented fixation group (20% and 29%, respectively). Among the studies, uncemented monopolar fixation had the lowest reoperation rate (14%), while cemented monopolar fixation had the highest reoperation rate (36%). Regarding complication rates, uncemented bipolar fixation yielded the lowest rate (12%), while cemented bipolar fixation yielded the highest rate (34%). The range of motion and clinical outcome scores were good in both groups.

Conclusion: Uncemented radial head prostheses had lower reoperation and complication rates than cemented prostheses. In particular, uncemented monopolar prostheses may yield the lowest reoperation rate, while uncemented bipolar prostheses may yield the lowest overall complication rate.

KEYWORDS
radial head, arthroplasty, replacement, prostheses, fixation

Introduction

Radial head fractures account for approximately 33% of elbow fractures and 1.7%–5.4% of all fractures (Mason ML, 1954; Kaas L et al., 2010). When dislocation or comminuted radial head fractures (modified Mason types III and IV) occur, it is crucial to restore radial head function because of its essential role in maintaining elbow stabilization (Morrey et al., 1991). Currently, radial head arthroplasty (RHA) is universally accepted for the treatment of comminuted radial head fractures. Sershon et al. reported that approximately 85% of patients achieved good-to-excellent outcomes after primary RHA (Sershon et al., 2018). Li et al. performed a systematic review and meta-analysis and concluded that the application of RHA led to better range of motion (ROM) and lower complication rates (Li and Chen, 2014). However, complications after RHA cannot be avoided, with varying reoperation rates ranging from 0% to 45% (Laumonerie et al., 2017). Among these complications, painful loosening is the primary reason for radial head fixation reoperation (Van Riet et al., 2010; O'Driscoll and Herald, 2012; Duckworth et al., 2014; Delclaux et al., 2015; Neuhaus et al., 2015; Kachooei et al., 2016); its cause is speculated to be related to the manner the prostheses stem is fixed.

Radial head prostheses fixation can be divided according to the stem fixation method: cemented and uncemented. Cemented fixation is defined as firm fixation of a prostheses in the medulla without micromotion. Meanwhile, uncemented fixation is described as fixation of a prostheses in the medullary region with micromotion owing to a 1–2 mm space existing between the prostheses stem and medullary cavity. Previous studies have reported that cemented prostheses can achieve good stability, with a lower loosening rate (Acevedo et al., 2014), while uncemented micromotion prostheses can avoid the oversizing effect, alleviate radial head impingement, and have fewer complications (Chanlalit et al., 2012; Laflamme et al., 2017). Nevertheless, there is still controversy regarding which type of prostheses has better performance.

The purpose of this study was to compare between cemented and uncemented radial head prostheses during long-term follow-up. We hypothesized that uncemented prostheses have lower complication and reoperation rates than cemented prostheses.

Methods

Search strategy

The study was performed in accordance with the Preferred Reporting Items for Systematic Reviews and Meta-Analyses (PRISMA) guidelines. The PubMed/MEDLINE, Embase, Cochrane Library, and Web of Science databases were searched from inception to April 2022 using the following search terms: radial head, radial head arthroplasty, prostheses, unipolar, monopolar, bipolar, cemented, uncemented, and not reviewed. Randomized controlled trials, retrospective cohort studies, and case series were included, and the average follow-up period was >24 months. The prostheses fixation methods were divided into cemented and uncemented fixation groups. Letters, comments, editorials, case reports, proceedings, and personal communications as well as studies in which the characteristics of elbow injury involved active infection, previous treatment failure or bilateral treatment were excluded. The list of potential references was reviewed, and data were extracted by two independent reviewers; a third reviewer was consulted to resolve any uncertainties regarding eligibility.

Data extraction and quality assessment

The following data were extracted from the studies that met the inclusion criteria: name of the first author, year of publication, design of the study, number of participants in each group, age and sex of the participants, implants used for RHA, complications, length of follow-up, and major clinical functional outcomes.

The quality of the included studies was evaluated using the modified 18-item Delphi checklist.

Outcome measures

The primary outcomes were the rates of reoperation and overall complications. The secondary outcomes were the average range of clinical functional outcomes, including the mean Mayo Elbow Performance Score (MEPS) and Disabilities of the Arm, Shoulder, and Hand (DASH), visual analog scale (VAS), The American Shoulder and Elbow Surgeons Elbow Questionnaire (ASES), and Broberg–Morrey scores, and the average ROM (flexion minus extension). For subgroup analysis, we would investigate the effect of prostheses polarity on the rates of reoperation and complications.

Statistical analysis

Event rates with 95% confidence intervals (Cis) were calculated for dichotomous outcomes and means with 95% Cis for continuous outcomes. Heterogeneity among the studies

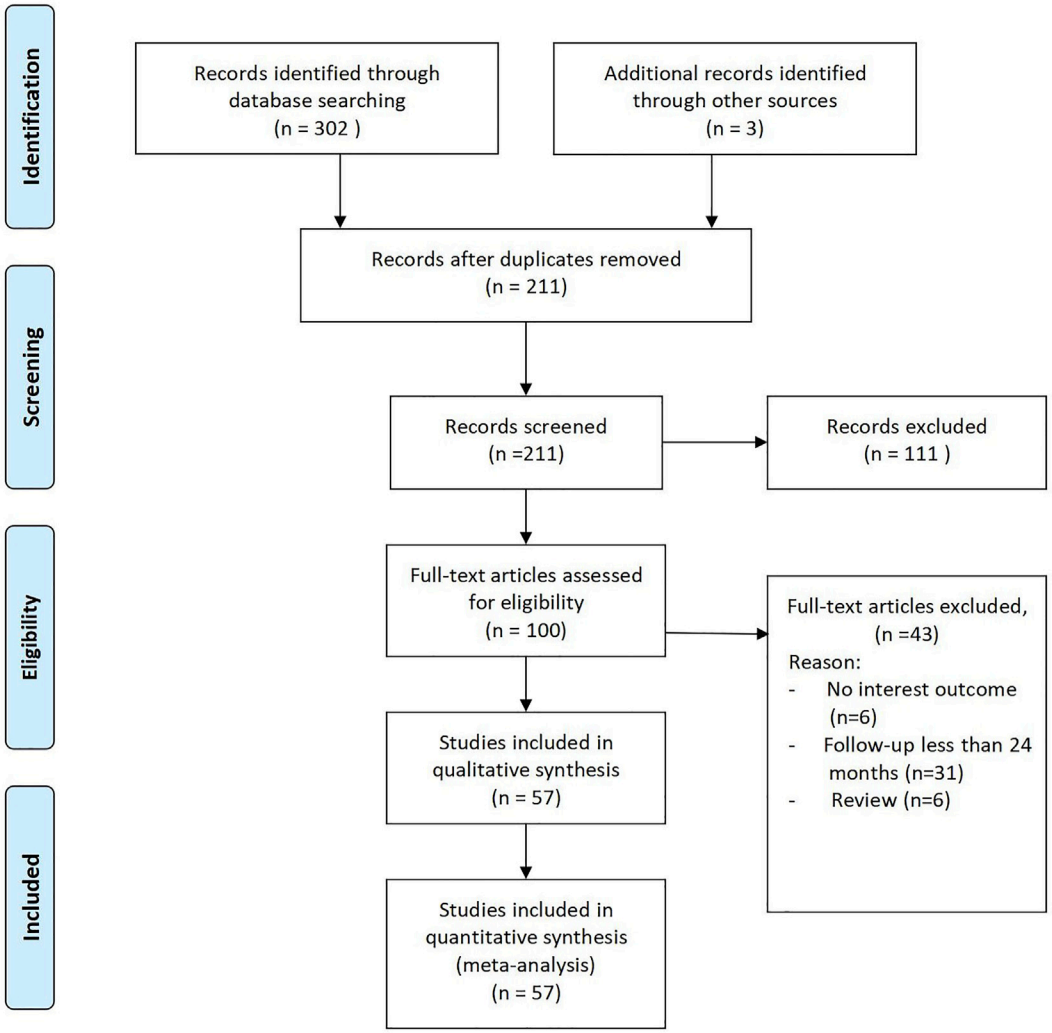

FIGURE. 1
PRISMA 2009 flow diagram.

was assessed using Cochran's Q and I^2 statistics. The I^2 statistic indicates the percentage of the observed between-study variability caused by heterogeneity. Heterogeneity was evaluated based on the I^2 statistic as follows: 0%–24%, no heterogeneity; 25%–49%, moderate heterogeneity; 50%–74%, large heterogeneity; and 75%–100%, extreme heterogeneity. When the I^2 statistic (>50%) indicated heterogeneity between the studies, the random-effects model (DerSimonian–Laird method) was used. Otherwise, the fixed-effects model was utilized (Mantel–Haenszel method). Pooled effects were calculated, and a two-sided p value of <0.05 was considered to indicate statistical significance. All statistical analyses were performed using the RevMan software version 5.3 (The Cochrane Collaboration, Oxford, United Kingdom).

Result

Of the 211 studies initially identified, 111 were excluded after preliminary screening of the abstracts and titles because they were not relevant (Figure 1). The remaining 100 articles underwent full-text review, and 42 were excluded for not reporting the outcomes of interest, not applying RHA, and not mentioning whether the periprosthetic fixation method was cemented fixation.

57 studies were finally included in the analysis, with a total of 2050 patients who received RHA implants: 618 patients received cemented implants, and 1,432 patients received uncemented implants. Two studies were prospective studies; eighteen, retrospective studies; and thirty-seven, case series (Table 1). Across all studies, the mean age in the cemented and

TABLE. 1 Baseline demographics of the selected studies for cemented fixation.

Author (year)	Type of studies	Patients	Average age	Gender (male)	Dominant	Average follow-up (month)	Indication of surgery	Implant of radial head arthroplasty	Polarity (monopolar VS. bipolar)	Clinical outcomes	Rang of motion (flexion minus extension)	Reoperation	Complications	QA
Luo2022	Case series	17	35	15	13	103	stiffness by trauma	Tornier	bipolar	MEPI: 95 ± 6; DASH: 8 ± 5; VAS: 0.2 ± 0.5	ROM: 113 ± 19°		ulnar nerve symptoms n = 1	13
Songy2021	Retrospective Cohort	29				78	acute, nonreconstructible radial head fractures	Evolve n = 60; SBI/Avanta/ Stryker n = 21; Anatomic n = 33	monopolar			4	stiffness:pain: Transverse instability/pain n = 1:2:1	15
Pehlivanoglu2021	Retrospective Cohort	26	48.85	15		132.2	acute and comminuted radial head fractures	OrtoPro	monopolar	VAS:0.8; MEPS:91.5; DASH:6.3; SF-36:55.5	ROM:117.5°	1	periprosthetic stem lucency and pain n = 1	11
Montbarbon2021	Case series	16	52.5	9	8	144		Tornier	bipolar	Quick-Dash: 23.01 ± 7.8	ROM: 132 ± 11°	3	recurrent dislocation n = 1; or chronic pain n = 1	17
Marcheix2021	Case series	41	59	14		86.9	acute elbow trauma	Judet-type RH prostheses with floating cup	bipolar	VAS:0.78, MEPI:88.7, DASH18.7	ROM: 13–139.3°	5	regional pain:nerve palsy n = 4:1	15
Laun2019	Case series	37	49.9	21	28	67.2	radial head fracture Mason III	Judet's bipolar prostheses	bipolar	VAS: 1.2; DASH:18.6; Broberg and Morrey score: 86.5; MEPS: 90.3	ROM: 12.5–131.7°	1		17
Kiechle2019	Retrospective cohort study	48	45			46	fracture associated with instability of the elbow	MoPyC; Tornier	monopolar	VAS:3.3; MEPS: 70 Broberg and Morrey score: 63 DASH:34	ROM: 20–118°		subluxation: loosening: ossifications:nerve affection:instability n = 1:1:1:1:1	16
Laumonerie2018	Retrospective cohort study	65	52.46	44		76.78	nonreconstructable fracture	GUEPAR n = 30; Evolutive n = 20; rHead STANDARD n = 6; rHead RECON prostheses n = 9	bipolar n = 59; monopolar n = 6	MEPS:87.4; DASH:16.57	ROM: 11–133.6°	14	painful loosening n = 14	14
Jungbluth2018	Case series	46	57.7	19	35	65.3	Monteggia-like lesion	Tornier	bipolar	VAS:1.0; Morrey and broberg score: 86.6; DASH:15.1	ROM: 8–133.2°	6		13
Cui2018	Retrospective cohort study	9	31	5	3	29	Terrible triad injury of the elbow	Edina	bipolar	MEPS:94	ROM: 5–126°			9
Laumonerie2017	Retrospective cohort study	77	52	54	42	74	nonreconstructable fracture	Guepar n = 36; Evolutive n = 24; rHead RECON; SBI/Stryker n = 10; rHead Standard n = 7	bipolar n = 70; monopolar n = 7	MEPS:88.8; DASH:15.5	ROM: 9.3–135.3°	30	painful loosening n = 29; nerve palsy n = 12	12

(Continued on following page)

10.3389/fbioe.2022.1041531

TABLE. 1 (*Continued*) Baseline demographics of the selected studies for cemented fixation.

Author (year)	Type of studies	Patients	Average age	Gender (male)	Dominant	Average follow-up (month)	Indication of surgery	Implant of radial head arthroplasty	Polarity (monopolar VS. bipolar)	Clinical outcomes	Rang of motion (flexion minus extension)	Reoperation	Complications	QA
Lopiz2016	Retrospective cohort study	14	54	6	6	42	radial head fractures	MoPyC	bipolar	DASH: 24.8 MEPI: 78.9	ROM:85.5°	4	stiffness n = 3; fracture n = 1; neurological injuries n = 2	15
Heijink2016	Case series	25	55	7	4	50	radial head fractures	Tornier	bipolar	MEPS:89.6	ROM:6–135°	1	neuropraxia n = 2; nerve paresthesia n = 2; stiffness n = 1	14
Alllavena2014	Case series	22	44	15	10	50	radial head fractures	The Guepar® radial head prostheses	bipolar	MEPS:79	ROM:100	4	postero-lateral subluxation n = 6; nerve dysfunction n = 5	13
Liu2013	Case series	8	31.7	7		26	elbow stiffness	Tornier, Edina, MN, United States	bipolar	MEPS:92.5	ROM: 7.5–120.6°			17
Leigh2012	Retrospective cohort study	11	45.5	6		40.7	terrible triad injuries	Avante or Evolve	monopolar	DASH: 10.83 ASES: 89	ROM:5–135°	4	stiffness n = 2	16
Celli2010	Case series	16	46.1	11	9	41.1	radial head fractures	Tornier, Edina	bipolar	VAS:1.38; MEPS:89.4; DASH:11.4	ROM:117°		ankylosis n = 2 synostosis n = 2	13
Burkhart2010	Case series	17	44.1	14		106	radial head fractures	Judet's bipolar radial head prostheses	bipolar	MEPS: 90.83 DASH: 9.8	ROM:21–124°		dislocation n = 2	14
Lim2008	Case series	7		2	4	29.7	radial head fractures	Howmedica	monopolar	VAS:1.8; Broberg and Morrey score: 78.4; DASH: 13.61; ASES:92.5	ROM:100°		neuropathy n = 1; loosening n = 4	14
Popovic2007	Case series	51	51	32	41	100.8	radial head fractures	Tornier	bipolar	MEPS:83	ROM:14–130°		regional pain syndrome n = 1; nerve palsy n = 5; subluxation n = 1	8
Dotzis2006	Case series	14	44.8	10	9	63.6	radial head fractures	Tornier	bipolar	DASH:23.9	ROM:14–140°		complex regional pain syndrome n = 1	16
Brinkman2005	Case series	11	43	8	6	24	treated previously with ORIF	Judet CRF II	bipolar		ROM: 14.5–135°	2		15
Popovic2000	Case series	11	52.7	6	7	32	radial head fractures associated with elbow dislocation	Tornier	bipolar		ROM: 14.5–130°			11

10.3389/fbioe.2022.1041531

uncemented fixation groups was 47.4 and 49.5 years, respectively; the number of the male patients in the cemented and uncemented fixation groups was 320 and 601, respectively, while that of the female patients was 214 and 631 in the studies that mentioned related item, respectively. In general, the average of follow-up in cemented group was 65.6 months, and that in uncemented group was 60.0 months. The detail is shown in Table 1 and 2.

Quality assessment

The study quality was assessed using the modified 18-item Delphi checklist (maximal [i.e., best] score: 18). In general, the studies were of good quality, with most (55/59) studies having a score of >10. Two studies had a score of nine and other two studies had scores of 7 and 8, respectively.

Cemented and uncemented fixation comparison

Twenty-three and thirty-five studies were included in the analysis of cemented and uncemented fixations, respectively. No significant heterogeneity was found in the rate of cemented and uncemented reoperations (cemented: Q = 7.9, I^2 = 0%; uncemented: Q = 7.47, I^2 = 0%); therefore, the fixed-effects model was used. The rate of cemented reoperation ranged from 3% to 39%, while that of uncemented reoperation ranged from 2% to 25%, with pooled estimates of 20% and 12%, respectively (cemented: 95% CI: 0.12–0.29, uncemented: 95% CI: 0.06–0.19) (Figures 2, 3). Heterogeneity was observed in the overall complication rate (cemented: Q = 41; I^2 = 61%, uncemented: Q = 61.67; I^2 = 68%). Therefore, the random-effects model was used. The pooled estimate of overall complications in the cemented and uncemented fixation groups was 29% and 22%, respectively (cemented: 95% CI: 0.16–0.41, uncemented: 95% CI: 0.11–0.34) (Figures 4, 5). Moreover, the mean MEPS and DASH, VAS, ASES, and Broberg–Morrey scores were 70–95, 6.5–34, 0–3.3, 86–92.5, and 63–90.1 in the cemented fixation group and 74–96, 6.17–31, 0.6–2.9, 70–94.7, and 85.5–94.2 in the uncemented fixation group, respectively. The mean ranges of flexion, extension, pronation, and supination between the cemented and uncemented fixation groups were 118–140 vs 124–145, 5–21 vs 4.7–34, 43–87.5 vs. 47.9–85, and 57–88 vs. 35–85, respectively. Seventeen and twenty-two studies reported complications in the cemented and uncemented fixation groups, respectively. The following complications were found in the cemented fixation group: painful loosening (10.1%), nerve symptoms (6.5%), elbow stiffness (2%), dislocation (2%), and regional pain syndrome (1%). Meanwhile, the following complications were reported in the uncemented fixation group: painful loosening (4.3%), nerve symptoms (3.7%), elbow stiffness (3.5%), regional pain syndrome (1.6%), and dislocation (0.5%).

Subgroup analysis

Eighteen studies used cemented bipolar prostheses; six, cemented monopolar prostheses; five, uncemented bipolar prostheses; and twenty-five, uncemented monopolar prostheses. In the meta-analysis, the lowest rate of reoperation was reported for uncemented monopolar fixation (14%, 95% CI: 0.08–0.20) and the lowest rate of complications for uncemented bipolar fixation (12%, 95% CI: 0.05–0.30). The highest rate of reoperation was reported for cemented monopolar fixation (36%, 95% CI: 0.15–0.56) and the highest rate of complications for cemented bipolar fixation (34%, 95% CI: 0.26–0.42) (Table 3). The range of clinical outcomes in cemented bipolar and monopolar was MEPS: 78.9–95 and 70–91.5, DASH: 8–23.9 and 6.3–34, VAS: 0.2–1.38 and 0.8–3.39, Broberg and Morrey: 86.5–86.6 and 63–78.4, while ASES score was only mentioned in two studies using cemented monopolar prostheses, it ranged from 89 to 92.5. And the range of that uncemented bipolar and monopolar was MEPS: 90–92 and 74–96.5, VAS: one and 0.6–2.1, while DASH and Broberg and Morrey reported in studies using uncemented monopolar were 7.7–31 and 88–92.1, respectively. For some of the more concerned complications, distribution of complications in cemented bipolar: nerve symptoms 0.05%, painful loosening 8%, elbow stiffness 2%, dislocation 2.9%, regional pain syndrome 2%, while that in studies using cemented monopolar: nerve symptoms 3.3%, painful loosening 33%, elbow stiffness 5%, dislocation 1.7%, regional pain syndrome 3.3%. Distribution of complications in uncemented bipolar: nerve symptoms 2%, painful loosening 17.5%, elbow stiffness 6%, dislocation 2%, while that in studies using uncemented monopolar: nerve symptoms 3.9%, painful loosening 3%, elbow stiffness 3.2%, dislocation 0.2%, regional pain syndrome 1.7%.

Discussion

The main finding of this study is that uncemented radial head prostheses had lower reoperation and overall complication rates than cemented radial head protheses. In particular, uncemented monopolar prostheses yielded the lowest reoperation rate and uncemented bipolar prostheses, the lowest overall complication rate.

Multiple radial head prostheses fixation can be classified according to the stem fixation method: uncemented or cemented. For uncemented fixation, there is often a gap of 1–2 mm between the prosthetic stem and medullary cavity,

TABLE 2 Baseline demographics of the selected studies for uncemented fixation.

Author (year)	Type of studies	Patients	Average age	Gender (male)	Dominant	Average follow-up (month)	Identification of surgery	Implant of radial head arthroplasty	Polarity (monopolar VS. bipolar)	Clinical outcomes	Rang of motion (flexion minus extension)	Reoperation	Complications	QA
Gramlich2021	Retrospective comparative treatment study	66	48	41		42.2	nonreconstructible radial head fractures	SBI rHead n = 31; Tornier MoPyC n = 35	bipolar n = 31; monopolar n = 35		ROM: 17.7–127.5°	13	painful loosening n = 6; joint stiffness n = 3	13
Raven2020	Retrospective cohort study	86	54	37	46	87.6	nonreconstructible radial head fractures	Evolve n = 75; MoPyC, Tornier n = 11	monopolar	MEPI:79.4; DASH: 24.5	ROM: 16.5–128.2°	4	painful loosening n = 5; nerve syndrome n = 3	14
Songy2021	Retrospective cohort study	85				78	persistent symptoms previously treated radial head fractures	Evolve n = 60; SBI/Avanta/ Stryker n = 21; Anatomic n = 33	monopolar			10	stiffness n = 1; pain n = 7	12
Mukka2020	Retrospective cohort study	14	45	7	7	72	comminuted radial head fractures	Explor n = 14	monopolar	VAS:2; DASH:26	ROM:17–125°			11
Claessen2020	Case series	24	48	8		27	nonreconstructible radial head fracture associated with elbow instability	Tornier						15
Chen2020	Retrospective cohort study	33	44.76	20	18	108.36	comminuted radial head fractures	Evolve	monopolar	MEPS:84; DASH:10.8	ROM:126.8°	1	stiffness n = 1	15
Carbonell-Escobar2020	Case series	62	54		32	62.4	nonreconstructible radial head fracture associated with elbow instability	Evolve n = 27; Anatomic Radial Head n = 35	monopolar	MEPS:83	ROM:10–125°		neurologic symptoms n = 10	16
Baek2020	Case series	24	49.8	13		58.9	complex radial head fractures with associated injuries	EVOLVE n = 10; Acumed n = 7; Zimmer-Biomet n = 5; Tornier n = 2	monopolar	VAS: 0.6 MEPS: 88.7; DASH: 19.4	ROM: 4.7–132.7°	1	stiffness n = 2; ulnar neuropathy n = 2	14
Jung2019	Retrospective cohort study	57	49	31	22	100.8	nonreconstructible radial head fracture	Evolve	monopolar	MEPS:74 ± 22; DASH: 31 ± 25; VAS: 2.1 ± 2.5	ROM:102°	12	loosening n = 7; instability n = 1; nerve syndrome n = 4; stiffness n = 1; pain syndrome n = 1	13
Gramlich2019	Retrospective cohort study	66	48	41		42	acute radial head fracture	rHead, SBI n = 31; MoPyc, Tornier n = 35	bipolar n = 31; monopolar n = 35			13	painful loosening n = 17; stiffness n = 3	12
Cristofaro2019	Case series	119	50	56		132			monopolar	DASH:13		30	painful loosening n = 6; stiffness n = 12	13
Ricon2018	Case series	18	48	13		79.8		MoPyC, Tornier	monopolar	MEPS:89.5	ROM:15–127°			15
Tarallo2017	Case series	31	49	26	26	30	radial head fractures	Acumed		MEPS:91.2	ROM:112°			14
Strelzow2017	Prospective study	148	55	43	66	56.4	radial head fractures	Evolve	monopolar	DASH:17.55	ROM:14–135°	5		12

(Continued on following page)

10.3389/fbioe.2022.1041531

TABLE 2 (*Continued*) Baseline demographics of the selected studies for uncemented fixation.

Author (year)	Type of studies	Patients	Average age	Gender (male)	Dominant	Average follow-up (month)	Identification of surgery	Implant of radial head arthroplasty	Polarity (monopolar VS. bipolar)	Clinical outcomes	Rang of motion (flexion minus extension)	Reoperation	Complications	QA
Laflamme2017	Retrospective cohort study	57	50.2	28	27	75.6		The EVOLVE n = 32; The ExploR n = 48	monopolar	VAS:1.11; DASH:7.7; MEPI:96.5		2		11
Han2016	Case series	3	53.3	0	2	24.6	isolated radial head fracture	SBI		MEPS: 95 DASH: 7.5 ASES:94.7	ROM: 6.6–140°			15
Gauci2016	Case series	65	52	30	36	46	radial head fractures	MoPyC, Tornier	monopolar	VAS:1; MEPS:96	ROM:9–136°	4		17
Yan2015	Retrospective cohort study	20	36.54	11		36	radial head fractures with terrible triad	Waldemar LINK GmbH & Co.	monopolar	MEPS:85.8	ROM:17–117°		stiffness n = 1; Secondary coronoid fragment displaced n = 1	7
Sarris2012	Case series	32	54	20	22	27		MoPyC, Tornier	monopolar		ROM:130°		stem neck dissociation n = 1	15
Rotini2012	Retrospective cohort study	30	44	19		24	radial head fractures with elbow stiffness or instability	SBI	monopolar n = 12; bipolar n = 19	MEPS:90		2		17
Ricon2012	Case series	28	54	11	15	32.6		MoPyC	bipolar	MEPS:92	ROM:15–120°		neuropathy n = 1	16
Flinkilla2012	Case series	42	56	16		53	acute unstable injury	Avanta Orthopedics n = 19; Acumed n = 23	monopolar	MEPS: 86 DASH:23	ROM:20–135°		nerve palsy n = 1; stiffness n = 4	14
Lamas2011	Case series	47	51	18	32	48	nonreconstructable radial head fracture	Mopyc, Bioprofile-Tornier	bipolar	VAS:1	ROM:6–140°	3	dislocation n = 2; neurologic symptoms n = 2	16
Chen2011	Prospective randomised controlled trial	22	37			33.6	nonreconstructable radial head fracture	Evolve	monopolar	Broberg and Morrey:92.1			stiffness n = 3	15
Chien2010	Case series	13	37	10		38.3	radial head fractures	Evolve	monopolar	MEPS:86.9	ROM: 6.2–126.5°	2	stiffness n = 2	15
Fehringer2009	Case series	16	55	9		32	comminuted radial head fractures	Evolve	monopolar					14
Shore2008	Case series	31	54		12	96	Chronic posttraumatic elbow disorders	Smith and Nephew Richards n = 22; Evolve n = 10	monopolar	MEPS:83			neuropathy n = 4; chronic regional pain syndrome n = 1	15
Anneluuk2008	Retrospective cohort study	31	47	22		24		EVOLVE n = 16; Swanson Titanium Radial Head Implant n = 1		MEPS:88; DASH:16.5	ROM:16–132°			13

(Continued on following page)

10.3389/fbioe.2022.1041531

TABLE 2 (*Continued*) Baseline demographics of the selected studies for uncemented fixation.

Author (year)	Type of studies	Patients	Average age	Gender (male)	Dominant	Average follow-up (month)	Identification of surgery	Implant of radial head arthroplasty	Polarity (monopolar VS. bipolar)	Clinical outcomes	Rang of motion (flexion minus extension)	Reoperation	Complications	QA
Doornberg2007	Case series	27	52	13	7	48	radial head fractures	Evolve		MEPS: 85 DASH: 17 ASES:84	ROM:20–131°			17
Wretenberg2006	Case series	18	52	11		44.4	radial head fractures	Waldemar Link, GmbH & Co.		VAS:0.8	ROM:15–130°			12
Grewal2006	Case series	26	54	9	11	24.5	radial head fractures	Evolve	monopolar	MEPI: 80.5 DASH: 24.4	ROM: 24.9–138.1°		neurologic n = 3	14
Ashwood2004	Case series	16	45	8	16	33.6	radial head fractures	Evolve	monopolar	MEPS: 87 VAS:1.7	ROM:15–125°		regional sympathetic mediated pain n = 1; ulnar nerve neuropathy n = 3	15
Moro2001	Case series	24	54	11		39	radial head fractures	Smith and Nephew Richards	monopolar	MEPI:80; DASH:17	ROM:8–140°		regional sympathetic mediated pain n = 1; ulnar nerve neuropathy n = 1	16
Harrington2001	Case series	20	46	7	11	145.2	radial head fractures	Smith and Nephew Richards	monopolar	Broberg and Morrey score:88	ROM:17–120°	4	pain n = 4	9
Knight1993	Case series	31	57	12		54	comminuted radial head fracture	Silastic: Dow Corning	monopolar				ulnar nerve paraesthesia n = 2	12

10.3389/fbioe.2022.1041531

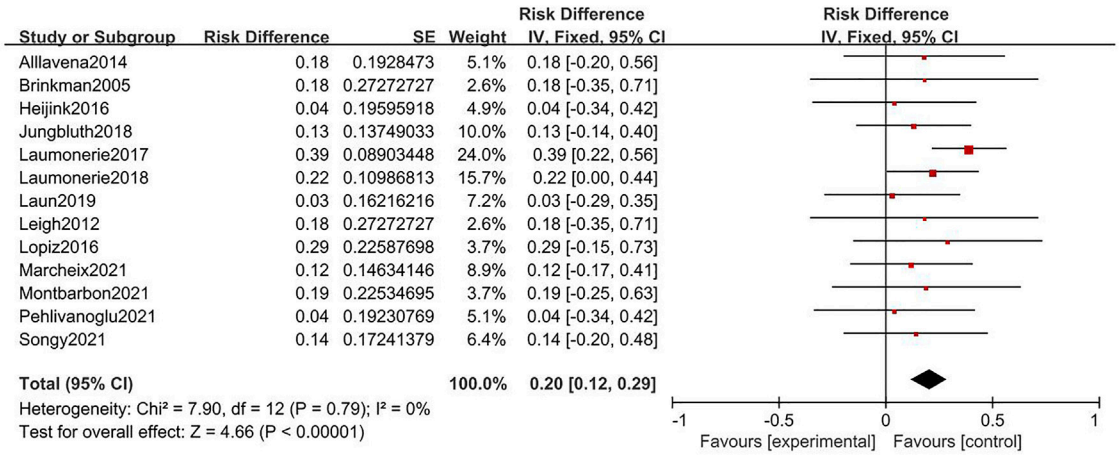

FIGURE. 2
Forest plot for rate of reoperation of cemented fixation.

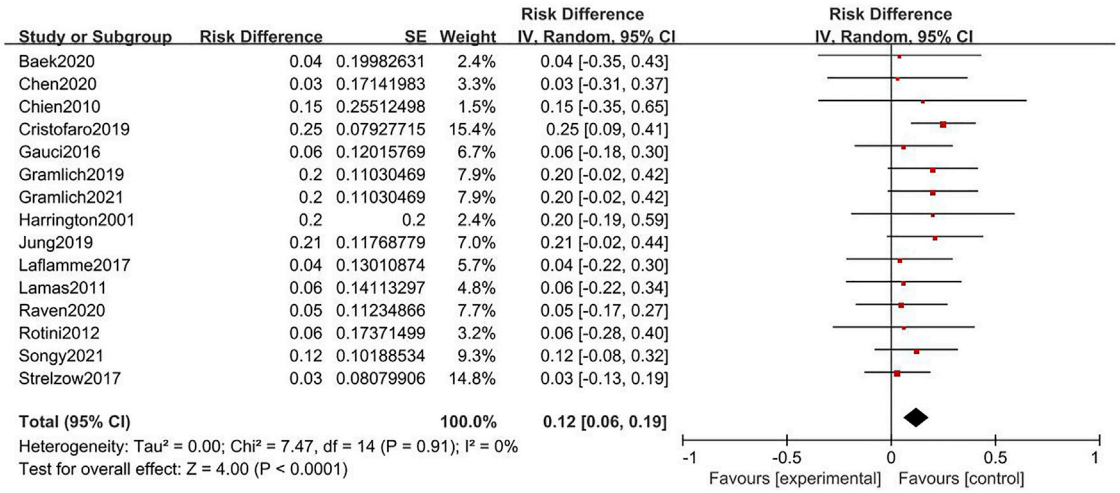

FIGURE. 3
Forest plot for rate of reoperation of uncemented fixation.

allowing micromotion, which can lead to excessive stress that is appropriately dispersed. Muhm et al. conducted a survey on the outcome of uncemented prostheses during mid-term follow-up; they found a mean Broberg–Morrey score of 85.5 ± 12.2, indicating good results observed in the group (Muhm et al., 2011). For cemented stem fixation, the prostheses was rigidly fixed to the medulla using bone cement. Cement fixation, including firm fixation, may reduce early prostheses loosening, and smaller-diameter stems avoid iatrogenic fracture during surgery. Agyeman et al. performed a systematic review and meta-analysis and found no significant outcome between the cemented prostheses group and the loose smooth stem group, although the cemented prostheses group had a higher risk of complications and reoperation than the other group (Agyeman et al., 2019). Laumonerie et al. conducted a survey of prostheses implanted *via* cemented fixation and found a relatively high rate of painful loosening (approximately 21.5%), osteolysis (53.8%), and overstuffing (46.2%) (Laumonerie et al., 2018). Szmit et al. performed a biomechanical study and found that using cemented fixation would make the radial head prostheses less effective in distributing high contact stress and easier to get abraded (Szmit et al., 2019). Although Kachooei et al. observed the lowest rate of revision with cemented fixation in their systematic review and meta-analysis, they thought that the rate may be related to

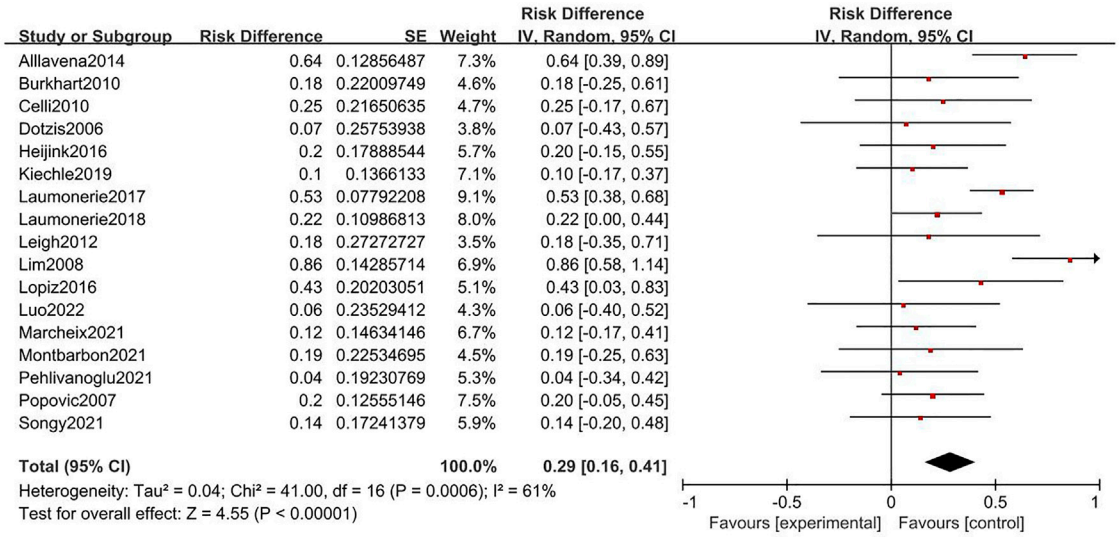

FIGURE. 4
Forest plot for rate of complication of cemented fixation.

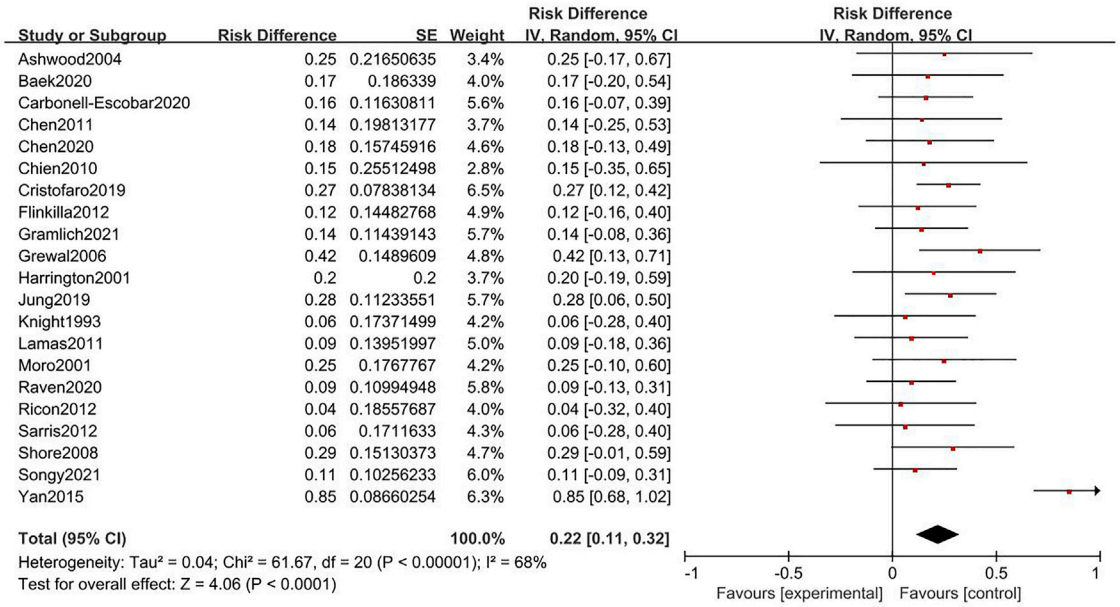

FIGURE. 5
Forest plot for rate of complication of uncemented fixation.

difficulties in removing the implant design (Kachooei et al., 2018). Regarding radiographic evaluation, Popovic et al. observed progressive radiographic loosening lines in 16 of 51 patients, and further 16 patients had loss of proximal bone support at the neck of the radius (Popovic et al., 2007). Similarly, Marcheix et al. found that 24% of elbows had radiographic loosening, and 54% of elbows developed lateral condyle demineralization (Marcheix et al., 2021). The results of the present study are comparable with those of previous studies. Herein, higher rates of reoperation and overall complications were found with

TABLE 3 Meta-analysis for secondary outcomes.

	Reoperation				Complications			
	Heterogeneity		Pooled results		Heterogeneity		Pooled results	
	Number of studies	I^2	Effect size (95% CI)	p value	Number of studies	I^2	Effect size (95% CI)	p value
Uncemented monopolar	16	0%	0.14(0.08,0.20)	<0.001	19	69%	0.24 (0.12,0.35)	<0.001
Cemented monopolar	4	0%	0.36(0.15,0.56)	<0.001	5	80%	0.32 (0.17,0.46)	<0.001
Uncemented bipolar	3	39%	0.20(0.02,0.37)	0.03	3	0%	0.12 (-0.05,0.30)	0.17
Cemented bipolar	12	34%	0.34(0.26,0.42)	<0.001	12	46%	0.34 (0.26,0.42)	<0.001

cemented fixation than with uncemented fixation; in particular, the painful loosening rate was higher with cemented fixation than with uncemented fixation (10% vs 5.5%).

In addition, radial head prostheses were divided into monopolar and bipolar prostheses. Most monopolar prostheses are one-piece unipolar metallic devices with a closely connected junction between the radial head and the stem. Strelzow et al. conducted a survey on monopolar prostheses and found that the final mean PREE and Quick-DASH scores were 17 ± 3 and 14 ± 3, respectively, with a complication rate of 26% (Strelzow et al., 2017). Baek et al. reported satisfactory results of monopolar prostheses for complex radial head fractures, with a mean MEPS of 88.7 ± 11.5 and a mean DASH score of 19.4 ± 7.8 (Baek et al., 2020). In the present study, the rates of complications and reoperation with uncemented monopolar protheses were 24% and 14%, respectively; the rates with cemented monopolar prostheses were 32% and 36%, respectively. The mean VAS score, MEPS, DASH score, and Broberg–Morrey score were 0.8–3.3, 70–91.5, 6.3–34, and 63–78.4, respectively. Bipolar radial head implants were invented to improve the junction and ROM of the elbow, and some experts suggest that their use leads to better elbow kinematics after surgery. Laun et al. reported good-to-excellent results of bipolar arthroplasty for radial head fractures at an average of 5.6 years of follow-up (Laun et al., 2019). Patients showed a mean DASH score of 18.6 and a mean MEPS of 90.3. Burkhart et al. also reported promising mid-to-long-term results with bipolar radial head prostheses. The mean MEPS reached approximately 90.8, and the mean DASH score reached approximately 9.8. However, Burkhart et al. reported degenerative changes in 71% and periarticular ossification after surgery in 76%, which were confirmed in the present study (Burkhart et al., 2010). Herein, the rates of complications and reoperation with uncemented bipolar protheses were 24% and 14%, respectively; the rates with cemented bipolar protheses were 32% and 36%, respectively. The mean VAS score, MEPS, DASH score, and Broberg–Morrey score were 0.2–1.4, 78.9–95, 8–23.9, and 86.5–86.6, respectively.

The efficacy of bipolar or monopolar prostheses is still controversial. Theoretically, bipolar designs reduce abrasion of the capitellar cartilage and stress at the implant-to-cement and cement-to-bone interfaces because of the free rotation between the stem and articular components. The radiocapitellar contact pressure may also decrease with bipolar designs compared with that with monopolar designs owing to the better alignment of the articular component onto the capitellum. Antoni et al. reported similar clinical and radiological results and complication and revision rates (Antoni et al., 2020). Hejink et al. reviewed 30 studies involving 727 patients and found that there was no significant difference in the ROM or clinical outcomes between bipolar and monopolar prostheses (Heijink et al., 2016). Mukka et al. conducted a mean follow-up of 6 years between two kinds of prostheses and found no significant difference in the QuickDASH score and ROM (Mukka et al., 2020). Van Riet et al. reviewed radial head prostheses revisions and observed a lower incidence of loosening with fixed-stem bipolar prostheses than with monopolar prostheses (Van Riet et al., 2010). In the survey by Antoni et al., the rate of ectopic ossification was higher in monopolar prostheses, which may be attributed to the longer follow-up in the monopolar prostheses group.

In our study, cemented monopolar prostheses yielded the highest reoperation rate, while uncemented monopolar prostheses yielded the lowest reoperation rate. Similarly, cemented bipolar prostheses had the highest complication rate, while uncemented bipolar prostheses had the lowest complication rate. Thus, the effect of cemented or uncemented fixation may be dominant in the outcome of RHA, with a minimal effect of bipolar or monopolar fixation. However, further biomechanical and clinical studies are required.

Limitation

As with any systematic review or meta-analysis, our study has several limitations. First, because data interpretation depends on the quality of the information gathered, the validity of our study may be

limited by the respective levels of evidence. Second, different prostheses differ in morphological design, which may have an impact on the results. Third, in the subgroup analysis, only three studies mentioned the rate of periprosthetic loosening in uncemented bipolar prostheses, while three studies mentioned the rate of overall complications in monopolar cemented prostheses, which would create a significant bias. Finally, we included only English literature; studies in other languages were not included, and the results may be affected by the fact that the prostheses used worldwide vary.

Conclusion

Uncemented radial head prostheses have lower rates of reoperation and overall complications than cemented radial head prostheses. In particular, uncemented monopolar prostheses may yield the lowest rate of reoperation, while uncemented bipolar prostheses may yield the lowest rate of overall complications.

Data availability statement

The original contributions presented in the study are included in the article/supplementary material, further inquiries can be directed to the corresponding author.

Author contributions

SL, HZ, and YL designed the study and collected the data. SL and GY analyzed and interpreted the patient data. GY was a major contributor in writing the manuscript. All authors read and approved the final manuscript.

Conflict of interest

The authors declare that the research was conducted in the absence of any commercial or financial relationships that could be construed as a potential conflict of interest.

The reviewer, JC, declared a shared parent affiliation with the authors to the handling editor at the time of review.

Publisher's note

References

Acevedo, D. C., Paxton, E. S., Kukelyansky, I., Abboud, J., and Ramsey, M. (2014). Radial head arthroplasty: State of the art. *J. Am. Acad. Orthop. Surg.* 22 (10), 633–642. doi:10.5435/JAAOS-22-10-633

Agyeman, K. D., Damodar, D., Watkins, I., and Dodds, S. D. (2019). Does radial head implant fixation affect functional outcomes? A systematic review and meta-analysis. *J. shoulder Elb. Surg.* 28 (1), 126–130. doi:10.1016/j.jse.2018.07.032

Antoni, M., Kempf, J. F., and Clavert, P. (2020). Comparison of bipolar and monopolar radial head prostheses in elbow fracture-dislocation. *Orthop. Traumatology Surg. Res.* 106 (2), 311–317. doi:10.1016/j.otsr.2019.10.027

Baek, C. S., Kim, B. S., Kim, D. H., and Cho, C. H. (2020). Short- to mid-term outcomes of radial head replacement for complex radial head fractures. *Clin. Shoulder Elb.* 23 (4), 183–189. doi:10.5397/cise.2020.00325

Burkhart, K. J., Mattyasovszky, S. G., Runkel, M., Schwarz, C., Küchle, R., Hessmann, M. H., et al. (2010). Mid- to long-term results after bipolar radial head arthroplasty. *J. shoulder Elb. Surg.* 19 (7), 965–972. doi:10.1016/j.jse.2010.05.022

Chanlalit, C., Shukla, D. R., Fitzsimmons, J. S., An, K. N., and O'Driscoll, S. W. (2012). Effect of hoop stress fracture on micromotion of textured ingrowth stems for radial head replacement. *J. shoulder Elb. Surg.* 21 (7), 949–954. doi:10.1016/j.jse.2011.05.001

Delclaux, S., Lebon, J., Faraud, A., Toulemonde, J., Bonnevialle, N., Coulet, B., et al. (2015). Complications of radial head prostheses. *Int. Orthop.* 39 (5), 907–913. doi:10.1007/s00264-015-2689-7

Duckworth, A. D., Wickramasinghe, N. R., Clement, N. D., Court-Brown, C. M., and McQueen, M. M. (2014). Radial head replacement for acute complex fractures: What are the rate and risks factors for revision or removal? *Clin. Orthop. Relat. Res.* 472 (7), 2136–2143. doi:10.1007/s11999-014-3516-y

Heijink, A., Kodde, I. F., Mulder, P., Van Dijk, C. N., and Eygendaal, D. (2016). Cemented bipolar radial head arthroplasty: Midterm follow-up results. *J. shoulder Elb. Surg.* 25 (11), 1829–1838. doi:10.1016/j.jse.2016.05.017

Kaas, L., van Riet, R. P., Vroemen, J. P., and Eygendaal, D. (2010). The epidemiology of radial head fractures. *J. shoulder Elb. Surg.* 19 (4), 520–523. doi:10.1016/j.jse.2009.10.015

Kachooei, A. R., Baradaran, A., Ebrahimzadeh, M. H., van Dijk, C. N., and Chen, N. (2018). The rate of radial head prosthesis removal or revision: A systematic review and meta-analysis. *J. hand Surg.* 43 (1), 39–53.e1. e1. doi:10.1016/j.jhsa.2017.08.031

Kachooei, A. R., Claessen, F. M., Chase, S. M., Verheij, K. K., van Dijk, C. N., and Ring, D. (2016). Factors associated with removal of a radial head prosthesis placed for acute trauma. *Injury* 47 (6), 1253–1257. doi:10.1016/j.injury.2016.02.023

Laflamme, M., Grenier-Gauthier, P. P., Leclerc, A., Antoniades, S., and Bédard, A. M. (2017). Retrospective cohort study on radial head replacements comparing results between smooth and porous stem designs. *J. shoulder Elb. Surg.* 26 (8), 1316–1324. doi:10.1016/j.jse.2017.04.008

Laumonerie, P., Reina, N., Gutierrez, C., Delclaux, S., Tibbo, M. E., Bonnevialle, N., et al. (2018). Tight-fitting radial head prosthesis: Does stem size help prevent painful loosening? *Int. Orthop.* 42 (1), 161–167. doi:10.1007/s00264-017-3644-6

Laumonerie, P., Reina, N., Kerezoudis, P., Declaux, S., Tibbo, M. E., Bonnevialle, N., et al. (2017). The minimum follow-up required for radial head arthroplasty: A meta-analysis. *bone & Jt. J.* 99-B (12), 1561–1570. doi:10.1302/0301-620X.99B12.BJJ-2017-0543.R2

Laun, R., Tanner, S., Grassmann, J. P., Schneppendahl, J., Wild, M., Hakimi, M., et al. (2019). Primary cemented bipolar radial head prostheses for acute elbow injuries with comminuted radial head fractures: Mid-term results of 37 patients. *Musculoskelet. Surg.* 103 (1), 91–97. doi:10.1007/s12306-018-0576-2

Li, N., and Chen, S. (2014). Open reduction and internal-fixation versus radial head replacement in treatment of Mason type III radial head fractures. *Eur. J. Orthop. Surg. Traumatol.* 24 (6), 851–855. doi:10.1007/s00590-013-1367-y

Marcheix, P. S., Cuenca, C., Vergnenegre, G., Mabit, C., Hardy, J., and Charissoux, J. L. (2021). Factors influencing the mid-term radiological and functional outcomes of 41 post-fracture bipolar radial head arthroplasty cases at

a mean follow-up of 87 months. *Orthop. Traumatology Surg. Res.* 107 (2), 102818. doi:10.1016/j.otsr.2021.102818

Mason, M. L. (1954). Some observations on fractures of the head of the radius with a review of one hundred cases. *Br. J. Surg.* 42 (172), 123–132. doi:10.1002/bjs.18004217203

Morrey, B. F., Tanaka, S., and An, K. N. (1991). Valgus stability of the elbow. A definition of primary and secondary constraints. *Clin. Orthop. Relat. Res.* 265 (265), 187–195. doi:10.1097/00003086-199104000-00021

Muhm, M., de Castro, R., and Winkler, H. (2011). Radial head arthroplasty with an uncemented modular metallic radial head prosthesis: Short- and mid-term results. *Eur. J. trauma Emerg. Surg.* 37. St. Pölten, Austria: official publication of the European Trauma Society, 85–95. doi:10.1007/s00068-010-0051-8

Mukka, S., Sjöholm, P., Perisynakis, N., Wahlström, P., Rahme, H., and Kadum, B. (2020). Radial head arthroplasty for radial head fractures: A clinical and radiological comparison of monopolar and bipolar radial head arthroplasty at a mean follow-up of 6 years. *Eur. J. trauma Emerg. Surg.*, 46. St. Pölten, Austria: official publication of the European Trauma Society, 565–572. doi:10.1007/s00068-018-1042-4

Neuhaus, V., Christoforou, D. C., Kachooei, A. R., Jupiter, J. B., Ring, D. C., and Mudgal, C. S. (2015). Radial head prosthesis removal: A retrospective case series of 14 patients. *Arch. Bone Jt. Surg.* 3 (2), 88–93.

O'Driscoll, S. W., and Herald, J. A. (2012). Forearm pain associated with loose radial head prostheses. *J. shoulder Elb. Surg.* 21 (1), 92–97. doi:10.1016/j.jse.2011.05.008

Popovic, N., Lemaire, R., Georis, P., and Gillet, P. (2007). Midterm results with a bipolar radial head prosthesis: Radiographic evidence of loosening at the bone-cement interface. *J. Bone Jt. Surg.* 89 (11), 2469–2476. doi:10.2106/JBJS.F.00723

Sershon, R. A., Luchetti, T. J., Cohen, M. S., and Wysocki, R. W. (2018). Radial head replacement with a bipolar system: An average 10-year follow-up. *J. shoulder Elb. Surg.* 27 (2), e38–e44. doi:10.1016/j.jse.2017.09.015

Strelzow, J. A., Athwal, G. S., MacDermid, J. C., Grewal, R., Faber, K. J., Drosdowech, D., et al. (2017). Effect of concomitant elbow injuries on the outcomes of radial head arthroplasty: A cohort comparison. *J. Orthop. Trauma* 31 (10), e327–e333. doi:10.1097/BOT.0000000000000921

Szmit, J., King, G., Johnson, J. A., and Langohr, G. (2019). The effect of stem fit on the radiocapitellar contact mechanics of a metallic axisymmetric radial head hemiarthroplasty: Is loose fit better than rigidly fixed? *J. shoulder Elb. Surg.* 28 (12), 2394–2399. doi:10.1016/j.jse.2019.05.019

Van Riet, R. P., Sanchez-Sotelo, J., and Morrey, B. F. (2010). Failure of metal radial head replacement. *J. Bone Jt. Surg. Br. volume* 92 (5), 661–667. doi:10.1302/0301-620X.92B5.23067

frontiers | Frontiers in Bioengineering and Biotechnology

TYPE Original Research
PUBLISHED 16 November 2022
DOI 10.3389/fbioe.2022.1055176

OPEN ACCESS

EDITED BY
Liqun Xu,
Southwest University, China

REVIEWED BY
Zheng-Zheng Zhang,
Sun Yat-Sen Memorial Hospital, China
Yi Ding,
Capital Medical University, China

*CORRESPONDENCE
Zhong Zhang,
wuhai_zhangzhong@126.com

†These authors have contributed equally to this work and share first authorship

SPECIALTY SECTION
This article was submitted to Biomaterials, a section of the journal Frontiers in Bioengineering and Biotechnology

RECEIVED 27 September 2022
ACCEPTED 02 November 2022
PUBLISHED 16 November 2022

CITATION
Ren X, Wang J, Yang S, Liu Z, Wang T, Zhang T, Li H and Zhang Z (2022), The safety, efficacy, and functional outcomes on arthroscopic fixation of posterior cruciate ligament avulsion fracture by a bio-absorbable anchor or traditional pull-out technique: A prospective cohort study.
Front. Bioeng. Biotechnol. 10:1055176.
doi: 10.3389/fbioe.2022.1055176

The safety, efficacy, and functional outcomes on arthroscopic fixation of posterior cruciate ligament avulsion fracture by a bio-absorbable anchor or traditional pull-out technique: A prospective cohort study

Xiangyu Ren[1†], Jianing Wang[2†], Shulong Yang[1], Zhe Liu[1], Tianda Wang[1], Teng Zhang[1], Haoxin Li[1] and Zhong Zhang[1*]

[1]Department of Sports Medicine, The People's Hospital of Wu Hai Inner Mongolia, Wuhai, China, [2]Department of Sports Medicine, Peking University Third Hospital. Institute of Sports Medicine of Peking University. Beijing Key Laboratory of Sports Injuries, Beijing, China

Background: The posterior cruciate ligament avulsion fracture (PCLAF) is a special type of PCL rupture, and arthroscopic fixation for PCLAF has been recommended currently. The bio-absorbable suture anchor is a novel internal fixation for PCLAF. This study aims to estimate and compare the safety, efficacy, and functional outcomes between the bio-absorbable anchor and the traditional suture pull-out technique for arthroscopic fixation of PCLAF.

Methods: This was a prospective cohort study. PCLAF patients were included from 1 January 2020, to 31 August 2021, in our department, and randomly divided into the absorbable anchor group and control group (pull-out suture fixation). Clinical assessments included: post drawer test, gravity test, anterior-posterior laxity (KT-2000), range of motion, Lysholm and International Knee Documentation Committee (IKDC) scores, total failure rate, and returning to sports rate. The minimum follow-up was 1 year (y).

Results: 31 patients had accomplished the 1 year follow-up (missing rate: 13.9%). We did not face any complications such as neurovascular injury, fever, infection, un-union, or re-rupture during the follow-up. CT scan showed that all of the patients in the two groups had a well bone union at 3 months in post-operation. At 1 year follow-up, the total failure rate of the bio-absorbable anchor group (1/17, $p = 0.036$) was lower than the control group (5/14), and the IKDC (86.24 $\pm$ 4.35, $p = 0.008$) and return to sports rate (11/17, $p = 0.045$) of the bio-absorbable anchor group were higher than that of the control group (81.43 $\pm$ 5.06) (4/14).

Conclusion: Both the bio-absorbable anchor and suture pull-out technique for arthroscopic fixation of PCLAF have acquired a well bone union and superior safety, but the bio-absorbable anchor group had better efficacy and functional outcomes than the traditional pull-out technique.

KEYWORDS

posterior cruciate ligament avulsion fracture, bio-absorbable anchor, bio-material, safety, efficacy, functional outcome

1 Introduction

The posterior cruciate ligament (PCL) is a main stabilizer of knee, maintaining the rotation stability and posterior stability during motion (Rosenthal et al., 2012). PCL avulsion fracture (PCLAF) is a special type of PCL rupture, which mostly occurs at its tibial insertion. As the PCL ligament is usually intact, a reduction and fixation operation for reconstructing the tendon-bone integrity can acquire a good efficacy and functional outcome in patients with a fresh PCLAF (Zhang et al., 2013; Sabat et al., 2016). Currently, arthroscopic operations of PCLAF have been recommended, because of the advantages of mini-invasive, reliable reduction, ease of operation, and less complication (Domnick et al., 2016; Nourbakhsh et al., 2016; Hooper et al., 2017).

Recently, the biomaterial science development has greatly advanced the arthroscopic fixation techniques of PCLAF. One of the most representative biomaterial fixations is the bio-absorbable suture anchor, which can be used to perform the arthroscopic "suture bridge" fixation for PCLAF. The suture bridge technique has been commonly used in arthroscopic repair of the rotator cuff, it is easy to perform, and has been described as an effective method for obtaining higher initial fixation strength, larger contact area, and higher contact pressure at the tendinous footprint, compared with the traditional former techniques (Kim et al., 2006). The novel bio-absorbable can produce a rigid fixation for PCLAF. The main component of the bio-absorbable suture anchor is polylactide, which melts over the suture during the fixation process, creating an inextricable connection between the anchor and suture, as well as a rigid fixation between the anchor and bone (Koch et al., 2021). What's more, Similar to the traditional pull-out suture fixation, the bio-absorbable suture anchor is also applicable to PCLAF with small or comminuted fragments (Willinger et al., 2019) (Nakagawa et al., 2017).

The clinical application of the novel bio-absorbable anchor has been paid more and more attention in the fields of biomaterial science and sports medicine. The first arthroscopic suture bridge fixation of PCLAF (non-absorbable) was reported in 2016 (Nourbakhsh et al., 2016), till now, clinical study on using the bio-absorbable suture anchor in this field is still limited, and only several cases were reported, lacking of systematic follow-up study and clinical comparisons. The purpose of this study is to estimate and compare the safety, efficacy, and functional outcomes of arthroscopic fixation of PCLAF between the bio-absorbable suture anchor and the traditional technique.

2 Materials and methods

2.1 Patient involvement

Patients diagnosed with PCLAF were included between 1 January 2020, and 31 August 2021, in our department. The inclusion criteria were: 1) age: 18–39 years old, BMI≤31; 2) acute PCLAF (injury less than 3 weeks) (Madi et al., 2021); 3) MRI showed a definite PCLAF with partial, complete, or comminuted fragment; 4) isolated PCLAF in a single knee; 5) agree to participate in this study after signing the informed consent; 6) agree to the arrangement of the grouping. The exclusion criteria were: 1) the periarticular fractures; 2) PCL re-rupture; 3) patients combined with ACL rupture, MCL rupture, or meniscus tears; 4) knee osteoarthritis with the Kellgren-Lawrence grade>2; 5) systematic diseases such as rheumatoid arthritis, gouty arthritis, nerve system diseases, diabetes.

Patients were randomly divided into the absorbable anchor group and control group (pull-out suture fixation). The protocol and procedure for protecting human subjects in the present study were approved by the Ethics Committee (IRB ethical approval: KS-ob202171) in our hospital before this study started.

2.2 Arthroscopic fixation of PCLAF with bio-absorbable anchor or pull-out technique

Operations of the two groups were performed by the same senior surgeon, with the patients supine, under spinal anesthesia, and using a tourniquet. A standard anterolateral (AL) and anteromedial (AM) portals were made, and an initial diagnostic arthroscopy and debridement were carried out until the posteromedial (PM) compartment is visualized, and then a high PM portal (arthroscope) and a low PM (working) portal were created by a guide needle. After identifying the bone fragment, debridement of the fracture bed was performed.

Bio-absorbable anchors (4.5 mm Healix BioCryl Rapide Suture Anchors, Depuy Mitek, Johnson & Johnson, Shanghai) was implanted superiorly to the fracture bed. The fragment of

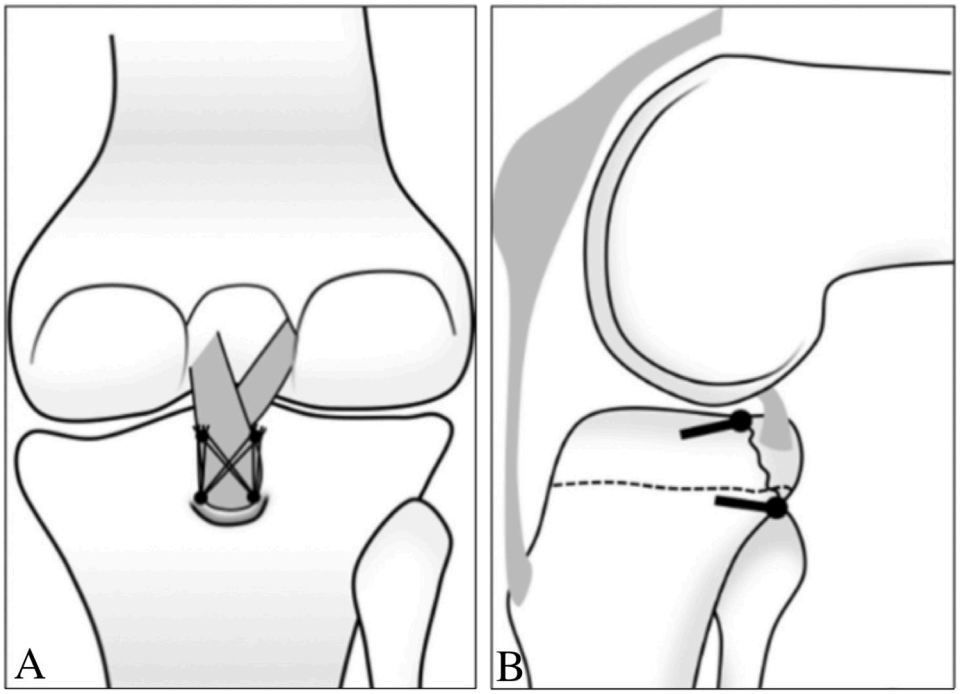

FIGURE 1
Schematic draw of the suture bridge fixation of PCLAF (Lee et al., 2015) (Copyright 2015; The Korean Orthopaedic Association). **(A)** 2 bio-absorbable anchors were implanted into the proximal-medical side and proximal-lateral side of the fracture bed, and the fragment of PCLAF was fixed by threading the 4 strands of the suture through the bone-tendon junction from anterior to posterior, and the 4 strands (2 strands of each anchor) were retrieved and located by external anchors; **(B)** lateral view, the internal anchors were located proximally, and the external row anchors were located distally of the fracture bed.

PCLAF is fixed using the suture bridge by threading the 4 strands of the suture through the bone-tendon junction from anterior to posterior (Figure 1A). After reducing the fragment by flexion at 90°, the external row anchor (5.5 mm, Healix Advance BioCryl Rapide Knot Free Suture Anchors, Depuy Mitek, Johnson & Johnson, Shanghai) was located at 1.5 cm proximally from the posterior edge of the fracture bed. The 4 strands were retrieved and passed through the external anchor, which was screwed into the bone until enough depth, creating a "suture bridge" fixation (Figure 1B). When the operation was completed, the patient's limb was placed in a long leg brace with a small pillow under the lower leg to support the lower leg against gravity (Nourbakhsh et al., 2016).

In the control group, the arthroscope was transferred to AM portal, and a Lasso and 2 sutures (no.2 Ethibond suture, Johnson & Johnson, United States) were used to do 2 figure-of-eight sutures through the bone-tendon junction. A 3 cm incision was made on the proximal tibia, which was 2 cm medial to the tibial tuberosity. Transferred the arthroscope to low PM portal, passed a PCL guide through AM portal and space between PCL and medial femur condyle, located it at the medial and lateral side of the fracture bed, and then drilled 2 transtibial tunnels. A beath pin with looped PDS was passed through the tunnels and retrieved with the 2 strands of sutures through the high PM portal, and then the strands were pulled out through the tunnels when reduced the fragment by flexion at 90° ("pulled out" technique). The 4 strands of 2 sutures were tied over a suture disc after maximum pulling and giving anterior drawer at the same time.

2.3 Follow-ups

The follow-up was started when the operation was completed. The end was re-operation of the PCL/re-rupture of the PCL/death/missing, whichever occurred first. The minimum follow-up was 1 year (y). Basic clinical parameters included: age, gender, body mass index (BMI), operation time, follow-up time, and complications.

Osseous union was assessed by knee CT scan at 3 months of the follow-up (Lamoria et al., 2020), and knee MRI was performed at 1 year follow-up. All of those data were checked and entered into a database by two researchers, and a double-entry is carried out for quality control.

2.4 Clinical assessments

The clinical examinations of PCLAF included the post drawer test (PDT) and gravity test (GT), which were used to assess the anterior-posterior (A-P) joint stability. PDT was classified as: normal (-, posterior shift< 5 mm), doubtable laxity (±, posterior shift between 5 and 10 mm), and laxity (+, posterior shift >10 mm). GT was classified as: normal (-), subsided tibial tuberosity (+). The clinical examinations were performed and recorded before the operation (under anesthesia) and at 1 year follow-up.

A-P laxity (backward shift) was measured by KT-2000 when the knee is flexed at 70°, and it is evaluated by comparing it to the healthy side, and it is classified as (Ranger et al., 2011): normal, grade 1 (difference between 1 and 5 mm), grade 2 (between 5 and 10 mm), and grade 3 (>10 mm). The KT-2000 exam was performed in pre-operation and at 1 year follow-up.

Knee range of motion (ROM) was measured by standardized goniometry technique in pre-operation and at 1 year follow-up. The knee flexion contracture (KFC) and knee flexion limitation (KFL) angles were assessed by passive physical examination of ROM. KFC is defined as the gap value of extension loss compared to the normal side, and KFC ≤5° is normal (Insall et al., 1989; Yi et al., 2020). KFC is classified as: grade 1 (KFC between 5° and 10°), grade 2 (moderate, between 10° and 15°), grade 3 (severe, between 15° and 20), grade 4 (very severe, KFC >20°), according to the Knee Society Score (KSS) system (Insall et al., 1989; Yi et al., 2020). KFL is defined as the gap value of flexion loss compared to the normal side, and KFL is classified as: grade 1 (mild, KFL between 5° and 10°), grade 2 (moderate, between 10° and 15°), grade 3 (severe, between 15° and 20), and grade 4 (very severe, KFL >20°).

2.5 Subjective assessments of knee function

To evaluate the functional outcomes of motor function, the Lysholm knee scoring scale (Wang et al., 2016), and International Knee Documentation Committee (IKDC) subjective-form score (Fu and Chan, 2011) were assessed by self-questionnaires at follow-ups. The IKDC score gives equal evaluations of the knee function, while the Lysholm score gives more points to the pain and instability (Lamoria et al., 2020). The full scores of IKDC and Lysholm are 100, and a higher score represents a better functional outcome. The rate of returning to sports was used to evaluate the outcome of physical activity.

2.6 Clinical failure

Clinical failure was judge as meeting any of the following results at 1 year follow-up: 1) the re-rupture; 2) overall IKDC score of grade C (60–70 score) or D (less than 60 scores) (Su et al., 2020); 3) PDT (+) or GT (+); 4) A-P laxity of grade 2 or 3 (Fu and Chan, 2011); 5) KFC>5 (grade 1) or KFL>15 (grade 3) (Su et al., 2020). The clinical failure rates were calculated.

2.7 Statistical analysis

The continuous data were expressed as mean ± SD, and the inter-group comparisons and intra-group comparisons of the continuous data were processed by the independent samples t-tests and Levene variance homogeneity tests between groups. Count data were expressed as number (n) and rate (/), and inter-group comparisons and intra-group comparisons of the count data were processed by the Chi-square test or Fisher's exact test. The level of significance was set at 0.05. All of the statistical analyses were performed using SPSS 20.0 (SPSS Inc., 2009; Chicago, IL, United States).

3 Results

3.1 Basic characteristics

36 patients were enrolled in this study initially, and the sample size of the two groups was set at 1:1. Finally, 31 patients had accomplished the 1 year follow-up, 1 patient of the suture anchor group and 4 patients of the control group were missing, and the total missing rate was 13.9% (5/36). Those missing subjects were excluded from the database, in order to control the bias. Most of the included patients (n = 31) were injured by sports or traffic accidents: 13 subjects suffered a sprain of the knee when doing competitive sports; 10 were caused by traffic accident; 2 sprained the knee by themselves when skiing or skating; 4 slipped and sprained the knee by themselves.

The general characteristics including age, gender, BMI, as well as the fracture type, and follow-up time between the suture anchor group (n = 17) and control group (n = 14) did not have significance (Table 1), while the operative time of the bio-absorbable anchor group was shorter than the control group (Table 1). We did not face any complications such as neurovascular injury, fever, or infection during the perioperative period.

3.2 Comparisons of the efficacy of the two groups

At 1 year follow-up, the positive rates of PDT and GT, as well as the grade of A-P laxity, KFC, and KFL did not have significance between the bio-absorbable suture anchor group and control group, however, the total failure rate of suture anchor group (1 case: A-P laxity of grade 2) was lower than

TABLE 1 Basic characteristics of PCLAF patients in the bio-absorbable suture anchor and control groups.

Characteristics	Suture anchor (n = 17)	Control (n = 14)	p-value
PCLAF type (partial/complete/comminute)	4/10/3	4/8/2	χ^2 = 0.133
			p = 0.936
Gender (male/female)	11/6	9/5	χ^2 = 0.001
			p = 0.981
Age (year)	24.6 ± 6.3	26.0 ± 6.0	t = -0.636
			p = 0.530
BMI	22.39 ± 1.19	22.76 ± 1.28	t = -0.825
			p = 0.416
Operation time (minute)	97.6 ± 13.4	142.6 ± 9.9	t = -10.423
			p < 0.001**
Follow-up (month)	13.6 ± 2.1	13.4 ± 1.6	t = 0.414
			p = 0.682

Note: PCLAF (posterior cruciate ligament avulsion fracture); BMI (Body Mass Index); p < 0.001**.

TABLE 2 The efficacy of PCLAF patients in the bio-absorbable suture anchor and control groups at 1 year follow-up.

Parameters		Suture anchor (n = 17)	Control (n = 14)	p-value
PDT	–	15	8	χ^2 = 4.165
	±	2	5	p = 0.125
	+	0	1	
GT	–	17	12	χ^2 = 2.596
	+	0	2	p = 0.107
A-P laxity	Normal	13	7	
	Grade 1	3	4	χ^2 = 3.206
	Grade 2	1	2	p = 0.361
	Grade 3	0	1	
KFC	Normal	17	13	
	Grade 1	0	1	χ^2 = 1.225
	Grade 2	0	0	p = 0.263
	Grade 3	0	0	
	Grade 4	0	0	
KFL	Normal	13	7	
	Grade 1	4	4	χ^2 = 4.552
	Grade 2	0	2	p = 0.208
	Grade 3	0	1	
	Grade 4	0	0	
Total failure rate		1/17	5/14	χ^2 = 4.377
				p = 0.036*

Note: PDT (post drawer test); GT (gravity test); A-P (anterior-posterior), KFC (knee flexion contracture); KFL (knee flexion limitation); p < 0.05*.

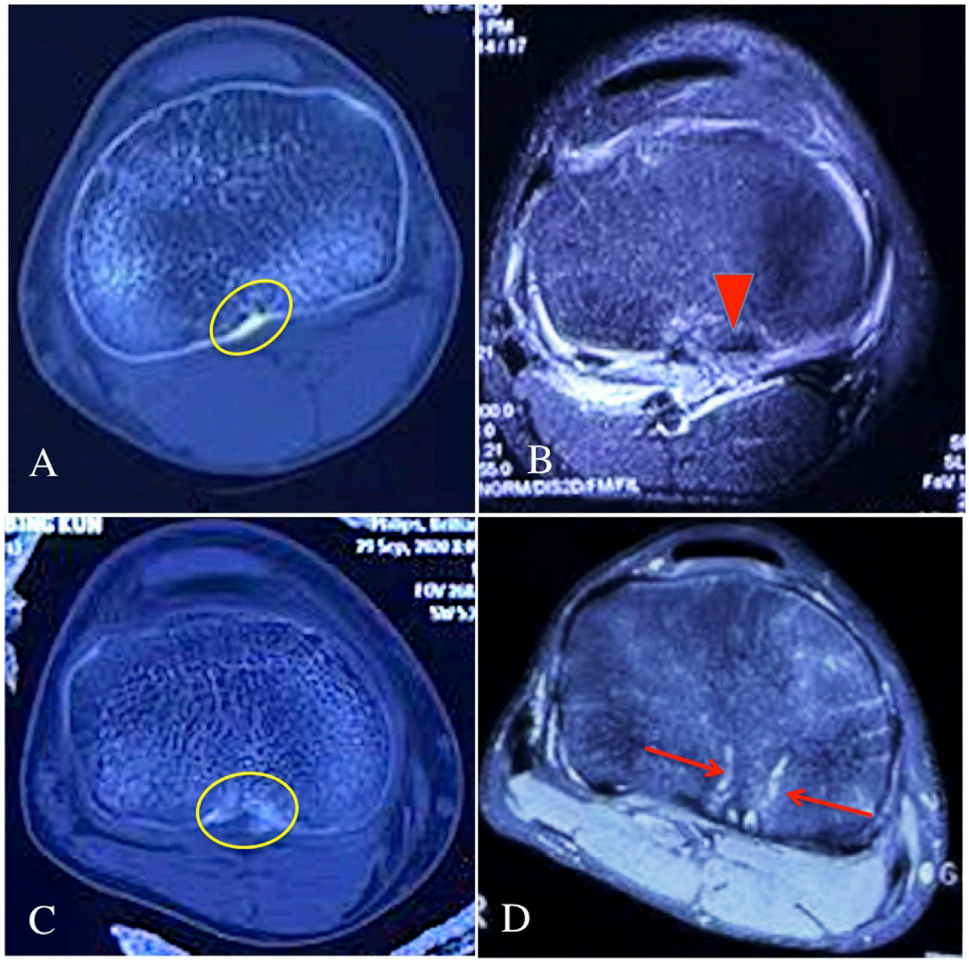

FIGURE 2
The CT scan and knee MRI of the two groups during the follow-ups. **(A)** knee CT scan of the bio-absorbable group at 3 months follow-up, the yellow circle showed a well bone union of the PCLAF in post-operation; **(B)** knee MRI of the bio-absorbable group at 1 year follow-up, the red triangle showed an intact PCL with the normal signal; **(C)** knee CT scan of the suture pull-out group at 3 months follow-up, the yellow circle showed a well bone union of the PCLAF in post-operation; **(D)** knee MRI of the suture pull-out group at 1 year follow-up, the red arrows showed the trans-tibial tunnels still existed.

TABLE 3 The functional outcomes of the bio-absorbable suture anchor and control groups at 1 year follow-up.

Parameters		Suture anchor (n = 17)	Control (n = 14)	p-value
Lysholm		86.88 ± 5.24	86.21 ± 3.26	t = 0.415
				p = 0.681
IKDC		86.24 ± 4.35	81.43 ± 5.06	t = 2.843
				p = 0.008**
Return to sports	Yes	11	4	χ^2 = 4.014
	No	6	10	p = 0.045*

Note: $p < 0.01$**; $p < 0.05$*.

the control group (3 case: A-P laxity of grade 2–3, 1 case of KFC of grade 1, 1 case of KFL of grade 3) (Table 2).

CT scan showed that all of the patients in the bio-absorbable group and control group had a well bone union of the PCLAF at 3 months in post-operation (Figures 2A,C). At 1 year follow-up, knee MRI showed that the patients in the bio-absorbable group had an intact PCL with the normal signal (Figure 2B), while the trans-tibial tunnels were still found in the control group (Figure 2D). We did not face any complications such as the bone un-union or re-rupture during the follow-up period.

3.3 The functional outcomes of the two groups at 1 year follow-up

No patients of the two groups had an IKDC or Lysholm score lower than 70 scores at 1 year follow-up, and the Lysholm score did not have significance between the bio-absorbable suture anchor group and control group, but the IKDC of bio-absorbable suture anchor group was higher than that of the control group (Table 3). The return to sports rate in the bio-absorbable anchor group was also higher than that in the control group (Table 3).

4 Discussion

4.1 PCLAF and sports-injury in the young population

PCLAF is a special type of PCL rupture, and it can occur in the setting of high-energy trauma such as motorcycle accidents, as well as in lower-energy sports-related injuries in young and active individuals (Schulz et al., 2003). However, the present study found that most of the included patients were injured by sports (13 cases of competitive sports, 2 cases of skiing or skating), high-energy trauma was ranked second (10 cases of traffic accidents), followed by lower-energy trauma (4 cases of slip and self-sprain). In our study, the included patients were young population with the age ranging from 18 to 38, who were physically active and prone to get injured during sports. The relatively young population may explain the reason why the lower-energy sports-related injuries ranked first in the PCLAF patients.

4.2 Arthroscopic fixations for PCLAF

PCLAF always needs surgical fixation in order to achieve sufficient knee stability and adequate bone healing (Willinger et al., 2019). Although it has been considered that a fragment with a displacement of more than 5 mm is an operative indication (Zhao et al., 2006), the failure rate of conservative treatment for PCLAF is relatively high as a matter of fact. Because the tibial insertion of PCL is located outside the capsule, the surrounding soft tissue of PCLAF is easy to be embedded into the fracture, causing non-union. Therefore, in the present study, we performed the arthroscopic fixation for all the patients, including PCLAF with the partial, complete, or comminuted fragment.

A whole arthroscopic fixation of PCLAF has been firstly presented by Dr. Dinshaw Pardiwala in 2009, until now, several arthroscopic techniques have been described for fixation of PCLAF, and which have been classified into the screw-based, anchor-based, and pull-out techniques (Lamoria et al., 2020). Correspondingly, there is a wide variety of biomaterials available for arthroscopic fixation of PCLAF, for example, the absorbable interference screw (Li et al., 2016), polyether-ether-ketone (PEEK)-based suture anchor, and absorbable polymer-based suture anchor. The screw-based PCLAF fixation has a series of disadvantages, which includes a risk of epiphyseal damage and destruction of the avulsed fragment, hence, it is not suitable for the PCLAF with a small fragment (Willinger et al., 2019). Therefore, the suture-bridge fixation based on suture anchors was developed to fixate the small and multi-fragment fractures, without the need for fragment drilling (Willinger et al., 2019), and it is possible to reduce the risk of bone fragment destruction (Kanayama et al., 2022). The first article about the arthroscopic suture bridge technique for PCLAF fixation has been reported in 2016 (Nourbakhsh et al., 2016), although it has been commonly used in the field of shoulder arthroscopy for many years. The pull-out technique is a traditional arthroscopic fixation method of PCLAF, similar to the suture bridge, it is not limited to the conditions of fragments either (Willinger et al., 2019) (Nakagawa et al., 2017). Hence, we compared the efficacy and outcomes of the bio-absorbable suture anchor with the pull-out technique on treatment of PCLAF, as both the two arthroscopic techniques have a general clinical application (Willinger et al., 2019) (Nakagawa et al., 2017).

4.3 Safety, complication, and bone union

The present compared the safety, complications, and bone union of the two arthroscopic fixation methods for PCLAF with or without the bio-absorbable fixation materials. Our results showed that no complication of neurovascular injury, fever, and infection was found during the perioperative period. It suggests that both of the arthroscopic fixation methods had superior safety. It has been generally recognized that these arthroscopic methods are safer and less invasive than the posterior open approach for PCLAF fixation (Nakagawa et al., 2017), which requires a large skin incision to avoid damage to the popliteal neurovascular structures located immediately behind the site (Nakagawa et al., 2017), and has a risk of neurovascular injury (Lopez-Vidriero et al., 2010). However, the operation time of the suture bridge was much shorter than the traditional pull-

out technique (97.6 ± 13.4 vs. 142.6 ± 9.9 min), hence, the suture bridge fixation for PCLAF may have more benefits in decreasing the peri-operation complication than the traditional technique.

Our results showed that both of the arthroscopic fixation groups did not have complications of bone un-union or re-rupture during the follow-up. It indicates that the arthroscopic fixation techniques can provide enough strength for the fixation and bone union of the avulsion fragment. We performed a double-row suture bridge in the bio-absorbable anchor group, similar to our results, Kanayama et al. found that PCLAF fixation by suture bridge can firmly fix the bone fragments, and it is supposed to reduce the risk of fragment destruction (Kanayama et al., 2022), such as non-union and re-rupture. We performed a pull-out fixation with Ethibond suture in the control group, and a biomechanical study has proved that the mechanical properties of the Ethibond suture were comparable with the screw fixation on tibial eminence fractures, in terms of cyclic load, stiffness, and maximum load (Eggers et al., 2007). The present study suggests that both the bio-absorbable suture anchor and pull-out technique on fixation of PCLAF can provide a rigid fixation and sufficient strength for the reduction and bone union.

4.4 Efficacy and knee functional outcomes

The present compared the efficacy, clinical failure rate, and complications, and the functional outcomes of the bio-absorbable anchor and pull-out technique for PCLAF fixation. Our results found that although the positive rates of PDT and GT, as well as the grade of A-P laxity, KFC, and KFL, did not have a significant difference between the two groups, the total failure rate of the suture anchor group (1/17) was significantly lower than the control group (5/14) at 1 year follow-up. In our study, the patient with PDT (+)/GT (+), A-P laxity≥2 (Su et al., 2020), KFC>5 (grade 1) (Su et al., 2020), and KFL>15 (grade 3) (Su et al., 2020) were considered as the clinical failure case, as those were important indicators for assessing knee stability and ROM, and which were closely associated with the patient's functional outcomes. What's more, our study also found that the IKDC and return to sports rate in the bio-absorbable anchor group were higher than the control group. IKDC is more sensitive compared to Lysholm score while evaluating knee ligament injuries (Farshad et al., 2011), and return to sports rate is the ultimate indication for evaluating the functional outcomes. Our results indicate that arthroscopic fixation of PCLAF with the bio-absorbable suture anchor has better efficacy and functional outcomes than the pull-out suture fixation.

The bio-absorbable suture anchor has less impact on the tibial cancellous bone and blood supply, which can explain the reason why it can acquire better efficacy and functional outcomes than the pull-out suture fixation. The local blood supply may be more important in patients with PCLAF. Patients with PCLAF may have a relatively weaker bone structure in comparison with the PCL, which makes they are prone to having a PCLAF rather than a PCL rupture (Kanayama et al., 2022). The pull-out suture fixation was based on a trans-tibial tunnel, which results in a bony defect and destruction of the local blood supply for a long period post-operatively. The local blood supply is extremely important to ligament recovery, for example, the stumps are always preserved as much as possible in ACL and PCL reconstruction, in order to preserve the blood supply (Yuanliang et al., 2020). Our results have shown that the trans-tibial tunnel and bony defect can still be found on 1 year post-operative MRI in the pull-out group, and it can be adverse to the local blood supply, as well as the recovery process of PCL. Similar to our results, a follow-up study reported the efficacy of the trans-tibial pull-out fixation for PCLAF (same with ours, trans-tibial cortical suspension with suture and suture disc), they found that 2 patients (2/22) had a grade 2 laxity (5–10 mm) at 1 year post-operatively, and 3 patients had a complication of KFL who eventually ended up with 110–120 of flexion (Lamoria et al., 2020). As the suture bridge fixation technique did not need the tunnel (Willinger et al., 2019), it is supposed to acquire a better efficacy and outcomes than the traditional pull-out technique. Kanayama et al. used the suture bridge technique for PCLAF open fixation, finally, no perioperative complication was found, and all patients returned to full sporting activity (Kanayama et al., 2022). On the other hand, the bio-absorbable suture anchor consists of 70% of polylactic acid-glycolic acid copolymer (PLGA, 85% L-lactic acid, 15% glycolic acid), and 30% of β-tricalcium phosphate, which have superior *in-vivo* safety, without impact on local cancellous bone and blood supply (Koch et al., 2021). Hence, the bio-absorbable suture anchor for arthroscopic fixation of PCLAF can result in a well-recovered PCL with the least impact on the blood supply.

The biomechanical mechanism may be another potential mechanism that explains the reason why the bio-absorbable suture anchor can acquire better efficacy and outcomes. Many studies have reported that fixation strength produced by suture-bridge is greater than pull-out suture fixation. A biomechanical comparison study by Willinger et al. found that the suture-bridge technique for PCLAF fixation resulted in a significant lower elongation (4.5 ± 2.9 mm) than the transtibial pull-out technique (11.9 ± 3.1 mm) during cyclic loading, suggesting that PCLAF with suture bridge can fix the bone fragments more firmly than the traditional pull-out technique (Willinger et al., 2019). The PCL post-operative elongation is associated with poor knee stability and physical function, which may contribute to the low IKDC and return to sports rate in the suture pull-out group.

Our study had several limitations. First, it was not an RCT study, which cannot avoid the selected bias. Second, our sample size was relatively small, and the follow-up time did not reach the long-term. As the present study was a pilot study, further RCTs and longitudinal studies with more samples and longer follow-up are needed as well as to explore and determine the long-term outcome of using bio-absorbable anchors for PCLAF fixation.

5 Conclusion

Both the bio-absorbable anchor and suture pull-out technique for arthroscopic fixation of PCLAF had superior perioperative safety and a well bone union at 3 months in post-operation. However, 1 year follow-up showed that the bio-absorbable anchor group had better efficacy and functional outcomes than the traditional suture pull-out technique, suggesting the novel bio-absorbable anchor has a wide clinical application prospect on treatment of PCLAF.

Data availability statement

The original contributions presented in the study are included in the article/Supplementary Material, further inquiries can be directed to the corresponding author.

Ethics statement

The studies involving human participants were reviewed and approved by The Ethics Committee Approval of the People's Hospital of Wu Hai Inner Mongolia. The patients/participants provided their written informed consent to participate in this study. Written informed consent was obtained from the individual(s) for the publication of any potentially identifiable images or data included in this article.

Author contributions

XR wrote the manuscript. JW and SY participated in critical revision of the manuscript for intellectual content and sorted out and screened the relevant literatures. ZL and TW revised the paper, TZ and HL conducted statistical analysis on clinical data, ZZ designed the outline and revised the paper. All authors have read and approved the final version of this manuscript.

Funding

This study was supported by the Science and Technology Innovation Guidance Project of Inner Mongolia.

Acknowledgments

We thank Yansong Qi from the Sports Medicine Center, Inner Mongolia People's Hospital for his language editing, which greatly improved the manuscript.

Conflict of interest

The authors declare that the research was conducted in the absence of any commercial or financial relationships that could be construed as a potential conflict of interest.

Publisher's note

References

Domnick, C., Kösters, C., Franke, F. F., Raschke, M. J., Petersen, W., Fink, C., et al. (2016). Biomechanical properties of different fixation techniques for posterior cruciate ligament avulsion fractures. *Arthrosc. J. Arthrosc. Relat. Surg.* 32 (6), 1065–1071. doi:10.1016/j.arthro.2015.10.013

Eggers, A. K., Becker, C., Weimann, A., Herbort, M., Zantop, T., Raschke, M. J., et al. (2007). Biomechanical evaluation of different fixation methods for tibial eminence fractures. *Am. J. Sports Med.* 35 (3), 404–410. doi:10.1177/0363546506294677

Farshad, M., Gerber, C., Szucs, T., and Meyer, D. C. (2011). Determining utility values in patients with anterior cruciate ligament tears using clinical scoring systems. *BMC Health Serv. Res.* 11, 182. doi:10.1186/1472-6963-11-182

Fu, S. N., and Chan, Y. H. (2011). Translation and validation of Chinese version of international knee documentation committee subjective knee form. *Disabil. Rehabil.* 33 (13-14), 1186–1189. doi:10.3109/09638288.2010.524274

Hooper, P. O., Silko, C., Malcolm, T. L., and Farrow, L. D. (2017). Management of posterior cruciate ligament tibial avulsion injuries: A systematic review. *Am. J. Sports Med.* 46, 734–742. doi:10.1177/0363546517701911

Insall, J., Dorr, L. D., Scott, R. D., and Norman, W. (1989). Rationale of the Knee Society clinical rating system. *Clin. Orthop. Relat. Res.* 248 (248), 13–14. doi:10.1097/00003086-198911000-00004

Kanayama, T., Nakase, J., Asai, K., Yoshimizu, R., Kimura, M., and Tsuchiya, H. (2022). Suture bridge fixation for posterior cruciate ligament tibial avulsion fracture in children. *Arthrosc. Tech.* 11 (4), e609–e613. doi:10.1016/j.eats.2021.12.012

Kim, D. H., ElAttrache, N. S., Tibone, J. E., Jun, B. J., DeLaMora, S. N., Kvitne, R. S., et al. (2006). Biomechanical comparison of a single-row versus double-row suture anchor technique for rotator cuff repair. *Am. J. Sports Med.* 34 (3), 407–414. doi:10.1177/0363546505281238

Koch, L., Bockstahler, B., Tichy, A., Peham, C., and Schnabl-Feichter, E. (2021). Comparison of extracapsular stabilization techniques using an ultrasonically implanted absorbable bone anchor (weldix) after cranial cruciate ligament rupture in cats-an *in vitro* study. *Anim. (Basel)* 11 (6), 1695. doi:10.3390/ani11061695

Lamoria, R., Goyal, D., Bansal, M., Kaler, S., and Upadhyay, R. (2020). Clinical experience with arthroscopic suture pull technique in isolated PCL avulsion injuries. *J. Clin. Orthop. Trauma* 11 (3), S362–S367. doi:10.1016/j.jcot.2019.06.020

Lee, K. W., Yang, D. S., Lee, G. S., and Choy, W. S. (2015). Suture bridge fixation technique for posterior cruciate ligament avulsion fracture. *Clin. Orthop. Surg.* 7 (4), 505–508. doi:10.4055/cios.2015.7.4.505

Li, Q., Song, K., Sun, Y., Zhang, H., Chen, D., and Jiang, Q. (2016). Severe cartilage damage from a broken absorbable screw head after fixation of an avulsion fracture of the tibial attachment of the posterior cruciate ligament: A case report. *Medicine* 95 (43), e5180. doi:10.1097/md.0000000000005180

Lopez-Vidriero, E., Simon, D. A., and Johnson, D. H. (2010). Initial evaluation of posterior cruciate ligament injuries: History, physical examination, imaging studies, surgical and nonsurgical indications. *Sports Med. Arthrosc. Rev.* 18 (4), 230–237. doi:10.1097/jsa.0b013e3181fbaf38

Madi, S. S., Pandey, V., Reddy, B., and Acharya, K. (2021). Clinical and radiological outcomes following arthroscopic dual tibial tunnel double sutures knot-bump fixation technique for acute displaced posterior cruciate ligament avulsion fractures. *Arch. Bone Jt. Surg.* 9 (1), 50–57. doi:10.22038/abjs.2020.47089.2300

Nakagawa, S., Arai, Y., Hara, K., Inoue, H., Hino, M., and Kubo, T. (2017). Arthroscopic pullout fixation for a small and comminuted avulsion fracture of the posterior cruciate ligament from the tibia. *Knee Surg. Relat. Res.* 29 (4), 316–320. doi:10.5792/ksrr.16.025

Nourbakhsh, S. T., Bahramian, F., Zafarani, Z., Alidousti, A., and Aslani, H. (2016). Arthroscopic bridge technique for PCL avulsion: Surgical technique and key points. *Arch. Bone Jt. Surg.* 4 (4), 393–395.

Ranger, P., Renaud, A., Phan, P., Dahan, P., De Oliveira, E., and Delisle, J. (2011). Evaluation of reconstructive surgery using artificial ligaments in 71 acute knee dislocations. *Int. Orthop.* 35 (10), 1477–1482. doi:10.1007/s00264-010-1154-x

Rosenthal, M., Rainey, C. E., Tognoni, A., and Worms, R. (2012). Evaluation and management of posterior cruciate ligament injuries. *Phys. Ther. Sport* 13 (4), 196–208. doi:10.1016/j.ptsp.2012.03.016

Sabat, D., Jain, A., and Kumar, V. (2016). Displaced posterior cruciate ligament avulsion fractures: A retrospective comparative study between open posterior approach and arthroscopic single-tunnel suture fixation. *Arthrosc. J. Arthrosc. Relat. Surg.* 32 (1), 44–53. doi:10.1016/j.arthro.2015.06.014

Schulz, M. S., Russe, K., Weiler, A., Eichhorn, H. J., and Strobel, M. J. (2003). Epidemiology of posterior cruciate ligament injuries. *Arch. Orthop. Trauma Surg.* 123 (4), 186–191. doi:10.1007/s00402-002-0471-y

Su, M., Jia, X., Zhang, Z., Jin, Z., Li, Y., Dong, Q., et al. (2020). Medium-term (least 5 Years) comparative outcomes in anterior cruciate ligament reconstruction using 4SHG, allograft, and LARS ligament. *Clin. J. Sport Med.* Publish Ahead of Print, e101–e110. publish ahead of print. doi:10.1097/jsm.0000000000000730

Wang, W., Liu, L., Chang, X., Jia, Z. Y., Zhao, J. Z., and Xu, W. D. (2016). Cross-cultural translation of the Lysholm knee score in Chinese and its validation in patients with anterior cruciate ligament injury. *BMC Musculoskelet. Disord.* 17 (1), 436. doi:10.1186/s12891-016-1283-5

Willinger, L., Lacheta, L., Deimmling, C. V., Lang, J., Imhoff, A., and Forkel, P. (2019). Suture-bridge technique for tibial avulsion fractures of the posterior cruciate ligament - a biomechanical comparison. *Orthop. J. Sports Med.* 7 (6), 2325967119S0022. doi:10.1177/2325967119s00226

Yi, D., Baoge, L., Hui, Q., Yin, L., He, W., Si, F., et al. (2020). Can knee flexion contracture affect cervical alignment and neck tension? A prospective self-controlled pilot study. *Spine J.* 20 (2), 251–260. doi:10.1016/j.spinee.2019.09.008

Yuanliang, D., Haifeng, D., Zhihui, W., Wu, D., Shi, C., Xiao, T., et al. (2020). A case report of traumatic osteoarthritis associated with LARS artificial ligament use in anterior cruciate ligament reconstruction. *BMC Musculoskelet. Disord.* 21 (1), 745. doi:10.1186/s12891-020-03764-7

Zhang, X., Cai, G., Xu, J., and Wang, K. (2013). A minimally invasive postero-medial approach with suture anchors for isolated tibial avulsion fracture of the posterior cruciate ligament. *Knee* 20 (2), 96–99. doi:10.1016/j.knee.2012.10.016

Zhao, J., He, Y., and Wang, J. (2006). Arthroscopic treatment of acute tibial avulsion fracture of the posterior cruciate ligament with suture fixation technique through Y-shaped bone tunnels. *Arthrosc. J. Arthrosc. Relat. Surg.* 22 (2), 172–181. doi:10.1016/j.arthro.2005.10.020

frontiers | Frontiers in Bioengineering and Biotechnology

TYPE Review
PUBLISHED 21 November 2022
DOI 10.3389/fbioe.2022.1045220

OPEN ACCESS

EDITED BY
Yansong Qi,
Inner Mongolia People's Hospital, China

REVIEWED BY
Bin Wang,
Zhejiang University, China
Peng Xiu,
Sichuan University, China
Sheng Xu,
Chinese Academy of Medical Sciences and Peking Union Medical College, China

*CORRESPONDENCE
Shanshan Chen,
sschen@imr.ac.cn
Shuai Wang,
wangshuai2011@foxmail.com
Meng Niu,
13998217255@163.com

SPECIALTY SECTION
This article was submitted to Biomaterials, a section of the journal Frontiers in Bioengineering and Biotechnology

RECEIVED 15 September 2022
ACCEPTED 07 November 2022
PUBLISHED 21 November 2022

CITATION
He J, Wang Z, Zhou YX, Ni H, Sun X, Xue J, Chen S, Wang S and Niu M (2022), The application of inferior vena cava filters in orthopaedics and current research advances.
Front. Bioeng. Biotechnol. 10:1045220. doi: 10.3389/fbioe.2022.1045220

The application of inferior vena cava filters in orthopaedics and current research advances

Jingchao He[1], Zhitao Wang[1], Yue Xin Zhou[1], Hongbo Ni[2], XiaoHanu Sun[2], Jian Xue[2], Shanshan Chen[3]*, Shuai Wang[2]* and Meng Niu[2]*

[1]China Medical University, Shenyang, China, [2]The First Affiliated Hospital of China Medical University, Shenyang, Liaoning, China, [3]Institute of Metal Research, Chinese Academy of Sciences (CAS), Shenyang, Liaoning, China

Deep vein thrombosis is a common clinical peripheral vascular disease that occurs frequently in orthopaedic patients and may lead to pulmonary embolism (PE) if the thrombus is dislodged. pulmonary embolism can be prevented by placing an inferior vena cava filter (IVCF) to intercept the dislodged thrombus. Thus, IVCFs play an important role in orthopaedics. However, the occurrence of complications after inferior vena cava filter placement, particularly recurrent thromboembolism, makes it necessary to carefully assess the risk-benefit of filter placement. There is no accepted statement as to whether IVCF should be placed in orthopaedic patients. Based on the problems currently displayed in the use of IVCFs, an ideal IVCF is proposed that does not affect the vessel wall and haemodynamics and intercepts thrombi well. The biodegradable filters that currently exist come close to the description of an ideal filter that can reduce the occurrence of various complications. Currently available biodegradable IVCFs consist of various organic polymeric materials. Biodegradable metals have shown good performance in making biodegradable IVCFs. However, among the available experimental studies on degradable filters, there are no experimental studies on filters made of degradable metals. This article reviews the use of IVCFs in orthopaedics, the current status of filters and the progress of research into biodegradable vena cava filters and suggests possible future developments based on the published literature by an electronic search of PubMed and Medline databases for articles related to IVCFs searchable by October 2022 and a manual search for citations to relevant studies.

KEYWORDS

deep vein thrombosis, pulmonary embolism, orthopaedic, biodegradable inferior vena cava filter, biodegradable metal material

1 Introduction

DVT is the abnormal clotting of blood in the deep veins and is a venous return disorder. It is commonly seen in patients who are bedridden and have limited limb movement and is one of the most common peripheral vascular diseases in clinical practice.

Venous thromboembolism (VTE) includes DVT and PE. Acute PE is the most serious clinical manifestation of venous thromboembolism (Konstantinides et al., 2014). When a DVT is dislodged in the body, the embolus travels down the IVC to the right atrium and into the right ventricle, where it reaches the pulmonary artery through the blood flow, causing a serious complication: PE.

The occurrence of PE is substantially associated with untreated lower leg deep vein thrombosis. Currently it is possible to prevent PE by placing an IVCF in the inferior vena cava (IVC) to intercept the dislodged thrombus.

Although all published guidelines agree that IVCFs are indicated in patients who have an acute VTE and who cannot receive anticoagulation medications or in whom adequate anticoagulation has clearly failed despite evidence of appropriate use and effect, some indications are more controversial (Weinberg et al., 2013). There has been considerable debate about whether IVCF is recommended for implantation as a preventive measure for patients in orthopedics (Cohen-Levy et al., 2019).

Currently for orthopaedics, patients undergoing orthopaedic surgery are at increased risk of DVT and PE due to factors such as limited mobility, prolonged bed rest and the use of intraoperative tourniquets, making them a high-risk group for the development of VTE (El-Daly et al., 2013).

The management of thromboprophylaxis in patients with pelvic and acetabular fractures remains a highly controversial topic within the trauma community. Despite anticoagulation, VTE remains the most common cause of surgical morbidity and mortality in this high-risk patient group (El-Daly et al., 2013).

Following surgically treated spinal injuries, the risk of epidural haematoma is low but the consequences are extremely harmful. Although some studies have concluded that well-controlled anticoagulation is not associated with an increased risk of postoperative spinal epidural haematoma (Awad et al., 2005). However, there is still insufficient evidence on the safety of postoperative chemoprophylaxis for patients who have undergone spinal surgery. Therefore, some physicians may be reluctant to start anticoagulation therapy soon after surgery to prevent thrombosis. So some doctors may be reluctant to start anticoagulation shortly after surgery to prevent thrombosis. The impact of anticoagulation therapy on wound healing also makes orthopaedic surgeons cautious about the use of anticoagulants postoperatively (Ploumis et al., 1976). Some surgeons therefore opt for prophylactic implantation of an IVCF to prevent PE and to avoid the risks associated with anticoagulation (Rosner et al., 2004).

However, some studies have now shown that the placement of IVCFs increases the probability of DVT and the long-term benefits of inferior vena cava filters have been questioned (Hirano et al., 2021), raising questions about whether orthopaedic patients would benefit from preoperative IVCF placement.

To perform a more visual assessment of the currently available studies on the inferior vena cava filter, we have visualized and analysed the relevant documentation through vosviewer.

Supplementary Figure S1 shows that the research available on vena cava filters is divided into four main topics: the causes, prevention, and treatment of PE; methods and placement sites of IVCFs in clinical use; complications associated with IVCF implantation; and causes of thrombosis. In Supplementary Figure S2, we can see that in recent years there has been an increased interest in complications related to filter implantation and surgical management.

2 Current orthopaedic preventive measures for VTE

In the 2020 Interventional Radiology Society clinical practice guideline for the treatment of patients with venous thromboembolic disease with IVCFs, it was mentioned that given the high efficacy of modern venous thromboembolic drug prophylaxis in surgical patients, future studies should focus on whether certain patients considered to be at high risk of venous thromboembolism (e.g., patients undergoing bariatric, orthopaedic, or cancer surgery) would benefit from IVCF placement (Kaufman et al., 2020).

Patients undergoing orthopaedic procedures, such as total knee arthroplasty (TKA) or total hip arthroplasty (THA), are considered to be at very high risk for the development of venous embolism because of the many factors that contribute to venous stasis, such as the age of the patient, the position on the operating table, the use of a thigh tourniquet to provide a blood-free area during knee arthroplasty, and prolonged resting of the patient before and after surgery.

Before 1980, after a patient underwent orthopaedic surgery, the incidence of symptomatic VTE events was 15–30% in the absence of venous thrombosis prevention, and with modern surgical techniques, postoperative care and effective pharmacological prophylaxis, the rate of symptomatic DVT was estimated at 0.8% and PE at 0.35% (Falck-Ytter et al., 2012).

In one study, it was also noted that the rarity of clinical VTE observation by surgeons may be due to the subclinical nature of coagulation masked by the postoperative inflammatory healing process and the short hospital stay of only a few days in most centres. With shorter hospital stays after major joint surgery, an increasing proportion of patients will be discharged with VTE (Bjørnarå et al., 2006).

A study of medical costs for orthopaedic patients showed that patients with DVT had more than $2,000 more in medical costs compared to patients who did not have DVT (Nutescu et al., 2008).

The above statistics show that patients are at significantly higher risk of developing VTE after all types of orthopaedic surgery, that VTE accounts for a greater proportion of serious adverse outcomes in the postoperative period and that the cost of care for patients with DVT complications after orthopaedic surgery is significantly higher. Therefore, the prevention of pulmonary embolism is particularly important for orthopaedic patients, from both a life and an economic point of view.

There are currently two main types of prevention methods for VTE: post-operative walking, mechanical prophylaxis and chemical prophylaxis.

In addition to reducing the incidence of postoperative thromboembolism, early postoperative ambulation has a positive impact on the patient's recovery of gastrointestinal function (Talec et al., 2016).

The main drugs commonly used for pharmacological prophylaxis include heparin, factor Xa inhibitors, vitamin K antagonists, direct coagulation inhibitors, and antiplatelets.

Heparin achieves anticoagulation mainly by inhibiting the function of prothrombin (X, IX, XI and XII) after binding to antithrombin (Olson and Chuang, 2002). The common heparin analogues are unfractionated heparin (UFH)and low molecular weight heparin (LMWH). Compared with heparin, LMWH has a longer half-life, and produces a more predictable anticoagulant response (Weitz, 1997).

Factor Xa inhibitors inhibit the production of thrombin by selectively inhibiting factor Xa to achieve anticoagulation (Bauer et al., 2002). Representative drugs include sodium fondaparinux and rivaroxaban. A study in 2019 (Lewis et al., 2019) showed that the use of rivaroxaban was the most effective strategy for preventing deep vein thrombosis in patients undergoing elective TKA.

Vitamin K antagonists inhibit the synthesis of coagulation factors II, VII, IX and X in the liver, which are involved in vitamin K. They are not resistant to coagulation factors II, VII, IX and X that are already present in the blood. Representative drugs include warfarin. In a 2016 guideline (Witt et al., 2016) on warfarin for the treatment of venous thromboembolism, it is stated that warfarin should be started as soon as possible after diagnosis of venous thromboembolism, preferably on the same day, in combination with UFH, LMWH or sulforaphane sodium.

Direct thrombin inhibitors such as dabigatran bind to the fibrin-specific binding site of thrombin and prevent the cleavage of fibrinogen to fibrin, thus blocking the final step in the coagulation waterfall network and thrombosis. This drug is already approved for the prevention of VTE after TKA and THA (Schulman and Majeed, 2011).

Antiplatelets such as aspirin has an antiplatelet effect by inhibiting the production of thromboxane.

The use of these anticoagulants can sometimes be accompanied by some negative effects. For example, the development of heparin-induced thrombocytopenia may occur with the use of heparin (Franchini, 2005), long-term use of aspirin increases the risk of gastrointestinal bleeding (Sostres and Lanas, 2011) and gastric ulcers, and the use of various anticoagulants increases the risk of bleeding (Lewis et al., 2019).

Mechanical prevention mainly includes compression stockings (Hui et al., 1996), external mechanical equipment (Zhao et al., 2014), *etc.* Devices such as compression stockings and external mechanical devices can reduce the chance of DVT by reducing stasis in venous blood flow, but external mechanical devices should not be used in patients with lower limb trauma and compression stockings are contraindicated in patients with peripheral arterial disease and atherosclerosis. These mechanical prophylaxis methods are only external to the body and are non-invasive and do not increase the risk of bleeding compared to pharmacological prophylaxis (Falck-Ytter et al., 2012).

3 IVCF for orthopaedic management of VTE

The IVCF is an intravascular interceptor device that intercepts foreign bodies flowing through the IVC and prevents them from reaching the pulmonary artery and causing PE. However, because the function of IVCF is strictly speaking to intercept thrombus and not to prevent thrombosis, IVCF has not been included in many studies as a mechanical prophylactic device. Because of the various risk factors for VTE in orthopaedic patients, IVCF is increasingly being used in the perioperative period in orthopaedic surgery, and the risk benefit of IVCF placement in orthopaedic patients is gaining attention, and the question of whether IVCF should be placed in patients undergoing orthopaedic surgery is beginning to be investigated.

However, these studies have shown mixed results, with some suggesting that vena cava filters may be beneficial in patients undergoing orthopaedic surgery (Stein et al., 2018), and others suggesting that IVCF implantation is unnecessary in orthopaedic patients (Segon et al., 1995). Therefore, determining which patients may not benefit from prophylactic filters and limiting unnecessary placement is one of the challenges of using inferior vena cava filters for prophylactic treatment (Stein et al., 2018).

The incidence of DVT and PE after various types of orthopaedic surgery has been statistically analysed by several researchers. The types of orthopaedic surgery involved in these studies are described separately below as a basis for classification.

3.1 The role of IVCF in joint surgery

The incidence of VTE in patients undergoing joint surgery ranges from 2.9% to 3.7% and is the most common postoperative complication after joint surgery (Bjørnarå et al., 2006). The risk of VTE persists for up to 3 months after hip surgery and 1 month after total knee replacement (TKR) (Bjørnarå et al., 2006). For patients who undergo total joint replacement, the incidence of postoperative pulmonary embolism is 1.07%, 81% within the first 3 days, 89% within the first week, and 94% within 2 weeks (Parvizi et al., 2015). For those who underwent joint replacement surgery, fatal pulmonary embolism resulted in 58% of deaths (Dahl et al., 2005).

It is easy to see from the above studies the high incidence and risk of VTE after arthroplasty. Thus, in a 1996 study on the treatment of PE after TJA, the risk of treating symptomatic PE with an IVCF was evaluated and the use of an IVCF for symptomatic PE was shown to be a viable option (Bicalho et al., 1996). This was followed by a 2007 study of arthroplasty patients undergoing IVCF, which again demonstrated that IVCF is a valuable and effective method of preventing fatal thromboembolic outcomes in patients with established thromboembolism (Austin et al., 2007).

However the small number of cases in the two studies mentioned above may have been more biased. Thus, a report in 2021 reviewed 2,857 hip or knee replacements between January 2013 and December 2018. The results showed that for high-risk patients with a history of preoperative VTE the use of an IVCF was associated with a significantly lower incidence of PE and that the incidence of postoperative VTE was more than twice as high in high-risk patients as in other patients. The results demonstrate the effectiveness of prophylactic placement of IVCFs during hip/knee arthroplasty.

In a study comparing approaches to PE prevention after TJA, it was found that among patients who received warfarin, IVCF was associated with fewer complications and lower overall hospital costs compared to the use of heparin for the treatment of PE after TJA (Raphael et al., 2014).

Although there is clear evidence of the efficacy of IVCF in arthroplasty, the complications associated with filter implantation have not been followed over time in the trials described above. In one case report from 2013 (Langlois et al., 2013), it was shown that prolonged placement of the filter led to vena cava thrombosis, which in turn led to intra-articular capsule oedema and ultimately to femoral separation of the prosthesis.

The 9-year cumulative risk of IVC occlusion due to permanent filters is estimated to be 33.2% (Crochet et al., 1999). The fact that IVC occlusion is long term and progressive, even without obvious symptoms, may result in a condition that is not observed by researchers in the short term. Although the use of recyclable filters is now mostly recommended, due to the low retrieval rate of filters, unretrieved filters can remain in the body for long periods of time leading to complications and some patients still choose to have permanent filters placed for various reasons.

Although there is debate as to which is the more effective strategy for the prevention of VTE after TKA, single- or combined-measure prevention strategies (Dorr et al., 2007; Gesell et al., 2013; Lewis et al., 2019). However, the role of IVCF placement in the prevention of PE in a high-risk group with a previous history of VTE after joint surgery is well established.

3.2 The role of IVCF in fractures

The studies found on the use of IVCF in fracture patients are mainly in the area of pelvic and acetabular fractures and to a lesser extent in lower limb fractures, the following will focus on pelvic and acetabular fractures and the use of IVCF in these patients.

Patients with pelvic and acetabular fractures have a high probability of developing VTE, with estimates of the incidence of DVT following pelvic trauma ranging from 35% to 61% (Godoy Monzon et al., 2012)and the risk of PE between 2% and 10% (Montgomery et al., 1996). The prevalence of VTE is more in pelvi-acetabular trauma in comparison to hip arthroplasty. This is attributed to multiple factors including high velocity injury, disruption of pelvic vessels, immobilization for long duration and manipulation during surgical procedure (Aggarwal et al., 2020). Comprehensive data show that pulmonary embolism accounts for 10–40% of all deaths in all cases undergoing hip fracture surgery (Dahl et al., 2005).

There are conflicting findings on whether IVCF should be placed in patients with pelvic and acetabular fractures. In two reports in 2005 and 2008, IVCF was placed prophylactically in patients with pelvic and acetabular fractures with preoperative DVT findings and both showed that the filter was safe and effective in preventing PE (Karunakar et al., 2005; Toro et al., 2008).

However, in a recent 2019 study showing a significant increase in prophylactic IVCF insertion during the study period, and the failure of increased prophylactic IVCF use to reduce the incidence of PE or DVT in patients with pelvic and acetabular fractures, it was ultimately concluded that the benefit of prophylactic IVCF placement in this patient population is unclear (Cohen-Levy et al., 2019).

It then becomes a question of whether or not the placement of IVCF will cause pelvic and acetabular fractures in patients. In the guidelines for the prevention of venous thromboembolism in hospitalised patients with pelvic-acetabular trauma, published in 2020, a grading scheme has been devised to classify patients into five categories. Among these, prophylactic IVCF is not recommended for patients in Category 3: Critically ill patient presenting to emergency department (strong recommendation, moderate evidence). For Category 4: Patient with established

DVT and planned for surgery placement of IVCF is recommended (weak recommendation, very low evidence) (Aggarwal et al., 2020).

In addition to this, the evidence-based recommendations published in 2021 on the perioperative management of acetabular and pelvic fractures also mention that IVCF cannot be routinely applied prophylactically in patients with pelvic and acetabular fractures, but can be considered in preoperative high-risk groups (Yakkanti et al., 2021).

For patients with lower limb bone fractures, there are fewer relevant studies available.

A 2016 study reported a 2.2% incidence of PE after femur fracture (28/453), with 57.1% of these occurring within 24 h of injury and 89.3% within 48 h of injury (Kim et al., 2016).

In a 1973 study (Fullen et al., 1973), researchers randomly assigned patients diagnosed with traumatic fractures of the proximal femur to either have an IVC filter inserted or no filter inserted. The results showed a lower incidence of PE in patients with a filter placed compared to those without (2% vs. 20%).

In another 2016 report, a retrospective analysis of 2,763 cases of patients with lower limb fractures or pelvic fractures complicated by DVT showed that recyclable IVCF makes a safe and effective approach to prevent PE in patients with fractures complicated by DVT (Pan et al., 2016). In the 2021 report, IVCF was implanted in 964 patients with fractures complicated by DVT. the final results also concluded that the retrievable filter was effective in preventing PE in patients with fractures complicated by DVT (Huang et al., 2021).

From the available studies the placement of IVCF has a significant effect on the prevention of PE in patients with lower limb bone fractures.

3.3 The role of IVCF in spine surgery

The incidence of VTE following spine surgery is poorly defined, with reported rates from 0.3% to 31%, suggesting substantial variability in the literature (Kepler et al., 2018). A study in 2018 (Cloney et al., 2018) showed a higher incidence of VTE in patients who underwent spinal fractures compared to those who underwent other spinal procedures.

The difference in postoperative thrombosis prevention strategies for spinal surgery compared to other orthopaedic procedures is the focus on the occurrence of epidural haematomas. Although epidural haematoma is a rare complication the incidence is about 0.2%, epidural haematomas can lead to serious neurological damage (Glotzbecker et al., 1976). Therefore, thromboprophylaxis in spinal surgery requires a balance between the various approaches to thromboprophylaxis and the development of epidural haematomas. Prior to starting treatment, the clinician must consider the appropriate dose, timing and alternatives available to avoid unnecessary complications (Moorthy et al., 2020).

Although some of the current studies have shown that well-controlled anticoagulation is not associated with the risk of spinal epidural haematoma (Awad et al., 2005), some studies have shown that the use of therapeutic doses of heparin is associated with a better risk of bleeding complications (Glotzbecker et al., 1976). However, some studies have also shown that the use of therapeutic doses of heparin results in a better risk of bleeding complications in patients undergoing spinal surgery. There are not enough studies to prove the safety of postoperative chemoprophylaxis for spinal surgery. Some orthopaedic surgeons have therefore chosen to place IVCF.

In a 2005 study (Leon et al., 2005), prophylactic placement of IVCF in 74 spinal surgery patients at high risk of VTE showed that despite the high incidence of postoperative DVT in these spinal surgery patients (23/74), prophylactic placement of IVCF did protect patients from developing PE. However, there was a flaw in this study in that the experiment did not have a control group.

In a 2012 report, a retrospective study of 219 patients who underwent spinal reconstruction surgery with IVCF placement showed that prophylactic placement of IVC filters significantly reduced venous thromboembolism-related events, including PE, compared to group controls. In this study, the incidence of VTE was also found to be significantly higher in patients who received Greenfield permanent filters than in those who received retrievable filters (OR = 2.8, p = 0.008).. (McClendon et al., 1976).

In another retrospective study in 2012, in which IVCF was prophylactically placed in 12 patients at high risk of VTE from spinal surgery, a total of 10 patients were eventually retrieved, two of whom had thrombotic entrapment at the time of retrieval. No complications or PEs occurred at subsequent follow-up (Dazley et al., 2012).

In a retrospective study in 2020 on the occurrence of VTE in patients hospitalised after spinal surgery and after discharge, it was shown that IVCF placement was associated with the formation of DVT in hospitalised patients (OR 6.380 [3.414–11.924]) (Cloney et al., 2020). This phenomenon has increased the risk associated with prophylactic placement of IVCF in patients undergoing spinal surgery, making the indications for IVCF placement more limited.

There is no consensus on a postoperative protocol for venous thrombosis prophylaxis after spinal surgery (Alvarado et al., 2020). Recommendations regarding mechanical *versus* chemical prophylaxis vary greatly among institutions. However, in the results of the above-mentioned studies on thromboprophylaxis in patients undergoing spinal surgery, the benefits of prophylactic placement of IVCF in high-risk patients were all shown to be favorable.

3.4 Summary of IVCF applications in orthopaedics

Most of the current literature and guidelines suggest that primary prophylaxis with IVCF is not recommended for major surgery in patients without known venous thromboembolism (Falck-Ytter et al., 2012; Mismetti et al., 2015; Kaufman et al., 2020).

This may be due to the problems associated with the prolonged placement of IVCF, which affects the haemodynamics within the IVC and has led to a higher incidence of DVT in patients with filters than in those without filters in some studies (Cloney et al., 2020). This and the occurrence of some other complications of IVCF make the risks of filter placement for the average patient undergoing orthopaedic surgery higher relative to the benefits. So if the filter is to be made more suitable for the general public, there are two improvements.

1. Use retrievable filters as much as possible, retrieve them as soon as possible after the patient is out of the danger period, increase the retrieval rate of filters by active postoperative follow-up and minimise the time they remain in the body.
2. Improve the structure of the filter to reduce the haemodynamic impact of the filter.

In patients at high risk of VTE undergoing orthopaedic surgery, the prophylactic placement of IVCF has been shown in several studies to protect patients and effectively reduce the incidence of PE in patients undergoing all types of orthopaedic surgery.

In summary, the opinion of this article is that IVCF placement is recommended for patients at high risk of VTE who undergo orthopaedic surgery, while for non-VTE orthopaedic patients there is no conclusive data to prove that the benefits of IVCF placement outweigh the risks and it is not recommended.

4 IVCF for the prevention of complications of percutaneous vertebroplasty

The function of the IVCF is to intercept foreign bodies in the IVC, so sometimes IVCF will intercept something other than a blood clot, such as bone cement.

Polymethyl methacrylate (PMMA), commonly known as bone cement, is widely used for its biocompatibility, malleability and physical properties to anchor prostheses during joint replacement surgery (Vaishya et al., 2013) and for the treatment of compression fractures, such as percutaneous vertebroplasty (PVP) (Laratta et al., 2017). Although uncommon in procedures such as THA, leakage of PMMA into the circulation is frequently observed during and after vertebroplasty, and PMMA 'migration' is the most commonly reported complication of PVP (Yoo et al., 1976).

There are three main mechanisms that cause bone cement to migrate into the venous system: (1) inadequate bone cement polymerization at the time of injection; (2) incorrect needle position; and (3) overfilling of the vertebral body (Baumann et al., 2006). Bone cement leaking outside the vertebral body may reach the IVC along tiny veins, such as the anterior external vertebral plexus, eventually leading to serious conditions such as PE.

4.1 Case reports related to filter interception of bone cement

By searching for the role of filters in orthopaedics, we found seven interesting and rare reports of IVCFs intercepting bone cement.

In the first case of IVCF interception of bone cement in 2006 (Herbstreit et al., 1976), a DVT in the femoral vein of the iliac vein was detected during the preoperative examination and a filter was implanted prior to surgery to prevent pulmonary embolism. Post-operatively, it was found that the bone cement from the procedure migrated into the venous blood stream and was captured by the filter, but the surgeon judged that the filter could not be removed conventionally, and the patient subsequently had successful removal of the filter by open surgery.

In the 2009 case (Athreya et al., 2009), during vertebroplasty of L4, the cement leaked into the IVC through the paravertebral vein and it formed a worm-like cast, over which a filter was subsequently placed. Radiographs taken 4 h after the procedure showed that the bone cement had been captured by the filter and that the patient had no corresponding symptoms of cement embolism in the lungs. On the second day after the operation, the surgeon used a Gooseneck snare to successfully capture the embolus and withdraw it into the right common femoral vein, where it was successfully removed by surgery. The patient recovered successfully.

In a 2010 case (Agko et al., 2010), after the discovery of bone cement infiltration into the IVC, no attempt was made to remove the bone cement fragment directly to avoid further damage to the patient, but a Greenfield IVCF was placed over the fragment to prevent embolization. The fragment was subsequently found to be dislodged and captured by the IVCF at follow-up. Initially, the cement fragment was successfully captured by the trap device, but due to the shape of the fragment itself, it could not be retrieved through the sheath. The captured cement fragment was eventually moved to the level of the right common femoral vein and successful retrieval by surgical means.

In the 2015 case report (Edwards et al., 2015), the patient developed DVT during his hospital stay after the first corrective spinal repair. The surgeon placed an IVCF as a means of DVT

prophylaxis prior to the second surgery. During the injection of bone cement into the L4 vertebral body during the second procedure, it was discovered that the bone cement had entered the retroperitoneal vein and the injection was stopped. Postoperative observations revealed no complications and the patient recovered function. The filter was then removed 5 months after the operation using an endovascular approach, but the operation was very difficult to perform and took 2 h.

Following the filter retrieval procedure, a CT scan of the patient revealed bone cement in the inferior vena cava where the filter had been placed, presumably during the injection of the bone cement not only had it infiltrated into the paravertebral vein, but some of the bone cement had also reached the IVC and was captured by the filter making the retrieval of the filter unusually difficult.

In a 2013 report (Li et al., 2013), a free thrombus was found in the patient's left femoral vein on preoperative ultrasound and a filter was implanted prior to PVP to prevent PE. The physician placed a permanent filter due to the patient's history of malignancy and, referring to the 2010 report (Agko et al., 2010), concluded that the IVCF with intercepted bone cement could not be removed solely by endovascular techniques and that surgical removal would have been extremely risky for this patient and ultimately did not consider removing the IVCF. There were no filter-related complications during the follow-up period of 8 months. In this report, and for the only time to date, the entire process of cement migration into the IVC and capture in the filter was documented intraoperatively by Digital Subtraction Angiography fluoroscopy. This evidence clearly confirms the ability of the filter to trap bone cement and prevent it from migrating into the pulmonary circulation and causing serious damage (Supplementary Figure S3).

In a report from 2021 (Prater et al., 2021), The patient had a retrievable filter placed 2 years ago but not retrieved due to a previous history of DVT. The patient was recently treated with a PVP. She presented several days after her procedure with pain and redness of the skin over the access site. The doctor's examination revealed that opaque bone cement material was visible along the entire length of the tiny vein extending from the vertebral body to the adjacent inferior vena cava and was intercepted by the filter (Supplementary Figure S4). At the subsequent outpatient follow-up at approximately 2 weeks, the patient reported that the skin changes had subsided, and the patient eventually chose to forgo further intervention in favour of observation.

In the 2022 case report (Han et al., 2022), an IVCF was implanted prior to surgery to prevent PE because of isolated distal DVT in the left calf vein revealed on preoperative ultrasound. Post-operative examination revealed that the bone cement had leaked into the IVC through the paravertebral vein and had become entangled with the filter, making it impossible to remove the filter by conventional means (Supplementary Figure S5). Because of the absence of other symptoms, the patient was eventually discharged from the hospital and given close follow-up and lifelong anticoagulation after discharge for the prevention of secondary IVC and collodion filter thrombosis.

4.2 The role of filters in bone cement migration

The anatomical basis for the migration of cement into the IVC lies in the fact that the lumbar veins enter the IVC below the level of the L1-L5 vertebral body and have many connections with the basal vein and segmental veins (Iwanaga et al., 2020) (Supplementary Figure S6). This requires a more accurate understanding of the anatomy of the lumbar veins at the time of surgery in order to avoid bone cement leakage as much as possible. The migration of bone cement observed in the case was through the paravertebral vein into the IVC.

In all of the above cases (Supplementary Table S2), the filter was inserted in the IVC prior to the PVP, except in the 2009 and 2010 cases where the filter was placed specifically to intercept the bone cement after it had migrated into the IVC. What is common to all of these cases is the increased difficulty in retrieving the filter after it has intercepted the bone cement. Some doctors opt out of recycling due to the difficulty of filter recycling. The above cases suggest that in PVP routine pre-operative and post-operative imaging and aggressive intra-operative X-ray fluoroscopy may help in the early diagnosis and treatment of cement leakage.

Because IVCF interception of leaking PMMA is uncommon, there is no recognized optimal remedy, but the aforementioned study demonstrates that IVCF works effectively to intercept leaking bone cement. When a postoperative leak of bone cement into the IVC is identified, if it cannot be removed immediately, consideration may be given to placing a filter over the bone cement and waiting for the debris to dislodge from the IVC wall before finding a way to remove it. In theory, the approach published in 2010 (Agko et al., 2010) is a good alternative if the bone cement does not cling to the filter, but if the bone cement is firmly linked to the filter and the filter itself is permanent, there is no viable solution other than open surgery, as reported in 2006 (Herbstreit et al., 1976).

In 2015 (Guo et al., 2015), it was found that IVCFs had a preventive effect on hypotension and decreased oxygen saturation during the development of cement implantation syndrome in sheep, which were used as experimental subjects to study whether IVCFs could prevent or stop cement implantation syndrome. This finding demonstrates the possible role of IVCFs in high-risk patients undergoing cemented arthroplasty. However, the risk-benefit of IVCF in preventing bone cement implantation syndrome is still unclear and a decision needs to be made on a case-by-case basis at the discretion of the physician.

In 2018 (Isaak et al., 2018), an attempt was made to remove bone cement leaking into the IVC through a "fishing net" technique, which was pretested in a 3D-printed model simulating the patient's body and was ultimately successful in removing the leaking bone cement from the patient's IVC. This provides a safe and feasible solution for the removal of bone cement leaking into the IVC (Supplementary Figure S7).

In conclusion, although the interception of leaking bone cement by IVCF is a low probability practice, bone cement leakage is the most common complication of PVP, and it is theoretically unlikely that prophylactic implantation of IVCFs will be used in the future to prevent the serious consequences of bone cement leakage into the IVC because of the difficulty of recycling the filters that intercept the bone cement and the high cost of the filters themselves. However, the successful interception of bone cement by the IVCF in the above case may provide an idea for the prevention of serious consequences of bone cement leaks into the IVC in the future. Is it possible to design a device that is simpler and cheaper, that only needs to have an interception function for a few hours and does not need to be stable in the body for a long time, and that can be recycled together with the leaking bone cement?

5 Current status of IVCFs

Initially, IVCFs were mainly made of stainless steel, but due to their mechanical strength, biocompatibility, thermal shape memorability and unsuitability for nuclear magnetic examination, most IVCFs used in clinical practice are now made of nickel-titanium alloy, which is widely used due to its good shape memory effect, superelasticity, corrosion resistance and biocompatibility (Prince et al., 1988). Inferior vena cava filters come in a variety of structures that differ in their capacity to prevent thromboembolism, their effect on haemodynamics, their capacity to maintain stability in the vasculature, and their imaging profile. The inferior vena cava filter is compressed into a delivery sheath at the time of fabrication and can be placed from the femoral, internal jugular, subclavian or anterior elbow veins, releasing the filter upon arrival at the designated location, which is usually the IVC below the lower edge of the renal vein opening (Caplin et al., 2011). The implantation of the filter intercepts the thrombus and effectively reduces the incidence of pulmonary embolism.

5.1 Classification of IVCFs

There is a wide range of inferior vena cava filters available, which vary in shape, material and design, and these characteristics have a direct impact on their use in clinical practice. Due to the many characteristics of filters, there are various ways of classifying them, but below, we classify them according to whether they can be recycled after being placed in the clinic and how they can be recycled. These classifications are permanent filters, recyclable filters and temporary filters.

Permanent filters were first employed in clinical practice, and they cannot be removed until the vena cava is surgically incised, and therefore, they remain in the IVC for a long time as a foreign body. A series of linked issues (filter tilt, displacement, fracture, *etc.*) have occurred as a result of its long-term installation in the body. Some patients who require long-term filter implantation but do not have the necessary health conditions for a filter retrieval surgery will still use this type of filter, but this filter is currently less commonly used clinically. Representative products of this type of filter are the Mobin-Uddin umbrella filter (Dupont, 1976), Greenfield filter (Kanter and Moser, 1988), Bird's Nest filter (Roehm, 1984), Vena Tech LGM filter (Crochet et al., 1993), Vena Tech LP filter (Ahmed et al., 2016), Simon nitinol filter (Poletti et al., 1998) and TrapEase filter (Liu et al., 2005).

The temporary filter is designed for short-term implantation and is released in the body with a rod at the closing end leading to the body surface, at the end of which an anti-dislodgement protection device is attached to prevent dislodgement and placement under the skin. The temporary filter has a connecting rod at the end that extends to the surface of the body to keep it stable in the body. There is therefore no barb fixation on the filter arm. Therefore, there is very little endothelial dilation of the vessel wall by the temporary filter, the filter is safer during recycling, the retrieval rate of the filter is high and no special instrumentation is required for recycling. Representative products of this type of filter are Tempofilter (Bovyn et al., 1997) and Angel Catheter (Tapson et al., 2017).

Retrievable filters usually have a fixed barb in contact with the vessel to maintain the normal position of the filter in the body and a retrieval hook at the retrieval end, which can be removed from the vena cava by a catheter technique, reducing the risk of infection without the need for an external device. It is the most widely used IVCF because it does not need to be removed within a specific period of time and can be retained for a long time if needed. Representative products of this type of filter are the Günther Tulip filter (Hoppe et al., 2006), Denali vena cava filter (Hahn, 2015), OptEase filter (Kalva et al., 2011) Celect filter (De Oliveira Leite et al., 2020), ALN filter (Pellerin et al., 2008) and Crux Vena Cava Filter (Murphy et al., 2009).

5.2 Recycling of IVCFs

The removal of retrievable filters requires a new percutaneous puncture and retrieval using a retrieval device. This step is technically demanding, and the filter will be more difficult to remove when it is tilted and in contact with the wall. Endothelial coverage is also one of the factors affecting the retrieval success rate of retrievable filters. Endothelial fixation

of the IVCF frame in contact with the vessel wall is usually completed 2 weeks after filter insertion, which maintains the stability of the filter in the body but increases the difficulty of retrieving it and the probability of retrieval complications.

When endothelialization is too high, forcing removal can break the vessel, and it can only be kept in the body as a permanent sort of filter. With longer filter retention times, the likelihood of filter-related complications, such as filter tilt, IVC perforation, filter fracture, filter displacement, inferior vena cava thrombotic obstruction, and recurrent DVT or PE, also increases.

There have been many statistical reports on vena cava filter retrieval rates in recent years (Marquess et al., 2008; Minocha et al., 2010; Iliescu and Haskal, 2012; Kalina et al., 2012; Al-Hakim et al., 2014; Sutphin et al., 2015; Inagaki et al., 2016), but most studies have had small sample sizes and extremely variable filter retrieval rates (8%–95%), which may be due to small sample sizes, differences in physician skill levels, and the adequacy of hospital return systems. Nonetheless, it is clear from these studies that IVCF retrieval rates can be significantly improved through more aggressive post-operative visits and the use of more advanced filter retrieval techniques.

5.3 Common complications after filter implantation

There are several complications associated with filter implantation, such as filter tilt, filter displacement, inferior vena cava perforation, filter fracture, recurrent thromboembolism, and incomplete expansion of the filter. Of these, filter tilt seems to have the least impact, but the occurrence of filter tilt greatly increases the likelihood of other complications or is a precomplication of other complications (except for incomplete filter expansion).

5.3.1 Filter tilt

Filter tilt is diagnosed when the angle between the central axis of the filter and the longitudinal axis of the IVC exceeds 15°. According to a review of the literature (Singer and Wang, 2011), the tilt of the filter was greater than 5° in approximately 33% of instances, and severe tilt (>15°–20°) occurred in approximately 3%–9% of cases. When the filter is excessively tilted (>15°), the efficacy of thrombus filtration is lowered, and *in vitro* investigations have shown that slanted filters have a lower filtration capacity for smaller thrombi (Günther et al., 2005). Furthermore, when the tilt of the filter is increased, the thrombus trapped at the filter tip promotes the production of *in situ* thrombi in the vena cava wall (Singer and Wang, 2011). (Supplementary Figure S8).

5.3.2 Filter displacement

Filter displacement is described as the filter being more than 10 mm away from the intended point, which is a dangerous complication. When the filter is placed too close to the renal vein, the risk of renal vein embolism or possibly renal failure increases (Janvier et al., 2010). Filter migration to the heart and lungs, which can lead to serious consequences, has also been reported in the past (Gelbfish and Ascer, 1991; Stösslein and Altmann, 1998). Incorrect size selection at the time of placement is one of the reasons for filter migration. (Supplementary Figure S9).

5.3.3 Inferior vena cava perforation

Vena cava perforation is defined when the filter penetrates the vena cava into structures surrounding the IVC wall, such as the aorta, psoas major, duodenum, and kidney. By more than 3 mm (Supplementary Figure S10). IVC perforation is linked to the filter's longer retention and tilting, with the angle between the barbs on the strainer arm and the vessel wall becoming sharper as the angle between the hook and the vessel wall grows, which could raise the chance of perforation.

5.3.4 Filter fracture

Filter fracture refers to the loss of structural integrity caused by filter shattering (Supplementary Figure S11).

Filter fracture, according to Xin Li et al. (Li et al., 2020), is caused by the IVC's rhythmic expansion and contraction during the cardiac cycle, subjecting the IVC filter to repetitive mechanical pressure. This mechanical stress eventually leads to wear and subsequent fracture of the cartridge joints. The fragments move with the circulatory system and may damage vital organs.

5.3.5 Recurrent thromboembolism

Most of the current research on the causes of recurrent thromboembolism suggests that it is due to the adverse haemodynamic effects of the filter on the body after the interception of the thrombus by the IVCF, which slows the blood flow and increases the probability of thrombosis. Computational models suggest that filters may lead to stagnation and turbulence in downstream blood flow after thrombus capture, with a significant increase in the probability of thrombosis (Leask et al., 2004) (Supplementary Figure S12).

5.3.6 Incomplete filter expansion

Incomplete deployment of the filter is usually caused by the structure of the filter itself or by the practitioner's operational error (Supplementary Figure S13). Early filters, such as Greenfield, were used in a small clinical study in which a large gap was found between poorly distributed filter legs in 17 of the 24 filters placed (Sweeney and Van Aman, 1993). When the filter is not fully deployed, it not only has a reduced ability to intercept the thrombus but also has a reduced radial support, which can result in filter displacement or even IVC perforation (Shimoo and Koide, 2020). This problem has been significantly reduced with improvements in filter construction design and

materials, with recent studies showing a low rate of incomplete opening in the range of 0.4–0.5% (Li et al., 2020).

6 Ideal IVCF

The various vena cava filters currently available are effective in intercepting blood clots to prevent pulmonary embolism, but complications can still occur after implantation. That is why the search for the ideal filter is ongoing. Depending on the role the filter should play and the needs in use, the ideal IVCF should have the following characteristics:

1. High filtering capacity for blood clots in PE prevention
2. Excellent biocompatibility with minimal haemodynamic effects for prevention of recurrent thromboembolism
3. Nonprocoagulant and nonelectrolytic corrosion capability
4. Strong radial support to prevent tilting and shifting
5. Excellent elasticity and compression qualities, allowing recovery of proper dimensions after release in the IVC
6. High mechanical stability, reducing the possibility of filter breakage
7. Ability to decrease vena cava endothelial damage and the occurrence of vena cava perforation
8. Insensitivity to thrombolytic drugs, such as urokinase heparin
9. Nonmagnetic materials that do not interfere with examinations such as MRI
10. Clear visualization under imaging release localization and postoperative review

7 Biodegradable IVCF

In recent years, IVCF has been used on a large scale in clinical practice to prevent PE, but there has been a growing interest in the series of problems associated with complications of filter implantation while preventing PE. Data from an article published by the British Society of Interventional Radiology in 2013 showed that 73% of patients with an IVCF implanted had a retrievable IVCF, with 78% of these patients undergoing an attempt to retrieve the filter and 83% experiencing successful removal, with a significantly lower retrieval rate for filters implanted >9 weeks (Uberoi et al., 2013). As the retention time of the filter in the body increases, the probability of complications during filter retrieval also increases (Grewal et al., 2016). For elderly patients and those with coexisting conditions, the filter retrieval rate is significantly lower (Geisbüsch et al., 2012). It can also be complicated by filter breakage and IVC injuries, such as bleeding and entrapment during filter retrieval (Grewal et al., 2016). Biodegradable IVCFs degrade spontaneously in the body, avoiding complications during retrieval and in long-term filter retention.

Biodegradable IVCFs are IVCFs made from biodegradable materials, also known as bioresorbable IVCFs. They can gradually degrade in the body according to a predetermined pattern after passing through the PE risk period, eliminating the need for secondary surgery for removal, reducing the physical burden of patients, and compensating for the occurrence of a series of complications (tilt, displacement, fracture, perforation, and so on) caused by existing filters that cannot be retrieved.

Biodegradable materials are frequently employed in medical sutures, drug release carriers, tissue engineering, and other sectors, such as orthopaedics, maxillofacial surgery, cardiovascular surgery, and plastic surgery (Spitalny, 2006). Yin et al. (2022) used 3D printing technology to investigate the phased degradation of poly-l-actide (PLLA) vascular scaffolds in mice, as well as the alteration of vascular endothelial cells during scaffold degradation, to elucidate the long-term effects of poly-l-actide vascular scaffolds (PLSs) on vascular repair and to demonstrate the potential of PLSs in promoting endothelial function and positive remodelling. Currently, LP Medical's NeoVas stent (Han et al., 2018) has received State Drug Administration permission for marketing and is believed to have ushered in a new era of coronary intervention. In the field of biliary stents, several types of biliary biodegradable stents have been developed, and some are already in clinical use (Song et al., 2022).

The above examples indicate the excellent potential of biodegradable materials in the medical field, which is progressively becoming a reality.

However, no therapeutic biodegradable IVCFs are currently available. Because of its potential for great performance, the biodegradable vena cava filter has been a prominent focus of research in China and internationally.

7.1 Classification of biodegradable IVCFs

According to a review of the literature on biodegradable IVCFs, there are two types of biodegradable filters explored by researchers: completely biodegradable filters and partially biodegradable filters. Completely degradable filters are made of degradable materials and can be completely degraded after reaching an expected time point; partially degradable filters are usually made of a combination of degradable filters and nondegradable metal stents, and the filter is completely degraded after reaching an expected time point, while the remaining part becomes a stent to support the inferior vena cava; partially degradable filters are also called autodeformable IVCFs or convertible IVCFs.

7.1.1 Partially biodegradable filter

Thors, Gao and Novate Medical Ltd. All use metal and biodegradable materials to create partially biodegradable filters. The common feature of these filters is that when the

filter is first implanted, the filter itself remains intact using a filter mesh to intercept the thrombus, but as the biodegradable material degrades in the body, the filter transforms, and the mesh structure disappears into a vascular stent in the inferior vena cava.

Thors and Muck (2011), Gao et al. (2011) have progressed to the animal stage but have had problems with severe endothelial hyperplasia and filter displacement, respectively, and both have yet to clarify the process of degradation of material fragments, their destination, and their effect on the organism.

The Sentry Bioconvertible Inferior Vena Cava Filter from Novate Medical Ltd. Was tested in animal trials in May 2018 (Gaines et al., 2018), and its performance was validated against the OptEase filter. In a 1-year analysis of the prospective multicentre SENTRY clinical trial published in August 2018 (Dake et al., 2018), it was shown that by month 12 post-implantation, morphological conversion was completed in 96.4% (106/110) of the filters, and no symptomatic pulmonary embolism was demonstrated at 12 months. In the November 2019 article (Dake et al., 2018), it was shown that 96.5% (82/85) of filters successfully converted morphologically at 24 months in the second year of follow-up, and there was no evidence of late inferior vena cava obstruction or thrombosis following filter conversion at 24 months of follow-up, nor was there evidence of a correlation between filter morphology conversion and thrombosis. In 2020 (Dake et al., 2020), the Sentry Bioconvertible Inferior Vena Cava Filter was clinically implanted in an 85-year-old female patient who did not experience any adverse events within 3 weeks of implantation, and no subsequent adverse events were reported in this patient, making the Sentry filter the first bioconvertible filter to be approved (Supplementary Figure S14).

After the filter cone has entirely dissolved, the semidegradable filter takes on the appearance of a vascular stent. Although not completely degraded *in vivo*, the remaining stent structure has minimal haemodynamic impact and reduces the incidence of recurrent thromboembolism. It also lowers the risk of recurrent thromboembolism, and the undegraded component can be used as a vascular stent to maintain vascular morphology, avoiding subsequent surgery and lowering the risk of problems associated with filter implantation.

7.1.2 Fully biodegradable filter

Zhang, Yang and Eggers have each produced fully biodegradable filters using various biodegradable materials, which are characterized by the fact that the filters degrade in the body over a predicted period of time, ultimately leaving no residual material in the body.

Zhang's study (Zhang et al., 2017) has progressed to the animal testing phase, with *in vivo* experiments in beagles. The results showed that all filters were mildly displaced, in one case to the right atrium, and that there was an inflammatory reaction in all inferior vena cava (Supplementary Figure S15).

Yang's study (Yang et al., 2019), which only progressed as far as *in vitro* simulations, confirmed that the filter degraded progressively more rapidly in the cone than in the stent and that the average *in vitro* thrombus capture efficiency of 90% was comparable to that of a conventional descending vein filter. This finding demonstrates the clinical potential of this filter, but the efficacy of this filter *in vivo* is not yet known, as animal studies have not yet been performed, and further studies are needed to investigate the degradation *in vivo*.

Eggers screened Poly (p-dioxanone) (PPDO) as a candidate material for a degradable descending interface filter in 2012 (Eggers and Reitman, 2012). The thrombus interception ability of the filter was initially validated in pigs in 2015 (Eggers et al., 2015) and further validated by *in vitro* simulations in 2016 (Dria and Eggers, 2016). The results suggest that the absorbable filters are likely to be comparable in efficacy to Greenfield filters. In 2017 (Huang et al., 2017), the safety of the absorbable inferior vena cava filter was again demonstrated in pigs, and in 2019 (Eggers et al., 2019), the filter was compared with the Cook Celect inferior vena cava filter, which demonstrated a good safety profile, particularly with regard to vena cava perforation, as all control metal filters showed perforation. For the first time in 2020 (Elizondo et al., 2020), biodegradable vena cava filters made of PPDO were placed prospectively in eight patients at high risk of lower limb deep vein thrombosis. In this trial, all filters were successfully implanted and intercepted the thrombus with a success rate of 100%, and no pulmonary embolism or filter-related complications occurred.

The above summary shows that the current research on fully degradable filters is based on the use of organic polymers for production, and the production process is mostly based on the use of weaving methods. However, research progress has varied from *in vitro* validation in a simulated environment to animal testing, with Eggers' research being the most advanced and rapid to date, having progressed to the stage of prospective implantation of filters in humans.

The most serious problem that has arisen thus far in these experiments is the inadequate mechanical properties of some of the filters to maintain radial support in the body, which has led to the displacement of the filters in several experiments. This issue will have a direct impact on the safety of the filter, causing a major safety hazard, and is the largest obstacle on the current path of research into fully degradable filters.

The reason for this phenomenon may be, on the one hand, that the filter itself does not have sufficient mechanical properties to maintain sufficient radial support in the IVC or, on the other hand, that the actual size of the filter is less than the theoretical value due to compression by the compression sheath, and it does not return to its proper size when it is released in the IVC. Consideration can be given to increasing the radial support force

directly by changing the structure of the filter so that the filter is fixed in position in the IVC, by directly increasing the mechanical properties of the filter itself by changing the material from which the filter is made, or by increasing the memory and elasticity of the filter so that the filter can return to its proper size after release.

In addition, the use of biodegradable polymers has the unavoidable problem of significantly reducing their ability to develop under radiation compared to metal filters. To solve this problem, the use of biodegradable metallic materials can be considered, or the composition of the material can be changed to increase the developing power of biodegradable polymers.

7.2 Increase the imaging capability

There have been numerous attempts by scholars to address the abovementioned situation where fully degradable materials do not develop well under X-ray through various methods. The development of organic polymer compounds with enhanced imaging capabilities may further expand the use of biodegradable scaffolds in tissue engineering. The main methods currently available are the blending of 2,3,5-triiodobenzoic acid (TIBA) (Singhana et al., 2015; Zhao et al., 2020), gold nanoparticles (AuNPs) (Tian et al., 2017; Tian et al., 2018; Huang et al., 2020) or bismuth nanoparticles (BiNPs) (Perez et al., 2021; Damasco et al., 2022) into PPDO to increase its imaging capacity.

Completely biodegradable IVCFs degrade completely after functioning and have less impact on the human body than partially biodegradable filters because they leave no residual material in the body and have a lower probability of related complications, but at the same time, they place higher demands on the overall degradation time, degradation rate, control of the degradation method and the manufacturing process.

The available studies on biodegradable filters have shown good thrombus interception and good thrombus capture in vitro and animal studies. However, displacement of the filters, which was reported in several papers (Gao et al., 2011; Zhang et al., 2017), is noteworthy and may be due to the inferior nature of the organic polymer materials used in these filters in terms of mechanical strength, radial support and the degree of recovery from deformation after release compared to metallic materials. Most of the above studies have not studied the specific degradation time, degradation process, and degradation products and their destination and effects on the body, and the formation process, size, destination and effects of the degradation products may become a constraint to the biodegradable filter in the clinic.

7.3 Biodegradable metal material

The most common materials for making biodegradable vena cava filters are organic polymers, such as polycaprolactone, PLLA, and PPDO. When compared to metallic materials, the radial force and mechanical strength of these organic polymer compounds, as well as their ability to recover from deformation after release, are weak; most of them cannot be fully expanded by the balloon and require additional energy, which is potentially dangerous for the vessel wall. Currently, biodegradable metals have demonstrated good performance in the health care field, with a variety of cardiovascular stents made from biodegradable metals emerging, demonstrating the good biocompatibility of biodegradable metals in vasculature (Bowen et al., 2016; Debieux et al., 2016; Shreenivas and Kereiakes, 2018), and biodegradable metals show significant promise in the direction of making biodegradable vena cava filters. Over the last few decades, biodegradable metals (BMs) as temporary implants have generated much scholarly interest in research.

BMs are metals expected to corrode gradually *in vivo*, with an appropriate host response elicited by the released corrosion products, which can pass through or be metabolized or assimilated by cells and/or tissue and then dissolve completely upon fulfilling the mission to assist with tissue healing with no implant residues (Liu et al., 2019). This is also known as an absorbable metal material.

In contrast to conventional metallic biomaterials, BMs consist mainly of essential metallic elements that are present in trace amounts in the human body. To date, there are three main BM systems that have been extensively studied, namely, Mg-based BM, Fe-based BM and Zn-based BM. For decades, Mg-based and Fe-based metals and zinc alloys have been a popular topic of research in the field of BMs (Yuan et al., 2022).

Although Fe-based BMs have excellent biocompatibility, corrosion resistance and mechanical properties, Fe-based alloys undergo degradation *in vivo* rather slowly without systemic iron toxicity, so implants can persist *in vivo* for a long time (Kraus et al., 2014). However, the corrosion products of Fe are stable in the organism and accumulate over time in the body, compromising the integrity of the vessel wall and causing damage to it, making this metal unavailable for the fabrication of absorbable implants that require a large volume or cross-sectional thickness (Peuster et al., 2006; Zhang et al., 2010; Pierson et al., 2012).

Existing BM research on zinc-based alloys, magnesium-based alloys, and zinc-magnesium alloys has revealed potentially outstanding qualities as material choices for biodegradable vena cava filters.

8 Summary

This article reviews the use of IVCFs in orthopaedics, the current status of filters and the progress of research into biodegradable vena cava filters and suggests possible future developments based on the published literature. With the

long-term use of IVCFs, the associated difficulties are receiving increasing attention, and IVCF perfection is increasingly desired. Although there are still certain issues with current biodegradable filters, their ability to gradually dissolve and absorb in the body without the need for further surgery, as well as their ability to reduce the occurrence of numerous complications, will continue to be of concern to people. It is believed that with further development and perfection of the biodegradable filter through improvements in the manufacturing process and design concept, it will eventually be suitable for clinical use and may even be further developed into a drug-eluting biodegradable IVCF in the future, which will have increasingly broad application prospects.

Author contributions

MN, SC, and SW developed the idea for the review, JH, ZW, XZ, SX, JX, and HN designed the review, collecting the literature, performed the review, analyzed data, and wrote the paper. All authors discussed the results and revised the manuscript.

Conflict of interest

The authors declare that the research was conducted in the absence of any commercial or financial relationships that could be construed as a potential conflict of interest.

Publisher's note

All claims expressed in this article are solely those of the authors and do not necessarily represent those of their affiliated organizations, or those of the publisher, the editors and the reviewers. Any product that may be evaluated in this article, or claim that may be made by its manufacturer, is not guaranteed or endorsed by the publisher.

Supplementary material

The Supplementary Material for this article can be found online at: https://www.frontiersin.org/articles/10.3389/fbioe.2022.1045220/full#supplementary-material

References

Aggarwal, S., Patel, S., Vashisht, S., Kumar, V., Sehgal, I. S., Chauhan, R., et al. (2020). Guidelines for the prevention of venous thromboembolism in hospitalized patients with pelvi-acetabular trauma. *J. Clin. Orthop. Trauma* 11, 1002–1008. doi:10.1016/j.jcot.2020.09.011

Agko, M., Nazzal, M., Jamil, T., Castillo-Sang, M., Clark, P., and Kasper, G. (2010). Prevention of cardiopulmonary embolization of polymethylmethacrylate c ement fragment after kyphoplasty with insertion of inferior vena cava filter. *J. Vasc. Surg.* 51, 210–213. doi:10.1016/j.jvs.2009.07.110

Ahmed, O., Madassery, S., Heussner, D., Tran, P., Masrani, A., Arslan, B., et al. (2016). VenaTech LP filter retrieval for filter-related thrombosis or malpositioning. *J. Vasc. Interv. Radiol.* 27, 1724–1726. doi:10.1016/j.jvir.2016.06.006

Al-Hakim, R., Kee, S. T., Olinger, K., Lee, E. W., Moriarty, J. M., and McWilliams, J. P. (2014). Inferior vena cava filter retrieval: Effectiveness and complications o f routine and advanced techniques. *J. Vasc. Interv. Radiol.* 25, 933–939. doi:10.1016/j.jvir.2014.01.019

Alvarado, A. M., Porto, G. B. F., Wessell, J., Buchholz, A. L., and Arnold, P. M. (2020). Venous thromboprophylaxis in spine surgery. *Glob. Spine J.* 10, 65s–70s. doi:10.1177/2192568219858307

Athreya, S., Mathias, N., Rogers, P., and Edwards, R. (2009). Retrieval of cement embolus from inferior vena cava after percutaneous vertebroplasty. *Cardiovasc. Interv. Radiol.* 32, 817–819. doi:10.1007/s00270-009-9550-6

Austin, M. S., Parvizi, J., Grossman, S., Restrepo, C., Klein, G. R., and Rothman, R. H. (2007). The inferior vena cava filter is effective in preventing fatal pulmonary embolus after hip and knee arthroplasties. *J. Arthroplasty* 22, 343–348. doi:10.1016/j.arth.2006.10.008

Awad, J. N., Kebaish, K. M., Donigan, J., Cohen, D. B., and Kostuik, J. P. (2005). Analysis of the risk factors for the development of post-operative spinal epidural haematoma. *J. Bone Jt. Surg. Br. volume* 87, 1248–1252. doi:10.1302/0301-620x.87b9.16518

Bauer, K. A., Hawkins, D. W., Peters, P. C., Petitou, M., Herbert, J. M., Boeckel, C. A. A., et al. (2002). Fondaparinux, a synthetic pentasaccharide: The first in a new class of antithrombotic agents - the selective factor Xa inhibitors. *Cardiovasc. Drug Rev.* 20, 37–52. doi:10.1111/j.1527-3466.2002.tb00081.x

Baumann, A., Tauss, J., Baumann, G., Tomka, M., Hessinger, M., and Tiesenhausen, K. (2006). Cement embolization into the vena cava and pulmonal arteries after ver tebroplasty: Interdisciplinary management. *Eur. J. Vasc. Endovasc. Surg.* 31, 558–561. doi:10.1016/j.ejvs.2005.11.008

Bicalho, P. S., Hozack, W. J., Rothman, R. H., and Eng, K. (1996). Treatment of early symptomatic pulmonary embolism after total joint arthroplasty. *J. Arthroplasty* 11, 522–524. doi:10.1016/s0883-5403(96)80103-3

Bjørnarå, B. T., Gudmundsen, T. E., and Dahl, O. E. (2006). Frequency and timing of clinical venous thromboembolism after major jo int surgery. *J. Bone Jt. Surg. Br. volume* 88, 386–391. doi:10.1302/0301-620X.88B3.17207

Bovyn, G., Gory, P., Reynaud, P., and Ricco, J. B. (1997). The tempofilter: A multicenter study of a new temporary caval filter implantable for up to six weeks. *Ann. Vasc. Surg.* 11, 520–528. doi:10.1007/s100169900084

Bowen, P. K., Shearier, E. R., Zhao, S., Guillory, R. J., Zhao, F., Goldman, J., et al. (2016). Biodegradable metals for cardiovascular stents: From clinical concerns to recent Zn-alloys. *Adv. Healthc. Mat.* 5, 1121–1140. doi:10.1002/adhm.201501019

Caplin, D. M., Nikolic, B., Kalva, S. P., Ganguli, S., Saad, W. E., and Zuckerman, D. A. (2011). Quality improvement guidelines for the performance of inferior vena ca va filter placement for the prevention of pulmonary embolism. *J. Vasc. Interv. Radiol.* 22, 1499–1506. doi:10.1016/j.jvir.2011.07.012

Cloney, M. B., Yamaguchi, J. T., Dhillon, E. S., Hopkins, B., Smith, Z. A., Koski, T. R., et al. (2018). Venous thromboembolism events following spinal fractures: A single center experience. *Clin. Neurol. Neurosurg.* 174, 7–12. doi:10.1016/j.clineuro.2018.08.030

Cloney, M. B., Driscoll, C. B., Yamaguchi, J. T., Hopkins, B., and Dahdaleh, N. S. (2020). Comparison of inpatient versus post-discharge venous thromboembolic events after spinal surgery: A single institution series of 6869 consecutive patients. *Clin. Neurol. Neurosurg.* 196, 105982. doi:10.1016/j.clineuro.2020.105982

Cohen-Levy, W. B., Liu, J., Sen, M., Teperman, S. H., and Stone, M. E., Jr. (2019). Prophylactic inferior vena cava filters for operative pelvic fractures: A twelve year experience. *Int. Orthop.* 43, 2831–2838. doi:10.1007/s00264-019-04384-0

Crochet, D. P., Stora, O., Ferry, D., Grossetete, R., Leurent, B., Brunel, P., et al. (1993). Vena tech-LGM filter: Long-term results of a prospective study. *Radiology* 188, 857–860. doi:10.1148/radiology.188.3.8351362

Crochet, D. P., Brunel, P., Trogrlic, S., Grossetete, R., Auget, J. L., and Dary, C. (1999). Long-term follow-up of vena tech-LGM filter: Predictors and frequency of caval occlusion. *J. Vasc. Interv. Radiol.* 10, 137–142. doi:10.1016/s1051-0443(99)70455-0

Dahl, O. E., Colwell, C., Frostick, S., Haas, S., Hull, R., Laporte, S., et al. (2005). Fatal vascular outcomes following major orthopedic surgery. *Thromb. Haemost.* 93, 860–866. doi:10.1160/TH04-11-0769

Dake, M. D., Murphy, T. P., Kramer, A. H., Darcy, M. D., Sewall, L. E., Curi, M. A., et al. (2018). One-year analysis of the prospective multicenter SENTRY clinical trial: Safety and effectiveness of the novate Sentry bioconvertible inferior vena cava filter. *J. Vasc. Interv. Radiol.* 29, 1350–1361. doi:10.1016/j.jvir.2018.05.009

Dake, M. D., Murphy, T. P., Kramer, A. H., Darcy, M. D., Sewall, L. E., Curi, M. A., et al. (2020). Final two-year outcomes for the Sentry bioconvertible inferior vena cava filter in patients requiring temporary protection from pulmonary embolism. *J. Vasc. Interv. Radiol.* 31, 221–230. doi:10.1016/j.jvir.2019.08.036

Damasco, J. A., Huang, S. Y., Perez, J. V. D., Manongdo, J. A. T., Dixon, K. A., Williams, M. L., et al. (2022). Bismuth nanoparticle and polyhydroxybutyrate coatings enhance the radiopacity of absorbable inferior vena cava filters for fluoroscopy-guided placement and longitudinal computed tomography monitoring in pigs. *ACS Biomater. Sci. Eng.* 8, 1676–1685. doi:10.1021/acsbiomaterials.1c01449

Dazley, J. M., Wain, R., Vellinga, R. M., Cohen, B., and Agulnick, M. A. (2012). Prophylactic inferior vena cava filters prevent pulmonary embolisms in high-risk patients undergoing major spinal surgery. *J. Spinal Disord. Tech.* 25, 190–195. doi:10.1097/BSD.0b013e31821532bd

De Oliveira Leite, T. F., Silva, T. O. E., Pereira, O. I., and Carnevale, F. C. (2020). Retrievable celect™ filter placement in the superior vena cava: A case report. *Int. J. Surg. Case Rep.* 73, 105–108. doi:10.1016/j.ijscr.2020.06.100

Debieux, P., Franciozi, C. E., Lenza, M., Tamaoki, M. J., Magnussen, R. A., Faloppa, F., et al. (2016). Bioabsorbable versus metallic interference screws for graft fixation in anterior cruciate ligament reconstruction. *Cochrane Database Syst. Rev.* 7, Cd009772. doi:10.1002/14651858.CD009772.pub2

Dorr, L. D., Gendelman, V., Maheshwari, A. V., Boutary, M., Wan, Z., and Long, W. T. (2007). Multimodal thromboprophylaxis for total hip and knee arthroplasty based on risk assessment. *J. Bone Jt. Surgery-American Volume* 89, 2648–2657. doi:10.2106/jbjs.F.00235

Dria, S. J., and Eggers, M. D. (2016). *In vitro* evaluation of clot capture efficiency of an absorbable vena cava filter. *J. Vasc. Surg. Venous Lymphatic Disord.* 4, 472–478. doi:10.1016/j.jvsv.2016.05.006

Dupont, P. A. (1976). The Mobin-Uddin umbrella filter in the management of proven and threatened pulmonary embolism. *Ann. R. Coll. Surg. Engl.* 58, 318–321.

Edwards, C., 2nd, Blight, A., Kim, K., and Edwards, C. (2015). Polymethylmethacrylate entrapped in inferior vena cava filter after a scheuermann kyphosis revision surgery. *Spine Deform.* 3, 604–607. doi:10.1016/j.jspd.2015.03.004

Eggers, M. D., and Reitman, C. A. (2012). *In vitro* analysis of polymer candidates for the development of absorbable vascular filters. *J. Vasc. Interv. Radiol.* 23, 1023–1030. doi:10.1016/j.jvir.2012.05.039

Eggers, M. D., McArthur, M. J., Figueira, T. A., Abdelsalam, M. E., Dixon, K. P., Pageon, L. R., et al. (2015). Pilot *in vivo* study of an absorbable polydioxanone vena cava filter. *J. Vasc. Surg. Venous Lymphatic Disord.* 3, 409–420. doi:10.1016/j.jvsv.2015.03.004

Eggers, M., Rousselle, S., Urtz, M., Albright, R., Will, A., Jourden, B., et al. (2019). Randomized controlled study of an absorbable vena cava filter in a porcine model. *J. Vasc. Interv. Radiol.* 30, 1487–1494. doi:10.1016/j.jvir.2019.03.010

El-Daly, I., Reidy, J., Culpan, P., and Bates, P. (2013). Thromboprophylaxis in patients with pelvic and acetabular fractures: A short review and recommendations. *Injury* 44, 1710–1720. doi:10.1016/j.injury.2013.04.030

Elizondo, G., Eggers, M., Falcon, M., Trevino, M., Marrufo, R., Perez, C., et al. (2020). First-in-Human study with eight patients using an absorbable vena cava filter for the prevention of pulmonary embolism. *J. Vasc. Interv. Radiol.* 31, 1817–1824. doi:10.1016/j.jvir.2020.07.021

Falck-Ytter, Y., Francis, C. W., Johanson, N. A., Curley, C., Dahl, O. E., Schulman, S., et al. (2012). Prevention of VTE in orthopedic surgery patients: Antithrombotic thera py and prevention of thrombosis, 9th ed: American college of chest phy sicians evidence-based clinical practice guidelines. *Chest* 141, e278S–e325S. doi:10.1378/chest.11-2404

Franchini, M. (2005). Heparin-induced thrombocytopenia: An update. *Thromb. J.* 3, 14. doi:10.1186/1477-9560-3-14

Fullen, W. D., Miller, E. H., Steele, W. F., and McDonough, J. J. (1973). Prophylactic vena caval interruption in hip fractures. *J. Trauma Inj. Infect. Crit. Care* 13, 403–410. doi:10.1097/00005373-197305000-00001

Gaines, P. A., Kolodgie, F. D., Crowley, G., Horan, S., MacDonagh, M., McLucas, E., et al. (2018). Sentry bioconvertible inferior vena cava filter: Study of stages of incorporation in an experimental ovine model. *Int. J. Vasc. Med.* 2018, 1–10. doi:10.1155/2018/6981505

Gao, X., Zhang, J., Chen, B., Yu, H., Li, J., Zhang, S., et al. (2011). A new self-convertible inferior vena cava filter: Experimental *in-vitro* and *in-vivo* evaluation. *J. Vasc. Interv. Radiol.* 22, 829–834. doi:10.1016/j.jvir.2011.02.018

Zhao, J. M., He, M. L., Xiao, Z. M., Li, T. S., Wu, H., and Jiang, H. (2014). Different types of intermittent pneumatic compression devices for preventing venous thromboembolism in patients after total hip replacement. doi:10.1002/14651858.CD009543.pub3

Geisbüsch, P., Benenati, J. F., Pena, C. S., Couvillon, J., Powell, A., Gandhi, R., et al. (2012). Retrievable inferior vena cava filters: Factors that affect retrieval success. *Cardiovasc. Interv. Radiol.* 35, 1059–1065. doi:10.1007/s00270-011-0268-x

Gelbfish, G. A., and Ascer, E. (1991). Intracardiac and intrapulmonary Greenfield filters: A long-term follow-up. *J. Vasc. Surg.* 14, a32195–a32617. doi:10.1067/mva.1991.32195

Gesell, M. W., Gonzalez Della Valle, A., Bartolome Garcia, S., Memtsoudis, S. G., Ma, Y., Haas, S. B., et al. (2013). Safety and efficacy of multimodal thromboprophylaxis following total knee arthroplasty: A comparative study of preferential aspirin vs. routine coumadin chemoprophylaxis. *J. Arthroplasty* 28, 575–579. doi:10.1016/j.arth.2012.08.004

Glotzbecker, M. P., Bono, C. M., Wood, K. B., and Harris, M. B. (1976). Postoperative spinal epidural hematoma: A systematic review. *Spine* 35, E413–E420. doi:10.1097/BRS.0b013e3181d9bb77

Godoy Monzon, D., Iserson, K. V., Cid, A., and Vazquez, J. A. (2012). Oral thromboprophylaxis in pelvic trauma: A standardized protocol. *J. Emerg. Med.* 43, 612–617. doi:10.1016/j.jemermed.2011.09.006

Grewal, S., Chamarthy, M. R., and Kalva, S. P. (2016). Complications of inferior vena cava filters. *Cardiovasc. Diagn. Ther.* 6, 632–641. doi:10.21037/cdt.2016.09.08

Günther, R. W., Neuerburg, J., Mossdorf, A., Pfeffer, J., Hoj, A. R., Molgaard-Nielsen, A., et al. (2005). New optional IVC filter for percutaneous retrieval--*in vitro* evaluatio n of embolus capturing efficiency. *Rofo* 177, 632–636. doi:10.1055/s-2005-858109

Guo, W., Zheng, Q., Li, B., Shi, X., Xiang, D., and Wang, C. (2015). An experimental study to determine the role of inferior vena cava filter in preventing bone cement implantation syndrome. *Iran. J. Radiol.* 12, e14142. doi:10.5812/iranjradiol.14142v2

Hahn, D. (2015). Retrievable filter update: The Denali vena cava filter. *Semin. Interv. Radiol.* 32, 379–383. doi:10.1055/s-0035-1564812

Han, Y., Xu, B., Fu, G., Wang, X., Xu, K., Jin, C., et al. (2018). A randomized trial comparing the NeoVas sirolimus-eluting bioresorbable scaffold and metallic everolimus-eluting stents. *JACC Cardiovasc. Interv.* 11, 260–272. doi:10.1016/j.jcin.2017.09.037

Han, X., Sheng, Y., Wu, J., and Wang, W. (2022). Unretrievable IVC filter due to cement intravasation. *Cardiovasc Interv. Radiol.* 45, 1048–1050. doi:10.1007/s00270-022-03122-1

Herbstreit, F., Kühl, H., and Peters, J. (1976). A cemented caval vein filter: Case report. *Spine* 31, E917–E919. doi:10.1097/01.brs.0000245824.63150.ef

Hirano, S., Funatsu, A., Nakamura, S., and Ikeda, T. (2021). Clinical evaluation of retrievable inferior vena cava filters for the prevention of pulmonary thromboembolism. *Heart Vessels* 36, 1756–1764. doi:10.1007/s00380-021-01856-5

Hoppe, H., Nutting, C. W., Smouse, H. R., Vesely, T. M., Pohl, C., Bettmann, M. A., et al. (2006). Günther Tulip filter retrievability multicenter study including CT follow-up: Final report. *J. Vasc. Interv. Radiol.* 17, 1017–1023. doi:10.1097/01.rvi.90000223689.49091.76

Huang, S. Y., Eggers, M., McArthur, M. J., Dixon, K. A., McWatters, A., Dria, S., et al. (2017). Safety and efficacy of an absorbable filter in the inferior vena cava to prevent pulmonary embolism in swine. *Radiology* 285, 820–829. doi:10.1148/radiol.2017161880

Huang, S. Y., Damasco, J. A., Tian, L., Lu, L., Perez, J. V. D., Dixon, K. A., et al. (2020). *In vivo* performance of gold nanoparticle-loaded absorbable inferior vena cava filters in a swine model. *Biomater. Sci.* 8, 3966–3978. doi:10.1039/d0bm00414f

Huang, J., Dai, X., Zhang, X., Li, J., Huang, M., Liu, C., et al. (2021). Retrievable inferior vena cava filter to prevent pulmonary embolism in patients with fractures and deep venous thrombosis of lower extremities: A single-center experience. *J. Int. Med. Res.* 49, 030006052110065. doi:10.1177/03000605211006591

Hui, A. C., Heras-Palou, C., Dunn, I., Triffitt, P. D., Crozier, A., Imeson, J., et al. (1996). Graded compression stockings for prevention of deep-vein thrombosis after hip and knee replacement. *J. Bone Jt. Surg. Br. volume* 78, 550–554. doi:10.1302/0301-620x.78b4.0780550

Iliescu, B., and Haskal, Z. J. (2012). Advanced techniques for removal of retrievable inferior vena cava filt ers. *Cardiovasc. Interv. Radiol.* 35, 741–750. doi:10.1007/s00270-011-0205-z

Inagaki, E., Farber, A., Eslami, M. H., Siracuse, J. J., Rybin, D. V., Sarosiek, S., et al. (2016). Improving the retrieval rate of inferior vena cava filters with a mult idisciplinary team approach. *J. Vasc. Surg. Venous Lymphatic Disord.* 4, 276–282. doi:10.1016/j.jvsv.2015.11.002

Isaak, A., Takes, M., Kingsmore, D., and Gürke, L. (2018). Endovascular retrieval of intracaval cement: A fishing net technique. *Cardiovasc. Interv. Radiol.* 41, 1958–1961. doi:10.1007/s00270-018-2061-6

Iwanaga, J., Rustagi, T., Ishak, B., Johal, J., David, G., Reina, M. A., et al. (2020). Venous drainage of lumbar vertebral bodies: Anatomic study with application to kyphoplasty, vertebroplasty, and pedicle screw complications. *World Neurosurg. x.* 137, e286–e290. doi:10.1016/j.wneu.2020.01.174

Janvier, A. L., Hamdan, H., and Malas, M. (2010). Bilateral renal vein thrombosis and subsequent acute renal failure due to IVC filter migration and thrombosis. *Clin. Nephrol.* 73, 408–412. doi:10.5414/cnp73408

Kalina, M., Bartley, M., Cipolle, M., Tinkoff, G., Stevenson, S., and Fulda, G. (2012). Improved removal rates for retrievable inferior vena cava filters with the use of a 'filter registry. *Am. Surg.* 78, 94–97. doi:10.1177/000313481207800143

Kalva, S. P., Marentis, T. C., Yeddula, K., Somarouthu, B., Wicky, S., and Stecker, M. S. (2011). Long-term safety and effectiveness of the "OptEase" vena cava filter. *Cardiovasc. Interv. Radiol.* 34, 331–337. doi:10.1007/s00270-010-9969-9

Kanter, B., and Moser, K. M. (1988). The Greenfield vena cava filter. *Chest* 93, 170–175. doi:10.1378/chest.93.1.170

Karunakar, M. A., Shah, S. N., and Jerabek, S. (2005). Body mass index as a predictor of complications after operative treatment of acetabular fractures. *J. Bone Jt. Surg.* 87, 1498–1502. doi:10.2106/jbjs.D.02258

Kaufman, J. A., Barnes, G. D., Chaer, R. A., Cuschieri, J., Eberhardt, R. T., Johnson, M. S., et al. (2020). Society of interventional radiology clinical practice guideline for in ferior vena cava filters in the treatment of patients with venous thro mboembolic disease: Developed in collaboration with the American college of cardiology, American college of chest physicians, American colle ge of surgeons committee on trauma, American heart association, societ y for vascular surgery, and society for vascular medicine. *J. Vasc. Interv. Radiol.* 31, 1529–1544. doi:10.1016/j.jvir.2020.06.014

Kepler, C. K., McKenzie, J., Kreitz, T., and Vaccaro, A. (2018). Venous thromboembolism prophylaxis in spine surgery. *J. Am. Acad. Orthop. Surg.* 26, 489–500. doi:10.5435/jaaos-d-17-00561

Kim, Y.-J., Choi, D. H., Ahn, S., Sohn, C. H., Seo, D. W., and Kim, W. Y. (2016). Timing of pulmonary embolisms in femur fracture patients: Incidence an d outcomes. *J. Trauma Acute Care Surg.* 80, 952–956. doi:10.1097/TA.0000000000001014

Konstantinides, S. V., Torbicki, A., Agnelli, G., Danchin, N., Fitzmaurice, D., Galie, N., et al. (2014). 2014 ESC Guidelines on the diagnosis and management of acute pulmonary embolism. *Eur. Heart J.* 35, 3033–3080. doi:10.1093/eurheartj/ehu283

Kraus, T., Moszner, F., Fischerauer, S., Fiedler, M., Martinelli, E., Eichler, J., et al. (2014). Biodegradable Fe-based alloys for use in osteosynthesis: Outcome of an *in vivo* study after 52 weeks. *Acta Biomater.* 10, 3346–3353. doi:10.1016/j.actbio.2014.04.007

Langlois, J., Nich, C., Courpied, J. P., and Hamadouche, M. (2013). An unreported cause of early postoperative dislocation following total hip revision: Massive intra-capsular oedema related to inferior vena cava filter thrombosis. *Orthop. Traumatology Surg. Res.* 99, 367–370. doi:10.1016/j.otsr.2012.10.015

Laratta, J. L., Shillingford, J. N., Lombardi, J. M., Mueller, J. D., Reddy, H., Saifi, C., et al. (2017). Utilization of vertebroplasty and kyphoplasty procedures throughout th e United States over a recent decade: An analysis of the nationwide in patient sample. *J. Spine Surg.* 3, 364–370. doi:10.21037/jss.2017.08.02

Leask, R. L., Johnston, K. W., and Ojha, M. (2004). Hemodynamic effects of clot entrapment in the TrapEase inferior vena cava filter. *J. Vasc. Interv. Radiol.* 15, 485–490. doi:10.1097/01.rvi.0000124941.58200.85

Leon, L., Rodriguez, H., Tawk, R. G., Ondra, S. L., Labropoulos, N., and Morasch, M. D. (2005). The prophylactic use of inferior vena cava filters in patients undergoing high-risk spinal surgery. *Ann. Vasc. Surg.* 19, 442–447. doi:10.1007/s10016-005-0025-1

Lewis, S., Glen, J., Dawoud, D., Dias, S., Cobb, J., Griffin, X. L., et al. (2019). Venous thromboembolism prophylaxis strategies for people undergoing elective total knee replacement: A systematic review and network meta-analysis. *Lancet Haematol.* 6, e530–e539. doi:10.1016/s2352-3026(19)30155-3

Li, Z., Ni, R.-f., Zhao, X., Yang, C., and Li, M.-m. (2013). Cement embolus trapped in the inferior vena cava filter during percuta neous vertebroplasty. *Korean J. Radiol.* 14, 451–454. doi:10.3348/kjr.2013.14.3.451

Li, X., Haddadin, I., McLennan, G., Farivar, B., Staub, D., Beck, A., et al. (2020). Inferior vena cava filter - comprehensive overview of current indications, techniques, complications and retrieval rates. *Vasa* 49, 449–462. doi:10.1024/0301-1526/a000887

Liu, W. C., Do, Y. S., Choo, S. W., Kim, D. I., Kim, Y. W., Kim, D. K., et al. (2005). The mid-term efficacy and safety of a permanent nitinol IVC filter(TrapEase). *Korean J. Radiol.* 6, 110–116. doi:10.3348/kjr.2005.6.2.110

Liu, Y., Zheng, Y., Chen, X., Yang, J., Pan, H., Chen, D., et al. (2019). Fundamental theory of biodegradable metals-definition, criteria, and design. *Adv. Funct. Mat.* 29, 1805402. doi:10.1002/adfm.201805402

Marquess, J. S., Burke, C. T., Beecham, A. H., Dixon, R. G., Stavas, J. M., Sag, A. A., et al. (2008). Factors associated with failed retrieval of the Günther Tulip inferior vena cava filter. *J. Vasc. Interv. Radiol.* 19, 1321–1327. doi:10.1016/j.jvir.2008.06.004

McClendon, J., Jr., O'Shaughnessy, B. A., Smith, T. R., Sugrue, P. A., Halpin, R. J., Morasch, M., et al. (1976). Comprehensive assessment of prophylactic preoperative inferior vena cava filters for major spinal reconstruction in adults. *Spine* 37, 1122–1129. doi:10.1097/BRS.0b013e31824abde2

Minocha, J., Idakoji, I., Riaz, A., Karp, J., Gupta, R., Chrisman, H. B., et al. (2010). Improving inferior vena cava filter retrieval rates: Impact of a dedic ated inferior vena cava filter clinic. *J. Vasc. Interv. Radiol.* 21, 1847–1851. doi:10.1016/j.jvir.2010.09.003

Mismetti, P., Laporte, S., Pellerin, O., Ennezat, P. V., Couturaud, F., Elias, A., et al. (2015). Effect of a retrievable inferior vena cava filter plus anticoagulation vs anticoagulation alone on risk of recurrent pulmonary embolism: A r andomized clinical trial. *JAMA* 313, 1627–1635. doi:10.1001/jama.2015.3780

Montgomery, K. D., Geerts, W. H., Potter, H. G., and Helfet, D. L. (1996). Thromboembolic complications in patients with pelvic trauma. *Clin. Orthop. Relat. Res.* 329, 68–87. doi:10.1097/00003086-199608000-00010

Moorthy, V., Wang, J. X., Tang, J. H., and Oh, J. Y. (2020). Postoperative spinal epidural hematoma following therapeutic anticoagulation: Case report and review of literature. *J. Spine Surg.* 6, 743–749. doi:10.21037/jss-20-636

Murphy, E. H., Johnson, E. D., Kopchok, G. E., Fogarty, T. J., and Arko, F. R. (2009). Crux vena cava filter. *Expert Rev. Med. Devices* 6, 477–485. doi:10.1586/erd.09.25

Nutescu, E. A., Shorr, A. F., Farrelly, E., Horblyuk, R., Happe, L. E., and Franklin, M. (2008). Burden of deep vein thrombosis in the outpatient setting following maj or orthopedic surgery. *Ann. Pharmacother.* 42, 1216–1221. doi:10.1345/aph.1L135

Olson, S. T., and Chuang, Y. J. (2002). Heparin activates antithrombin anticoagulant function by generating new interaction sites (exosites) for blood clotting proteinases. *Trends cardiovasc. Med.* 12, 331–338. doi:10.1016/s1050-1738(02)00183-4

Pan, Y., Zhao, J., Mei, J., Shao, M., Zhang, J., and Wu, H. (2016). Evaluation of nonpermanent inferior vena cava filter placement in patients with deep venous thrombosis after lower extremity fracture: A single-center retrospective study. *Phlebology.* 31, 564–572. doi:10.1177/0268355515597632

Parvizi, J., Huang, R., Raphael, I. J., Maltenfort, M. G., Arnold, W. V., and Rothman, R. H. (2015). Timing of symptomatic pulmonary embolism with warfarin following arthr oplasty. *J. Arthroplasty* 30, 1050–1053. doi:10.1016/j.arth.2015.01.004

Pellerin, O., Barral, F. G., Lions, C., Novelli, L., Beregi, J. P., and Sapoval, M. (2008). Early and late retrieval of the ALN removable vena cava filter: Results from a multicenter study. *Cardiovasc. Interv. Radiol.* 31, 889–896. doi:10.1007/s00270-008-9357-x

Perez, J. V. D., Jacobsen, M. C., Damasco, J. A., Melancon, A., Huang, S. Y., Layman, R. R., et al. (2021). Optimization of the differentiation and quantification of high-Z nanoparticles incorporated in medical devices for CT-guided interventions. *Med. Phys.* 48, 300–312. doi:10.1002/mp.14601

Peuster, M., Hesse, C., Schloo, T., Fink, C., Beerbaum, P., and von Schnakenburg, C. (2006). Long-term biocompatibility of a corrodible peripheral iron stent in the porcine descending aorta. *Biomaterials* 27, 4955–4962. doi:10.1016/j.biomaterials.2006.05.029

Pierson, D., Edick, J., Tauscher, A., Pokorney, E., Bowen, P., Gelbaugh, J., et al. (2012). A simplified *in vivo* approach for evaluating the bioabsorbable behavior of candidate stent materials. *J. Biomed. Mat. Res.* 100, 58–67. doi:10.1002/jbm.b.31922

Ploumis, A., Ponnappan, R. K., Sarbello, J., Dvorak, M., Fehlings, M. G., Baron, E., et al. (1976). Thromboprophylaxis in traumatic and elective spinal surgery: Analysis of questionnaire response and current practice of spine trauma surgeons. *Spine* 35, 323–329. doi:10.1097/BRS.0b013e3181ca652e

Poletti, P. A., Becker, C. D., Prina, L., Ruijs, P., Bounameaux, H., Didier, D., et al. (1998). Long-term results of the Simon nitinol inferior vena cava filter. *Eur. Radiol.* 8, 289–294. doi:10.1007/s003300050382

Prater, S., Awan, M. A., Antuna, K., and Colon, J. Z. (2021). Prevention of pulmonary cement embolism by inferior vena cava filter f ollowing vertebroplasty-related cement intravasation. *J. Radiol. Case Rep.* 15, 17–27. doi:10.3941/jrcr.v15i4.4139

Prince, M. R., Salzman, E. W., Schoen, F. J., Palestrant, A. M., and Simon, M. (1988). Local intravascular effects of the nitinol wire blood clot filter. *Invest. Radiol.* 23, 294–300. doi:10.1097/00004424-198804000-00009

Raphael, I. J., McKenzie, J. C., Zmistowski, B., Brown, D. B., Parvizi, J., and Austin, M. S. (2014). Pulmonary embolism after total joint arthroplasty: Cost and effectiveness of four treatment modalities. *J. Arthroplasty* 29, 933–937. doi:10.1016/j.arth.2013.09.033

Roehm, J. O. F. (1984). The bird's nest filter: A new percutaneous transcatheter inferior vena cava filter. *J. Vasc. Surg.* 1, 498–501. doi:10.1016/0741-5214(84)90092-2

Rosner, M. K., Kuklo, T. R., Tawk, R., Moquin, R., and Ondra, S. L. (2004). Prophylactic placement of an inferior vena cava filter in high-risk patients undergoing spinal reconstruction. *Neurosurg. Focus* 17, 1–6. doi:10.3171/foc.2004.17.4.6

Schulman, S., and Majeed, A. (2011). A benefit-risk assessment of dabigatran in the prevention of venous thromboembolism in orthopaedic surgery. *Drug Saf.* 34, 449–463. doi:10.2165/11587290-000000000-00000

Segon, Y. S., Summey, R. D., Slawski, B., and Kaatz, S. (1995). Surgical venous thromboembolism prophylaxis: Clinical practice update. *Hosp. Pract. (1995).* 48, 248–257. doi:10.1080/21548331.2020.1788893

Shimoo, S., and Koide, M. (2020). Incomplete opening of an ALN-type inferior vena cava filter due to entanglement of the filter legs resulting in filter migration and inferior vena cava perforation. *Radiol. Case Rep.* 15, 1231–1234. doi:10.1016/j.radcr.2020.05.019

Shreenivas, S. S., and Kereiakes, D. J. (2018). Evolution of the SYNERGY bioresorbable polymer metallic coronary stent. *Future Cardiol.* 14, 307–317. doi:10.2217/fca-2018-0040

Singer, M. A., and Wang, S. L. (2011). Modeling blood flow in a tilted inferior vena cava filter: Does tilt a dversely affect hemodynamics? *J. Vasc. Interv. Radiol.* 22, 229–235. doi:10.1016/j.jvir.2010.09.032

Singhana, B., Chen, A., Slattery, P., Yazdi, I. K., Qiao, Y., Tasciotti, E., et al. (2015). Infusion of iodine-based contrast agents into poly(p-dioxanone) as a radiopaque resorbable IVC filter. *J. Mat. Sci. Mat. Med.* 26, 124. doi:10.1007/s10856-015-5460-0

Song, G., Zhao, H. Q., Liu, Q., and Fan, Z. (2022). A review on biodegradable biliary stents: Materials and future trends. *Bioact. Mat.* 17, 488–495. doi:10.1016/j.bioactmat.2022.01.017

Sostres, C., and Lanas, A. (2011). Gastrointestinal effects of aspirin. *Nat. Rev. Gastroenterol. Hepatol.* 8, 385–394. doi:10.1038/nrgastro.2011.97

Spitalny, A. D. (2006). Bioabsorbable implants. *Clin. Podiatr. Med. Surg.* 23, 673–694. doi:10.1016/j.cpm.2006.06.001

Stein, P. D., Matta, F., and Hughes, M. J. (2018). Prophylactic inferior vena cava filters in patients with fractures of the pelvis or long bones. *J. Clin. Orthop. Trauma* 9, 175–180. doi:10.1016/j.jcot.2017.09.018

Stösslein, F., and Altmann, E. (1998). A rare complication with an Anthéor vena cava filter. *Cardiovasc. Interv. Radiol.* 21, 165–167. doi:10.1007/s002709900235

Sutphin, P. D., Reis, S. P., McKune, A., Ravanzo, M., Kalva, S. P., and Pillai, A. K. (2015). Improving inferior vena cava filter retrieval rates with the define, m easure, analyze, improve, control methodology. *J. Vasc. Interv. Radiol.* 26, 491–498. doi:10.1016/j.jvir.2014.11.030

Sweeney, T. J., and Van Aman, M. E. (1993). Deployment problems with the titanium Greenfield filter. *J. Vasc. Interv. Radiol.* 4, 691–694. doi:10.1016/s1051-0443(93)71950-8

Talec, P., Gaujoux, S., and Samama, C. M. (2016). Early ambulation and prevention of post-operative thrombo-embolic risk. *J. Visc. Surg.* 153, S11–s14. doi:10.1016/j.jviscsurg.2016.09.002

Tapson, V. F., Hazelton, J. P., Myers, J., Robertson, C., Gilani, R., Dunn, J. A., et al. (2017). Evaluation of a device combining an inferior vena cava filter and a central venous catheter for preventing pulmonary embolism among critically ill trauma patients. *J. Vasc. Interv. Radiol.* 28, 1248–1254. doi:10.1016/j.jvir.2017.05.001

Thors, A., and Muck, P. (2011). Resorbable inferior vena cava filters: Trial in an *in-vivo* porcine model. *J. Vasc. Interv. Radiol.* 22, 330–335. doi:10.1016/j.jvir.2010.11.030

Tian, L., Lee, P., Singhana, B., Chen, A., Qiao, Y., Lu, L., et al. (2017). Radiopaque resorbable inferior vena cava filter infused with gold nanoparticles. *Sci. Rep.* 7, 2147. doi:10.1038/s41598-017-02508-3

Tian, L., Lee, P., Singhana, B., Chen, A., Qiao, Y., Lu, L., et al. (2018). *In vivo* imaging of radiopaque resorbable inferior vena cava filter infused with gold nanoparticles. *Proc. SPIE. Int. Soc. Opt. Eng.* 10576, 105762S. doi:10.1117/12.2293738

Toro, J. B., Gardner, M. J., Hierholzer, C., Sama, D., Kosi, C., Ertl, W., et al. (2008). Long-term consequences of pelvic trauma patients with thromboembolic disease treated with inferior vena caval filters. *J. Trauma* 65, 25–29. doi:10.1097/TA.0b013e318075e97a

Uberoi, R., Tapping, C. R., Chalmers, N., and Allgar, V. (2013). British society of interventional Radiology (BSIR) inferior vena cava (IVC) filter registry. *Cardiovasc. Interv. Radiol.* 36, 1548–1561. doi:10.1007/s00270-013-0606-2

Vaishya, R., Chauhan, M., and Vaish, A. (2013). Bone cement. *J. Clin. Orthop. Trauma* 4, 157–163. doi:10.1016/j.jcot.2013.11.005

Weinberg, I., Kaufman, J., and Jaff, M. R. (2013). Inferior vena cava filters. *JACC Cardiovasc. Interv.* 6, 539–547. doi:10.1016/j.jcin.2013.03.006

Weitz, J. I. (1997). Low-molecular-weight heparins. *N. Engl. J. Med. Overseas. Ed.* 337, 688–698. doi:10.1056/nejm199709043371007

Witt, D. M., Clark, N. P., Kaatz, S., Schnurr, T., and Ansell, J. E. (2016). Guidance for the practical management of warfarin therapy in the treatment of venous thromboembolism. *J. Thromb. Thrombolysis* 41, 187–205. doi:10.1007/s11239-015-1319-y

Yakkanti, R. R., Mohile, N. V., Cohen-Levy, W. B., Haziza, S., Lavelle, M. J., Bellam, K. G., et al. (2021). Perioperative management of acetabular and pelvic fractures: Evidence-based recommendations. *Arch. Orthop. Trauma Surg.* doi:10.1007/s00402-021-04278-0

Yang, C., Ma, F., Gao, C., Kang, Y., Zhang, G., Liu, P., et al. (2019). Design and evaluation of a novel biodegradable inferior vena cava filter. *J. Biomater. Appl.* 33, 1060–1069. doi:10.1177/0885328218824203

Yin, T., Du, R., Wang, Y., Huang, J., and Huang, Y. (2022). Two-stage degradation and novel functional endothelium characteristics of a 3-D printed bioresorbable scaffold. *Bioact. Mat.* 10, 378–396. doi:10.1016/j.bioactmat.2021.08.020

Yoo, K. Y., Jeong, S. W., Yoon, W., and Lee, J. (1976). Acute respiratory distress syndrome associated with pulmonary cement e mbolism following percutaneous vertebroplasty with polymethylmethacryl ate. *Spine* 29, E294–E297. doi:10.1097/01.brs.0000131211.87594.b0

Yuan, W., Xia, D., Wu, S., Zheng, Y., Guan, Z., and Rau, J. V. (2022). A review on current research status of the surface modification of Zn-based biodegradable metals. *Bioact. Mat.* 7, 192–216. doi:10.1016/j.bioactmat.2021.05.018

Zhang, E., Chen, H., and Shen, F. (2010). Biocorrosion properties and blood and cell compatibility of pure iron as a biodegradable biomaterial. *J. Mat. Sci. Mat. Med.* 21, 2151–2163. doi:10.1007/s10856-010-4070-0

Zhang, F., Li, H., Liang, G., and Zhang, H. (2017). Development and evaluation of a new biodegradable vena cava filter in a canine model. *Asian J. Surg.* 40, 12–16. doi:10.1016/j.asjsur.2015.05.002

Zhao, F., Xu, H., Xue, W., Li, Y., Sun, J., Wang, F., et al. (2020). Iodinated poly(p-dioxanone) as a facile platform for X-ray imaging of resorbable implantable medical devices. *J. Biomater. Appl.* 35, 39–48. doi:10.1177/0885328220912842

frontiers | Frontiers in Bioengineering and Biotechnology

TYPE Original Research
PUBLISHED 12 December 2022
DOI 10.3389/fbioe.2022.1069804

OPEN ACCESS

EDITED BY
Yansong Qi,
Inner Mongolia People's Hospital, China

REVIEWED BY
Marley Dewey,
University of Pittsburgh, United States
Virginia Brancato,
Italian Institute of Technology (IIT), Italy
Lei Yang,
Hebei University of Technology, China

*CORRESPONDENCE
Jianhao Lin,
linjianhao@pkuph.edu.cn
Dan Xing,
xingdan@bjmu.edu.cn

†These authors have contributed equally to this work

SPECIALTY SECTION
This article was submitted to Biomaterials, a section of the journal Frontiers in Bioengineering and Biotechnology

RECEIVED 14 October 2022
ACCEPTED 28 November 2022
PUBLISHED 12 December 2022

CITATION
Li H, He Z, Li W, Li JJ, Lin J and Xing D (2022), Self-assembled microtissues loaded with osteogenic MSCs for *in vivo* bone regeneration.
Front. Bioeng. Biotechnol. 10:1069804.
doi: 10.3389/fbioe.2022.1069804

Self-assembled microtissues loaded with osteogenic MSCs for *in vivo* bone regeneration

Hui Li[1,2†], Zihao He[1,2†], Wenjing Li[3], Jiao Jiao Li[4], Jianhao Lin[1,2*] and Dan Xing[1,2*]

[1]Arthritis Clinic and Research Center, Peking University People's Hospital, Peking University, Beijing, China, [2]Arthritis Institute, Peking University, Beijing, China, [3]MOE Key Laboratory of Bioorganic Phosphorus Chemistry and Chemical Biology, Department of Biomedical Engineering, School of Medicine, Tsinghua-Peking Center for Life Sciences, Tsinghua University, Beijing, China, [4]Kolling Institute, University of Sydney, Sydney, NSW, Australia

Bone regeneration strategies based on mesenchymal stem cell (MSC) therapy have received widespread attention. Although MSC incorporation into bone scaffolds can help with the repair process, a large number of studies demonstrate variable effects of MSCs with some noting that the inclusion of MSCs does not provide better outcomes compared to unseeded scaffolds. This may in part be related to low cell survival following implantation and/or limited ability to continue with osteogenic differentiation for pre-differentiated cells. In this study, we incorporated MSCs into gelatin microcryogels to form microtissues, and subjected these microtissues to osteogenic induction. We then mixed as-formed microtissues with those subjected to 6 days of osteogenic induction in different ratios, and investigated their ability to induce *in vitro* and *in vivo* osteogenesis during self-assembly. Using a full-thickness rat calvarial defect model, we found that undifferentiated and osteogenically induced microtissues mixed in a ratio of 2:1 produced the best outcomes of bone regeneration. This provides a new, customizable cell-based therapeutic strategy for *in vivo* repair of bone defects.

KEYWORDS

bone regeneration, microtissues, gelatin microcryogel, mesenchymal stem cells, self-assembly

Introduction

Between 5% and 20% of all bone fractures result in delayed healing or non-union, with the overall rate of non-union estimated at 1.9%–10%, leading to chronic morbidity, prolonged hospitalization and increased costs (Gómez-Barrena et al., 2015; Zura et al., 2016). The rate of fracture non-union varies depending on the anatomical region. For instance, femoral shaft non-union is estimated to occur in 8% of patients treated with intramedullary nailing (Rupp et al., 2018). The cost of fracture non-union poses a significant healthcare burden, for example, tibial shaft non-union amounts to a median total cost of $25,556 in the United States, more than double the cost compared to tibial shaft fractures that achieve union within 24 months after fracture (Antonova et al., 2013).

Mesenchymal stem cell (MSC)-based bone regeneration strategies have received increasing attention in the past decades. Both autologous (Bhattacharjee et al., 2019) and allogeneic (Arinzeh et al., 2003) MSC therapy can play an important role in bone reconstruction and have been adopted using various approaches. These approaches include MSC cell therapy, MSC secretome therapy (including conditioned medium, extracellular vesicles, and other secretory products), and MSC-loaded carriers (including cell-seeded demineralized bone matrix, bone substitutes, and scaffolds) (Liebergall et al., 2013). Among these, scaffold-based approaches and cell carriers have distinct advantages, as they provide a supportive matrix for MSCs to be implanted into the bone defect area, and can directly participate in promoting local bone reconstruction. The scaffold or cell carrier should ideally mimic the structure and function of the bone extracellular matrix (ECM) (Yu et al., 2015), and provide a functional three-dimensional space for the adhesion, migration, proliferation, and differentiation of osteoblast progenitors (Venkataiah et al., 2021), as well as help to maintain the osteogenic activity of loaded cells following implantation.

Although MSC incorporation into bone scaffolds has been shown to help with bone reconstruction, a large number of studies have also demonstrated variable outcomes of cell-seeded scaffolds, with some noting that the inclusion of MSCs does not necessarily provide better outcomes compared to cell-free scaffolds in preclinical models of bone repair. The beneficial effects of MSCs might be hindered by a range of factors including low cell survival after implantation and limited ability of the scaffold to sustain osteogenic differentiation and continuous bone formation (Shang et al., 2021). These factors can often lead to failure of bone repair particularly in large bone defects (Scarano et al., 2017).

Previous experimental strategies combining MSCs with a cell carrier or scaffold to induce bone regeneration have focused almost exclusively on improving the properties of the supporting matrix to sustain cell survival and osteogenic capacity. However, the potential benefits of modulating the composition of the transplanted cells should not be ignored. During the process of osteoblastic differentiation, various osteogenically inducing factors are produced at different stages including RUNX2, ALP, COL1A1, OPN, and OCN. These factors can help propel the proliferation, collagen expression, mineralization, and other osteogenic processes to sustain ongoing bone formation (Nakashima et al., 2002; Ai-Aql et al., 2008; Vimalraj, 2020). On the other hand, transplanting undifferentiated MSCs makes better use of their paracrine functions that reduce inflammation and improve tissue healing. Current cell-based bone regeneration strategies have generally focused on incorporating either osteogenically primed or undifferentiated stem cells into implantable matrices. In this study, we hypothesize that better osteogenic outcomes can be achieved by mixing populations of undifferentiated and osteogenically primed MSCs, which draws benefits both from shared osteogenic factors in the microenvironment produced by osteogenic cells, and undifferentiated MSCs which provide stronger stemness as well as anti-apoptosis and anti-senescence characteristics.

To deliver the mixed MSC populations in a suitable carrier, we have chosen gelatin carriers due to their good biocompatibility, biodegradability, and demonstrated use in bone tissue engineering (Kuttappan et al., 2016). In our previous studies, we have successfully developed and applied gelatin microcryogels loaded with MSCs in a variety of tissue regeneration applications (Xing et al., 2020). Using this strategy, we can produce self-assembled MSC-containing microtissues which help to maintain MSC secretory activity and pro-regenerative functions both *in vitro* and *in vivo*. In this study, we explore for the first time the effects of mixing microtissues containing undifferentiated MSCs together with microtissues containing osteogenically primed MSCs in bone regeneration. We demonstrate that undifferentiated and osteogenically primed microtissues mixed in different ratios can significantly change *in vivo* bone regeneration outcomes, and coupling the paracrine activity of undifferentiated MSCs with an osteogenic microenvironment provided by osteogenic MSCs is beneficial for bone repair.

Materials and methods

Isolation, culture and identification of rat bone marrow-derived MSCs

Bone marrow was collected from the femur of 8 week old healthy Sprague Dawley rats. The extracted bone marrow was cultured in complete growth medium (α-MEM (Hyclone, United States) supplemented with 10% fetal bovine serum (FBS, Gibco, United States) and 1% penicillin/streptomycin (Hyclone, United States)) in a 10 cm cell culture dish. Each dish contained 5 ml bone marrow and the culture medium was replaced every two days. Adherent cells remaining in the dish were identified as bone marrow MSCs, and cells from the third passage were used for subsequent experiments.

To verify the multilineage differentiation ability of isolated rat bone marrow MSCs, cells were cultured in osteogenic, chondrogenic, and adipogenic medium. To evaluate osteogenesis, cells were stained for alkaline phosphatase at 14 days using BCIP/NBT kit (Beyotime, China) according to the manufacturer's instructions. To evaluate chondrogenesis, pelleted cells were stained with Alcian blue staining solution at 21 days (Solarbio, China) to visualize proteoglycan deposition. To evaluate adipogenesis, cells were stained with Oil Red O at 21 days (Beyotime, China) to visualize lipid droplets.

To identify MSC-related surface markers, 1 × 106 cells were incubated with the following monoclonal antibodies: PE-CD90 (Invitrogen, United States), PE-CD105 (Invitrogen,

10.3389/fbioe.2022.1069804

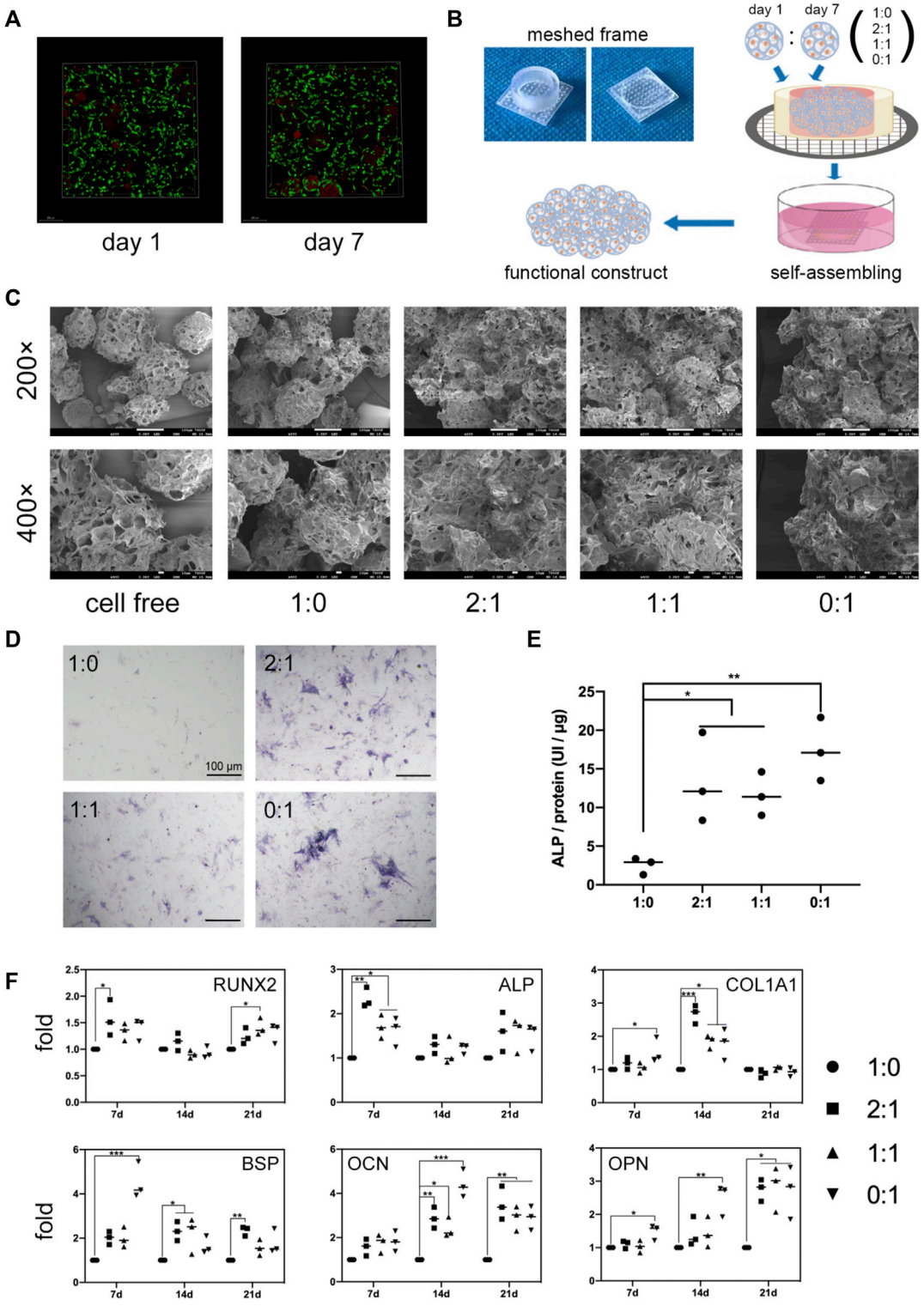

FIGURE 1
In vitro microtissue construct formation and osteogenic differentiation. **(A)**. Live/dead staining of MSCs after 24 h culture in growth medium within microcryogels (day 1) or after additional 6-day osteogenic induction within microcryogels (day 7). **(B)**. Schematic of the process of forming different group of microtissue constructs by *in vitro* self-assembly of MSC-loaded microtissues within meshed frames. **(C)**. Scanning electron microscope (SEM) images of different groups of microtissue constructs cultured in meshed frames for 7 days. **(D)**. ALP staining images of MSCs lysed from different groups of microtissue constructs after 7-day self-assembly. Scale bar = 100 μm. **(E)**. ALP quantitative analysis of different groups of microtissue constructs after 7-day self-assembly (*$p < 0.05$, **$p < 0.01$). **(F)**. The mRNA levels of osteogenic differentiation related genes in different groups of microtissue constructs over 21 days (*$p < 0.05$, **$p < 0.01$, ***$p < 0.001$).

United States), FITC-CD34 (proteintech, United States), and FITC-CD45 (proteintech, United States). Unstained cells were used as negative controls. Cells incubated with antibodies at 25°C for 30 min, followed by washing with phosphate buffered saline (PBS) and analysis by flow cytometry (BD Biosciences, United States).

Fabrication of gelatin microcryogels

Gelatin microcryogels were synthesized according to our published methods (Xing et al., 2020). Briefly, poly (methyl methacrylate) (PMMA) stencil array chips were made by a laser fabrication system. Each chip contained 600 circular micro-wells with diameter of 200 μm. Gelatin solution (4% w/v) was dissolved at 65°C for 45 min, followed by ice bath for 5 min, and 0.5% glutaraldehyde solution was used as crosslinking agent. Gelatin solution was pipetted into the PMMA chip, which then underwent cryogelation for 16 h at −20°C, followed by lyophilization for 1 h. The resulting gelatin microcryogels were washed with 0.1 M $NaBH_4$ (Aladdin, China) solution and distilled water. Microcryogels were lyophilised and vacuum-packaged until use for subsequent experiments.

Preparation and characterization of self-assembled microtissues

Osteogenic medium containing 89% α-MEM, 10% FBS, 1% penicillin/streptomycin, 10 mM β-glycerophosphate, 50 nM ascorbic acid, and 100 nM dexamethasone. Gelatin microcryogels were loaded with MSCs and dispersedly cultured for either 1 day in growth medium (day 1 microtissues in Figure 1A) or additional 6 days in osteogenic medium (day 7 microtissues in Figure 1A). They were then added in different ratios into a meshed frame to induce self-assembly and form microtissue constructs (Figure 1B). Meshed frames were designed using AUTOCAD software and made by 3D printing using poly (lactic acid) (PLA) with 5.5 mm (diameter) × 2.5 mm (height) inner dimensions. The diameter of mesh spacing was set at 100 μm to prevent overflow of microcryogels. The undifferentiated and osteogenically induced MSC-loaded microtissues were mixed in different ratios (1:0, 2:1, 1:1, and 0:1) and cultured in meshed frames within a 6-well plate for 7 days to form microtissue constructs for further analysis.

Characterization of MSCs in microtissues

The viability of MSCs within microtissues was characterized by live/dead staining (Life Technologies, United States). Morphological observation was performed by scanning electron microscopy (SEM, FEI Quanta 200, Netherlands). Microtissue constructs were completely removed from the meshed frames after 7 days culture, fixed by 2.5% glutaraldehyde, dehydrated by graded ethanol, lyophilised, and sputtered with gold for SEM analysis.

Characterization of osteogenic differentiation

To evaluate osteogenic differentiation, microtissue constructs grown in meshed frames for 7 days were removed from the frame, and MSCs were digested from the constructs using 0.1% collagenase I for 30 min at 37°C. MSCs were then seeded in 48-well plates and cultured for 8 h in growth medium. An ALP staining kit (Beyotime, China) was used to visualize ALP expression according to the manufacturer's instructions. Whole microtissue constructs were used to quantitatively analyze ALP protein level, where 0.2% Triton X-100 was used to repeatedly blow the constructs after 7-day self-assembly. After centrifugation, the supernatant was used to quantify ALP levels using an ALP quantitative analysis kit (Beyotime, China) according to the manufacturer's instructions.

Microtissue constructs cultured in meshed frames for 3, 7, and 14 days were subjected to gene expression analysis for markers of osteogenic differentiation by quantitative real-time PCR (qPCR). The constructs were homogenized in TRIZOL reagent (Life Technologies. United States), and total RNA extraction was performed following the manufacturer's instructions. cDNA was synthesized from 500 ng of DNA-free total RNA using PrimeScript RT Reagent Kit (Taraka. Japan). Gene-specific transcription was analyzed by qPCR using SYBR Premix Ex Taq II (Taraka. Japan) on a CFX96 instrument (Bio-Rad. United States). All genes were normalized to GAPDH. Primers used are listed in Table 1.

Characterization of cell apoptosis and senescence

For cell apoptosis analysis, MSCs were digested from microtissue constructs using the same procedures as above. The MSC suspension was stained using annexin V/propidium iodide (PI) double staining apoptosis detection kit (Beyotime, China) according to the manufacturer's instructions, and analyzed by flow cytometry (BD Fortessa, United States).

The β-galactosidase (β-Gal) activity of MSCs was measured using a senescence β-galactosidase staining kit (Beyotime, China) according to the manufacturer's instructions. MSCs were digested from microtissue constructs, seeded in a 6-well plate and cultured for 8 h. The MSCs were observed using an inverted microscope (Olympus, Japan), and the number of senescent cells were counted in three randomly selected high-power fields.

TABLE 1 Primer sequences.

	Forward primer	Reverse primer
RUNX2	GGTGGAGCTACGGACAATGAATGG	GCTTGAGGCACTGACTGAGACTG
ALP	CACGGCGTCCATGAGCAGAAC	CAGGCACAGTGGTCAAGGTTGG
COL1A1	TGTTGGTCCTGCTGGCAAGAATG	GTCACCTTGTTCGCCTGTCTCAC
BSP	AAGCGACGAGGAAGAGGAAGAGG	TTGGTGCTGGTGCCGTTGAC
OCN	GGACCCTCTCTCTGCTCACTCTG	ACCTTACTGCCCTCCTGCTTGG
OPN	GACGATGATGACGACGACGATGAC	GTGTGCTGGCAGTGAAGGACTC

In vivo study and analysis of bone regeneration

Sprague-Dawley female rats (8 week old, 220–260 g) were used for *in vivo* evaluation of bone regeneration using microtissues. A full-thickness calvarial defect with a diameter of 5 mm was constructed on the top of the rat skull. Rats were divided into 5 groups (n = 6) and implanted with: cell free microcryogels, and microtissues comprising undifferentiated/osteogenically primed MSC-loaded microcryogels in ratios of 1:0, 2:1, 1:1, and 0:1. PLA mesh was removed before implantation. Rats were sacrificed by excessive administration of anesthesia at 3 months after surgery. Explanted calvarial samples containing the defect were fixed in 4% paraformaldehyde for 24 h, and then evaluated by micro-CT (SCANCO μCT-100, Switzerland). The bone volume/tissue volume (BV/TV) and bone mineral density (BMD) of the regenerated bone was measured by Evaluation V6.5 (SCANCO, Switzerland).

For histological analysis, the samples were decalcified in 10% EDTA for 4 weeks. After dehydration by graded ethanol, samples were embedded in paraffin. Decalcified paraffin sections with 7 mm thickness were stained using hematoxylin and eosin (H&E) and Masson's trichrome.

For mineralization rate analysis, alizarin red (30 mg/kg, Sigma-Aldrich, United States) and calcein (30 mg/kg, Sigma-Aldrich, United States) with fluorescent labeling were injected intraperitoneally at 3 and 21 days before euthanasia, respectively. Sample collection and histological processing were performed as described above. Non-decalcified sections were observed using a fluorescence microscope (Olympius, Japan).

Statistical analysis

All data were obtained from at least 3 independent experiments, and expressed as mean ± standard deviation. After testing for homogeneity of variances, one-way analysis of variance (ANOVA) followed by Tukey's multiple comparisons test were used to determine significant differences between groups. $p < 0.05$ was considered a significant difference between groups.

Results

In vitro microtissue formation and osteogenic differentiation

The trilineage differentiation ability (Supplementary Figure S1A) and surface markers (Supplementary Figure S1B) of isolated rat bone marrow MSCs were verified. Microcryogels loaded with MSCs for 24 h were defined as day 1 microtissues, while day 1 microtissues subjected to osteogenic induction in differentiation medium for additional 6 days were defined as day 7 microtissues. Both day 1 and day 7 microtissues underwent dispersed culture. Live/dead staining showed that MSCs in the day 1 and day 7 microtissue had good cell activity (Figure 1A). Taking advantage of the ability of cell-laden microtissues to self-assemble *in vitro*, we combined day 1 and day 7 microtissues in different proportions (1:0, 2:1, 1:1, and 0:1) to form customized microtissue constructs, and investigated the cell survival and osteogenic differentiation potential of MSCs in these self-assembly constructs (Figure 1B).

We used SEM to characterize the self-assembly of microtissues with different proportions in meshed frames for 7 days. SEM images showed that all groups of microtissues containing MSCs underwent self-assembly, and fusion between adjacent microtissues was achieved through ECM-like substance. Meanwhile, the cell free microcryogels remained separate and were not joined to each other. The degree of self-assembly appeared to be higher for constructs containing day 7 (osteogenic) microtissues (2:1, 1:1, 0:1 groups) compared to constructs containing only day 1 microtissues. This suggests the introduction of an osteogenic microenvironment may promote ECM production by MSCs and lead to better self-assembly.

The state of osteogenic differentiation for different groups of microtissue constructs was measured after 7 days of culture in meshed frames. MSCs extracted from microtissue constructs

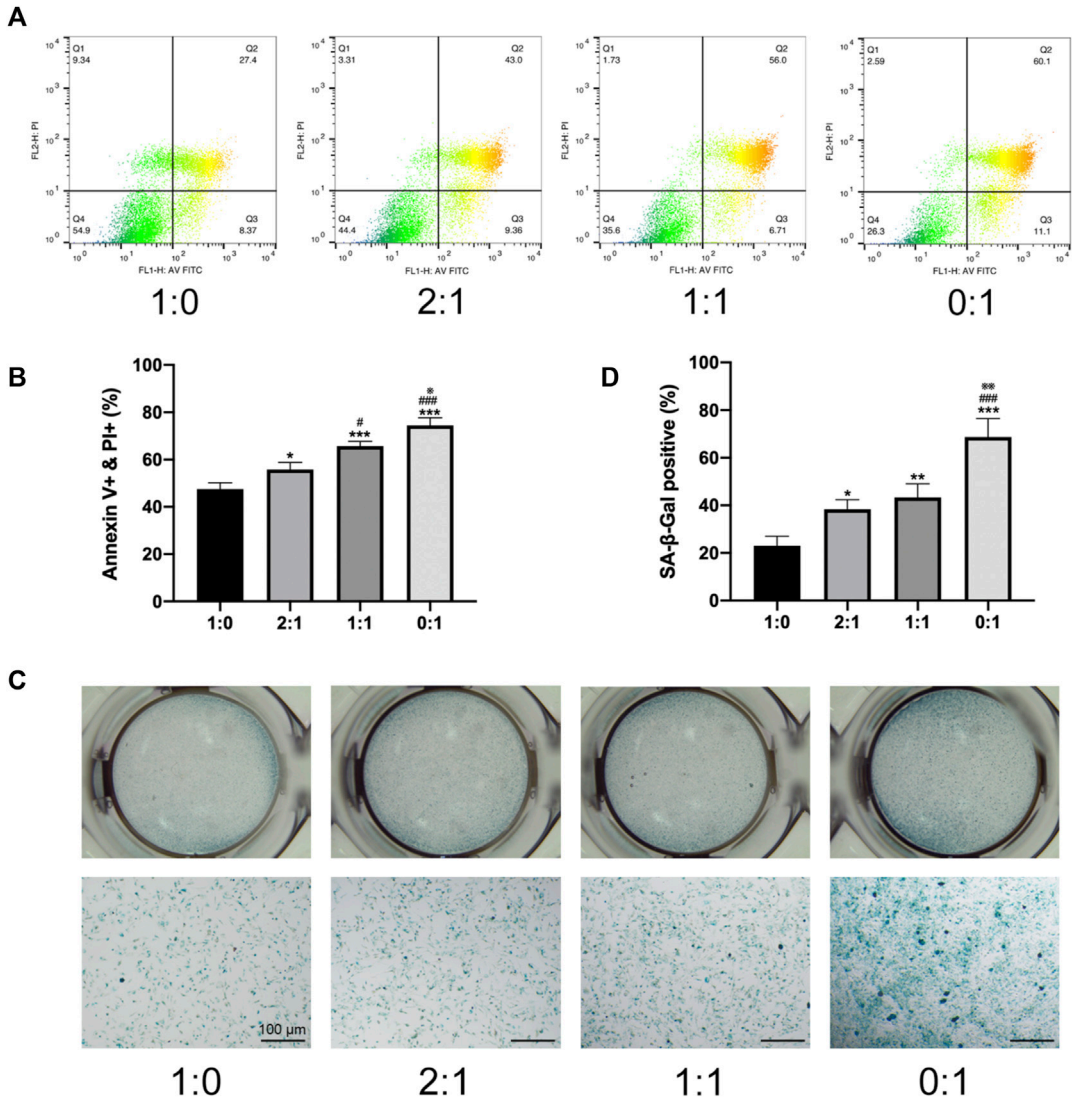

FIGURE 2
In vitro survival of MSCs within microtissue constructs. **(A)**. Apoptosis of MSCs in different groups of microtissue constructs measured by flow cytometry. **(B)**. Quantitative analysis of the proportion of Annexin V positive and PI positive cells. **(C)**. SA-β-Gal staining images of for cells lysed from different groups of microtissue constructs. Scale bar = 100 μm. **(D)**. Quantitative analysis of SA-β-Gal positive cells. (* compared to 1:0 group. # compared to 2:1 group. ※ compared to 1:1 group. */#/※$p < 0.05$, **/##$p < 0.01$, ***/###$p < 0.001$).

showed more staining and higher protein levels of ALP for constructs containing day 7 (osteogenic) microtissues (2:1, 1:1, 0:1 groups) compared to the group that contained only day 1 microtissues (Figures 1D,E). qPCR results showed that the same groups containing day 7 (osteogenic) microtissues had significantly higher transcription levels of key osteogenic genes over 21 days, including RUNX2 and ALP indicating early-stage osteogenic differentiation, COL1A1 and BSP indicating middle-stage differentiation, and OCN and OPN indicating later stage differentiation (Figure 1F). Although the constructs containing day 7 (osteogenic) microtissues showed better osteogenic potential compared to the group without, their osteogenic potential was not correlated with the ratio of incorporation of day 7 microtissues within the constructs.

In vitro survival of MSCs within microtissues

To investigate changes in the survival of MSCs in different groups of microtissue constructs during the process of *in vitro* self-assembly, MSC apoptosis was evaluated after 3 days of

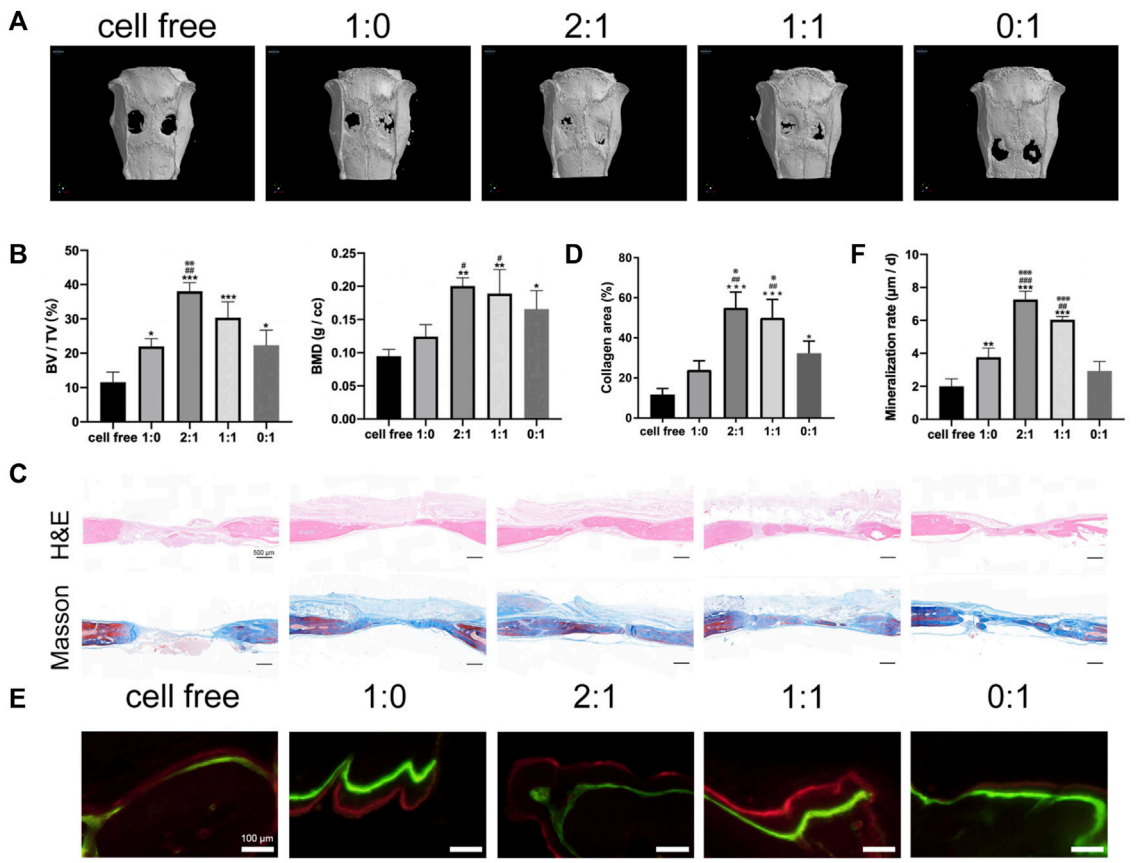

FIGURE 3
Bone repair using microtissue constructs in rat calvarial bone defects. **(A)**. Micro-CT images of calvarial defect repair effect at 3 months after surgery. **(B)**. Quantitative analysis of new bone volume/tissue volume (BV/TV) and bone mineral density (BMD). **(C)**. Histological analysis by H&E and Masson's trichrome staining. Scale bar = 500 μm. **(D)**. Quantitative analysis of percentage of collagen in defect area. (* compared to cell free group. # compared to 1:0 group. ※ compared to 0:1 group. */※ $p < 0.05$, ##$p < 0.01$, ***$p < 0.001$). **(E)**. Tissue mineralization shown by: green = calcein injected 3 weeks before euthanasia, red = alizarin red injected 3 days before euthanasia. Scale bar = 100 μm. **(F)**. Quantitative analysis of mineralization rate (MAR, the average distance between two lines divided by the number of days). (* compared to cell free group. # compared to 1:0 group. ※ compared to 0:1 group. */#$p < 0.05$, **/##/※※ $p < 0.01$, ***/###/※※※ $p < 0.001$).

culturing MSC-loaded microtissues in meshed frames, by flow cytometry (Figure 2A) and quantitative analysis of the proportion of Annexin V and PI positive cells (Figure 2B), as well as SA-β-Gal staining (Figure 2C) and quantitative analysis (Figure 2D). MSCs in non-differentiated constructs containing only day 1 microtissues (1:0 group) showed the lowest level of apoptosis, and the proportion of apoptotic cells progressively increased when higher ratios of day 7 (osteogenic) microtissues were incorporated within the constructs (progressively higher apoptosis for 2:1, 1:1, and 0:1 groups). The different analysis methods showed consistent results on the level of MSC apoptosis in different groups. Constructs that contained both undifferentiated (day 1) and osteogenic (day 7) microtissues were considered to provide the best balance between enhanced osteogenic potential and reduced senescence/apoptosis of MSCs.

Bone repair using microtissues in rat calvarial bone defects

Different groups of microtissue constructs were implanted in a critical-sized rat calvarial defect model, using cell free microcryogels as a control group. The outcomes of bone healing were evaluated by micro-CT (Figures 3A,B), histology (Figures 3C,D), and mineralization (Figures 3E,F) at 3 months after implantation. Micro-CT analysis showed limited bone healing in the cell free control group. New bone formation was most pronounced in the construct groups with a mixed ratio of day 1 and day 7 microtissues (2:1 and 1:1 groups), with macroscopically better defect healing (Figure 3A) and higher BV/TV as well as BMD compared to construct groups containing only day 1 or only day 7 microtissues (Figure 3B). This was further verified by histological staining using H&E and Masson's trichrome, where continuous bone formation was observed in the

defects treated with 2:1 and 1:1 groups, while the 1:0 and 0:1 groups showed irregular and discontinuous new tissue (Figures 3C,D). The amount of mineralization in the newly formed bone area showed similar findings as micro-CT and histology, where the 2:1 and 1:1 groups produced the highest mineralization as seen in images (Figure 3E) and quantitative analysis (Figure 3F) compared to the 1:0 and 0:1 groups. Combining all *in vivo* study results, it appears that the 2:1 group gave the highest level of defect filling with new tissue, while the amount of mineralized tissue formation was highest in the 1:1 group.

Discussion

This study provided a new approach that could potentially be applied to improve the outcomes of regeneration in large bone defects using MSC-based therapy. By introducing MSCs embedded within self-assembled microtissue constructs, and mixing different proportions of undifferentiated and osteogenically induced MSCs, this approach creates an osteogenic microenvironment in the implanted constructs while still incorporating significant "stemness" or strong regenerative activity of the MSCs. Microtissues with a mixture of undifferentiated and osteogenic MSCs were shown to provide better regenerative characteristics *in vitro* and *in vivo* compared to a homogenous population of MSCs which were all at the same differentiation stage.

The qPCR results of microtissue constructs grown *in vitro* were consistent with a number of expected pathways during different stages of *in vivo* osteogenesis. RUNX2 is a master regulator of osteogenesis and initiates early-stage commitment of undifferentiated MSCs to form pre-osteoblasts (Nakashima et al., 2002), acting as a downstream effector the ERK1/2-RUNX2 pathway (Yuh et al., 2020). Following RUNX2 induction, ALP becomes highly expressed during the early-mid stage of osteogenic differentiation and prepares the osteogenic matrix for mineralization (Vimalraj, 2020). This is followed by the expression of mid-late stage osteogenesis markers including OPN and OCN. Osteopontin encoded by OPN is a highly acidic glycoprotein secreted by differentiating cells, which can bind to collagen type I and help promote osteogenesis (McKee and Nanci, 1996; Wang et al., 2016). Osteocalcin encoded by OCN is a vitamin K dependent non-collagen protein in bone tissue specifically produced by non-proliferative osteoblasts, which acts as a late stage osteogenic marker. Both OPN and OCN are involved in the synthesis of bone matrix and maintenance of bone mineralization (Mizokami et al., 2017). The sequence of this expected sequence of osteogenic marker expression was observed in our qPCR data for microtissues containing osteogenically induced MSCs, indicating that these microtissue constructs have osteogenic potential which was also verified by our *in vivo* data.

During skeletal development, MSCs differentiate into osteoblast progenitor cells which are capable of proliferating before becoming mature osteoblasts (Beeravolu et al., 2016). Therefore, a potential method for encouraging bone regeneration is to use immature osteoblastic precursors (Aino et al., 2014). In our study, we found that microtissue constructs consisting solely of osteogenically induced MSCs tended to undergo mineralization and osteoblastic maturation earlier *in vivo* with limited proliferation potential, and may not be the ideal candidate for regeneration of large bone defects. The higher proportion of senescent cells in these microtissue constructs can also produce undesirable inflammatory and degenerative effects within the microenvironment and further deter bone regeneration (Ambrosi et al., 2021). On the other hand, mixing osteogenically primed MSCs with their undifferentiated counterparts makes maximum use of both an osteogenic microenvironment created by the osteogenic MSCs, as well as the paracrine anti-inflammatory and pro-regenerative functions of the undifferentiated MSCs. In our study, this approach produced the best bone regeneration outcomes and may provide new ideas for developing engineered bone grafts.

Some limitations of our study should be considered when interpreting the results. The mechanical microenvironment plays an important role during *in vivo* osteogenesis (Giannoudis et al., 2007) and is responsible for directing the structure and orientation of load-bearing for the newly formed bone. In this study, we used a calvarial defect model to demonstrate proof-of-concept which was a non-loadbearing model. The outcomes and mechanisms of bone regeneration using microtissue constructs need to be investigated in a load-bearing bone regeneration model to demonstrate greater physiological relevance. In addition, osteoblastic differentiation is a complex and continuous process that is coordinated by multiple factors with tight temporal control at different stages of differentiation (Lee et al., 2018). In our study, we have not conducted specific characterization of the activity of MSCs within the microtissue constructs to elucidate their contribution to the differentiation process and therefore progressive bone formation. Future studies analyzing the secretome, such as markers of inflammation, or transcriptome of MSCs within microtissue constructs undergoing *in vivo* osteogenesis will provide insights into the activation of relevant signaling pathways and reveal the precise mechanisms of improved bone healing using microtissue constructs with mixed undifferentiated and osteogenically primed MSCs. Nevertheless, our study provides a new therapeutic perspective and may help the further development of cell-based therapies for the effective treatment of clinically encountered bone defects.

Data availability statement

The original contributions presented in the study are included in the article/Supplementary Material, further inquiries can be directed to the corresponding authors.

Ethics statement

The animal study was reviewed and approved by the ethics committee of Peking University People's Hospital.

Author contributions

Conception and design: DX and JL. Implementation the experiments: HL and ZH. Analysis and interpretation of data: all authors. Drafting of the article: HL and JL. Critical revision of the article for important intellectual content: all authors. Final approval of the article: all authors.

Funding

This study was supported by grants from the National Natural Science Foundation of China (81973606), Peking University People's Hospital Scientific Research Development Funds (RDY 2019-11 and RDJP 2022-04), Peking University Medicine Fund of Fostering Young Scholars' Scientific & Technological Innovation (BMU2022PYB004), Beijing Science and Technology Projects (Z181100001818008), and Beijing Natural Science Foundation (L222087, 7214261, and 7212118).

Conflict of interest

The authors declare that the research was conducted in the absence of any commercial or financial relationships that could be construed as a potential conflict of interest.

Publisher's note

All claims expressed in this article are solely those of the authors and do not necessarily represent those of their affiliated organizations, or those of the publisher, the editors and the reviewers. Any product that may be evaluated in this article, or claim that may be made by its manufacturer, is not guaranteed or endorsed by the publisher.

Supplementary material

The Supplementary Material for this article can be found online at: https://www.frontiersin.org/articles/10.3389/fbioe.2022.1069804/full#supplementary-material

References

Ai-Aql, Z. S., Alagl, A. S., Graves, D. T., Gerstenfeld, L. C., and Einhorn, T. A. (2008). Molecular mechanisms controlling bone formation during fracture healin g and distraction osteogenesis. *J. Dent. Res.* 87 (2), 107–118. doi:10.1177/154405910808700215

Aino, M., Nishida, E., Fujieda, Y., Orimoto, A., Mitani, A., Noguchi, T., et al. (2014). Isolation and characterization of the human immature osteoblast cultur e system from the alveolar bones of aged donors for bone regeneration therapy. *Expert Opin. Biol. Ther.* 14 (12), 1731–1744. doi:10.1517/14712598.2014.960387

Ambrosi, T. H., Marecic, O., McArdle, A., Sinha, R., Gulati, G. S., Tong, X., et al. (2021). Aged skeletal stem cells generate an inflammatory degenerative niche. *Nature* 597 (7875), 256–262. doi:10.1038/s41586-021-03795-7

Antonova, E., Le, T. K., Burge, R., and Mershon, J. (2013). Tibia shaft fractures: costly burden of nonunions. *BMC Musculoskelet. Disord.* 14, 42. doi:10.1186/1471-2474-14-42

Arinzeh, T. L., Peter, S. J., Archambault, M. P., Van Den Bos, C., Gordon, S., Kraus, K., et al. (2003). Allogeneic mesenchymal stem cells regenerate bone in a critical-sized canine segmental defect. The Journal of bone and joint surgery. *J. Bone Jt. Surgery-American Volume* 85 (10), 1927–1935. doi:10.2106/00004623-200310000-00010

Beeravolu, N., Khan, I., McKee, C., Dinda, S., Thibodeau, B., Wilson, G., et al. (2016). Isolation and comparative analysis of potential stem/progenitor cells from different regions of human umbilical cord. *Stem Cell Res.* 16 (3), 696–711. doi:10.1016/j.scr.2016.04.010

Bhattacharjee, A., Kuiper, J. H., Roberts, S., Harrison, P. E., Cassar-Pullicino, V. N., Tins, B., et al. (2019). Predictors of fracture healing in patients with recalcitrant nonunions treated with autologous culture expanded bone marrow-derived mesenchy mal stromal cells. *J. Orthop. Res.* 37 (6), 1303–1309. doi:10.1002/jor.24184

Giannoudis, P. V., Einhorn, T. A., and Marsh, D. (2007). Fracture healing: The diamond concept. *Injury* 38, S3–S6. doi:10.1016/s0020-1383(08)70003-2

Gómez-Barrena, E., Rosset, P., Lozano, D., Stanovici, J., Ermthaller, C., and Gerbhard, F. (2015). Bone fracture healing: Cell therapy in delayed unions and nonunions. *Bone* 70, 93–101. doi:10.1016/j.bone.2014.07.033

Kuttappan, S., Mathew, D., and Nair, M. B. (2016). Biomimetic composite scaffolds containing bioceramics and collagen/gelatin for bone tissue engineering - a mini review. *Int. J. Biol. Macromol.* 93, 1390–1401. doi:10.1016/j.ijbiomac.2016.06.043

Lee, J., Byun, H., Madhurakkat Perikamana, S. K., Lee, S., and Shin, H. (2018). Current Advances in Immunomodulatory biomaterials for bone Regeneratio n. *Adv. Healthc. Mater.* 8 (4), e1801106. doi:10.1002/adhm.201801106

Liebergall, M., Schroeder, J., Mosheiff, R., Gazit, Z., Yoram, Z., Rasooly, L., et al. (2013). Stem cell–based therapy for prevention of delayed fracture union: A Randomized and Prospective Preliminary study. *Mol. Ther.* 21 (8), 1631–1638. doi:10.1038/mt.2013.109

McKee, M. D., and Nanci, A. (1996). Osteopontin: An Interfacial extracellular matrix protein in mineralize d tissues. *Connect. Tissue Res.* 35 (1-4), 197–205. doi:10.3109/03008209609029192

Mizokami, A., Kawakubo-Yasukochi, T., and Hirata, M. (2017). Osteocalcin and its endocrine functions. *Biochem. Pharmacol.* 132, 1–8. doi:10.1016/j.bcp.2017.02.001

Nakashima, K., Zhou, X., Kunkel, G., Zhang, Z., Deng, J. M., Behringer, R. R., et al. (2002). The novel zinc finger-containing transcription factor osterix is required for osteoblast differentiation and bone formation. *Cell* 108 (1), 17–29. doi:10.1016/s0092-8674(01)00622-5

Rupp, M., Biehl, C., Budak, M., Thormann, U., Heiss, C., and Alt, V. (2018). Diaphyseal long bone nonunions — Types, aetiology, economics, and treatment recommendations. *Int. Orthop.* 42 (2), 247–258. doi:10.1007/s00264-017-3734-5

Scarano, A., Crincoli, V., Di Benedetto, A., Cozzolino, V., Lorusso, F., Podaliri Vulpiani, M., et al. (2017). Bone regeneration induced by bone Porcine Block with bone marrow Strom al Stem cells in a Minipig model of Mandibular "critical size" defect. *Stem cells Int.* 2017, 1–9. doi:10.1155/2017/9082869

Shang, F., Yu, Y., Liu, S., Ming, L., Zhang, Y., Zhou, Z., et al. (2021). Advancing application of mesenchymal stem cell-based bone tissue regen eration. *Bioact. Mater.* 6 (3), 666–683. doi:10.1016/j.bioactmat.2020.08.014

Venkataiah, V. S., Yahata, Y., Kitagawa, A., Inagaki, M., Kakiuchi, Y., Nakano, M., et al. (2021). Clinical applications of cell-scaffold constructs for bone Regeneratio n therapy. *Cells* 10 (10), 2687. doi:10.3390/cells10102687

Vimalraj, S. (2020). Alkaline phosphatase: Structure, expression and its function in bone m ineralization. *Gene* 754, 144855. doi:10.1016/j.gene.2020.144855

Wang, Y-G., Qu, X-H., Yang, Y., Han, X. g., Wang, L., Qiao, H., et al. (2016). AMPK promotes osteogenesis and inhibits adipogenesis through AMPK-Gfi1-OPN axis. *Cell. Signal.* 28 (9), 1270–1282. doi:10.1016/j.cellsig.2016.06.004

Xing, D., Liu, W., Li, J. J., Liu, L., Guo, A., Wang, B., et al. (2020). Engineering 3D functional tissue constructs using self-assembling cell-laden microniches. *Acta Biomater.* 114, 170–182. doi:10.1016/j.actbio.2020.07.058

Yu, X., Tang, X., Gohil, S. V., and Laurencin, C. T. (2015). Biomaterials for bone regenerative engineering. *Adv. Healthc. Mater.* 4 (9), 1268–1285. doi:10.1002/adhm.201400760

Yuh, D-Y., Maekawa, T., Li, X., Kajikawa, T., Bdeir, K., Chavakis, T., et al. (2020). The secreted protein DEL-1 activates a β3 integrin-FAK-ERK1/2-RUNX2 pa thway and promotes osteogenic differentiation and bone regeneration. *J. Biol. Chem.* 295 (21), 7261–7273. doi:10.1074/jbc.ra120.013024

Zura, R., Mehta, S., Della Rocca, G. J., and Steen, R. G. (2016). Biological Risk factors for Nonunion of bone fracture. *JBJS Rev.* 4 (1), e5. doi:10.2106/jbjs.rvw.o.00008

frontiers | Frontiers in Bioengineering and Biotechnology

TYPE Review
PUBLISHED 23 December 2022
DOI 10.3389/fbioe.2022.1069932

OPEN ACCESS

EDITED BY
Yansong Qi,
Inner Mongolia People's Hospital, China

REVIEWED BY
Jie Yang,
Tianjin University, China
Aleksandr Urakov,
Izhevsk State Medical Academy, Russia
Paolo Mercorelli,
Leuphana University Lüneburg, Germany

*CORRESPONDENCE
Zhiming Song,
zmsong@jlu.edu.cn
Yuhao Zheng,
zhengyuh@jlu.edu.cn

SPECIALTY SECTION
This article was submitted to Biomaterials, a section of the journal Frontiers in Bioengineering and Biotechnology

RECEIVED 14 October 2022
ACCEPTED 09 December 2022
PUBLISHED 23 December 2022

CITATION
Wang C, Xu P, Li X, Zheng Y and Song Z (2022), Research progress of stimulus-responsive antibacterial materials for bone infection.
Front. Bioeng. Biotechnol. 10:1069932. doi: 10.3389/fbioe.2022.1069932

Research progress of stimulus-responsive antibacterial materials for bone infection

Changqing Wang, Peng Xu, Xiaoxu Li, Yuhao Zheng* and Zhiming Song*

Department of Sports Medicine, Orthopaedic Center, The First Hospital of Jilin University, Changchun, China

Infection is one of the most serious complications harmful to human health, which brings a huge burden to human health. Bone infection is one of the most common and serious complications of fracture and orthopaedic surgery. Antibacterial treatment is the premise of bone defect healing. Among all the antibacterial strategies, irritant antibacterial materials have unique advantages and the ability of targeted therapy. In this review, we focus on the research progress of irritating materials, the development of antibacterial materials and their advantages and disadvantages potential applications in bone infection.

KEYWORDS

stimulus response, infection, antibiotics, nanomaterials, metal nanoparticles, antimicrobial peptides, drug resistance

1 Introduction

Bacterial infection was an important challenge in the fields of medicine, environment or food, etc. Antibiotics play an indelible role as an important drug to control infection. However, the resistance of bacteria to antibiotics is gradually increasing, due to the previous neglect of drug management (Rasigade and Vandenesch, 2014; Tacconelli et al., 2018). Methicillin-resistant *Staphylococcus aureus*, vancomycin intermediate *Staphylococcus aureus*, vancomycin-resistant enterococci and *Clostridium* labile are common species with antibiotic resistance (AMR) or multiple drug resistance (MDR). According to the statistics from World Health Organization (WHO), lower respiratory tract infection was the fourth leading cause of death, from 2000 to 2019. AMR is one of the greatest dangers to global health and development. Bacterial infection can lead to sepsis, bacteremia and even death. By 2050, 10 million people are expected to die from diseases caused by bacteria and other microbial infections (da Rosa et al., 2020).

Compared with other infections, bone tissue infections are more difficult to diagnose and treat, especially those involving bone related implants (Tande Aaron and Patel, 2014). The main infection routes of osteomyelitis, purulent arthritis and implant related infection are blood borne, adjacent tissue infection, or infection after trauma, surgery or foreign body implantation (such as joint replacement) (Brady et al., 2006; Wright and Nair, 2010). In orthopedic implant infection, *staphylococcus* infection accounts for two-thirds of all pathogen infections. Implant infection is prone to repeated infection, leading

to chronic bone infection. It is unlikely to rely solely on antibiotic treatment, which is more difficult to cure than other infections. Many bone infections still require antibiotic treatment for 4–6 weeks after surgical debridement (Marculescu et al., 2006; Del Pozo and Patel, 2009; Lee et al., 2010). Bone loss is a major complication of osteomyelitis. The osteoclast precursor of bone marrow is induced to differentiate into active macrophages by live *Staphylococcus aureus*, and secretes many proinflammatory cytokines. These cytokines can enhance the bone absorption capacity of mature osteoclasts and promote the differentiation of uninfected osteoclasts (Trouillet-Assant et al., 2015).

Bone infection can be caused by continuous transmission of surrounding tissues, direct bone trauma caused by surgery or injury, or blood borne transmission caused by systemic bacteremia. It is still a major medical burden. In the United States, there are about 22 cases per 100,000 people, and the incidence rate has been rising, especially among the elderly and diabetes patients. The infection of bone is mainly due to the destruction of the Haves system, the loss of blood supply support and necrosis of bone, the inability to remove bacteria, the formation of pus cavity or bone erosion, resulting in prolonged healing and repeated attacks. Soft tissue infection mainly occurs in areas with sufficient blood supply. The pus can be drained out through surgery or the granulation tissue can be promoted by changing the dressing. The granulation tissue with blood supply can be cured when it grows and heals.

At present, there are two main strategies to deal with infection: One is to build an antifouling surface to resist the adhesion of bacteria, and the other is to use fungicides to kill bacteria (Campoccia et al., 2013; Berne et al., 2018). Bacteria can produce extracellular matrix on the contact surface to form a biofilm to protect themselves, which usually requires 10 to 1,000 times the concentration of antibiotics to completely remove the bacteria (Yang et al., 2012; Wang et al., 2016). Bacteria that produce biofilms are resistant to antibiotics, which explains the root cause why biofilm removal is difficult. The uptake of nutrients by the outer layer of the biofilm is faster than that of the inner layer, and it has higher metabolic activity and faster growth rate, which makes it more difficult to develop effective antibiotics. The biofilm outer layer cells take in nutrients faster than the inner layer cells, and have higher metabolic activity and faster growth rate, which makes it more difficult to develop effective antimicrobials (Werner et al., 2004; Stewart and Franklin, 2008).

In the 1970s, the stimulus response system was first introduced, beginning with the use of locally released drugs from thermosensitive liposomes (Wang et al., 2018). In recent years, due to the sensitivity to external environmental signals or pathological abnormalities, the release rate of antimicrobials was adjusted when needed to effectively kill bacteria. Irritant response materials have made great progress in the field of antimicrobials (Lu et al., 2016; Wei et al., 2017). This review mainly introduces the source and research progress of irritating materials, the development of antibacterial materials and their advantages and disadvantages.

2 Stimulus-responsive antibacterial material

In the last century, people began to make and utilize stimulus-responsive systems. In the seventies, it has been reported that by heating neomycin-containing liposomes to their phase transition temperature to control the release of antibacterial drugs, inhibit the protein synthesis of *E. coli* and kill bacteria (Kim et al., 2017). Thermally responsive stimulation systems have evolved in subsequent studies and mainly include polymer-solvent mixtures transitioning from single-phase systems at low temperatures to two-phase systems at high temperatures and polymer-solvent mixtures transitioning from two-phase systems at low temperatures to single-phase at high temperatures (Schmaljohann, 2006; Zhao et al., 2019). In the early 20th century, von Tappeiner described the principles that underlie photodynamic therapy (PDT) (Felsher, 2003; Li et al., 2018a). Due to the lack of an ideal molecular photosensitizer and an efficient activation process, the full ideal of PDT has not yet been realized (Lovell et al., 2010). Through so many years of development, many nanodelivery systems have been designed to overcome these problems (Lucky et al., 2015; Li et al., 2018a). PDT is highly efficient, spatiotemporal selective, not easy to produce drug resistance, and its killing effect is limited to tens of nanometers. However, most current PDT systems promote the formation of ROS through type II mechanisms, which makes the activation of PDT systems very dependent on oxygen (Mukai et al., 2018). In recent years, some scholars have also studied the use of type I mechanism photosensitizers to reduce dependence on oxygen (Huynh and Zheng, 2013; Li et al., 2018b). Due to the composition of multiple components, especially materials with low biocompatibility, most PDT systems require cumbersome toxicity studies and complex manufacturing procedures, and clinical application is still a difficult challenge. Magnetic drug-controlled delivery was first proposed in the 80s of the last centuries (Williams et al., 2009; Price et al., 2018). In later developments, more versatile magnetic probes were developed that allowed for a combination of diagnosis and treatment, including targeted drug delivery and drug delivery, among others (Peng et al., 2017; Tang et al., 2018). The magnetic field is largely unabsorbed by tissue, penetrates deeper than infrared and visible light, and philately is easy to use and the ability to target carriers deeper into tissues (Kumar and Mohammad, 2011; Owen et al., 2012). External magnetic fields can increase heat in magnetic nanoparticles for local hyperthermia, or increase polymer permeability to the matrix or disrupt temperature-sensitive drug envelopes to induce drug release (Kumar and Mohammad, 2011; Thirunavukkarasu et al., 2018). However, using an external magnet to attract a magnetic

drug carrier is difficult to accurately locate to an area below 5 cm under the skin, and there is a lack of mechanism for delivery to the depths of the body (Shapiro, 2009; Price et al., 2018). In the 90s, pH response systems have reported that when ionizable groups are attached to polymers, they cause conformational changes in soluble polymers as well as changes in hydrogel swelling (Nakamae et al., 1992; Miyata et al., 1994; Nakamae et al., 1997). pH differences between tissues have been widely used in the design of pH-sensitive drug delivery systems in stimuli-responsive drug delivery systems for their thermal/chemical stability, polymer species morphology, and biocompatibility (Nakamae et al., 1992; Zhu and Chen, 2015; Shin et al., 2021). At the beginning of the 21st century, polymers with enzyme-responsive systems have been considerably developed in the field of hydrogels and nanoparticles (Ulijn, 2006; Ghadiali and Stevens, 2008; Hahn and Gianneschi, 2011). As a key component of bionanotechnology, enzymes have excellent biorecognition capabilities and excellent catalytic performance, and the combination of enzymes and nanomaterials has been successfully used in diagnosis and drug treatment (Andresen et al., 2005; Minelli et al., 2010). The precise identification of substrates by enzymes can effectively reduce the amount of drugs used and thus reduce the toxicological effects of drugs without ensuring efficacy (Minelli et al., 2010). Over the past 20 years, great progress has been made in the development of redox-responsive nanocarriers, typically glutathione-responsive nanocarriers (Cheng et al., 2011; Lee et al., 2013). As an ideal internal stimulator, glutathione can be used for the rapid unstable resolution of intracellular nanocarriers, and this method of drug delivery acting on intracellular cells is beneficial to overcome multidrug resistance and reduce drug side effects (Li et al., 2020a). In the 90s, there was an interest in precisely controlled drug delivery by electrical stimulation (Pernaut and Reynolds, 2000; Murdan, 2003; Abidian et al., 2006). Compared to other stimuli, electrical stimulation can be applied to biological systems quickly, reversibly and locally. Thanks to the development of MEMS, implantable devices can shine in controlled drug release (Schmidt et al., 2010). Stimulus-responsive materials are divided into endogenous and exogenous response systems. According to the type of response factors, the endogenous stimulus response system is divided into PH responsiveness, redox sensitivity, enzyme responsiveness, etc. Exogenous stimulus response system includes light sensitivity, ultrasonic trigger, magnetic trigger, electrical trigger, etc. Multiple stimulus response systems have developed rapidly in recent years, such as: topologically integrating temperature-responsive Nisopropylacrylamide (NIPAM), photoresponsive azobenzene/cyclodextrin (Azo/CD) complex, hydrophilic PHEMA segments, and nanobactericides (AgNPs) on one single substrate (Ni et al., 2021). The antibacterial substances in the stimulus response system are constantly updated and optimized. Now the mainstream antibacterial substances are antibiotics, metal nanomaterials, cationic antimicrobial agents and antimicrobial enzymes, each of which has its own advantages and disadvantages. Stimulus-responsive materials have good development and application prospects in the field of medicine, such as medical equipment, drug delivery, therapeutic diagnostics, tissue engineering, etc. (Smith et al., 2012; Duque Sanchez et al., 2016; Gao et al., 2017; Morgese et al., 2018; Zhou et al., 2018; Xue et al., 2019) The stimulus response system is shown in Table 1.

2.1 Endogenous stimulus response system

2.1.1 Enzyme responsive material

In the past 10 years, enzyme responsive polymers have made great progress, Many enzymes have been used in the design of antimicrobial stimuli responsive drugs (Ma et al., 2020a), such as, lipase, phosphatase, protease, etc. As the most important catalytic substance in the body, enzymes play an important role in a series of physiological processes, and their expression levels will also change in the state of disease. The high selectivity and biocompatibility of enzyme responsive materials determine that they can play a role in many biomedical applications. As the original trigger factor, the change of specific enzyme expression level can cause enzyme responsive biomaterial reaction and control the release of antibacterial drugs at the required sites, so as to kill bacteria。Enzymes are highly expressed in the infected site, and some specific enzymes were used to identify stimuli, thus achieving the release of antibacterial substances (Wei et al., 2022). Glutamyl endonuclease (V8 enzyme) is a product of *Staphylococcus aureus*. Ag nanoparticles were encapsulated in mesoporous silica nanoparticles (MSN), and then poly L-glutamic acid (PG) and polyallylamine hydrochloride (PAH) were assembled layer by layer on MSN-Ag to form LBL@MSN-Ag nanoparticles. When V8 enzyme cleaves the PG amide bond, the Ag ion in the polymer is released, thus killing bacteria at the bacterial infection site (Ding et al., 2020), as shown in Figure 1A. Through the reaction with the substrate, the enzyme achieves the precise location of bacteria and control the release of antimicrobials, thus killing bacteria (Hu et al., 2012; Haas et al., 2015; Zuo et al., 2020). It is also a good strategy to kill drug-resistant bacteria. In addition to specific enzymes, wound infection causes macrophages to accumulate and secrete cholesterol esterase cholesterol esterase (CE) in the wound, which catalyze the hydrolysis of ester bonds to sterols and fatty acids, and be used to prepare enzyme-responsive antibacterial materials (Ye et al., 2020), as shown in Figure 1B.

Most *Staphylococcus aureus*, some *Escherichia coli* and *Pseudomonas aeruginosa* can produce lipase and connect ciprofloxacin to the surface of polyethylene glycol (PEG) by anhydride, which shows good biocompatibility in physiological conditions. Once a bacterial infection occurs, the

TABLE 1 Stimulus response materials.

Response type (material)	Loading drugs	Loading pathway	Biological evaluation	Reference
Glutamyl endonuclease	AgNPs encapsulated by mesoporous silica nanoparticles (MSN) (MSN-Ag)	Physical encapsulation	***In vitro.*** (*Staphylococcus aureus*) and *in vivo* (rat)	Ding et al. (2020)
serine protease-like B enzyme proteins (SplB)	$AgNO_3$	Physical encapsulation	***In vitro.*** (MRSA) and *in vivo* (rat MRSA infection model)	Zuo et al. (2020)
Lipase	Vancomycin	Physical encapsulation	***In vitro.*** (*Staphylococcus aureus*)	Xiong et al. (2012)
β-lactamase	Nanoparticles (AgNPs, etc.)	Physical encapsulation	***In vitro.*** (*Staphylococcus aureus*, *Klebsiella pneumoniae*, *Pseudomonas aeruginosa*, cloaca and *Bacillus cereus*)	Alkekhia et al. (2022)
polyDVBAPS	TCS (triclosan)	Drug binding	***In vitro.*** (*Escherichia coli* and *Staphylococcus aureus*)	Wang et al. (2019)
polyDVBAPS	AgNPs	Physical encapsulation	***In vitro.*** (*Escherichia coli* and *Staphylococcus aureus*)	Zhang et al. (2018)
Salt responsiveness	Poly (trimethylamino) ethyl methacrylate (pTMAEMA)	Drug binding	***In vitro.*** (*Staphylococcus epidermidis Escherichia coli*)	Huang et al. (2019)
human cathelicidin LL-37	Antibacterial peptides (AMP)	Physical encapsulation	***In vitro.*** (*Escherichia coli*)	Gontsarik et al. (2019)
pH-sensitive quaternary pyridinium salt (QPS)	(E)-1-hexadecyl-4-((4-(methacryloyloxy) phenyl)diazenyl)-pyridinium bromide (named Azo-QPS-C16)	Drug binding	***In vitro.*** (*Escherichia coli* and *Mutant streptococci*)	Yang et al. (2018)
poly (N-vinylpyrrolidone-co-N-vinylformamide)	Doxorubicin	Drug binding	***In vitro***	Peng et al. (2019)
Light stimulus response	Reactive oxygen species produced by excitation (ROS)	Drug binding or physical encapsulation	***In vitro.*** (*Escherichia coli*)	Chong et al. (2012)
phthalocyanine molecules (NanoPcA)	Reactive oxygen species produced by excitation (ROS)	Drug binding	***In vitro.*** (*Escherichia coli* and *Staphylococcus aureus*)	Li et al. (2018b)
P(BMA-co-AAm-co-MAA)	AgNPs and ofloxacin	Physical encapsulation	***In vitro***	Amoli-Diva et al. (2017)
PEDOT		Drug binding	***In vitro.*** (*Salmonella typhimurium*)	Gomez-Carretero et al. (2017)
Magnetic stimulus response	Isoniazid (INH)	Physical encapsulation	***In vitro***	Zhao et al. (2017)
Fe3O4 MNP	Vancomycin	Physical encapsulation	***In vitro***	Harris et al. (2017)

Poly DVBAPS: poly (3-(dimethyl (4-vinylbenzyl) ammonio) propyl sulfonate). P (BMA-co-AAm-co-MAA): poly butyl methacrylate-co-acrylamide-co-methacrylic acid. PEDOT: poly (3,4-ethylenedioxythiophene). MNP: superparamagnetic nanoparticles.

bacteria begin to secrete lipase, and the polymer releases ciprofloxacin, which almost completely kills the bacterial strain at the initial stage of biofilm formation (Hasan et al., 2009; Xiong et al., 2012), as shown in Figure 1C.

The production of β-lactam hydrolase by bacteria is the main cause of bacterial drug resistance, which could be produced by a variety of bacterial pathogens. Maleimide functionalized cephalosporins were used as cross-linking agents by terminal cross-linking polymerization with polyethylene glycol macromonomers, to development of hydrogels for specific degradation of β-lactamases as a platform to trigger drug delivery, which could effective against infection without increasing the dose (Alkekhia et al., 2022), as shown in Figure 1D. Enzyme stimulation response system can overcome the challenges of bacterial drug resistance, controlled release of antibiotics and biofilm formation. It has high histocompatibility and great potential in the field of biomedicine.

2.1.2 Salt responsive material

At the earliest time, some scholars studied the ability of zwitterionic polymers to repeatedly switch from bactericidal cationic form to protein repellent zwitterionic form under

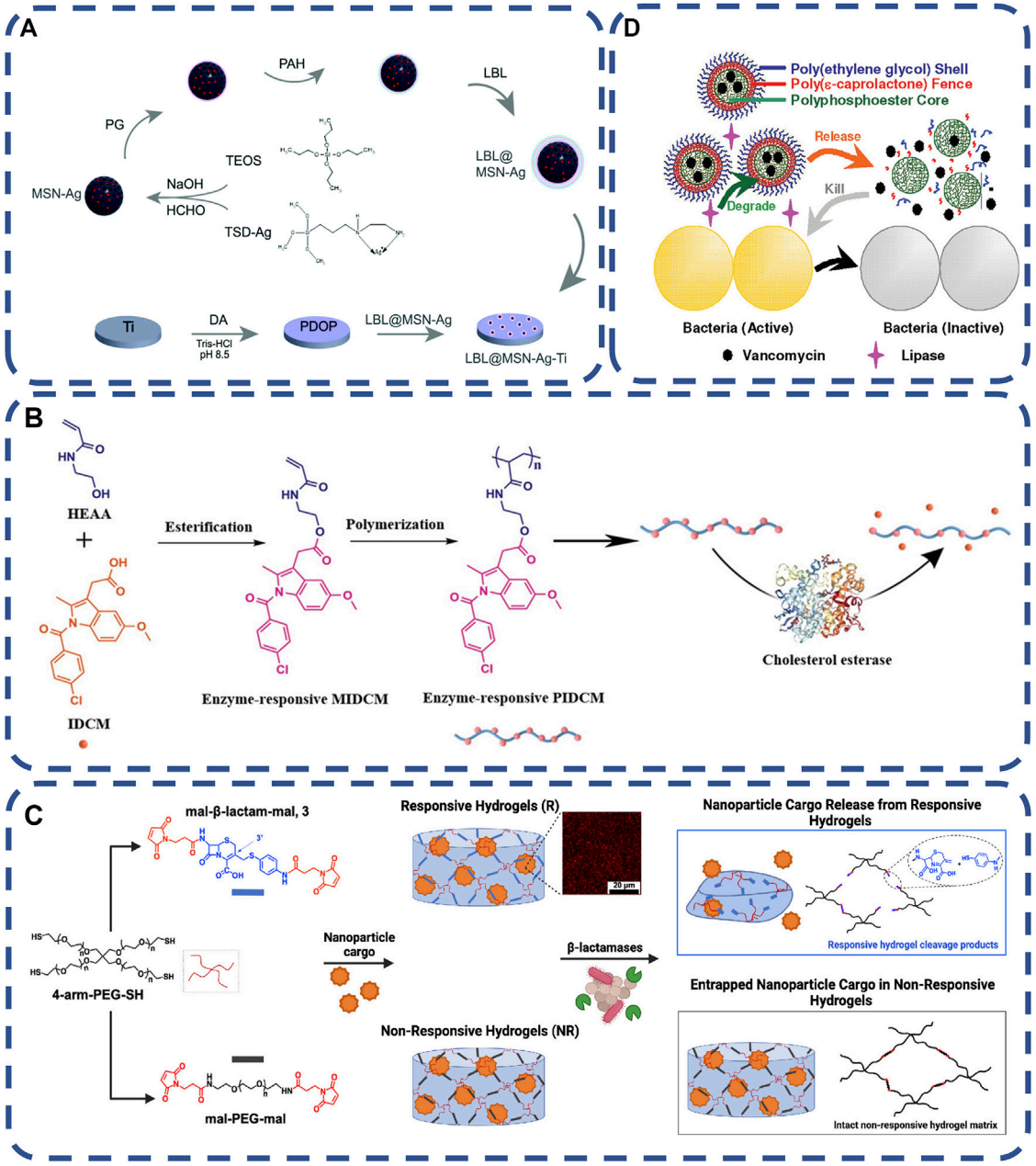

FIGURE 1
(A) schematic diagram of preparation process of LBL@MSN-Ag modified Ti substrate (Ding et al., 2020). Copyright 2020, Biomater Sci. **(B)** Schematic diagram of on-demand drug delivery triggered by bacterial lipase in the treatment of bacterial infection using polymerized three-layer nanogels (TLN) (Xiong et al., 2012) Copyright 2012, J Am Chem Soc. **(C)** Schematic Representation of β-Lactamase-Responsive (R) Hydrogel Fabrication *via* Thiol–ene Michael-Type Addition, β- The hydrolysis of lactam leads to the splitting of the main chain of the polymer, which releases nanomaterials, and the manufacturing process and stability of unresponsive hydrogels (Alkekhia et al., 2022) Copyright 2022, ACS Appl Mater Interfaces. **(D)** Schematic showing the synthesis procedures of the enzyme-responsive prodrug that allows for the triggered release of indomethacin (Ye et al., 2020). Copyright 2020, Macromol Biosci.

controlled switching in alkaline/acidic solutions (Cao et al., 2012). Later, more and more researchers began to pay attention to the development of materials based on this strategy. In recent years, the research on the sterilization and release of salt responsive materials has made progress. The regenerative surface of polyampholytic ions shows a transition between the repulsive state of biomolecules and the adhesion state of biomolecules when the counter ion type and the

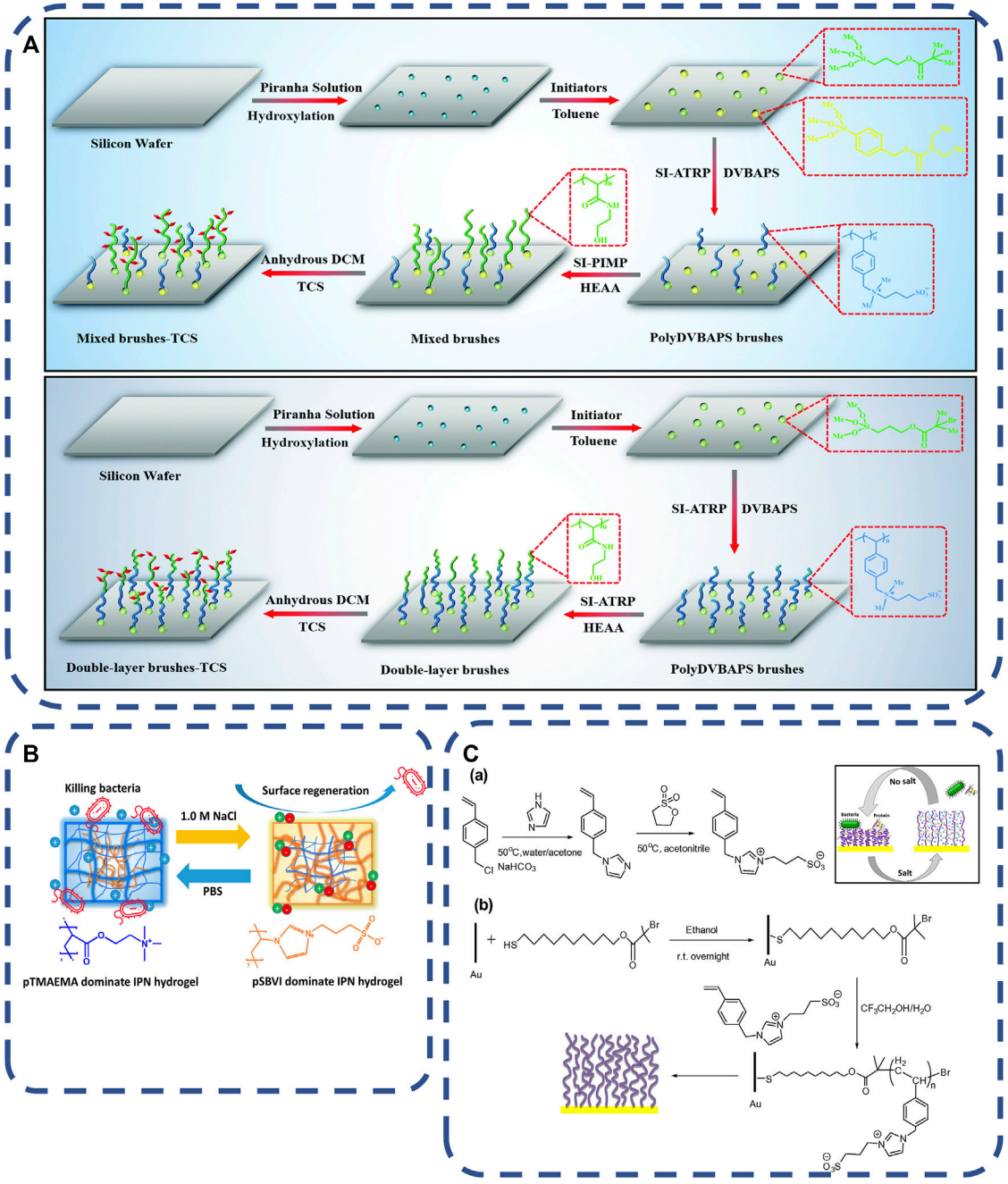

FIGURE 2
(A) Schematic of the two types of antibacterial polymer brushes with hierarchical structures of a mixed polyDVBAPS/polyHEAA brush and a double-layer poly (DVBAPS-b-HEAA) brush (Wang et al., 2019). Copyright 2019, J Mater Chem B. **(B)** schematic diagram of exchangeable salt to kill bacteria and IPN hydrogel to release bacteria in PBS and NaCl solutions (Huang et al., 2019). Copyright 2019, Biomacromolecules. **(C)** (a) Synthesis of VBIPS monomer in response to salt and (b) schematic diagram of SI-ATRP process by brushing the poly vein double shrinkage analyzer to the gold surface coated with fixed initiator (Chen et al., 2016). Copyright 2016, Acta Biomater.

concentration of responsive salts are used (Li et al., 2020b). It is the most commonly used method to achieve sterilization and release functions by introducing bactericides to achieve the regeneration of antibacterial surfaces.

Mainly, Salt-responsive materials are used to eliminate bacteria-release dead bacteria to prevent bacterial attachment and biofilm formation (Sundaram et al., 2014; Wang et al., 2019). In the process of contact killing strategy, the accumulation and

covering of dead bacteria on the antibacterial surface leads to the decrease of antibacterial effect, that develop new materials with dual characteristics of antifouling and antibacterial are necessarily (Blummel et al., 2007; Klein et al., 2011; Ma et al., 2016). Some studies have integrated salt-responsive PolyDVBAPS (poly (3-(dimethyl (4-vinylbenzyl) ammonium) propyl sulfonate), antifouling PolyHEAA (poly (N-hydroxyethyl acrylamide)) and bactericidal TCS (triclosan) onto a single surface. PolyDVBAPS and PolyHEAA were polymerized and grafted onto the substrate in different ways to form two kinds of PlyDVBAPS/Poly (HEAA-G-TCS) with different hierarchical structures, As shown in Figure 2A. The polymer has three functions of preventing bacterial attachment, killing attached bacteria on the germicidal surface and stimulating the response material to release bacteria from the surface, and the salt response material surface has high regeneration ability (Wang et al., 2019). Salt-responsive materials are usually anti-fouling, sterilization, release of three different properties of materials together, have the ability of regeneration and in a short time can play a role for many times (Sundaram et al., 2014; Zhang et al., 2018). However, it is easily affected by the environment, such as electrolyte concentration.

Salt responsive renewable surface is an ideal choice for antibacterial materials. Huang et al. (2019) synthesized salt responsive pTMAEMA/pSBVI hydrogels using antibacterial hydrogel poly (trimethylamino) ethyl methacrylate (pTMAEMA) and antifouling material amphoteric poly (sulfonbutylvinylimidazole) (pSBVI), As shown in Figure 2B. The bactericidal rate and release rate did not show obvious reusability after five germicidal release cycles. As shown in Figure 2C. Chen et al. (2016) issued salt-responsive polymer brushes of poly (3-(1-(4vinylbenzyl)-1H-imidazol-3-ium-3-yl) propane-1-sulfonate) (polyVBIPS) to realize the reversible and repeated switching of protein capture/release and surface wettability in a controllable square. The reversible switching of multiple cycles is shown in the table from ~ 40°to 25°. Here, the collapsed chain conformation is used to achieve surface adhesion at low ionic strength, and the extended chain conformation is used to achieve antifouling performance at high ionic strength.

2.1.3 PH responsive materials

The pH of blood is maintained by the dynamic stability of the concentration of carbon dioxide, bicarbonate and other examples. Under some pathological conditions, tissues will have pH values different from the physiological pH values. The local acidic environment of the infected site is caused by immune reaction and anaerobic glycolysis (Ma et al., 2020b). This feature makes researchers begin to develop pH responsive carriers. pH responsive carriers have been developed earlier in the field of tumor therapy, similar to tumor microenvironment (Kanamala et al., 2016). The microenvironment of the infection site is different from that of normal tissues. Therefore, pH responsive nano carriers also have a greater impact in the field of bacterial infection therapy. The change of pH affects the state of the gel (the transition between gel and solution), significantly. pH response materials can respond to bacterial acids, such as acetic acid, lactic acid and malic acid, etc. In PH response system, polyacrylamide (PAAm) (Lee et al., 2015; Bellingeri et al., 2018; Zhong et al., 2018), tannic acid (TA) (Jing et al., 2019), polyacrylic acid (PAA) (Modarresi-Saryazdi et al., 2018; Raju et al., 2018), polymethacrylic acid (PMAA) (Rasib et al., 2018; Sharpe et al., 2018; Qu et al., 2019) and chitosan (CS) (Zhou et al., 2013) are widely used because of their biocompatibility. Cross-linking agents such as glutaraldehyde, carbodiimide, transglutaminase, Glyoxal and binders with bifunctional groups are commonly used in the chemical modification of hydrogels (Kaul and Amiji, 2005; Lee et al., 2012). They could bind ammonium ions produced by infected bacteria and release antibacterial materials such as antimicrobial peptides (AMP) (Traba and Liang, 2015). Local pH environmental changes trigger structural changes, locally activate the bactericidal effect of antibacterial substances, and improve germicidal efficacy (Gontsarik et al., 2019), as shown in Figure 3A. Yang et al. (2018) reported a new pH-sensitive quaternary pyridine salt (QPS). Its antibacterial activity is enhanced when the low pH value decreases, and the activity can be controlled by regulating pH between four and eight of pH. The compound selectively inhibits the growth of acid-producing bacteria, which could be used to kill acid-producing bacteria and to regulate the pH value of the environment to provide antibacterial protection, as shown in Figure 3B pH responsive polymers were designed to be responsive to a specific range of environmental pH, controlling drug release and killing bacteria only in the target tissue (Du et al., 2010; Liechty et al., 2013; Sim et al., 2017).

In clinical application, pH responds to the direct contact between the outer layer of the germicidal system and the tissue, requiring the outer layer material pH responsiveness, biocompatibility, inner layer response to stimulation and drug adjustable release properties (Lee et al., 2015; Gontsarik et al., 2019). Such as a charge-switchable and pH-responsive nanocomplex is fabricated *via* a facile aqueous one-pot zeolitic imidazolate framework-8 (ZIF8) encapsulation of proteinase K(PK) and photosensitizer Rose Bengal (RB), for enzymatic and photodynamic therapies (PDT) against biofilm infections (Ding et al., 2022). The nanocomposite (PRZ) is negatively charged in physiological environment and becomes positively charged when stimulated by acidic substances. Positive charge can enhance the penetration of PRZ into the biofilm and promote competition and the release of RB. RB produces reactive oxygen species under light to further eliminate the remaining bacteria. pH responsive materials were used for gastrointestinal infections, wound healing, treatment of osteomyelitis and implantable medical devices

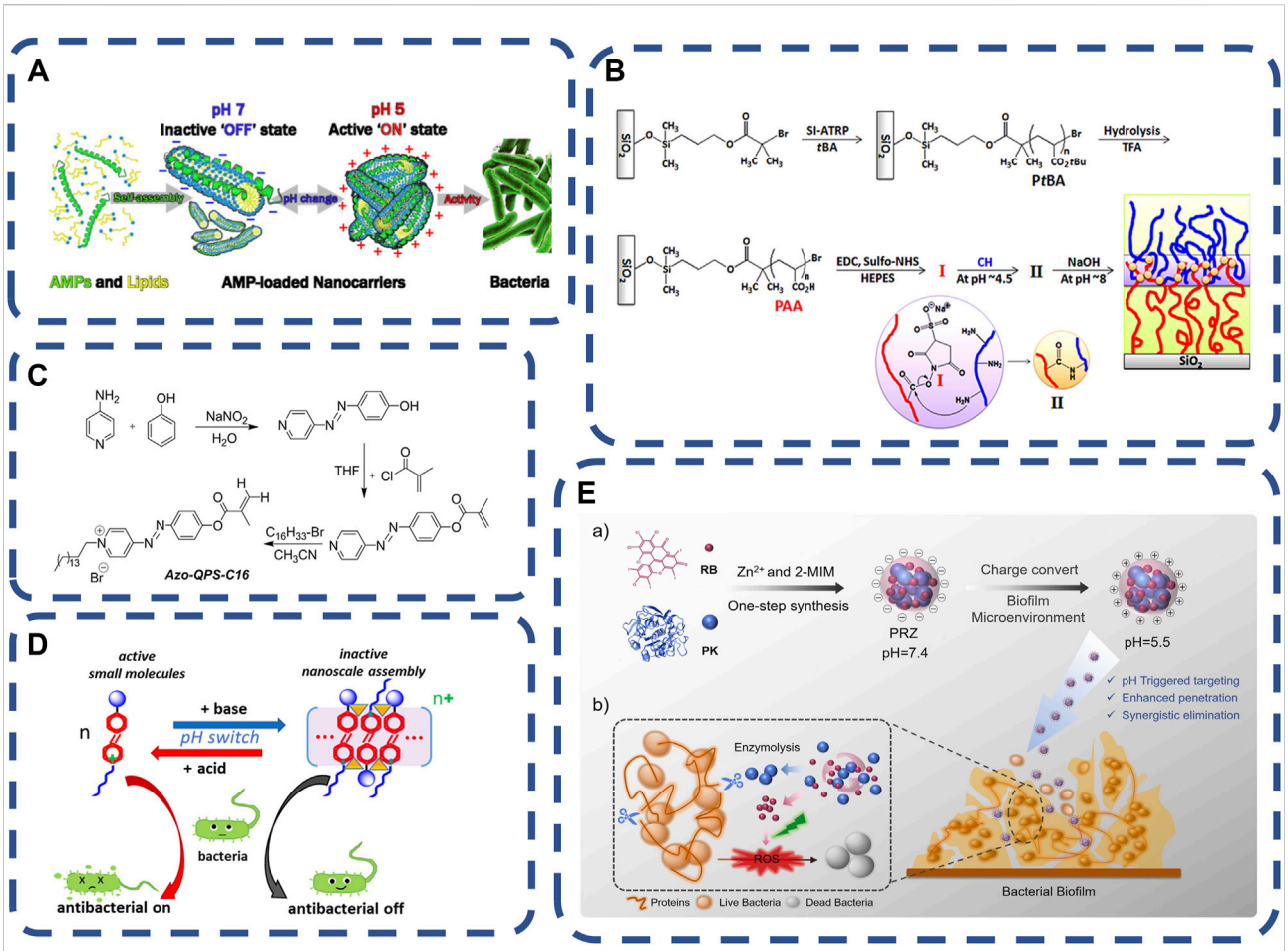

FIGURE 3
(A) Amphiphilic antimicrobial peptides are transformed from core-shell cylindrical micelles with a cross-sectional diameter of 5.5 nm and a length of 23 nm at pH 7.0 to branched chain linear micelle aggregates at pH 5.0. At pH 5.0, positively charged LL-37/OA aggregates have high antibacterial activity (Gontsarik et al., 2019). Copyright 2019, ACS Appl Mater Interfaces. **(B)** Synthesis of pH responsive materials (Lee et al., 2015).Copyright 2015, Biomacromolecules. **(C,D)** pH responds to the characteristics and assembly behavior of azo QPS-C16 (Yang et al., 2018). Copyright 2018, ACS Appl Mater Interfaces. **(E)** Synthesis and mechanism of pH responsive PRZ (Ding et al., 2022) Copyright 2022, ELSEVIER.

(Chung et al., 2014; Lee et al., 2015; Anandhakumar et al., 2016; Yang et al., 2018; Ding et al., 2022), as shown in Figure 3C.

2.1.4 Redox response material

Bacterial infection produces metabolites, such as cysteine, glutathione, etc. In the past 10 years, the development of redox responsive materials has made great progress. Many redox responsive matrices have been developed to extend the cycle time and immediately release drugs at biologically relevant concentrations. Redox responsive nanocarriers can be designed from organic and/or inorganic materials. Inorganic nanomaterials have attracted more attention due to their unique physical and chemical properties and ability to experience the modification process. Liposomes, dendrimers, micelles or protein-based nanomaterials can be used as redox responsive nanocarriers for drug delivery. Some nanocarriers have been approved by the US Food and Drug Administration (FDA) and used in clinical practice. Inflammation lead to a high concentration of reactive oxygen species (ROS) at the infection site. The method of using redox responsive cross-linking agents with various functional groups to manufacture drug delivery carriers through a variety of synthesis strategies has made good progress (Howard et al., 2008). The basic principle is that the redox active substances embedded in the polymerization system will be cleaved by substances such as glutathione (GSH) when they are internalized by cells (Cao et al., 2014; Krisch et al., 2016). Pegylated nanogels are decorated by capturing, adsorbing or covalently grafting PEG chains. Cross-linking agents are the main components in the preparation of redox responsive nanogels, which are generally redox active units containing tellurium bonds, disulfide bonds and diselenide

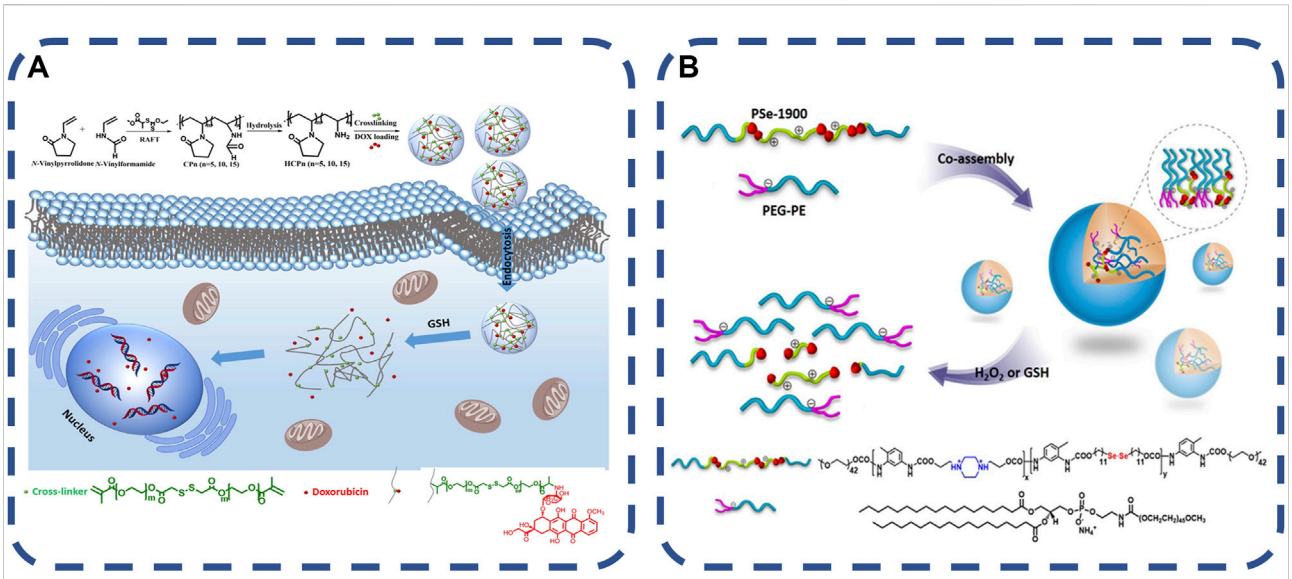

FIGURE 4
(A) redox response. The synthesis of prodrug nanogels is based on amine-functionalized polymers, which are integrated into fine cells in a reduced environment and trigger intracellular drug release (Peng et al., 2019).Copyright 2019, J Colloid Interface Sci. **(B)** Redox responsive co assemblies formed from block copolymers containing selenides and polymer lipids (Wang et al., 2014). Copyright 2014, Langmuir.

bonds, which are broken in response to redox triggers to achieve the effective release and degradation of antibiotics (Ren et al., 2012; Wang et al., 2014; Sun et al., 2017). The synthesis strategies of the polymer (Kumar et al., 2019) are as follows: 1. Free radical polymerization with redox responsive cross-linking agent; 2. Adding redox response cross-linking agent to ring-opening polymerization; 3. Michael Additionreaction method, coupling a large number of nucleophiles with electron-deficient olefins to synthesize a simple and efficient dynamic controlled polymerization of hyperbranched polymers under mild conditions. 4. Self-crosslinking of mercaptan groups. Two polymer chains containing mercaptan (SH) side chains are cross-linked by a simple thiol-disulfide bond exchange reaction to form nanogels. 5. Disulfide crosslinked branched chain nanogels have the potential to be used as redox responsive drug delivery carriers. Peng et al. (2019) synthesized a series of water-soluble poly (N-vinylpyrrolidone-co-N-vinylformamide) copolymers. The copolymers were hydrolyzed under alkaline conditions to obtain primary amine functional reactive copolymers. After that, the copolymer and doxorubicin (DOX) were covalently coupled with the redox response crosslinking agent in the water-in-oil emulsion, and the prodrug nanogels were formed by Michael addition, as shown in Figures 4A, B. The gel has good biocompatibility and sustained drug release. Advanced technologies related to nanosynthesis can provide better drug delivery carriers, which can show their role in the precise location of lesions, and continue to develop towards highly sensitive materials.

2.2 Exogenous stimulus response system

2.2.1 Light/heat triggered material

Photodynamic therapy (PDTA) began to be used for tumor treatment in the last century. In recent years, the drug resistance of traditional antibiotics has become increasingly serious. Due to the advantages of non-invasive and broad antibacterial properties, researchers have paid attention to it and designed a variety of light response systems to achieve on-demand drug release in response to light in specific wavelength areas. Moreover, PDTA has also demonstrated its strong ability to eliminate biofilm, and has now developed into a broad antibacterial system (Misba et al., 2018). Polymer antibacterial materials, light response materials induce antibacterial substances generally have two effective ways: photothermal triggering and photodynamic triggering. Compared with other response materials, the corresponding operation of light is simple, and the irradiation site, time and dose can be controlled, easily (Gohy and Zhao, 2013). Photoresponsive materials can be obtained by introducing photoresponsive groups, but most of the photoresponsive groups are sensitive to ultraviolet rays, such as azobenzene, o-nitrobenzyl ester and so on. Due to the low tissue penetration and phototoxicity of ultraviolet light, it is not suitable for practical application. Visible light and infrared light are more attractive to researchers. And combined with photothermal agent, the thermal stimulation response platform can also be constructed.

Among the available stimuli, non-invasive and essentially clean light is particularly attractive and suitable for biological

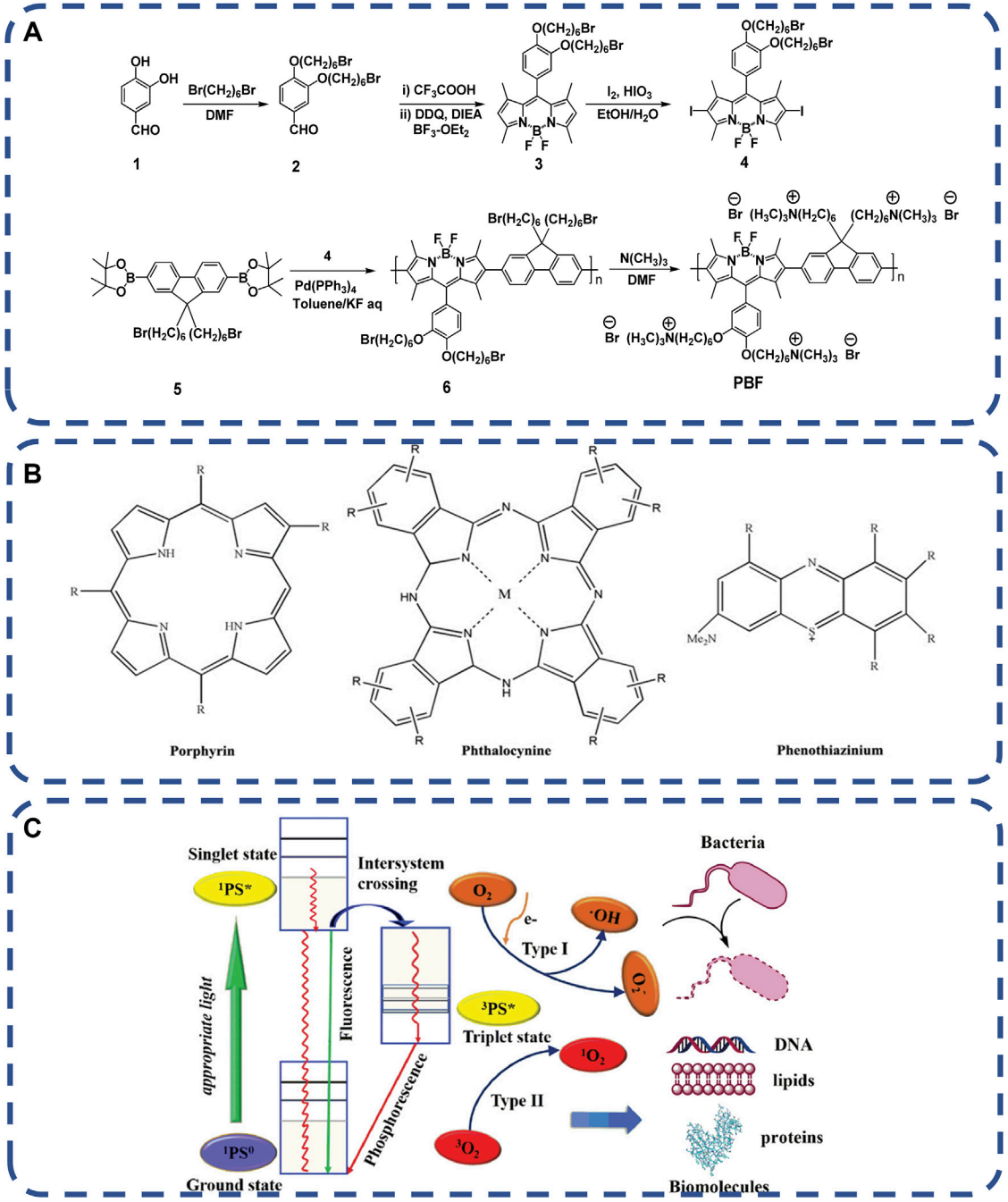

FIGURE 5
(A) Synthesis route of water-soluble polymer PBF (Gontsarik et al., 2019). Copyright 2012, Langmuir. **(B)** The basic chemical structure of classical PS used in PDAT, including porphyrins, phthalocyanines and phenothiazines, and the PDAT mechanism of **(C)** PSs under appropriate light emission (Jia et al., 2019). Copyright 2019, Adv Healthc Mater.

systems without compromising normal function (Browne and Feringa, 2009; Szymanski et al., 2013; Borges et al., 2014; Qu et al., 2015). Photodynamic therapy (APDT) with non-invasive and spectral antimicrobial activity is a traditional technique. Active oxygen (ROS) produced by photosensitizer (PS) kills bacteria. Based on electrostatic interaction, positively charged ionic antimicrobial agents can efficiently destroy negatively charged bacterial cell membranes (Muñoz-Bonilla and Fernández-García, 2012; Xiong et al., 2014; Jiao et al., 2017). Azobenzene (Azo) is one of the commonly used light response molecules, which

reversibly converts between the extended trans form and the dense cis form when exposed to ultraviolet and visible light (Jiao et al., 2017). Chong et al. (2012) synthesized fluorene and boron-dipyrromethene repeat units in the backbones (PBF). PBF can form uniform nanoparticles with disodium salt 3-dithiodipropionic acid (SDPA) through electrostatic interaction in aqueous solution, as shown in Figure 5A. Excited by 400 and 800 nm white light, PBF nanoparticles activate oxygen molecules and produce reactive oxygen species (ROS) to damage biomolecules, such as lipids, DNA and proteins, to quickly kill bacteria and cancer cells. In particular, PDAT does not require specific targeted interactions between photosensitizers (PSS) and bacteria, and bacteria are unlikely to develop drug resistance. The commonly used photosensitizers include macrocyclic compound-based PSs, non-self-quenching PSs, conjugated polymer-based PSs and nano-PSs (Jia et al., 2019), as shown in Figures 5B, C. Xing shuli et al. (Li et al., 2018b) demonstrated that a new phthalocyanine assembly, NanoPcA, has the ability to promote efficient ROS production through class I mechanisms.

Compared with the pure light response group, the photothermal response group is relatively more. APTT refers to photothermal agent (PTA), which converts light energy into heat energy to produce local hyperthermia to cleave the target bacteria (Ray et al., 2012; Pallavicini et al., 2014). The phenomenon of photothermal release is that electrons on the surface of conductive materials convert the light energy absorbed into thermal energy dissipation (Canaparo et al., 2019). Plasma active metal particles are very effective photothermal agents, such as silver nanoparticles, copper nanoparticles and gold nanoparticles. They have controllable optical properties, large light absorption cross section and high efficiency of converting light energy into thermal energy (Jaque et al., 2014). Graphene-based nanomaterials are typical PTA (Fan et al., 2018). Amoli Diva et al. embedded AgNPs into poly (butyl methacrylate-co-acrylamide-co-methacrylic acid) hydrogel to control the release of ofloxacin. The rats were irradiated with 405 nm laser for 15 s at 10, 30 and 50 min. After 70 min, the amount of ofloxacin released from these samples was significantly higher than that of unirradiated samples (Amoli-Diva et al., 2017). Photothermal conversion materials increase the Designability of photoresponsive nanoparticles and fabricate photoresponsive nano-platforms by simply combining photothermal agents and thermal response materials. Photothermal/antimicrobial therapy has great potential in eliminating bacterial infections (Moorcroft et al., 2020; Huang et al., 2022). Compared with other synthesis methods, photochemistry has several key advantages, including fine space-time control, and no need for heating or any solvent. Together with green organic chemistry, this field highlights the great potential of natural compounds (terpenes, polyphenols, polysaccharides, etc.) as cheap, renewable and safe basic materials (Versace et al., 2021). However, in some cases, the high temperature healthy tissue of APTT cannot be tolerated, resulting in healthy tissue damage. In addition, the efficacy of APDT is limited by local oxygen content, and the site of infection is always in anoxic environment. Beside of the combination of APTT or APDT with antimicrobials, the combination of both can also enhance the antibacterial efficacy (Wei et al., 2019).

2.2.2 Electrical stimulation responsive material

In the field of skin and transdermal drug delivery, there have been a large number of literatures on the research of current used *in vivo*, which have determined the safety limit of applied electric field strength (Vanbever and Préat, 1999). Moreover, conductive polymers have been used to detect and regulate bacterial colonization, diagnose bacterial infection and prevent biofilm formation. Electric response delivery systems are often used to release drugs at specific locations and at specific times (Gomez-Carretero et al., 2017; Butina et al., 2019). The release location and drug dosage depend on the implantable polymer or electronic equipment using an external electric field. Compared with other methods, electrical stimulation has the advantages of rapid induction, high controllability of time and space, non-invasive, etc. (Pranzetti et al., 2013; Cantini et al., 2016). Bacteria are sensitive to electrical pulses, and electroactive materials containing specific compounds may allow bacterial biofilms to grow (Czerwinska-Glowka et al., 2021). One of the most studied polymers is poly (3mine4-ethylene dioxythiophene) (PEDOT), which has good environmental and electrochemical stability. When oxidized, PEDOT can promote bacterial adhesion and growth, as well as biofilm formation. This behavior may be caused by the existence of available sites for bacterial electron transfer. On the contrary, the reduced PEDOT film can express antibacterial activity. It is likely that the electron saturation on the surface of PEDOT prevents the electron transfer of bacteria (Pranzetti et al., 2013; Gomez-Carretero et al., 2017), as shown in Figures 6A, B. Because of its good biocompatibility, PEDOT is considered as an ideal candidate for various bioengineering applications. Dominika et al. (Czerwinska-Glowka et al., 2021) added antibiotics (tetracycline, Tc) to poly (3pyr4-ethylene dioxythiophene) (PEDOT) matrix to produce a new coating with obvious antibacterial activity against Gram-negative strains. The polymer can be used as a Tc carrier to participate in the design of powerful antibacterial systems with electrically triggered response, which provides a solid foundation for further medical applications, especially transplantation. The switching mechanism of electrical response to stimulation is based on the skeleton or end group of charged molecules, which has been proved to control the interaction between non-specific and specific biomolecules. Through the study of various dynamic molecular structures, it has become a powerful tool for regulating the interaction between the surface and proteins, bacteria and mammalian cells (Cantini et al., 2016). It is expected to open up new prospects in tissue engineering, drug delivery, biological imaging and regenerative medicine.

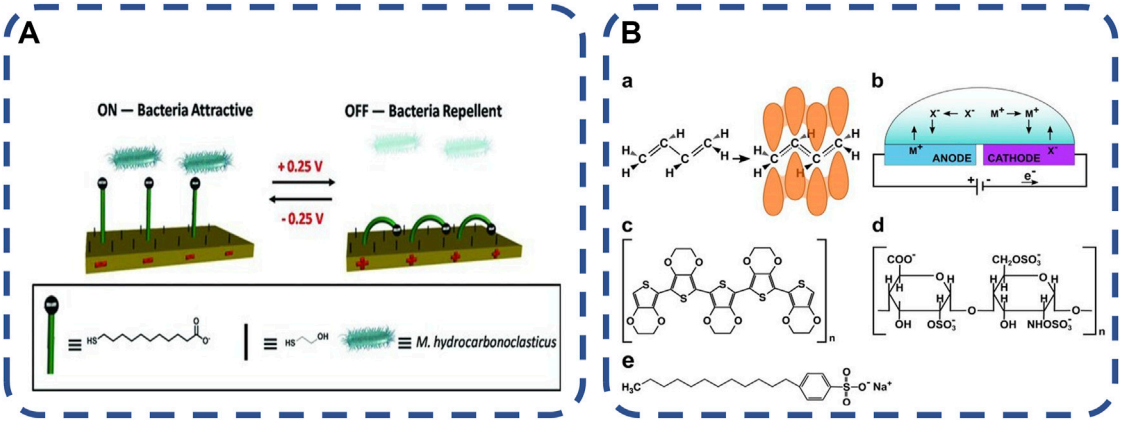

FIGURE 6
(A) Schematic diagram of an electrically switchable two-component SAM, which can switch its molecular conformation reversibly and rapidly according to the applied potential (Pranzetti et al., 2013). Copyright 2013, Adv Mater, **(B)** Chemical structure and electrochemical redox reaction in conductive polymer. a Chemical structure of the conductive polymer polyacetylene (left) and its resonance hybrid (right). b Ion flux in a conductive polymer-based electrochemical cell. m+ and x− represent positively and negatively charged ions, respectively. The blue color of the anode and the purple color of the cathode represent the electrochromic effect occurring in oxidized and reduced conducting polymers. c chemical structure of PEDOT. d chemical structure of heparin. (Gomez-Carretero et al., 2017). Copyright 2017, NPJ Biofilms Microbiomes.

2.2.3 Magnetic responsive material

The literature on the use of magnetic particles in drug delivery experiments first appeared in the 1960s. Freeman et al. (1960) proposed that magnetic nanoparticles can be transported through the blood system and concentrated in specific parts of the body through the external magnetic field. In the later development, some researchers used them in the research of tumors and developed new drug delivery systems containing drugs and magnetic nanoparticles (Hafeli et al., 1994). In recent years, researchers have combined this stimulus response system with infection treatment to develop a local drug delivery system for orthopaedic surgery or post-traumatic infection control (Harris et al., 2017).

In recent years, more and more attention has been paid to magnetic responsive drug delivery system. This is an efficient drug delivery system designed to target the delivery of drugs to specific organs or tissues of the body, improve therapeutic effectiveness and reduce or eliminate adverse drug side effects (Dobson, 2006; El-Husseiny et al., 2011). It is easy to use and easy to target to deeper tissue carriers (Kumar and Mohammad, 2011). The most commonly used superparamagnetic nanoparticles (MNP) in magnetic responsive delivery systems are Fe_3O_4, which can be magnetized under the influence of an external magnetic field for *in vivo* applications. However, the exposed Fe_3O_4 nanoparticles have poor stability and are easy to agglomerate. Therefore, it is a correct choice to choose the nanocomposite carrier with good biodegradability, good mechanical properties and biocompatibility as the matrix for Fe_3O_4 incorporation (Zhao et al., 2017). Hyperbranched polyester HBPE can provide structural support and functionalize Fe_3O_4, thereby improving the dispersion and stability of Fe_3O_4 particles, as shown in Figures 7A, B. Chi lizhao et al. (Zhao et al., 2017) synthesized HBPE-DDSA polymer from dodecenyl succinic anhydride (DDSA) functional group and hyperbranched polyester (HBPE). Then superparamagnetic iron oxide Fe_3O_4 nanoparticles were dispersed in HBPE-DDSA to synthesize magnetic nanocomposites Fe_3O_4/HBPE-DDSA. Finally, Fe_3O_4/HBPE-DDSA was combined with isoniazid. The experimental results show that the nanocomposites show good superparamagnetic behavior, non-toxic and good biocompatibility, and have great potential as targeted drug delivery carriers.

Chitosan is also a magnetic responsive drug carrier. Paramagnetic Fe_3O_4 nanoparticles and antibiotic vancomycin were encapsulated into chitosan beads and crosslinked with polyethylene glycol dimethacrylate of different lengths to obtain magnetic responsive polymers (Harris et al., 2017). 30 min of magnetic stimulation increased the daily drug elution rate of the polymer. Magnetic stimulation can be used to increase drug delivery after implantation to obtain maximum drug concentration or to maintain therapeutic drug levels after controlling the elution rate required by traditional delivery systems, it can be used as a potential infection prevention and treatment device.

2.3 Multiple stimulus responsive antibacterial materials

The multi-stimulus response antibacterial system can detect bacteria in time, respond to bacterial metabolites and release drugs according to the infection site, which improves the germicidal efficacy and biocompatibility (Li et al., 2018c). Many double stimulus or multiple stimulus response materials have been developed. This multiple stimulus response

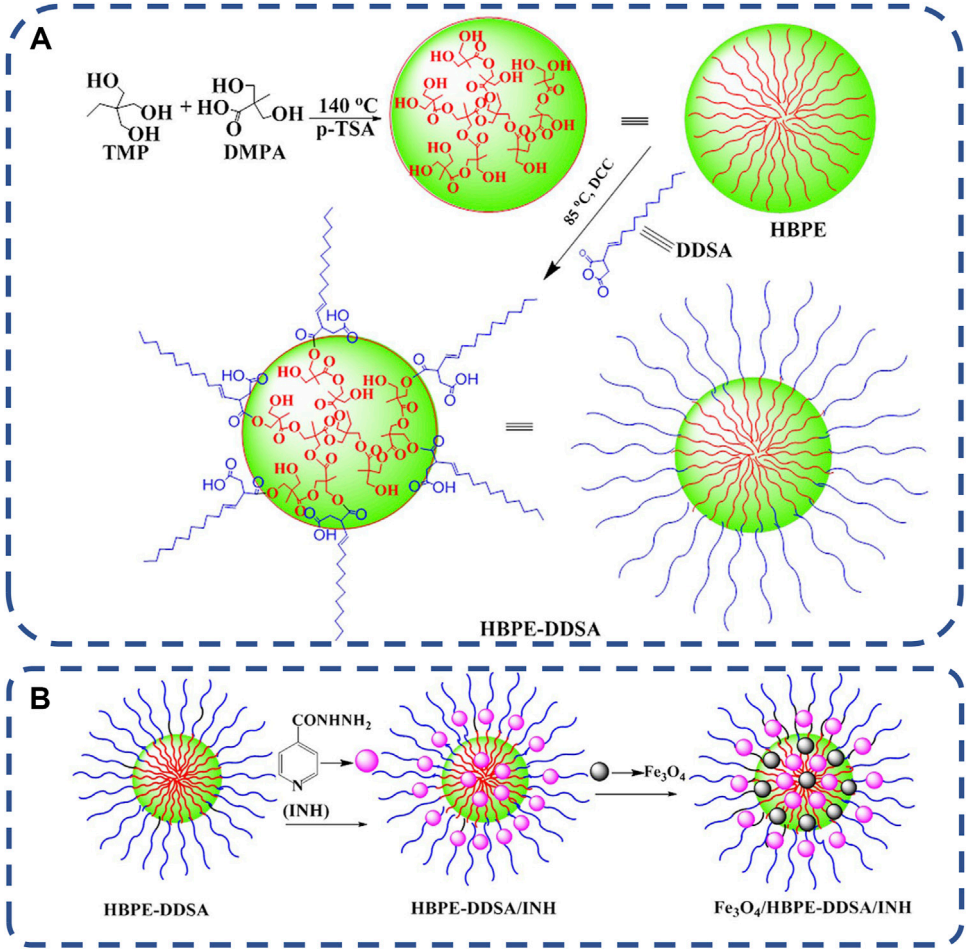

FIGURE 7
(A) Synthetic route of HBPE-DDSA. **(B)** The formation of the nanocomposites of HBPE-DDSA/INH and Fe3O4/HBPE-DDSA/INH (Zhao et al., 2017).Copyright 2017, J Biomater Sci Polym Ed.

antibacterial material has the advantages of drug release and enhancing therapeutic efficacy. Lot's of stimulus-responsive materials showed surface renewable properties through the changes of response light, pH value and temperature because of their interfacial properties (Cole et al., 2007; Zhao et al., 2012).

The dual response of thermal response and pH response can effectively enhance the antibacterial effect of the material and inhibit the attachment of bacteria (Elashnikov et al., 2022). Stimulation-responsive antibacterial nanofibers were prepared by electrospinning poly (caprolactone) (PCL), poly (N-isopropylacrylamide-co-acrylamide) PNIPAm-co-AAm with different concentrations and ciprofloxacin (CIP). The low critical solution temperature (LCST) of PNIPAm-co-AAm was determined by refractometry in distilled water and buffer solution of pH4 and 7.4. The nanofibers showed enhanced release at temperatures lower than LCST. Compared with PCL nanofibers loaded only with CIP, the adhesion of two kinds of bacteria on PCL/PNIPAM-Co-AAM containing CIP decreased significantly. Ni et al. (2021) designed triple functional smart surfaces by topologically integrating temperature-responsive poly (N-isopropylacrylamide) NIPAM, photoresponsive dissociation of azobenzene/cyclodextrin (Azo/CD) complexes, hydrophilic PHEMA fragments and nano-fungicides (AgNPs) on a single substrate. Due to the thermosensitive conformational changes of PNIPAM fragments and the synergy of host-guest interactions between Azo and CD derivatives, it can further release more than 94.9% of previously killed bacteria.

pH and Redox response Materials. The pH values of different organs/tissues were significantly different in the state of disease, and the pH value of extracellular fluid was 7.35–7.45 normally. The pH of different organelles is also slightly different, Golgi 6.4, endosome 5.0–6.0 and lysosome 4.0–5.0 (De Arco et al., 2009). The difference in pH between normal and diseased tissues has been used as a response to stimuli that trigger drug release (Ganta

et al., 2008; Pan et al., 2012). Curcio et al. (2017) prepared pH/redox double-response nanogels (DEX-SS) using methacrylate dextran (DEXMA) and 2-aminoethyl methacrylate (AEMA) as the response part of pH/and N-mathyl-bis (acryloyl) cystamine (BAC) as redox response cross-linking agent. Then loaded with methotrexate (MTX), pH/redox double-response nanogels (DEX-SS) were obtained. GSH released methotrexate (MTX) in the environment of pH 5.0 and 7.4, respectively, which proved the pH and redox response of DEX-SS nanogels. The results showed that the release rate of methotrexate increased by 5 times in acidic environment.

PH and high reactive oxygen species (ROS) dual response materials. Ye et al. (2021) reported a dextran-coated stimulus-responsive nanoparticles (NP) encapsulated with a hydrophobic antibiotic rifampicin. NP showed strong affinity for a variety of pathogens *in vitro* and could effectively accumulate in bacterial infected tissues. NP is activated by low pH and high reactive oxygen species in the infective microenvironment, releasing cationic polymers and rifampicin, which have synergistic activity against AMR pathogens. Poly (β-aminoester)-guanidine-phenylboric acid (PBAE-G-B) polymer with disulfide bond in its main chain is easy to degrade into non-toxic by-products, which further enhances its biocompatibility (Hwang et al., 2011). NP can effectively eliminate biofilm and intracellular infections and resist AMR pathogens *in vitro* and *in vivo*. Shi et al. (2021) developed a novel dynamic hydrogel based on dynamic covalent bond of borate esters using phenylboric acid modified hyaluronic acid (HA-PBA) and polyphenol-tannic acid (TA). Dynamic hydrogels can be used for pH responsive and reactive oxygen species (ROS) responsive release of antibiotics without obvious cytotoxicity and hemolysis and good histocompatibility.

Double response of electricity and pH. The drug release of conductive nanoparticles can be controlled by applying a weak external DC electric field. This method represents a new responsive drug delivery system that effectively controls the time, space and dose of drug release. A drug delivery system based on temperature and electric field stimulation. Qu et al. (2018) proposed an electric field and pH stimulus response system and developed injectable conductive hydrogels with electrical responsiveness, pH sensitivity and inherent antibacterial activity as drug carriers. Chitosan-graft-Polyaniline (CP) copolymer and oxidized dextran (OD) were mixed as crosslinking agents to prepare hydrogels. When the applied voltage increased the release rate of the model drug loaded in CP/OD hydrogel increased significantly. Both chitosan and Polyaniline have inherent antibacterial properties, which make hydrogels have excellent antibacterial properties.

PH/glucose double response. Liang et al. (2022) developed a class of antibacterial hydrogel dressings with good antioxidant capacity, appropriate mechanical properties, good hemostasis and conductivity, and pH/glucose double reactive drug release ability. It is used to repair the wound of exercise-induced diabetic foot. The polymer is based on the double dynamic bond of Schiff base and phenylborate bond. The structure of Schiff base is easy to dissociate under acidic conditions. The competitive binding of phenylboric acid with glucose leads to the dissociation of the coordination structure of catechol and phenylboric acid. This double dynamic bond makes the gel have double reactivity between pH and glucose, which is beneficial to the release of therapeutic drugs (Shan et al., 2017; Shi et al., 2020).

2.4 Antibacterial substances

Bacterial extracellular matrix (ECM) is mainly composed of proteins, extracellular polysaccharides and eDNA polymers (EPS) matrix structure. Provide a barrier for biofilm bacteria to resist the killing of antibiotics, or pump antibiotics through an efflux pump (Limoli et al., 2015). In recent years, for the control of antibiotic drugs, the development of bacterial drug resistance has slowed down, but there is urgent to develop the next-generation of spectral antibiotics or alternative therapy. In this section, we describe the current situation and development prospects of antibiotics.

2.4.1 Antibiotic

Antibiotics have been a popular treatment against bacterial infection in clinic in recent decades, saving countless infected patients. The main categories of antibiotics are β- Lactamides, glycopeptides, macrolides, oxazolidones, amphetamines, lincomamides, fluoroquinolones, nitroimidazoles, lipopeptides and polymyxin, etc. (Singh et al., 2017). β- Lactam antibiotics inhibit cell wall synthesis by combining with a series of enzymes and bacteria, thereby inhibiting bacterial growth. Vancomycin, the representative drug of glycopeptide antibiotics, can bind with d-alanine-d-alanine, the terminal dipeptide of Lipid II, the precursor of bacterial cell wall peptidoglycan chain, thereby preventing cell wall synthesis (Dougherty and Pucci, 2012). Lipopeptides such as daltomycin can be inserted into the cell membrane, leading to cell depolarization and the formation of cell membrane pores, ion leakage and the destruction/rupture of the cell membrane, leading to bacterial death. Aminoglycoside and tetracycline antibiotics bind to 16S rRNA of 30S ribosomal subunit to inhibit bacterial protein synthesis (Armstrong et al., 2012). Macrolide antibiotics bind to 23S rRNA of bacterial 50S ribosomal subunits to inhibit bacterial protein synthesis (Chellat et al., 2016). Oxazolidinone is a kind of synthetic antibacterial agent represented by linezolid, which also binds to 23S rRNA of 50S ribosomal subunit of bacteria to inhibit protein synthesis (Chellat et al., 2016). Quinolones inhibit bacterial growth by inhibiting bacterial DNA helicase, DNA synthetase and topoisomerase IV (Jacoby and Hooper, 2012). For orthopedic infectious diseases, no matter whether

surgical treatment is performed or not, antibiotics are indispensable weapons in the hands of surgeons. Especially for patients infected with drug-resistant bacteria, scientific drug programs should be used to quickly kill possible pathogens and prevent infection complications. For patients infected with drug-resistant bacteria, the following medication principles are generally adopted: 1) When there is an infection beyond the control of an antibiotic and a mixed infection caused by multiple bacteria, combined medication is often required, such as β-lactam antibiotics (penicillin and ceftazidime) inhibit the synthesis of bacterial cell wall, belonging to the bactericide of reproductive period; Aminoglycoside antibiotics (tobramycin and gentamicin) inhibit bacterial protein synthesis, which belongs to the stationary phase bactericide. The combination of the two can strengthen each other; 2) The dosage of drugs should be controlled within the range that can form effective concentrations in blood and tissues without toxic and side effects. For example, glycosides and quinolones have concentration dependent bactericidal effects, that is, increasing the concentration can enhance the effect. Therefore, taking instantaneous high concentration pulse administration can not only enhance the efficacy, but also reduce the toxic and side effects; 3) For non-dose dependent drugs, such as β- Lactam antibiotics have different characteristics of action. Ultra-high concentration cannot strengthen its bactericidal effect, while maintaining the effective concentration in blood and tissue for a long time can improve the efficacy. Continuous release of drugs can enhance the efficacy. However, the combination of β-lactam antibiotics and aminoglycoside antibiotics has the risk of antagonism. The mechanism is that the amino groups of aminoglycoside antibiotics β-Amides with no biological activity are formed between the lactam rings, which will reduce each other's efficacy. How to accurately manage the drug delivery mode is particularly important. However, the drug resistance of bacteria has also been increasing in recent years. Some studies have suggested that bacterial drug resistance exists long before clinical use (Bhullar et al., 2012; Waglechner et al., 2021), but bacteria that abuse antibiotics in clinical and agricultural fields that lead to antibiotic resistance (AMR) or multiple drug resistance (MDR) have been screened out. At present, pharmaceutical companies and experimental centers are carrying out the development of antibiotics (Hutchings et al., 2019), and 45 drugs are being tested, among which there are also categories of new modes of action. In the future, it is necessary to use computer simulation calculation, which is similar to the research of epidemic diseases (Chen et al., 2021; Wieland and Mercorelli, 2021). For example, through the computer simulation of targeting combined with bacterial modeling, *in vitro* activity of antibiotic molecules, safety screening, *in vitro* antibacterial activity of clinical strains and other screening processes, the best bactericidal mechanism will be finally determined, and a series of antibiotics suitable for orthopedic treatment will be designed to form a new antibiotic library.

2.4.2 Metal nanoparticles

With the rapid development of nanotechnology, metal nanoparticles (NPs) have shown excellent properties in the field of antibacterial and conducive to medical applications, including excellent photoelectrochemical activity, large surface area-volume ratio and strong particle surface activity (Jaque et al., 2014; Pallavicini et al., 2014; Canaparo et al., 2019). Metal nanoparticles can kill microorganisms through a variety of mechanisms, so drug resistance is unlikely (Fan et al., 2018). Metal nanoparticles are mainly silver (Ag), zinc (Zn), copper (Cu), magnesium (Mg) and titanium (Ti). Metal nanoparticles containing alumina particles (Al2O3NP) are an exception and may promote the development of drug resistance (Huang et al., 2022).

Silver nanoparticles (AgNPs) are the most common. AgNPs can destroy the bacterial cell wall, dissociate its peptidoglycan structure from inactivation, disrupt bacterial permeability, but also destroy respiratory proteases, disrupt the respiratory chain, leading to bacterial death biofilm disintegration (Morones-Ramirez et al., 2013; Jia et al., 2016; Ding et al., 2020), as shown in Figure 8. By inactivating bacterial proteins, AgNPs can penetrate bacteria, dephosphorylate tyrosine residues, and inactivate bacterial growth-related enzymes to inhibit bacterial growth (Cozzone, 2005; Welburn et al., 2007). Ag nanoparticles hinder the transfer of electrons, and oxygen is forced to become an electron acceptor, leading to the production of reactive oxygen species (ROS), such as hydroxyl radicals and superoxide radicals. Affecting DNA replication, Ag can transform DNA into a condensed state, thus organizing DNA replication (Marambio-Jones and Hoek, 2010; Xu et al., 2021a). There have been studies on the combination of stimulus response platform and AgNPs to develop a silver nano platform with stimulus response and controlled release (Guo et al., 2019). In the future, it is possible to achieve the controlled release of Ag ion and selectively kill bacteria, and alleviate the biological toxicity caused by the high concentration of Ag ion.

Zinc oxide nanoparticles (ZnONPs) also have a variety of mechanisms for killing bacteria, such as destroying lipids and proteins, resulting in the formation of Zn^{2+} ions and reactive oxygen species (ROS) to damage cells (Blecher et al., 2011; Huh and Kwon, 2011; Hajipour et al., 2012). Other metal ions have similar mechanisms for killing bacteria, but they are different. In general, it is difficult for bacteria to produce resistance (Pelgrift and Friedman, 2013). However, attention should be paid to the side effects of some metal ions, such as the toxicity of AgNPs and the skin hypersensitivity caused by TiO_2.

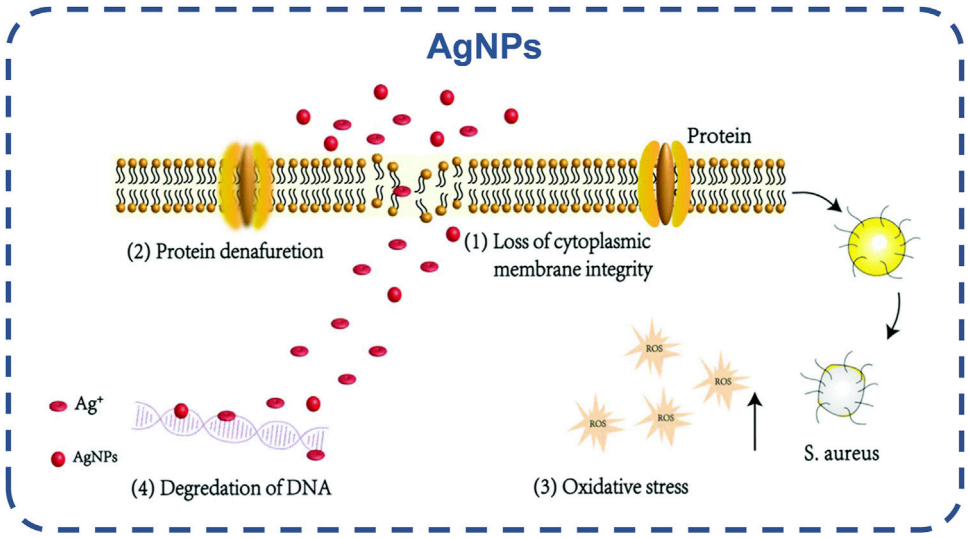

FIGURE 8
Schematic diagram of the potential antibacterial mechanism of AgNPs and Ag (Ding et al., 2020). Copyright 2020, Biomater Sci.

2.4.3 Antibacterial peptides (AMP)

Most eukaryotic biosynthetic AMP can target the plasma membrane of bacteria, dissolve the plasma membrane and destroy the bacterial structure (Ageitos et al., 2017; Torres et al., 2019). The main bactericidal mechanisms are membrane lytic activity, active oxygen (ROS) induction, enzyme inactivation, etc (Andoy et al., 2020). Antimicrobial peptides can also destroy the bacterial biofilm through three aspects: cleavage of eDNA (Whitchurch et al., 2002), destruction of bacterial quorum sensing (QS) (Herget et al., 2017; Whiteley et al., 2017) and destruction of the whole biofilm (Chen et al., 2018). According to its source, AMP can be divided into two types (Xu et al., 2021b): one is natural antibacterial enzyme, which is called host defense peptide (HDP) or defensin. Because of its targeted antibacterial mechanism, HDP has spectral antibacterial activity, but it is easy to be hydrolyzed, poor stability, moderate activity and expensive. The other is the synthetic peptide (HDPs) that mimics HDP artificially, which is the modification or improvement of HDP, has higher stability, resistance to protein hydrolysis and cheap. Peptides synthesized by bacterial ribosomes, called bacteriocins, should never be removed by bacteria. Compared with antibiotics, cationic amphiphilic bacteriocin can also penetrate phospholipase when adhering to bacteria. Bacteriocin exerts its antibacterial effect by inhibiting cell wall synthesis, inhibiting cell membrane formation and interfering with DNA and protein synthesis at high concentrations (Meade et al., 2020). Antimicrobial peptides can also have self-assembly properties. Liu and his colleagues (Liu et al., 2013) selected a Gram-positive antimicrobial peptide as the basic framework and developed a self-assembly material. When exposed to pH, ion or thermal stimulation, the sequence containing antimicrobial peptides can make a reversible transition from random structure to β-fold structure, and further self-assemble into hydrogels with antibacterial function on their surface. Similar to antibiotics, bacteria can evolve resistance to AMP, which will become more and more obvious in the future (Andersson et al., 2016). Because of their specific binding, some antimicrobial peptides show high selectivity for anticancer and killing cancer cells, and are harmless to normal cells. Vectors constructed with functional polymers can help kill cancer cells that escape from immune system monitoring (Sun et al., 2018).

3 Conclusion and prospect

In general, all material systems have their own characteristics, but the general policy is to precisely control the release of drugs. For various substances, their modes of action, ways and possible application prospects are different. The enzyme stimulating response material system can react with certain specific enzymes produced by bacteria, such as glutamyl endonuclease, lipase, β- The lactamase, combined with antibacterial substances such as Ag ions, has an adaptive drug release function to play a good antibacterial role. It has good application prospects in biological materials, tissue engineering and regenerative medicine, such as integrating the response system with the orthopedic implant system to prevent infection. The advantages of the salt responsive material system can be switched between the antibacterial surface that kills and resists living bacteria and the antifouling release surface that releases dead bacteria. It can be easily regenerated through simple salt solution treatment to maintain its high antibacterial and antifouling activities,

thus playing an antibacterial role, having good biocompatibility and high bacterial clearance rate. It is expected to provide a new idea for the design of orthopedic built-in functional materials with ideal antibacterial surfaces. The advantage of pH responsive material system is that it is sensitive to pH changes and will not release drugs under physiological pH. For acidic inflamed environment, it can rapidly increase the local concentration of antibacterial drugs and has a strong antibacterial effect. For example, based on the acidic environment in osteomyelitis, this material system has the potential of bone substitute and can also be used as the stimulus response nano carrier of macro drug delivery system. For different design schemes, there are different uses. For the application of redox response material system, due to different metabolites of bacteria, this material can be used to distinguish Gram negative and Gram-positive bacteria, identify different reduction products secreted by different bacterial strains, and select and specifically detect or kill bacteria. The photosensitizer of light stimulated antibacterial therapy does not need the antibacterial method of bacterial target, and is not easy to produce drug resistance. It is suitable for local infection. The research of new photosensitizer and optical technology can improve its antibacterial depth. The electric trigger response system has many characteristics and fast response speed. Using the low drive voltage and magnetic field compatible with the biological system, multiple switchable regions can be created on the same surface. Applying potential to change the surface characteristics will change the effect of the antibacterial surface on bacteria, thus affecting their viability. Combining antibacterial drugs with them can form materials with adjustable antibacterial properties. In active stimulation, the magnetic stimulation system is easy to use and targets deep tissues. Magnetic stimulation can be used to increase the drug delivery after implantation to obtain the maximum drug concentration, or maintain the therapeutic drug level after the traditional delivery system is lower than the required release rate. In this paper, the research status of stimulus response system and the development of antibacterial substances and potential applications in bone infection were reviewed. Bacterial biofilm and drug resistance are the main problems in dealing with bacterial infection, and the resistance of bacteria to antibiotics is becoming more and more intense. Although many countries and organizations have regulated and restricted the use of antibiotics, they only slow down the growth trend. Stimulus-response antibacterial system has developed rapidly in recent years, and various components and metabolites of bacteria have been studied. The endogenous stimulus response system includes pH response, salt response, enzyme response, etc. The response systems of exogenous stimuli include light response, thermal response, magnetic response, electrical response, etc. Each system has its own applicable environment. When the tissue has pathological changes, the changes are in many aspects, and the pH value and metabolites are constantly changing. Therefore, when a defect in the single response system, it can be combined with other systems to form a multi-stimulus response system, which is conducive to the better role of therapeutic drugs. At present, with the increasing resistance to antibiotics, the research and development of antibacterial substances is accelerating. There are not only the improvement of traditional antibiotics and the optimization of antibiotic discovery pathway. With the development of nanotechnology, a variety of fungicides began to enter people's field of vision, such as metal nanoparticles, which have advantages in sterilization. However, the development of its technology is not enough to be used in bone clinic. The development prospect of stimulus response system and antibacterial materials has partial unity, towards highly sensitive materials, precise control of drug release, and selective action on bacteria. This method has a good prospect, but it requires considerable energy and effort, and at the same time, it is necessary to make these systems and antibacterial materials as simple and efficient as possible.

Author contributions

YZ and ZS contributed to conception and design of the study. ZS and XL organized the database. YZ and PX performed the statistical analysis. CW wrote the first draft of the manuscript. YZ wrote sections of the manuscript. All authors contributed to manuscript revision, read, and approved the submitted version.

Funding

This work was supported by grants from Special Project for Medical and Sanitary Talent of Finance Department of Jilin Province of China (No. 3D5205133428), Department of Science and Technology of Jilin Province of China (Nos. 20220204126YY&20200201478JC).

Conflict of interest

The authors declare that the research was conducted in the absence of any commercial or financial relationships that could be construed as a potential conflict of interest.

Publisher's note

References

Abidian, M. R., Kim, D. H., and Martin, D. C. (2006). Conducting-polymer nanotubes for controlled drug release. *Adv. Mater* 18 (4), 405–409. doi:10.1002/adma.200501726

Ageitos, J. M., Sanchez-Perez, A., Calo-Mata, P., et al. (2017). Antimicrobial peptides (AMPs): Ancient compounds that represent novel weapons in the fight against bacteria. *Biochem. Pharmacol.* 133, 117–138. doi:10.1016/j.bcp.2016.09.018

Alkekhia, D., LaRose, C., and Shukla, A. (2022). β-Lactamase-Responsive hydrogel drug delivery platform for bacteria-triggered cargo release. *ACS Appl. Mater Interfaces* 14 (24), 27538–27550. doi:10.1021/acsami.2c02614

Amoli-Diva, M., Sadighi-Bonabi, R., and Pourghazi, K. (2017). Laser-assisted triggered-drug release from silver nanoparticles-grafted dual-responsive polymer. *Mater Sci. Eng. C Mater Biol. Appl.* 76, 536–542. doi:10.1016/j.msec.2017.03.089

Anandhakumar, S., Gokul, P., and Raichur, A. M. (2016). Stimuli-responsive weak polyelectrolyte multilayer films: A thin film platform for self triggered multi-drug delivery. *Mater Sci. Eng. C Mater Biol. Appl.* 58, 622–628. doi:10.1016/j.msec.2015.08.039

Andersson, D. I., Hughes, D., and Kubicek-Sutherland, J. Z. (2016). Mechanisms and consequences of bacterial resistance to antimicrobial peptides. *Drug Resist Updat* 26, 43–57. doi:10.1016/j.drup.2016.04.002

Andoy, N. M. O., Jeon, K., Kreis, C. T., and Sullan, R. M. A. (2020). Multifunctional and stimuli-responsive polydopamine nanoparticle-based platform for targeted antimicrobial applications. *Adv. Funct. Mater.* 30 (40), 2004503. doi:10.1002/adfm.202004503

Andresen, T. L., Jensen, S. S., and Jorgensen, K. (2005). Advanced strategies in liposomal cancer therapy: Problems and prospects of active and tumor specific drug release. *Prog. Lipid Res.* 44 (1), 68–97. doi:10.1016/j.plipres.2004.12.001

Armstrong, E. S., Kostrub, C. F., and Cass, R. T. (2012). *Aminoglycosides [M]// Dougherty TJ, Pucci MJ. Antibiotic discovery and development*. Boston, MA: Springer US, 229–269.

Bellingeri, R., Mulko, L., Molina, M., Picco, N., Alustiza, F., Grosso, C., et al. (2018). Nanocomposites based on pH-sensitive hydrogels and chitosan decorated carbon nanotubes with antibacterial properties. *Mater Sci. Eng. C Mater Biol. Appl.* 90, 461–467. doi:10.1016/j.msec.2018.04.090

Berne, C., Ellison, C. K., Ducret, A., and Brun, Y. V. (2018). Bacterial adhesion at the single-cell level. *Nat. Rev. Microbiol.* 16 (10), 616–627. doi:10.1038/s41579-018-0057-5

Bhullar, K., Waglechner, N., Pawlowski, A., Koteva, K., Banks, E. D., Johnston, M. D., et al. (2012). Antibiotic resistance is prevalent in an isolated cave microbiome. *PLoS* 7 (4), e34953. doi:10.1371/journal.pone.0034953

Blecher, K., Nasir, A., and Friedman, A. (2011). The growing role of nanotechnology in combating infectious disease. *J. Virulence* 2 (5), 395–401. doi:10.4161/viru.2.5.17035

Blummel, J., Perschmann, N., Aydin, D., Drinjakovic, J., Surrey, T., Lopez-Garcia, M., et al. (2007). Protein repellent properties of covalently attached PEG coatings on nanostructured SiO2-based interfaces. *Biomaterials* 28 (32), 4739–4747. doi:10.1016/j.biomaterials.2007.07.038

Borges, J., Rodrigues, L. C., Reis, R. L., and Mano, J. F. (2014). Layer-by-Layer assembly of light-responsive polymeric multilayer systems. *Adv. Funct. Mater.* 24 (36), 5624–5648. doi:10.1002/adfm.201401050

Brady, R. A., Leid, J. G., Costerton, J. W., and Shirtliff, M. (2006). Osteomyelitis: Clinical overview and mechanisms of infection persistence. *Clin. Microbiol. Newsl.* 28 (9), 65–72. doi:10.1016/j.clinmicnews.2006.04.001

Browne, W. R., and Feringa, B. L. (2009). Light switching of molecules on surfaces. *Annu. Rev. Phys. Chem.* 60, 407–428. doi:10.1146/annurev.physchem.040808.090423

Butina, K., Löffler, S., Rhen, M., and Richter-Dahlfors, A. (2019). Electrochemical sensing of bacteria via secreted redox active compounds using conducting polymers. *Sensors Actuators, B Chem.* 297, 126703. doi:10.1016/j.snb.2019.126703

Campoccia, D., Montanaro, L., and Arciola, C. R. (2013). A review of the biomaterials technologies for infection-resistant surfaces. *Biomaterials* 34 (34), 8533–8554. doi:10.1016/j.biomaterials.2013.07.089

Canaparo, R., Foglietta, F., Giuntini, F., Della Pepa, C., Dosio, F., and Serpe, L. (2019). Recent developments in antibacterial therapy: Focus on stimuli-responsive drug-delivery systems and therapeutic nanoparticles. *Molecules* 24 (10), 1991. doi:10.3390/molecules24101991

Cantini, E., Wang, X., Koelsch, P., Preece, J. A., Ma, J., and Mendes, P. M. (2016). Electrically responsive surfaces: Experimental and theoretical investigations. *Acc. Chem. Res.* 49 (6), 1223–1231. doi:10.1021/acs.accounts.6b00132

Cao, W., Gu, Y., Meineck, M., Li, T., and Xu, H. (2014). Tellurium-containing polymer micelles: Competitive-Ligand-Regulated coordination responsive systems. *J. Am. Chem. Soc.* 136 (13), 5132–5137. doi:10.1021/ja500939m

Cao, Z., Mi, L., Mendiola, J., Ella-Menye, J. R., Zhang, L., Xue, H., et al. (2012). Reversibly switching the function of a surface between attacking and defending against bacteria. *Angew. Chem. Int. Ed. Engl.* 51 (11), 2602–2605. doi:10.1002/anie.201106466

Chellat, M. F., Raguž, L., and Riedl, R. (2016). Targeting antibiotic resistance. *Angew. Chem. Int. Ed.* 55 (23), 6600–6626. doi:10.1002/anie.201506818

Chen, H., Haus, B., and Mercorelli, P. (2021). Extension of SEIR compartmental models for constructive lyapunov control of COVID-19 and analysis in terms of practical stability. *Mathematics* 9 (17), 2076. doi:10.3390/math9172076

Chen, H., Yang, J., Xiao, S., Hu, R., Bhaway, S. M., Vogt, B. D., et al. (2016). Salt-responsive polyzwitterionic materials for surface regeneration between switchable fouling and antifouling properties. *Acta Biomater.* 40, 62–69. doi:10.1016/j.actbio.2016.03.009

Chen, Z., Wang, Z., Ren, J., and Qu, X. (2018). Enzyme mimicry for combating bacteria and biofilms. *Acc. Chem. Res.* 51 (3), 789–799. doi:10.1021/acs.accounts.8b00011

Cheng, R., Feng, F., Meng, F., Deng, C., Feijen, J., and Zhong, Z. (2011). Glutathione-responsive nano-vehicles as a promising platform for targeted intracellular drug and gene delivery. *J. Control Release* 152 (1), 2–12. doi:10.1016/j.jconrel.2011.01.030

Chong, H., Nie, C., Zhu, C., Yang, Q., Liu, L., Lv, F., et al. (2012). Conjugated polymer nanoparticles for light-activated anticancer and antibacterial activity with imaging capability. *Langmuir* 28 (4), 2091–2098. doi:10.1021/la203832h

Chung, M. F., Chia, W. T., Liu, H. Y., Hsiao, C. W., Hsiao, H. C., Yang, C. M., et al. (2014). Inflammation-induced drug release by using a pH-responsive gas-generating hollow-microsphere system for the treatment of osteomyelitis. *Adv. Healthc. Mater* 3 (11), 1854–1861. doi:10.1002/adhm.201400158

Cole, M. A., Voelcker, N. H., and Thissen, H. (2007). Electro-induced protein deposition on low-fouling surfaces. *Smart Mater. Struct.* 16 (6), 2222–2228. doi:10.1088/0964-1726/16/6/025

Cozzone, A. J. (2005). Role of protein phosphorylation on serine/threonine and tyrosine in the virulence of bacterial pathogens. *J. Mol. Microbiol. Biotechnol.* 9 (3-4), 198–213. doi:10.1159/000089648

Curcio, M., Diaz-Gomez, L., Cirillo, G., Concheiro, A., Iemma, F., and Alvarez-Lorenzo, C. (2017). pH/redox dual-sensitive dextran nanogels for enhanced intracellular drug delivery. *Eur. J. Pharm. Biopharm.* 117, 324–332. doi:10.1016/j.ejpb.2017.05.002

Czerwinska-Glowka, D., Przystas, W., Zablocka-Godlewska, E., Student, S., Cwalina, B., Łapkowski, M., et al. (2021). Electrically-responsive antimicrobial coatings based on a tetracycline-loaded poly(3, 4-ethylenedioxythiophene) matrix. *Mater Sci. Eng. C Mater Biol. Appl.* 123, 112017. doi:10.1016/j.msec.2021.112017

da Rosa, T. F., Coelho, S. S., Foletto, V. S., Bottega, A., Serafin, M. B., Machado, C. d. S., et al. (2020). Alternatives for the treatment of infections caused by ESKAPE pathogens. *J. Clin. Pharm. Ther.* 45 (4), 863–873. doi:10.1111/jcpt.13149

De Arco, L. G., Yi, Z., Kumar, A., and Zhou, C. (2009). Synthesis, transfer, and devices of single- and few-layer graphene by chemical vapor deposition. *IEEE Trans. Nanotechnol.* 8 (2), 135–138. doi:10.1109/tnano.2009.2013620

Del Pozo, J. L., and Patel, R. (2009). Infection associated with prosthetic joints. *N. Engl. J. Med.* 361 (8), 787–794. doi:10.1056/nejmcp0905029

Ding, M., Zhao, W., Zhang, X., Song, L., and Luan, S. (2022). Charge-switchable MOF nanocomplex for enhanced biofilm penetration and eradication. *J. Hazard Mater* 439, 129594. doi:10.1016/j.jhazmat.2022.129594

Ding, Y., Hao, Y., Yuan, Z., Tao, B., Chen, M., Lin, C., et al. (2020). A dual-functional implant with an enzyme-responsive effect for bacterial infection therapy and tissue regeneration. *Biomater. Sci.* 8 (7), 1840–1854. doi:10.1039/c9bm01924c

Dobson, J. (2006). Magnetic nanoparticles for drug delivery. *Drug Dev. Res.* 67 (1), 55–60. doi:10.1002/ddr.20067

Dougherty, T. J., and Pucci, M. J. (2012). *Antibiotic discovery and development [M]*. Waltham, NH

Du, J. Z., Sun, T. M., Song, W. J., Wu, J., and Wang, J. (2010). A tumor-acidity-activated charge-conversional nanogel as an intelligent vehicle for promoted tumoral-cell uptake and drug delivery. *Angew. Chem. Int. Ed. Engl.* 49 (21), 3621–3626. doi:10.1002/anie.200907210

Duque Sanchez, L., Brack, N., Postma, A., Pigram, P. J., and Meagher, L. (2016). Surface modification of electrospun fibres for biomedical applications: A focus on

radical polymerization methods. *Biomaterials* 106, 24–45. doi:10.1016/j.biomaterials.2016.08.011

El-Husseiny, M., Patel, S., MacFarlane, R. J., and Haddad, F. S. (2011). Biodegradable antibiotic delivery systems. *J. Bone Jt. Surg. Br.* 93 (2), 151–157. doi:10.1302/0301-620X.93B2.24933

Elashnikov, R., Rimpelova, S., Lyutakov, O., Pavlickova, V. S., Khrystonko, O., Kolska, Z., et al. (2022). Ciprofloxacin-loaded poly(*N*-isopropylacrylamide-*co*-acrylamide)/Polycaprolactone nanofibers as dual thermo- and pH-responsive antibacterial materials. *ACS Appl. Bio Mater* 5 (4), 1700–1709. doi:10.1021/acsabm.2c00069

Fan, X., Yang, F., Nie, C., Yang, Y., Ji, H., He, C., et al. (2018). Mussel-Inspired synthesis of NIR-responsive and biocompatible Ag–graphene 2D nanoagents for versatile bacterial disinfections. *ACS Appl. Mater Interfaces* 10 (1), 296–307. doi:10.1021/acsami.7b16283

Felsher, D. W. (2003). Cancer revoked: Oncogenes as therapeutic targets. *Nat. Rev. Cancer* 3 (5), 375–379. doi:10.1038/nrc1070

Freeman, M. W., Arrott, A., and Watson, J. H. L. (1960). Magnetism in medicine. *J. Appl. Phys.* 31 (5), S404–S405. doi:10.1063/1.1984765

Ganta, S., Devalapally, H., Shahiwala, A., and Amiji, M. (2008). A review of stimuli-responsive nanocarriers for drug and gene delivery. *J. Control Release* 126 (3), 187–204. doi:10.1016/j.jconrel.2007.12.017

Gao, Q., Yu, M., Su, Y., Xie, M., Zhao, X., Li, P., et al. (2017). Rationally designed dual functional block copolymers for bottlebrush-like coatings: *In vitro* and *in vivo* antimicrobial, antibiofilm, and antifouling properties. *Acta Biomater.* 51, 112–124. doi:10.1016/j.actbio.2017.01.061

Ghadiali, J. E., and Stevens, M. M. (2008). Enzyme-responsive nanoparticle systems. *Adv. Mater.* 20 (22), 4359–4363. doi:10.1002/adma.200703158

Gohy, J. F., and Zhao, Y. (2013). Photo-responsive block copolymer micelles: Design and behavior. *Chem. Soc. Rev.* 42 (17), 7117–7129. doi:10.1039/c3cs35469e

Gomez-Carretero, S., Libberton, B., Rhen, M., Persson, K., Jager, E., Berggren, M., et al. (2017). Redox-active conducting polymers modulate Salmonella biofilm formation by controlling availability of electron acceptors. *NPJ Biofilms Microbiomes* 3, 19. doi:10.1038/s41522-017-0027-0

Gontsarik, M., Yaghmur, A., Ren, Q., Maniura-Weber, K., and Salentinig, S. (2019). From structure to function: pH-switchable antimicrobial nano-self-assemblies. *ACS Appl. Mater Interfaces* 11 (3), 2821–2829. doi:10.1021/acsami.8b18618

Guo, Y., Wang, S., Du, H., Chen, X., and Fei, H. (2019). Silver ion-histidine interplay switches peptide hydrogel from antiparallel to parallel β-assembly and enables controlled antibacterial activity. *Biomacromolecules* 20 (1), 558–565. doi:10.1021/acs.biomac.8b01480

Haas, S., Hain, N., Raoufi, M., Handschuh-Wang, S., Wang, T., Jiang, X., et al. (2015). Enzyme degradable polymersomes from hyaluronic acid-*block*-poly(ε-caprolactone) copolymers for the detection of enzymes of pathogenic bacteria. *Biomacromolecules* 16 (3), 832–841. doi:10.1021/bm501729h

Hafeli, U. O., Sweeney, S. M., Beresford, B. A., Sim, E. H., and Macklis, R. M. (1994). Magnetically directed poly(lactic acid)90Y-microspheres: Novel agents for targeted intracavitary radiotherapy. *J. Biomed. Mater Res.* 28 (8), 901–908. doi:10.1002/jbm.820280809

Hahn, M. E., and Gianneschi, N. C. (2011). Enzyme-directed assembly and manipulation of organic nanomaterials. *Chem. Commun. (Camb)* 47 (43), 11814–11821. doi:10.1039/c1cc15220c

Hajipour, M. J., Fromm, K. M., Ashkarran, A. A., Jimenez de Aberasturi, D., de Larramendi, I. R., Rojo, T., et al. (2012). Antibacterial properties of nanoparticles. *Trends Biotechnol.* 30 (10), 499–511. doi:10.1016/j.tibtech.2012.06.004

Harris, M., Ahmed, H., Barr, B., LeVine, D., Pace, L., Mohapatra, A., et al. (2017). Magnetic stimuli-responsive chitosan-based drug delivery biocomposite for multiple triggered release. *Int. J. Biol. Macromol.* 104, 1407–1414. doi:10.1016/j.ijbiomac.2017.03.141

Hasan, F., Shah, A. A., and Hameed, A. (2009). Methods for detection and characterization of lipases: A comprehensive review. *Biotechnol. Adv.* 27 (6), 782–798. doi:10.1016/j.biotechadv.2009.06.001

Herget, K., Hubach, P., Pusch, S., Deglmann, P., Gotz, H., Gorelik, T. E., et al. (2017). Haloperoxidase mimicry by CeO_{2-x}Nanorods combats biofouling. *Adv. Mater* 29 (4), 1603823. doi:10.1002/adma.201603823

Howard, M. D., Jay, M., Dziubla, T. D., and Lu, X. (2008). PEGylation of nanocarrier drug delivery systems: State of the art. *J. Biomed. Nanotechnol.* 4 (2), 133–148. doi:10.1166/jbn.2008.021

Hu, J., Zhang, G., and Liu, S. (2012). Enzyme-responsive polymeric assemblies, nanoparticles and hydrogels. *Chem. Soc. Rev.* 41 (18), 5933–5949. doi:10.1039/c2cs35103j

Huang, K. T., Ishihara, K., and Huang, C. J. (2019). Polyelectrolyte and antipolyelectrolyte effects for dual salt-responsive interpenetrating network hydrogels. *Biomacromolecules* 20 (9), 3524–3534. doi:10.1021/acs.biomac.9b00796

Huang, Y., Zou, L., Wang, J., Jin, Q., and Ji, J. (2022). Stimuli-responsive nanoplatforms for antibacterial applications. *Wiley Interdiscip. Rev. Nanomed Nanobiotechnol* 14 (3), e1775. doi:10.1002/wnan.1775

Huh, A. J., and Kwon, Y. J. (2011). "Nanoantibiotics": A new paradigm for treating infectious diseases using nanomaterials in the antibiotics resistant era. *J. Control Release* 156 (2), 128–145. doi:10.1016/j.jconrel.2011.07.002

Hutchings, M. I., Truman, A. W., and Wilkinson, B. (2019). Antibiotics: Past, present and future. *Curr. Opin. Microbiol.* 51, 72–80. doi:10.1016/j.mib.2019.10.008

Huynh, E., and Zheng, G. (2013). Engineering multifunctional nanoparticles: All-in-one versus one-for-all. *Wiley Interdiscip. Rev. Nanomed Nanobiotechnol* 5 (3), 250–265. doi:10.1002/wnan.1217

Hwang, D. W., Son, S., Jang, J., Youn, H., Lee, S., Lee, D., et al. (2011). A brain-targeted rabies virus glycoprotein-disulfide linked PEI nanocarrier for delivery of neurogenic microRNA. *Biomaterials* 32 (21), 4968–4975. doi:10.1016/j.biomaterials.2011.03.047

Jacoby, G. A., and Hooper, D. C. (2012). *Review of the quinolone family [M]// Dougherty TJ, Pucci MJ. Antibiotic discovery and development*. Boston, MA: Springer US, 119–146.

Jaque, D., Martinez Maestro, L., del Rosal, B., Haro-Gonzalez, P., Benayas, A., Plaza, J. L., et al. (2014). Nanoparticles for photothermal therapies. *Nanoscale* 6 (16), 9494–9530. doi:10.1039/c4nr00708e

Jia, Q., Song, Q., Li, P., and Huang, W. (2019). Rejuvenated photodynamic therapy for bacterial infections. *Adv. Healthc. Mater* 8 (14), e1900608. doi:10.1002/adhm.201900608

Jia, Z., Xiu, P., Li, M., Xu, X., Shi, Y., Cheng, Y., et al. (2016). Bioinspired anchoring AgNPs onto micro-nanoporous TiO2 orthopedic coatings: Trap-killing of bacteria, surface-regulated osteoblast functions and host responses. *Biomaterials* 75, 203–222. doi:10.1016/j.biomaterials.2015.10.035

Jiao, Y., Niu, L. N., Ma, S., Li, J., Tay, F. R., and Chen, J. h. (2017). Quaternary ammonium-based biomedical materials: State-of-the-art, toxicological aspects and antimicrobial resistance. *Prog. Polym. Sci.* 71, 53–90. doi:10.1016/j.progpolymsci.2017.03.001

Jing, J., Liang, S., Yan, Y., Tian, X., and Li, X. (2019). Fabrication of hybrid hydrogels from silk fibroin and tannic acid with enhanced gelation and antibacterial activities. *ACS Biomater. Sci. Eng.* 5 (9), 4601–4611. doi:10.1021/acsbiomaterials.9b00604

Kanamala, M., Wilson, W. R., Yang, M., Palmer, B. D., and Wu, Z. (2016). Mechanisms and biomaterials in pH-responsive tumour targeted drug delivery: A review. *Biomaterials* 85, 152–167. doi:10.1016/j.biomaterials.2016.01.061

Kaul, G., and Amiji, M. (2005). Tumor-targeted gene delivery using poly(ethylene glycol)-modified gelatin nanoparticles: *In vitro* and *in vivo* studies. *Pharm. Res.* 22 (6), 951–961. doi:10.1007/s11095-005-4590-3

Kim, S., Chen, Y., Ho, E. A., and Liu, S. (2017). Reversibly pH-responsive polyurethane membranes for on-demand intravaginal drug delivery. *Acta Biomater.* 47, 100–112. doi:10.1016/j.actbio.2016.10.006

Klein, F., Richter, B., Striebel, T., Franz, C. M., Freymann, G. v., Wegener, M., et al. (2011). Two-component polymer scaffolds for controlled three-dimensional cell culture. *Adv. Mater* 23 (11), 1341–1345. doi:10.1002/adma.201004060

Krisch, E., Messager, L., Gyarmati, B., Ravaine, V., and Szilagyi, A. (2016). Redox- and pH-responsive nanogels based on thiolated poly(aspartic acid). *Macromol. Mater. Eng.* 301 (3), 260–266. doi:10.1002/mame.201500119

Kumar, C. S., and Mohammad, F. (2011). Magnetic nanomaterials for hyperthermia-based therapy and controlled drug delivery. *Adv. Drug Deliv. Rev.* 63 (9), 789–808. doi:10.1016/j.addr.2011.03.008

Kumar, P., Liu, B., and Behl, G. (2019). A comprehensive outlook of synthetic strategies and applications of redox-responsive nanogels in drug delivery. *Macromol. Biosci.* 19 (8), e1900071. doi:10.1002/mabi.201900071

Lee, E. J., Khan, S. A., Park, J. K., and Lim, K. H. (2012). Studies on the characteristics of drug-loaded gelatin nanoparticles prepared by nanoprecipitation. *Bioprocess Biosyst. Eng.* 35 (1-2), 297–307. doi:10.1007/s00449-011-0591-2

Lee, H. S., Dastgheyb, S. S., Hickok, N. J., Eckmann, D. M., and Composto, R. J. (2015). Targeted release of tobramycin from a pH-responsive grafted bilayer challenged with *S. aureus*. *Biomacromolecules* 16 (2), 650–659. doi:10.1021/bm501751v

Lee, J., Kang, C. I., Lee, J. H., Joung, M., Moon, S., Wi, Y., et al. (2010). Risk factors for treatment failure in patients with prosthetic joint infections. *J. Hosp. Infect.* 75 (4), 273–276. doi:10.1016/j.jhin.2010.03.012

Lee, M. H., Yang, Z., Lim, C. W., Lee, Y. H., Dongbang, S., Kang, C., et al. (2013). Disulfide-cleavage-triggered chemosensors and their biological applications. *Chem. Rev.* 113 (7), 5071–5109. doi:10.1021/cr300358b

Li, D., Wei, Q., Wu, C., Zhang, X., Xue, Q., Zheng, T., et al. (2020). Superhydrophilicity and strong salt-affinity: Zwitterionic polymer grafted surfaces with significant potentials particularly in biological systems. *Adv. Colloid Interface Sci.* 278, 102141. doi:10.1016/j.cis.2020.102141

Li, D., Zhang, R., Liu, G., Kang, Y., and Wu, J. (2020). Redox-responsive self-assembled nanoparticles for cancer therapy. *Adv. Healthc. Mater* 9 (20), e2000605. doi:10.1002/adhm.202000605

Li, X., Lee, D., Huang, J. D., and Yoon, J. (2018). Phthalocyanine-assembled nanodots as photosensitizers for highly efficient Type I photoreactions in photodynamic therapy. *Angew. Chem. Int. Ed. Engl.* 57 (31), 9885–9890. doi:10.1002/anie.201806551

Li, X., Lee, S., and Yoon, J. (2018). Supramolecular photosensitizers rejuvenate photodynamic therapy. *Chem. Soc. Rev.* 47 (4), 1174–1188. doi:10.1039/c7cs00594f

Li, X., Wu, B., Chen, H., Nan, K., Jin, Y., Sun, L., et al. (2018). Recent developments in smart antibacterial surfaces to inhibit biofilm formation and bacterial infections. *J. Mater Chem. B* 6 (26), 4274–4292. doi:10.1039/c8tb01245h

Liang, Y., Li, M., Yang, Y., Qiao, L., Xu, H., and Guo, B. (2022). pH/glucose dual responsive metformin release hydrogel dressings with adhesion and self-healing via dual-dynamic bonding for athletic diabetic foot wound healing. *ACS Nano* 16 (2), 3194–3207. doi:10.1021/acsnano.1c11040

Liechty, W. B., Scheuerle, R. L., and Peppas, N. A. (2013). Tunable, responsive nanogels containing t-butyl methacrylate and 2-(t-butylamino)ethyl methacrylate. *Polymer* 54 (15), 3784–3795. doi:10.1016/j.polymer.2013.05.045

Limoli, D. H., Jones, C. J., and Wozniak, D. J. (2015). Bacterial extracellular polysaccharides in biofilm formation and function. *Microbiol. Spectr.* 3 (3). doi:10.1128/microbiolspec.mb-0011-2014

Liu, Y., Yang, Y., Wang, C., and Zhao, X. (2013). Stimuli-responsive self-assembling peptides made from antibacterial peptides. *Nanoscale* 5 (14), 6413–6421. doi:10.1039/c3nr00225j

Lovell, J. F., Liu, T. W., Chen, J., and Zheng, G. (2010). Activatable photosensitizers for imaging and therapy. *Chem. Rev.* 110 (5), 2839–2857. doi:10.1021/cr900236h

Lu, Y., Aimetti, A. A., Langer, R., and Gu, Z. (2016). Bioresponsive materials. *Nat. Rev. Mater.* 2 (1), 16075. doi:10.1038/natrevmats.2016.75

Lucky, S. S., Soo, K. C., and Zhang, Y. (2015). Nanoparticles in photodynamic therapy. *Chem. Rev.* 115 (4), 1990–2042. doi:10.1021/cr5004198

Ma, L., Jiang, F., Fan, X., Wang, L., He, C., Zhou, M., et al. (2020). Metal–organic-framework-engineered enzyme-mimetic catalysts. *Adv. Mater* 32 (49), e2003065. doi:10.1002/adma.202003065

Ma, Y., Sun, Y., Fu, Y., Fang, G., Yan, X., and Guo, Z. (2016). Swelling behaviors of porous lignin based poly (acrylic acid). *Chemosphere* 163, 610–619. doi:10.1016/j.chemosphere.2016.08.035

Ma, Z., Li, J., Bai, Y., Zhang, Y., Sun, H., and Zhang, X. (2020). A bacterial infection-microenvironment activated nanoplatform based on spiropyran-conjugated glycoclusters for imaging and eliminating of the biofilm. *Chem. Eng. J.* 399, 125787. doi:10.1016/j.cej.2020.125787

Marambio-Jones, C., and Hoek, E. M. V. (2010). A review of the antibacterial effects of silver nanomaterials and potential implications for human health and the environment. *J. Nanoparticle Res.* 12 (5), 1531–1551. doi:10.1007/s11051-010-9900-y

Marculescu, C. E., Berbari, E. F., Hanssen, A. D., Steckelberg, J. M., Harmsen, S. W., Mandrekar, J. N., et al. (2006). Outcome of prosthetic joint infections treated with debridement and retention of components. *Clin. Infect. Dis.* 42 (4), 471–478. doi:10.1086/499234

Meade, E., Slattery, M. A., and Garvey, M. (2020). Bacteriocins, potent antimicrobial peptides and the fight against multi drug resistant species: Resistance is futile? *J. Antibiot. (Basel)* 9 (1), 32. doi:10.3390/antibiotics9010032

Minelli, C., Lowe, S. B., and Stevens, M. M. (2010). Engineering nanocomposite materials for cancer therapy. *Small* 6 (21), 2336–2357. doi:10.1002/smll.201000523

Misba, L., Zaidi, S., and Khan, A. U. (2018). Efficacy of photodynamic therapy against Streptococcus mutans biofilm: Role of singlet oxygen. *J. Photochem Photobiol. B* 183, 16–21. doi:10.1016/j.jphotobiol.2018.04.024

Miyata, T., Nakamae, K., Hoffman, A. S., and Kanzaki, Y. (1994). Stimuli-sensitivities of hydrogels containing phosphate groups. *Macromol. Chem. Phys.* 195 (4), 1111–1120. doi:10.1002/macp.1994.021950401

Modarresi-Saryazdi, S. M., Haddadi-Asl, V., and Salami-Kalajahi, M. N. (2018). N, N'-methylenebis(acrylamide)-crosslinked poly(acrylic acid) particles as doxorubicin carriers: A comparison between release behavior of physically loaded drug and conjugated drug via acid-labile hydrazone linkage. *J. Biomed. Mater Res. A* 106 (2), 342–348. doi:10.1002/jbm.a.36240

Moorcroft, S. C. T., Roach, L., Jayne, D. G., Ong, Z. Y., and Evans, S. D. (2020). Nanoparticle-loaded hydrogel for the light-activated release and photothermal enhancement of antimicrobial peptides. *ACS Appl. Mater Interfaces* 12 (22), 24544–24554. doi:10.1021/acsami.9b22587

Morgese, G., Gombert, Y., Ramakrishna, S. N., and Benetti, E. M. (2018). Mixing poly(ethylene glycol) and poly(2-alkyl-2-oxazoline)s enhances hydration and viscoelasticity of polymer brushes and determines their nanotribological and antifouling properties. *ACS Appl. Mater Interfaces* 10 (48), 41839–41848. doi:10.1021/acsami.8b17193

Morones-Ramirez, J. R., Winkler, J. A., Spina, C. S., and Collins, J. J. (2013). Silver enhances antibiotic activity against gram-negative bacteria. *Sci. Transl. Med.* 5 (190), 190ra81. doi:10.1126/scitranslmed.3006276

Mukai, T., Sevostyanova, A., Suzuki, T., Fu, X., and Soll, D. (2018). Eine einfache Methode zur Produktion von Selenoproteinen. *Angew. Chem.* 130 (24), 7333–7337. doi:10.1002/ange.201713215

Muñoz-Bonilla, A., and Fernández-García, M. (2012). Polymeric materials with antimicrobial activity. *Prog. Polym. Sci.* 37 (2), 281–339. doi:10.1016/j.progpolymsci.2011.08.005

Murdan, S. (2003). Electro-responsive drug delivery from hydrogels. *J. Control Release* 92 (1-2), 1–17. doi:10.1016/s0168-3659(03)00303-1

Nakamae, K., Miyata, T., and Hoffman, A. S. (1992). *Die Makromol. Chem.* 193 (4), 983–990. doi:10.1002/macp.1992.021930414

Nakamae, K., Nizuka, T., Miyata, T., Furukawa, M., Nishino, T., Kato, K., et al. (1997). Lysozyme loading and release from hydrogels carrying pendant phosphate groups. *J. Biomater. Sci. Polym. Ed.* 9 (1), 43–53. doi:10.1163/156856297x00254

Ni, Y., Zhang, D., Wang, Y., He, X., He, J., Wu, H., et al. (2021). Host–guest interaction-mediated photo/temperature dual-controlled antibacterial surfaces. *ACS Appl. Mater Interfaces* 13 (12), 14543–14551. doi:10.1021/acsami.0c21626

Owen, J., Pankhurst, Q., and Stride, E. (2012). Magnetic targeting and ultrasound mediated drug delivery: Benefits, limitations and combination. *Int. J. Hyperth.* 28 (4), 362–373. doi:10.3109/02656736.2012.668639

Pallavicini, P., Dona, A., Taglietti, A., Minzioni, P., Patrini, M., Dacarro, G., et al. (2014). Self-assembled monolayers of gold nanostars: A convenient tool for near-IR photothermal biofilm eradication. *Chem. Commun. (Camb)* 50 (16), 1969–1971. doi:10.1039/c3cc48667b

Pan, Y. J., Chen, Y. Y., Wang, D. R., Wei, C., Guo, J., et al. (2012). Redox/pH dual stimuli-responsive biodegradable nanohydrogels with varying responses to dithiothreitol and glutathione for controlled drug release. *Biomaterials* 33 (27), 6570–6579. doi:10.1016/j.biomaterials.2012.05.062

Pelgrift, R. Y., and Friedman, A. J. (2013). Nanotechnology as a therapeutic tool to combat microbial resistance. *Adv. Drug Deliv. Rev.* 65 (13-14), 1803–1815. doi:10.1016/j.addr.2013.07.011

Peng, H., Huang, X., Melle, A., Karperien, M., and Pich, A. (2019). Redox-responsive degradable prodrug nanogels for intracellular drug delivery by crosslinking of amine-functionalized poly(N-vinylpyrrolidone) copolymers. *J. Colloid Interface Sci.* 540, 612–622. doi:10.1016/j.jcis.2019.01.049

Peng, Y., Zhao, Z., Liu, T., Li, X., Hu, X., Wei, X., et al. (2017). Smart human-serum-albumin-as$_2$O$_3$Nanodrug with self-amplified folate receptor-targeting ability for chronic myeloid leukemia treatment. *Angew. Chem. Int. Ed. Engl.* 56 (36), 10845–10849. doi:10.1002/anie.201701366

Pernaut, J-M., and Reynolds, J. R. (2000). Use of conducting electroactive polymers for drug delivery and sensing of bioactive molecules. A redox chemistry approach. *J. Phys. Chem. B* 104 (17), 4080–4090. doi:10.1021/jp994274o

Pranzetti, A., Mieszkin, S., Iqbal, P., Rawson, F. J., Callow, M. E., Callow, J. A., et al. (2013). An electrically reversible switchable surface to control and study early bacterial adhesion dynamics in real-time. *Adv. Mater* 25 (15), 2181–2185. doi:10.1002/adma.201204880

Price, P. M., Mahmoud, W. E., Al-Ghamdi, A. A., and Bronstein, L. M. (2018). Magnetic drug delivery: Where the field is going. *Front. Chem.* 6, 619. doi:10.3389/fchem.2018.00619

Qu, D. H., Wang, Q. C., Zhang, Q. W., Ma, X., and Tian, H. (2015). Photoresponsive host–guest functional systems. *Chem. Rev.* 115 (15), 7543–7588. doi:10.1021/cr5006342

Qu, J., Zhao, X., Ma, P. X., and Guo, B. (2018). Injectable antibacterial conductive hydrogels with dual response to an electric field and pH for localized "smart" drug release. *Acta Biomater.* 72, 55–69. doi:10.1016/j.actbio.2018.03.018

Qu, Y., Chu, B., Wei, X., Lei, M., Hu, D., Zha, R., et al. (2019). Redox/pH dual-stimuli responsive camptothecin prodrug nanogels for "on-demand" drug delivery. *J. Control Release* 296, 93–106. doi:10.1016/j.jconrel.2019.01.016

Raju, R., Bandyopadhyay, S., Sharma, A., Gonzalez, S., Carlsen, P., Gautun, O., et al. (2018). Synthesis, characterization and drug loading of multiresponsive p[NIPAm-co-PEGMA] (core)/p[NIPAm-co-AAc] (shell) nanogels with monodisperse size distributions. *Polym. (Basel)* 10 (3), 309. doi:10.3390/polym10030309

Rasib, S. Z. M., Ahmad, Z., Khan, A., Akil, H., Othman, M., Hamid, Z., et al. (2018). Synthesis and evaluation on pH- and temperature-responsive chitosan-p(MAA-co-NIPAM) hydrogels. *Int. J. Biol. Macromol.* 108, 367–375. doi:10.1016/j.ijbiomac.2017.12.021

Rasigade, J. P., and Vandenesch, F. (2014). *Staphylococcus aureus*: A pathogen with still unresolved issues. *Infect. Genet. Evol.* 21, 510–514. doi:10.1016/j.meegid.2013.08.018

Ray, P. C., Khan, S. A., Singh, A. K., Senapati, D., and Fan, Z. (2012). Nanomaterials for targeted detection and photothermal killing of bacteria. *Chem. Soc. Rev.* 41 (8), 3193–3209. doi:10.1039/c2cs15340h

Ren, H., Wu, Y., Ma, N., Xu, H., and Zhang, X. (2012). Side-chain selenium-containing amphiphilic block copolymers: Redox-controlled self-assembly and disassembly. *Soft Matter* 8 (5), 1460–1466. doi:10.1039/c1sm06673k

Schmaljohann, D. (2006). Thermo- and pH-responsive polymers in drug delivery☆. *Adv. Drug Deliv. Rev.* 58 (15), 1655–1670. doi:10.1016/j.addr.2006.09.020

Schmidt, D. J., Moskowitz, J. S., and Hammond, P. T. (2010). Electrically triggered release of a small molecule drug from a polyelectrolyte multilayer coating. *Chem. Mater* 22 (23), 6416–6425. doi:10.1021/cm102578j

Shan, M., Gong, C., Li, B., and Wu, G. (2017). A pH, glucose, and dopamine triple-responsive, self-healable adhesive hydrogel formed by phenylborate–catechol complexation. *Polym. Chem.* 8 (19), 2997–3005. doi:10.1039/c7py00519a

Shapiro, B. (2009). Towards dynamic control of magnetic fields to focus magnetic carriers to targets deep inside the body. *J. Magn. Magn. Mater* 321 (10), 1594–1599. doi:10.1016/j.jmmm.2009.02.094

Sharpe, L. A., Vela Ramirez, J. E., Haddadin, O. M., Ross, K. A., Narasimhan, B., and Peppas, N. A. (2018). pH-responsive microencapsulation systems for the oral delivery of polyanhydride nanoparticles. *Biomacromolecules* 19 (3), 793–802. doi:10.1021/acs.biomac.7b01590

Shi, W., Hass, B., Kuss, M. A., Zhang, H., Ryu, S., Zhang, D., et al. (2020). Fabrication of versatile dynamic hyaluronic acid-based hydrogels. *Carbohydr. Polym.* 233, 115803. doi:10.1016/j.carbpol.2019.115803

Shi, W., Kong, Y., Su, Y., Kuss, M. A., Jiang, X., Li, X., et al. (2021). Tannic acid-inspired, self-healing, and dual stimuli responsive dynamic hydrogel with potent antibacterial and anti-oxidative properties. *J. Mater Chem. B* 9 (35), 7182–7195. doi:10.1039/d1tb00156f

Shin, Y., Husni, P., Kang, K., Lee, D., Lee, S., Lee, E., et al. (2021). Recent advances in pH- or/and photo-responsive nanovehicles. *Pharmaceutics* 13 (5), 725. doi:10.3390/pharmaceutics13050725

Sim, T., Lim, C., Hoang, N. H., and Oh, K. T. (2017). Recent advance of pH-sensitive nanocarriers targeting solid tumors. *J. Pharm. Investigation* 47 (5), 383–394. doi:10.1007/s40005-017-0349-1

Singh, S. B., Young, K., and Silver, L. L. (2017). What is an "ideal" antibiotic? Discovery challenges and path forward [J]. *Biochem. Pharmacol.* 133, 63–73. doi:10.1016/j.bcp.2017.01.003

Smith, R. S., Zhang, Z., Bouchard, M., et al. (2012). Vascular catheters with a nonleaching poly-sulfobetaine surface modification reduce thrombus formation and microbial attachment [J]. *Sci. Transl. Med.* 4 (153), 153ra32–ra32.

Stewart, P. S., and Franklin, M. J. (2008). Physiological heterogeneity in biofilms. *Nat. Rev. Microbiol.* 6 (3), 199–210. doi:10.1038/nrmicro1838

Sun, C., Ji, S., Li, F., and Xu, H. (2017). Diselenide-containing hyperbranched polymer with light-induced cytotoxicity. *ACS Appl. Mater Interfaces* 9 (15), 12924–12929. doi:10.1021/acsami.7b02367

Sun, H., Hong, Y., Xi, Y., Zou, Y., Gao, J., and Du, J. (2018). Synthesis, self-assembly, and biomedical applications of antimicrobial peptide–polymer conjugates. *Biomacromolecules* 19 (6), 1701–1720. doi:10.1021/acs.biomac.8b00208

Sundaram, H. S., Ella-Menye, J-R., Brault, N. D., Shao, Q., and Jiang, S. (2014). Reversibly switchable polymer with cationic/zwitterionic/anionic behavior through synergistic protonation and deprotonation. *Chem. Sci.* 5 (1), 200–205. doi:10.1039/c3sc52233d

Szymanski, W., Beierle, J. M., Kistemaker, H. A., Velema, W. A., and Feringa, B. L. (2013). Reversible photocontrol of biological systems by the incorporation of molecular photoswitches. *Chem. Rev.* 113 (8), 6114–6178. doi:10.1021/cr300179f

Tacconelli, E., Carrara, E., Savoldi, A., Harbarth, S., Mendelson, M., Monnet, D. L., et al. (2018). Discovery, research, and development of new antibiotics: The WHO priority list of antibiotic-resistant bacteria and tuberculosis. *Lancet Infect. Dis.* 18 (3), 318–327. doi:10.1016/S1473-3099(17)30753-3

Tande Aaron, J., and Patel, R. (2014). Prosthetic joint infection. *Clin. Microbiol. Rev.* 27 (2), 302–345. doi:10.1128/cmr.00111-13

Tang, H., Guo, Y., Peng, L., Fang, H., Wang, Z., Zheng, Y., et al. (2018). *In vivo* targeted, responsive, and synergistic cancer nanotheranostics by magnetic resonance imaging-guided synergistic high-intensity focused ultrasound ablation and chemotherapy. *ACS Appl. Mater Interfaces* 10 (18), 15428–15441. doi:10.1021/acsami.8b01967

Thirunavukkarasu, G. K., Cherukula, K., Lee, H., Jeong, Y. Y., Park, I. K., and Lee, J. Y. (2018). Magnetic field-inducible drug-eluting nanoparticles for image-guided thermo-chemotherapy. *Biomaterials* 180, 240–252. doi:10.1016/j.biomaterials.2018.07.028

Torres, M. D. T., Sothiselvam, S., Lu, T. K., and de la Fuente-Nunez, C. (2019). Peptide design principles for antimicrobial applications. *J. Mol. Biol.* 431 (18), 3547–3567. doi:10.1016/j.jmb.2018.12.015

Traba, C., and Liang, J. F. (2015). Bacteria responsive antibacterial surfaces for indwelling device infections. *J. Control Release* 198, 18–25. doi:10.1016/j.jconrel.2014.11.025

Trouillet-Assant, S., Gallet, M., Nauroy, P., Rasigade, J. P., Flammier, S., Parroche, P., et al. (2015). Dual impact of live *Staphylococcus aureus* on the osteoclast lineage, leading to increased bone resorption. *J. Infect. Dis.* 211 (4), 571–581. doi:10.1093/infdis/jiu386

Ulijn, R. V. (2006). Enzyme-responsive materials: A new class of smart biomaterials. *J. Mater. Chem.* 16 (23), 2217. doi:10.1039/b601776m

Vanbever, R., and Préat, V. (1999). *In vivo* efficacy and safety of skin electroporation. *Adv. Drug Deliv. Rev.* 35 (1), 77–88. doi:10.1016/s0169-409x(98)00064-7

Versace, D. L., Breloy, L., Palierse, E., and Coradin, T. (2021). Contributions of photochemistry to bio-based antibacterial polymer materials. *J. Mater Chem. B* 9 (47), 9624–9641. doi:10.1039/d1tb01801a

Waglechner, N., Culp, E. J., and Wright, G. D. (2021). Ancient antibiotics, ancient resistance. *EcoSal Plus* 9 (2). doi:10.1128/ecosalplus.esp-0027-2020

Wang, J., Xue, Z., Li, G., Wang, Y., Fu, X., Zhong, W. H., et al. (2018). A UV-curable epoxy with "soft" segments for 3D-printable shape-memory materials. *J. Mater. Sci.* 53 (17), 12650–12661. doi:10.1007/s10853-018-2520-0

Wang, L., Cao, W., Yi, Y., and Xu, H. (2014). Dual redox responsive coassemblies of diselenide-containing block copolymers and polymer lipids. *Langmuir* 30 (19), 5628–5636. doi:10.1021/la501054z

Wang, L. S., Gupta, A., and Rotello, V. M. (2016). Nanomaterials for the treatment of bacterial biofilms. *ACS Infect. Dis.* 2 (1), 3–4. doi:10.1021/acsinfecdis.5b00116

Wang, Y., Wu, J., Zhang, D., Chen, F., Fan, P., Zhong, M., et al. (2019). Design of salt-responsive and regenerative antibacterial polymer brushes with integrated bacterial resistance, killing, and release properties. *J. Mater Chem. B* 7 (38), 5762–5774. doi:10.1039/c9tb01313j

Wei, H., Song, X., Liu, P., Yan, X., and Yu, L. (2022). Antimicrobial coating strategy to prevent orthopaedic device-related infections: Recent advances and future perspectives. *Biomater. Adv.* 135, 212739. doi:10.1016/j.bioadv.2022.212739

Wei, T., Tang, Z., Yu, Q., and Chen, H. (2017). Smart antibacterial surfaces with switchable bacteria-killing and bacteria-releasing capabilities. *ACS Appl. Mater Interfaces* 9 (43), 37511–37523. doi:10.1021/acsami.7b13565

Wei, T., Yu, Q., and Chen, H. (2019). Responsive and synergistic antibacterial coatings: Fighting against bacteria in a smart and effective way. *Adv. Healthc. Mater* 8 (3), e1801381. doi:10.1002/adhm.201801381

Welburn, J. P., Tucker, J. A., Johnson, T., Lindert, L., Morgan, M., Willis, A., et al. (2007). How tyrosine 15 phosphorylation inhibits the activity of cyclin-dependent kinase 2-cyclin A. *J. Biol. Chem.* 282 (5), 3173–3181. doi:10.1074/jbc.m609151200

Werner, E., Roe, F., Bugnicourt, A., Franklin, M. J., Heydorn, A., Molin, S., et al. (2004). Stratified growth in *Pseudomonas aeruginosa* biofilms. *Appl. Environ. Microbiol.* 70 (10), 6188–6196. doi:10.1128/aem.70.10.6188-6196.2004

Whitchurch, C. B., Tolker-Nielsen, T., Ragas, P. C., and Mattick, J. S. (2002). Extracellular DNA required for bacterial biofilm formation. *Science* 295 (5559), 1487. doi:10.1126/science.295.5559.1487

Whiteley, M., Diggle, S. P., and Greenberg, E. P. (2017). Progress in and promise of bacterial quorum sensing research. *Nature* 551 (7680), 313–320. doi:10.1038/nature24624

Wieland, J., and Mercorelli, P. (2021). "Simulation of SARS-CoV-2 pandemic in Germany with ordinary differential equations in MATLAB [Z]," in *2021 25th international conference on system theory, control and computing* (Luneburg, Germany: ICSTCC), 564–569. doi:10.1109/icstcc52150.2021.9607181

Williams, P. S., Carpino, F., and Zborowski, M. (2009). Magnetic nanoparticle drug carriers and their study by quadrupole magnetic field-flow fractionation. *Mol. Pharm.* 6 (5), 1290–1306. doi:10.1021/mp900018v

Wright, J. A., and Nair, S. P. (2010). Interaction of staphylococci with bone. *Int. J. Med. Microbiol.* 300 (2), 193–204. doi:10.1016/j.ijmm.2009.10.003

Xiong, M. H., Bao, Y., Yang, X. Z., Wang, Y. C., Sun, B., and Wang, J. (2012). Lipase-sensitive polymeric triple-layered nanogel for "on-demand" drug delivery. *J. Am. Chem. Soc.* 134 (9), 4355–4362. doi:10.1021/ja211279u

Xiong, M. H., Bao, Y., Yang, X. Z., Zhu, Y. H., and Wang, J. (2014). Delivery of antibiotics with polymeric particles. *Adv. Drug Deliv. Rev.* 78, 63–76. doi:10.1016/j.addr.2014.02.002

Xu, Q., Hu, X., and Wang, Y. (2021). Alternatives to conventional antibiotic therapy: Potential therapeutic strategies of combating antimicrobial-resistance and biofilm-related infections. *Mol. Biotechnol.* 63 (12), 1103–1124. doi:10.1007/s12033-021-00371-2

Xu, Z., Zhang, C., Wang, X., and Liu, D. (2021). Release strategies of silver ions from materials for bacterial killing. *ACS Appl. Bio Mater* 4 (5), 3985–3999. doi:10.1021/acsabm.0c01485

Xue, J., Wu, T., Dai, Y., and Xia, Y. (2019). Electrospinning and electrospun nanofibers: Methods, materials, and applications. *Chem. Rev.* 119 (8), 5298–5415. doi:10.1021/acs.chemrev.8b00593

Yang, L., Liu, Y., Wu, H., Song, Z., Hoiby, N., Molin, S., et al. (2012). Combating biofilms. *FEMS Immunol. Med. Microbiol.* 65 (2), 146–157. doi:10.1111/j.1574-695x.2011.00858.x

Yang, Y., Reipa, V., Liu, G., Meng, Y., Wang, X., Mineart, K. P., et al. (2018). pH-sensitive compounds for selective inhibition of acid-producing bacteria. *ACS Appl. Mater Interfaces* 10 (10), 8566–8573. doi:10.1021/acsami.8b01089

Ye, J., Zhang, X., Xie, W., Gong, M., Liao, M., Meng, Q., et al. (2020). An enzyme-responsive prodrug with inflammation-triggered therapeutic drug release characteristics. *Macromol. Biosci.* 20 (9), e2000116. doi:10.1002/mabi.202000116

Ye, M., Zhao, Y., Wang, Y., Yodsanit, N., Xie, R., et al. (2021). A dual-responsive antibiotic-loaded nanoparticle specifically binds pathogens and overcomes antimicrobial-resistant infections. *Adv. Mater* 33 (9), e2006772. doi:10.1002/adma.202006772

Zhang, D., Fu, Y., Huang, L., Zhang, Y., Ren, B., Zhong, M., et al. (2018). Integration of antifouling and antibacterial properties in salt-responsive hydrogels with surface regeneration capacity. *J. Mater Chem. B* 6 (6), 950–960. doi:10.1039/c7tb03018e

Zhao, C., Chen, Q., Patel, K., Li, L., Li, X., Wang, Q., et al. (2012). Synthesis and characterization of pH-sensitive poly(N-2-hydroxyethyl acrylamide)–acrylic acid (poly(HEAA/AA)) nanogels with antifouling protection for controlled release. *Soft Matter* 8 (30), 7848. doi:10.1039/c2sm25861g

Zhao, C., Han, Q., Qin, H., Yan, H., Qian, Z., Ma, Z., et al. (2017). Biocompatible hyperbranched polyester magnetic nanocarrier for stimuli-responsive drug release. *J. Biomater. Sci. Polym. Ed.* 28 (7), 616–628. doi:10.1080/09205063.2017.1289630

Zhao, J., Lee, V. E., Liu, R., and Priestley, R. D. (2019). Responsive polymers as smart nanomaterials enable diverse applications. *Annu. Rev. Chem. Biomol. Eng.* 10, 361–382. doi:10.1146/annurev-chembioeng-060718-030155

Zhong, J. X., Clegg, J. R., Ander, E. W., and Peppas, N. A. (2018). Tunable poly(methacrylic acid-co-acrylamide) nanoparticles through inverse emulsion polymerization. *J. Biomed. Mater Res. A* 106 (6), 1677–1686. doi:10.1002/jbm.a.36371

Zhou, J., Yao, D., Qian, Z., Hou, S., Jenkins, A. T. A., et al. (2018). Bacteria-responsive intelligent wound dressing: Simultaneous *in situ* detection and inhibition of bacterial infection for accelerated wound healing. *Biomaterials* 161, 11–23. doi:10.1016/j.biomaterials.2018.01.024

Zhou, T., Xiao, C., Fan, J., Chen, S., Shen, J., Wu, W., et al. (2013). A nanogel of on-site tunable pH-response for efficient anticancer drug delivery. *Acta Biomater.* 9 (1), 4546–4557. doi:10.1016/j.actbio.2012.08.017

Zhu, Y. J., and Chen, F. (2015). pH-responsive drug-delivery systems. *Chem. Asian J.* 10 (2), 284–305. doi:10.1002/asia.201402715

Zuo, Y. M., Yan, X., Xue, J., Guo, L. Y., Fang, W. W., Sun, T. C., et al. (2020). Enzyme-responsive Ag nanoparticle assemblies in targeting antibacterial against methicillin-resistant *Staphylococcus aureus*. *ACS Appl. Mater Interfaces* 12 (4), 4333–4342. doi:10.1021/acsami.9b22001

frontiers | Frontiers in Bioengineering and Biotechnology

TYPE Systematic Review
PUBLISHED 03 January 2023
DOI 10.3389/fbioe.2022.1065314

OPEN ACCESS

EDITED BY
Yansong Qi,
Inner Mongolia People's Hospital, China

REVIEWED BY
Ning Liang,
First Hospital of Tsinghua University, China
Bo Ren,
Xi'an Honghui Hospital, China
Hosam Alzahrani,
Taif University, Saudi Arabia

*CORRESPONDENCE
Hui Zhang,
zhui76@126.com

SPECIALTY SECTION
This article was submitted to Biomaterials, a section of the journal Frontiers in Bioengineering and Biotechnology

RECEIVED 09 October 2022
ACCEPTED 21 November 2022
PUBLISHED 03 January 2023

CITATION
Zheng T, Cao Y, Song G, Li Y, Zhang Z, Feng Z and Zhang H (2023), Suture tape augmentation, a novel application of synthetic materials in anterior cruciate ligament reconstruction: A systematic review.
Front. Bioeng. Biotechnol. 10:1065314.
doi: 10.3389/fbioe.2022.1065314

Suture tape augmentation, a novel application of synthetic materials in anterior cruciate ligament reconstruction: A systematic review

Tong Zheng, Yanwei Cao, Guanyang Song, Yue Li, Zhijun Zhang, Zheng Feng and Hui Zhang*

Sports Medicine Department, Beijing Jishuitan Hospital, Beijing, China

Objective: Suture tape (ST) is a common synthetic material in the repairing surgery of soft tissue. Recently, ST augmentation (STA) technique has been described as a novel way to improve the mechanical property of grafts in the anterior cruciate ligament (ACL) reconstruction (ACLR). However, the clinical outcomes of ACLR using ST-augmented grafts have not been clarified. This systematic review aimed to summarize the specific technique of STA and evaluate the clinical outcomes after ACLR with STA.

Methods: A electronic search of PubMed and Embase databases with a manual search of Google Scholar was performed to identify studies that reported the clinical outcomes of ACLR with STA. Each included study was abstracted regarding the study features, patient data, surgical information, and outcome measures.

Results: Nine studies were included, representing 314 knees in 314 patients undergoing ACLR with STA. Technically, ST was fixed independently from grafts in six studies and along with grafts in two studies. Most studies applied an equal or slightly less tension on ST than ACL graft. Clinically, significant improvements were found in the Lysholm, IKDC, and KOOS scores after a mean follow-up of 16.7 months. Physical examinations of 220 patients showed significant restoration of knee stability at the final follow-up. 59 of 80 (73.8%) patients returned to preinjury sports level at a minimum 2 year follow-up. Six of 266 (2.3%) patients had a graft failure during the first 2 years postoperatively. The use of ST was significantly associated with better Tegner scores and a trend toward significantly higher rates of return to sport compared to standard ACLR. No significant difference was found in most subjective scores, knee laxity, and graft failures between ACLR with or without STA.

Conclusion: ACLR with STA achieved overall favorable clinical outcomes. Patients using ST-augmented grafts were seemingly associated with better sports performance compared to standard ACLR. But ACLR with STA was not superior to ACLR alone in most functional scores, knee stability measures, and graft failure rates. A tension equal to or slightly less than the ACL graft should be carefully applied on ST during fixation to avoid stress shielding of the graft.

KEYWORDS
anterior cruciate ligament, suture tape, synthetic materials, augmentation, outcomes

Introduction

Anterior cruciate ligament (ACL) injury is a common sports-related knee trauma with steadily increasing incidence over recent years, exceeding seven injuries per 100,000 games among adolescent athletes (Bram et al., 2021). Due to the critical role of an intact ACL in maintaining knee kinematics (Markolf et al., 2009), ligament reconstruction has long time been the gold standard treatment for ACL injury in restoring stability, preventing early degeneration, and achieving return to preinjury sports (Lai et al., 2018). Despite the well-accepted clinical outcomes of arthroscopic ACL reconstruction (ACLR) using soft tissue grafts, the long process of ligamentization could make the grafts vulnerable to reinjury (Claes et al., 2011), and a high risk of graft failure would be worrying (Samuelsen et al., 2017). Previous studies demonstrated that outcomes after ACLR was related to graft choices (Mouarbes et al., 2019). Considering the inherent biological characteristics of commonly used grafts, interest in methods to increase the strength of graft construct has gradually risen in past decades.

Although synthetic devices to replace the ACL graft have been available since the 1970s, high failure rates and complications such as effusion and synovitis have been reported and limited their wide use (Batty et al., 2015). Other than total substitution, an addition of a broad, braided, ultrahigh-molecular-weight polyethylene/polyester suture tape (ST) is frequently applied in the repairing surgery for soft tissue, including at least the rotator cuff tendon (Boksh et al., 2022), ulnar collateral ligament (Carr et al., 2020), and lateral ankle ligament (Lewis et al., 2021). For the ACL injury, adding an ST as an internal brace was reported to improve the clinical outcomes of ACL suture repair, with comparable results in subjective scores, knee stability, and graft failure rate to standard ACLR (Murray et al., 2020; Hoogeslag et al., 2022). Such inspiring findings indicate that adding an ST to the ACL graft might promote graft healing and remodeling and probably reduce the residual laxity and graft rupture for patients undergoing ACLR.

Currently, the ST augmentation (STA) technique has been described as a novel way to enhance the graft for ACLR (Figure 1), supporting the graft in a load-sharing manner and acting as a "safety belt" to prevent the graft from excessive tension, especially in the early phase of ligamentization (Bachmaier et al., 2018). This effect was supported by biomechanical studies demonstrating that ACLR with STA improved graft stiffness and failure load compared to ACLR alone, reducing tibial displacement under anterior load (Torres et al., 2022). In the clinical scenario, the STA technique has been used for ACLR in several sports medicine centers worldwide in recent 5 years (Mackenzie et al., 2022). However, the clinical superiority of ST-augmented grafts remained unclear, and a summary of available literature on clinical outcomes of ACLR with STA is lacking.

Therefore, the purpose of this study was to systematically 1) summarize the specific technique of STA and 2) evaluate the clinical outcomes after ACLR with STA. It was hypothesized that ACLR using ST-augmented grafts would be associated with better functional outcome measures and lower graft failure rates compared to standard ACLR.

Methods

This systematic review was performed following the Preferred Reporting Items for Systematic Reviews and Meta-Analyses (PRISMA) 2020 statement (Page et al., 2021) and was registered in INPLASY (registration number: INPLASY2022100125).

Search strategy

An electronic search of PubMed and Embase databases was conducted on 12 September 2022 to explore studies reporting clinical outcomes of ACLR using ST-augmented grafts. The following key terms were used for the electronic search: (*anterior cruciate ligament* OR *ACL*) AND (*tape* OR *augment* OR *reinforce* OR *internal brace*). The full search strategies used for each of these electronic databases are available in Supplementary Appendix Tables S1, S2. A manual search of Google Scholar was then performed to identify studies not indexed by the Web of Science.

Two authors (Z.Z. and Z.F.) independently assessed all studies and cross-checked the finalized ones according to the inclusion and exclusion criteria (Table 1). The titles and abstracts were initially screened for relevance, then the full texts were critically retrieved for further selection. Reference lists of all included articles were reviewed for potentially eligible studies. Any disagreement about a study's inclusion was resolved by discussion with a third senior author (H.Z.) involved if consensus could not be achieved.

Data extraction

Each finally included study was abstracted regarding the study features, patient data, surgical information, and outcome measures. Two authors (G.S. and Y.L.) independently extracted the original data, and the final decision on the disagreement was made by a third senior author (H.Z.).

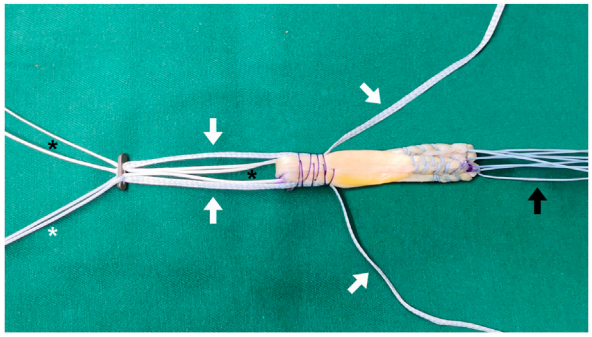

FIGURE 1
The final construct of ST-augmented quadrupled (8-strand) semitendinosus and gracilis tendon autograft, with the ST passing through the femoral button eyelets. White arrow: ST; black arrow: braided nonabsorbable suture; white asterisk: pull suture; black asterisk: adjustable loop suture. ST, suture tape.

Study features consisted of author name, publication year, journal, study design, level of evidence, and methodological quality. Patient data comprised number of cases, sex, age, length of follow-up, and meniscal status. Surgical information was extracted from the specific descriptions in the original studies, including graft details (choice, construct, diameter, and fixation), tape details (indication, product, and fixation), and concomitant procedures. For outcome measures, all subjective and objective results including pain and function scores, knee laxity measurements, return to sports, graft failures, and other complications were documented. Comparison analysis between pre- and postoperative conditions and between patients with and without STA was recorded. Radiographic and arthroscopic outcomes extracted by follow-up magnetic resonance imaging (MRI) and second-look arthroscopy were not reviewed in this systematic review, as there was no available data in the original studies.

TABLE 1 Study inclusion and exclusion criteria.

(1) Studies reporting clinical outcomes of suture tape-augmented auto- or allografts for ACL reconstructions	(1) Studies unrelated to the suture tape
	(2) Studies with the suture tape used for partial ACL injuries
(2) Studies with an adequate description of the construct of augmented grafts	(3) Studies with the suture tape used for ACL repairs
(3) Level of evidence, 1–4	(4) Studies with the suture tape used for other knee ligaments
(4) English-language articles	
(5) Studies without limits placed on the date of publication	(5) Studies with other artificial synthetic devices used for ACL reconstructions
(6) Studies published online or in print in a peer-reviewed journal	(6) Biomechanical studies, reviews, case reports, or technical notes

ACL, anterior cruciate ligament.

Descriptive statistics were used to report study characteristics, patient data, surgical information, and outcome measures. A quantitative comparison (meta-analysis) of the data was considered inappropriate due to the heterogeneity between studies.

Quality appraisal

The methodologic quality of each included study was assessed with the Methodological Index for Non-Randomized Studies (MINORS). The items in the MINORS criteria for non-randomized studies were scored as 0 (not reported), 1 (reported but inadequate), or 2 (reported and adequate) (Slim et al., 2003). For comparative studies, the ideal MINORS score was 24, and a study was considered at low risk of bias when it scored 21–23 and at high risk of bias when it scored ≤20. For non-comparative studies, corresponding thresholds were 16, 13–15, and ≤12 (Slim et al., 2003). The MINORS score of each study was calculated independently by two authors (G.S. and Y.L.). Any disagreement was resolved by discussion until a consensus was reached.

Results

Literature search

The electronic and manual search identified 1,250 studies for initial screening, and 74 studies proceeded to full-text review. Critical application of the inclusion and exclusion criteria finally yielded nine studies (Figure 2). One was a prospective cohort study (level 2) (Shantanu et al., 2019), six were retrospective cohort studies (level 3) (Bodendorfer et al., 2019; Parkes et al., 2021; Allom et al., 2022; Kitchen et al., 2022; Szakiel et al., 2022; von Essen et al., 2022), and two were case series (level 4) (Lavender et al., 2021; Duong et al., 2022). All seven comparative studies were designed to compare patients who underwent ACLR with and without ST-augmented grafts (Table 2).

Quality appraisal

A high risk of bias was confirmed in all seven comparative studies with a mean MINORS value of 18.0 ± 1.6 (range, 16–20). The two non-comparative studies were also at high risk of bias with a MINORS value of 11 for each (Table 2). The risk of bias mainly came from an unblinded assessment of the study endpoint, followed by a lack of prospective calculation of the study size and a historical comparison between the study and control group. The full appraisal for each study is available in Supplementary Appendix Table S3.

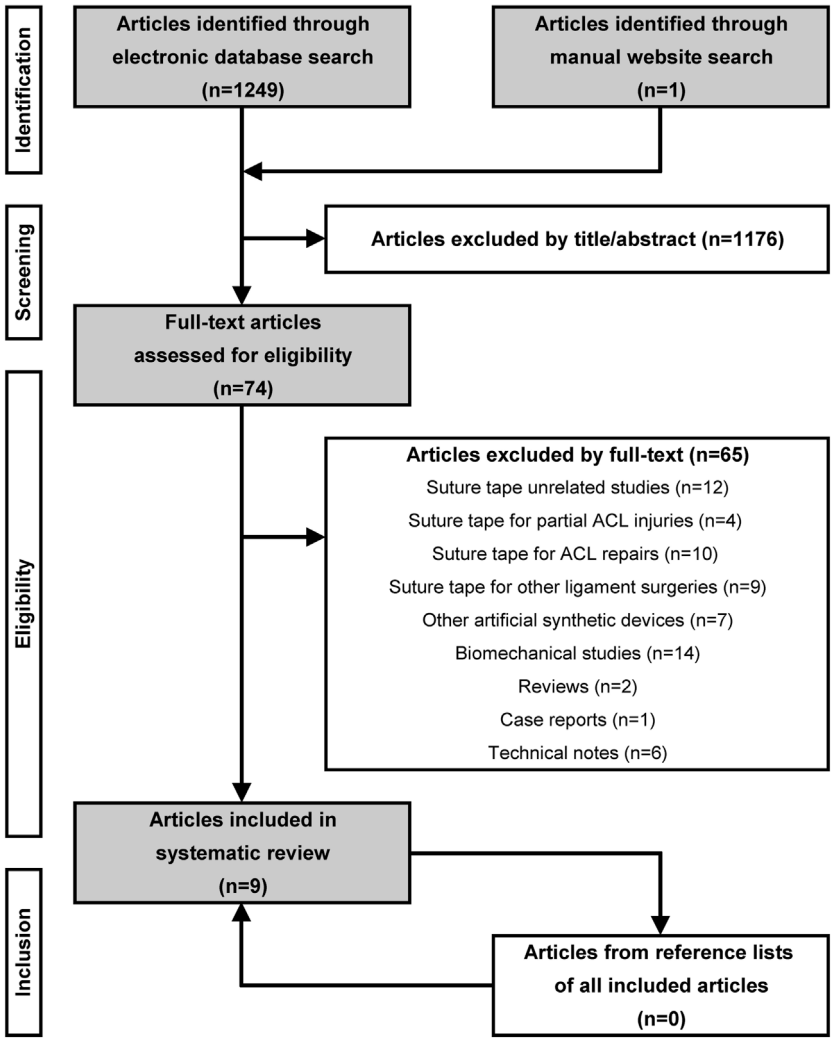

FIGURE 2
Flowchart of search strategy following the PRISMA 2020 statement (Page et al., 2021). ACL, anterior cruciate ligament.

Patient characteristics

A total of 314 knees of 314 patients undergoing ACLR with STA were enrolled in this systematic review (Table 3). There were 190 (60.5%) males and 124 females (39.5%) with a mean age of 26.6 years (range, 15.7–33.0 years). The mean clinical follow-up was 16.7 months (range, 6.0–29.0 months). The meniscal status at the time of ACLR was documented in six studies, and the incidence of meniscal tears was 49.0% (125/255) overall, 32.0% (72/225) for the medial, and 32.9% (74/225) for the lateral.

Surgical information

ACLRs were performed with 283 hamstring tendon auto- or allografts in eight studies, 20 quadriceps tendon autografts in one study, and 11 bone-patellar tendon-bone autografts in one study (Table 4). ACL grafts were augmented with FiberTape (Arthrex, United States) in 231 patients and InternalBrace (Arthrex, United States) in 11 patients, and the product used in the rest 72 patients was not described. Different fixation methods of the graft-ST construct were applied. On the femoral side, the suspensory device was used in eight studies, with the ST

TABLE 2 Study feature and methodologic quality.

First author	Year	Journal	Design	LOE	MINORS	Subjective score	Laxity	RTS	Failure
Shantanu	2019	Int J Orthop Sci	Pro cohort	2	16/24	Lysholm	Yes	No	Yes
Allom	2022	Arthrosc Sports Med Rehabil	Retro cohort	3	16/24	No	Yes	No	Yes
Kitchen	2022	Orthop J Sports Med	Retro cohort	3	17/24	Lysholm, SANE, Tegner, VAS	No	Yes	No
von Essen	2022	J Exp Orthop	Retro cohort	3	19/24	KOOS	Yes	No	Yes
Parkes	2021	Arthroscopy	Retro cohort	3	20/24	Lysholm, IKDC, Tegner	Yes	No	Yes
Bodendorfer	2019	Arthroscopy	Retro cohort	3	20/24	IKDC, KOOS, SANE, VAS, WOMAC	No	Yes	No
Szakiel	2022	J Orthop	Retro cohort	3	18/24	KOOS	No	No	No
Lavender	2021	Arthrosc Sports Med Rehabil	Case series	4	11/16	IKDC	Yes	Yes	Yes
Duong	2022	Asia Pac J Sports Med Arthrosc Rehabil Technol	Case series	4	11/16	Lysholm, IKDC (grade)	Yes	No	Yes

LOE, level of evidence; MINORS, Methodological Index for Non-Randomized Studies; RTS, return to sports; pro, prospective; retro, retrospective; IKDC, international knee documentation committee; KOOS, knee injury and osteoarthritis outcome score; SANE, single assessment numeric evaluation; VAS, visual analogue scale; WOMAC, Western Ontario and McMaster Universities Osteoarthritis Index.

TABLE 3 Patient characteristics between anterior cruciate ligament reconstruction with or without suture tape augmentation.

First author	Size		Sex (M/F)		Age (y)		F-U (mo)		Meniscal tear		MM tear		LM tear	
	Tape	No tape	Tape	No tape	Tape	No tape	Tape	No tape	Tape	No tape	Tape	No tape	Tape	No tape
Shantanu	25	25	21/4	20/5*	27.8	32.2*	6.0	6.0*	NR	NR	NR	NR	NR	NR
Allom	72	97	41/31	53/44*	25.6	27.6*	6.0	6.0*	22	46*	11	29*	11	17*
Kitchen	40	40	19/21	18/22*	15.7	14.9*	27.6	29.0*	19	27*	9	7*	23	15*
von Essen	40	40	23/17	23/17*	29.2	29.2*	12.0	12.0*	23	20*	14	10*	9	10*
Parkes	36	72	25/11	50/22*	25.3	24.9*	26.1	31.3*	27	48*	18	48*	21	48*
Bodendorfer	30	30	13/17	13/17*	29.3	29.7*	29.0	30.1*	8	10*	NR	NR	NR	NR
Szakiel	23	23	12/11	11/12*	31.5	31.5*	24.0	24.0*	NR	NR	NR	NR	NR	NR
Lavender	11	NN	8/3	NN	25.5	NN	24.0	NN	NR	NN	NR	NN	NR	NN
Duong	37	NN	28/9	NN	33.0	NN	12.0	NN	26	NN	20	NN	10	NN
Overall	314	327	190/124	188/139	26.6	26.5	16.7	18.6	125	151	72	94	74	90

M, male; F, female; F-U, follow-up; MM, medial meniscus; LM, lateral meniscus; NR, not reported; NN, not needed.
*no significant difference ($p > 0.05$) between grafts with or without suture tape.

passing through the eyelets of the suspensory button in eight studies and the loop of the suspensory button in two studies. On the tibial side, the suspensory device was used in seven studies and the interference screw in two studies, with the ST fixed independently from the graft using an additional anchor before graft fixation in six studies and along with the graft using the same fixation device in two studies. Most studies applied an equal or slightly less tension on the ST than the ACL graft during fixation. For all studies, the use of ST was based on the surgeon's preference, except for one prospective cohort study with randomized selection. Concomitant lateral extra-articular tenodesis was performed in one study (Allom et al., 2022) for 84/169 patients with risk factors for graft rupture.

Subjective scores

Overall, eight subjective scores were reported in eight out of nine studies: the Lysholm score in four studies, International Knee Documentation Committee (IKDC) score in three studies,

TABLE 4 Surgical technique of anterior cruciate ligament reconstruction with suture tape augmentation.

First author	Size	Graft					Suture tape		
		Choice	Strand	Diameter, mm	Fem fix	Tib fix	Product	Fem fix	Tib fix
Shantanu	25	HT (ST + G)	Quadrupled	NR	SD	NR	FiberTape	Loop	NR
Allom	72	HT (ST ± G)	Quadrupled	≥8.5 (M), ≥8 (F)	SD	SD	NR	Eyelets/loop	Add anchor
Kitchen	40	HT (ST + G)	Quadrupled	<8 (29), ≥8 (11)	SD	IS	FiberTape	Eyelets	With graft
von Essen	20	HT (ST)	Quadrupled	8–10	SD	SD	FiberTape	Eyelets	With graft
	20	QT	Quad	10 (width)	SD	SD	FiberTape	Eyelets	With graft
Parkes	36	HT (ST ± G)	Quadrupled	NR	SD	SD	FiberTape	Eyelets	Add anchor
Bodendorfer	30	HT (ST, auto ± allo)	Quadrupled	8–10	SD	SD	FiberTape	Eyelets	Add anchor
Szakiel	23	HT (ST)	Quadrupled	NR	SD	SD	FiberTape	Eyelets	Add anchor
Lavender	11	BPTB (auto/allo)	Quad	NR	SD	SD	InternalBrace	Eyelets	Add anchor
Duong	37	HT (ST)	Quadrupled	7–8	SD	SD	FiberTape	Eyelets	Add anchor

fem, femoral; tib, tibial; fix, fixation; HT, hamstring tendon; ST, semitendinosus tendon; G, gracilis tendon; QT, quadriceps tendon; BPTB, bone-patellar tendon-bone; auto, autograft; allo, allograft; M, male; F, female; SD, suspensory device; IS, interference screw; loop, suture tape passed through the loop of the femoral button; eyelets, suture tape passed through the eyelets of the femoral button; add, additional, NR, not reported.

Knee injury and Osteoarthritis Outcome Score (KOOS) score in three studies, Single Assessment Numeric Evaluation (SANE) score in two studies, Tegner activity score in two studies, visual analogue scale (VAS) score in two studies, Western Ontario and McMaster Universities Osteoarthritis (WOMAC) score in one study, and IKDC grade in one study. The remaining one study (Allom et al., 2022) not reporting any subjective score (Table 2).

Seven studies compared subjective scores between pre- and postoperative status for ACLR with STA, and significant improvement was reported in six studies. Those used at least in two studies included the Lysholm score from 61.2 to 91.2 (Shantanu et al., 2019; Duong et al., 2022), IKDC score from 30.7 to 85.8 (Bodendorfer et al., 2019; Lavender et al., 2021), and KOOS score from 60.9 to 89.1 (Bodendorfer et al., 2019; Szakiel et al., 2022; von Essen et al., 2022). The IKDC grade was reported in one study (Duong et al., 2022) with the grade (A/B/C/D) from 0/0/19/18 to 30/7/0/0. The comparison of the other three scores was only performed in one study (Bodendorfer et al., 2019) with the SANE score from 96.0 to 90.0, VAS score from 7.1 to 1.6, and WOMAC score from 35.5 to 2.2. Only one study (Parkes et al., 2021) demonstrated no significant improvement in the Tegner score (from 7.2 to 7.1).

Six studies compared subjective scores between ACLR with or without STA at the final follow-up. The Tegner score used in two studies (Parkes et al., 2021; Kitchen et al., 2022) both yielded superior results in the augmentation group. Results of other scores were inconsistent across studies. Only one study (Bodendorfer et al., 2019) reported that the VAS (1.6 *versus* 3.4), IKDC (87.6 *versus* 73.2), KOOS (92.2 *versus* 87.1), SANE (90.0 *versus* 80.0), and WOMAC (2.2 *versus* 6.2) score were all significantly better in augmentation group. However, no significant superiority of any score other than the Tenger was found in the augmentation group among other studies (Table 5).

Objective knee laxity

Knee laxity was evaluated by the Lachman test in five studies, pivot shift test in four studies, and KT-1000/2000 arthrometer test in two studies (Table 6). In all these studies, significant improvement in objective stability was reported in patients with ST-augmented grafts at the final follow-up. The comparative analysis of knee laxity between ACLR using ST-augmented grafts and not was performed in four studies. No studies reported superior objective stability in the augmentation group at the final follow-up, although one of which (Shantanu et al., 2019) reported better improvement in grades of the Lachman test as the preoperative laxity in the augmentation group was severer.

Return to sports

The ability to return to preinjury sports level was evaluated in three studies, with an overall rate of 73.8% (range, 69.2%–81.8%) in patients with ST-augmented ACL grafts (Table 7). The ability to return to sports between patients with or without STA was compared in two studies. Both demonstrated no (but a trend toward) significant difference in the rate of return to sports at a minimum 2-year follow-up, and one of them (Bodendorfer et al., 2019) reported that the use of ST was significantly correlated with earlier time to return (9.2 months *versus* 12.9 months).

Graft failures and other complications

The graft failure and other major complications were recorded in seven studies (Table 8). The overall failure rate of ST-augmented grafts was 2.3% (range, 0%–6.7%) among

TABLE 5 Postoperative subjective scores between anterior cruciate ligament reconstruction with or without suture tape augmentation.

First author	Graft choice	Size		Mean VAS		Mean Lysholm		Mean IKDC		Mean KOOS		Mean SANE		Mean Tegner	
		Tape	No tape	Tape	No tape	Tape	No tape	Tape	No tape	Tape	No tape	Tape	No tape	Tape	No tape
Shantanu	HT	25	25	NR	NR	87.0	87.0**	NR	NR	NR	NR	NR	NR	NR	NR
Kitchen	HT	40	40	1.0	1.0**	92.7	92.1**	NR	NR	NR	NR	90.6	87.6**	7.4	6.3*
von Essen	HT	14	19	NR	NR	NR	NR	NR	NR	83.9	88.4**	NR	NR	NR	NR
	QT	15	9	NR	NR	NR	NR	NR	NR	87.2	77.0**	NR	NR	NR	NR
Parkes	HT	36	72	NR	NR	95.6	94.0**	94.4	93.8**	NR	NR	NR	NR	7.1	6.4*
Bodendorfer	HT	30	30	1.6	3.4*	NR	NR	87.6	73.2*	92.2	87.1*	90.0	80.0*	NR	NR
Szakiel	HT	23	22	NR	NR	NR	NR	NR	NR	92.1	87.5**	NR	NR	NR	NR
Overall		183	217	1.3	2.0	92.3	92.2	91.3	87.7	89.8	86.4	90.3	84.3	7.3	6.4

VAS, visual analogue scale; IKDC, international knee documentation committee; KOOS, knee injury and osteoarthritis outcome score; SANE, single assessment numeric evaluation; HT, hamstring tendon; QT, quadriceps tendon; NR, not reported; NN, not needed.
*, significant difference ($p < 0.05$) between grafts with or without suture tape.
**, no significant difference ($p > 0.05$) between grafts with or without suture tape.

TABLE 6 Postoperative objective knee laxity between anterior cruciate ligament reconstruction with or without suture tape augmentation.

First author	Graft choice	Minimum F-U, mo	Size		KT-1000/ 2000 SSD, mm		Lachman, nor/ abnor		Pivot shift, nor/ abnor	
			Tape	No tape	Tape	No tape	Tape	No tape	Tape	No tape
Shantanu	HT	6	25	25	NR	NR	23/2**	21/4***	NR	NR
Allom	HT	6	72	97	1.2**	1.3***	NR	NR	NR	NR
von Essen	HT	6	20 (16*)	20 (20*)	1.4**	2.3***	16/4**	17/3***	20/0**	20/0***
	QT	6	20 (16*)	20 (12*)	1.8**	2.0***	17/3**	17/3***	20/0**	20/0***
Parkes	HT	24	35	68	NR	NR	34/1**	65/3***	35/0**	66/2***
Lavender	BPTB	6	11	NN	NR	NN	11/0**	NN	11/0**	NN
Duong	HT	12	37	NN	NR	NN	37/0**	NN	37/0**	NN
Overall			220	230	1.3	1.5	138/10	120/13	123/0	106/2

F-U, follow-up; SSD, side-to-side difference; nor, normal; abnor, abnormal; HT, hamstring tendon; QT, quadriceps tendon; BPTB, bone-patellar tendon-bone; NR, not reported; NN, not needed.
*, number of patients who underwent KT-1000/2000 arthrometer test.
**, significant difference ($p < 0.05$) between pre- and postoperative status for grafts with suture tape.
***, no significant difference ($p > 0.05$) between grafts with or without suture tape.

TABLE 7 Return to preinjury sports level between anterior cruciate ligament reconstruction with or without suture tape augmentation.

First author	Graft choice	Minimum follow-up	Size		Able to return		
			Tape	No tape	Tape, n (%)	No tape, n (%)	value
Kitchen	HT	24 months	39	33	27 (69.2)	17 (51.5)	$p = 0.124$
Bodendorfer	HT	24 months	30	30	23 (76.7)	17 (56.7)	$p = 0.100$
Lavender	BPTB	24 months	11	Not needed	9 (81.8)	Not needed	Not needed
Overall			80	63	59 (73.8)	34 (54.0)	

HT, hamstring tendon; BPTB, bone-patellar tendon-bone.

TABLE 8 Graft failure and other complications between anterior cruciate ligament reconstruction with or without suture tape augmentation.

First author	Graft choice	Minimum F-U, mo	Size		Graft failure, n (%)		Other complications	
			Tape	No tape	Tape	No tape	Tape	No tape
Allom	HT	6	72	97	0 (0.0)	0 (0.0)*	1 meniscal tear	1 cyclops lesion
Kitchen	HT	24	40	40	2 (5.0)	7 (17.5)*	2 meniscal tears, 1 infection	2 meniscal tears
Von Essen	HT	24	20	20	1 (5.0)	0 (0.0)*	1 meniscal tear, 1 cyclops lesion	2 meniscal tears, 2 cyclops lesions
	QT	24	20	20	0 (0.0)	2 (10.0)*	None	2 meniscal tears, 1 cyclops lesion
Parkes	HT	24	36	72	1 (2.8)	4 (5.6)*	2 meniscal tears, 2 arthrofibrosis, 1 cyclops lesion	3 meniscal tears, 3 arthrofibrosis, 1 infection
Bodendorfer	HT	24	30	30	2 (6.7)	2 (6.7)*	2 arthrofibrosis	1 arthrofibrosis
Lavender	BPTB	24	11		0 (0.0)	NN	1 arthrofibrosis	Not needed
Duong	HT	12	37		0 (0.0)	NN	None	Not needed
Overall			266	279	6 (2.3)	15 (5.4)		

F-U, follow-up; HT, hamstring tendon; QT, quadriceps tendon; BPTB, bone-patellar tendon-bone; NN, not needed.
*, no significant difference ($p > 0.05$) between grafts with or without suture tape.

266 patients. The comparison of failure between grafts with or without ST proceeded in five studies. Almost all studies reported a lower failure rate in ST-augmented grafts, but the difference did not meet statistical significance. Other complications including further meniscal tear, arthrofibrosis, cyclops lesion, and infection were also not significantly different in any of these studies.

Discussion

The most important findings of this systematic review could be summarized as follows: 1) patients with ST-augmented grafts obtained overall favorable clinical outcomes after ACLR; 2) the use of ST was associated with significantly higher Tegner activity score and a trend toward significantly better ability to return to sports compared with standard ACLR; 3) no significant differences in most subjective scores, knee laxity, and graft failure were found between patients undergoing ACLR with STA and ACLR alone; and 4) most authors preferred an equal or slightly less tension on the ST than the ACL graft during fixation.

In recent 2–5 years, the use of ST to improve the biomechanical performance of ACL graft has been a hot topic in the field of sports medicine, intending to protect the graft from over-loads during the early rehabilitation phase when the graft is weak secondary to necrosis and remodeling process during this time (Claes et al., 2011). As suggested by animal models, adding an ST improved the mechanical properties of the ACL graft by the load-sharing effect, characterized by reduced graft elongation and increased load to failure (Bachmaier et al., 2018), and this function was especially dramatic in smaller -diameter grafts (Noonan et al., 2020), occurring earlier and carrying final loads with a greater extent (Bachmaier et al., 2022). Cadaveric studies further demonstrated that the increased graft-ST construct stiffness was associated with improved knee stability after ACLR, manifested as decreased tibial displacement under anterior load when the ACL graft was augmented with ST (Torres et al., 2022).

Despite increased mechanical strength, an over-tensioned ST possibly led to stress shielding of the ACL graft, compromising the graft ligamentization process (Muellner et al., 2001). Therefore, proper tension of the ST should be carefully applied during fixation in clinical practice to avoid stress shielding of the graft. Among the included studies, the majority preferred to fix the ST independent from the graft on the tibial side, with equal or slightly less manual tension on the ST. If fixed together, the ST was pulled to just remove the slack but without applying tension on the ST. For the same purpose, some suggested fixing the ST in full or hyperextension and the graft in 30° of flexion. As proposed by biomechanical studies, an ideal augmentation effect should be dynamic, permitting lower loads transferred by the graft and only acting as a "safety belt" when strains exceed (Bachmaier et al., 2018). However, whether mechanically improved graft constructs would achieve better surgical outcomes of ACLR in clinical scenarios needs to be further verified.

For the functional outcomes in patients with ACLR and STA, this systematic review showed consistent improvements in nearly all subjective scores at a mean follow-up of 16.7 months, indicating amelioration of clinical symptoms. Meanwhile,

significant improvement in objective knee stability was reported in five studies, and no positive pivot shift was observed at the final follow-up. However, as opposed to the study hypothesis, the addition of ST failed to show superiority in either subjective scores or objective stability compared to standard ACLR among nearly all included studies. Based on this evidence, improved mechanical behavior of ST-augmented grafts would not necessarily lead to better subjective function and mechanical stability after ACLR, and the clinical implication of STA requires assessments from specific aspects.

Interestingly, the only subjective score exhibiting superiority in STA was the Tegner activity score, implying better maintenance of sports level in patients using augmented grafts. Such findings were consistent with the results on the ability to return to sports that patients with STA had a significantly earlier time to return to preinjury level and a trend toward a significantly higher proportion to return to preinjury level. Meanwhile, the rate (69.2%–81.8%) of return to preinjury level in patients undergoing ACLR and STA was comparable with the literature. In a recent systematic review of ACLR in the athletic population, the rate of return to preinjury level was 32%–64% in bone-patellar tendon-bone autografts and 9%–65% in hamstring tendon autografts (DeFazio et al., 2020). The causes of better sports performance in patients with STA was unable to be clarified according to the current data since the objective stability was similar and the rehabilitation protocol was identical between patient with or without STA. A potential explanation could be the better confidence in return to sports in patients with STA as they were aware of the use of ST (Keays et al., 2022).

One of the expectations for the use of STA is to protect the ACL graft from a high risk of failure. In this systematic review, the failure rate of ST-augmented ranged from 0% to 6.7%, considered satisfactory and compared similarly to the results of previous studies that 0%–6.1% of athletes experienced graft ruptures at a minimum 2-year follow-up after standard ACLR (DeFazio et al., 2020). Nevertheless, although the use of ST was seemingly associated with a lower failure rate, the difference between grafts with or without ST was not of statistical significance. Considering that half to three-quarters of graft failures would occur in the first 1–2 years following ACLR (Webster and Feller, 2016), the mechanical protection of ST to the ACL graft might not reduce the risk of failures.

The biocompatibility of synthetic material is another concern about the intra-articular use of ST. Even for the more recent designs of synthetic ligament devices, the chronic inflammatory response of the synovium was still reported to be a common finding after ACLR using the Ligament Augmentation and Reconstruction System, which comprises fibers of terephthalic polyethylene polyester (Tulloch et al., 2019). However, histologic assessments in an animal model did not confirm any ST-associated immune responses or cartilage erosions at 6 months following ACLR and STA (Smith et al., 2019). In this systematic review, complications including arthrofibrosis, cyclops lesion, and infection were at a low incidence and similar between ACLR with or without STA, supporting the safety of ST added in ACL grafts.

Clinically, the signal intensity on MRI has been commonly used to monitor the graft ligamentization process after ACLR, with a higher intensity revealing a poor structural strength (Fleming et al., 2011). According to radiological studies, the signal intensity of ACL graft reached its peak at 6 months, followed by a gradual decline until 2–3 years postoperatively (Lansdown et al., 2020; Warth et al., 2020). Unfortunately, no included studies conducted an MRI analysis of ACL grafts. A serial evaluation of the graft signal is necessary to explore if the ligamentization process would be improved with the STA technique in future studies.

Limitations

The limitations of this systematic review were largely from the results of input literature. Firstly, the low level of evidence and high risk of bias within the majority of included studies lowered the validity of this review. Second, the heterogeneity and insufficient data across the original literature restricted the application of a formal meta-analysis. Third, variable reports of outcome measures made this review unable to draw a firm conclusion on the superiority of STA from the clinical perspective. Fourth, the surgical indication of STA lacked a specific description, leading to uncertainty that patients with what features would more benefit from the ST-augmented grafts. Fifth, no radiological or arthroscopic methods were used to evaluate the intra-articular condition after ACLR with STA. Despite the limitations, this is the first study to systematically review the clinical outcomes of ACLR with STA, with a comparison to standard ACLR. This study could be helpful to direct future studies that seek to explore the clinical effectiveness of STA in ACLR.

Conclusion

Clinically, the application of STA achieved overall favorable outcomes in patients with ACLR. ACLR using ST-augmented grafts was seemingly associated with better sports performance compared to standard ACLR. However, despite inconsistent reports across original studies, ACLR with STA did not yield superior results in most functional scores, knee stability measures, and graft failure rates than ACLR alone. Technically, proper tension of the ST should be carefully applied during fixation with an equal or slightly less tension on the ST than the ACL graft to avoid stress shielding of the graft.

Data availability statement

The data analyzed in this study is subject to the following licenses/restrictions: This is a systematic review using data extracted from previously published literature. Requests to access these datasets should be directed to TZ, zhengtong2020@pku.edu.cn.

Author contributions

TZ conducted the descriptive statistics and drafted the manuscript. YC participated in the data analysis and helped to draft the manuscript. GS and YL extracted the original data and assessed the methodologic quality. ZZ and ZF retrieved the literature and completed the study inclusion. HZ conceived the study and was involved in the study inclusion and data extraction. All authors reviewed and approved the final version of the manuscript.

Funding

GS has received funding from the National Natural Science Foundation of China (82002288) and Beijing Municipal Health Commission (BJRITO-RDP-2023). YL has received funding from the Beijing Municipal Excellent Talents Foundation (2018000021469G224). HZ has received funding from the National Natural Science Foundation of China (82172514), Beijing Municipal Science and Technology Commission (Z211100002921043), Capital Health Research and Development of Special Fund (CFH 2020-1-2071 and CFH 2020-2-2075), and Beijing Jishuitan Hospital High-Level Talent Program (XKGG202109).

Conflict of interest

The authors declare that the research was conducted in the absence of any commercial or financial relationships that could be construed as a potential conflict of interest.

Publisher's note

All claims expressed in this article are solely those of the authors and do not necessarily represent those of their affiliated organizations, or those of the publisher, the editors and the reviewers. Any product that may be evaluated in this article, or claim that may be made by its manufacturer, is not guaranteed or endorsed by the publisher.

Supplementary material

The Supplementary Material for this article can be found online at: https://www.frontiersin.org/articles/10.3389/fbioe.2022.1065314/full#supplementary-material

References

Allom, R. J., Wood, J. A., Chen, D. B., and Macdessi, S. J. (2022). The addition of suture tape to the hamstring graft construct does not reduce instrumented knee laxity following ACL reconstruction. *Arthrosc. Sports Med. Rehabilitation* 4 (2), e545–e551. doi:10.1016/j.asmr.2021.11.015

Bachmaier, S., Smith, P. A., Argintar, E. H., Chahla, J., Higgins, L. D., and Wijdicks, C. A. (2022). Independent suture augmentation with all-inside anterior cruciate ligament reconstruction reduces peak loads on soft-tissue graft. A biomechanical full-construct study. *Arthrosc. J. Arthrosc. Relat. Surg.* 38 (1), 88–98. doi:10.1016/j.arthro.2021.09.032

Bachmaier, S., Smith, P. A., Bley, J., and Wijdicks, C. A. (2018). Independent suture tape reinforcement of small and standard diameter grafts for anterior cruciate ligament reconstruction: A biomechanical full construct model. *Arthrosc. J. Arthrosc. Relat. Surg.* 34 (2), 490–499. doi:10.1016/j.arthro.2017.10.037

Batty, L. M., Norsworthy, C. J., Lash, N. J., Wasiak, J., Richmond, A. K., and Feller, J. A. (2015). Synthetic devices for reconstructive surgery of the cruciate ligaments: A systematic review. *Arthrosc. J. Arthrosc. Relat. Surg.* 31 (5), 957–968. doi:10.1016/j.arthro.2014.11.032

Bodendorfer, B. M., Michaelson, E. M., Shu, H. T., Apseloff, N. A., Spratt, J. D., Nolton, E. C., et al. (2019). Suture augmented versus standard anterior cruciate ligament reconstruction: A matched comparative analysis. *Arthrosc. J. Arthrosc. Relat. Surg.* 35 (7), 2114–2122. doi:10.1016/j.arthro.2019.01.054

Boksh, K., Haque, A., Sharma, A., Divall, P., and Singh, H. (2022). Use of suture Tapes versus conventional sutures for arthroscopic rotator cuff repairs: A systematic review and meta-analysis. *Am. J. Sports Med.* 50 (1), 264–272. doi:10.1177/0363546521998318

Bram, J. T., Magee, L. C., Mehta, N. N., Patel, N. M., and Ganley, T. J. (2021). Anterior cruciate ligament injury incidence in adolescent athletes: A systematic review and meta-analysis. *Am. J. Sports Med.* 49 (7), 1962–1972. doi:10.1177/0363546520959619

Carr, J. B., Camp, C. L., and Dines, J. S. (2020). Elbow ulnar collateral ligament injuries: Indications, management, and outcomes. *Arthrosc. J. Arthrosc. Relat. Surg.* 36 (5), 1221–1222. doi:10.1016/j.arthro.2020.02.022

Claes, S., Verdonk, P., Forsyth, R., and Bellemans, J. (2011). The "ligamentization" process in anterior cruciate ligament reconstruction: What happens to the human graft? A systematic review of the literature. *Am. J. Sports Med.* 39 (11), 2476–2483. doi:10.1177/0363546511402662

Defazio, M. W., Curry, E. J., Gustin, M. J., Sing, D. C., Abdul-Rassoul, H., Ma, R., et al. (2020). Return to sport after ACL reconstruction with a btb versus hamstring tendon autograft: A systematic review and meta-analysis. *Orthop. J. Sports Med.* 8 (12), 232596712096491. doi:10.1177/2325967120964919

Duong, T. D., Tran, D. T., Do, B. N. T., Nguyen, T. T., Le, S. M., and Le, H. H. (2022). All-inside arthroscopic anterior cruciate ligament reconstruction with internal brace ligament augmentation using semitendinosus tendon autograft: A case series. *Asia-Pacific J. Sports Med. Arthrosc. Rehabilitation Technol.* 29, 15–21. doi:10.1016/j.asmart.2022.05.002

Fleming, B. C., Vajapeyam, S., Connolly, S. A., Magarian, E. M., and Murray, M. M. (2011). The use of magnetic resonance imaging to predict ACL graft structural properties. *J. Biomechanics* 44 (16), 2843–2846. doi:10.1016/j.jbiomech.2011.09.004

Hoogeslag, R. a. G., T Veld, R., Brouwer, R. W., De Graaff, F., and Verdonschot, N. (2022). Huis inAcute anterior cruciate ligament rupture: Repair or reconstruction? Five-year results of a randomized controlled clinical trial. *Am. J. Sports Med.* 50 (7), 1779–1787. doi:10.1177/03635465221090527

Keays, S. L., Mellifont, D. B., Keays, A. C., Stuelcken, M. C., Lovell, D. I., and Sayers, M. G. L. (2022). Long-term return to sports after anterior cruciate ligament injury: Reconstruction vs No reconstruction-A comparison of 2 case series. *Am. J. Sports Med.* 50 (4), 912–921. doi:10.1177/03635465211073152

Kitchen, B. T., Mitchell, B. C., Cognetti, D. J., Siow, M. Y., Howard, R., Carroll, A. N., et al. (2022). Outcomes after hamstring ACL reconstruction with suture tape reinforcement in adolescent athletes. *Orthop. J. Sports Med.* 10 (4), 232596712210855. doi:10.1177/23259671221085577

Lai, C. C. H., Ardern, C. L., Feller, J. A., and Webster, K. E. (2018). Eighty-three per cent of elite athletes return to preinjury sport after anterior cruciate ligament reconstruction: A systematic review with meta-analysis of return to sport rates, graft rupture rates and performance outcomes. *Br. J. Sports Med.* 52 (2), 128–138. doi:10.1136/bjsports-2016-096836

Lansdown, D. A., Xiao, W., Zhang, A. L., Allen, C. R., Feeley, B. T., Li, X., et al. (2020). Quantitative imaging of anterior cruciate ligament (ACL) graft demonstrates longitudinal compositional changes and relationships with clinical outcomes at 2 years after ACL reconstruction. *J. Orthop. Res.* 38 (6), 1289–1295. doi:10.1002/jor.24572

Lavender, C., Singh, V., Berdis, G., Fravel, W., Lamba, C., and Patel, T. (2021). Anterior cruciate ligament (ACL) reconstruction augmented with bone marrow concentrate, demineralized bone matrix, autograft bone, and a suture tape (the fertilized ACL). *Arthrosc. Sports Med. Rehabilitation* 3 (6), e1719–e1722. doi:10.1016/j.asmr.2021.07.030

Lewis, T. L., Joseph, A., Patel, A., Ahluwalia, R., and Ray, R. (2021). Modified brostrom repair with suture tape augmentation for lateral ankle instability: A systematic review. *Foot Ankle Surg.* 27 (3), 278–284. doi:10.1016/j.fas.2020.12.004

Mackenzie, C. E. A., Huntington, L. S., and Tulloch, S. (2022). Suture tape augmentation of anterior cruciate ligament reconstruction increases biomechanical stability: A scoping review of biomechanical, animal, and clinical studies. *Arthrosc. J. Arthrosc. Relat. Surg.* 38 (6), 2073–2089. doi:10.1016/j.arthro.2021.12.036

Markolf, K. L., Park, S., Jackson, S. R., and Mcallister, D. R. (2009). Anterior-posterior and rotatory stability of single and double-bundle anterior cruciate ligament reconstructions. *J. Bone Jt. Surgery-American Volume* 91 (1), 107–118. doi:10.2106/JBJS.G.01215

Mouarbes, D., Menetrey, J., Marot, V., Courtot, L., Berard, E., and Cavaignac, E. (2019). Anterior cruciate ligament reconstruction: A systematic review and meta-analysis of outcomes for quadriceps tendon autograft versus bone-patellar tendon-bone and hamstring-tendon autografts. *Am. J. Sports Med.* 47 (14), 3531–3540. doi:10.1177/0363546518825340

Muellner, T., Kwasny, O., Loehnert, V., Mallinger, R., Unfried, G., Schabus, R., et al. (2001). Light and electron microscopic study of stress-shielding effects on rat patellar tendon. *Archives Orthop. Trauma Surg.* 121 (10), 561–565. doi:10.1007/s004020100281

Murray, M. M., Fleming, B. C., Badger, G. J., Team, B. T., Freiberger, C., Henderson, R., et al. (2020). Bridge-enhanced anterior cruciate ligament repair is not inferior to autograft anterior cruciate ligament reconstruction at 2 Years: Results of a prospective randomized clinical trial. *Am. J. Sports Med.* 48 (6), 1305–1315. doi:10.1177/0363546520913532

Noonan, B. C., Bachmaier, S., Wijdicks, C. A., and Bedi, A. (2020). Independent suture tape reinforcement of tripled smaller-diameter and quadrupled grafts for anterior cruciate ligament reconstruction with tibial screw fixation: A biomechanical full construct model. *Arthrosc. J. Arthrosc. Relat. Surg.* 36 (2), 481–489. doi:10.1016/j.arthro.2019.06.036

Page, M. J., Moher, D., Bossuyt, P. M., Boutron, I., Hoffmann, T. C., Mulrow, C. D., et al. (2021). PRISMA 2020 explanation and elaboration: Updated guidance and exemplars for reporting systematic reviews. *BMJ* 372, n160. doi:10.1136/bmj.n160

Parkes, C. W., Leland, D. P., Levy, B. A., Stuart, M. J., Camp, C. L., Saris, D. B. F., et al. (2021). Hamstring autograft anterior cruciate ligament reconstruction using an all-inside technique with and without independent suture tape reinforcement. *Arthrosc. J. Arthrosc. Relat. Surg.* 37 (2), 609–616. doi:10.1016/j.arthro.2020.09.002

Samuelsen, B. T., Webster, K. E., Johnson, N. R., Hewett, T. E., and Krych, A. J. (2017). Hamstring autograft versus patellar tendon autograft for ACL reconstruction: Is there a difference in graft failure rate? A meta-analysis of 47, 613 patients. *Clin. Orthop. Relat. Res.* 475 (10), 2459–2468. doi:10.1007/s11999-017-5278-9

Shantanu, K., Singh, S., Ratha, S., Kumar, D., and Sharma, V. (2019). Comparative study of functional outcomes of arthroscopic ACL reconstruction by augmented hamstring graft with fiber tape and hamstring graft alone: A prospective study. *Int. J. Orthop. Sci.* 5 (3), 165–173. doi:10.22271/ortho.2019.v5.i3d.1526

Slim, K., Nini, E., Forestier, D., Kwiatkowski, F., Panis, Y., and Chipponi, J. (2003). Methodological index for non-randomized studies (minors): Development and validation of a new instrument. *ANZ J. Surg.* 73 (9), 712–716. doi:10.1046/j.1445-2197.2003.02748.x

Smith, P. A., Bozynski, C. C., Kuroki, K., Henrich, S. M., Wijdicks, C. A., and Cook, J. L. (2019). Intra-articular biocompatibility of multistranded, long-chain polyethylene suture tape in a canine ACL model. *J. Knee Surg.* 32 (6), 525–531. doi:10.1055/s-0038-1655765

Szakiel, P. M., Aksu, N. E., Kirloskar, K. M., Gruber, M. D., Zittel, K. W., Grieme, C. V., et al. (2022). Rehabilitation and functional outcomes in internally braced and standard ACL reconstructions. *J. Orthop.* 33, 95–99. doi:10.1016/j.jor.2022.07.002

Torres, S. J., Nelson, T. J., Pham, N., Uffmann, W., Limpisvasti, O., and Metzger, M. F. (2022). Suture tape augmentation increases the time-zero stiffness and strength of anterior cruciate ligament grafts: A cadaveric study. *Arthrosc. Sports Med. Rehabilitation* 4 (4), e1253–e1259. doi:10.1016/j.asmr.2022.02.008

Tulloch, S. J., Devitt, B. M., Norsworthy, C. J., and Mow, C. (2019). Synovitis following anterior cruciate ligament reconstruction using the LARS device. *Knee Surg. Sports Traumatol. Arthrosc.* 27 (8), 2592–2598. doi:10.1007/s00167-018-5280-0

Von Essen, C., Sarakatsianos, V., Cristiani, R., and Stalman, A. (2022). Suture tape reinforcement of hamstring tendon graft reduces postoperative knee laxity after primary ACL reconstruction. *J. Exp. Orthop.* 9 (1), 20. doi:10.1186/s40634-022-00454-2

Warth, R. J., Zandiyeh, P., Rao, M., Gabr, R. E., Tashman, S., Kumaravel, M., et al. (2020). Quantitative assessment of *in vivo* human anterior cruciate ligament autograft remodeling: A 3-dimensional UTE-T2* imaging study. *Am. J. Sports Med.* 48 (12), 2939–2947. doi:10.1177/0363546520949855

Webster, K. E., and Feller, J. A. (2016). Exploring the high reinjury rate in younger patients undergoing anterior cruciate ligament reconstruction. *Am. J. Sports Med.* 44 (11), 2827–2832. doi:10.1177/0363546516651845

frontiers | Frontiers in Bioengineering and Biotechnology

TYPE Systematic Review
PUBLISHED 09 February 2023
DOI 10.3389/fbioe.2023.1111386

OPEN ACCESS

EDITED BY
Yansong Qi,
Inner Mongolia People's Hospital, China

REVIEWED BY
Sara Ferraris,
Polytechnic University of Turin, Italy
Geetha Manivasagam,
VIT University, India
Yue-li Sun,
Longhua Hospital, Shanghai University of Traditional Chinese Medicine, China

*CORRESPONDENCE
Cheng Xu,
xuchengngh@163.com
Wanheng Liu,
liuwanheng301@163.com
Jiantao Li,
lijiantao618@163.com

†These authors have contributed equally to this work

SPECIALTY SECTION
This article was submitted to Biomaterials, a section of the journal Frontiers in Bioengineering and Biotechnology

RECEIVED 29 November 2022
ACCEPTED 31 January 2023
PUBLISHED 09 February 2023

CITATION
Li H, Wang D, Zhang W, Xu G, Xu C, Liu W and Li J (2023), Potential side effects of antibacterial coatings in orthopaedic implants: A systematic review of clinical studies.
Front. Bioeng. Biotechnol. 11:1111386.
doi: 10.3389/fbioe.2023.1111386

Potential side effects of antibacterial coatings in orthopaedic implants: A systematic review of clinical studies

Hua Li[1,2†], Daofeng Wang[1,2†], Wupeng Zhang[1,2,3†], Gaoxiang Xu[1,2], Cheng Xu[1,2*], Wanheng Liu[1,2*] and Jiantao Li[1,2*]

[1]Senior Department of Orthopedics, The Fourth Medical Center of Chinese PLA General Hospital, Beijing, China, [2]National Clinical Research Center for Orthopedics, Sports Medicine and Rehabilitation, Beijing, China, [3]School of Medicine, Nankai University, Tianjin, China

Objective: The systematic review aimed to determine the potential side effects of antibacterial coatings in orthopaedic implants.

Methods: Publications were searched in the databases of Embase, PubMed, Web of Science and Cochrane Library using predetermined keywords up to 31 October 2022. Clinical studies reporting side effects of the surface or coating materials were included.

Results: A total of 23 studies (20 cohort studies and three case reports) reporting the concerns about the side effects of antibacterial coatings were identified. Three types of coating materials, silver, iodine and gentamicin were included. All of studies raised the concerns regarding safety of antibacterial coatings, and the occurrence of adverse events was observed in seven studies. The main side effect of silver coatings was the development of argyria. For iodine coatings, only one anaphylactic case was reported as an adverse event. No systemic or other general side effects were reported for gentamicin.

Conclusion: Clinical studies on the side effects of antibacterial coatings were limited. Based on the available outcomes, the most reported side effects of antibacterial coatings in clinical use were argyria with silver coatings. However, researchers should always pay attention to the potential side effects of antibacterial materials, such as systematic or local toxicity and allergy.

KEYWORDS

antibacterial coatings, clinical studies, side effect, implant, systematic review

1 Introduction

Implant-related infection (IRI) is one of the most devastating complications after orthopaedic procedures (Van Belleghem et al., 2020). The frequency of IRI after arthroplasty ranges from 0.5% to 15% (Cats-Baril et al., 2013; Lenguerrand et al., 2017). Spinal implant infection affects between 2% and 13% of patients (McClelland et al., 2016). Postoperative infection following trauma surgeries has an incidence of 0.5%–50% (Bonnevialle et al., 2012; Oliveira et al., 2016). With some reporting an annual number of 1,000,000 IRIs occurring in the United States (US), over $1.6 billion is spent for the treatment against the IRI (Edmiston et al., 2011). The socio-economic burden of IRI is heavy, with relatively high morbidity and mortality (Berbari et al., 2012).

Previous studies have demonstrated that the formation of biofilm plays an important role in the pathogenesis of IRI (Josse et al., 2019; van Vugt et al., 2019). In general, there are two important steps in the formation of biofilm. Initially, the bacteria attach to the implant surface through physicochemical interactions. Subsequently, the bacteria replicate to form multilayered cell colonies on the surface through molecular and cellular interactions, producing an extracellular matrix forming a complex community called biofilm (Costerton et al., 1999). The formation of biofilm can render the bacteria extremely resistant to the human immune system and antibiotics (Zimmerli et al., 2004; Gbejuade et al., 2015; Riool et al., 2017). Gristina et al. coined the term "race for the surface" to illustrate the competition between host cells and bacteria for adhesion to the surface (Gristina et al., 1988). This concept leads to a promising strategy of modifying the implant surface with antibacterial coatings.

Numerous studies have examined the ability of antibacterial-coated implants against infections. Many of these studies have demonstrated excellent antibacterial properties (Shirai et al., 2016; Wilding et al., 2016; Hardes et al., 2017). Sambri et al. investigated the use of silver-coated megaprostheses *versus* uncoated megaprostheses in patients with tumor prostheses infections and found that the reinfection rate in coated group was lower than that in uncoated group (10.3% VS. 17.5%) (Sambri et al., 2020). Kabata et al. used an iodine-coated hip implant for 28 patients who had IRI, pyogenic arthritis or immunosuppressive condition. In their cohort, no signs of infection were observed after a 3-year follow up (Kabata et al., 2015). Savvidou et al. conducted a systematic review and meta-analysis on the efficacy of antibacterial surface in preventing IRI. The authors included seven comparative studies regarding different antibacterial coatings and found that implants with antibacterial coatings could reduce the risk of infection with an odds ratio of 2.9 as compared with general implants (Savvidou et al., 2020).

However, the coating procedure should ensure not only antibacterial resistance but also safety, as antibacterial materials may be toxic to host cells. In this regard, a few clinical studies focused on the potential side effects of the coated surface. To our knowledge, few systematic reviews have been published on this subject. Alt analyzed the risk and benefit of antibacterial coatings using the method of systematic review. Nevertheless, the author focused the gentamicin- and silver-coated implants only at the initial search and did not complete a comprehensive search. Studies reporting the potential side effects of antibacterial coatings may be missed, as many materials have been used to modify the implant surface (Alt, 2017). Therefore, the aim of this systematic review was to ascertain the potential side effects of antibacterial-coated implants reported in clinical studies.

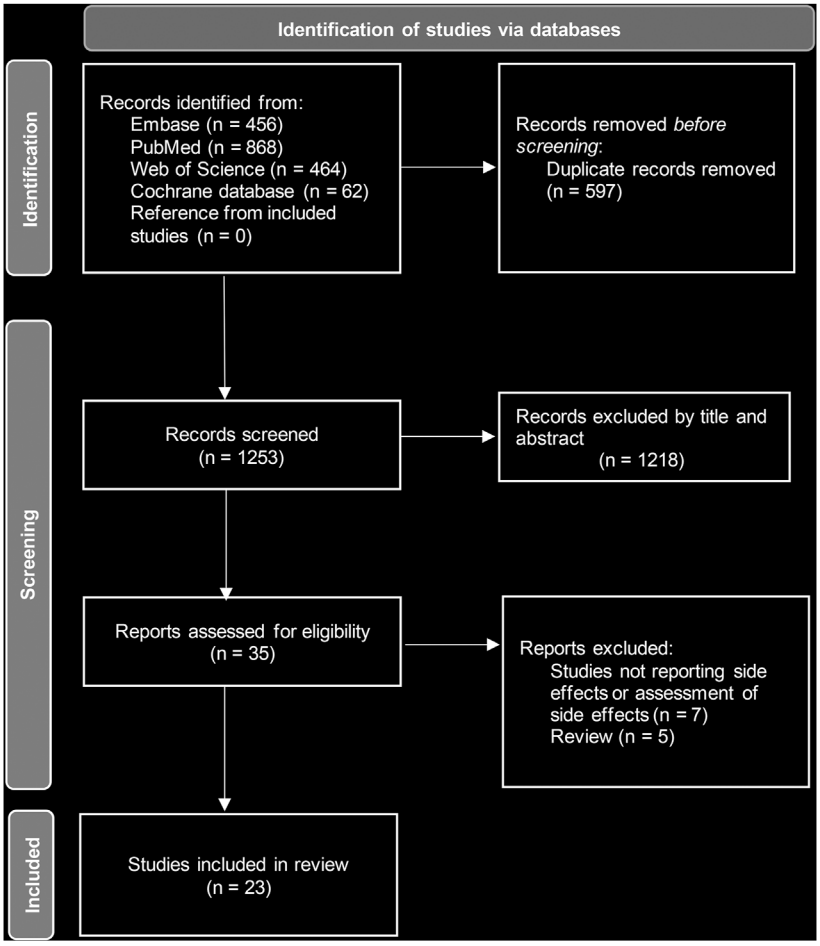

FIGURE 1
Flowchart of PRISMA.

2 Methods

This study was registered in the International Prospective Register of Systematic Reviews (PROSPERO) (CRD42018102464). This systematic review was conducted according to the Preferred Reporting Items for Systematic reviews and Meta-Analyses (PRISMA) Statement protocol (Shamseer et al., 2015).

2.1 Search strategy

Embase, PubMed, Web of Science and the Cochrane library databases were searched up to October 2022. The search keywords included antibacterial, coating and orthopaedic implants (Supplementary Table S1). We developed specific search strategies for each database. The bibliographies of included articles and relevant review articles were also assessed for potential eligibility.

2.2 Eligibility criteria and study selection

The inclusion criteria encompassed the following: 1) clinical studies or case reports regarding the antibacterial surface for orthopaedic surgeries; 2) modifying the implant surface using physical and/or chemical methods; 3) outcomes including the data of any side effect with regard to the surface or coating materials. We excluded studies that imparted antibacterial materials directly to the implant surface using cement or hydrogel which carried these materials, because these two materials were added to implant surface by surgeons freehand, which could jeopardize the uniformity and consistence. Non-English language publications, *in vitro* studies, brief reports, reviews and conference proceedings were also excluded. After dropping the duplicates, two authors reviewed the titles and abstracts to identify potentially eligible studies independently. Full texts were then read independently by the same two authors to determine the final list of included studies. A senior doctor was consulted for the final consensus if there occurred a disagreement.

2.3 Data extraction

The primary goal of this systematic review was to determine the side effects of antibacterial coatings against the IRI. Therefore, we extracted any possible negative results as a consequence of antibacterial modification. Other information was also extracted, including the year of publication, study design, type of surface coating, coating procedure, load of antibacterial materials, patients' attributes and orthopaedic procedure. We contacted the corresponding author in an attempt to obtain any additional unclear or missing data.

2.4 Assessment of quality and bias

Two authors estimated the quality of the included studies independently. For cohort studies, the Newcastle-Ottawa Scale was used (Stang, 2010). For case reports, we applied the Joanna Briggs Institute Critical Appraisal Checklist (Munn et al., 2015; Wang et al., 2022), which has been widely used to assess the quality of case reports.

3 Results

3.1 Overview of study selection

Initially, a total of 1850 studies were identified. After removing duplicates, 1,253 studies were available for review. We screened the titles and abstracts and excluded 1,218 papers that did not meet the criteria. The full texts of the remaining 35 papers were read, and finally, 23 studies (20 cohort studies and three case reports) were included (Figure 1). Of these studies, 14 reported on silver coatings, six on iodine coatings and three on gentamicin coatings. These studies were mainly published from Japan ($n = 8$), followed by Germany ($n = 6$) and Italy ($n = 5$). All the studies regarding iodine coatings were from Japan. The coated implants were mainly used for tumor resections, open fractures, revision of prosthetic joint infection, arthroplasty of pyogenic arthritis and so on. The mean age of recruited patients ranged from 14 to 80 years (Table 1).

3.2 Coating technologies

The included studies revealed four different antibacterial modification technologies with silver. Modular universal Tumor and Revision System (MUTARS) megaprostheses (Implantcast, Buxtehude, Germany) were modified by galvanic deposition of pure silver (Hardes et al., 2007; Hardes et al., 2010; Glehr et al., 2013; Hussmann et al., 2013; Karakasli et al., 2014; Donati et al., 2016; Piccioli et al., 2016; Denes et al., 2022; Smolle et al., 2022). A mean amount of 0.91 g (range 0.7–1.2 g) silver was coated on the implant surface. Porous Argentum (PorAg) MegaC prostheses (Waldemar, Hamburg, Germany) used the vapor deposition of $TiAg_{20}N$ to modify the surface with a silver content of 0.33 g (Scoccianti et al., 2016; Sambri et al., 2020). Another coating method, thermal plasma spraying, was used by Eto et al. to load a mixture of silver oxide and hydroxyapatite (Ag-HA) onto the implant surface, and only 0.003 g silver was added (Eto et al., 2016; Hashimoto et al., 2020). Massè et al. reported the clinical use of silver-coated stainless-steel pins for external fixation in patients with open fractures (Massè et al., 2000). Silver was coated to the pins based on ion-beam-assisted deposition from vapor.

Iodine coatings were produced by the Chiba Institute of Technology (Narashino, Japan) (Tsuchiya et al., 2012; Shirai et al., 2014a; Shirai et al., 2014b; Hayashi et al., 2015; Kabata et al., 2015; Shirai et al., 2019). This type of coating is an adhesive anodic oxide film, which forms through the anodization of povidone-iodine electrolyte. The thickness of the coating was between 5 and 10 μm with the capacity to support 10–12 $\mu g/cm^2$ iodine.

Gentamicin-coated technology is now only used in tibia nails (Unreamed Tibial Nail [UTN] PROtect, DePuy Synthes, Bettlach, Switzerland; Expert Tibial Nail [ETN] PROtect, DePuy Synthes, Johnson & Johnson, New Brunswick, New Jersey) (Fuchs et al., 2011; Moghaddam et al., 2016; Schmidmaier et al., 2017). This coating consisted of a poly (L-lactic acid) (PLLA) matrix containing gentamicin sulphate. The surface modification was achieved by the dip coating process. The total amount of gentamicin on an implant ranged from 10 to 50 mg.

TABLE 1 Characteristics of the included studies.

Authors	Year	Country	Study design	Case number	Patient age [a]	Indications	Coating	Implant
Smolle et al	2022	Austria	Cohort study	46	47.1	ReTJA, Oncology	Silver	MUTARS megaprostheses
Denes et al	2022	France	Case report	1	75	Oncology	Silver	MUTARS megaprostheses
Hashimoto et al	2020	Japan	Case report	1	80	TJA of SA	Silver	Ag-HA TJA prostheses
Sambri et al	2020	Italy	Cohort study	68	30	PJI	Silver	PorAg megaprostheses
Shirai et al	2019	Japan	Cohort study	72	59.3	PJI, ReTJA, Spinal surgery, Fracture, Oncology	Iodine	Iodine-coated megaprostheses, spinal instruments, nails and TJA prostheses
Schmidmaier et al	2017	Germany	Cohort study	100	46.6	Fracture	Gentamicin	Tibial nails
Moghaddam et al	2016	Germany	Cohort study	25	50.9	Fracture	Gentamicin	Tibial nails
Eto et al	2016	Japan	Cohort study	20	77.0	TJA	Silver	Ag-HA TJA prostheses
Piccioli et al	2016	Italy	Cohort study	30	56.2	Oncology	Silver	MUTARS megaprostheses
Donati et al	2016	Italy	Cohort study	68	61.6	Oncology	Silver	MUTARS megaprostheses
Scoccianti et al	2016	Italy	Cohort study	33	55	ReTJA, Oncology	Silver	PorAg megaprostheses
Hayashi et al	2015	Japan	Cohort study	69	55.1	Spinal surgery	Iodine	Iodine-coated spinal instruments
Kabata et al	2015	Japan	Cohort study	30	56	PJI, TJA of SA	Iodine	Iodine-coated megaprostheses
Shirai et al	2014	Japan	Cohort study	47	53.6	Oncology, TJA of SA	Iodine	Iodine-coated megaprostheses
Shirai et al	2014	Japan	Cohort study	38	33.6	Fracture	Iodine	Iodine-coated pins
Karakasli et al	2014	Turkey	Case report	1	14	Oncology	Silver	MUTARS megaprostheses
Glehr et al	2013	Austria	Cohort study	32	46	ReTJA, Oncology	Silver	MUTARS megaprostheses
Hussmann et al	2013	Germany	Cohort study	18	60.1	ReTJA, Oncology	Silver	MUTARS megaprostheses
Tsuchiya et al	2012	Japan	Cohort study	222	49.4	PJI, TJA of SA	Iodine	Iodine-coated megaprostheses, spinal instruments, nails and TJA prostheses
Fuchs et al	2011	Germany	Cohort study	21	47.7	Fracture	Gentamicin	Tibial nails
Hardes et al	2010	Germany	Cohort study	51	37	Oncology	Silver	MUTARS megaprostheses
Hardes et al	2007	Germany	Cohort study	20	61.8	Oncology	Silver	MUTARS megaprostheses
Massè et al	2000	Italy	Cohort study	24	34.7	Fracture	silver	Silver-coated pins

[a], year; ReTJA, revision total joint arthroplasty; MUTARS, modular universal tumor and revision system; SA, septic arthritis; Ag-HA, silver oxide and hydroxyapatite; PJI, periprosthetic joint infection; PorAg, Porous Argentum.

3.3 Concerns about side effects

All of the studies reported the concerns regarding the safety of antibacterial coatings and seven studies detected the development of side effects (Table 2).

3.3.1 Silver coating

Fourteen studies reported concerns regarding the side effects of silver, including a high concentration of silver in blood, impairment of liver and/or kidney function, implication on ossification and osteointegration, argyria and neurotoxicity (Massè et al., 2000;

TABLE 2 Reported side effects of antibacterial coatings.

Coating and concerns regarding safety	Implant	Encountered side effects
Silver: argyria, high blood silver levels, damage to organ function, suppression on osteointegration, neurotoxicity	MUTARS megaprostheses	Argyria: the incidence of 23% (7/32) in Glehr et al.'s study, 8.7% (4/46) in Smolle et al.'s study and 2.0% (1/51) in Hardes et al.'s study; two cases in two case reports The other studies did not detect argyria and any other adverse events
	Ag-HA TJA prostheses	Not seen
	PorAg megaprostheses	Not seen
	Silver-coated pins	Increase in blood silver levels: PreOP, 0.20 μg/L; PostOP 3.12 (range 0.2–20.55) μg/L
Iodine: allergy, abnormality of thyroid function	Iodine-coated implants	Allergy: only one case among 222 patients in Tsuchiya et al.'s study The other studies did not report any adverse events
Gentamicin: allergy, high gentamicin blood levels, nephrotoxicity, hepatotoxicity	Tibial nails	Not seen

MUTARS, modular universal tumor and revision system; Ag-HA, silver oxide and hydroxyapatite; TJA, total joint arthroplasty; PorAg, Porous Argentum. PreOP, preoperatively; PostOP, postoperatively.

Hardes et al., 2007; Hardes et al., 2010; Glehr et al., 2013; Hussmann et al., 2013; Karakasli et al., 2014; Donati et al., 2016; Eto et al., 2016; Piccioli et al., 2016; Scoccianti et al., 2016; Hashimoto et al., 2020; Sambri et al., 2020; Denes et al., 2022; Smolle et al., 2022). Five studies reported the occurrence of argyria when using the silver-coated megaprostheses (Hardes et al., 2010; Glehr et al., 2013; Karakasli et al., 2014; Denes et al., 2022; Smolle et al., 2022). The highest incidence of argyria was 23% (7/32) in Glehr et al.'s study (Glehr et al., 2013), followed by 8.7% (4/46) in Smolle et al.'s study (Smolle et al., 2022). Massè et al. conducted a study using external fixation with silver-coated stainless-steel pins to prevent pin tract infection. The researchers found that the postoperative blood silver levels increased to 3.12 ppb from the preoperative 0.2 ppb. This intervention was finally cancelled due to concerns about the significant increase in the concentration of silver in the blood (Massè et al., 2000). The other eight studies stated that none of the specific adverse events related to silver coatings was detected.

3.3.2 Iodine coating

Six studies that reported the use of iodine coating were all conducted by the group of Shirai and Tsuchiya (Tsuchiya et al., 2012; Shirai et al., 2014a; Shirai et al., 2014b; Hayashi et al., 2015; Kabata et al., 2015; Shirai et al., 2019). The main concerns regarding the side effects of iodine coatings were the allergy and impairment of thyroid function. A total of 479 patients following different orthopaedic procedures (including trauma, spine surgery, arthroplasty, revision and tumor resection) received iodine-coated implants. Only one suspicious episode of allergy to iodine after arthroplasty revision was observed (Tsuchiya et al., 2012). No patients showed thyroid malfunction.

3.3.3 Gentamicin coating

The major side effects of gentamicin coating involved allergy, nephrotoxicity and hepatotoxicity. The gentamicin-coated tibial nails were used in a total of 145 patients from the three studies (Fuchs et al., 2011; Moghaddam et al., 2016; Schmidmaier et al., 2017). The results showed no systemic or other general side effects. In the study by Fuchs et al., the researchers estimated the gentamicin serum levels and the values were below 0.3 μg/mL in all patients (Fuchs et al., 2011).

3.4 Quality assessment

Table 3 summarized the quality assessment of the cohort studies and the Newcastle-Ottawa rank represented high quality. The quality of the three case reports was considered high-quality (Supplementary Table S2).

4 Discussion

IRI is a disastrous complication faced by orthopaedic patients and surgeons due to the substantial morbidity and mortality, as well as heavy financial and psychological burdens. The formation of biofilm plays a critical role in the development of IRI, and various prophylactic methods against biofilm formation have been developed (Parvizi et al., 2017). Among them, antibacterial modification of implant surface has been proven as a powerful method for its promising antibacterial capability by numerous *in vitro*, *in vivo* and clinical studies (Wafa et al., 2015; Alt, 2017; Wang et al., 2021; Zhang et al., 2022; Zhao et al., 2022). However, there were only limited studies reporting the potential side effects of antibacterial coatings, and no systematic review has been published to summarize these concerns. To the best of our knowledge, the present systematic review is the first that identify the possible problems when using implants with antibacterial coatings. In order to demonstrate a comprehensive panorama of this topic, we also reviewed relevant case reports. In these studies, the main concerns of researchers regarding antibacterial coatings were a high concentration of antibacterial materials in blood, neurotoxicity, harm to organs/glands function, allergy and suppression on osteointegration. Based on available evidence, dermal discoloration was the most commonly-reported problem when using silver-coated implants. Iodine coatings might be associated with a possibility of anaphylactic adverse events, while the studies on gentamicin-coated nails did not report any side effects.

4.1 Silver

In our review, the main side effect of silver coatings was argyria, which was thought to be related to exposure to large amounts of silver

10.3389/fbioe.2023.1111386

TABLE 3 The Newcastle-Ottawa Scale for the included cohort studies.

Authors	Selection				Comparability	Outcome			Total
	Representativeness	Non-exposed cohort	Ascertainment of exposure	Absence of the outcome		Assessment of outcome	Adequate duration	Accuracy	
Smolle et al	*	-	*	*	-	*	*	*	6
Sambri et al	*	*	*	*	-	*	*	*	7
Shirai et al	*	-	*	*	-	*	*	*	6
Schmidmaier et al	*	-	*	*	-	*	*	*	6
Moghaddam et al	*	-	*	*	-	*	*	*	6
Eto et al	*	-	*	*	-	*	*	*	6
Piccioli et al	*	-	*	*	-	*	*	*	6
Donati et al	*	*	*	*	-	*	*	*	7
Scoccianti et al	*	-	*	*	-	*	*	*	6
Hayashi et al	*	*	*	*	-	*	*	*	7
Kabata et al	*	-	*	*	-	*	*	-	5
Shirai et al. (megaprostheses)	*	-	*	*	-	*	*	*	6
Shirai et al. (pins)	*	-	*	*	-	*	*	-	5
Glehr et al	*	-	*	*	-	*	*	*	6
Hussmann et al	*	-	*	*	-	*	*	*	6
Tsuchiya et al	*	-	*	*	-	*	*	*	6
Fuchs et al	*	-	*	*	-	*	*	*	6
Hardes et al	*	-	*	*	-	*	*	*	6
Hardes et al	*	-	*	*	-	*	*	*	6
Massè et al	*	*	*	*	-	*	*	-	5

(Lansdown, 2006). Silver has a long history of clinical use against infections (Alexander, 2009). It can cause harm to bacteria including membrane destruction, DNA condensation and so on (Aldabaldetrecu et al., 2018). However, an overdose of silver can damage host cells. Many clinical studies have shown the excellent antibacterial capability of silver-coated implants in orthopaedic procedures (Schmolders et al., 2017; Zajonz et al., 2017). Diez-Escudero et al. reviewed the published data on silver-coated arthroplasty components and found that silver coatings could reduce the risk of IRI, particularly in tumor patients with megaprostheses (Diez-Escudero and Hailer, 2021). However, silver-coated megaprostheses usually indicated a high silver content in the implant surface. This might explain why all reported argyria cases were those in whom the megaprostheses (MUTARS) were used. Nearly 1 G of silver was added to the surface of this megaprosthesis. The two highest incidences of argyria occurrence were 23% reported by Glehr et al. and 8.7% reported by Smolle et al. (Glehr et al., 2013; Smolle et al., 2022), respectively, and all patients in their studies received MUTARS reconstruction. Other silver-coated implants, such as PorAg megaC prostheses and Ag-HA prostheses (Eto et al., 2016; Scoccianti et al., 2016; Hashimoto et al., 2020; Sambri et al., 2020), contained a relatively lower amount of silver (0.33 g silver in PorAg megaC and 0.003 g silver in Ag-HA), and none of the cases with these implants had argyria. Fortunately, these reported cases of argyria were not associated with neurological deficits or systematic toxicity. Previous studies have identified that blood silver levels exceeding 300 ppb would lead to argyria, hepato- and nephrotoxicity (Noda et al., 2009; Ando et al., 2010). Among the five studies in our review that encountered argyria, two reported blood silver levels, ranging from 9.1 to 29.1 ppb (Denes et al., 2022; Smolle et al., 2022), and the occurrence of argyria was not related to the blood silver levels. Blood silver levels were also estimated in some other studies using PorAg MegaC prostheses or Ag-HA prostheses. Scoccianti et al. reported that the blood silver levels in patients receiving PorAg MegaC prostheses ranged from 0.82 to 20 ppb (Scoccianti et al., 2016). Eto et al. reported the clinical outcomes of Ag-HA prostheses and the blood silver levels ranged from 0 to 6 ppb (Eto et al., 2016). It seems that the blood silver levels may be lower in patients receiving implants with a relatively lower content of silver. Surgeons should monitor laboratory analyses and blood silver levels after the implantation of silver-coated prostheses. In addition, several *in vitro* and *in vivo* studies have shown that elevated silver ions might influence the activity of osteoblasts and thus inhibit osteointegration (Yonekura et al., 2011; Hauschild et al., 2015; Croes et al., 2018). We also noticed that the age of patients occurring argyria in our review was variable, ranging from 14 to 75 years, which might suggest that the occurrence of argyria was not associated with age. However, the elderly patients were at higher risk of organ dysfunction and thus should be treated carefully when they were about to receive antibacterial-coated implants. Silver has also been used in other clinical settings to prevent infections, such as wound dressings and bone cement (polymethylmethacrylate). These applications were also associated with several adverse events. Trop et al. reported that a burn patient represented argyria with liver dysfunction after using silver-coated dressings (Trop et al., 2006). Sudmann et al. reported a case of severe neurological paralysis after total hip arthroplasty with silver-impregnated bone cement (Sudmann et al., 1994). Although tthese severe side effects have not been reported when using silver-coated implants, they should also be concerned.

Apart from silver, other metals including zinc (Zn) and copper (Cu) are also investigated as antibacterial materials for surface modification. Zinc ions can inhibit bacteria by inactivating enzymes, destroying colonization plaques and so on (Osinaga et al., 2003). Copper ions can interact with bacterial membrane proteins and penetrate bacterial cells, inducing reactive oxygen species (Fan et al., 2021). Nevertheless, no clinical study has been published until now. Li et al. produced a coating with titania nanotubes incorporated with zinc and found that this coating could enhance bone formation and reduce bacterial adhesion in a rat model. However, if the zinc content was tripled in the coating, cytotoxicity would occur (Li et al., 2014). Several studies have demonstrated the promising antibacterial activity of copper in experiments (Ingle et al., 2014; Huang et al., 2018; Shimabukuro et al., 2020). However, even though copper is the essential nutrient required for normal body function, it is also toxic with a concentration-dependent feature. Prabhu et al. exposed rat ganglion cells to different concentrations of copper (10–100 μM) and found that significant cytotoxicity was observed and a higher concentration of copper revealed the maximum cytotoxicity (Prabhu et al., 2010). More studies should be conducted to find a balancing concentration of these metals between antibacterial capacity and cytotoxicity.

4.2 Iodine and gentamicin

Iodine has been widely used as an antibacterial substance in surgical hygiene, such as sterilizing operative areas and instruments (Lepelletier et al., 2020). It is also an indispensable component of the thyroid hormone. Therefore, after the implantation of an iodine-laden prosthesis in a patient, the thyroid hormone levels should be dynamically investigated. Our review reflected that none of the patients who received iodine-coated implants in the involved studies showed significant changes in thyroid function. As the possibility of iodine-induced allergy existed, Shirai et al. recommended preoperative patch tests to confirm the absence of allergy (Shirai et al., 2014a). Nevertheless, we noticed that the only case with suspected allergy also passed this test. Thus, careful assessment after implantation is also important. Previous *in vitro* studies also demonstrated concerns about toxicity of iodine, such as delaying healing (Taga et al., 2018). Schmidlin et al. found that higher concentrations of povidone-iodine could impair the differentiation of osteoblasts (Schmidlin et al., 2009). However, Shirai et al. tested the cytotoxicity of iodine-coated titanium using the fibroblasts and found that its toxicity was low and similar to that of normal uncoated titanium and stainless steel (Shirai et al., 2011). The results of non-clinical studies were still uncertain. Up to present, iodine-coated technologies or implants are not commercially available, and the published data of clinical studies were with a relatively small sample size. Studies with long-term follow-ups and larger sample sizes for iodine coatings are required.

Gentamicin belongs to the aminoglycoside group and its systematic use for infection prevention is gradually limited due to serious dose-dependent side effects, including nephrotoxicity and ototoxicity (Jiang et al., 2017). Other contraindications contain allergy to aminoglycoside, pregnancy, myasthenia gravis and so on. Nowadays, gentamicin is mainly added to bone cement to prevent infection (Cara et al., 2020). In the surface coatings, gentamicin is carried by PLLA to be released locally without high systematic doses. One of the three included studies reported the serum gentamicin levels and the value was below 0.3 μg/mL, which was recognized as the threshold of toxicity (Fuchs et al., 2011). In the study by Moghaddam et al., the authors also found that the serum gentamicin levels were

lower than 0. 2 μg/mL. These results indicated that the gentamicin-coated surface generated by the dip process did not cause the accumulation of gentamicin. To date, gentamicin coatings are only available for tibial nails (Schmidmaier et al., 2006). This coating might be limited because of a relatively high gentamicin resistance of 2%–50% (Romanò et al., 2019), especially to *Staphylococcus aureus*, the main pathogen causing IRI. There are several *in vivo* and *in vitro* studies on PLLA-vancomycin, which is much more effective against Gram-positive bacteria. However, clinical applications of vancomycin coatings are lacking (Kankilic et al., 2011; Kankilic et al., 2014).

4.3 Limitations

There are several limitations of this systematic review. First, the methodology of systematic review may introduce bias due to the possibly unavoidable missing of relevant studies. However, we have registered this systematic review and followed the PRISMA guideline to complete a thorough search of four main databases. We tried our best to identify any reported side effects of antibacterial coatings. Second, due to the paucity of publications, we could not aggregate the data to perform a meta-analysis. Thus, the incidences of side effects, such as argyria, were given individually rather than as pooled results. The overall estimation of the occurrence of side effects was then compromised. Third, the study designs of the included studies were different and case reports were also involved in the present review, which jeopardised the level of evidence for the present systematic review.

5 Conclusion

The present data reporting the side effects of antibacterial coatings were inadequate. Based on the limited available evidence, the incidence of side effects was low. The most reported side effects of antibacterial coatings in clinical use were argyria with silver coatings, of which the incidence could even reach 23%. Coating-related argyria might be related to a high amount of silver (MUTARS). Other coatings such as iodine and gentamicin coatings are also concerned due to their potential toxicity, while no episode of relevant complications has been reported in clinical studies up to now. Even though few adverse events and no fatal complications of antibacterial coatings were observed, researchers should always be aware of the doses of antibacterial materials in blood as well as the potential side effects, such as systematic or local toxicity and allergy. Further clinical studies with longer durations, larger sample sizes and higher levels of evidence are appealed to demonstrate a more comprehensive summary of side effects in antibacterial coatings and to confirm their ability against IRI.

Data availability statement

The original contributions presented in the study are included in the article/Supplementary Material, further inquiries can be directed to the corresponding authors.

Author contributions

HL, DW, and WZ contributed to conception and design of the study. HL, JL, and WL contributed to methodology of the study. HL and DW completed the data extraction. GX, CX, and WZ completed the investigation. WZ and GX completed the visualization of tabulation. HL wrote the first draft of the manuscript. DW, WZ, GX, and WL wrote sections of the manuscript. JL and CX reviewed and edited the manuscript. All authors contributed to manuscript revision, read, and approved the submitted version.

Funding

This study is funded by the Beijing Natural Science Foundation (7222180) and the 13th Five-year Plan for Key Discipline Construction Project of PLA (A350109).

Conflict of interest

The authors declare that the research was conducted in the absence of any commercial or financial relationships that could be construed as a potential conflict of interest.

Publisher's note

All claims expressed in this article are solely those of the authors and do not necessarily represent those of their affiliated organizations, or those of the publisher, the editors and the reviewers. Any product that may be evaluated in this article, or claim that may be made by its manufacturer, is not guaranteed or endorsed by the publisher.

Supplementary material

The Supplementary Material for this article can be found online at: https://www.frontiersin.org/articles/10.3389/fbioe.2023.1111386/full#supplementary-material

References

Aldabaldetrecu, M., Tamayo, L., Alarcon, R., Walter, M., Salas-Huenuleo, E., Kogan, M. J., et al. (2018). Stability of antibacterial silver carboxylate complexes against Staphylococcus epidermidis and their cytotoxic effects. *Molecules* 23 (7), 1629. doi:10.3390/molecules23071629

Alexander, J. W. (2009). History of the medical use of silver. *Surg. Infect. (Larchmt)* 10 (3), 289–292. doi:10.1089/sur.2008.9941

Alt, V. (2017). Antimicrobial coated implants in trauma and orthopaedics-A clinical review and risk-benefit analysis. *Injury* 48 (3), 599–607. doi:10.1016/j.injury.2016.12.011

Ando, Y., Miyamoto, H., Noda, I., Miyaji, F., Shimazaki, T., Yonekura, Y., et al. (2010). Effect of bacterial media on the evaluation of the antibacterial activity of a biomaterial containing inorganic antibacterial reagents or antibiotics. *Biocontrol Sci.* 15 (1), 15–19. doi:10.4265/bio.15.15

Berbari, E. F., Osmon, D. R., Lahr, B., Eckel-Passow, J. E., Tsaras, G., Hanssen, A. D., et al. (2012). The mayo prosthetic joint infection risk score: Implication for surgical site infection reporting and risk stratification. *Infect. Control Hosp. Epidemiol.* 33 (8), 774–781. doi:10.1086/666641

Bonnevialle, P., Bonnomet, F., Philippe, R., Loubignac, F., Rubens-Duval, B., Talbi, A., et al. (2012). Early surgical site infection in adult appendicular skeleton trauma surgery: A multicenter prospective series. *Orthop. Traumatol. Surg. Res.* 98 (6), 684–689. doi:10.1016/j.otsr.2012.08.002

Cara, A., Ballet, M., Hemery, C., Ferry, T., Laurent, F., and Josse, J. (2020). Antibiotics in bone cements used for prosthesis fixation: An efficient way to prevent *Staphylococcus aureus* and Staphylococcus epidermidis prosthetic joint infection. *Front. Med. (Lausanne)* 7, 576231. doi:10.3389/fmed.2020.576231

Cats-Baril, W., Gehrke, T., Huff, K., Kendoff, D., Maltenfort, M., and Parvizi, J. (2013). International consensus on periprosthetic joint infection: Description of the consensus process. *Clin. Orthop. Relat. Res.* 471 (12), 4065–4075. doi:10.1007/s11999-013-3329-4

Costerton, J. W., Stewart, P. S., and Greenberg, E. P. (1999). Bacterial biofilms: A common cause of persistent infections. *Science* 284 (5418), 1318–1322. doi:10.1126/science.284.5418.1318

Croes, M., Bakhshandeh, S., van Hengel, I. A. J., Lietaert, K., van Kessel, K. P. M., Pouran, B., et al. (2018). Antibacterial and immunogenic behavior of silver coatings on additively manufactured porous titanium. *Acta Biomater.* 81, 315–327. doi:10.1016/j.actbio.2018.09.051

Denes, E., El Balkhi, S., and Fiorenza, F. (2022). Local argyria due to silver-coated megaprosthesis. *Am. J. Med.* 135 (6), e116. doi:10.1016/j.amjmed.2022.01.026

Diez-Escudero, A., and Hailer, N. P. (2021). The role of silver coating for arthroplasty components. *Bone Jt. J.* 103-b (3), 423–429. doi:10.1302/0301-620x.103b3.Bjj-2020-1370.R1

Donati, F., Di Giacomo, G., D'Adamio, S., Ziranu, A., Careri, S., Rosa, M., et al. (2016). Silver-coated hip megaprosthesis in oncological limb savage surgery. *Biomed. Res. Int.* 2016, 9079041–9079046. doi:10.1155/2016/9079041

Edmiston, C. E., Spencer, M., Lewis, B. D., Brown, K. R., Rossi, P. J., Henen, C. R., et al. (2011). Reducing the risk of surgical site infections: Did we really think SCIP was going to lead us to the promised land? *Surg. Infect. (Larchmt)* 12 (3), 169–177. doi:10.1089/sur.2011.036

Eto, S., Kawano, S., Someya, S., Miyamoto, H., Sonohata, M., and Mawatari, M. (2016). First clinical experience with thermal-sprayed silver oxide-containing hydroxyapatite coating implant. *J. Arthroplasty* 31 (7), 1498–1503. doi:10.1016/j.arth.2015.12.034

Fan, X., Yahia, L., and Sacher, E. (2021). Antimicrobial properties of the Ag, Cu nanoparticle system. *Biol. (Basel)* 10 (2), 137. doi:10.3390/biology10020137

Fuchs, T., Stange, R., Schmidmaier, G., and Raschke, M. J. (2011). The use of gentamicin-coated nails in the tibia: Preliminary results of a prospective study. *Arch. Orthop. Trauma Surg.* 131 (10), 1419–1425. doi:10.1007/s00402-011-1321-6

Gbejuade, H. O., Lovering, A. M., and Webb, J. C. (2015). The role of microbial biofilms in prosthetic joint infections: A review. *Acta Orthop.* 86 (2), 147–158. doi:10.3109/17453674.2014.966290

Glehr, M., Leithner, A., Friesenbichler, J., Goessler, W., Avian, A., Andreou, D., et al. (2013). Argyria following the use of silver-coated megaprostheses: No association between the development of local argyria and elevated silver levels. *Bone Jt. J.* 95-b (7), 988–992. doi:10.1302/0301-620x.95b7.31124

Gristina, A. G., Naylor, P., and Myrvik, Q. (1988). Infections from biomaterials and implants: A race for the surface. *Med. Prog. Technol.* 14 (3-4), 205–224.

Hardes, J., Ahrens, H., Gebert, C., Streitbuerger, A., Buerger, H., Erren, M., et al. (2007). Lack of toxicological side-effects in silver-coated megaprostheses in humans. *Biomaterials* 28 (18), 2869–2875. doi:10.1016/j.biomaterials.2007.02.033

Hardes, J., Henrichs, M. P., Hauschild, G., Nottrott, M., Guder, W., and Streitbuerger, A. (2017). Silver-coated megaprosthesis of the proximal tibia in patients with sarcoma. *J. Arthroplasty* 32 (7), 2208–2213. doi:10.1016/j.arth.2017.02.054

Hardes, J., von Eiff, C., Streitbuerger, A., Balke, M., Budny, T., Henrichs, M. P., et al. (2010). Reduction of periprosthetic infection with silver-coated megaprostheses in patients with bone sarcoma. *J. Surg. Oncol.* 101 (5), 389–395. doi:10.1002/jso.21498

Hashimoto, A., Sonohata, M., Kitajima, M., Kawano, S., Eto, S., and Mawatari, M. (2020). First experience with a thermal-sprayed silver oxide-containing hydroxyapatite coating implant in two-stage total hip arthroplasty for the treatment of septic arthritis with hip osteoarthritis: A case report. *Int. J. Surg. Case Rep.* 77, 434–437. doi:10.1016/j.ijscr.2020.11.032

Hauschild, G., Hardes, J., Gosheger, G., Stoeppeler, S., Ahrens, H., Blaske, F., et al. (2015). Evaluation of osseous integration of PVD-silver-coated hip prostheses in a canine model. *Biomed. Res. Int.* 2015, 1–10. doi:10.1155/2015/292406

Hayashi, H., Murakami, H., Demura, S., Kato, S., Yoshioka, K., Shinmura, K., et al. (2015). Surgical site infection after total *en bloc* spondylectomy: Risk factors and the preventive new technology. *Spine J.* 15 (1), 132–137. doi:10.1016/j.spinee.2014.08.007

Huang, Q., Li, X., Elkhooly, T. A., Liu, X., Zhang, R., Wu, H., et al. (2018). The Cu-containing TiO(2) coatings with modulatory effects on macrophage polarization and bactericidal capacity prepared by micro-arc oxidation on titanium substrates. *Colloids Surf. B Biointerfaces* 170, 242–250. doi:10.1016/j.colsurfb.2018.06.020

Hussmann, B., Johann, I., Kauther, M. D., Landgraeber, S., Jäger, M., and Lendemans, S. (2013). Measurement of the silver ion concentration in wound fluids after implantation of silver-coated megaprostheses: Correlation with the clinical outcome. *Biomed. Res. Int.* 2013, 1–11. doi:10.1155/2013/763096

Ingle, A. P., Duran, N., and Rai, M. (2014). Bioactivity, mechanism of action, and cytotoxicity of copper-based nanoparticles: A review. *Appl. Microbiol. Biotechnol.* 98 (3), 1001–1009. doi:10.1007/s00253-013-5422-8

Jiang, M., Karasawa, T., and Steyger, P. S. (2017). Aminoglycoside-induced cochleotoxicity: A review. *Front. Cell Neurosci.* 11, 308. doi:10.3389/fncel.2017.00308

Josse, J., Valour, F., Maali, Y., Diot, A., Batailler, C., Ferry, T., et al. (2019). Interaction between staphylococcal biofilm and bone: How does the presence of biofilm promote prosthesis loosening? *Front. Microbiol.* 10, 1602. doi:10.3389/fmicb.2019.01602

Kabata, T., Maeda, T., Kajino, Y., Hasegawa, K., Inoue, D., Yamamoto, T., et al. (2015). Iodine-Supported hip implants: Short term clinical results. *Biomed. Res. Int.* 2015, 1–6. doi:10.1155/2015/368124

Kankilic, B., Bayramli, E., Kilic, E., Dağdeviren, S., and Korkusuz, F. (2011). Vancomycin containing PLLA/β-TCP controls MRSA *in vitro*. *Clin. Orthop. Relat. Res.* 469 (11), 3222–3228. doi:10.1007/s11999-011-2082-9

Kankilic, B., Bilgic, E., Korkusuz, P., and Korkusuz, F. (2014). Vancomycin containing PLLA/β-TCP controls experimental osteomyelitis *in vivo*. *J. Orthop. Surg. Res.* 9, 114. doi:10.1186/s13018-014-0114-3

Karakasli, A., Hapa, O., Akdeniz, O., and Havitcioğlu, H. (2014). Dermal argyria: Cutaneous manifestation of a megaprosthesis for distal femoral osteosarcoma. *Indian J. Orthop.* 48 (3), 326–328. doi:10.4103/0019-5413.132528

Lansdown, A. B. (2006). Silver in health care: Antimicrobial effects and safety in use. *Curr. Probl. Dermatol* 33, 17–34. doi:10.1159/000093928

Lenguerrand, E., Whitehouse, M. R., Beswick, A. D., Toms, A. D., Porter, M. L., and Blom, A. W. (2017). Description of the rates, trends and surgical burden associated with revision for prosthetic joint infection following primary and revision knee replacements in england and wales: An analysis of the national joint registry for england, wales, northern Ireland and the Isle of Man. *BMJ Open* 7 (7), e014056. doi:10.1136/bmjopen-2016-014056

Lepelletier, D., Maillard, J. Y., Pozzetto, B., and Simon, A. (2020). Povidone iodine: Properties, mechanisms of action, and role in infection control and *Staphylococcus aureus* decolonization. *Antimicrob. Agents Chemother.* 64 (9), e00682. doi:10.1128/aac.00682-20

Li, Y., Xiong, W., Zhang, C., Gao, B., Guan, H., Cheng, H., et al. (2014). Enhanced osseointegration and antibacterial action of zinc-loaded titania-nanotube-coated titanium substrates: *In vitro* and *in vivo* studies. *J. Biomed. Mater Res. A* 102 (11), 3939–3950. doi:10.1002/jbm.a.35060

Massè, A., Bruno, A., Bosetti, M., Biasibetti, A., Cannas, M., and Gallinaro, P. (2000). Prevention of pin track infection in external fixation with silver coated pins: Clinical and microbiological results. *J. Biomed. Mater Res.* 53 (5), 600–604. doi:10.1002/1097-4636(200009)53:5<600::aid-jbm21>3.0.co;2-d

McClelland, S., 3rd, Takemoto, R. C., Lonner, B. S., Andres, T. M., Park, J. J., Ricart-Hoffiz, P. A., et al. (2016). Analysis of postoperative thoracolumbar spine infections in a prospective randomized controlled trial using the centers for disease control surgical site infection criteria. *Int. J. Spine Surg.* 10, 14. doi:10.14444/3014

Moghaddam, A., Graeser, V., Westhauser, F., Dapunt, U., Kamradt, T., Woerner, S. M., et al. (2016). Patients' safety: Is there a systemic release of gentamicin by gentamicin-coated tibia nails in clinical use? *Ther. Clin. Risk Manag.* 12, 1387–1393. doi:10.2147/tcrm.S107398

Munn, Z., Moola, S., Lisy, K., Riitano, D., and Tufanaru, C. (2015). Methodological guidance for systematic reviews of observational epidemiological studies reporting prevalence and cumulative incidence data. *Int. J. Evid. Based Healthc.* 13 (3), 147–153. doi:10.1097/xeb.0000000000000054

Noda, I., Miyaji, F., Ando, Y., Miyamoto, H., Shimazaki, T., Yonekura, Y., et al. (2009). Development of novel thermal sprayed antibacterial coating and evaluation of release properties of silver ions. *J. Biomed. Mater Res. B Appl. Biomater.* 89 (2), 456–465. doi:10.1002/jbm.b.31235

Oliveira, P. R., Carvalho, V. C., da Silva Felix, C., de Paula, A. P., Santos-Silva, J., and Lima, A. L. (2016). The incidence and microbiological profile of surgical site infections following internal fixation of closed and open fractures. *Rev. Bras. Ortop.* 51 (4), 396–399. doi:10.1016/j.rboe.2015.09.012

Osinaga, P. W., Grande, R. H., Ballester, R. Y., Simionato, M. R., Delgado Rodrigues, C. R., and Muench, A. (2003). Zinc sulfate addition to glass-ionomer-based cements: Influence on physical and antibacterial properties, zinc and fluoride release. *Dent. Mater* 19 (3), 212–217. doi:10.1016/s0109-5641(02)00032-5

Parvizi, J., Shohat, N., and Gehrke, T. (2017). Prevention of periprosthetic joint infection: New guidelines. *Bone Jt. J.* 99-B, 3–10. doi:10.1302/0301-620X.99B4.BJJ-2016-1212.R1

Piccioli, A., Donati, F., Giacomo, G. D., Ziranu, A., Careri, S., Spinelli, M. S., et al. (2016). Infective complications in tumour endoprostheses implanted after pathological fracture of the limbs. *Injury* 47, S22–s28. doi:10.1016/j.injury.2016.07.054

Prabhu, B. M., Ali, S. F., Murdock, R. C., Hussain, S. M., and Srivatsan, M. (2010). Copper nanoparticles exert size and concentration dependent toxicity on somatosensory neurons of rat. *Nanotoxicology* 4 (2), 150–160. doi:10.3109/17435390903337693

Riool, M., de Breij, A., Drijfhout, J. W., Nibbering, P. H., and Zaat, S. A. J. (2017). Antimicrobial peptides in biomedical device manufacturing. *Front. Chem.* 5, 63. doi:10.3389/fchem.2017.00063

Romanò, C. L., Tsuchiya, H., Morelli, I., Battaglia, A. G., and Drago, L. (2019). Antibacterial coating of implants: Are we missing something? *Bone Jt. Res.* 8 (5), 199–206. doi:10.1302/2046-3758.85.Bjr-2018-0316

Sambri, A., Zucchini, R., Giannini, C., Zamparini, E., Viale, P., Donati, D. M., et al. (2020). Silver-coated (PorAg(®)) endoprosthesis can be protective against reinfection in the treatment of tumor prostheses infection. *Eur. J. Orthop. Surg. Traumatol.* 30 (8), 1345–1353. doi:10.1007/s00590-020-02705-3

Savvidou, O. D., Kaspiris, A., Trikoupis, I., Kakouratos, G., Goumenos, S., Melissaridou, D., et al. (2020). Efficacy of antimicrobial coated orthopaedic implants on the prevention of periprosthetic infections: A systematic review and meta-analysis. *J. Bone Jt. Infect.* 5 (4), 212–222. doi:10.7150/jbji.44839

Schmidlin, P. R., Imfeld, T., Sahrmann, P., Tchouboukov, A., and Weber, F. E. (2009). Effect of short-time povidone-iodine application on osteoblast proliferation and differentiation. *Open Dent. J.* 3, 208–212. doi:10.2174/1874210600903010208

Schmidmaier, G., Kerstan, M., Schwabe, P., Südkamp, N., and Raschke, M. (2017). Clinical experiences in the use of a gentamicin-coated titanium nail in tibia fractures. *Injury* 48 (10), 2235–2241. doi:10.1016/j.injury.2017.07.008

Schmidmaier, G., Lucke, M., Wildemann, B., Haas, N. P., and Raschke, M. (2006). Prophylaxis and treatment of implant-related infections by antibiotic-coated implants: A review. *Injury* 37, S105–S112. doi:10.1016/j.injury.2006.04.016

Schmolders, J., Koob, S., Schepers, P., Pennekamp, P. H., Gravius, S., Wirtz, D. C., et al. (2017). Lower limb reconstruction in tumor patients using modular silver-coated megaprostheses with regard to perimegaprosthetic joint infection: A case series, including 100 patients and review of the literature. *Arch. Orthop. Trauma Surg.* 137 (2), 149–153. doi:10.1007/s00402-016-2584-8

Scoccianti, G., Frenos, F., Beltrami, G., Campanacci, D. A., and Capanna, R. (2016). Levels of silver ions in body fluids and clinical results in silver-coated megaprostheses after tumour, trauma or failed arthroplasty. *Injury* 47, S11–s16. doi:10.1016/j.injury.2016.07.042

Shamseer, L., Moher, D., Clarke, M., Ghersi, D., Liberati, A., Petticrew, M., et al. (2015). Preferred reporting items for systematic review and meta-analysis protocols (PRISMA-P) 2015: Elaboration and explanation. *Bmj* 350, g7647. doi:10.1136/bmj.g7647

Shimabukuro, M., Tsutsumi, Y., Nozaki, K., Chen, P., Yamada, R., Ashida, M., et al. (2020). Investigation of antibacterial effect of copper introduced titanium surface by electrochemical treatment against facultative anaerobic bacteria. *Dent. Mater J.* 39 (4), 639–647. doi:10.4012/dmj.2019-178

Shirai, T., Shimizu, T., Ohtani, K., Zen, Y., Takaya, M., and Tsuchiya, H. (2011). Antibacterial iodine-supported titanium implants. *Acta Biomater.* 7 (4), 1928–1933. doi:10.1016/j.actbio.2010.11.036

Shirai, T., Tsuchiya, H., Nishida, H., Yamamoto, N., Watanabe, K., Nakase, J., et al. (2014a). Antimicrobial megaprostheses supported with iodine. *J. Biomater. Appl.* 29 (4), 617–623. doi:10.1177/0885328214539365

Shirai, T., Tsuchiya, H., Terauchi, R., Tsuchida, S., Mizoshiri, N., Igarashi, K., et al. (2016). The outcomes of reconstruction using frozen autograft combined with iodine-coated implants for malignant bone tumors: Compared with non-coated implants. *Jpn. J. Clin. Oncol.* 46 (8), 735–740. doi:10.1093/jjco/hyw065

Shirai, T., Tsuchiya, H., Terauchi, R., Tsuchida, S., Mizoshiri, N., Mori, Y., et al. (2019). A retrospective study of antibacterial iodine-coated implants for postoperative infection. *Med. Baltim.* 98 (45), e17932. doi:10.1097/md.0000000000017932

Shirai, T., Watanabe, K., Matsubara, H., Nomura, I., Fujiwara, H., Arai, Y., et al. (2014b). Prevention of pin tract infection with iodine-supported titanium pins. *J. Orthop. Sci.* 19 (4), 598–602. doi:10.1007/s00776-014-0561-z

Smolle, M. A., Bergovec, M., Scheipl, S., Gössler, W., Amerstorfer, F., Glehr, M., et al. (2022). Long-term changes in serum silver concentrations after extremity reconstruction with silver-coated megaprostheses. *Sci. Rep.* 12 (1), 13041. doi:10.1038/s41598-022-16707-0

Stang, A. (2010). Critical evaluation of the Newcastle-Ottawa scale for the assessment of the quality of nonrandomized studies in meta-analyses. *Eur. J. Epidemiol.* 25 (9), 603–605. doi:10.1007/s10654-010-9491-z

Sudmann, E., Vik, H., Rait, M., Todnem, K., Andersen, K. J., Julsham, K., et al. (1994). Systemic and local silver accumulation after total hip replacement using silver-impregnated bone cement. *Med. Prog. Technol.* 20 (3-4), 179–184.

Taga, T., Kabata, T., Kajino, Y., Inoue, D., Ohmori, T., Yamamoto, T., et al. (2018). Comparison with the osteoconductivity and bone-bonding ability of the iodine supported titanium, titanium with porous oxide layer and the titanium alloy in the rabbit model. *J. Orthop. Sci.* 23 (3), 585–591. doi:10.1016/j.jos.2018.01.007

Trop, M., Novak, M., Rodl, S., Hellbom, B., Kroell, W., and Goessler, W. (2006). Silver-coated dressing acticoat caused raised liver enzymes and argyria-like symptoms in burn patient. *J. Trauma* 60 (3), 648–652. doi:10.1097/01.ta.0000208126.22089.b6

Tsuchiya, H., Shirai, T., Nishida, H., Murakami, H., Kabata, T., Yamamoto, N., et al. (2012). Innovative antimicrobial coating of titanium implants with iodine. *J. Orthop. Sci.* 17 (5), 595–604. doi:10.1007/s00776-012-0247-3

Van Belleghem, J. D., Manasherob, R., Międzybrodzki, R., Rogóż, P., Górski, A., Suh, G. A., et al. (2020). The rationale for using bacteriophage to treat and prevent periprosthetic joint infections. *Front. Microbiol.* 11, 591021. doi:10.3389/fmicb.2020.591021

van Vugt, T. A. G., Arts, J. J., and Geurts, J. A. P. (2019). Antibiotic-Loaded polymethylmethacrylate beads and spacers in treatment of orthopedic infections and the role of biofilm formation. *Front. Microbiol.* 10, 1626. doi:10.3389/fmicb.2019.01626

Wafa, H., Grimer, R. J., Reddy, K., Jeys, L., Abudu, A., Carter, S. R., et al. (2015). Retrospective evaluation of the incidence of early periprosthetic infection with silver-treated endoprostheses in high-risk patients: Case-control study. *Bone Jt. J.* 97 (2), 252–257. doi:10.1302/0301-620x.97b2.34554

Wang, G., Zhu, Y., Zan, X., and Li, M. (2021). Endowing orthopedic implants' antibacterial, antioxidation, and osteogenesis properties through a composite coating of nano-hydroxyapatite, tannic acid, and lysozyme. *Front. Bioeng. Biotechnol.* 9, 718255. doi:10.3389/fbioe.2021.718255

Wang, Q., Guo, S., Wei, X., Dong, Q., Xu, N., Li, H., et al. (2022). Global prevalence, treatment and outcome of tuberculosis and COVID-19 coinfection: A systematic review and meta-analysis (from november 2019 to march 2021). *BMJ Open* 12 (6), e059396. doi:10.1136/bmjopen-2021-059396

Wilding, C. P., Cooper, G. A., Freeman, A. K., Parry, M. C., and Jeys, L. (2016). Can a silver-coated arthrodesis implant provide a viable alternative to above knee amputation in the unsalvageable, infected total knee arthroplasty? *J. Arthroplasty* 31 (11), 2542–2547. doi:10.1016/j.arth.2016.04.009

Yonekura, Y., Miyamoto, H., Shimazaki, T., Ando, Y., Noda, I., Mawatari, M., et al. (2011). Osteoconductivity of thermal-sprayed silver-containing hydroxyapatite coating in the rat tibia. *J. Bone Jt. Surg. Br.* 93 (5), 644–649. doi:10.1302/0301-620x.93b5.25518

Zajonz, D., Birke, U., Ghanem, M., Prietzel, T., Josten, C., Roth, A., et al. (2017). Silver-coated modular Megaendoprostheses in salvage revision arthroplasty after periimplant infection with extensive bone loss - a pilot study of 34 patients. *BMC Musculoskelet. Disord.* 18 (1), 383. doi:10.1186/s12891-017-1742-7

Zhang, H., Shen, X., Fei, Z., Fan, X., Ma, L., Wang, H., et al. (2022). Ag-incorporated polydopamine/tannic acid coating on titanium with enhanced cytocompatible and antibacterial properties. *Front. Bioeng. Biotechnol.* 10, 877738. doi:10.3389/fbioe.2022.877738

Zhao, Q., Wu, J., Li, Y., Xu, R., Zhu, X., Jiao, Y., et al. (2022). Promotion of bone formation and antibacterial properties of titanium coated with porous Si/Ag-doped titanium dioxide. *Front. Bioeng. Biotechnol.* 10, 1001514. doi:10.3389/fbioe.2022.1001514

Zimmerli, W., Trampuz, A., and Ochsner, P. E. (2004). Prosthetic-joint infections. *N. Engl. J. Med.* 351 (16), 1645–1654. doi:10.1056/NEJMra040181

frontiers | Frontiers in Bioengineering and Biotechnology

TYPE Original Research
PUBLISHED 14 February 2023
DOI 10.3389/fbioe.2023.1107209

OPEN ACCESS

EDITED BY
Yansong Qi,
Inner Mongolia People's Hospital, China

REVIEWED BY
Feza Korkusuz,
Hacettepe University, Türkiye
Zhiguo Yuan,
Shanghai Jiao Tong University, China

*CORRESPONDENCE
Dan Xing,
xingdan@bjmu.edu.cn
Jianhao Lin,
linjianhao@pkuph.edu.cn

†These authors have contributed equally to this work

SPECIALTY SECTION
This article was submitted to Biomaterials, a section of the journal Frontiers in Bioengineering and Biotechnology

RECEIVED 24 November 2022
ACCEPTED 03 February 2023
PUBLISHED 14 February 2023

CITATION
Yang Z, Fan Z, Wang D, Li H, He Z, Xing D and Lin J (2023), Bibliometric and visualization analysis of stem cell therapy for meniscal regeneration from 2012 to 2022.
Front. Bioeng. Biotechnol. 11:1107209.
doi: 10.3389/fbioe.2023.1107209

Bibliometric and visualization analysis of stem cell therapy for meniscal regeneration from 2012 to 2022

Zhen Yang[1,2†], Zejun Fan[3†], Du Wang[1,2], Hui Li[1,2], Zihao He[1,2], Dan Xing[1,2*] and Jianhao Lin[1,2*]

[1]Arthritis Clinical and Research Center, Peking University People's Hospital, Beijing, China, [2]Arthritis Institute, Peking University, Beijing, China, [3]Department of Biomedical Engineering, School of Medicine, Tsinghua-Peking Center for Life Sciences, Tsinghua University, Beijing, China

Background: Meniscus injuries, a common joint disease caused by long-term wear, trauma and inflammation, usually cause chronic dysfunction and pain in the joint. Current clinical surgeries mainly aim to remove the diseased tissue to alleviate patient suffering instead of helping with meniscus regeneration. As an emerging treatment, stem cell therapy has been verified to facilitate meniscus regeneration effectively. The purpose of this study is to investigate the publication conditions of stem cell therapy for meniscal regeneration and to visualize the research trends and frontiers.

Methods: Relevant publications relevant to stem cells for meniscal regeneration was retrieved SCI-Expanded of the Web of Science database from 2012 to 2022. Research trends in the field were analysed and visualized by CiteSpace and VOSviewer.

Results: A total of 354 publications were collected and analysed. The United States contributed the largest number of publications (118, 34.104%). Tokyo Medical Dental University has contributed the largest number of publications (34) among all full-time institutions. *Stem cell research therapy* has published the largest number of researches on stem cells for meniscal regeneration (17). SEKIYA. I contributed the majority of publications in this field (31), while Horie, M was the most frequently cited authors (166). #1 tissue engineering, #2 articular cartilage, #3 anterior cruciate ligament, #4 regenerative medicine, #5 scaffold are the chief keywords. This indicates that the current research hotspot has been transformed from basic surgical research to tissue engineering.

Conclusion: Stem cell therapy is a promising therapeutic method for meniscus regeneration. This is the first visualized and bibliometric study to thoroughly construct the development trends and knowledge structure in the research field of stem cell therapy for meniscal regeneration in the past 10 years. The results thoroughly summarize and visualize the research frontiers, which will shed light on the research direction of stem cell therapy for meniscal regeneration.

KEYWORDS

stem cell, meniscal regeneration, bibliometric, citespace, vosviewer

1 Introduction

The meniscus acts as a shock absorber between the shinbone and the thighbone, which is a C-shaped piece of tough, rubbery cartilage (Markes et al., 2020). In this sense, the meniscus plays a key role in normal knee movement and transmission of loading force, although the meniscus is smaller in size. Due to its high mechanical burden and continuous friction in the joint, it hurts easily and consequently becomes one of the most common knee injuries (Chambers and Chambers, 2019). On the one hand, while bearing weight on it, the meniscus can be torn if the knee is twisted suddenly due to inappropriate mechanical stimulation. On the other hand, excessive exercise and degeneration of articular cartilage usually cause meniscus wear, especially in aged individuals. Due to its avascular nature, the meniscus has a very weak ability to regenerate (Kurzweil et al., 2018). Thus, the chondrocytes are not able to proliferate fast enough and generate sufficient extracellular matrix to repair a defect (Kurzweil et al., 2018).

Researchers from all over the world are focusing on this field to find a way to alleviate the suffering and relieve symptoms of patients. For instance, some surgical accesses, already used in clinical treatment, can slightly alleviate patients' suffering, including meniscectomy, which means removing the meniscus of the patients to reduce local chronic inflammatory reactions (Brown et al., 2021). Recent research results show that meniscectomy can only improve athletic ability in the beginning and has an adverse effect on the joint in several post-surgery years, although surgical technology provides symptomatic relief (Brown et al., 2021). When the knee joint moves, the friction between the femoral condyle and the tibial condyle increases. Under the same load, whether the meniscus is damaged or removed, the stress on the articular cartilage surface increases greatly. The decrease in stability promotes the subsequent formation of cartilage degeneration and osteoarthritis (Sun and Mauerhan, 2012).

As one type of stem cell, mesenchymal stem cells (MSCs) as the word implies, are named for their ability to differentiate into mesenchymal tissues (Yu et al., 2015). They have subpluripotent differentiation potential and can be induced into a variety of tissue cells in both natural and artificial environments. MSC therapy for meniscal regeneration is a relatively promising treatment, the main mechanism of which comes from its pluripotent differentiation potential (Caminal et al., 2014). Accordingly, when suffering from meniscal disease, the use of stem cell therapy may have corresponding therapeutic effects, especially for patients with mild articular meniscus wear and tears. In fact, mild patients are usually treated conservatively with no cure. With the development of regenerative medicine, MSC therapy has been tested for more than 10 years in the field of meniscus defects and meniscus regeneration (Joyce et al., 2010).

MSCs function mainly through two mechanisms of action (Hatsushika et al., 2013). On the one hand, stem cells directly repair damaged tissues through multidirectional differentiation potential, which means that stem cells are transformed into osteocytes and chondrocytes under specific induction conditions to repair bone and meniscus. On the other hand, stem cells activate the repair function of other cells, such as chondrocytes, by secreting various cytokines (Wang et al., 2017), such as transforming growth factor-β1 and insulin-like growth factor-1. These cytokines could inhibit the development of local inflammation and promote the self-repairing ability of local damaged tissues, thus accomplishing the purpose of meniscal regeneration.

In the last 10 years, many advances and achievements in stem cell-based therapy for meniscus repair have been made both clinically (Rinonapoli et al., 2021) and preclinically (Khalifeh Soltani et al., 2019). In addition to MSCs, many other cell types have also been utilized and further clinical applications require the effectiveness of clinical trials. In addition, in preclinical studies, different types of stem cells accompanied by fantastic biomaterials have been utilized to repair the meniscus, demonstrating a huge potential and a research hotspot. Despite the increasing results and interest in the topic of stem cell therapy for meniscal regeneration, the analysis of publication trends in this research area is still insufficient. Considering some researchers has summarized the specific advances (Le et al., 2020), there is a missing to comprehensively conclude the research development. Hence, it is necessary to explore, identify and analyse the trends in this field to help us predict and guide research directions.

As is widely acknowledged, the literature is the carrier of scientific progress. Bibliometric analysis uses mathematical and statistical methods to quantitatively and quantitatively analyse publications in medical databases, revealing the development history, research focus and future trends of a certain field. Among the literature, generous information was ignored. We are going to excavate useful information behind the data to help conclude and analyze the research development.

With advances in statistics science, bibliometric analysis has been utilized gradually, analysing current scientific research data and identifying developing trends (Wu et al., 2022a; IsmailSaqr, 2022). Furthermore, although a visualized network and comprehensive analysis, it is feasible to investigate the publication condition, predict research trends, and thus analyses research hotspots in specific fields (Zhang et al., 2022; Zhao et al., 2022). It is widely acknowledged that the combination of several bibliometric and mathematical tools, such as CiteSpace, the R package "bibliometrix" and VOSviewer, has also been widely used to visualize specific research literature analysis fields (Wu et al., 2022b; Zhang et al., 2022; Zhao et al., 2022). Accordingly, in this study, a new bibliometric statistics analysis with a visual network is performed to meet the unmet need and fill this knowledge gap. No related analysis of stem cell therapy for meniscal regeneration has been performed. This study comprehensively analysed the literature related to stem cell therapy for meniscal regeneration and performed visualization analysis over the last decade (2012–2022) to identify its research focus and even predict research hotspots. The study is significant because it is the first bibliometric analysis to scientifically and comprehensively analyze the researches related to stem cell therapy for meniscal regeneration and visualize the development trends in the past 10 years. Besides, the study would also benefit the audience a lot because it sheds light on the research direction of stem cell therapy for meniscal regeneration. On the one hand, current articles mainly focus on some specific therapy, which means, in fact, there is a lack of an all-round level bibliometric analysis of stem cell therapy for meniscus regeneration. On the other hand, researchers are in great need of such a summary, looking forward to understand the current status and hot spots in the field. An all-round level can

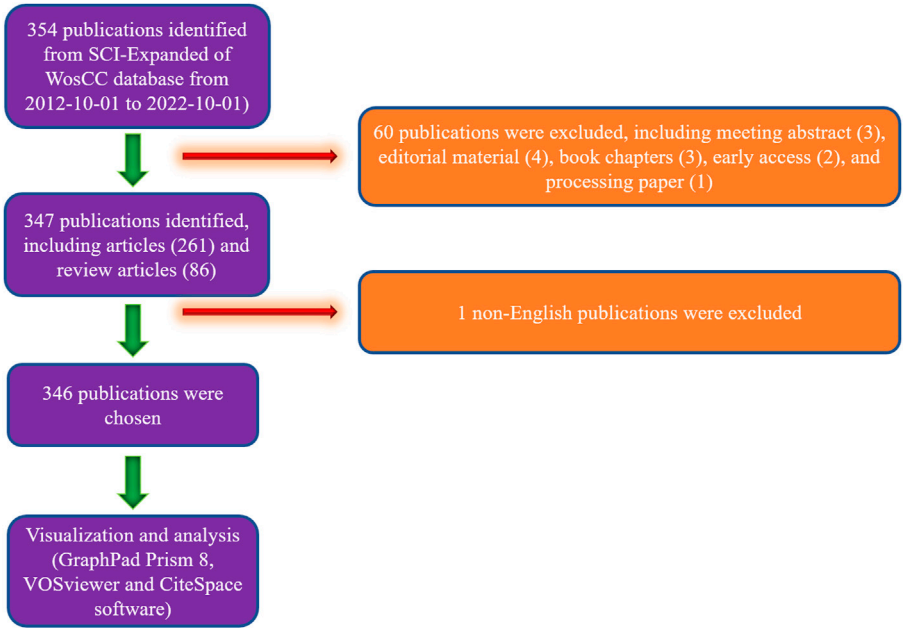

FIGURE 1
Flowchart depicting the article selection process.

help think clearly and avoid detours. Besides, a big data aggregation in the field can improve efficiency by reducing duplication of labor, sharing information resources, and improving researchers' comprehensive capabilities. Furthermore, researchers could formulate more reasonable work goals and find more suitable scientific research directions when they read this study.

2 Materials and methods

2.1 Data source and search strategy

As one of the most authoritative and comprehensive database platforms, the SCI-Expanded of Web of Science Core Collection (WoSCC) originates from Clarivate Analytics, which contains more than 12000 international academic journals (Wu et al., 2022b). Consequently, it was chosen to obtain global academic information for bibliometric analysis based on previous publications (Ekici et al., 2022). All the published literature was extracted from SCI-Expanded database, and the searching time was set from 1 October 2012 to 1 October 2022. The searching date is set to 3 November 2022, which means the update time of the dataset is determined. In present study, through the Advanced Search Section function, the searching terms were as follows (Figure 1): Theme = menisc* regeneration AND theme = stem cells AND publishing year = (2012.10.1–2022.10.1) AND Document types = (Article or Review) AND Language = (English). We indexed country/region to acquire further information of countries/regions in the SCI-Expanded database. The inclusion criteria are as follows: (1) Peer-reviewed publications mainly focused on the research field regarding stem cells for meniscal regeneration; (2) The document types must be Article and Review; (3) The publications should be written in English; (4) The publishing data must be between 2012 and 2022. The exclusion criteria were also as follows: (1) The themes of publications were not related to stem cells for meniscal regeneration; (2) Papers were news, meetings, abstract, briefings, etc.

In addition, all detailed data of the publications, including nationalities, name of journals, title, publishing year, author names, affiliations, abstract and keywords were saved in the format of download. txt files from the SCI-Expanded database and subsequently imported into Excel 2021. Coauthors (YZ and FZJ) searched and extracted all data from these studies independently. All disagreements were addressed by consulting with experts to reach the ultimate consensus. Finally, all data were cleaned and analysed individually by the coauthors and separately cleaned using GraphPad Prism 8 and Origin 2021.

2.2 Bibliometric analysis and visualization

The basic features of eligible studies were characterized by the intrinsic function of WoSCC.

Accordingly, the publishing number of studies and citations were analysed and visualized. We chose GraphPad Prism 8 and Origin 8 to perform the following bibliometric analysis. First, the year was taken as the *x*-axis and the number of documents published each year was set as *y*-axis to explore the trend of the number of documents issued. The relative research interest (RRI) was considered as the number of publications in a certain field by all field literatures per year (Shah et al., 2022). A combination of R software, including Python, NumPy, SciPy and Matplotlib, helped acquire the world map. Meanwhile, the time curve of publications has also been drawn. The H-index, which refers to a scholar who has published H papers and has been cited at least H times, was also calculated to measure the impact of scientific research (Hu et al., 2022).

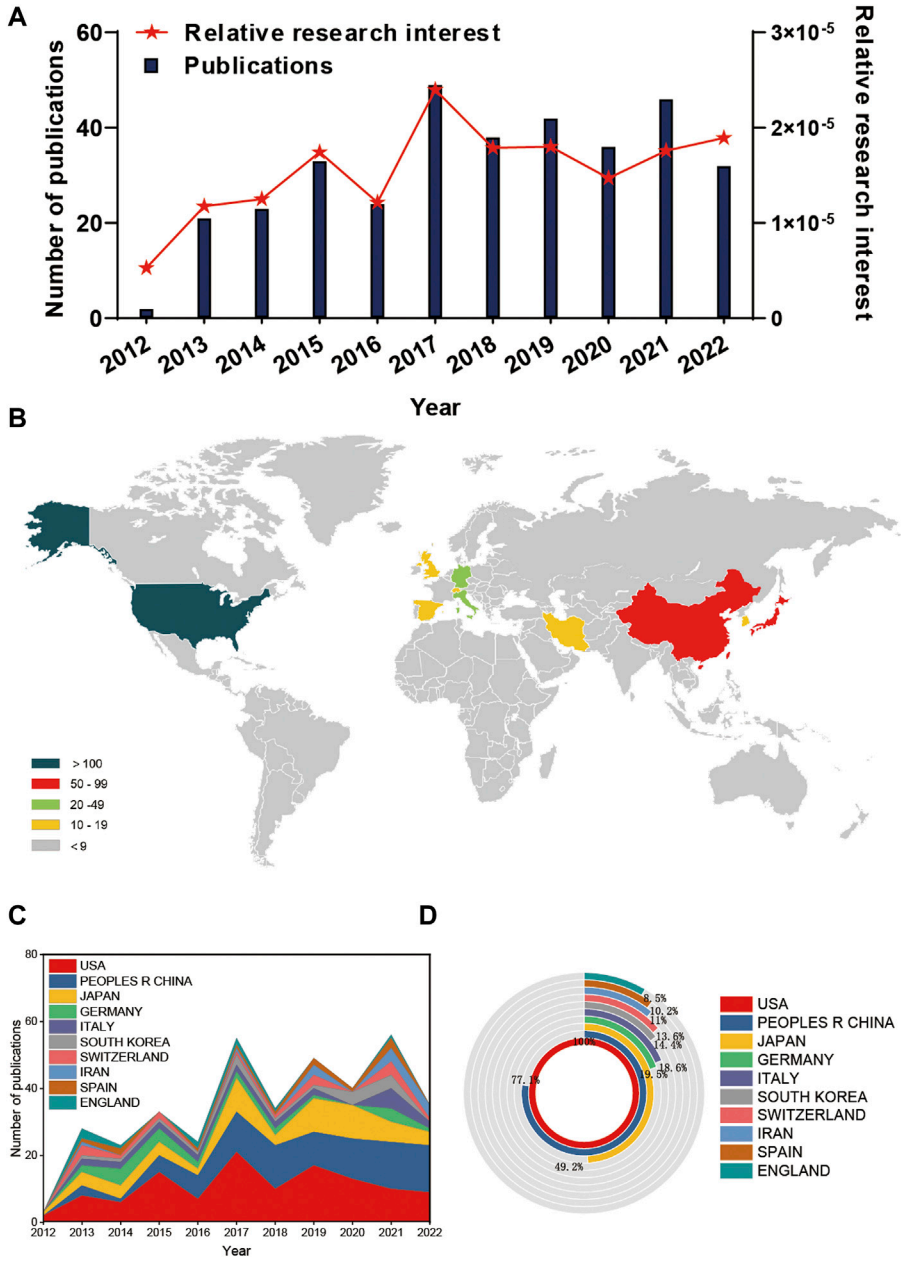

FIGURE 2
Global trends and countries/regions contributing to the research field regarding stem cells for meniscal regeneration from 2012 to 2022. **(A)** The annual number of publications related to stem cells for meniscal regeneration. **(B)** A world map depicting the distribution of stem cells for meniscal regeneration. The annual number **(C)** and total number **(D)** of publications in the top 10 most productive countries from 2012 to 2022.

To comprehensively visualize bibliometric networks of the publications, VOSviewer (Leiden University, Netherlands) software was used in this study. Deep down, bibliographic coupling, cocitation, and co-occurrence analysis were also performed and visualized in detail using VOSviewer. The relative parameter settings main about the minimum number of documents/citations/times. In details, 1) for bibliographic coupling analysis, the minimum number of documents of the Country, Journal, Author, and Institution was defied as more than 2; 2) for co-citation analysis, the minimum number of citations of the Author, Reference, and Journal was defined as more than10; 3) for co-authorship analysis, the minimum number of documents of the Country, Author, and Institution was defied as more than 2; 4) for co-occurrence analysis, the keyword was defined as the words used more than 2 times in titles/abstracts among all papers.

Moreover, CiteSpace (6.1. R2) served to construct a dual-map overlay for journals, visualize the diagram of country/regional collaboration, institutional collaboration and author collaboration, cluster analysis of co-cited keywords, and detection of references and keywords with intense citation bursts, which was developed by Professor Chen C. The parameters of CiteSpace were set as follows: link retaining factor (LRF = 3), look back years (LBY = 5), e for top N (e = 1),

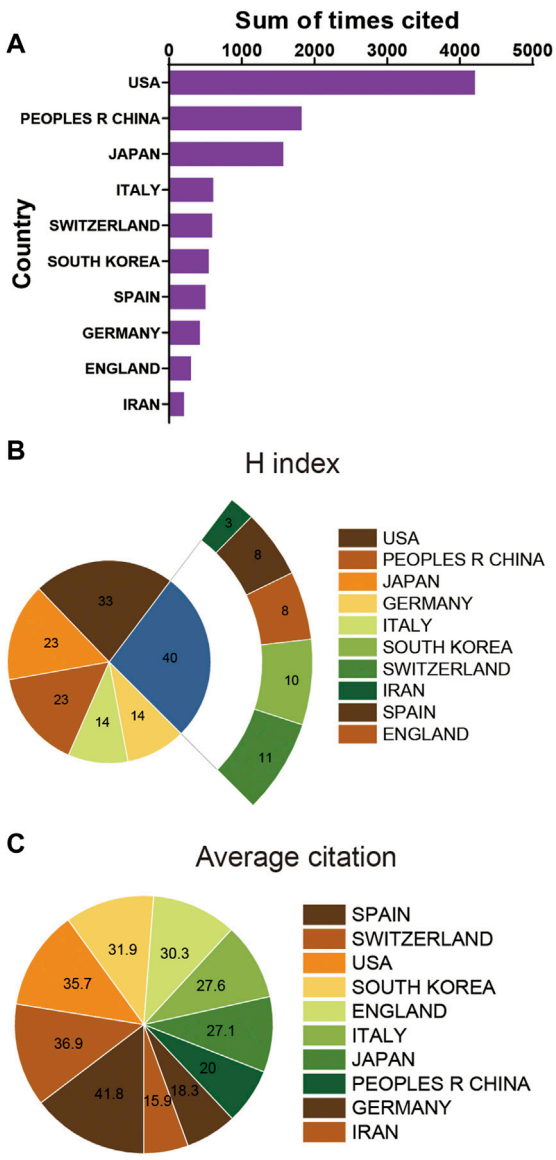

FIGURE 3
(A) The top 10 countries/regions of total citations related to stem cells for meniscal regeneration. **(B)** The top 10 countries/regions of the publication H-index related to stem cells for meniscal regeneration. **(C)** The top 10 countries/regions of the average citations per publication related to stem cells for meniscal regeneration.

time span (2012–2022), years per slice (1), links (strength: Cosine, scope: Within slices), selection criteria (g-index: k = 25), and minimum duration (MD = 2 for keywords; MD = 5 for references).

3 Results

3.1 Overall performance of global literature

Based on the search criteria, a total of 354 studies were collected and analyzed from 2012 to 2022. Second, 347 studies were identified, excluding the editorial material (4), meeting abstract (3), early access (2), correction book chapter (3), and processing paper (1). Consequently, 346 studies were identified, and 1 non-English study (Figure 1) was removed. As shown in Figure 2A, the trend of global literature experienced a steady increase almost year by year. The number of total global studies rose from 3 (2012) to 33 (2022). In the past decade, the year most studies were published was 2017 (Figure 2A). Additionally, there is ongoing increase in the research interest in this field over the past years in a not dissimilar way (Figure 2A).

Generally, 31 countries/regions have made contributions to the literature in this field according to VOSviewer. As suggested in Figures 2B, C, the United States contributed the most papers (117), followed by the four countries: China (91), Japan (58), Germany (23) and Italy (22). It is shown in Figure 2D that the United States proceeds much more in this the number of publications for the top 10 countries/regions. The number of publications of the second and third countries—China and Japan—are only equivalent to 77.1% and 49.2% of that of the United States, respectively.

From a temporal perspective, there is a slight decline in the annual number of publications in the United States and an increase in the number of publications in China in Figure 2C during 2019–2022. Overall, research on stem cells associated with meniscal regeneration has drawn increasing attention of global researchers and has arrived in a stage of rapid development.

TABLE 1 The top 10 most productive countries/regions related to stem cells for meniscal regeneration.

Rank	Country/region	Article counts	Percentage
1	United States	118	34.10
2	Peoples R China	91	26.30
3	Japan	58	16.76
4	Germany	23	6.64
5	Italy	22	6.36
6	South Korea	17	4.91
7	Switzerland	16	4.62
8	Iran	13	3.76
9	Spain	12	3.47
10	England	10	2.89

3.2 Distribution of publications in countries

As seen from Figure 3A and Table 1, the publications with the highest total citation frequencies were form the United States (4184). China ranked second concerning total citation frequencies (1822), followed by Japan (1569), Italy (608) and Switzerland (591). Additionally, the United States (33) played a dominant role in this field in the relative publications of the H-index, followed by China (23), Japan (23), Germany (14) and Italy (14) (Figure 3B). Interestingly, when it comes to average citation frequency, publications from Spain possessed the highest average citation frequencies (41.8). Switzerland ranked in the second position in the aspect of average citation frequency (36.9) prior to the United States (36.9), South Korea (31.9) and England (30.3) (Figure 3C).

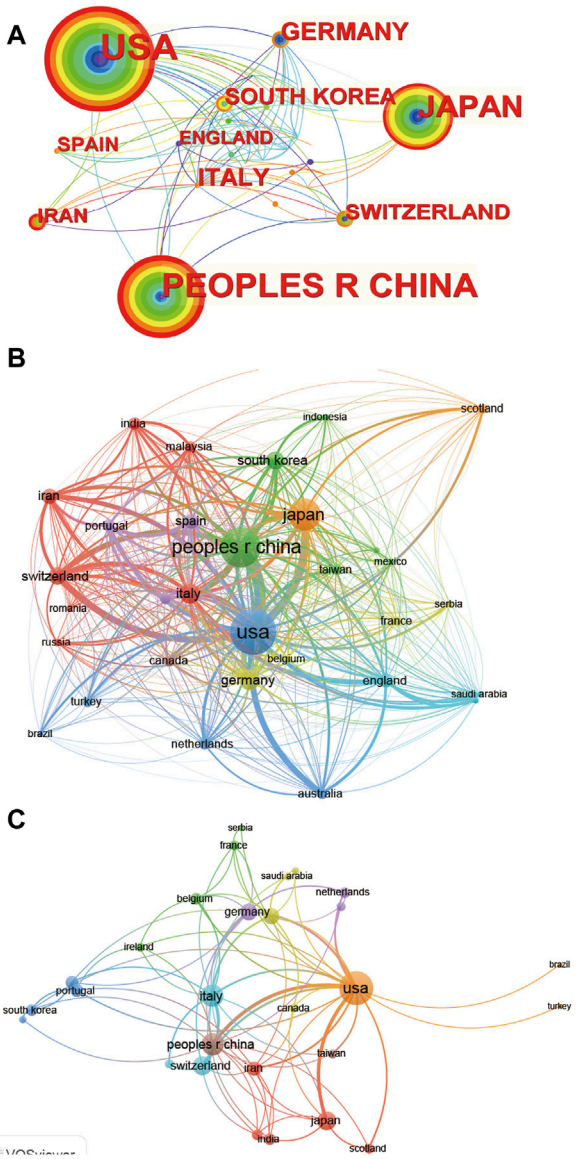

FIGURE 4
Mapping of countries/regions associated with stem cells for meniscal regeneration. Country/regional collaboration analysis derived based on CiteSpace **(A)** and Vosviewer **(B)**. **(C)** The authorship-country collaboration analysis *via* Vosviewer. The nodes represent countries/regions, and the lines connect them. The number of publications grows proportionally to the size of the nodes. The lines between the nodes represent the cooperation relationship, and the thickness of the connecting lines represents the strength of their cooperation; the closer the cooperation is, the thicker the connecting lines. The nodes with the outermost orange circles have higher centrality.

3.3 Analysis of country/regional collaboration

The global collaboration network analysis was also carried out; Figure 4A shows that the United States exhibited the highest output area and worked closely with other countries using CiteSpace, which means it had the strongest international collaboration. In detail, the size of the circle represents the collaboration strength, while the color represents the distribution of collaboration time from 2012 to 2022. From Figure 4A, the United States, China and Japan have maintained a steady collaboration strength in the last decade. However, Germany experiences shrinking international collaboration with other countries.

Additionally, the collaboration of the 31 countries is visualized in Figures 4B, C. Figures 4B, C shows that the United States (link strength 5255.64), Japan (link strength 3377.95) and China (link strength 1722.27) have the most frequent international collaborations. In addition, the majority of international partners of the United States are Australia, Japan and Switzerland. The transformation of collaboration with time can also be acquired from the color of the circle of country and the link between different countries, which did not represent obvious changes for most countries.

3.4 Analysis of institutions

Regarding publication ranking, the top 10 contributing institutions are listed in Table 2 and visualized in Figures 5A, B. Based on CiteSpace in Figures 5A, B, in terms of international collaboration between institutions, the first institution was Tokyo Medical and Dental University, which also possessed a high yield of publication. Interestingly, the time of the main collaboration lasted from 2012 to 2017, which means that there is currently a decrease in collaboration. In contrast, the two Chinese institutions, Peking University and Shanghai Jiao Tong University, display an intense collaboration strength from 2017 to the present, ranking second and third, respectively. Based on Vosviewer in Figure 5B, the impact of each research is estimated by the citations, considering the citations in the 161 institutions. In that sense, the first institution is Peking University (link strength 1646.14), followed by People's Liberation Army General Hospital (link strength 1567.14) and Nankai University (link strength 1041.34). Especially concerning Nankai University, the research number is not very high, yet the research impact is relatively strong. Figure 5C demonstrated the network diagram of collaboration between institutions. As suggested, there is a close cooperative relationship between institutions in East Asia, such as Shanghai Jiao Tong University, Tokyo Medical and Dental University, People's Liberation Army General Hospital and Peking University.

3.5 Analysis of authors

In general, a total of 326 authors in this field that have more than 2 articles are considered and calculated by Vosviewer and CiteSpace. The relatedness of the items depending on the numbers they together co-operated in one study was calculated in the collaboration analysis.

All required authors were analysed using CiteSpace (Figure 6A) and Vosviewer (Figure 6B). Based on CiteSpace (Figure 6A), the top 5 authors with the largest total link and circle strength were as follows: SEKIYA I, KOGA H, MUNETA T, TSUJI K, MIZUNO M. In detail, Sekiya published 27 articles with 748 citations, which proves its contribution and leading role in the field from these two aspects. It is also suggested that collaborations between American

TABLE 2 The top 10 institutions published literature related to stem cells for meniscal regeneration.

Rank	Institution	Article counts	Percentage	Country	Total citations	Average citation
1	Tokyo Medical Dental University Tmdu	34	9.83	Japan	1231	34.19
2	Peking University	29	8.38	China	508	17.52
3	Chinese People S Liberation Army General Hospital	15	4.36	China	272	18.13
4	Pennsylvania Commonwealth System of Higher Education Pcshe	13	3.76	United States	593	45.62
5	Shanghai Jiao Tong University	13	3.76	China	319	24.54
6	Zhejiang University	13	3.76	China	413	31.77
7	Harvard University	11	3.18	United States	319	26.58
8	University of Regensburg	11	3.18	Germany	253	23.00
9	Mayo Clinic	10	2.89	United States	244	24.40
10	Nanjing Medical University	10	2.89	China	142	14.20

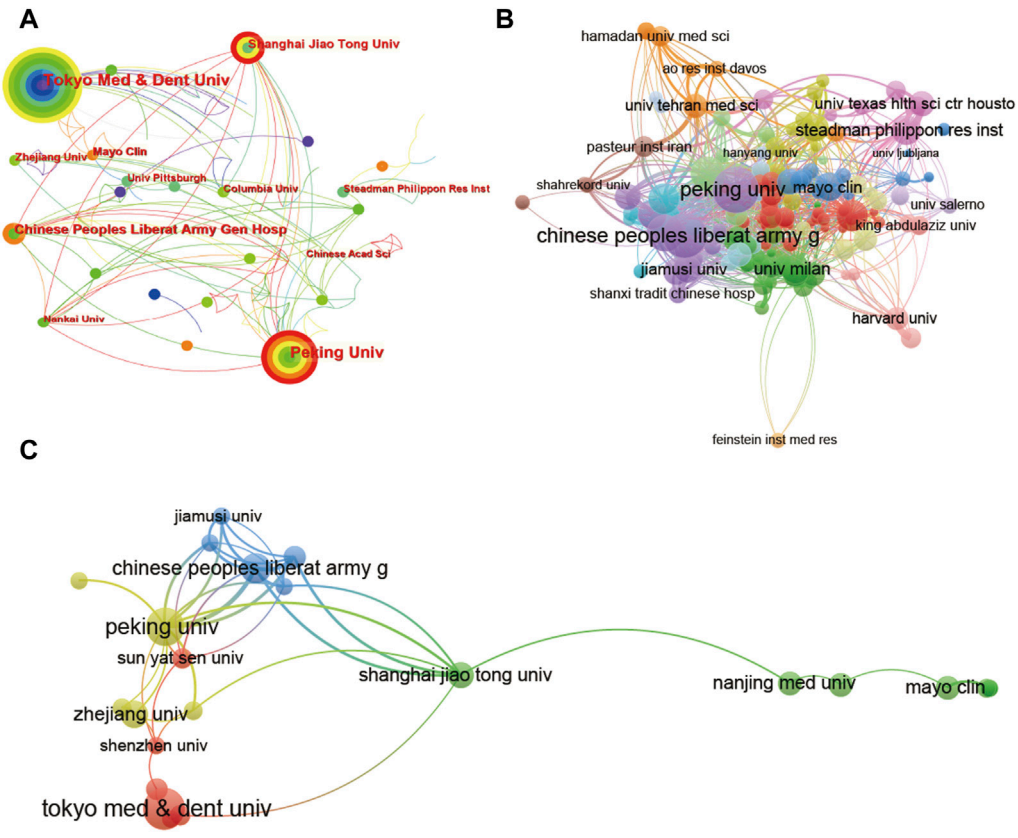

FIGURE 5
Mapping of institutions associated with stem cells for meniscal regeneration. Institutional collaboration analysis based on CiteSpace **(A)** and Vosviewer **(B)**. **(C)** The authorship-institution collaboration analysis *via* Vosviewer. The nodes represent countries/regions or institutions, and the lines connect them. The number of publications grows proportionally to the size of the nodes. The lines between the nodes represent the cooperation relationship, and the thickness of the connecting lines represents the strength of their cooperation; the closer the cooperation is, the thicker the connecting lines. The nodes with the outermost red circles have higher centrality.

and Japanese researchers are much more frequent and closer. Based on Vosviewer (Figure 6B), the visualization of author collaboration shows that there exist some collaboration circles of researchers, the central authors of which are Guo, Sekiya, Chen and Angele. In Figure 6C, a clear transition of collaboration with time from 2012 to 2022 has been displayed, predicting a possible transfer of academic

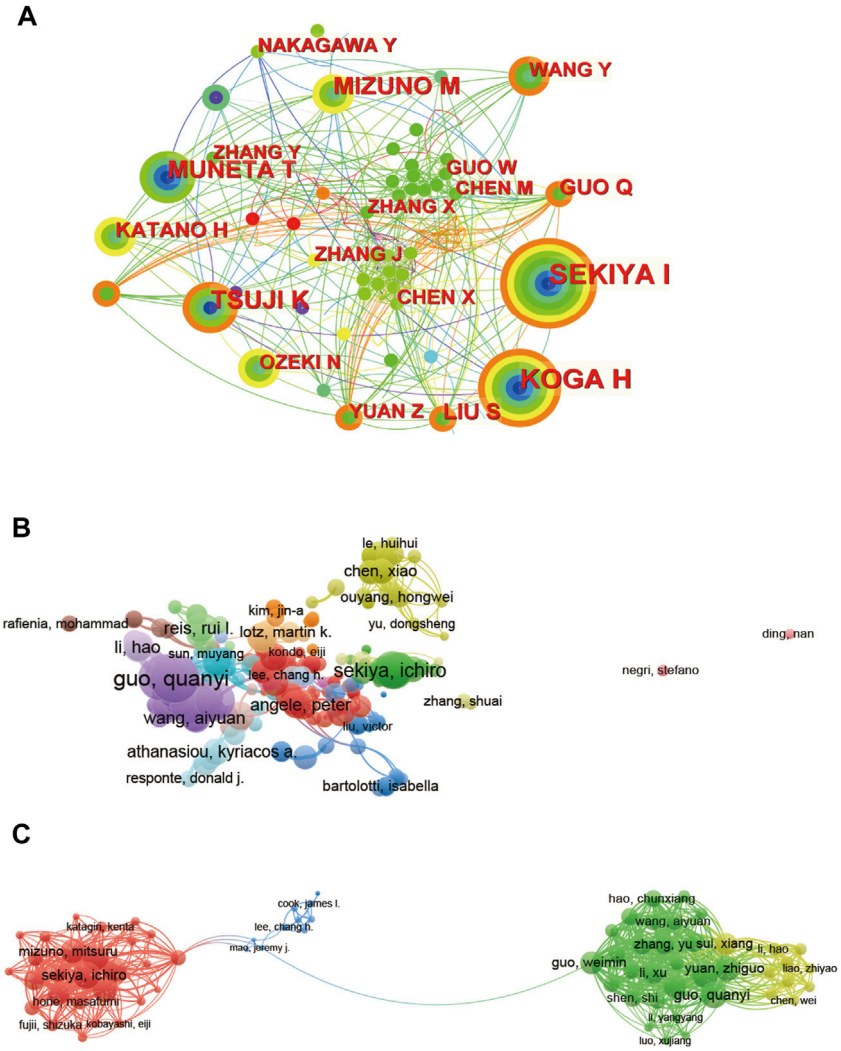

FIGURE 6
CiteSpace and Vosviewer network visualizations of author collaboration analysis regarding stem cells for meniscal regeneration. Author collaboration analysed by CiteSpace **(A)** and Vosviewer **(B)**. **(C)** Network visualization diagram of authorship-author analysis based on Vosviewer. Author collaboration authors are indicated by the node. The collaboration relationship is indicated by the line connecting the nodes. The node area grows as the number of collaborations increases. The colors from green to orange represent different years from 2012 to 2022.

center. According to Figure 6C, it seems that during 2012–2022, a hot collaboration will transfer from Guo to Mao and then to Sekiya.

3.6 Citation and Co-Citation analysis

In terms of citation and cocitation analysis, a total of 367 researches in this field have been collected. These publications collected are more than 10 citations (Figure 7A). The leading 5 most cited documents are listed in Table 3. There were 301 citations for "Treatment of Knee Osteoarthritis with Autologous Mesenchymal Stem Cells: A Pilot Study", followed by "Adult Human Mesenchymal Stem Cells Delivered *via* Intraarticular Injection to the Knee Following Partial Medial Meniscectomy a Randomized, Double-Blind, Controlled Study", with 255 citations. The third-dominant article with the largest number of citations was "Poly (lactic acid)-based biomaterials for orthopaedic regenerative engineering", with 223 citations. Cocitation means that an article is cited by two different articles but not necessarily linked. Moreover, cocited authors were analysed by CiteSpace (Figure 7B) to show the top 5 most influential studies.

What can't be ignored is citation burst, which is a valuable indicator in a particular domain in a period, reflecting the references of interest to researchers. In our analysis, the top strongest citation bursts were characterized and identified. In details, a total of 20 publications have been summarized by CiteSpace and are presented in Figure 7C. The study by Weinand C maintains the strongest citation burst with a strength of 3.84, lasting from 2013 to 2015.

3.7 Analysis of research areas and journals

The 10 most productive journals involved in this study have been displayed in Table 4. For visualization, the dual-map overlay of journals related to stem cells for meniscal regeneration is plotted

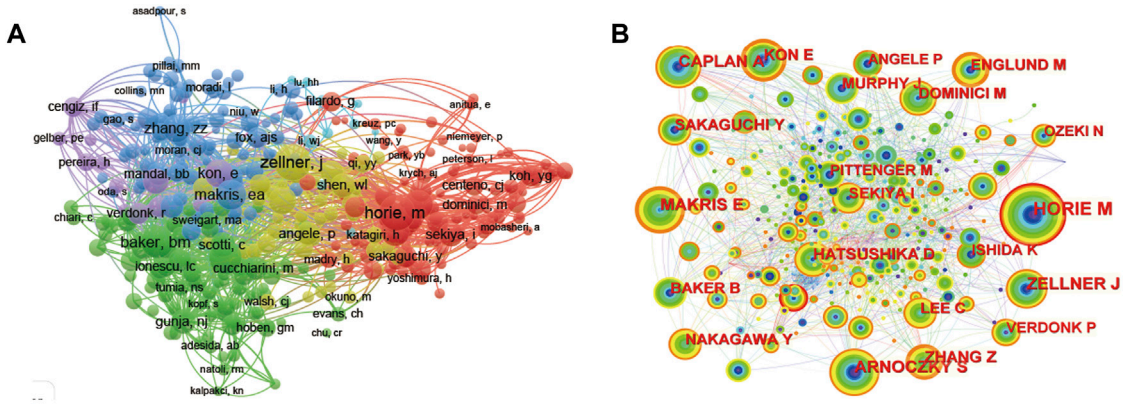

C

Top 20 Cited Authors with the Strongest Citation Bursts

Cited Authors	Year	Strength	Begin	End	2012 - 2022
WEINAND C	2012	3.84	2013	2015	
JOHNSTONE B	2012	3.83	2013	2017	
STONE K	2012	3.48	2013	2016	
PERETTI G	2012	3.41	2013	2016	
PETERSEN W	2012	3.26	2013	2015	
MURPHY J	2012	4	2014	2016	
CAPLAN A	2012	3.66	2014	2016	
AL F	2012	2.92	2014	2016	
KOH Y	2012	3.57	2016	2019	
SHEN W	2012	3.03	2017	2019	
LEE C	2012	3.78	2018	2020	
YAN L	2012	3.7	2018	2020	
MCNULTY A	2012	3.37	2018	2020	
MORADI L	2012	5.02	2019	2022	
SHIMOMURA K	2012	4.72	2019	2022	
ZHANG Z	2012	4.65	2019	2022	
LEE J	2012	3.83	2019	2022	
BILGEN B	2012	3.83	2019	2022	
GAO S	2012	3.83	2019	2022	
MORIGUCHI Y	2012	3.54	2019	2022	

FIGURE 7
CiteSpace network visualization of cocitation author analysis regarding stem cells for meniscus regeneration. Author cocitation analysed by Vosviewer **(A)** and CiteSpace **(B)**. **(C)** Top 25 references with the strongest citation bursts of publications related to stem cells for meniscal regeneration. Author cocitations are indicated by the node. The cocitation relationship is indicated by the line connecting the nodes. The node area grows as the number of cocitations increases. The colors from green to orange represent different years from 2012 to 2022.

after analysis in Figures 8A, B, 9. The journal *Stem Cells Research Therapy* published the most, with 17 publications. There were 15 publications in *American Journal of Sports Medicine*, 13 publications in *Journal of Orthopaedic Research*, 12 publications in *Acta Biomaterialia* and 9 articles in *Osteoarthritis and Cartilage*. Concerning the analysis of journals of cocitation using VOSviewer, the collection standard is that the journal with a number of citations less than 10 will be ignored. As visualized in Figure 8C, 300 journals are collected in the total link strength. The 5 journals, as follows: *Biomaterials* (total citations = 1229 times), *American Journal of Sports Medicine* (total citations = 1180 times), *Osteoarthritis and Cartilage* (total citations = 896 times), *Journal of Orthopedic Research* (total citations = 645 times), and *Arthroscopy* (total citations = 642 times), owned best total link strength, as shown in Table 5.

A list of research orientations is summarized using VOSviewer in Table 6. As a matter of fact, the most prevalent research fields are cell biology, orthopedics, engineering, materials science and research experimental medicine. The main research orientation points out the current research focus and potential.

3.8 Analysis of references and funds

Moreover, to show the most influential literature, cocited references were analysed by VOSviewer (Figure 10A). In this

TABLE 3 The top 5 documents with the most citations in the field of stem cells for meniscal regeneration.

Rank	Title	First author	Journal	IF	Publication year	Total citations
1	Treatment of Knee Osteoarthritis with Autologous Mesenchymal Stem Cells: A Pilot Study	Orozco, L	Transplantation	5.385	2013	301
2	Adult Human Mesenchymal Stem Cells Delivered *via* Intra-Articular Injection to the Knee Following Partial Medial Meniscectomy A Randomized, Double-Blind, Controlled Study	Vangsness, CT	Journal of Bone and Joint Surgery-American Volume	6.558	2014	255
3	Poly (lactic acid)-based biomaterials for orthopaedic regenerative engineering	Narayanan, G	Advanced Drug Delivery Reviews	17.873	2016	223
4	Surgical and tissue engineering strategies for articular cartilage and meniscus repair	Kwon, H	Nature Reviews Rheumatology	32.286	2019	201
5	Secreted trophic factors of mesenchymal stem cells support neurovascular and musculoskeletal therapies	Hofer, HR	Stem Cell Research & Therapy	8.079	2016	201

TABLE 4 The top 10 most productive journals related to stem cells for meniscal regeneration.

Rank	Journal	Article counts	Percentage
1	Stem Cell Research Therapy	17	4.91
2	American Journal of Sports Medicine	15	4.34
3	Journal of Orthopaedic Research	13	3.76
4	Acta Biomaterialia	12	3.47
5	Osteoarthritis and Cartilage	9	2.60
6	Arthroscopy the Journal of Arthroscopic and Related Surgery	8	2.31
7	International Journal of Molecular Sciences	8	2.31
8	Journal of Tissue Engineering and Regenerative Medicine	8	2.31
7	Stem Cells International	7	2.02
10	Tissue Engineering Part C Methods	7	2.02

research, the publications were identified by CiteSpace and are presented in Figure 10B, as the 20 influential articles with the strongest citation bursts and the cocitation relationship between each article is presented in the network map. Moreover, cocited references were analysed by CiteSpace (Table 7), showing the top 5 most influential studies. The article titled "The knee meniscus: structure–function, pathophysiology, current repair techniques, and prospects for regeneration", published in 2011, was cited 85 times. In addition, more details of related articles are displayed in Figure 10C, including the citation burst for the duration of references. The paper by Horie M published in 2009 has the strongest reference citation burst, lasting from 2012 to 2014.

A list of the funds for stem cells in meniscal regeneration is summarized in Table 8. According to Table 8, the National Natural Science Foundation of China supports the most articles with 60 articles, followed by the National Institutes of Health with 54 articles and the United States Department of Health Human Services with 54 articles. Interestingly, the first three funds that support most articles are funds from the United States and China, which is consistent with previous analyses of countries.

3.9 Analysis of keywords and hotspots

Using CiteSpace's algorithm, the burst of keywords based on burst detection was also analysed and visualized. The top 25 keywords with the highest frequency of occurrence are shown in Figure 11A. It has been reported that the keyword with the most frequent citations is "mesenchymal stem cell", which means it is probably a hotspot for using mesenchymal stem cells for meniscal regeneration. Furthermore, "scaffold", "knee osteoarthritis", and "*in vitro*" also occur frequently as the key words in the period of 2012–2022 about stem cells for meniscus regeneration. The three key words mentioned above demonstrated the attention of researchers from three perspectives: "auxiliary materials", "experiment method", and "disease association".

A network map was also built to visualize keyword clusters (Figure 11B), and each node represents a hot key word using Vosviewer. Accordingly, the top ten keywords in order are #1tissue engineering, #2 articular cartilage, #3 anterior cruciate ligament, #4 regenerative medicine, #5 scaffold, #6 human serum, #7 bone morphogenetic protein 2, #8 behavior, #9 decellularized

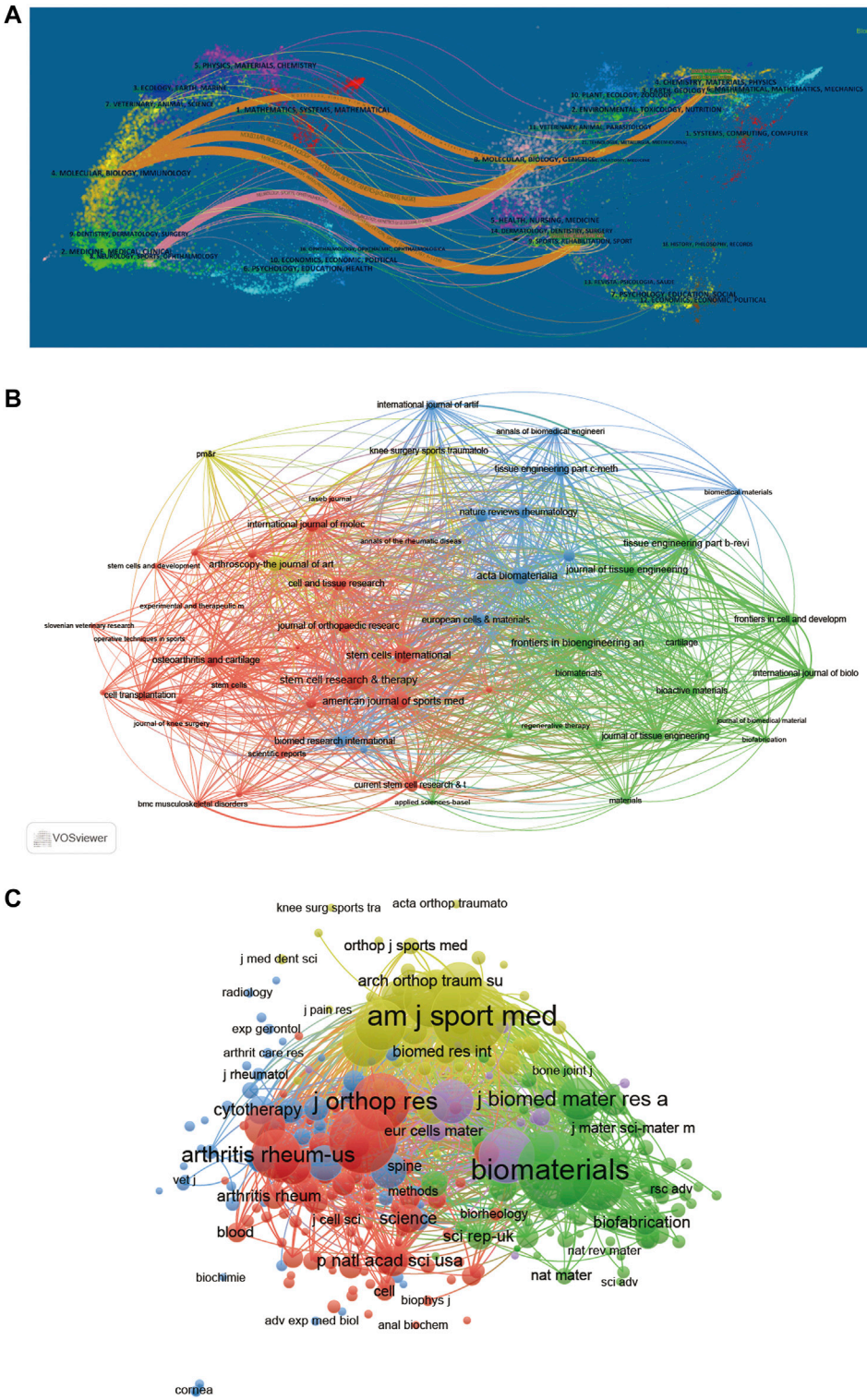

FIGURE 8
Articles published in different journals on stem cells for meniscal regeneration. **(A)** The dual-map overlay of journals related to stem cells for meniscal regeneration. **(B)** Bibliographic analysis of journals based on Vosviewer. **(C)** Network map of journals that were cocited in more than 50 citations based on Vosviewer.

extracellular matrix, and #10 4D printing. In terms of the information, we analyse the key word transform during 2012–2022 and visualize the timeline of the related key words. As Figure 11C suggests, the frequency of key words displays a large difference with time, which undoubtedly indicates a change in research direction.

TABLE 5 The top 10 cocited journals related to stem cells for meniscal regeneration.

Rank	Cited journal	Citations	JCR (2021)	IF
1	Biomaterials	1229	Q1	15.30
2	American Journal of Sports Medicine	1180	Q1	7.01
3	Osteoarthritis and Cartilage	896	Q1	7.51
4	Journal of Orthopedic Research	645	Q2	3.10
5	Arthroscopy	642	Q1	5.97
6	Tissue Engineering Part A	596	Q2	4.08
7	Journal of Bone Joint Surgery-American	502	Q1	6.56
8	Acta Biomaterialia	501	Q1	10.63
9	Arthritis Rheumatology	484	Q1	15.48
10	Clinical Orthopedic and Related Research	421	Q1	4.76

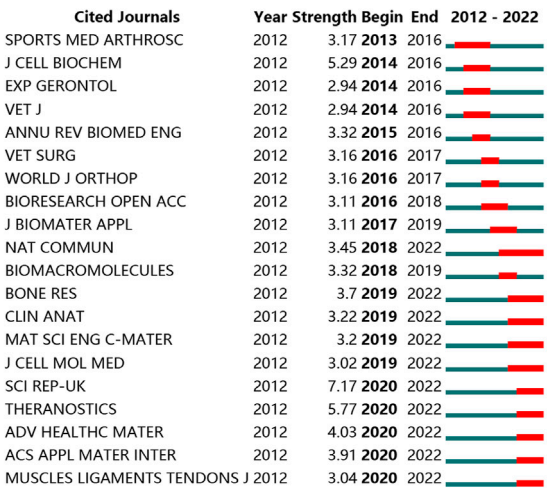

FIGURE 9
Top 20 cited journals with the strongest citation bursts of publications related to stem cells for meniscal regeneration.

4 Discussion

In the past decade, enormous efforts have been made in stem cell therapy for meniscal regeneration (Pillai et al., 2018; Zhang et al., 2018), and considerable advances have been achieved in both clinical and preclinical experiments for meniscal disease. This study provided a bibliometric and visualization analysis of stem cells for meniscal regeneration from 2012 to 2022. With the development of bibliometric software, bibliometric analysis is now broadly pursued. It can favor beginners understand the development process and trends of a specific field intuitively and systematically. Additionally, it is also beneficial to find new research hotspots and milestone achievements.

4.1 Trend overview of the development of stem cell treatment for meniscal regeneration

As suggested in the visualized figures, there is a considerable increase in the number of publications from 1 October 2012 to 1 October 2022 despite a slight decrease in 2016. Meanwhile, the relative research interest has also increased over the past few years, indicating that the popularity of this field is also experiencing a boom.

When it comes to national contributions, in this analysis, roughly 31 countries published papers on stem cell therapy for the meniscus regeneration field. In particular, the United States

TABLE 6 The top 10 well-represented research areas.

Rank	Research areas	Records	Percentage
1	Cell Biology	103	29.77
2	Orthopedics	87	25.15
3	Engineering	75	21.68
4	Materials Science	67	19.36
5	Research Experimental Medicine	47	13.58
6	Sport Sciences	38	10.98
7	Biotechnology Applied Microbiology	36	10.41
8	Science Technology Other Topics	26	7.51
9	Surgery	23	6.65
10	Rheumatology	22	6.36

contributed the most papers (117) compared to China (90), Japan (58), Germany (23), and Italy (22). The main research regions are located in North America, North America and East Asia, which have both developed economies and large populations. It is widely acknowledged that the number of total citations, average citation and the H-index are significant statistic indexes for bibliometric studies. What is interesting in Figure 3 is that the United States published the most papers (117), contributed the most extensive total citations (4233), and the largest H-index (33). These indexes suggest United States has an outstanding role in the aspects of the quality and academic impact among different countries. This phenomenon perhaps resulted from the rich resources of researchers and institutions worldwide, guaranteeing the USA's dominant position in the field of stem cell therapy for meniscal regeneration resulting the United States, an extremely productive and chief country in this field.

Interestingly, Spain ranked top 1 in terms of average citations (41.6), with Switzerland (36.9) and the United States (35.7) following. Allowing for top 10 total publications, Spain, ranking seventh in terms of the publishing number, is still making a significant progression in this field. Considering the high number of total publications, however, China shows a disappointing performance in average citations. As a matter of fact, China ranks only eighth, which means a pretty low acceptance in the global academic research field of stem cell therapy for meniscal regeneration. The incongruity between the quality and quantity of studies also indicates that China requires more influential studies.

As for the scientific institutions, Tokyo Medical Dental University ranked first (34 publications), Peking University (29 publications), and Chinese People Liberation Army General Hospital (15 publications) have contributed a lot to the research field effectively. What is interesting is that the leading top 2 institutes have contributed considerably concerning publication number, while there exists a huge difference in average citations. In detail, the average citation of Peking University is only 17.52, while that of Tokyo Medical Dental University is up to 34.19. It is contended that the prevailing role of first-group institutes guarantees one country's

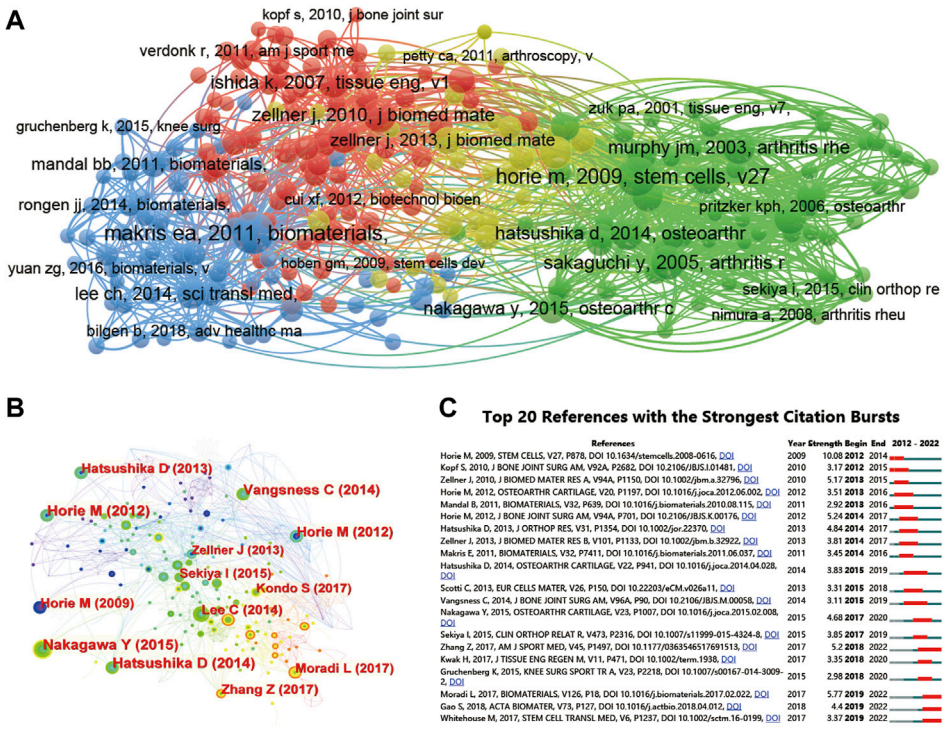

FIGURE 10
Mapping of references in studies on stem cells for meniscal regeneration. **(A)** Network map of publishing document analysis based on Vosviewer. **(B)** Network map of cocitation analysis of references with more than 50 citations based on CiteSpace. **(C)** Top 20 references with the strongest citation bursts of publications related to stem cells for meniscal regeneration.

TABLE 7 The top 5 cocitation analyses of cited references on stem cells for meniscal regeneration.

Rank	Title	First author	Journal	IF	Publication year	Total citations
1	The knee meniscus: structure-function, pathophysiology, current repair techniques, and prospects for regeneration	Makris, Eleftherios A	Biomaterials	15.304	2011	85
2	Intra-articular Injected synovial stem cells differentiate into meniscal cells directly and promote meniscal regeneration without mobilization to distant organs in rat massive meniscal defect	Horie, Masafumi	Stem cells	5.845	2009	75
3	Comparison of human stem cells derived from various mesenchymal tissues: superiority of synovium as a cell source	Sakaguchi, Yusuke	Arthritis and rheumatism	—	2005	56
4	Role of mesenchymal stem cells in tissue engineering of meniscus	Zellner, Johannes	Journal of biomedical materials research. Part A	4.854	2010	52
5	Repetitive allogeneic intraarticular injections of synovial mesenchymal stem cells promote meniscus regeneration in a porcine massive meniscus defect model	Hatsushika, D	Osteoarthritis and cartilage	7.507	2014	51

TABLE 8 The top 10 funds related to stem cells for meniscal regeneration.

Rank	Journal	Article counts	Percentage
1	National Natural Science Foundation of China Nsfc	60	17.34
2	National Institutes of Health Nih Usa	54	15.61
3	United States Department of Health Human Services	54	15.61
4	Nih National Institute of Arthritis Musculoskeletal Skin Diseases Niams	24	6.94
5	Ministry of Education Culture Sports Science and Technology Japan Mext	23	6.65
6	Japan Society for The Promotion of Science	21	6.07
7	Grants in Aid for Scientific Research Kakenhi	17	4.91
8	National High Technology Research and Development Program of China	16	4.62
7	Japan Agency For Medical Research and Development Amed	14	4.05
10	National Key R D Program of China	14	4.05

academic research ranking, allowing for approximately the top 10 institutes come from the several related countries. It can be concluded that the following related studies with cooperation could make a big difference in meniscus research, benefitting researchers producing more impactful researches across disciplines.

4.2 Status of authors and studies

What is surprising is that Japanese and Chinese are the first-ranked authors with the most articles, instead of the United States. However, the largest fund provided in the field is the US National Institutes of Health, which is strange. In Table 9, the top-ranked authors with the most researches were scientists with longer career and research time. In that sense, they possibly have turned attention to advancements in stem cell therapy for meniscal regeneration ahead of time. In fact, Sekiya I, the researcher with the most publications, tried to perform intraarticular injections of MSCs to promote meniscus regeneration in a porcine massive meniscal defect model and proved the protection efficiency at the medial femoral articular cartilage before 2014 (Hatsushika et al., 2014).

What can't be ignored is that the collaboration analysis in Figure 6B indicated a shortage of academic collaboration and close communication among authors form different countries. It can be seen that the academic relationship basically located in the same countries and is scattered in different countries. The collaboration circle mainly consists of Chinese authors and Japanese authors separately, however, with almost no intersection. Therefore, authors may enhance their collaboration in this field jointly.

For cocitation frequency, as shown in Table 10, Horie, Zellner and Arnoczky are with the highest cocitation frequency. It undoubtedly reflected the international impact and recognition of these researchers in this field. Zellner, using a combination of mesenchymal stem cells and a hyaluronan collagen-based scaffold, attempted to repair meniscal tears in the avascular zone of meniscus (Zellner et al., 2013). In addition to the authors' analysis, the related journals concerning researches were further explored,

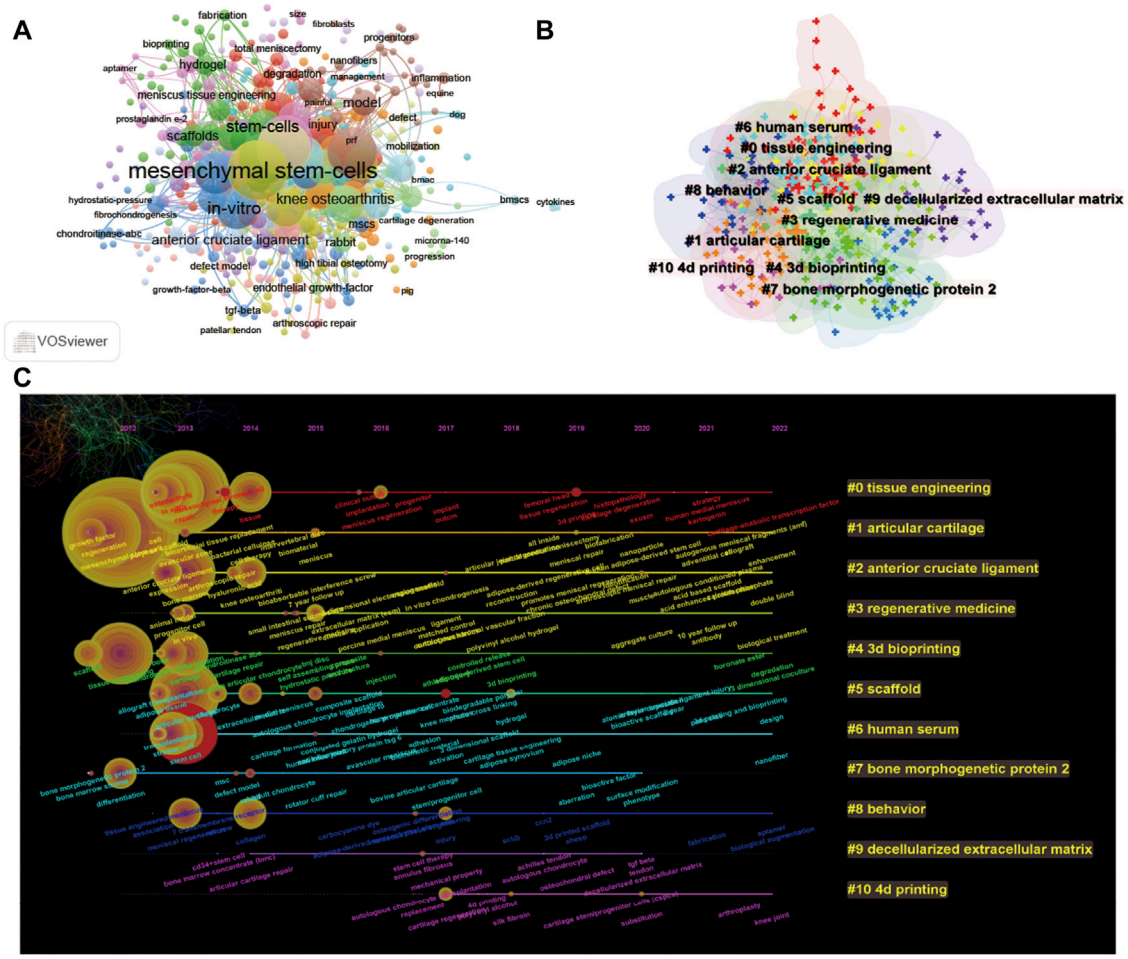

FIGURE 11
Mapping of keywords in studies on stem cells for meniscal regeneration. **(A)** Network visualization of keywords based on Vosviewer. **(B)** Keyword clustering visualization from 2012 to 2022. **(C)** Keyword timeline visualization from 2012 to 2022.

TABLE 9 The top 10 authors with the most publications on stem cells for meniscal regeneration.

Rank	High published authors	Country	Article counts	Percentage
1	Sekiya I	Japan	31	8.96
2	Koga H	Japan	27	7.80
3	Tsuji K	Japan	22	6.36
4	Muneta T	Japan	21	6.07
5	Mizuno M	Japan	19	5.49
6	Guo QY	China	16	4.62
7	Liu SY	China	16	4.62
8	Ozeki N	Japan	15	4.34
9	Yuan ZG	China	13	3.76
10	Katano H	Japan	12	3.47

TABLE 10 The top 10 cocited authors on stem cells for meniscal regeneration.

Rank	High Co-cited authors	Total citations
1	Horie, M	166
2	Zellner, J	125
3	Arnoczky, Sp	111
4	Makris, Ea	104
5	Caplan, Ai	101
6	Hatsushika, D	96
7	Sekiya, I	94
8	Baker, Bm	90
9	Englund, M	84
10	Zhang, Zz	77

analyzed and then shown in Table 4. The journal *Stem Cells Research Therapy*, *American Journal of Sports Medicine*, and *Journal of Orthopaedic Research* published the most papers. Meanwhile, the related journals only occupy a limited percentage, and articles are relatively scattered in different journals without aggregations. What is interesting is that more than 60 articles were published in only the top 5 journals, indicating the focus and relevance in this field. Accordingly, the listed top 10 journals might be possible choices for researchers to publish related research in the future. Furthermore, this study has also conducted cocitation analysis based on journals for investigation of the impacts of publications after analysing the total number of citations. Figure 8C shows that *Biomaterials* (IF = 15.304) made the best contributions in this field, with 1229 citations. The article published on *Biomaterials*, The knee meniscus: Structure–function, pathophysiology, current repair techniques, and prospects for regeneration (Makris et al., 2011), systematically investigated the properties of a series of scaffolds and cell types for meniscus regeneration, which produced great academic impact.

In addition, the top 10 research orientations are composed of biology, medicine and material engineering, which means it is a multidisciplinary field of deep intersection. More specifically, both focus and relevance of research in tissue engineering studies were reflected by the dual-map analysis.

Based on the citation analysis of documents (Figure 10A) the impact of each publication was analysed. Besides, the cocitation network analysis (Figure 10B). Table 3 shows that the most cited article is Treatment of Knee Osteoarthritis with Autologous Mesenchymal Stem Cells: A Pilot Study (Orozco et al., 2013), which may be a target for meniscus defect treatment. Another study reported a clinical double-blind controlled study using MSC for meniscectomy written by Vangsness (Vangsness et al., 2014). Among the publications, the basic research type consists of main type of publications, involving pathology, biomaterial, and preclinical research.

Notably, cocitation analysis can determine which publications have contributed most in this field. As shown in Figure 10B and Table 7, "The knee meniscus: structure–function, pathophysiology, current repair techniques, and prospects for regeneration" (Makris et al., 2011) authored by Makris, Eleftherios et al., as the top publication, possess the highest citation frequency, which, as mentioned before, reviewed the structure, pathophysiology, repair and prospects of the meniscus. In Figure 10C, as for the strongest citation bursts, meniscus pathophysiology, diagnosis, and therapy are the aspects with most attention for the top 20 cited articles, suggesting which way hot topics exist in this research field.

4.3 Analysis of research hotspots

The research trends and frontiers in stem cell therapy for meniscus regeneration research could be demonstrated by the co-occurrence analysis of keywords and bursts. From Figure 11A, as the keyword with the highest citation outbreaks, "mesenchymal stem cells" shows the prevailing status of this hotspots in meniscus research. As a matter of fact, as early as 2005, Yasunori Izuta et al. attempted to utilize bone marrow-derived mesenchymal stem cells to treat meniscal tears in rats and verified a reduction in meniscus destruction in this therapy (Izuta et al., 2005). As shown in Figures 11B, C, it can be argued that the primary research clusters mainly refer to "tissue engineering", "articular cartilage", "anterior cruciate ligament", "regeneration medicine", and "bioprinting", indicating that there is a huge similarity and connection in the whole joint cartilage and biomaterial and engineering method, all contributing greatly to meniscus regeneration.

In our study, the keyword timeline visualization network is plotted depending on the keywords in the titles/abstracts of all included publications. Figure 11C shows the 10 main research clusters, which include some more detailed secondary research keywords with their occurrence and variation over time. Not only could these keyword clusters comply with promising hotspots in the field of stem cell therapy for meniscus regeneration research, but these timelines also forecast the promising perspectives of future studies, as follows.

(I). Tissue engineering: Co-occurrence analysis of keywords identified "mesenchymal stem cell", "regeneration", and "implantation" as important research hotspots that deserve further attention. It is commonly known that cartilage (including the meniscus) regeneration is an important component in tissue regeneration, meaning that there is a similarity between these two fields. As a result, some advanced biomaterials or mechanisms in tissue regeneration may promote and inspire meniscal regeneration. As reviewed in this review, poly (lactic acid)-based biomaterials for orthopedic regenerative engineering suggest that the architecture, topography, and biochemical cues that influence cellular outcomes in tissue engineering can inspire research related to meniscus regeneration (Narayanan et al., 2016). Considering the specificity of the meniscus, however, implantation and regenerative effects are the main therapy and evaluation gold standards (Bansal et al., 2017). The blood supply to the meniscus comes from branches of the internal and external knee arteries, which form a network of blood vessels within the joint capsule. These arterial networks from the joint capsule and synovium only provide blood supply to 30% of the fibers around the meniscus, which is called the red zone under arthroscopy, and can be

repaired after injury (Wang et al., 2022). In contrast, the central part has no blood supply, so it is called the white area. It relies on the penetration of synovial fluid for nutrition, so it lacks the ability to repair and regenerate after injury. Even worse, repetitive movement can easily induce inflammation. Therefore, exogenous implants, including MSCs, generally have a better therapeutic effect (Chen et al., 2018). Overall, both similarities and differences exist in meniscal regeneration and the keyword cluster "tissue engineering", which may bring about benefits for future studies.

(II). Articular cartilage: Due to the low vascularization and slow metabolism, the tissue in the joint faces a similar conundrum in regeneration medicine, including the meniscus, articular cartilage and anterior cruciate ligament (Kwon et al., 2019). In fact, after injections of allogeneic synovial MSCs, articular cartilage, subchondral bone and meniscus at the medial femoral condyle were also significantly more preserved (Hatsushika et al., 2014), indicating a strong similarity and interaction in the whole joint (Chen et al., 2017). In these three clusters, "extracellular matrix *in vitro* chondrogenesis" and "hydrogel"occur with high frequency as keywords, suggesting that research on the interaction of ECM and chondrocytes would probably help with field promotion, including the mechanism, material design and application for different parts of whole joint regeneration.

(III). Regeneration medicine: Most studies share the belief that clinical experiments are the most convincing evaluation of the efficacy of stem cell therapy for regeneration medicine. In this cluster, "double blind", "matched control" and "several years follow up" make demands on the related studies in the future. As a general rule, double-blind experiments with matched groups are compulsive in a clinical trial. Deep down, it is better to design a follow-up in a clinical trial, which will absolutely broaden the influence and scope. The chief reason is that the treatment of the meniscus is a long process, and it is impossible to obtain immediate results (Andia and Maffulli, 2017). In this sense, a suitable follow-up will undoubtedly enhance comprehensiveness and reasonableness. Moreover, according to a highly cited review of surgical and tissue engineering strategies for articular cartilage and meniscus repair (Kwon et al., 2019), strategies of tissue engineering are indispensable for meniscus repair in regeneration medicine and clinical translation.

Most human clinical trials have been highly cited, suggesting most researchers pay attention on clinical trials which only contains cells. And some stem cell therapies for meniscal regeneration based on animal model including rats, pigs and horse involve both cells and biomaterial. The two types of researches respectively represent feasibility and innovation.

(IV). 3D bioprinting

One important technology for meniscus treatment is 3D bioprinting. It is generally agreed that the repaired meniscus can function well based on the assumption that the meniscus has a correct shape and good topography that allows a stable load force transfer between the tibia and femur in the joint (Hao et al., 2021). Moreover, whether on the size or the angle, there always exists a slight difference in the patients' menisci (Deng et al., 2021). Faced with this problem, 3D bioprinting can be used to manufacture artificial menisci containing MSCs with any shape and angle, which will certainly facilitate the individualized treatment of patients (Filardo et al., 2019). There is much potential about the association with 3D bioprinting, which needs more updated and fantastic studies.

(V). Scaffold:

Both chondrocytes and mesenchymal stem cells tend to grow in scaffolds with good activity, a higher surface area and abundant adhesion sites. Accordingly, microspheres and porous scaffolds are usually utilized in stem cell therapy for meniscal regeneration (Itose et al., 2022). In addition, it has been reported that the stiffness and viscoelasticity of the matrix significantly induce the differentiation of MSCs into chondrogenic cells, osteogenic cells and adipogenic cells (Duarte Campos et al., 2015). In the meniscus, the red zone and the white zone result in different demands for scaffolds for regeneration. It has been reported that the optimal strategy for avascular zone regeneration is a combination of scaffolds and MSCs, which is even better than growth factors alone (Zellner et al., 2010). As a result, it is likely to control stem cell differentiation to focus on different therapeutic effects by tailoring scaffolds with different physical and chemical properties.

In terms of cell types, various stem cells have been used to treat meniscal disease, including BM-MSCs (bone marrow-derived mesenchymal stem cells), AD-MSCs (adipose tissue-derived mesenchymal stem cells), US-MSCs (umbilical cord mesenchymal stem cells), ESCs (embryonic stem cells), and iPSCs (Induced pluripotent stem cells), which own different mechanism and treatment effects. BM-MSCs is the most commonly used cell types in meniscal regeneration due to its low inflammation reaction, good biocompatibility and stable therapeutic effects while AD-MSCs are easily accessible *via* minimally invasive procedures.

4.4 Future research trends

Stem cell therapy aims to alleviate local symptoms, help regenerate the meniscus and promote the function of patients' movement. Accordingly, there are many urgent problems to be solved, although some clinical trials are in progress around the world. Not only safety, side effects, and long-term efficiency but also suitable cell types, ethical considerations, reasonable therapeutic courses and doses are totally unclear and unconfirmed, thus leading to serious concern and an intense debate about cell therapy for meniscal regeneration. In fact, these studies mainly focus on the possible benefits of cell therapy, the final therapeutic results and therapeutic potential, which means that the great majority of studies are not comprehensive and not specific. It is likely caused by the deficiency of the pathology and mechanism. First, meniscus defects are commonly accompanied by chronic physiological changes and intense inflammation. Meanwhile, the normal formation of the meniscus during development relates to a rich variety of cells. Unfortunately, most researchers are vague about the disease process due to complexity, which undoubtedly requires further

efforts, especially at the molecular and cellular levels. In addition, the main therapeutic mechanism is uncertain, despite several hypotheses proposed and good therapeutic effects. In a highly cited review (Hofer and Tuan, 2016), it was summarized that recent mechanistic insights into trophic activities focus on ultimate regulation by nitric oxide, nuclear factor-kB, and indoleamine, among other signaling pathways, to alleviate patients' pain and help tissue regeneration.

For instance, it is to be determined whether MSCs function mainly through differentiation into chondrocyte or paracrine forms to help meniscal regeneration. Further studies concerning pathology and mechanism will surely have a greater impact, benefiting the improvement of cell types, therapeutic course and dose, treatment method and adverse effects.

4.5 Limitation

There are still some limitations to be discussed: (1) Only research and review articles in English were extracted, and as a matter of fact, the articles written in non-English language or non-research/review articles were excluded in this study, which perhaps bring about some omissions. (2) Due to the limitation of our bibliometric software, publication bias may occur when some databases have not been included. In that sense, more data sources and powerful software are supposed to be included in future research. (3) Prediction bias in hotspots would result from the neglect of temporal data since the keywords with a timeline haven't been visualized. (4) Allowing for new studies to be updated daily, some influential newly published studies would inevitably be neglected. (5) Encountered problems were resolved by consulting with experts to reach the final consensus because the data selection was performed by two authors. (6) Other public databases including Scopus could be involved to guarantee the analysis more comprehensive and representative, which is widely utilized in many similar bibliometrics and visual analysis. (7) All data were cleaned and analysed individually by the coauthors. Problems in this research was generally solved by the repeated discussion by the two authors. However, this method cannot guarantee absolute accuracy and may cause some mistakes.

5 Conclusion

To conclude, this study is the first bibliometric and visualization analysis to scientifically and systematically analyse global stem cell therapy for meniscal regeneration research trends over the last decade. This study systematically summarized and analyzed the global publication trends and supported researchers to identify the essential authors, journals and institutions in this field. Furthermore, the keyword and cocitation clustering analysis also inspire researchers to choose research frontiers mainly in five directions: "Tissue engineering", "Articular cartilage", "Regeneration medicine", "3D-bioprinting", and "Scaffold". Further cooperation among authors, institutions, and countries is waiting to see, which points out the research potential and perhaps facilitates the development of stem cell therapy for meniscus regeneration research.

Data availability statement

The original contributions presented in the study are included in the article/Supplementary Material, further inquiries can be directed to the corresponding authors.

Author contributions

Conceptualization, ZY and ZF; methodology, ZY and ZF; software, ZY and ZF; validation, DW and HL; formal analysis, DW and ZH; investigation, ZY and ZF; resources, DX; data curation, ZY; writing original draft preparation, ZY and ZF; writing review and editing, DX and JL; visualization, ZY; supervision, DX and JL; funding acquisition, DX and JL. All authors have read and agreed to the published version of the manuscript.

Funding

This study was funded by grants from the Natural Science Foundation of Beijing Municipality (7214261) and Peking University People's Hospital Scientific Research Development Funds (RDX2020-02).

Conflict of interest

The authors declare that the research was conducted in the absence of any commercial or financial relationships that could be construed as a potential conflict of interest.

Publisher's note

All claims expressed in this article are solely those of the authors and do not necessarily represent those of their affiliated organizations, or those of the publisher, the editors and the reviewers. Any product that may be evaluated in this article, or claim that may be made by its manufacturer, is not guaranteed or endorsed by the publisher.

References

Andia, I., and Maffulli, N. (2017). Biological therapies in regenerative Sports medicine. *Sports Med.* 47 (5), 807–828. doi:10.1007/s40279-016-0620-z

Bansal, S., Keah, N. M., Neuwirth, A. L., O'Reilly, O., Qu, F., Seiber, B. N., et al. (2017). Large animal models of meniscus repair and regeneration: A systematic review of the state of the field. *Tissue Eng. Part C Methods* 23 (11), 661–672. doi:10.1089/ten.tec.2017.0080

Brown, A. C., Ross, P. P., Brown, S. M., and Mulcahey, M. K. (2021). The 50 most cited articles on meniscus injuries and surgery from 2000 to 2019 focus on arthroscopic repair

or removal, originate from institutions within the United States and were published before 2010. *Arthrosc. Sports Med. Rehabil.* 3 (6), e2103–e2116. doi:10.1016/j.asmr.2021.09.013

Caminal, M., Fonseca, C., Peris, D., Moll, X., Rabanal, R. M., Barrachina, J., et al. (2014). Use of a chronic model of articular cartilage and meniscal injury for the assessment of long-term effects after autologous mesenchymal stromal cell treatment in sheep. *N. Biotechnol.* 31 (5), 492–498. doi:10.1016/j.nbt.2014.07.004

Chambers, H. G., and Chambers, R. C. (2019). The natural history of meniscus tears. *J. Pediatr. Orthop.* 39, S53–S55. doi:10.1097/bpo.0000000000001386

Chen, M., Guo, W., Gao, S., Hao, C., Shen, S., Zhang, Z., et al. (2018). Biochemical stimulus-based strategies for meniscus tissue engineering and regeneration. *Biomed. Res. Int.* 2018, 1–15. doi:10.1155/2018/8472309

Chen, S., Fu, P., Wu, H., and Pei, M. (2017). Meniscus, articular cartilage and nucleus pulposus: A comparative review of cartilage-like tissues in anatomy, development and function. *Cell Tissue Res.* 370 (1), 53–70. doi:10.1007/s00441-017-2613-0

Deng, X., Chen, X., Geng, F., Tang, X., Li, Z., Zhang, J., et al. (2021). Precision 3D printed meniscus scaffolds to facilitate hMSCs proliferation and chondrogenic differentiation for tissue regeneration. *J. Nanobiotechnology* 19 (1), 400. doi:10.1186/s12951-021-01141-7

Duarte Campos, D. F., Blaeser, A., Korsten, A., Neuss, S., Jakel, J., Vogt, M., et al. (2015). The stiffness and structure of three-dimensional printed hydrogels direct the differentiation of mesenchymal stromal cells toward adipogenic and osteogenic lineages. *Tissue Eng. Part A* 21 (3-4), 740–756. doi:10.1089/ten.tea.2014.0231

Ekici, A., Alkan, S., Aydemir, S., Gurbuz, E., and Unlu, A. H. (2022). Trends in naegleria fowleri global research: A bibliometric analysis study. *Acta Trop.* 234, 106603. doi:10.1016/j.actatropica.2022.106603

Filardo, G., Petretta, M., Cavallo, C., Roseti, L., Durante, S., Albisinni, U., et al. (2019). Patient-specific meniscus prototype based on 3D bioprinting of human cell-laden scaffold. *Bone Jt. Res.* 8 (2), 101–106. doi:10.1302/2046-3758.82.bjr-2018-0134.r1

Hao, L., Tianyuan, Z., Zhen, Y., Fuyang, C., Jiang, W., Zineng, Y., et al. (2021). Biofabrication of cell-free dual drug-releasing biomimetic scaffolds for meniscal regeneration. *Biofabrication* 14 (1), 015001. doi:10.1088/1758-5090/ac2cd7

Hatsushika, D., Muneta, T., Horie, M., Koga, H., Tsuji, K., and Sekiya, I. (2013). Intraarticular injection of synovial stem cells promotes meniscal regeneration in a rabbit massive meniscal defect model. *J. Orthop. Res.* 31 (9), 1354–1359. doi:10.1002/jor.22370

Hatsushika, D., Muneta, T., Nakamura, T., Horie, M., Koga, H., Nakagawa, Y., et al. (2014). Repetitive allogeneic intraarticular injections of synovial mesenchymal stem cells promote meniscus regeneration in a porcine massive meniscus defect model. *Osteoarthr. Cartil.* 22 (7), 941–950. doi:10.1016/j.joca.2014.04.028

Hofer, H. R., and Tuan, R. S. (2016). Secreted trophic factors of mesenchymal stem cells support neurovascular and musculoskeletal therapies. *Stem Cell Res. Ther.* 7 (1), 131. doi:10.1186/s13287-016-0394-0

Hu, W., Chen, N., Yan, W., Pei, P., Wei, Y., and Zhan, X. (2022). Knowledge mapping of olfactory dysfunction: A bibliometric study. *Front. Syst. Neurosci.* 16, 904982. doi:10.3389/fnsys.2022.904982

IsmailII, and Saqr, M. (2022). A quantitative synthesis of eight decades of global multiple sclerosis research using bibliometrics. *Front. Neurol.* 13, 845539. doi:10.3389/fneur.2022.845539

Itose, M., Suzawa, T., Shibata, Y., Ohba, S., Ishikawa, K., Inagaki, K., et al. (2022). Knee meniscus regeneration using autogenous injection of uncultured adipose tissue-derived regenerative cells. *Regen. Ther.* 21, 398–405. doi:10.1016/j.reth.2022.09.003

Izuta, Y., Ochi, M., Adachi, N., Deie, M., Yamasaki, T., and Shinomiya, R. (2005). Meniscal repair using bone marrow-derived mesenchymal stem cells: Experimental study using green fluorescent protein transgenic rats. *Knee* 12 (3), 217–223. doi:10.1016/j.knee.2001.06.001

Joyce, N., Annett, G., Wirthlin, L., Olson, S., Bauer, G., and Nolta, J. A. (2010). Mesenchymal stem cells for the treatment of neurodegenerative disease. *Regen. Med.* 5 (6), 933–946. doi:10.2217/rme.10.72

Khalifeh Soltani, S., Forogh, B., Ahmadbeigi, N., Hadizadeh Kharazi, H., Fallahzadeh, K., Kashani, L., et al. (2019). Safety and efficacy of allogenic placental mesenchymal stem cells for treating knee osteoarthritis: A pilot study. *Cytotherapy* 21 (1), 54–63. doi:10.1016/j.jcyt.2018.11.003

Kurzweil, P. R., Cannon, W. D., and DeHaven, K. E. (2018). Meniscus repair and replacement. *Sports Med. Arthrosc. Rev.* 26 (4), 160–164. doi:10.1097/jsa.0000000000000224

Kwon, H., Brown, W. E., Lee, C. A., Wang, D., Paschos, N., Hu, J. C., et al. (2019). Surgical and tissue engineering strategies for articular cartilage and meniscus repair. *Nat. Rev. Rheumatol.* 15 (9), 550–570. doi:10.1038/s41584-019-0255-1

Le, H. X., Xu, W. G., Zhuang, X. L., Chang, F., Wang, Y. N., and Ding, J. X. (2020). Mesenchymal stem cells for cartilage regeneration. *J. Tissue Eng.* 11, 204173142094383. doi:10.1177/2041731420943839

Makris, E. A., Hadidi, P., and Athanasiou, K. A. (2011). The knee meniscus: Structure-function, pathophysiology, current repair techniques, and prospects for regeneration. *Biomaterials* 32 (30), 7411–7431. doi:10.1016/j.biomaterials.2011.06.037

Markes, A. R., Hodax, J. D., and Ma, C. B. (2020). Meniscus form and function. *Clin. Sports Med.* 39 (1), 1–12. doi:10.1016/j.csm.2019.08.007

Narayanan, G., Vernekar, V. N., Kuyinu, E. L., and Laurencin, C. T. (2016). Poly (lactic acid)-based biomaterials for orthopaedic regenerative engineering. *Adv. Drug Deliv. Rev.* 107, 247–276. doi:10.1016/j.addr.2016.04.015

Orozco, L., Munar, A., Soler, R., Alberca, M., Soler, F., Huguet, M., et al. (2013). Treatment of knee osteoarthritis with autologous mesenchymal stem cells: A pilot study. *Transplantation* 95 (12), 1535–1541. doi:10.1097/tp.0b013e318291a2da

Pillai, M. M., Gopinathan, J., Selvakumar, R., and Bhattacharyya, A. (2018). Human knee meniscus regeneration strategies: A review on recent advances. *Curr. Osteoporos. Rep.* 16 (3), 224–235. doi:10.1007/s11914-018-0436-x

Rinonapoli, G., Gregori, P., Di Matteo, B., Impieri, L., Ceccarini, P., Manfreda, F., et al. (2021). Stem cells application in meniscal tears: A systematic review of pre-clinical and clinical evidence. *Eur. Rev. Med. Pharmacol. Sci.* 25 (24), 7754–7764. doi:10.26355/eurrev_202112_27622

Shah, M. W., Ahmad, T., Khan, M., Muhammad, S., and Sun, G. (2022). Global research on vitamin D and coronavirus disease 2019: A bibliometric and visualized study. *Med. Baltim.* 101 (27), e29768. doi:10.1097/md.0000000000029768

Sun, Y., and Mauerhan, D. R. (2012). Meniscal calcification, pathogenesis and implications. *Curr. Opin. Rheumatol.* 24 (2), 152–157. doi:10.1097/bor.0b013e32834e90c1

Vangsness, C. T., Jr., Farr, J., 2nd, Boyd, J., Dellaero, D. T., Mills, C. R., and LeRoux-Williams, M. (2014). Adult human mesenchymal stem cells delivered via intra-articular injection to the knee following partial medial meniscectomy: A randomized, double-blind, controlled study. *J. Bone Jt. Surg. Am.* 96 (2), 90–98. doi:10.2106/jbjs.m.00058

Wang, X., Ding, Y., Li, H., Mo, X., and Wu, J. (2022). Advances in electrospun scaffolds for meniscus tissue engineering and regeneration. *J. Biomed. Mater Res. B Appl. Biomater.* 110 (4), 923–949. doi:10.1002/jbm.b.34952

Wang, Y., Yu, D., Liu, Z., Zhou, F., Dai, J., Wu, B., et al. (2017). Exosomes from embryonic mesenchymal stem cells alleviate osteoarthritis through balancing synthesis and degradation of cartilage extracellular matrix. *Stem Cell Res. Ther.* 8 (1), 189. doi:10.1186/s13287-017-0632-0

Wu, K., Liu, Y., Liu, L., Peng, Y., Pang, H., Sun, X., et al. (2022). Emerging trends and research foci in tumor microenvironment of pancreatic cancer: A bibliometric and visualized study. *Front. Oncol.* 12, 810774. doi:10.3389/fonc.2022.810774

Wu, T., Duan, Y., Zhang, T., Tian, W., Liu, H., and Deng, Y. (2022). Research trends in the application of artificial intelligence in oncology: A bibliometric and network visualization study. *Front. Biosci. (Landmark Ed.* 27 (9), 254. doi:10.31083/j.fbl2709254

Yu, H., Adesida, A. B., and Jomha, N. M. (2015). Meniscus repair using mesenchymal stem cells - a comprehensive review. *Stem Cell Res. Ther.* 6, 86. doi:10.1186/s13287-015-0077-2

Zellner, J., Hierl, K., Mueller, M., Pfeifer, C., Berner, A., Dienstknecht, T., et al. (2013). Stem cell-based tissue-engineering for treatment of meniscal tears in the avascular zone. *J. Biomed. Mater Res. B Appl. Biomater.* 101 (7), 1133–1142. doi:10.1002/jbm.b.32922

Zellner, J., Mueller, M., Berner, A., Dienstknecht, T., Kujat, R., Nerlich, M., et al. (2010). Role of mesenchymal stem cells in tissue engineering of meniscus. *J. Biomed. Mater Res. A* 94 (4), 1150–1161. doi:10.1002/jbm.a.32796

Zhang, N., Li, C., Chen, J., Liu, X., Wang, Z., and Ni, J. (2022). Research hotspots and frontiers about role of visual perception in stroke: A bibliometric study. *Front. Neurol.* 13, 958875. doi:10.3389/fneur.2022.958875

Zhang, Z., Guo, W., Gao, S., Chen, M., Li, X., Zhang, X., et al. (2018). Native tissue-based strategies for meniscus repair and regeneration. *Cell Tissue Res.* 373 (2), 337–350. doi:10.1007/s00441-017-2778-6

Zhao, Z., Fan, W., and Chu, Q. (2022). Mapping knowledge structure and global status of sarcopenia in geriatric hip fractures: A bibliometric and visualized study. *Front. Surg.* 9, 1019985. doi:10.3389/fsurg.2022.1019985

frontiers | Frontiers in Bioengineering and Biotechnology

TYPE Original Research
PUBLISHED 27 February 2023
DOI 10.3389/fbioe.2023.1141790

OPEN ACCESS

EDITED BY
Yansong Qi,
Inner Mongolia People's Hospital, China

REVIEWED BY
Dehao Fu,
Shanghai General Hospital, China
Yongjun Rui,
Soochow University, China

*CORRESPONDENCE
Peifu Tang,
pftang301@163.com

SPECIALTY SECTION
This article was submitted to Biomaterials, a section of the journal Frontiers in Bioengineering and Biotechnology

RECEIVED 10 January 2023
ACCEPTED 20 February 2023
PUBLISHED 27 February 2023

CITATION
Li H, Wang D, Zhang W, Xu C, Xiong D, Li J, Zhang L and Tang P (2023), Evaluating the biomechanical performance of Ti6Al4V volar plates in patients with distal radius fractures. *Front. Bioeng. Biotechnol.* 11:1141790. doi: 10.3389/fbioe.2023.1141790

Evaluating the biomechanical performance of Ti6Al4V volar plates in patients with distal radius fractures

Hua Li[1,2], Daofeng Wang[1,2], Wupeng Zhang[1,2,3], Cheng Xu[1,2], Dou Xiong[2], Jiantao Li[1,2], Licheng Zhang[1,2] and Peifu Tang[1,2]*

[1]Senior Department of Orthopedics, The Fourth Medical Center of Chinese PLA General Hospital, Beijing, China, [2]National Clinical Research Center for Orthopedics, Sports Medicine and Rehabilitation, Beijing, China, [3]School of Medicine, Nankai University, Tianjin, China

Purpose: This study aimed to investigate the biomechanical performance of three Ti6Al4V volar plates with the latest designs using a finite element model.

Methods: An AO type 23-A3 distal radius fracture and the models of T plate (2.4 mm LCP Volar Distal Radius Plate), V plate (2.4 mm LCP Two-Column Volar Distal Radius Plate) and π Plate (2.4 mm Volar Rim Distal Radius Plate) (all from Depuy Synthes, West Chester, PA, USA, Ti6Al4V) were built in 3D-matic software. After assembling the internal fixation and fractures, we imported these models into the finite element analysis software (ABAQUS). An axial loading of 100 N was added to the distal end of each model. The displacements of total models and implants, the principal strains and the von Mises stresses in the plates were calculated and compared to capture the biomechanical features of the three plates.

Results: The T plate, V plate and π plate represented a model displacement of 0.8414 mm, 1.134 mm and 1.936 mm, respectively. The T plate was with the implant displacement of 0.7576 mm, followed by the V plate (0.8802 mm) and the π plate (1.545 mm). The T plate had the smallest principal strain of 0.23%, the V plate showed an intermediate level of 0.28%, and the π plate had a value of 0.72%. The least peak von Mises stress was observed in the V plate with 263.6MPa, and this value was 435.6 MPa and 1050 MPa in the T plate and π plate, respectively.

Conclusion: The biomechanical features of three Ti6Al4V volar locking plates in an AO type 23-A3 fracture were described in our analysis. The T plate and the V plate showed similar biomechanical performance while the π plate represented worse performance than the other two plates.

KEYWORDS

biomechanical performance, Ti6Al4V, volar plates, distal radius fractures, simulation analysis

1 Introduction

Distal radius fractures are the second most common type of fracture in elderly population, accounting for almost 10%–25% of all fractures, and the prevalence increases yearly for all-age individuals (Letsch et al., 2003; Nellans et al., 2012). These fractures usually necessitate surgical interventions to obtain secure fixation.

Open reduction and internal fixation with locking plates is recommended to be the standard procedure for distal radius fractures according to the consensus of the American Academy of Orthopaedic Surgeons (Hammert et al., 2013). However, the selection of plates for internal fixation continues to be a subject of debate, given the variety of plates with different designs and materials available for clinical use. Of these materials, Ti6Al4V is known to provide a lower stress-shielding effect to the bone as compared with the stainless steel due to its low-profile stiffness (Mugnai et al., 2018). Ahirwar et al. developed a femoral fracture model using the finite element method to compare biomechanical performance of Ti6Al4V plates and stainless steel plates and found that Ti6Al4V plates represented a lower deformation and stress (Ahirwar et al., 2021). Though a promising material, polyetheretherketone (PEEK), has been used for plates at present, a 3-year follow-up comparative study showed no difference in clinical outcomes between Ti6Al4V plates and PEEK plates (Berger-Groch et al., 2021). Ti6Al4V is still the most applied material.

In terms of plate designs, the use of double dorsal plates is a traditional technique for the management of distal radius fractures, based on the three-column distal radius and ulna concept to achieve early and secure fixation. This approach facilitates the exposure of posterior displaced fragments and the implantation of internal fixation. However, dorsal plates can be associated with a relatively larger surgical dissection and a higher risk of tendon irritation (Knežević et al., 2017). Currently, volar locking plates are the most common type of internal fixation for distal radius fractures, accounting for 80% of the treatments (Miyashima et al., 2019). This type of internal fixation is preferred by many researchers due to its reduced risk of tendon complications and superior biomechanical stability. A meta-analysis of 38 studies conducted by found that distal radius fractures treated with volar plates exhibited lower complication rates and higher hand function scores compared to dorsal plates (Beyer et al., 2021).

Many volar locking plates are commercially available now, and some researchers have compared their stability and biomechanical features to determine the appropriate selection of plates for different types of distal radius fractures (Koh et al., 2006; Kamei et al., 2010). Reported favorable clinical results in patients with volar rim fractures (AO type 23-B3) using volar plates (Kachooei et al., 2016). Found that volar plates could also provide satisfactory outcomes in cases of dorsally comminuted distal radius fractures, as compared with dorsal plates (Chou et al., 2011). While recent studies have reported positive results with the latest-generation volar plates (Yamamoto et al., 2017; Alter and Ilyas, 2018; Selles et al., 2021), information is lacking on the mechanical attributes of volar plates, particularly with regard to the comparison among different designs. The finite element analysis is a useful tool for evaluating fracture models as it can simulate mechanical responses in a controllable manner and offer reliable data on the biomechanical behaviors of different models. This method is popular for evaluating fracture models (Liu et al., 2020). Used a finite element analysis to investigate the stability of distal radius fractures by volar and dorsal planting (Ghaem-Maghami et al., 2021). The present study aimed to investigate the mechanical performance of three widely-used volar plates with the latest designs using a non-linear finite element analysis.

2 Methods

2.1 Model construction

In this analysis, three finite element models of extra-articular distal radius fractures (AO type 23-A3) were utilized. The geometric model of the radius was derived from a computed tomography (CT) scan from a 50-year-old female patient who underwent CT angiography for the upper extremities, with ethical approval from our institutional review board (S2020-114-04). The helical CT scan was performed with a slice thickness of 1.0 mm and an interval of 0.8 mm (TOSHIBA Aquilion) and the data was restored as DICOM format and imported into 3D-matic (Materialize, Belgian). The three-dimensional reconstruction of the distal radius was then completed. Subsequently, an extra-articular distal radius fracture was built by a 10 mm dorsal wedge osteotomy (Synek et al., 2021) (Figure 1A). According to the method by (Baumbach et al., 2012), we produced a transverse osteotomy plane at a point 20 mm below the articular surface, and a 10 mm dorsal opening was created.

Geometric three-dimensional models of three volar plates with different designs (T Plate, V Plate and π Plate) and screws were reconstructed using the Unigraphics NX 8.5 software (Siemens PLM Software, Co., Ltd, Plano, TX, United States) based on the vendor-provided engineering drawings. The T plate is a 2.4 mm LCP Volar Distal Radius Plate (Figure 1B), the V plate is a 2.4 mm LCP Two-Column Volar Distal Radius Plate (Figure 1C) and the π Plate is a 2.4 mm Volar Rim Distal Radius Plate (Figure 1D) (all from Depuy Synthes, West Chester, PA, United States, Ti6Al4V), all of which are anatomically-contoured low-profile implants. The screws were created without threads and assumed to be 20 mm long, and have continuous connections with plates, cortical and cancellous bones, for the purpose of model simplification. The screw insertion was in accordance with the vendor's recommendations.

We assembled the implants and bones in 3D-matic. The models were exported and then meshed using the HyperMesh 11.0 software (Altair Engineering, Inc., Troy, MI, United States) and imported into the ABAQUS software (Simulia, Suresnes, France).

2.2 Assumption and boundary settings

Each model was 10 cm long with the proximal end fixed in all directions (Figure 2). Non-linear contact interactions were implementedto mimic the interfacial adaptation between the plates and bones as well as between the osteotomy sites, with a friction coefficient of 0.3 (Liu et al., 2020).

Bonded constraints were employed to connect the screws to the plates and the screws to the bones. The plates were meshed using quadratic tetrahedral elements. The total number of elements and nodes, which varied depending on the type of plate, ranged from 1185403 to 1238464 and from 256012 to 265991, respectively. The material properties were assumed to be isotropic and linear. The elastic modulus of plates and screws was 105 GPa with a Poisson's ratio of 0.35. The elastic moduli used for the cortical and trabecular bone were 16.7 GPa and 0.155 GPa, respectively. The Poisson's ratio for cortical bone and trabecular bone was set at 0.26 and 0.3, respectively (Zhang et al., 2018).

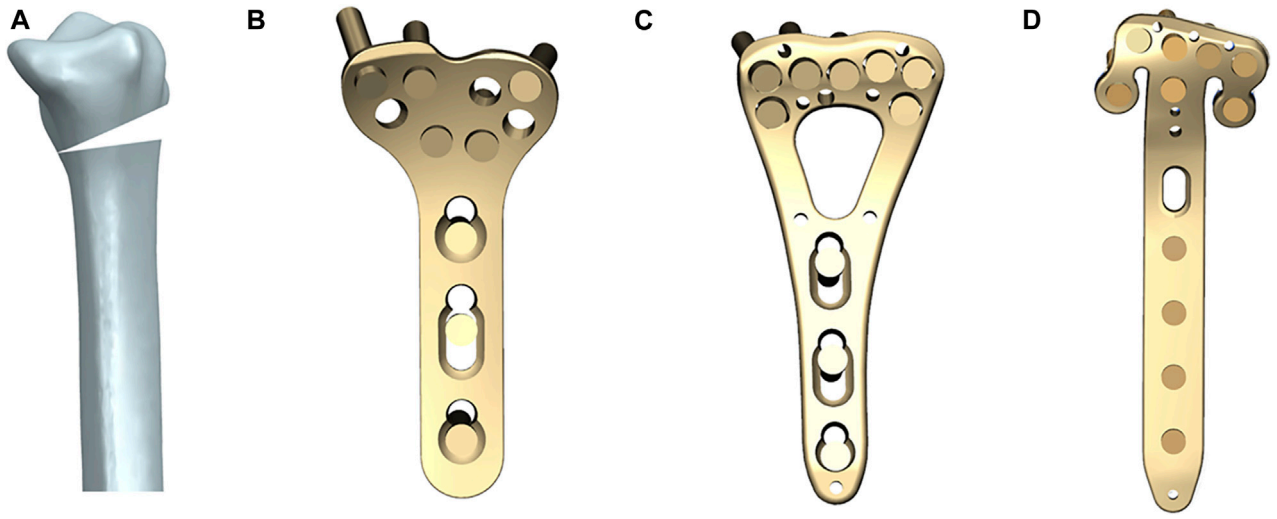

FIGURE 1
The models of a distal radius fracture and three volar plates (all from Depuy Synthes, West Chester, PA, United States, Ti6Al4V). **(A)** AO type 23-A3 distal radius fracture built by a 10 mm dorsal wedge osteotomy; **(B)** 2.4 mm LCP Volar Distal Radius Plate (T plate); **(C)** 2.4 mm LCP Two-Column Volar Distal Radius Plate (V plate); **(D)** 2.4 mm Volar Rim Distal Radius Plate (π Plate).

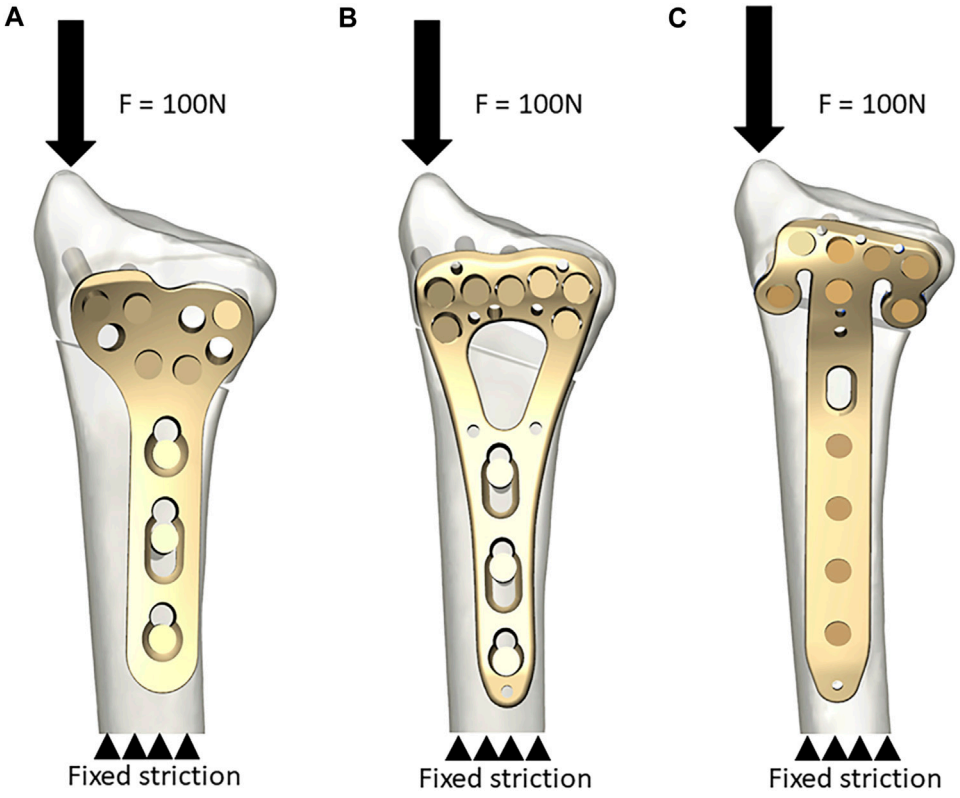

FIGURE 2
Model construction. Model A was used to clarify the simulation procedure. **(A)** The T plate. An axial load of 100 N was added to the distal end and the proximal end was fixed in all directions; **(B)** The V plate; **(C)** The π plate.

TABLE 1 Analysis results after axial loading simulation.

Parameters	T plate	V plate	π plate	V/T (ratio)	π/T (ratio)
Displacement of total models	0.8414 mm	1.134 mm	1.936 mm	1.35	2.30
Displacement of implants	0.7576 mm	0.8802 mm	1.545 mm	1.16	2.04
Principal strain in plates	0.2268%	0.2809%	0.7226%	1.24	3.19
Peak von Mises stress in plates	435.6 MPa	263.6 MPa	1050 MPa	0.61	2.41

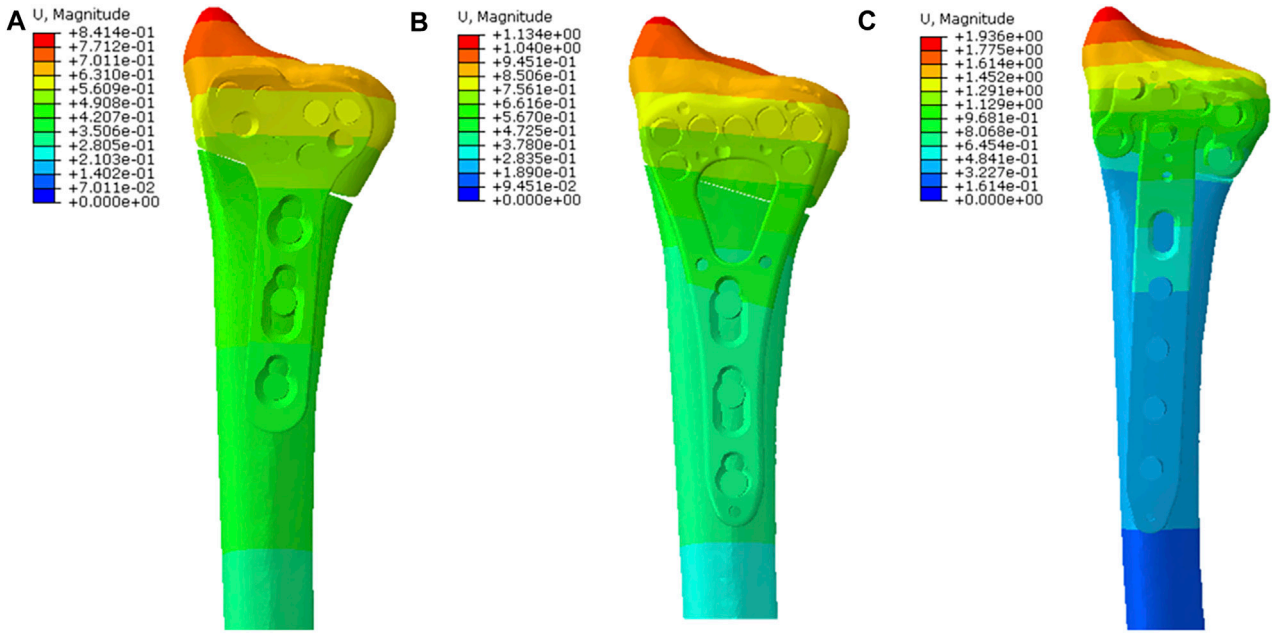

FIGURE 3
The displacement nephogram of total models and the most obvious displacement was observed at the distal end. **(A)** The nephogram in the T plate; **(B)** The nephogram in the V plate and the total displacement was similar to that in the T plate; **(C)** The nephogram in the π plate and the total displacement was higher than those in the other two plates.

2.3 Assessment and output parameters

Non-linear computational simulations were conducted using an axial load of 100 N to the distal end to facilitate the identification of reference points (Liu et al., 2020; Synek et al., 2021). The displacements of total models and implants were calculated to reflect the stability of internal fixation systems (Lv et al., 2022). The principal strains and the peak von Mises stresses of plates were also determined and compared to evaluate the biomechanical performance (Wong et al., 2020; Zheng et al., 2022). The values obtained from the model of T plate were used as references, as recommended by Klos et al. (Klos et al., 2010).

3 Results

Different biomechanical performance was observed on three models after the axial load simulation (Table 1).

The T plate represented the lowest model displacement of 0.8414 mm, while the V plate and the π plate displayed 1.4 times and 2.3 times more model displacement than the T plate, respectively (Figure 3). The T plate also had the smallest implant displacement of 0.7576mm, followed by the V plate (0.8802 mm) and the π plate (1.545 mm) (Figure 4).

The principal strains were concentrated at the similar area, the junction of plate head and body, in the three models. The T plate had the smallest strain of 0.23%, with the V plate displaying an intermediate level of 0.28% and the π plate showing the highest strain of 0.72% (Figure 5). Peak von Mises stresses of three plates were also concentrated at the junction site. In this regard, the least peak von Mises stress was observed in the V plate with 263.6 MPa, which was 61% of that of the T plate (435.6 MPa). The π plate represented a peak von Mises stress of 1050 MPa (Figure 6).

4 Discussion

Nearly one-sixth of all fractures in the emergency room are distal radius fractures (Bunch et al., 2016), which can be managed through various modalities including closed reduction, intramedullary fixation,

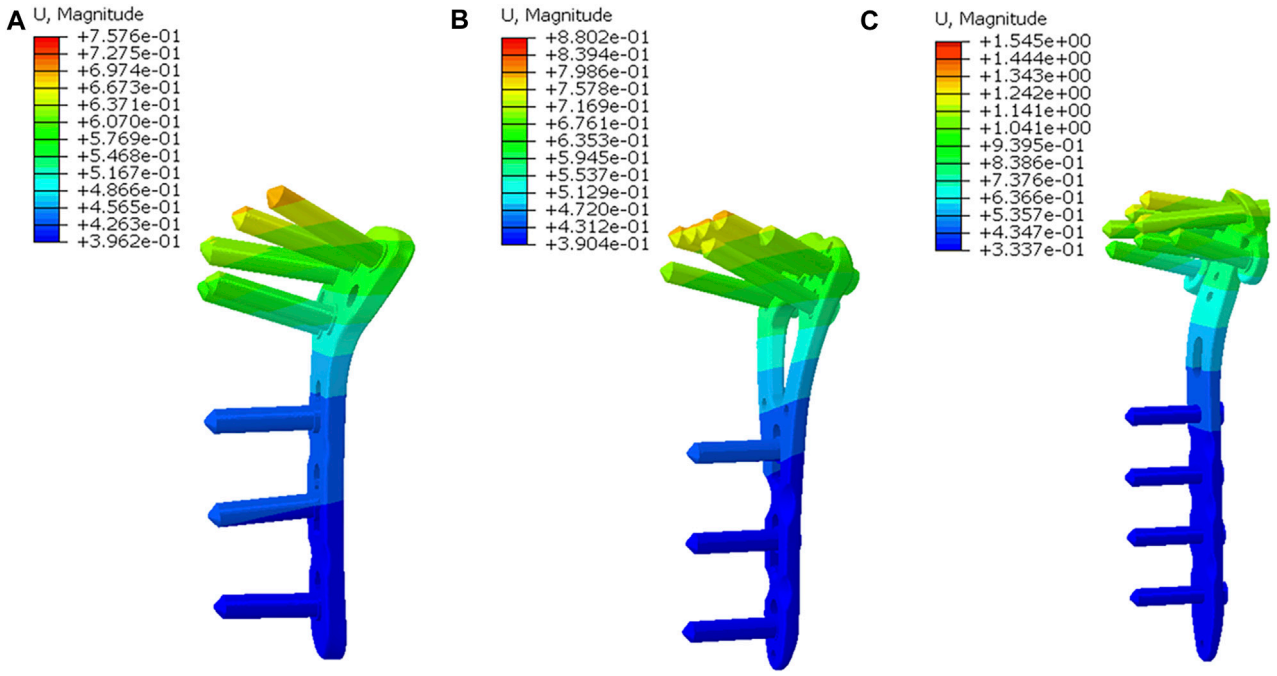

FIGURE 4
The displacement nephogram of implants. **(A)** The nephogram in the T plate; **(B)** The nephogram in the V plate and the plate displacement was similar to that in the T plate; **(C)** The nephogram in the π plate and the plate displacement was higher than those in the other two plates.

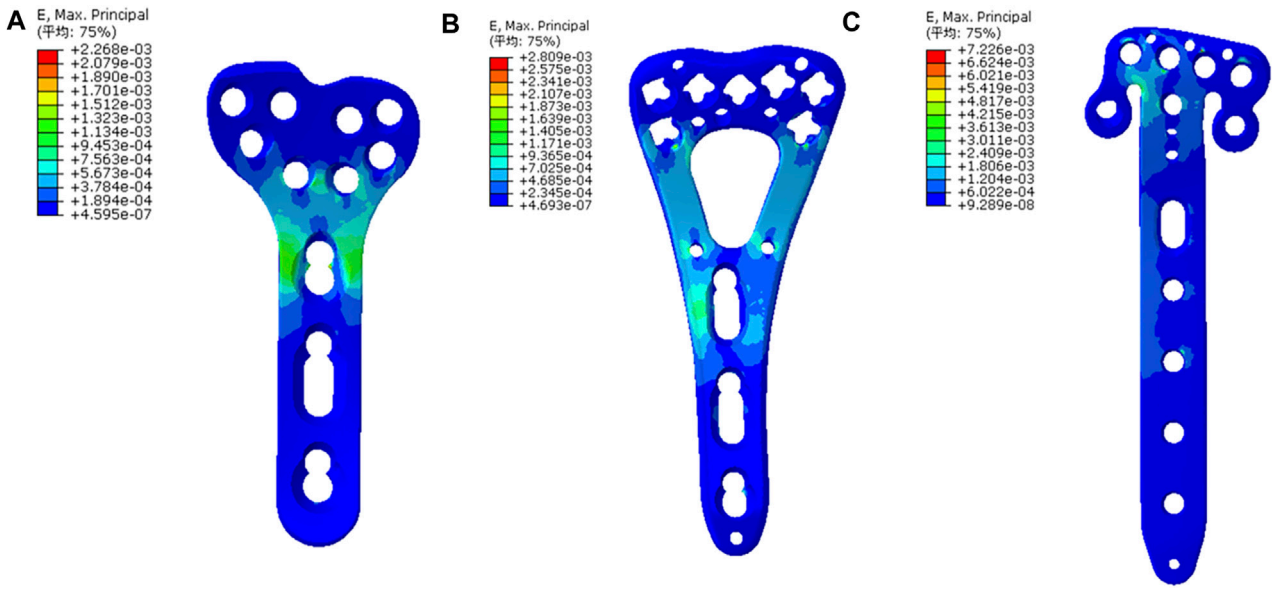

FIGURE 5
The strain nephogram of implants and the most obvious strain distribution was observed at the junction of plate head and body. **(A)** The strain nephogram in the T plate; **(B)** The nephogram in the V plate and the principal strain was similar to that in the T plate. **(C)** The nephogram in the π plate and the principal strain was higher than those in the other two plates.

external fixation and open reduction and internal fixation. Among these treatment strategies, open reduction and internal fixation with Ti6Al4V plates has shown faster recovery and improved wrist alignment (Oldrini et al., 2022). Volar locking plates are the most commonly employed type of plates, because of their lower incidences of tendon irritation and superior biomechanical stability over dorsal locking plates. However, to the best of our knowledge, a comprehensive comparison of volar locking plates with different designs has yet to be thoroughly investigated.

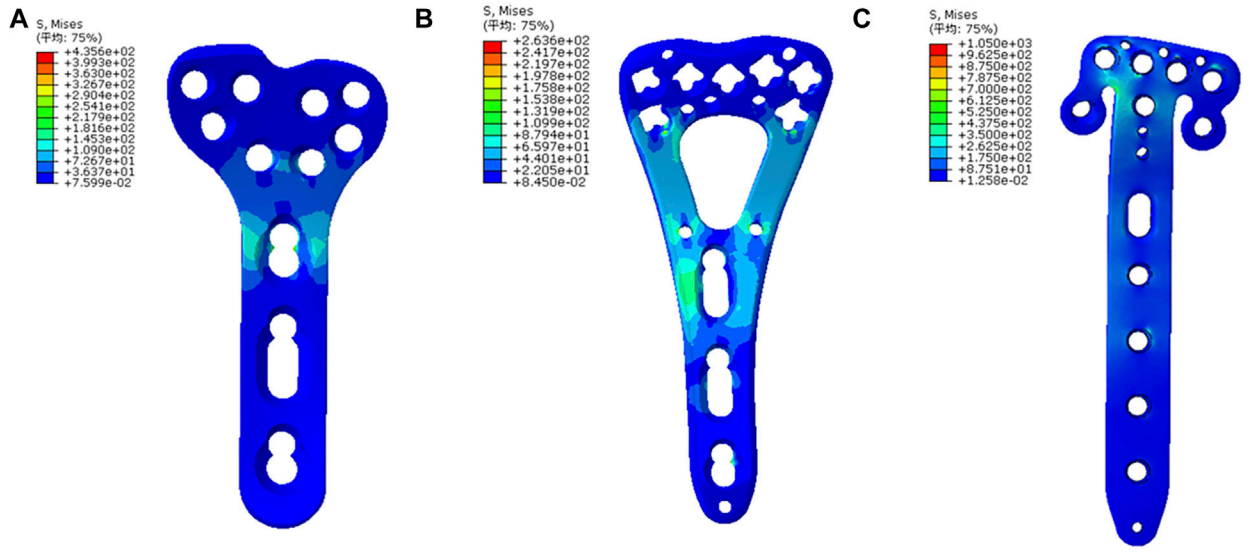

FIGURE 6
The von Mises stress nephogram of implants and the stresses were mainly concentrated at the junction of plate head and body. **(A)** The stress nephogram in the T plate; **(B)** The nephogram in the V plate and the peak stress was lower than that in the T plate. **(C)** The nephogram in the π plate and the peak stress was higher than those in the other two plates.

Ti6Al4V is one of the most commonly used biomaterials for internal fixation implants. Performed a comparative study regarding the stiffness of three volar plates by Ti6Al4V, stainless steel and PEEK using cadaveric models of distal radius fracture (Mugnai et al., 2018). They found that Ti6Al4V plates were associated with a significantly higher load to failure. Evaluated the postoperative Disabilities of the Arm, Shoulder and Hand (DASH) score for patients with distal radius fractures and found that the patients treated with Ti6Al4V plates showed a higher mean DASH score (15.3) *versus* those treated with PEEK plates (13.2), even though the results were not statistically significant (Perugia et al., 2017).

The present study is the first finite element analysis regarding the comparison among three Ti6Al4V volar plates with latest designs for distal radius fractures. We compared these three plates that were widely utilized in clinical procedures, aiming to investigate which type of plates would have better biomechanical features, as there are few clinical or biomechanical comparative studies in this area. We applied a simple and widely-used test, axial loading test, to simulate the loading pattern of distal radius fractures (Varga et al., 2009). This method can quantify resistance against external stress directly (Cheng et al., 2007). In our analysis, we found that most of results were in favor of the T plate. Both the T plate and the V plate exhibited superior advantages in various dimensions, including model displacements, stresses and strains, when compared with the π plate. The values of these parameters in the π plate were over 2 times amounts than those in the T plate. The findings suggested that distal radius fractures fixed with a π plate might be associated with a higher risk of implant displacement and failure, while a T plate might be a more suitable choice for simple extra-articular distal radius fractures. It should also be noted that, though the T plate appeared to be more stable and solid with lower displacement and strain than the V plate, the V plate showed lower peak von Mises stresses, indicating a lower probability of plates breakage. To our knowledge, among the three types of plates, only one case report of plate breakage was encountered in the T-type plate (volar column plate, The Matrix SmartLock Distal Radius system, Stryker, GmbH & Co. KG, Freiburg, Germany) (Yukata et al., 2009). The plate was broken through the fracture line where the screw holes were unfilled. The authors attributed this to a higher stress concentration in the broken site. Conducted a cadaveric biomechanical analysis of distal radius fractures and proved that the hole at the site of osteotomy is potentially a site of weakness in volar plates (Trease et al., 2005). Our findings, which demonstrated that obvious stresses and strains were distributed at the site of osteotomy, aligned with their results and theories.

The evaluation of displacements and strains indicated a slight superiority the T plate over the V plate. The displacement of V plate was 1.2 times greater than that of T plate. Previous publications mainly focused on the biomechanical/clinical outcomes of a single volar plate. Klos et al. recommended the T plate as a reference due to its good clinical outcomes and acceptable biomechanical features (Klos et al., 2010). The study by Khatri et al. reported that all 23 distal radius fractures following internal fixation with a V plate demonstrated excellent postoperative function with minimal complications (Khatri et al., 2016). Compared the biomechanical features of the V plate with those of the dorsal double plates and those of a juxta-articular distal radius volar plate in cadaveric models (Rausch et al., 2011; Rausch et al., 2013). They found that the V plate had higher initial and final stiffness and less loss of reduction after cyclical testing than the juxta-articular plate, and exhibited biomechanically equivalent stiffness to the dorsal double plates. Abdel-Wahed et al. followed up 96 patients with distal radius fractures for a mean period of 14 months and compared the clinical outcomes of T plates *versus* those of V plates. In their study, the V plates yielded slightly higher postoperative DASH scores over the T plates, while the complication rates and survivorships were comparable (Abdel-Wahed et al., 2022). The study by compared the stiffness of T plates and V plates after cyclical loading in sawbone phantoms of distal radius fractures (Stanbury et al., 2012). The authors discovered that in the extra-articular models, the mean load to failure of T plates (1548 N) was significantly less than that of V plates (2154 N). However, in the

intra-articular models, the mean load to failure of T plates (2146 N) was found to be higher than that of V plates (1495 N). Our results of peak von Mises stress were partially consistent with their findings regarding the extra-articular models, as our analysis illustrated that the stress in the V plate (263.6 MPa) was lower than that in the T plate (435.6 MPa) when receiving a 100 N axial loading. This might be associated with the cross-sectional sharps of plates. The V plate had two columns at the junction site while the T plate had only one column.

As for the π plate, many studies have demonstrated its superior clinical outcomes, particularly for the comminuted or intra-articular distal radius fractures (Kachooei et al., 2016; Spiteri et al., 2017b; Goorens et al., 2017; Chen et al., 2019; Chua et al., 2022). Reported satisfactory outcomes of π plates in 26 patients with complex intra-articular distal radius fractures (Spiteri et al., 2017a). No implant failure was observed in their study. Reviewed the records of 36 patients treated with a π plate and found that postoperative Lidstrom wrist scores were deemed as "excellent" in 32 patients (Kara et al., 2016). However, there is a lack of studies comparing the clinical outcomes of π plates to other plate types, and biomechanical studies on π plates are insufficient. In our analysis, the π plate showed inferior outcomes including larger displacements, stresses and strains than the V plate and T plate. This might be attributed to the more distal placement of the π plate and the narrower body passing through the osteotomy site, which could lead to a higher stress concentration. To our knowledge, there have been no clinical comparative analyses between the outcomes of π plates and those of V plates or T plates in patients with distal radius fractures. Thus, the further clinical investigation is need to identify the appropriate plate selection.

Our research is not without limitations. First, this is a numerical analysis using the finite element method to compare the biomechanical performance of three specific Ti6Al4V plates. The three-dimensional model was reconstructed based on the data from a 50-year-old female. We did not consider the anatomical variations, bone mineral density or other plate designs. The fracture pattern is a simple transverse extra-articular distal radius fracture. These issues can compromise the generalizability of our results in clinical scenarios. Nevertheless, we contend that our numerical estimation could provide a rough description and serve as a supplement for clinical research that is currently lacking. Second, according to the manufacturer (Depuy Synthes), the three plates in our study are intended for the fixation of both intra- and extra-articular fractures. However, some researchers have raised concerns regarding the consistency of the indications for these plates (Soong et al., 2011). Inadequate overlap in indications may also jeopardize the performance of each plate in specific situations. Third, we simplified the models in following aspects: (i) all screws were added to the plate using the assemble function and thus, each screw was placed along the center of each hole; (ii) all screws were modified without threads; (iii) the models did not comprise tendons and thus, the forces transferred onto the bone *via* attached tendons were not taken into account. Fourth, we only performed the axial loading test to simulate the loading pattern after fracture fixation. This method can not reflect the biomechanical properties of plates under loads in other directions, or multiple repetitive loads, which can be investigated by the cycling loading test. Additionally, the torsional loading simulation was not performed, which is important when considering the movement of the forearm in pronation and supination.

5 Conclusion

Our analysis compared the biomechanical features of three Ti6Al4V volar locking plates in an AO type 23-A3 fracture, and the results may provide information for surgeons when identifying the optimal plates among different designs for this particular type of fracture. Our findings indicated that the T plate was associated with a smaller model displacement, lower strain and higher stress over the V plate, though their overall performance was comparable. In contrast, the π plate appeared to be less effective than the two aforementioned plates in the scenarios of simple extra-articular distal radius fractures.

Data availability statement

The original contributions presented in the study are included in the article/supplementary material, further inquiries can be directed to the corresponding author.

Ethics statement

The studies involving human participants were reviewed and approved by The institutional ethic board of Chinese PLA general hospital. The patients/participants provided their written informed consent to participate in this study.

Written informed consent was obtained from the individual(s) for the publication of any potentially identifiable images or data included in this article.

Author contributions

JL, LZ, and PT contributed to conception and design of the study. HL, WZ, DW, and JL contributed to methodology of the study. HL, DX, JL, and CX completed the model construction. HL, CX, and DW completed data presentation. HL wrote the first draft of the manuscript. WZ, DX, DW, CX, and JL wrote sections of the manuscript. JL, LZ, and PT reviewed and edited the manuscript. All authors contributed to manuscript revision, read, and approved the submitted version.

Funding

This study is funded by the Beijing Natural Science Foundation (7222180) and the 13th Five-year Plan for Key Discipline Construction Project of PLA (A350109).

Conflict of interest

The authors declare that the research was conducted in the absence of any commercial or financial relationships that could be construed as a potential conflict of interest.

Publisher's note

References

Abdel-Wahed, M., Khater, A. A., and El-Desouky, M. A. (2022). Volar locking plate fixation for distal radius fractures: Did variable-angle plates make difference? *Int. Orthop.* 46 (9), 2165–2176. doi:10.1007/s00264-022-05469-z

Ahirwar, H., Gupta, V. K., and Nanda, H. S. (2021). Finite element analysis of fixed bone plates over fractured femur model. *Comput. Methods Biomech. Biomed. Engin* 24 (15), 1742–1751. doi:10.1080/10255842.2021.1918123

Alter, T. H., and Ilyas, A. M. (2018). Complications associated with volar locking plate fixation of distal radial fractures. *JBJS Rev.* 6 (10), e7. doi:10.2106/jbjs.Rvw.18.00004

Baumbach, S. F., Dall'Ara, E., Weninger, P., Antoni, A., Traxler, H., Dörr, M., et al. (2012). Assessment of a novel biomechanical fracture model for distal radius fractures. *BMC Musculoskelet. Disord.* 13, 252. doi:10.1186/1471-2474-13-252

Berger-Groch, J., Stodtmeister, A. C., Petersen, J. P., and Hoffmann, M. (2021). Palmar plating of distal radius fractures: 3-year follow-up with titanium and PEEK plates give similar outcomes. *Acta Orthop. Belg* 87 (3), 521–527. doi:10.52628/87.3.18

Beyer, J., Wynkoop, E., Liu, J., and Ebraheim, N. A. (2021). Interventions for distal radius fractures: A meta-analysis of comparison studies. *J. Wrist Surg.* 10 (5), 440–457. doi:10.1055/s-0041-1723793

Bunch, P. M., Sheehan, S. E., Dyer, G. S., Sodickson, A., and Khurana, B. (2016). A biomechanical approach to distal radius fractures for the emergency radiologist. *Emerg. Radiol.* 23 (2), 175–185. doi:10.1007/s10140-015-1363-0

Chen, M., Gittings, D. J., Yang, S., Liu, G., and Xia, T. (2019). Variable-Angle locking compression plate fixation of distal radius volar rim fractures. *Iowa Orthop. J.* 39 (2), 55–61.

Cheng, H. Y., Lin, C. L., Lin, Y. H., and Chen, A. C. (2007). Biomechanical evaluation of the modified double-plating fixation for the distal radius fracture. *Clin. Biomech. (Bristol, Avon)* 22 (5), 510–517. doi:10.1016/j.clinbiomech.2006.12.010

Chou, Y. C., Chen, A. C., Chen, C. Y., Hsu, Y. H., and Wu, C. C. (2011). Dorsal and volar 2.4-mm titanium locking plate fixation for AO type C3 dorsally comminuted distal radius fractures. *J. Hand Surg. Am.* 36 (6), 974–981. doi:10.1016/j.jhsa.2011.02.024

Chua, W. S., Hassan, S., and Anoar, A. F. (2022). Incidence of flexor tendon injuries in complex intra-articular distal radius fractures fixed with volar rim plate osteosynthesis. *Cureus* 14 (10), e29852. doi:10.7759/cureus.29852

Ghaem-Maghami, A., Fallah, E., Namazi, H., Karimi, M. T., and Hosseini, S. I. (2021). The comparison of biomechanical volar and dorsal plating in distal Part Radius fractures; a finite element analysis study. *Bull. Emerg. Trauma* 9 (1), 9–14. doi:10.30476/beat.2020.86681

Goorens, C. K., Geeurickx, S., Wernaers, P., Staelens, B., Scheerlinck, T., and Goubau, J. (2017). Midterm follow-up of treating volar marginal rim fractures with variable angle lcp volar rim distal radius plates. *J. Hand Surg. Asian Pac* 22 (2), 184–187. doi:10.1142/s0218810417500228

Hammert, W. C., Kramer, R. C., Graham, B., and Keith, M. W. (2013). AAOS appropriate use criteria: Treatment of distal radius fractures. *J. Am. Acad. Orthop. Surg.* 21 (8), 506–509. doi:10.5435/jaaos-21-08-506

Kachooei, A. R., Tarabochia, M., and Jupiter, J. B. (2016). Distal radius volar rim fracture fixation using DePuy-synthes volar rim plate. *J. Wrist Surg.* 5 (1), 002–008. doi:10.1055/s-0035-1570740

Kamei, S., Osada, D., Tamai, K., Kato, N., Takai, M., Kameda, M., et al. (2010). Stability of volar locking plate systems for AO type C3 fractures of the distal radius: Biomechanical study in a cadaveric model. *J. Orthop. Sci.* 15 (3), 357–364. doi:10.1007/s00776-010-1466-0

Kara, A., Celik, H., Oc, Y., Uzun, M., Erdil, M., and Tetik, C. (2016). Flexor tendon complications in comminuted distal radius fractures treated with anatomic volar rim locking plates. *Acta Orthop. Traumatol. Turc* 50 (6), 665–669. doi:10.1016/j.aott.2016.04.001

Khatri, K., Sharma, V., Farooque, K., and Tiwari, V. (2016). Surgical treatment of unstable distal radius fractures with a volar variable-angle locking plate: Clinical and radiological outcomes. *Arch. Trauma Res.* 5 (2), e25174. doi:10.5812/atr.25174

Klos, K., Rausch, S., Löffler, M., Fröber, R., Hofmeier, K., Lenz, M., et al. (2010). A biomechanical comparison of a biodegradable volar locked plate with two titanium volar locked plates in a distal radius fracture model. *J. Trauma* 68 (4), 984–991. doi:10.1097/TA.0b013e3181b28962

Knežević, J., Kodvanj, J., Čukelj, F., Pamuković, F., and Pavić, A. (2017). A biomechanical comparison of four fixed-angle dorsal plates in a finite element model of dorsally-unstable radius fracture. *Injury* 48 (5), S41–s46. doi:10.1016/s0020-1383(17)30738-6

Koh, S., Morris, R. P., Patterson, R. M., Kearney, J. P., Buford, W. L., Jr., and Viegas, S. F. (2006). Volar fixation for dorsally angulated extra-articular fractures of the distal radius: A biomechanical study. *J. Hand Surg. Am.* 31 (5), 771–779. doi:10.1016/j.jhsa.2006.02.015

Letsch, R., Infanger, M., Schmidt, J., and Kock, H. J. (2003). Surgical treatment of fractures of the distal radius with plates: A comparison of palmar and dorsal plate position. *Arch. Orthop. Trauma Surg.* 123 (7), 333–339. doi:10.1007/s00402-003-0538-4

Liu, H. C., Jiang, J. S., and Lin, C. L. (2020). Biomechanical investigation of a novel hybrid dorsal double plating for distal radius fractures by integrating topology optimization and finite element analysis. *Injury* 51 (6), 1271–1280. doi:10.1016/j.injury.2020.03.011

Lv, M. L., Ni, M., Sun, W., Wong, D. W., Zhou, S., Jia, Y., et al. (2022). Biomechanical analysis of a novel double-point fixation method for displaced intra-articular calcaneal fractures. *Front. Bioeng. Biotechnol.* 10, 791554. doi:10.3389/fbioe.2022.791554

Miyashima, Y., Kaneshiro, Y., Yano, K., Teraura, H., Sakanaka, H., and Uemura, T. (2019). Size and stabilization of the dorsoulnar fragment in AO C3-type distal radius fractures. *Injury* 50 (11), 2004–2008. doi:10.1016/j.injury.2019.08.003

Mugnai, R., Tarallo, L., Capra, F., and Catani, F. (2018). Biomechanical comparison between stainless steel, titanium and carbon-fiber reinforced polyetheretherketone volar locking plates for distal radius fractures. *Orthop. Traumatol. Surg. Res.* 104 (6), 877–882. doi:10.1016/j.otsr.2018.05.002

Nellans, K. W., Kowalski, E., and Chung, K. C. (2012). The epidemiology of distal radius fractures. *Hand Clin.* 28 (2), 113–125. doi:10.1016/j.hcl.2012.02.001

Oldrini, L. M., Feltri, P., Albanese, J., Lucchina, S., Filardo, G., and Candrian, C. (2022). Volar locking plate vs cast immobilization for distal radius fractures: A systematic review and meta-analysis. *EFORT Open Rev.* 7 (9), 644–652. doi:10.1530/eor-22-0022

Perugia, D., Guzzini, M., Mazza, D., Iorio, C., Civitenga, C., and Ferretti, A. (2017). Comparison between Carbon-Peek volar locking plates and titanium volar locking plates in the treatment of distal radius fractures. *Injury* 48 (3), S24–s29. doi:10.1016/s0020-1383(17)30653-8

Rausch, S., Schlonski, O., Klos, K., Gras, F., Gueorguiev, B., Hofmann, G. O., et al. (2013). Volar versus dorsal latest-generation variable-angle locking plates for the fixation of AO type 23C 2.1 distal radius fractures: A biomechanical study in cadavers. *Injury* 44 (4), 523–526. doi:10.1016/j.injury.2012.08.048

Rausch, S., Klos, K., Stephan, H., Hoffmeier, K., Gras, F., Windolf, M., et al. (2011). Evaluation of a polyaxial angle-stable volar plate in a distal radius C-fracture model--a biomechanical study. *Injury* 42 (11), 1248–1252. doi:10.1016/j.injury.2010.12.005

Selles, C. A., Mulders, M. A. M., Winkelhagen, J., van Eerten, P. V., Goslings, J. C., and Schep, N. W. L. (2021). Volar Plate fixation versus cast immobilization in acceptably reduced intra-articular distal radial fractures: A randomized controlled trial. *J. Bone Jt. Surg. Am.* 103 (21), 1963–1969. doi:10.2106/jbjs.20.01344

Soong, M., Earp, B. E., Bishop, G., Leung, A., and Blazar, P. (2011). Volar locking plate implant prominence and flexor tendon rupture. *J. Bone Jt. Surg. Am.* 93 (4), 328–335. doi:10.2106/jbjs.J.00193

Spiteri, M., Ng, W., Matthews, J., and Power, D. (2017a). Functional outcome of fixation of complex intra-articular distal radius fractures with a variable-angle distal radius volar rim plate. *J. Hand Microsurg* 9 (1), 011–016. doi:10.1055/s-0037-1601325

Spiteri, M., Roberts, D., Ng, W., Matthews, J., and Power, D. (2017b). Distal radius volar rim plate: Technical and radiographic considerations. *World J. Orthop.* 8 (7), 567–573. doi:10.5312/wjo.v8.i7.567

Stanbury, S. J., Salo, A., and Elfar, J. C. (2012). Biomechanical analysis of a volar variable-angle locking plate: The effect of capturing a distal radial styloid fragment. *J. Hand Surg. Am.* 37 (12), 2488–2494. doi:10.1016/j.jhsa.2012.09.009

Synek, A., Baumbach, S. F., and Pahr, D. H. (2021). Towards optimization of volar plate fixations of distal radius fractures: Using finite element analyses to reduce the number of screws. *Clin. Biomech. (Bristol, Avon)* 82, 105272. doi:10.1016/j.clinbiomech.2021.105272

Trease, C., McIff, T., and Toby, E. B. (2005). Locking versus nonlocking T-plates for dorsal and volar fixation of dorsally comminuted distal radius fractures: A biomechanical study. *J. Hand Surg. Am.* 30 (4), 756–763. doi:10.1016/j.jhsa.2005.04.017

Varga, P., Baumbach, S., Pahr, D., and Zysset, P. K. (2009). Validation of an anatomy specific finite element model of Colles' fracture. *J. Biomech.* 42 (11), 1726–1731. doi:10.1016/j.jbiomech.2009.04.017

Wong, C. E., Hu, H. T., Hsieh, M. P., and Huang, K. Y. (2020). Optimization of three-level cervical hybrid surgery to prevent adjacent segment disease: A finite element study. *Front. Bioeng. Biotechnol.* 8, 154. doi:10.3389/fbioe.2020.00154

Yamamoto, M., Fujihara, Y., Fujihara, N., and Hirata, H. (2017). A systematic review of volar locking plate removal after distal radius fracture. *Injury* 48 (12), 2650–2656. doi:10.1016/j.injury.2017.10.010

Yukata, K., Doi, K., Hattori, Y., and Sakamoto, S. (2009). Early breakage of a titanium volar locking plate for fixation of a distal radius fracture: Case report. *J. Hand Surg. Am.* 34 (5), 907–909. doi:10.1016/j.jhsa.2009.01.004

Zhang, W., Li, J., Zhang, H., Wang, M., Li, L., Zhou, J., et al. (2018). Biomechanical assessment of single liss versus double-plate osteosynthesis in the AO type 33-C2 fractures: A finite element analysis. *Injury* 49 (12), 2142–2146. doi:10.1016/j.injury.2018.10.011

Zheng, L., Wang, C., Hu, M., Apicella, A., Wang, L., Zhang, M., et al. (2022). An innovative additively manufactured implant for mandibular injuries: Design and preparation processes based on simulation model. *Front. Bioeng. Biotechnol.* 10, 1065971. doi:10.3389/fbioe.2022.1065971

frontiers | Frontiers in Bioengineering and Biotechnology

TYPE Review
PUBLISHED 04 April 2023
DOI 10.3389/fbioe.2023.1127939

OPEN ACCESS

EDITED BY
Yansong Qi,
Inner Mongolia People's Hospital, China

REVIEWED BY
Kai Zhang,
Sichuan University, China
Alideertu Dong,
Inner Mongolia University, China

*CORRESPONDENCE
Hui Xie,
xiehui424@163.com
Benjie Wang,
wangbenjie@dlu.edu.cn

†These authors have contributed equally to this work

SPECIALTY SECTION
This article was submitted to Biomaterials, a section of the journal Frontiers in Bioengineering and Biotechnology

RECEIVED 20 December 2022
ACCEPTED 22 March 2023
PUBLISHED 04 April 2023

CITATION
Wang X, Zhou K, Li Y, Xie H and Wang B (2023), Preparation, modification, and clinical application of porous tantalum scaffolds.
Front. Bioeng. Biotechnol. 11:1127939.
doi: 10.3389/fbioe.2023.1127939

Preparation, modification, and clinical application of porous tantalum scaffolds

Xinyi Wang†, Ke Zhou†, Yada Li, Hui Xie* and Benjie Wang*

Affiliated Zhongshan Hospital of Dalian University, Dalian, China

Porous tantalum (Ta) implants have been developed and clinically applied as high-quality implant biomaterials in the orthopedics field because of their excellent corrosion resistance, biocompatibility, osteointegration, and bone conductivity. Porous Ta allows fine bone ingrowth and new bone formation through the inner space because of its high porosity and interconnected pore structure. It contributes to rapid bone integration and long-term stability of osseointegrated implants. Porous Ta has excellent wetting properties and high surface energy, which facilitate the adhesion, proliferation, and mineralization of osteoblasts. Moreover, porous Ta is superior to classical metallic materials in avoiding the stress shielding effect, minimizing the loss of marginal bone, and improving primary stability because of its low elastic modulus and high friction coefficient. Accordingly, the excellent biological and mechanical properties of porous Ta are primarily responsible for its rising clinical translation trend. Over the past 2 decades, advanced fabrication strategies such as emerging manufacturing technologies, surface modification techniques, and patient-oriented designs have remarkably influenced the microstructural characteristic, bioactive performance, and clinical indications of porous Ta scaffolds. The present review offers an overview of the fabrication methods, modification techniques, and orthopedic applications of porous Ta implants.

KEYWORDS

porous Ta, preparation, surface modification, clinical application, porous tantalum scaffolds

1 Introduction

Tantalum (Ta) has been used in clinical practice as a surgical suture, bone fixation component, bone implant, vascular stent coating, and medical imaging contrast agent since its discovery because of its high biological affinity and superior physicochemical and biological properties (Yang et al., 2020a). Ta possesses excellent biocompatibility, corrosion resistance, mechanical ductility, osteoconductivity, osteoinductivity, and vascular inductivity. Furthermore, it has a high affinity for oxygen and tends to form a self-passivation surface oxide layer (Ta_2O_5), thus allowing the formation of bone-like apatite coating [(Wang et al., 2016a)· (Rupérez et al., 2015)]. Moreover, Ta oxide coatings exhibit remarkable antibacterial properties (Chang et al., 2014). These features make Ta ideal for orthopedic applications.

In the 1990s, porous Ta scaffolds were prepared through chemical vapor deposition (CVD), and their structures and properties were analyzed (Yang et al., 2020b). Porous Ta possesses a completely interconnected structure, high osteoconductivity, and low elastic modulus compared with dense Ta. Because the elastic modulus of porous Ta is equivalent to

that of human cancellous bone, stress load is evenly distributed on a porous Ta implant, thereby minimizing the risk of dissolution around the prosthesis and implant failure caused by stress shielding. Furthermore, porous Ta has a high friction coefficient for the bone, and thus, it exhibits high stability as an implant. Porous Ta scaffolds facilitate the attachment, proliferation, differentiation, and mineralization of osteoblasts, leading to better osteogenesis and osteointegration *in vivo* (Smith et al., 2014; Wang et al., 2015a).

Over the past 2 decades, porous Ta has been clinically used to repair defective bone tissues and treat various bone diseases. These clinical applications include hip/knee arthroplasty, spinal fusion, and femoral head necrosis treatment (Gao et al., 2021). Emerging manufacturing technologies, surface modification, and clinical applications have substantially eased manufacturing upgrades, structural and performance optimization, and application of Ta scaffolds. For instance, additive manufacturing (AM) has led to the production of patient-specific and anatomically matched Ta implants with well-designed porous structures. Levine et al. (Russell Levine et al., 2006) and George et al. (George, 2018) investigated the performance and clinical application, respectively, of porous Ta scaffolds produced through CVD. Liu et al. (Liu et al., 2015a) summarized the usefulness of porous Ta scaffolds in dental applications. Qian et al. (Hu et al., 2020) reviewed the physicochemical, cellular, animal, and clinical studies of porous Ta scaffolds prepared through AM. Han et al. (Han et al., 2019) compared the progress of porous Ta scaffolds and porous Ti-based scaffolds in orthopedics field.

The aforementioned studies have primarily summarized certain characteristics of porous Ta scaffolds; however, their properties have not been systematically examined. The present review summarizes the latest advances in the manufacturing, modification, and orthopedic applications of these scaffolds, providing a comprehensive reference for porous Ta-based implants.

2 Mechanical properties

Bone implant materials used to replace human bone tissue should fulfill certain conditions. First, they must have appropriate stiffness and compressive strength to provide support for the joints and a mechanical environment conducive to bone tissue regeneration for the implant because too high stiffness and compressive strength can reduce the load required for new bone formation. Second, the implant materials should possess the ability to resist fatigue fracture. Finally, the elastic modulus of the implant material should match the elastic modulus of the human bone to avoid stress shielding, which may cause implantation failure. Bone tissue grows normally only when it is subjected to an appropriate mechanical load. Insufficient force will cause bone absorption, whereas excessive stress can destroy the bone tissues (Ao et al., 2022).

2.1 Compressive strength

Bone tissue is sensitive to stress, and its growth is strongly associated with the stress of the surrounding bone tissue after implantation. In healthy mammals, the cortical lamellar bone can withstand a threshold of ultimate strength or fracture strength of approximately 120 MPa (or strain exceeding 25,000 με). The stress threshold for bone resorption ranges from 1 to 2 MPa (or strains less than 50–100 με), resulting in decreased bone stiffness and density. The stress threshold for bone growth is 20 MPa (or strains exceeding 1,000–1,500 με), which further results in increased bone strength. When the stress threshold of fatigue damage is 60 MPa (or the strain exceeds 3,000 με), the corresponding bone tissue is more prone to damage. Therefore, the compressive strength of the prepared porous tantalum implants is sufficient to meet the reconstruction of the mechanical function of bone tissue. Table 1 shows the results of porous tantalum compression experiment, indicating that the differences in compressive strength may be attributed to the differences in the structure and process of porous structures. The compressive strength of porous tantalum scaffolds is negatively correlated with porosity. Therefore, future studies should focus on the design of reasonable pore size or porosity to balance the compressive strength of porous tantalum scaffolds.

2.2 Fatigue strength

Bone implants can bear high cyclic loads *in vivo* (HEDAYATI et al., 2016); therefore, the fatigue performance of porous tantalum scaffolds should also be considered in the design process. Ghouse et al. (GHOUSE et al., 2018) compared the high periodic fatigue strength of four metal alloys (CP-Ti, Ti-6Al-4VELI, Ta, and Ti-30Ta), and the results showed that porous tantalum and titanium alloys had the highest fatigue strength under the same stiffness, which was 8% higher than that of CP-Ti and 19% higher than that of Ti-6Al-4VELI. At the same time, the fatigue strength of porous materials could be increased by 7%–8% by optimizing the process parameters of AM preparation. The study by Wauthle et al. (AMIN-YAVARI et al., 2013) also found that the fatigue strength of porous tantalum was significantly higher than that of porous titanium alloy (Ti-6Al-4VELI) (7.35 MPa vs 4.18 MPa) after 106 cycles. Due to its high ductility, the former allowed more plastic deformation and reduced the generation and diffusion of cracks (RITCHIE, 1999).

2.3 Elastic modulus

In the human body, the porosity of cortical bone is 3%–5%, and the elastic modulus is 7–30 Gpa; the porosity and elastic modulus of cancellous bone are 50%–90% and 0.01–3.0 Gpa, respectively (ZHANG et al., 1999). The elastic modulus of solid tantalum is 185 GPa, which is far higher than that of bone tissue, while the elastic modulus of porous tantalum is 2.3–30 GPa and the porosity is 27%–85% (WEI et al., 2016), thereby providing more variable space compared with cortical bone or spongy bone. According to the data in Table 1, the elastic modulus is also affected by the processing technology. Zhou et al. (ZHOU et al., 2017) determined the effect of energy density and scanning speed in selective laser melting (SLM) process on product density and used optimized SLM technology to prepare tantalum samples with the highest density of 96.92%. The microhardness increased from 120 HV to 445 HV. The tensile strength increased from 310 MPa to 739 MPa. Compared with those of powder metallurgy products, the mechanical properties

TABLE 1 Preparation technology, porosity, and mechanical properties of porous tantalum.

Material	Manufacturing method	Porosity/%	Elastic modulus/GPa	Compressive strength/MPa	Compressive yield strength/MPa	Reference
Cancellous bone		50–90	0.01–3.0		2–12	Yang et al. (2020a)
Unalloyed Ta(F560)			185		138–345	Zhou and Zhu (2013)
Porous Ta	CVD	75–85	2.3 ± 3.9	50–70	35–51	Zhou and Zhu (2013)
	PM	66.7	2.21 ± 0.16	61.5 ± 4.5		Rupérez et al. (2015)
		50	1.17 ± 0.08	34.12 ± 3.67		Xie et al. (2019)
		60	0.48 ± 0.03	20.01 ± 2.59		Xie et al. (2019)
		70	0.14 ± 0.03	8.57 ± 1.43		Xie et al. (2019)
	LENS	27–55	1.5–20			Hu et al. (2020)
	SLM	79.7 ± 0.2	1.22 ± 0.07	3.61 ± 0.4	12.7 ± 0.6	Wang et al. (2020)
	SLM	68.3 ± 1.1	2.34 ± 0.2	78.54 ± 9.1		Ma et al. (2016)

were increased by more than two times. The elastic modulus of a porous structure is not only affected by its preparation technology and related parameters but also by its pore characteristics. Through numerical simulation, it is found that in porous structures, cubic hole scaffolds have higher structural modulus than inclined hole scaffolds, and the elastic modulus of porous scaffolds is negatively correlated with porosity (WIEDING et al., 2014).

3 Preparation of porous Ta

Ta is a refractory metal having a melting point of up to 2,980°C. Theoretically, the method for preparing porous Ta materials is the same as that for preparing other porous refractory metals. Nevertheless, Ta can react with C and O at high temperatures, and therefore, limited processing methods are available for porous Ta materials (Van Steenkiste and Gorkiewicz, 2004). The reported methods mainly include CVD, powder metallurgy (PM), and AM.

3.1 Foam impregnation

The aqueous solution of polyvinyl alcohol (PVA) is used as a binder, to which the Ta powder is added for obtaining a slurry of appropriate viscosity and fluidity. A polyurethane foam with three-dimensional connected pores is used as the porous support. After compression and exhaust, the foam is placed in the slurry, and the foam body is repeatedly compressed. The elastic expansion property of polyurethane facilitates the absorption of the slurry. After impregnation, the surplus slurry in the foam is removed to obtain the green body. This green body is vacuum dried. Finally, the dried green body is sintered to obtain the porous Ta (Xu and Jiang, 2016).

The PVA concentration greatly influences slurry viscosity, which in turn affects the porosity of porous Ta. Porous Ta prepared through foam impregnation is disadvantageous because pore plugging formed inevitably during slurry impregnation affects the three-dimensional interconnected pore structure and hinders the complete bone tissue growth. Therefore, this method is rarely used.

3.2 Powder metallurgy

PM is a less-cutting or no-cutting material processing method that offers unique advantages in preparing porous metals having complex structures. The main steps are illustrated in Figure 1. First, Ta powders and space-holding particles are homogenously mixed. This mixture is compacted under an appropriate pressure (350 or 450 MPa), which is applied using a uniaxial hydraulic press with a 10-mm-diameter die. The green compact obtained is then dissolved in distilled water generally maintained at 60°C to ensure a quick dissolution process, complete removal of the space-holding particles, and formation of a porous structure. Lastly, the porous sample is oven-dried for 2 h and sintered at 1,300°C–2000°C in vacuum to produce porous Ta scaffolds (Wang et al., 2015b; Rupérez et al., 2015; Raja Sukumar et al., 2019; Wang et al., 2020).

Zhou et al. (Zhou and Zhu, 2013) first mixed glutinous rice flour and NaCl particles to produce spherical particles for use as a pore-forming agent. After isostatic pressure treatment, this agent was evenly mixed with Ta powder to obtain raw billet. The billet was sintered at 1800°C, and a preliminary spongy porous Ta sample was produced after removing the glutinous rice flour. To remove NaCl, the sample was placed in circulating water, and the final porous Ta scaffolds were fabricated. The as-prepared scaffolds exhibit a connected pore structure, with a pore size of 100–400 mm, compressive strength of 50.3 ± 0.5 MPa, and elastic modulus of

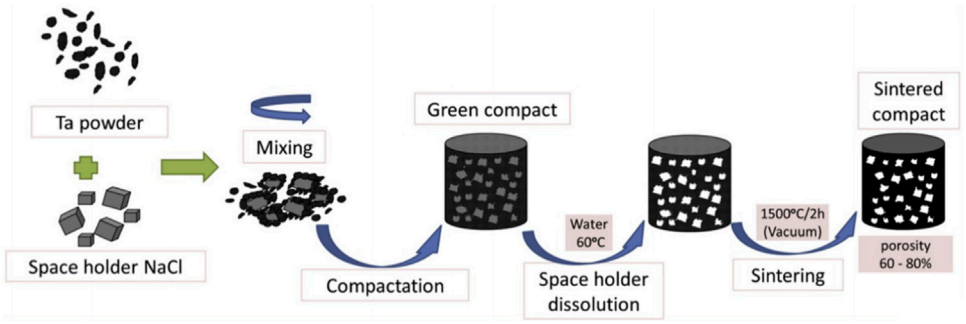

FIGURE 1
Schematic of the powder metallurgy technique (Rupérez et al., 2015). *Copyright © 2015 Published by Elsevier Ltd.*

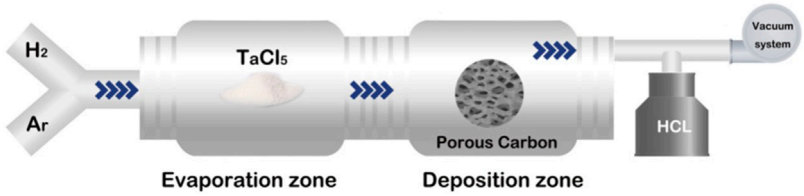

FIGURE 2
Schematic of the CVD system.

2.0 ± 0.3 GPa, which are comparable to those of the cancellous bone, and thus, they can minimize the stress shielding effect.

Notably, numerous closed pores are inevitably formed during PM because of the inherent limitation of this approach. Thus, the pores of Ta scaffolds fabricated through PM have lower interconnectivity than those of scaffolds fabricated through CVD. This hinders the enhancement of osteoconductivity *in vivo* of Ta scaffolds fabricated through PM. Despite extensive material, mechanical, *in vitro*, and preclinical animal studies on PM-generated porous Ta scaffolds, their clinical applications are limited.

3.3 Chemical vapor deposition

CVD is a mainstream commercial manufacturing method for porous Ta and was invented by Implex Company, which has now been taken over by Zimmer. Porous Ta implants are made through the pyrolysis of porous thermosetting polymers, which confer 98% porosity and form a low-density carbon skeleton with a repeating dodecahedral array. Pure Ta is deposited on the support through chemical vapor infiltration. For example, porous carbon is produced by pyrolysis of the polyurethane foam precursor, which leads to a glassy pyrolytic carbon skeleton with a spongy porous structure. Subsequently, commercially pure Ta serves as the raw material, and CVD is adopted to allow the pure Ta to react with Cl_2 and generate gaseous $TaCl_5$. Next, H_2 is used to reduce Ta from $TaCl_5$ and deposit Ta onto the carbon skeleton to form a unique porous structure (Xie et al., 2019). A typical CVD system is schematized in Figure 2.

The porous Ta produced using the aforementioned method maintains a skeleton with a spongy porous structure, comprising crisscross grids and pores. The grids are arranged in multiple dodecahedral structures. Thickness of Ta coating on the carbon skeleton is between a few micrometers to several hundred micrometers; this thickness is achieved by adjusting the reaction time. The Ta coating thickness is generally 40–60 μm, with the pore size being approximately 400–600 μm and the porosity being 75%–85%. These values indicate that the coating meets the clinical requirements in terms of mechanical properties and for bone penetration.

Ma et al. (Ma et al., 2016; Ma et al., 2020a) generated porous Ta scaffolds with a bone trabecular structure on the surface of a porous SiC scaffold through CVD. In such cases, the Ta coating thickness is linearly related to the deposition time and is accurately regulated from a few micrometers to hundreds of micrometers. Consequently, the scaffold porosity and pore size are customized, thereby resulting in various mechanical performances and in turn meeting the demand of different implantation sites. The elastic modulus of porous Ta scaffolds obtained through the aforementioned process is 1–30 GPa, and the corresponding compressive strength is 10–200 MPa (Ma et al., 2020a).

Despite the widespread use of CVD-manufactured Ta scaffolds in bone defect repair and bone disease treatment, more advanced manufacturing techniques are required because of the following

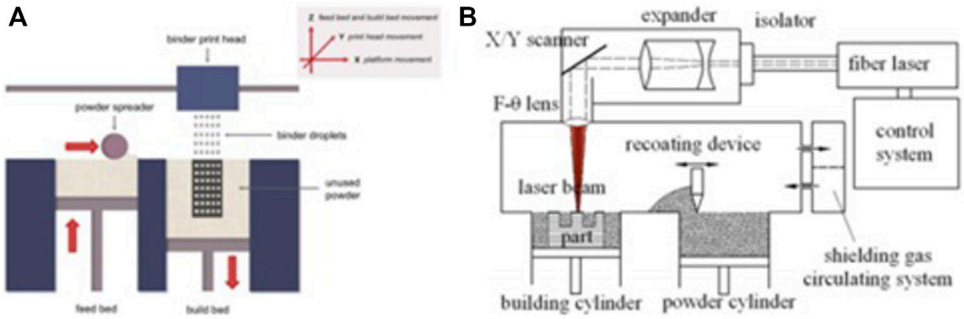

FIGURE 3
Schematics of the powder bed method **(A)** and the SLM method **(B)**, reproduced with the permission (Brunello et al., 2016) *Copyright © 2016 Elsevier Inc.* and the permission (Liu et al., 2015b) *Copyright © 2015 Published by Elsevier Ltd.*, respectively.

reasons. First, CVD is a conventional, high-cost manufacturing process. Second, fabrication of patient-specific and anatomically matched shapes is difficult. Furthermore, CVD lacks designability and controllability of porous structures.

3.4 Additive manufacturing

Customized patient-specific bone implants are required for proper matching of anatomical shapes at different anatomical sites, and personalized treatment is the current trend in orthopedic clinical practice. AM, a powerful and multi-functional processing technique, also known as rapid prototyping technology or 3D printing (Hu et al., 2020), has emerged in the past few years. It is based on 3D model data and adopts layer-by-layer superposition. AM techniques include powder bed laser fusion, powder bed electron fusion, selective laser sintering, directed energy deposition, direct metal deposition, direct metal printing, fused deposition modeling, direct metal writing, and binder jetting (Yang et al., 2020c). Highly customized porous implants with complex geometric shapes that match real anatomical shapes can be manufactured through AM. Moreover, the porosity of such implants can be designed and adjusted to regulate the compressive strength and elastic modulus and avoid stress shielding (Wauthle et al., 2015a; Zhao et al., 2018a; Amit et al., 2019).

SLM and electron beam melting are the most extensively applied AM techniques for porous metal scaffolds because of their high precision, high efficiency, and excellent stability. The first layer of the metallic powder is applied and fused into a solid part by using a heat source of a laser or electron beam. When the construction platform drops, the next layer of powder is applied from the material distribution platform and fused. Once the whole structure is completed, the produced object is cut from the support body (Wang et al., 2017a). Panels A and B in Figure 3 present the schematics of the powder bed system and SLM, respectively.

By using the laser 3D printing method, Balla et al. (Krishna Balla et al., 2010) obtained porous Ta with 27% and 55% porosity. *In vitro* cell characterization showed that the biocompatibility of porous Ta is superior to that of porous Ti. The expression of alkaline phosphatase (ALP) of human fetal osteoblasts cultured on the porous Ta surface was higher, suggesting that Ta has higher osteogenic activity than Ti. Wauthle et al. (Wauthle et al., 2015b) obtained a porous Ta implant (porosity: 80%) and used it to repair large bone defects. The porous Ta had a yield strength of 12.7 MPa, a compressive strength of 36.1 MPa, an elastic modulus of 1.22 GPa, and a fatigue strength of approximately 7.35 MPa, thus meeting the criteria for a bone implant material. Porous Ta exhibited no cytotoxicity in vitro tests. Twelve weeks after implantation, bone ingrowth was observed. Complete bone contacts were observed in certain cases. The anti-torsion test showed that porous Ta has a strong ability to bind to the surrounding bone tissue. Dou (Dou et al., 2019) et al. prepared porous Ta scaffolds through CVD combined with chemical meteorological deposition. The *in vitro* test results indicated that the adhesion and proliferation of bone marrow mesenchymal stem cells (BMSCs) on porous Ta are significantly superior to those on porous Ti. Moreover, the ALP activity assay suggested that the osteogenic activity of porous Ta is higher than that of porous Ti. The q-PCR test showed higher expressions of osteogenic genes encoding ALP, osterix, collagen-I (Col-I), osteonectin, and osteocalcin (OCN) on porous Ta. The Western blotting assay revealed higher p-ERK protein expression on porous Ta. The aforementioned analyses suggested that porous Ta facilitates BMSC adhesion and proliferation and exhibits excellent osteogenic activity and osteoinductivity compared with widely used Ti and its alloys.

In brief, different pore formation mechanisms of the aforementioned approaches contribute to differences in the porous structure characteristics. The foam impregnation method is rarely used because of its excessive disadvantages such as pore plugging. The PM-manufactured scaffold has low pore interconnectivity, which results in limited osteoconductivity and bone penetration capacity. CVD generates trabecular-like pores with high interconnectivity, thereby promoting bone tissue ingrowth. CVD still lacks control of the porous structure. By contrast, AM-fabricated scaffolds exhibit high interconnectivity and controllable pore characteristics (strut diameter, pore diameter, pore geometry, and porosity). Highly customized Ta scaffolds with well-designed porous structures and anatomically matched geometry can be produced using AM, which makes AM the most extensively used and the most efficient approach for generating porous Ta implants. With advances in AM-related technologies, AM is expected to be the mainstream method for preparing porous Ta scaffolds.

4 Surface modification of porous Ta

The surface microenvironment is of great significance in orthopedic implants. Appropriate surface characteristics improve the area and quality of bone–implant contact, thereby facilitating osseointegration. Osseointegration is the direct connection between the bone and implant, which is critical to implant stability and for ensuring successful implantation (Turkyilmaz, 2011). However, osteointegration is a lengthy process, usually spanning weeks to months, and has four stages: hemostasis, inflammation, proliferation, and remodeling (Hendrik et al., 2012). Guglielmotti et al. (Guglielmotti María et al., 2000) conducted several experiments to determine the factors for osteointegration. The results showed that surfaces with higher roughness facilitate osseointegration. Hence, surface modification of implants is essential for enhancing the binding between the bone tissue and implant. Moreover, the corrosion resistance, wear resistance, and biocompatibility of the implants need to be improved (Sasikumar et al., 2019). Since the 1970s, studies have focused on the surface modifications of Ta and porous Ta to facilitate bone healing and offer more durable and stable bone binding. The current main surface modification techniques include biomimetic calcium phosphate coating, anodic oxidation, micro-arc oxidation (MAO), alkali–heat treatment, and surface functional modification.

4.1 *Alkali–heat treatment*

In alkali–heat treatment, the implant is soaked in NaOH solution and heated at a high temperature. During heating, biomimetic apatite is formed on the implant surface (Miyazaki et al., 2000). In the alkali treatment, the sodium salt gel is produced that weakens the bonding between the apatite and substrate and interferes with the bone–implant bonding. After the heat treatment, the gel dehydrates into a dense and stable amorphous structure, leading to a cohesive bonding between the apatite and substrate. Li et al. (Li et al., 2010a) suggested that the activated surface of the porous Ta alloy contributes to SaOS2 cell adhesion and spread. Kuo and colleagues (Kuo et al., 2019) recently used alkali–heat treatment to activate Ta. First, the sample was immersed in a 1 M NaOH aqueous solution at 60°C for 24 h, heated to 300°C at a rate of 5°C/min, and kept at this temperature for 1 h. The resulting mixture was cooled to room temperature. Subsequently, bone-like apatite was inducted through immersion in the simulated body fluid. This proved that the alkali–heat treatment accelerates the apatite growth rate. In addition, the *in vitro* test revealed better adhesion and spread of MG-63 cells cultured on alkali–heat-treated coating.

4.2 Anodic oxidation

In anodic oxidation, a potential between the anode (the metal) and the cathode (the electrode, e.g., graphite, platinum, and lead) is applied to transfer charges and ions and form an oxide layer. The process leads to the production of protective oxide layers with controlled thickness (Chang and Webster Thomas, 2006). When the voltage is applied, the anode surface undergoes oxidation, forming a dense oxide film. This film effectively inhibits the release of metal ions and improves corrosion resistance and bioactivity. Moreover, the adjustment of process parameters, including the electrolyte composition and concentration, as well as the temperature, applied potential, process duration, and power supply mode, regulates the morphology, roughness, and physical and chemical properties of the coating (Ercan et al., 2011; Minagar et al., 2012; Fialho and Carvalho, 2019). Anodic oxidation has been successfully used with titanium and other metals to produce ordered nanostructures, which promote the adsorption of proteins, ions, and cells (Wang et al., 2019a; Dias-Netipanyj et al., 2020).

L. Fialho et al. (Fialho et al., 2020) prepared a Ta_2O_5 nanoporous surface through anodic oxidation in an HF-free electrolyte composed of ethylene glycol, water, and ammonium fluoride (NH_4F) with different anodic oxidation parameters (Figure 4). The parameters included electrolyte concentration, applied potential, and time. The samples with more uniform porous nanostructures were characterized in terms of their cross-sectional morphologies, chemical compositions, and crystal structures. The results proved that the Ta_2O_5 coating is well prepared on the porous Ta surface and facilitates cell adhesion. Ding et al. (Ding et al., 2018) prepared micro/nanostructures on Ta-coated surfaces by combining anodic oxidation and plasma spraying. The experimental results showed that the coating facilitates the proliferation, adhesion, and diffusion of human BMSCs, and the nanocoating increased gene expression by 1.5–2.1 times compared with the microporous Ta coating. An *in vitro* study (Wang et al., 2012) suggested that the modified Ta scaffold enhances rabbit BMSC adhesion and proliferation and upregulates the expression of osteogenic markers, ALP, Col-I, and OCN. Other *in vitro* experiments indicated that the anodic oxidation-modified Ta surface can facilitate the adhesion and proliferation of human osteoblasts, upregulate ALP expression in these osteoblasts, and promote bone nodule production and mineralization and deposition of the bone matrix (Frandsen et al., 2014).

4.3 Micro-arc oxidation

MAO, also known as plasma electrolytic oxidation, is an optimized version of anodic oxidation because of the formation of a ceramic coating mainly composed of substrate oxides and compounds containing electrolyte components (Kung et al., 2010). Studies have suggested that MAO coating incorporates bioactive elements (e.g., calcium, phosphorus) with certain electrolytes (Deng et al., 2010; Bai et al., 2011). MAO is superior to anodic oxidation in all aspects. The surface layer prepared by MAO has better corrosion resistance and wear resistance and cannot be easily separated. Gao et al. (Gao et al., 2014) employed MAO combined with alkali treatment to form an oxide coating on the porous Ta surface. *In vivo* and *in vitro* tests have confirmed that the coating enhances bioactivity *in vitro*, promotes angiogenesis and new bone formation, and facilitates new bone tissue infiltration into the scaffold. Huang et al. (Huang et al., 2018) used MAO to prepare oxide coating on the surface of Ti–Ta composites. The surface roughness and hydrophilicity of the treated area improved, which

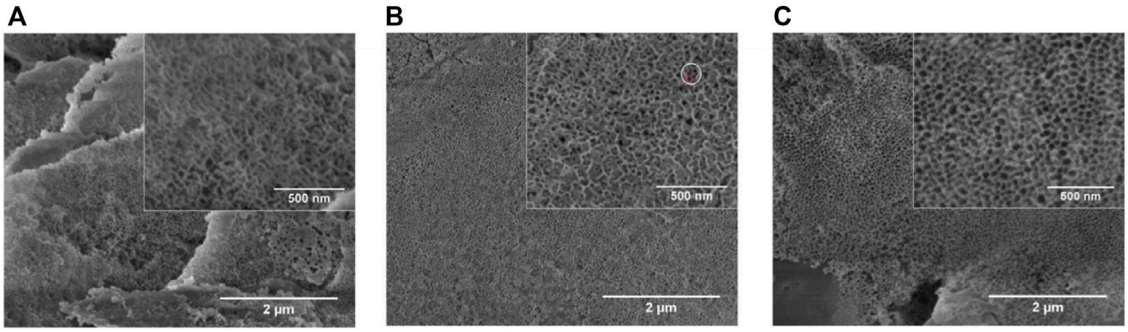

FIGURE 4
Scanning electron microscopy (SEM) images of Ta with different NH_4F concentrations (Fialho et al., 2020). *Copyright ©2020 Published by Elsevier Ltd.*

promoted the proliferation and differentiation of osteoblast-like SaOS-2 cells (Figures 5, 6).

4.4 Biomimetic calcium phosphate coating

Calcium phosphate coating has bone conductivity and promotes bone inward growth because of its physical and chemical similarities to human bones. Technological breakthroughs have recently been made in depositing the calcium phosphate layer on the substrate, such as electrochemical deposition, sol-gel, plasma immersion injection, and plasma spraying. Moreover, the formed crystals are more similar to natural bone minerals in structure than hydroxyapatite (HA) and tri-or tetra-calcium phosphate (Klein et al., 1994). The calcium phosphate biomimetic coating is more conducive to the differentiation of bone marrow stromal cells into osteoblasts than conventional coatings (Ohgushi and Caplan, 1999). Antonio et al. (Antonio et al., 2019) recently prepared a HA coating on a pure Ta surface through MAO. Compared with Ta coating, the HA coating significantly improved surface bioactivity. In addition, Ta_2O_5 added to the HA coating provides more calcium absorption sites and increases HA formation, thereby accelerating bone integration (Horandghadim et al., 2019).

4.5 Surface functional modification

Surface functionalization refers to modifying the implant surfaces by using growth factors, extracellular matrix proteins, peptides, and drugs to form surfaces with specific functions (García-Gareta et al., 2017). An ideal functional coating comprises uniformly incorporated natural or synthetic bioactive substances, such as bone morphogenetic proteins (BMPs), vascular endothelial growth factor, transforming growth factor, and antibiotics, which are stably released in a localized and controlled manner (Tobin, 2017). In this process, a minimum effective dose is essential for avoiding toxicity and side effects.

Wang et al. (Qian et al., 2018) used a rabbit osteochondral defect model of the femoral condyle and implanted BMP-7-coated porous Ta or uncoated porous Ta into the bone defect area. At 16 weeks after surgery, the micro-CT examination revealed that the new bone volume fraction and the quality and quantity of new bone trabeculae in the coated porous Ta group were superior to those in the uncoated group. Histological studies confirmed that more bone tissue was formed in the pores of the Ta scaffold in the coated group. The biomechanical analysis revealed that the maximum pullout force was significantly higher in the coated group than in the uncoated group. By building a 15-mm segmental defect model in the middle segment of the right radius of New Zealand white rabbits, Wang et al. (Wang et al., 2017b) verified the performance of an RGD peptide-coated porous Ta scaffold. The results indicated that bone formation at the interface and in the pores increased after application of the RGD peptide coating, thereby enhancing bone defect repair. Ma et al. (Ma et al., 2020b) used polydopamine (PDA) to load magnesium (Mg) on the surface of a porous 3D-printed Ta scaffold to enhance their surface bioactivity (Figure 7). The Ta-PDA-Mg scaffold released Mg ions and exhibited excellent biocompatibility (Figure 8). The Ta-PDA-Mg scaffold effectively promoted angiogenesis and osseointegration in a rat femoral condylar bone defect model. Through the formation of drug-doped self-assembled films, bioactive agents could be continuously released through the functionalized porous Ta surface. Garbuz et al. (Garbuz et al., 2008) designed a porous Ta scaffold for the local release of alendronate, which was fixed by immersing calcium phosphate-coated porous Ta in an alendronate buffer solution at room temperature for 7 days. During the whole release process, compared with the control group, the locally released alendronate inhibited osteoclast activity, resulting in an increase in osteoblast activity, and eventually, promoting the formation of more new bone on the scaffold surface.

Although surface modifications have been widely used and continually improved, their clinical applications have been rare. Many studies need to be conducted for their effective and reliable clinical translations.

5 Biological performance research

After implants are placed in the body, they remain in the body as a foreign body for a long time. The implant interacts with the specific

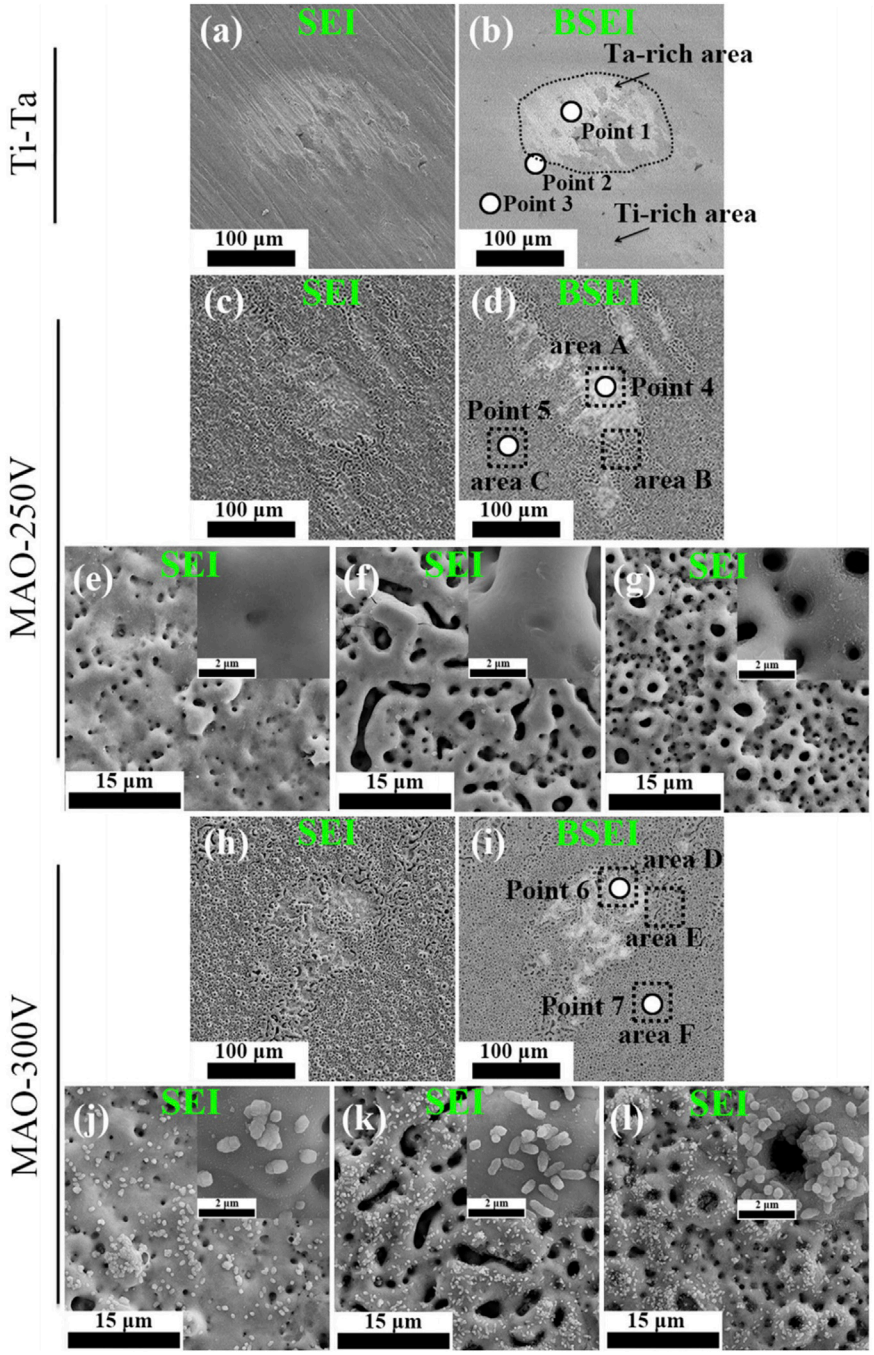

FIGURE 5
Secondary electron and backscattered electron SEM images showing the morphological features of various surfaces. Figures **(E–G)** and **(J–L)** correspond to areas **(A–F)** indicated by the black dashed lines in Figures **(D)** and **(I)**, respectively (Huang et al., 2018). *Copyright ©2018 Published by Elsevier Ltd.*

biological environment in the body until equilibrium is attained or the implant is removed from the body. As a bone implant material, porous tantalum allows a large number of new bone tissues to grow into the implant, showing excellent bone integration performance. Numerous scientific studies have attempted to quantitatively evaluate the biocompatibility and osteogenic properties of porous tantalum through *in vitro* cytotoxicity assay, *in vivo* segmental bone defect model, and histological analysis.

5.1 Cytotoxicity studies

Tantalum has been reported to show low cytotoxicity *in vivo* or *in vitro*, tissue or cell implants of various shapes. Liu et al. (Liu et al., 2022a) used FDA/PI dye solution to dye live and dead cells on the scaffold surface, respectively, and observed and photographed them through CLSM; live cells stained green and dead cells stained red, and fewer dead cells (red) were observed. Li et al. (LI et al., 2010b)

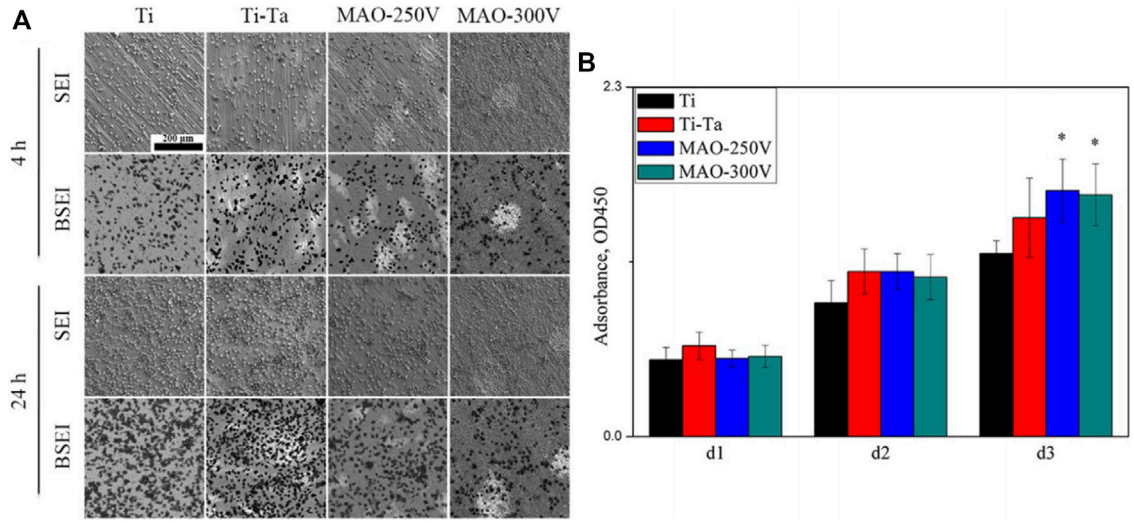

FIGURE 6
SEM images **(A)** and CCK-8 assay **(B)** showing the distribution and proliferation of SaOS-2 cells cultured on various surfaces. (Huang et al., 2018). *Copyright ©2018 Published by Elsevier Ltd.*

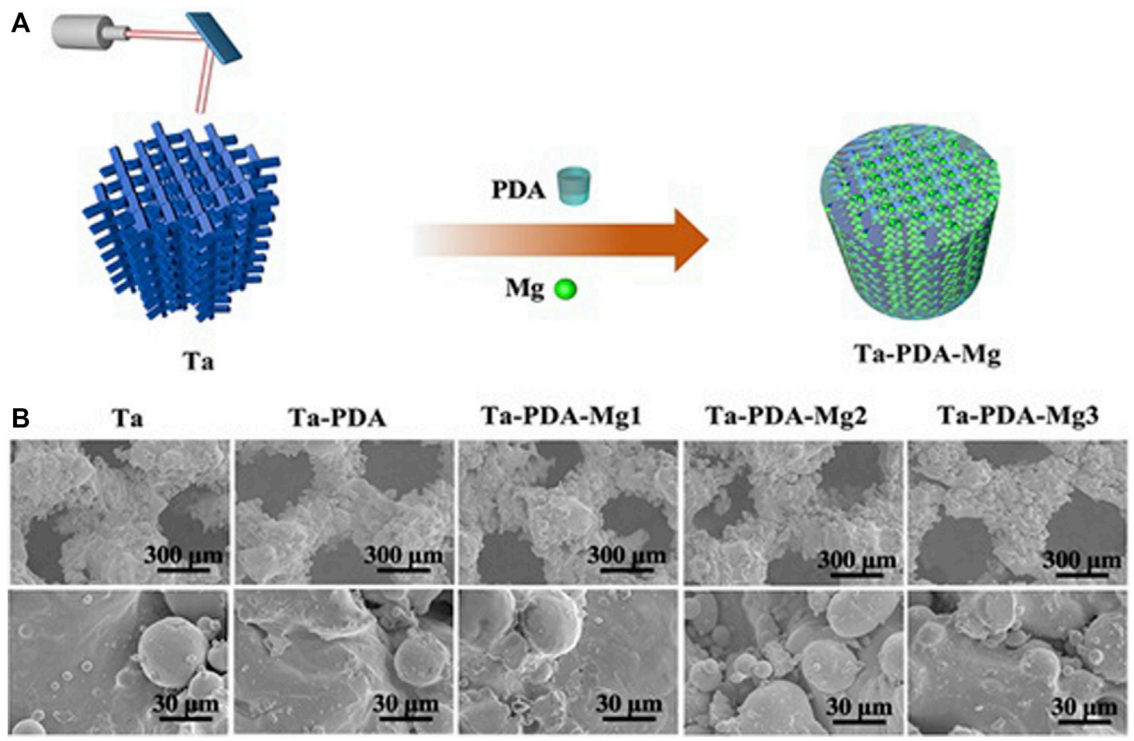

FIGURE 7
Schematics of Ta-PDA-Mg scaffold fabrication process **(A)**, and SEM images of the scaffold **(B)** (Ma et al., 2020b) *Copyright ©2020 Published by Elsevier Ltd.*

used osteoblast SaOS2 to evaluate the cytotoxicity of tantalum, titanium, niobium, molybdenum, niobium, and other common elements in titanium alloy and observed the cytotoxicity of these elements in powder and block. Cell experiments confirmed the cytotoxicity of titanium, niobium, molybdenum, and other metal powders, and molybdenum showed cytotoxicity in block. The safe ion concentrations of molybdenum, titanium and niobium were 8.5, 15.5, and 172.0 μg/L, respectively (a concentration lower than the

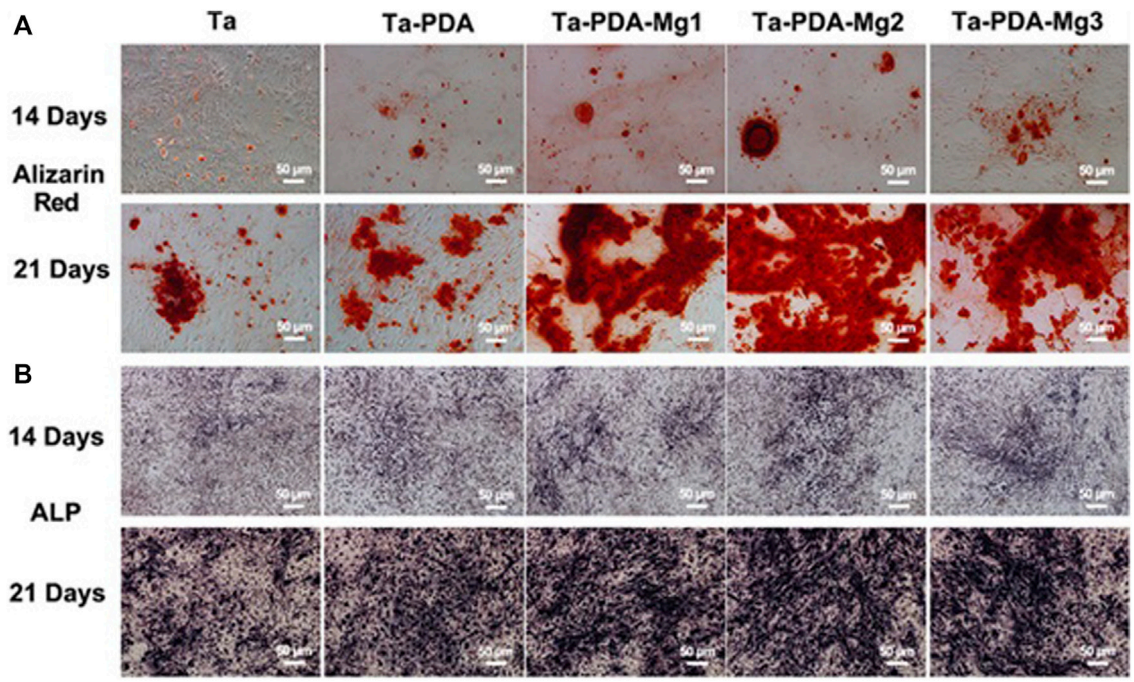

FIGURE 8
In vitro osteogenic evaluation of the Ta-PDA-Mg scaffold. Alizarin red staining **(A)** and ALP **(B)** of rBMSCs cultured with various extracts at 14 and 21 days (Ma et al., 2020b). *Copyright ©2020 Published by Elsevier Ltd.*

safe ion concentration is non-toxic), but no obvious cell damage was observed in tantalum. Wauthle et al. (WAUTHLE et al., 2015) placed mouse fibroblasts in the extract of porous tantalum scaffolds for 41 h and conducted *in vitro* experiments to evaluate their cytotoxicity. The results showed good biocompatibility and no cytotoxicity of scaffolds. In addition, tantalum metal can be easily combined with oxygen to form an oxide layer (Ta_2O_5) on the surface of porous tantalum implants, which not only prevents corrosion of the implants *in vivo* but also ensures stability over a wide pH range (Wang et al., 2012). Cell morphology and cell activity are also indicators to evaluate cytotoxicity. Gee, etc. (GEE et al., 2019) evaluated the porous tantalum between human fibroblasts and osteoblasts and proliferation of mesenchymal stem cells (MSCs). *In vitro* studies have shown that porous tantalum exerts neither any significant negative effect on fibroblasts after 28 days of continuous culture nor any inhibitory effect on the proliferation and behavior of osteoblasts or human MSCs.

5.2 Osseogenesis study

Osseointegration is the direct integration of phalanges and metals that allows the structural and functional integration of the living bone on implant surface (GEE et al., 2019). The process of bone integration may be affected by various factors (WANG et al., 2016b), which can be divided into two aspects: the bone–implant interface environment and the implant itself. Environmental factors include loading conditions, host bone characteristics, interface distance, local osteoblast, osteoclast concentration, systemic disease (diabetes, rheumatoid arthritis), and smoking (WANG et al., 2018), whereas implant factors include geometry, surface topography, and line design (KOBAYASHI et al., 2016). In general, tantalum metal is bioinert, that is, it does not stimulate bone growth (CHEN et al., 2012). However, porous tantalum has been shown to have satisfactory bone integration and bone conductivity. It allows the proliferation and differentiation of osteoblasts and promotes the growth of bones, tendons, and ligaments. Wei et al. (SHI et al., 2017) implanted porous tantalum rods into the hind legs of dogs. Three to 6 weeks after implantation, new osteoblast adhesion and new bone ingrosion were observed at the tantalum–host bone interface and pores through hard tissue biopsy. Fraser et al. (FRASER et al., 2019) implanted a dental implant with a titanium neck and root tip connected to an intermediate portion made of porous tantalum in a rabbit tibial repair model. They found that the middle part was in close contact with the surrounding soft and hard tissues. Studies have shown that tantalum surface properties affect the implant–bone interface microenvironment and play a crucial role in osteoblast proliferation and reconstruction as well as interfacial bone integration.

Many studies have attempted to explain the action mechanism of tantalum in bone tissue growth through the osteogenic signaling pathways including Wnt//β-catenin signaling pathway, BMP signaling pathway, TGF-β signaling pathway, and integrin signaling pathway (Figure 9). However, there are only a few biological studies and known mechanisms related to porous tantalum, despite complex crosstalk effects between these signaling pathways. More comprehensive, detailed, and in-depth mechanistic studies need to be conducted in the future.

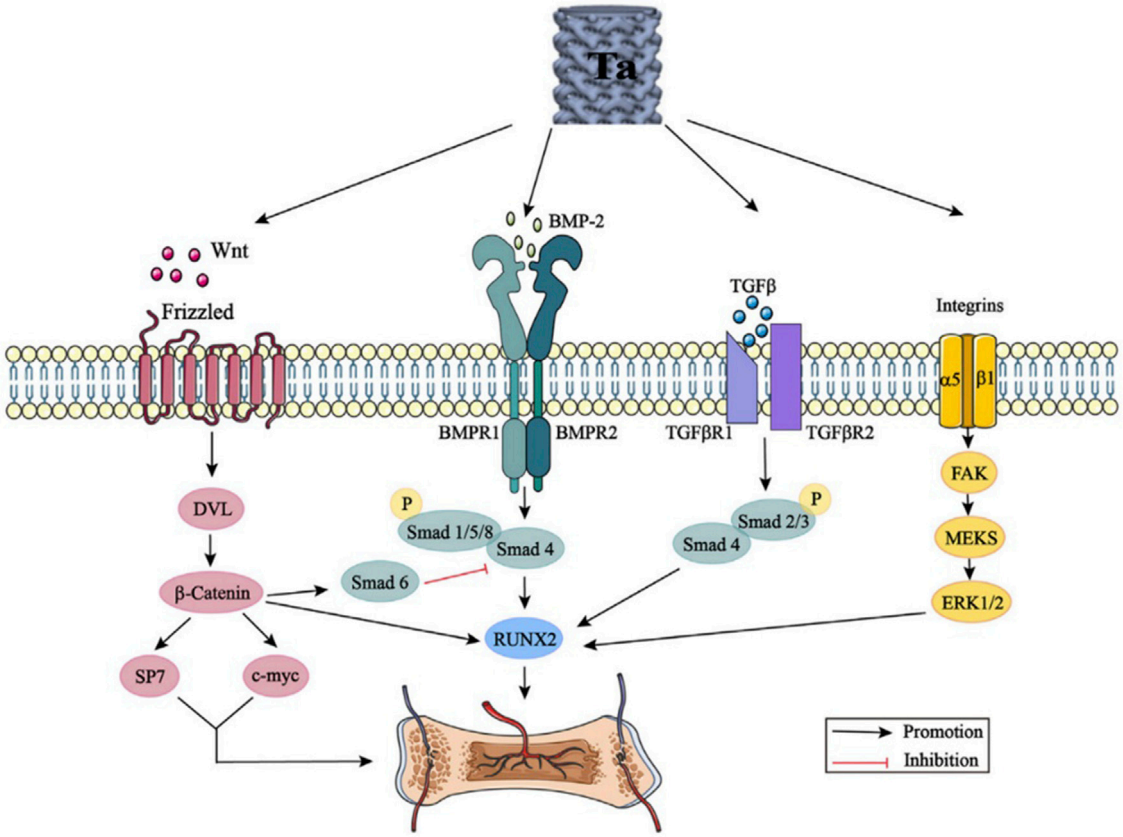

FIGURE 9
Tantalum activates the Wnt/β-catenin signaling pathway, BMP signaling pathway, TGF-β signaling pathway, and integrin signaling pathway by promoting the expression of Wnt, BMP-2, TGF-β, and integrins. DVL: disheveled; BMP: bone morphogenic proteins; Smad: small mother against decapentaplegic; Runx2: runt-related transcription factor 2; TGF-β: transforming growth factor-beta; FAK: focal adhesion kinase; and ERK: extracellular signal regulated kinase (Wang et al., 2022). From Wang et al., 2022 (Figure 3)

6 Clinical applications

Over the past decades, porous Ta implants have gained considerable attention, especially in the clinical orthopedics field. Porous metals applied in clinical practice mainly refer to trabecular metal (TM) produced by Zimmer (Minneapolis, MN, United States). TM is composed of porous Ta. Porous Ta scaffolds have been extensively used for clinical orthopedic applications, including the hip joint, knee joint, spine, foot and ankle joints, and oral cavity.

6.1 Hip joint

6.1.1 Femur head osteonecrosis

Necrosis of the femoral head (ONFH) is a pathological state, wherein the blood supply of the subchondral bone is reduced. Changes in bone trabecular structures and articular surface collapse are caused by multiple factors. According to the Steinberg classification, ONFH is divided into five phases. In Phase I and Phase II, when the non-operative treatment fails, doctors prefer core decompression with Ta TM rod implantation. Core decompression has long been a hip preservation treatment for early ONFH, whereas the lack of mechanical support for subchondral bone after necrotic bone debridement may lead to femoral head collapse (SCULLY Sean and Urbaniak, 1998). Thus, porous Ta rods, as a plausible substitute for the vascularized autofibular allograft, have allowed the maintenance of the bone defect portion after core decompression (Tsao et al., 2005; Wei et al., 2019).

Porous Ta rods are primarily used to maintain the subchondral plate structure and stimulate host bone osteogenesis, which can alleviate ONFH deterioration and delay the final conversion to total hip arthroplasty (THA), as indicated in most studies conducted in early- or middle-stage patients (Veillette et al., 2006; Shuler et al., 2007; Liu et al., 2010).

Although the long-term efficacy of Ta rods remains controversial, patient survival after the insertion of porous Ta rods is known to be affected by multiple factors such as disease stage, corticosteroid use, volume and location of osteonecrosis lesions, bone marrow edema, and joint effusion (Zhang et al., 2016; Zhang et al., 2021; Liu et al., 2022b). Accordingly, numerous optimized surgical techniques have been applied to improve the osteogenic capacity of porous Ta rods such as the combined technique involving bone marrow extraction from the iliac crest (Emilios et al., 2015), BMSCs, and graft (Pakos et al., 2015;

FIGURE 10
Multiple orthopedic applications for porous tantalum. Top row: monoblock acetabulum and a revision acetabular augment. Middle row: monoblock tibia, revision total knee arthroplasty augments, and salvage patella button. Bottom row: osteonecrosis implant and spine arthrodesis implants (Courtesy of Zimmer, Warsaw, IN) (Russell Levine et al., 2006). *Copyright ©2006 Published by Elsevier Ltd.*

Zhao et al., 2015). Nevertheless, long-term follow-up clinical trials are required to validate the effectiveness of the aforementioned modification methods.

6.1.2 Acetabular components of porous metals

Acetabular cups made of porous Ta that are used for primary THA are assembled by compressing ultra-high molecular polyethylene into elliptical porous Ta shells. For THA revision, modular and revision multi-hole porous Ta shells are available (Figure 10). Owing to their low elastic modulus, high friction coefficient, and superior osteoconductivity, porous Ta shells are beneficial for maintaining or even increasing the bone mass of the adjacent acetabulum and contribute to revision surgery, when needed (Vutescu et al., 2017; Beckmann et al., 2020). In a prospective study (Macheras et al., 2008) with 8–10 years of follow-up of 151 hips after primary THA, although the periacetabular gaps of length 1–5 mm were found in the early 25 acetabular cups, the aforementioned gaps disappeared after 24 weeks. Follow-up X-ray images confirmed the absence of light transmittance, osteolysis of the adjacent bone, polyethylene wear debris, and cup loosening. The aforementioned analyses verified the advantage of porous Ta cups in design and their clinical efficacy.

In a prospective clinical study (Duan et al., 2021) on the clinical application of Ta, eight patients (two male and six female patients, 12 hips, mean age: 43.75 ± 7.81 years) with Crowe I developmental dysplasia of the hip (DDH) were subjected to hip reconstruction by using an additional customized porous Ta acetabular patch. After computerized modeling of the patients' hip joint separately, a software was used to design the best acetabular patch, and then, the finite element analysis was performed to ensure biomechanical requirements. Finally, an AM-generated customized and personalized porous Ta acetabular patch was implanted. After an average follow-up of 8.2 months, the visual analog score (VAS) decreased significantly from 2.92 ± 0.79 before the operation to 0.83 ± 0.72 after the operation, and the Harris score decreased significantly from 69.67 ± 4.62 before the operation to 84.25 ± 4.14 after the operation. Imaging revealed that the acetabular patch was in close contact with the iliac bone, and no loosening or progression of osteoarthritis occurred. Therefore, the application of AM-produced individualized porous Ta patch for reconstructing

acetabular bone defects can reduce the difficulty of surgery and delay osteoarthritis progression.

6.2 Knee joint replacement

Porous Ta prostheses for knee replacement comprise single tibial components, tibial or femoral cones and prostheses, and patellar prostheses (Huang et al., 2021). The mechanical and biological properties of the porous Ta help achieve the primary stability of the tibial component and the patients' long-term survival. Short-term and long-term results suggest that the cemented or non-cemented single tibial assembly has high efficacy in relatively young and active patients (Ivan et al., 2016; Defrancesco et al., 2018; De-Wei et al., 2019). Histological examination of the porous Ta tibial component removed from a chronically infected knee prosthesis revealed significant inward bone outgrowth at the pile and pile–substrate interfaces (rather than the substrate), which suggested remarkable bone–implant integration even in an infected environment (Sambaziotis et al., 2012; Peter et al., 2018).

6.3 Spinal surgery

In cervical and lumbar surgery, porous Ta has been successfully applied as an effective intervertebral device because of its unique biomechanical properties (Marko et al., 2016).

A prospective randomized controlled clinical trial (Fernandez-Fairen et al., 2008) confirmed the efficacy of a porous Ta cage for anterior cervical fusion. Compared with the conventional autogenous iliac bone transplantation in combination with the anterior plate, the porous Ta cage exhibited a considerable fusion rate (89% vs. 85%) and postoperative stability at 2-year follow-up, without additional fixation and graft harvest-related damage. At 11-year follow-up, although the implant settlement ranged from 2 to 3 mm, the clinical and radiological results of patients who received a single-hole Ta inter body fusion cage for inter body fusion were satisfactory, and 12 patients exhibited no obvious complications. Furthermore, several observational studies have confirmed that porous Ta is efficacious in terms of the intervertebral fusion rate, low complication rate, and improved short-term or long-term postoperative assessment scores, including SF-36, neck disability index, and VAS (Papacci et al., 2016; Rissmann, 1055; Wen-Qiang et al., 2019; Wang et al., 2019b).

6.4 Shoulder replacement

Zimmer launched three types of TM implants for shoulder replacement. X-ray images of at least 2 years of one-stage shoulder replacement with porous Ta prosthesis for the treatment of complex proximal humeral fractures were satisfactory (Li and Jiang, 2013). TM prosthesis demonstrated a better healing effect than traditional prostheses in a hemi joint replacement. The first-generation glenoid components (Zimmer) were introduced for total shoulder arthroplasty in 2003 but were withdrawn after the reports of prosthesis failures in 2005. In 2009, the second-generation glenoid components with a changed design were introduced. The satisfactory function, subjective satisfaction, and clinical manifestation of 3-year average follow-up were reported (Merolla et al., 2016). Porous Ta is not omnipotent, and complications should be avoided based on the clinical experience. In addition to bone growth, antibacterial performance is crucial for porous implants both in the short and long term. Thus, future studies should pay more attention to the development of implants with antibacterial properties.

6.5 Fractures

Internal fixation materials used for clinical fracture treatment usually involve high-strength stainless steel and Ti alloys. Using Ta-coated Ti6Al4V bone plates, Liu et al. (Liu et al., 2021b) treated tibia fractures in goats. The Ta-coated bone plates effectively fixed the fractures. Histologically, the new bone was formed at the interface with excellent osseointegration with the host bone.

A randomized controlled trial (Zhao et al., 2022) compared the clinical efficacy of cannulated compression screws and pressurized porous tantalum screws (PTS) in femoral neck fracture (FNF) treatment. The PTS exhibited a higher fusion rate and better postoperative stability than the cannulated compression screws at the 3-month follow-up. The fixation PTS for FNF at the center could avoid blood supply destruction in the femoral head, reduced the incidence of FNF postoperative complications, induced early bone ingrowth, and promoted fracture healing.

6.6 Foot and ankle surgery

The porous Ta spacer, considered a promising alternative to a conventional autograft or bone allograft, has been used for ankle arthrodesis without limitation by size, volume, and origin (Sagherian and Claridge, 2019; Tiusanen et al., 2019). Sundet et al. (Ms et al., 2021) used retrograde intramedullary nails, porous Ta spacers, and bone induction pads combined with an autologous bone marrow concentrate to perform revision surgeries on 30 patients (31 ankles) with failed total ankle arthroplasties. The mean fusion rate at the mean 23-month follow-up was 93. Most patients expressed satisfaction with the procedure in terms of pain relief and activity improvement. Kreulen et al. (Kreulen et al., 2017) introduced a novel strategy for reconstructive surgery in two patients with failed total ankle replacements and four patients with ankle collapses after infection. They introduced the porous Ta spacer to autologous bone marrow obtained from the femoral bone marrow cavity by using a reamer/irrigator/aspirator and fixed it with a tibial calcaneal nail and then supplemented with BMP-2 or platelet-derived growth factor to facilitate bone fusion. Using this novel approach, a thorough bone fusion occurred at the bone–implant interface in the early stages of 4–6 weeks after surgery, and no failed cases were reported.

6.7 Oral cavity

Rough surfaces extensively employed in dental implants facilitate osseointegration and angiogenesis by increasing the surface energy, expanding the bone–implant contact area, improving surface hydrophilicity, and promoting the adhesion of

mesenchymal cells or osteoblast progenitors (Maxim et al., 2014; Bencharit et al., 2019). Porous Ta is superior to several other metals in bone growth and bone–implant contact. A clinical study (Brauner et al., 2015) suggests that dental implants made using porous Ta TM (PTTM) are safe and effective and cause no serious complications. Edelmann et al. (Edelmann et al., 2018) compared the peri-implant bone remodeling of PTTM-enhanced titanium implants and conventional titanium alloy implants in the first year after implantation. They found that the patients with PTTM-enhancing implants had lower bone loss rates than the controls (David et al., 2019; Piglionico et al., 2020).

7 Future development

Tantalum possesses extremely stable physical and chemical properties, in addition to excellent biocompatibility and other properties. Tantalum is one of the most promising bone graft replacement materials and has been increasingly favored by researchers. Bone implants made of porous tantalum materials are currently used in the treatment of bone defects in various parts of the body, and the short-term follow-up results also show relatively ideal clinical effects. However, as a material implanted in patients for a long time, it has some limitations. Combined with the research progress at home and abroad, we acknowledge the following problems:

(1) Porous tantalum is an inert material that cannot provide growth factors. Hence, surface modification studies are needed to determine whether it can be applied in combination with growth factors. Attempts can also be made to load antibiotics into the porous structure or to establish composite systems on the surface to prevent or treat infection of the joint around the implant.
(2) Tantalum is relatively rare, expensive, and difficult to process, which limit its clinical application. Therefore, breaking through the bottleneck of processing technology, reducing the development cost, and exploiting the excellent performance of porous tantalum implant materials for medical use are major research directions.
(3) The mechanical properties of porous tantalum can be matched with those of bone tissues by optimizing the design of the internal structure.
(4) Tantalum and porous tantalum surface modification technology is in a stage of rapid development. With the continuous optimization of this technology, its clinical application is expected to increase greatly. Presently, porous tantalum coating applied in clinic has not reached the ideal state, and long-term clinical follow-up data of large samples and multi-centers are lacking; hence, conducting a comprehensive evaluation of the safety and effectiveness of porous tantalum bone implants is challenging.

8 Summary

This systematic review elaborates on the preparation techniques, surface modification, and orthopedic applications of porous Ta scaffolds. Porous Ta scaffolds manufactured using different techniques exhibit excellent corrosion resistance, biocompatibility, osseointegration, and osteoconductivity, which highlight their great potential as orthopedic implants. The preparation and surface modification techniques of these scaffolds have been the focus of research.

CVD, an early manufacturing approach, is a well-established technique for manufacturing porous Ta scaffolds. Porous Ta implants in clinics are fabricated using this method. However, the shape of bone defects varies among patients depending on the anatomical sites and other conditions. Commercial CVD-manufactured porous Ta implants usually do not meet personalized requirements. An emerging technique, AM, can tailor patient-specific implants. AM-produced Ta implants are expected to be extensively used in orthopedic surgery. Regarding the modification of porous Ta, various methods (e.g., surface chemical modification and surface functionalization modification) have been developed to improve bioactivity. Modified porous Ta exhibits great potential in resolving various pathological conditions (e.g., osteoporosis, infection, diabetes, and even tumors).

Additional studies are required to explore the potential of porous Ta. With the booming evolution of porous Ta fabrication techniques, the clinical application of porous Ta is expected to expand in the future.

Author contributions

Literature search and data analysis, XW; writing—original draft preparation, XW; writing—review and editing, KZ, YL, HX; supervision, BW. All authors have read and agreed to the published version of the manuscript.

Funding

This work was supported by China Postdoctoral Science Foundation (grant numbers 2020M670715, 2021T140079); Dalian University Doctoral Foundation (grant numbers 2020QL015); Dalian high-level talent innovation support plan (grant numbers 2019RQ016).

Conflict of interest

The authors declare that the research was conducted in the absence of any commercial or financial relationships that could be construed as a potential conflict of interest.

Publisher's note

References

Amin-Yavari, S., Wauthle, R., VanDer Stok, J., Riemslag, A., Janssen, M., Mulier, M., et al. (2013). Fatigue behavior of porous biomaterials manufactured using selective laser melting. *Mater. Sci. Eng. C* 33 (8), 4849–4858. doi:10.1016/j.msec.2013.08.006

Amit, B., Mitra, I., Shivaram, A., Dasgupta, N., and Bose, S. (2019). Direct comparison of additively manufactured porous titanium and tantalum implants towards *in vivo* osseointegration. *Addit. Manuf.* 28, 259–266. doi:10.1016/j.addma.2019.04.025

Antonio, R. F., Rangel, E. C., Mas, B. A., Duek, E. A., and Cruz, N. C. (2019). Growth of hydroxyapatite coatings on tantalum by plasma electrolytic oxidation in a single step. *Surf. Coat. Technol.* 357, 698–705. doi:10.1016/j.surfcoat.2018.10.079

Ao, Y., Guo, L., Chen, H., He, C., Yang, P., Fu, D., et al. (2022). Application of three-dimensional-printed porous tantalum cones in total knee arthroplasty revision to reconstruct bone defects. *Front. Bioeng. Biotechnol.* 10. doi:10.3389/fbioe.2022.925339

Bai, Y., Park, I. S., Lee, S. J., Bae, T. S., Duncan, W., Swain, M., et al. (2011). One-step approach for hydroxyapatite-incorporated TiO2 coating on titanium via a combined technique of micro-arc oxidation and electrophoretic deposition. *Appl. Surf. Sci.* 257 (15), 7010–7018. doi:10.1016/j.apsusc.2011.03.058

Beckmann, N. A., Bitsch, R. G., Schonhoff, M., Siebenrock, K. A., Schwarze, M., and Jaeger, S. (2020). Comparison of the primary stability of porous tantalum and titanium acetabular revision constructs. *Materials* 13 (7), 1783. doi:10.3390/ma13071783

Bencharit, S., Morelli, T., Barros, S., Seagroves, J. T., Kim, S., Yu, N., et al. (2019). Comparing initial wound healing and osteogenesis of porous tantalum trabecular metal and titanium alloy materials. *J. Oral Implant.* 45, 173–180. doi:10.1563/aaid-joi-d-17-00258

Brauner, E., Guarino, G., Jamshir, S., Papi, P., Valentini, V., Pompa, V., et al. (2015). Evaluation of highly porous dental implants in postablative oral and maxillofacial cancer patients: A prospective pilot clinical case series report. *Implant Dent.* 24 (5), 631–637. doi:10.1097/id.0000000000000295

Brunello, G., Sivolella, S., Meneghello, R., Ferroni, L., Gardin, C., Piattelli, A., et al. (2016). Powder-based 3D printing for bone tissue engineering. *Biotechnol. Adv.* 34 (5), 740–753. doi:10.1016/j.biotechadv.2016.03.009

Chang, Yao, and Webster Thomas, J. (2006). Anodization: A promising nano-modification technique of titanium implants for orthopedic applications. *J. Nanosci. Nanotechnol.* 6 (9-10), 2682–2692. doi:10.1166/jnn.2006.447

Chang, Y-Y., Huang, H-L., Chen, H-J., Lai, C-H., and Wen, C-Y. (2014). Antibacterial properties and cytocompatibility of tantalum oxide coatings. *Surf. Coatings Technol.* 32, 259. doi:10.1116/1.4862543

Chen, G., Deng, C., and Li, Y. P. (2012). TGF-β and BMP signaling in osteoblast differentiation and bone formation. *Int. J. Biol. Sci.* 8 (2), 272–288. doi:10.7150/ijbs.2929

David, F., Paul, F., Carlo, E., and Luiz, M. (2019). Biomechanical analysis of the osseointegration of porous tantalum implants. *J. Prosthet. Dent.* 123, 811. doi:10.1016/j.prosdent.2019.09.014

De-Wei, Z., Zhao, Z-J., and Bao-yi, L. (2019). Biocompatible porous tantalum metal plates in the treatment of tibial fracture. *Orthop. Surg.* 11, 325. doi:10.1111/os.12432

Defrancesco, C., Canseco, J., José, A., Nelson, C. L., and Kamath, A. F. (2018). Uncemented tantalum monoblock tibial fixation for total knee arthroplasty in patients less than 60 Years of age: Mean 10-year follow-up. *JBJS* 100 (10), 865–870. doi:10.2106/jbjs.17.00724

Deng, F., Zhang, W., Zhang, P., Liu, C., and Ling, J. (2010). Improvement in the morphology of micro-arc oxidised titanium surfaces: A new process to increase osteoblast response. *Mater. Sci. Eng. C* 30 (1), 141–147. doi:10.1016/j.msec.2009.09.010

Dias-Netipanyj, M. F., Sopchenski, L., Gradowski, T., Elifio-Esposito, S., Popat, K. C., and Soares, P. (2020). Crystallinity of TiO(2) nanotubes and its effects on fibroblast viability, adhesion, and proliferation. *J. Mat. Sci. Mat. Med.* 31, 94. doi:10.1007/s10856-020-06431-4

Ding, D., outao, X., Kai, L., Huang, L., and Zheng, X. (2018). Micro/Nano structural tantalum coating for enhanced osteogenic differentiation of human bone marrow stem cells. *Materials* 11 (4), 546. doi:10.3390/ma11040546

Dou, X., Wei, X., Liu, G., Wang, S.i, Lv, Y., Li, J.i, et al. (2019). Effect of porous tantalum on promoting the osteogenic differentiation of bone marrow mesenchymal stem cells *in vitro* through the MAPK/ERK signal pathway. *J. Orthop. Transl.* 19 (C), 81–93. doi:10.1016/j.jot.2019.03.006

Duan, X., Wang, B., Yang, L., and Kadakia Anish, R. (2021). Applications of 3D printing technology in orthopedic treatment[J]. *Biomed Res. Int.* doi:10.1155/2020/7250528

Edelmann, A. R., Patel, D., Allen, R. K., Chad, J. G., Al, M. B., Sompop, B., et al. (2018). Retrospective analysis of porous tantalum trabecular metal–enhanced titanium dental implants. *J. Prosthet. Dent.* 121, 404. doi:10.1016/j.prosdent.2018.04.022

Emilios, E., Pakos, P., Nikolaos, K. P., Spyridon, A. S., Antonios, K., Georgios, G., et al. (2015). Modified porous tantalum rod technique for the treatment of femoral head osteonecrosis. *World J. Orthop.* 6, 829. doi:10.5312/wjo.v6.i10.829

Ercan, B., Taylor, E., Alpaslan, E., and Webster, T. J. (2011). Diameter of titanium nanotubes influences anti-bacterial efficacy. *Nanotechnology* 22 (29), 295102. doi:10.1088/0957-4484/22/29/295102

Fernandez-Fairen, M., Sala, P., Dufoo, M., Ballester, J., Murcia, A., and Merzthal, L. (2008). Anterior cervical fusion with tantalum implant: A prospective randomized controlled study. *Spine* 33 (5), 465–472. doi:10.1097/brs.0b013e3181657f49

Fialho, L., Alves, C., Marques, L. S., and Carvalho, S. (2020). Development of stacked porous tantalum oxide layers by anodization. *Appl. Surf. Sci.* 511, 145542. doi:10.1016/j.apsusc.2020.145542

Fialho, L., and Carvalho, S. (2019). Surface engineering of nanostructured Ta surface with incorporation of osteoconductive elements by anodization. *Appl. Surf. Sci.* 495, 143573. doi:10.1016/j.apsusc.2019.143573

Frandsen, C. J., Brammer, K. S., Noh, K., Johnston, G., and Jin, S. (2014). Tantalum coating on TiO2 nanotubes induces superior rate of matrix mineralization and osteofunctionality in human osteoblasts. *Mater. Sci. Eng. C* 37, 332–341. doi:10.1016/j.msec.2014.01.014

Fraser, D., Mendonca, G., Sartori, E., Funkenbusch, P., Ercoli, C., and Meirelles, L. (2019). Bone response to porous tantalum implants in a gap-healing model. *Clin. Oral Implants Res.* 30 (2), 156–168. doi:10.1111/clr.13402

Gao, H., Jie, Y. F., Wang, Z. Q., Wan, H., Gong, L., Lu, R. C., et al. (2014). Bioactive tantalum metal prepared by micro-arc oxidation and NaOH treatment. *J. Mater. Chem. B* 2 (9), 1216. doi:10.1039/c3tb21521k

Gao, H., Yang, J., Jin, X., Qu, X., Zhang, F., Zhang, D., et al. (2021). Porous tantalum scaffolds: Fabrication, structure, properties, and orthopedic applications. *Mater. Des.* 210, 110095. doi:10.1016/j.matdes.2021.110095

Garbuz, D. S., Hu, Y., Kim, W. Y., Duan, K., Masri, B. A., Oxland, T. R., et al. (2008). Enhanced gap filling and osteoconduction associated with alendronate-calcium phosphate-coated porous tantalum. *J. Bone Jt. Surg. Am.* 90, 1090–1100. doi:10.2106/jbjs.g.00415

García-Gareta, E., Hua, J., Orera, A., Kohli, N., Knowles, J. C., and Blunn, G. W. (2017). Biomimetic surface functionalization of clinically relevant metals used as orthopaedic and dental implants. *Biomed. Mat. (Bristol, Engl.* 13, 015008. doi:10.1088/1748-605x/aa87e6

Gee, E. C. A., Eleotério, R., Bowker, L. M., Saithna, A., and Hunt, J. A. (2019). The influence of tantalum on human celll ineages important for healing in soft-tissue reattachment surgery: Anin-vitroanalysis. *J. Exp. Orthop.* 6 (1), 40–46. doi:10.1186/s40634-019-0210-8

George, A. B. Nair (2018). *Porous tantalum: A new biomaterial in orthopedic surgery, fundamental biomater.* Metals: Elsevier.

Ghouse, S., Babu, S., Nai, K., Hooper, P. A., and Jeffers, J. R. (2018). The influence of laser parameters,scanning strategies and material on the fatigue strength of a stochastic porous structure. *Addit. Manuf.* 22, 290–301. doi:10.1016/j.addma.2018.05.024

Guglielmotti María, B., Olmedo Daniel, G., and Cabrini Rómulo, L. (2000). Research on implants and osseointegration. *Periodontology* 2019 (1), 79. doi:10.1111/prd.12254

Han, Q., Wang, C., Chen, H., Zhao, X., and Wang, J. (2019). Porous tantalum and titanium in orthopedics: A review. *ACS Biomaterials Sci. Eng.* 5 (11), 5798–5824. doi:10.1021/acsbiomaterials.9b00493

Hedayati, R., Hosseini-Toudeshky, H., Sadighi, M., Mohammadi-Aghdam, M., and Zadpoor, A. (2016). Computational prediction of the fatigue behavior of additively manufactured porous metallic biomaterials. *Int. J. Fatigue* 84, 67–79. doi:10.1016/j.ijfatigue.2015.11.017

Hendrik, T, Lang, N P., Susanne, . B., and Stadlinger, B. (2012). Osseointegration – communication of cells. *Clin. Oral Implants Res.* 23 (10), 1127–1135. doi:10.1111/j.1600-0501.2011.02327.x

Horandghadim, N., Khalil-Allafi, J., and Urgen, M. (2019). Effect of Ta(2)O(5) content on the osseointegration and cytotoxicity behaviors in hydroxyapatite-Ta(2)O(5) coatings applied by EPD on superelastic NiTi alloys. *Mat. Sci. Eng. C Mat. Biol. Appl.* 102, 683–695. doi:10.1016/j.msec.2019.05.005

Hu, Q., Ting, L., Lei, P. E., and Hu, Y. (2020). Additively manufactured tantalum implants for repairing bone defects: A systematic review. *Tissue Eng.* 27, 166. doi:10.1089/ten.TEB.2020.0134

Huang, G., Pan, S. T., and Qiu, J. X. (2021). The clinical application of porous tantalum and its new development for bone tissue engineering. *Materials* 14 (10), 2647. doi:10.3390/ma14102647

Huang, Q., Li, X., Elkhooly, T. A., Xu, S., Liu, X., Feng, Q., et al. (2018). The osteogenic, inflammatory and osteo-immunomodulatory performances of biomedical Ti-Ta metal-metal composite with Ca-and Si-containing bioceramic coatings. *Colloids Surf. B Biointerfaces* 169, 49–59. doi:10.1016/j.colsurfb.2018.05.010

Ivan, D., D'Apolito, R., Sculco, P. K., Poultsides, L. A., and Gasparini, G. (2016). Total knee arthroplasty using cementless porous tantalum monoblock tibial component: A minimum 10-year follow-up. *J. Arthroplasty* 31 (10), 2193–2198. doi:10.1016/j.arth.2016.03.057

Klein, C. P., Patka, P., Wolke, J. G., de Blieck-Hogervorst, J. M., and de Groot, K. (1994). Long-term *in vivo* study of plasma-sprayed coatings on titanium alloys of tetracalcium phosphate, hydroxyapatite and α-tricalcium phosphate. *Biomaterials15* 15, 146–150. doi:10.1016/0142-9612(94)90264-x

Kobayashi, Y., Uehara, S., Udagawa, N., and Takahashi, N. (2016). Regulation of bone metabolism by Wnt signals. *J. Biochem.* 159 (4), 387–392. doi:10.1093/jb/mvv124

Kreulen, C., Lian, E., and Giza, E. (2017). Technique for use of trabecular metal spacers in tibiotalocalcaneal arthrodesis with large bony defects. *Foot Ankle Int.* 38 (1), 96–106. doi:10.1177/1071100716681743

Krishna Balla, V., Bodhak, S., Bose, S., and Amit, B. (2010). Porous tantalum structures for bone implants: Fabrication, mechanical and *in vitro* biological properties. *Acta Biomater.* 6 (8), 3349–3359. doi:10.1016/j.actbio.2010.01.046

Kung, K. C., Lee, T. M., and Lui, T. S. (2010). Bioactivity and corrosion properties of novel coatings containing strontium by micro-arc oxidation. *J. Alloys Compd.* 508 (2), 384–390. doi:10.1016/j.jallcom.2010.08.057

Kuo, T.-Y., Chin, W.-H., Chien, C.-S., and Hsieh, Y.-H. (2019). Mechanical and biological properties of graded porous tantalum coatings deposited on titanium alloy implants by vacuum plasma spraying. *Surf. Coat. Technol.* 372, 399–409. doi:10.1016/j.surfcoat.2019.05.003

Li, F., and Jiang, C. (2013). Trabecular metal shoulder prosthesis in the treatment of complex proximal humeral fractures. *Int. Orthop.* 37 (11), 2259–2264. doi:10.1007/s00264-013-2061-8

Li, Y., Wong, C., Xiong, J., Hodgson, P., and Wen, C. (2010a). Cytotoxicity of titanium and titanium alloying elements. *J. Dent. Res.* 89 (5), 493–497. doi:10.1177/0022034510363675

Li, Y., Xiong, J., Hodgson, P. D., and Wen, C. (2010b). Effects of structural property and surface modification of Ti6Ta4Sn scaffolds on the response of SaOS2 cells for bone tissue engineering. *J. Alloys Compd.* 494 (1-2), 323–329. doi:10.1016/j.jallcom.2010.01.026

Liu, B., Ma, Z., Li, J., Xie, H., Wei, X., Wang, B., et al. (2021). Experimental study of a 3D printed permanent implantable porous Ta-coated bone plate for fracture fixation. *Bioact. Mater.* 10, 269–280. doi:10.1016/j.bioactmat.2021.09.009

Liu, G., Wang, J., Yang, S., Xu, W., Ye, S., and Xia, T. (2010). Effect of a porous tantalum rod on early and intermediate stages of necrosis of the femoral head. *Biomed. Mater.* 5 (6), 065003. doi:10.1088/1748-6041/5/6/065003

Liu, P., Yuan, B., Xiao, Z., Xie, H., Zhu, X., and Zhang, X. (2022). Construction of bioactive HA coating on porous tantalum scaffolds and its preliminary biological evaluation. *Rare metal Mater. Eng.* 51 (01), 225–231.

Liu, W., Hu, Y., Huang, Z., Shi, Z., and Xiao, J. (2022). Analysis of peripheral bone reconstruction after the failure of hip osteonecrosis treatment with porous tantalum rod implantation. *Int. Orthop.* 46, 1323–1330. doi:10.1007/s00264-022-05334-z

Liu, Y., Yang, Y., Mai, S., Wang, D., and Song, C. (2015). Investigation into spatter behavior during selective laser melting of AISI 316L stainless steel powder. *Mater. Des.* 87, 797–806. doi:10.1016/j.matdes.2015.08.086

Liu, Y., Bao, C., Wismeijer, D., and Wu, G. (2015). The physicochemical/biological properties of porous tantalum and the potential surface modification techniques to improve its clinical application in dental implantology. *Mater. Sci. Eng. C* 49, 323–329. doi:10.1016/j.msec.2015.01.007

Ma, L., Cheng, S., Ji, X., Zhou, Y., Zhang, Y., Li, Q., et al. (2020). Immobilizing magnesium ions on 3D printed porous tantalum scaffolds with polydopamine for improved vascularization and osteogenesis. *Mater. Sci. Eng. C* 117, 111303. doi:10.1016/j.msec.2020.111303

Ma, Z., Li, J., Cao, F., Yang, J., Liu, R., and Zhao, .Di (2020). Porous silicon carbide coated with tantalum as potential material for bone implants. *Regen. Biomater.* 7 (5), 453–459. doi:10.1093/rb/rbaa021

Ma, Z., Xie, H., Wang, B., Wei, X.i, and Zhao, D. (2016). A novel Tantalum coating on porous SiC used for bone filling material. *Mater. Lett.* 179, 166–169. doi:10.1016/j.matlet.2016.05.065

Macheras, G., Kateros, K., Kostakos, A., Koutsostathis, S., Danomaras, D., and Papagelopoulos, P. J. (2008). Eight-to ten-year clinical and radiographic outcome of a porous tantalum monoblock acetabular component. *J. arthroplasty* 24 (5), 705–709. doi:10.1016/j.arth.2008.06.020

Marko, H., Matjaž, V., Andrej, M., and Gregor, R. (2016). Porous tantalum in spinal surgery: An overview. *Eur. J. Orthop. Surg. traumatology Orthop. traumatologie* 26 (1), 1–7. doi:10.1007/s00590-015-1654-x

Maxim, G., Gintaras, J., and Valdas, V. (2014). Titanium surfaces with nanostructures influence on osteoblasts proliferation: A systematic review. *J. Oral Maxillofac. Res.* 5 (3), e1. doi:10.5037/jomr.2014.5301

Merolla, G., Sasyniuk, T. M., Paladini, P., and Porcellini, G. (2016). Total shoulder arthroplasty with a secondgeneration tantalum trabecular metal-backed glenoid component. *Bone & Jt. J.* 98-B (1), 75–80. doi:10.1302/0301-620x.98b1.36620

Minagar, S., Berndt, C. C., Wang, J., Ivanova, E., and Wen, C. (2012). A review of the application of anodization for the fabrication of nanotubes on metal implant surfaces. *Acta Biomater.* 8 (8), 2875–2888. doi:10.1016/j.actbio.2012.04.005

Miyazaki, T., Kato, H., Nakamura, T., and Miyaji, F. (2000). Bioactive tantalum metal prepared by NaOH treatment. *J. Biomed. Mater. Res.* 50 (1), 35–42. doi:10.1002/(sici)1097-4636(200004)50:1<35::aid-jbm6>3.0.co;2-8

Ms, A., Ej, B., Khe, C., and Eriksen, M. L. (2021). Retrograde nailing, trabecular metal implant and use of bone marrow aspirate concentrate after failed ankle joint replacement. *Foot Ankle Surg.* 27 (2), 123–128. doi:10.1016/j.fas.2020.03.003

Ohgushi, H., and Caplan, A. I. (1999). Stem cell technology and bioceramics: From cell to gene engineering. *J. Biomed. Mat.* 48, 913–927. doi:10.1002/(sici)1097-4636(1999)48:6<913::aid-jbm22>3.0.co;2-0

Pakos, E. E., Megas, P., and Paschos, N. K. (2015). Modified porous tantalum rod technique for the treatment of femoral head osteonecrosis. *World J. Orthop.* 6 (10), 829. doi:10.5312/wjo.v6.i10.829

Papacci, F., Rigante, L., Fernandez, E., Meglio, M., and Montano, N. (2016). Anterior cervical discectomy and interbody fusion with porous tantalum implant. Results in a series with long-term follow-up. *J. Clin. Neurosci.* 33, 159–162. doi:10.1016/j.jocn.2016.03.036

Peter, W., ChristophMeier, C., Milz, S., Gautier, E., et al. (2018). Successful bony integration of a porous tantalum implant despite longlasting and ongoing infection: Histologic workup of an explanted shoulder prosthesis. *J. Biomed. Mater. Res. Part B Appl. Biomaterials* 106, 2924–2931. doi:10.1002/jbm.b.34174

Piglionico, S., Bousquet, J., Fatima, N., Renaud, M., Collart-Dutilleul, P. Y., and Bousquet, P. (2020). Porous tantalum VS. Titanium implants: Enhanced mineralized matrix formation after stem cells proliferation and differentiation. *J. Clin. Med.* 9 (11), 3657. doi:10.3390/jcm9113657

Qian, W., Zhang, H., Gan, H., Li, Q., and Wang, Z. (2018). Application of combined porous tantalum scaffolds loaded with bone?morphogenetic protein 7 to repair of osteochondral defect in rabbits. *Int. Orthop.* 42, 1437–1448. doi:10.1007/s00264-018-3800-7

Raja Sukumar, V., Raju Golla, B., Ali Shaik, M., Yadav, A., ChandraTaraka, S., and Khaple, S.r (2019). Modeling and characterization of porous tantalum scaffolds. *Trans. Indian Inst. Metals* 72 (4), 935–949. doi:10.1007/s12666-018-01556-1

Rissmann, P., Anterior cervical fusion with stand-alone trabecular metal cages to treat cervical myelopathy caused by degenerative disk disease. Observations in 88 cases with minimum 12-month follow-up. *J. Neurological Surg. Part A Central Eur. Neurosurgery* 49, 496. doi:10.1055/s-0038-1642008

Ritchie, R. O. (1999). Mechanisms of fatigue-crack propagation in ductile and brittle solids. *Int. J. Fract.* 100 (1), 55–83. doi:10.1023/A:1018655917051

Rupérez, E., Manero, J. M., Riccardi, K., Li, Y., Aparicio, C., and Gil, F. J. (2015). Development of tantalum scaffold for orthopedic applications produced by space-holder method. *Mater. Des.* 83, 112. doi:10.1016/j.matdes.2015.05.067

Russell Levine, B., Scott, S., Poggie, R. A., CraigDella Valle, J., and JoshuaJacobs, J. (2006). Experimental and clinical performance of porous tantalum in orthopedic surgery. *Biomaterials* 27 (27), 4671–4681. doi:10.1016/j.biomaterials.2006.04.041

Sagherian, B. H., and Claridge, R. J. (2019). The use of tantalum metal in foot and ankle surgery. *Orthop. Clin. N. Am.* 50 (1), 119–129. doi:10.1016/j.ocl.2018.08.006

Sambaziotis, C., Lovy, A. J., Koller, K. E., Bloebaum, R. D., Hirsh, D. M., and Kim, S. J. (2012). Histologic retrieval analysis of a porous tantalum metal implant in an infected primary total knee arthroplasty. *J. Arthroplasty* 27 (7), 1413.e5–1413.e9. doi:10.1016/j.arth.2011.10.025

Sasikumar, Y., Indira, K., and Rajendran, N. (2019). Surface modification methods for titanium and its alloys and their corrosion behavior in biological environment: A review. *J. Bio- Tribo-Corrosion* 5 (2), 36. doi:10.1007/s40735-019-0229-5

SCULLYSean, P., and Urbaniak, J. R. (1998). Survival analysis of hips treated with core decompression or vascularized fibular grafting because of avascular necrosis. *J. Bone & Jt. Surg. Am. Volume* 80 (9), 1270–1275. doi:10.2106/00004623-199809000-00004

Shi, L. Y., Wang, A., Zang, F. Z., Wang, J. X., Pan, X. W., and Chen, H. J. (2017). Tantalum-coated pedicle screws enhance implant integration. *Colloids Surfaces B* 160, 22–32. doi:10.1016/j.colsurfb.2017.08.059

Shuler, M. S., Rooks, M. D., and Roberson, J. R. (2007). Porous tantalum implant in early osteonecrosis of the hip: Preliminary report on operative, survival, and outcomes results. *J. Arthroplasty* 22 (1), 26–31. doi:10.1016/j.arth.2006.03.007

Smith, J. O., Sengers, B. G., Aarvold, A., Tayton, E. R., Dunlop, D. G., and Oreffo, R. O. C. (2014). Tantalum trabecular metal - addition of human skeletal cells to enhance bone implant interface strength and clinical application. *J. tissue Eng. Regen. Med.* 8 (4), 304–313. doi:10.1002/term.1525

Tiusanen, H., Kormi, S., Kohonen, I., and Saltychev, M. (2019). Results of trabecular-metal total ankle arthroplasties with transfibular approach. *Foot Ankle Int.* 41 (4), 411–418. doi:10.1177/1071100719894929

Tobin, Eric J. (2017). Recent coating developments for combination devices in orthopedic and dental applications: A literature review. *Adv. Drug Deliv. Rev.* 112, 88–100. doi:10.1016/j.addr.2017.01.007

Tsao, A. K ., Roberson, J., Christie, M., Dore, D., Heck, D., Robertson, D., et al. (2005). Biomechanical and clinical evaluations of a porous tantalum implant for the treatment of early-stage osteonecrosis. *J. Bone & Jt. Surg. Am. Volume* 87, 22–27. doi:10.2106/jbjs.e.00490

Turkyilmaz, I. (2011). Implant dentistry - a rapidly evolving practice. *Dent. A Rapidly Evol. Pract.* 11, 1. doi:10.5772/706

Van Steenkiste, D., and Gorkiewicz, W. (2004). Analysis of tantalum coatings produced by the kinetic spray process. *Process. Therm. Spray Technol.* 13 (2), 265–273. doi:10.1361/10599630419418

Veillette, C. J. H., Mehdian, H., Schemitsch, E. H., and McKee, M. D. (2006). Survivorship analysis and radiographic outcome following tantalum rod insertion for osteonecrosis of the femoral head. *J. Bone & Jt. Surgery-american Volume* 88, 48–55. doi:10.2106/jbjs.f.00538

Vutescu, E. S., Hsiue, P., Paprosky, W., and Nandi, S. (2017). Comparative survival analysis of porous tantalum and porous titanium acetabular components in total hip arthroplasty. *Hip Int. J. Clin. Exp. Res. Hip Pathology Ther.* 27 (5), 505–508. doi:10.5301/hipint.5000479

Wang, H., Li, Q., Wang, Q., Zhang, H., Shi, W., Gan, H., et al. (2017). Enhanced repair of segmental bone defects in rabbit radius by porous tantalum scaffolds modified with the RGD peptide. *J. Mater. Sci. Mater. Med.* 28 (3), 50. doi:10.1007/s10856-017-5860-4

Wang, N., Li, H., Wang, J., Chen, S., Ma, Y., and Zhang, Z. (2012). Study on the anticorrosion, biocompatibility, and osteoinductivity of tantalum decorated with tantalum oxide nanotube array films. *Acs Appl. Mater Interfaces* 4 (9), 4516–4523. doi:10.1021/am300727v

Wang, Q., Qiao, Y., Cheng, M., Jiang, G., He, G., et al. (2016a). Tantalum implanted entangled porous titanium promotes surface osseointegration and bone ingrowth. *ScientificReports* 6 (1), 26248–26313. doi:10.1038/srep26248

Wang, Q., Zhang, H., GanhWang, H., Li, Q., and Wang, Z. (2018). Application of combined porous tantalum scaffolds loaded with bone morphogenetic protein 7 to repair of osteochondral defect in rabbits. *Int. Orthop.* 42 (7), 1437–1448. doi:10.1007/s00264-018-3800-7

Wang, Q., Qiao, Y., Cheng, M.i, Jiang, G., Guo, H., Chen, Y., et al. (2016b). Tantalum implanted entangled porous titanium promotes surface osseointegration and bone ingrowth. *Sci. Rep.* 6 (1), 26248. doi:10.1038/srep26248

Wang, Q., Zhang, H., Li, Q., Lei, Y., Gan, H., Liu, Y., et al. (2015). Biocompatibility and osteogenic properties of porous tantalum. *Exp. Ther. Med.* 9 (3), 780–786. doi:10.3892/etm.2015.2208

Wang, Q., Zhang, H., Li, Q., Lei, Y., Gan, H., Liu, Y., et al. (2015). Biocompatibility and osteogenic properties of porous tantalum. *Exp. Ther. Med.* 9 (3), 780–786. doi:10.3892/etm.2015.2208

Wang, T., Wang, L., Lu, Q., and Fan, Z. (2019). Changes in the esthetic, physical, and biological properties of a titanium alloy abutment treated by anodic oxidation. *J. Prosthet. Dent.* 121, 156–165. doi:10.1016/j.prosdent.2018.03.024

Wang, X., Liu, W., Yu, X., Wang, B., Xu, Y., Xu, Y., et al. (2022). Advances in surface modification of tantalum and porous tantalum for rapid osseointegration: A thematic review. *Front. Bioeng. Biotechnol.* 10, 983695. doi:10.3389/fbioe.2022.983695

Wang, X., Zhu, Z., Xiao, H., Luo, C., Luo, X., Lv, F., et al. (2020). Three-dimensional, MultiScale, and interconnected trabecular bone mimic porous tantalum scaffold for bone tissue engineering. *ACS omega* 5 (35), 22520–22528. doi:10.1021/acsomega.0c03127

Wang, Y., Wei, R., and Subedi, D. (2019). Tantalum fusion device in anterior cervical discectomy and fusion for treatment of cervical degeneration disease: A systematic review and meta-analysis. *Clin. Spine Surg.* 33, 111. doi:10.1097/BSD.0000000000000875

Wang, Z., Wang, C., Chen, L., Qin, Y, Zhong, L., Chen, B., et al. (2017). Analysis of factors influencing bone ingrowth into three-dimensional printed porous metal scaffolds: A review. *J. Alloys Compd.* 717, 271–285. doi:10.1016/j.jallcom.2017.05.079

Wauthle, R., Van Der Stok, J., Amin-Yavari, S., Van Humbeeck, J., Kruth, J. P., Zadpoor, A. A., et al. (2015). Additively manufactured porous tantalum implants. *Acta Biomater.* 14, 217–225. doi:10.1016/j.actbio.2014.12.003

Wauthle, R., van der Stok, J., Van Humbeeck, J., Kruth, J-P., Weinans, H., Mulier, M., et al. (2015). Additively manufactured porous tantalum implants. *Acta Biomater.* 14, 217–225. doi:10.1016/j.actbio.2014.12.003

Wauthle, R., van der Stok, J., Van Humbeeck, J., Kruth, J-P., Weinans, H., Mulier, M., et al. (2015). Additively manufactured porous tantalum implants. *Acta Biomater.* 14, 217–225. doi:10.1016/j.actbio.2014.12.003

Wei, B., Huang, X., Sandiford, S., He, X., Li, F., Li, Y., et al. (2019). Outcome after a new porous tantalum rod implantation for treatment of early-stage femoral head osteonecrosis. *Ann. Transl. Med.* 7 (18), 441. doi:10.21037/atm.2019.08.86

Wei, X., Zhao, D., Wang, B., Wang, W., Kang, K., Xie, H., et al. (2016). Tantalum coating of porous carbon scaffold supplemented with autologous bone marrow stromal stem cells for bone regeneration *in vitro* and invivo. *Exp. Biol. Med.* 241 (6), 592–602. doi:10.1177/1535370216629578

Wen-Qiang, Xin, Xin, W., Li, Q., and Tian, P. (2019). Comparison between porous tantalum metal implants and autograft in anterior cervical discectomy and fusion: A meta-analysis. *J. Comp. Eff. Res.* 8, 511–521. doi:10.2217/cer-2018-0107

Wieding, J., Wolf, A., and Bader, R. (2014). Numerical optimization of open-porous bone scaffold structures to match the elastic properties of human cortical bone. *J. Mech. Behav. Biomed. Mater.* 37, 56–68. doi:10.1016/j.jmbbm.2014.05.002

Xie, H., Xiao, Y., Wang, B. J., Hui, Y J., QinRong, K., and ZhaoWei, D. (2019). Deposition and biological evaluation of Ta coating on porous SiC scaffold for orthopedic application. *Sci. Adv. Mater.* 11 (10), 1443–1448. doi:10.1166/sam.2019.3548

Xu, Y., and Jiang, D. (2016). Physicochemical properties and biological characteristics of porous tantalum and its application progress in spinal surgery. *Zhongguo xiu fu chong jian wai ke za zhi = Zhongguo xiufu chongjian waike zazhi = Chin. J. reparative Reconstr. Surg.* 30 (6), 781–784. doi:10.7507/1002-1892.20160159

Yang, J., Jin, X., Gao, H., Zhang, D., Chen, H., Zhang, S., et al. (2020). Additive manufacturing of trabecular tantalum scaffolds by laser powder bed fusion: Mechanical property evaluation and porous structure characterization. *Mater. Charact.* 170, 110694. (prepublish). doi:10.1016/j.matchar.2020.110694

Yang, J., Jin, X., Gao, H., Zhang, D., Chen, H., Zhang, S.i, et al. (2020). Additive manufacturing of trabecular tantalum scaffolds by laser powder bed fusion: Mechanical property evaluation and porous structure characterization. *Mater. Charact.* 170, 110694. (prepublish). doi:10.1016/j.matchar.2020.110694

Yang, M., Ma, H., Shen, Z., Huang, Z., Tian, Q., and Tian, J. (2020). Dissimilar material welding of tantalum foil and Q235 steel plate using improved explosive welding technique. *Mater. Des.* 186 (C), 108348. doi:10.1016/j.matdes.2019.108348

Zhang, X., Wang, J., Xiao, J., and Shi, Z. (2016). Early failures of porous tantalum osteonecrosis implants: A case series with retrieval analysis. *Int. Orthop.* 40 (9), 1827–1834. doi:10.1007/s00264-015-3087-x

Zhang, Y., Ahnp, B., Fitzpatrick, D. C., Heiner, A. D., Poggie, R. A., and Brown, T. D. (1999). Interfacial frictional behavior: Cancellous bone, cortical bone, and a novel porous tantalum biomaterial. *J. Musculoskelet. Res.* 3 (4), 245–251. doi:10.1142/s0218957799000269

Zhang, Y., Chen, W., Yang, Z., Sun, J. N., Hu, Z. H., Hua, Z. J., et al. (2021). Porous tantalum implant for treatment of early-stage osteonecrosis of the femoral head: A minimum 5-year follow-up study. *BMC Surg.* 21, 360. doi:10.1186/s12893-021-01352-7

Zhao, D., Liu, B., Wang, B., Yang, L., Xie, H., Huang, S., et al. (2015). Autologous bone marrow mesenchymal stem cells associated with tantalum rod implantation and vascularized iliac grafting for the treatment of end-stage osteonecrosis of the femoral head. *Biomed. Res. Int.* 2015, 1–9. doi:10.1155/2015/240506

Zhao, D., Ma, Z., Liu, B., Yang, L., Qiu, X., Tian, S., et al. (2022). A new method to protect blood supply in the treatment of femoral neck fractures: Bidirectional compression porous tantalum screws. *Orthop. Surg.* 14 (9), 1964–1971. doi:10.1111/os.13285

Zhao, G., Li, S., Chen, Xu, Qu, X., Chen, R., Wu, Y., et al. (2018). Porous tantalum scaffold fabricated by gel casting based on 3D printing and electrolysis. *Mater. Lett.* 239, 5–8. doi:10.1016/j.matlet.2018.12.047

Zhou, L., Yuan, T., Li, R., Tang, J., Wang, G., and Guo, K. (2017). Selective laser melting of pure tantalum: Densification, microstructure and mechanical behaviors. *Mater. Sci. Eng. A* 707, 443–451. doi:10.1016/j.msea.2017.09.083

Zhou, Y., and Zhu, Y. (2013). Three-dimensional Ta foams produced by replication of NaCl space-holders. *Mater. Lett.* 99, 8–10. doi:10.1016/j.matlet.2013.02.068

frontiers | Frontiers in Bioengineering and Biotechnology

TYPE Original Research
PUBLISHED 06 April 2023
DOI 10.3389/fbioe.2023.1123459

OPEN ACCESS

EDITED BY
Liqun Xu,
Southwest University, China

REVIEWED BY
Aibing Huang,
Nanjing Medical University, China
Miroslav Trajanovic,
University of Niš, Serbia
Yansong Qi,
Inner Mongolia People's Hospital, China

*CORRESPONDENCE
Hua Wu,
wuhua@hust.edu.cn

SPECIALTY SECTION
This article was submitted to Biomaterials, a section of the journal Frontiers in Bioengineering and Biotechnology

RECEIVED 20 December 2022
ACCEPTED 28 March 2023
PUBLISHED 06 April 2023

CITATION
Li J, Wang J, Lv J, Bai J, Meng S, Li J and Wu H (2023), The application of additive manufacturing technology in pelvic surgery: A bibliometrics analysis. *Front. Bioeng. Biotechnol.* 11:1123459. doi: 10.3389/fbioe.2023.1123459

The application of additive manufacturing technology in pelvic surgery: A bibliometrics analysis

Jian Li[1], Jiani Wang[2], Jia Lv[3], Junjun Bai[3], Shichao Meng[1], Jinxuan Li[1] and Hua Wu[1,4]*

[1]Department of Orthopaedics, Third Hospital of Shanxi Medical University, Shanxi Bethune Hospital, Shanxi Academy of Medical Sciences, Tongji Shanxi Hospital, Taiyuan, China, [2]Department of Paediatric Medicine, Shanxi Medical University, Taiyuan, China, [3]Department of Orthopaedics, The Second Affiliated Hospital of Shanxi Medical University, Taiyuan, China, [4]Department of Orthopaedics, Tongji Hospital, Tongji Medical College, Huazhong University of Science and Technology, Wuhan, China

With the development of material science, additive manufacturing technology has been employed for pelvic surgery, addressing the challenges, such as the complex structure of the pelvis, difficulty in exposing the operative area, and poor visibility, of the traditional pelvic surgery. However, only limited studies have been done to review the research hotspots and trends of the additive manufacturing technology applied for pelvic surgery. In this study, we comprehensively analyzed the literatures related to additive manufacturing technology in pelvic surgery by a bibliometrics analysis and found that additive manufacturing technology is widely used in several aspects of preoperative diagnosis, preoperative planning, intraoperative navigation, and personalized implants for pelvic surgery. Firstly, we searched and screened 856 publications from the Web of Science Core Collection (WoSCC) with TS = (3D printing OR 3D printed OR three-dimensional printing OR additive manufacturing OR rapid prototyping) AND TS = (pelvis OR sacrum OR ilium OR pubis OR ischium OR ischia OR acetabulum OR hip) as the search strategy. Then, 565 of these were eliminated by evaluating the titles and abstracts, leaving 291 pieces of research literature whose relevant information was visually displayed using VOSviewer. Furthermore, 10 publications with high citations were selected by reading all publications extensively for carefully evaluating their Titles, Purposes, Results, Limitations, Journal of affiliation, and Citations. Our results of bibliometric analysis demonstrated that additive manufacturing technology is increasingly applied in pelvic surgery, providing readers with a valuable reference for fully comprehending the research hotspots and trends in the application of additive manufacturing technology in pelvic surgery.

KEYWORDS

pelvic surgery, three-dimensional printing technology, additive manufacturing technology, rapid prototyping, bibliometric analysis

Background

Additive manufacturing (AM), also referred to as three-dimensional (3D) printing technology, was invented in the 1980s and had been initially used for dentistry and maxillofacial surgery (Moss et al., 1991; Fuhrmann et al., 1996). Later, various types of additive manufacturing technology, such as 3D printing models, 3D virtual software, and 3D navigation systems, are developed and successfully applied in the medical field, particularly in pelvic surgery, including complex pelvic fractures (Wu et al., 2015), pelvic tumors (Wong et al., 2015), total hip arthroplasty (Arabnejad et al., 2017), and a variety of other pelvic surgeries (Wong et al., 2015; Upex et al., 2017). Additive manufacturing technology not only resolved the challenges of traditional pelvic surgery which occurred owing to the unique anatomical structure, limited visibility, and restricted working space of the pelvis (Coccolini et al., 2017), but also can be applied to preoperative planning, intraoperative navigation, and prosthetic plants, which can effectively improve surgical security and achieve individuation and accuracy in pelvic surgery (Wei et al., 2017). However, the progress and trends of the additive manufacturing technology in pelvic surgery were not systematically discussed by the bibliometrics analysis, limiting its wider application and inhibiting us from identifying the hotpots in pelvic surgery.

As a new discipline, bibliometrics is a good candidate for describing and analyzing the dynamics and progress of a specific research field (Peng et al., 2022). Bibliometrics analysis can comprehensively and systematically derive and visualize the detailed information (countries, institutions, authors, keywords, journals, references, and so on) of the published papers related to a specific research field. In addition, according to some scholars' opinions (Zhao et al., 2022), visual co-citation analysis can help with data interpretation and make the results more comprehensive. Simultaneously, the internal relationships of these data can be extracted, allowing complex and difficult-to-understand data to be presented in the form of images. In addition, VOSviewer (Zhu et al., 2021), a research tool widely employed in the field of bibliometrics, offers three visual views, including network visualization, overlay visualization, and density visualization.

Therefore, with the help of the bibliometrics analysis, we may better understand the current research status and future research trends in a specific field, allowing us to better identify research hotspots. In this study, bibliometric was employed for systematic and specific analyzing the application of additive manufacturing technology in pelvic surgery. The purpose of this study is to describe the application status and future development trends of additive manufacturing technology in pelvic surgery by analyzing existing relevant literature in order to discover research hotspots in this field.

Materials and methods

Search strategies

The Web of Science Core Collection (WoSCC) (Yeung et al., 2021), served as the database for this paper, is widely regarded as the best database for bibliometrics. Specific literature retrieval strategies were shown in Table 1. A total of 856 documents were discovered using the established retrieval strategy. 565 of these were eliminated by reviewing the titles and abstracts, leaving 291 pieces of research literature. The original data from the selected literature was exported to a text format, from which we extracted the year of publication, title, language, abstract, journal, author, affiliation, document type, keywords, and citation count. Finally, we extensively read all publications and opted for the 10 highly cited publications for deep analysis, extracting relevant data such as author, title, journal, purpose, results, limitations, and citations.

Data processing

VOSviewer (version 1.6.18) was employed to analyze the data for keywords, country, year of publication, institution, and journal, which were visually presented. Furthermore, read all publications extensively and choose highly 10 cited publications for detailed analysis and discussion.

Results

Publication outputs

All 291 articles were published from January 2009 to November 2022 in 148 journals, written by 1,506 authors from

TABLE 1 Summary of date source and selection.

category	Specific standard requirements
Research database	Web of science Core Collection
Citation indexes	SCI-EXPANDED
Searching period	January 2009 to November 2022
Language	"English"
Searching keywords	TS = (3D printing OR 3D printed OR three-dimensional printing OR additive manufacturing OR rapid prototyping) AND TS = (pelvis OR sacrum OR ilium OR pubis OR ischium OR ischia OR acetabulum OR hip)
Document types	"Articles"
Date extraction	Export with full records and cited references in plain text format
Sample size	856

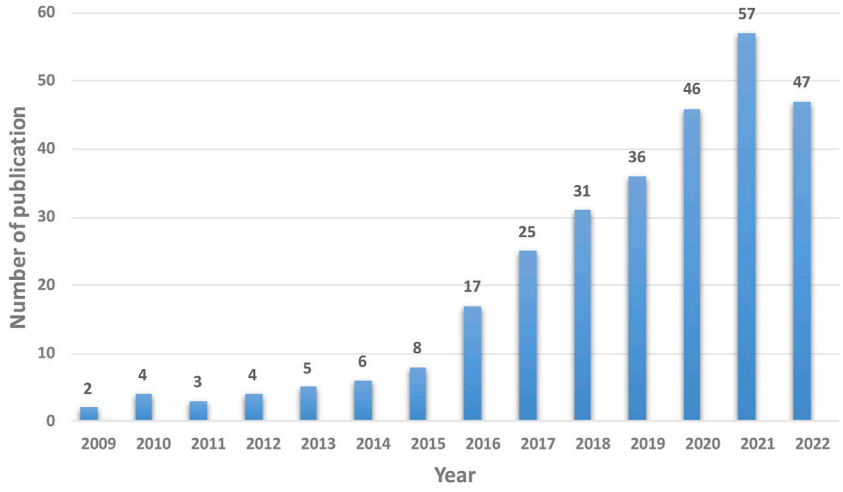

FIGURE 1
The annual trends of publications.

TABLE 2 Top 5 countries contributed to research publications in the field of additive manufacturing technology in pelvic surgery.

Rank	Country	Publications	Percentage	Average citation
1	China	120	41.2	12.2
2	United State	37	12.7	10.8
3	Germany	14	4.8	9.5
4	Italy	14	4.8	6.9
5	Australia	12	4.1	9.6

452 institutions in 45 countries, and cited 6,256 times by 1,835 different journals. During this period, the overall trends of research on the use of additive manufacturing technology in pelvic surgery increased from 2 articles in 2009 to 47 articles in 2022. The number of papers published between 1999 and 2015 was sporadic and modest. However, this number has rapidly increased since 2016, with the highest number of papers (57) published in 2021. The details were shown in Figure 1.

Analysis of countries

The selected articles on additive manufacturing technology in pelvic surgery were published in 54 countries. 41.2% (120/291) articles were published by China, followed by the United States (12.7%; 37/291), Germany (4.8%; 14/291), Italy (4.8%; 14/291), and Australia (4.1%; 12/291) (Table 2). Literature, published by China, had the most participants from other countries, indicating that they have more cooperation with other countries (Figure 2). In addition, as shown in Table 2, literature, published by China, had the highest average citation of 12.2, followed by that of the United States at 10.8, Australia at 9.6, Germany at 9.5, and Italy at 6.9.

Analysis of institutions

In terms of institutions, Southern Medical University published the highest number of articles (17, 5.8%), followed by Shanghai Jiao Tong University (16, 5.4%), Peking University (9, 3.1%), Huazhong University of Science and Technology (7, 2.4%), and Sichuan University (7, 2.4%). All top 5 institutions are from China (Table 3). The differences in publication volume were represented by the size of the bubbles, as shown in Figure 3, while the difference in publication time was symbolized by the color of the bubbles, with brighter colors indicating the most recent publications. More wires connecting bubbles means more collaboration between institutions. The top 5 institutions' average citation was analyzed and shown in Table 3. Literature, published by Peking University, had the highest average citation of 28.1, followed by that of Shanghai Jiao Tong University at 16.1, Southern Medical University at 15, Huazhong University of Science and Technology at 11.3, and Sichuan University at 4.

Analysis of journals

The 291 articles on additive manufacturing technology in pelvic surgery published in different journals. International Orthopaedics has published the most literature (15 articles, 10.1%), followed by the

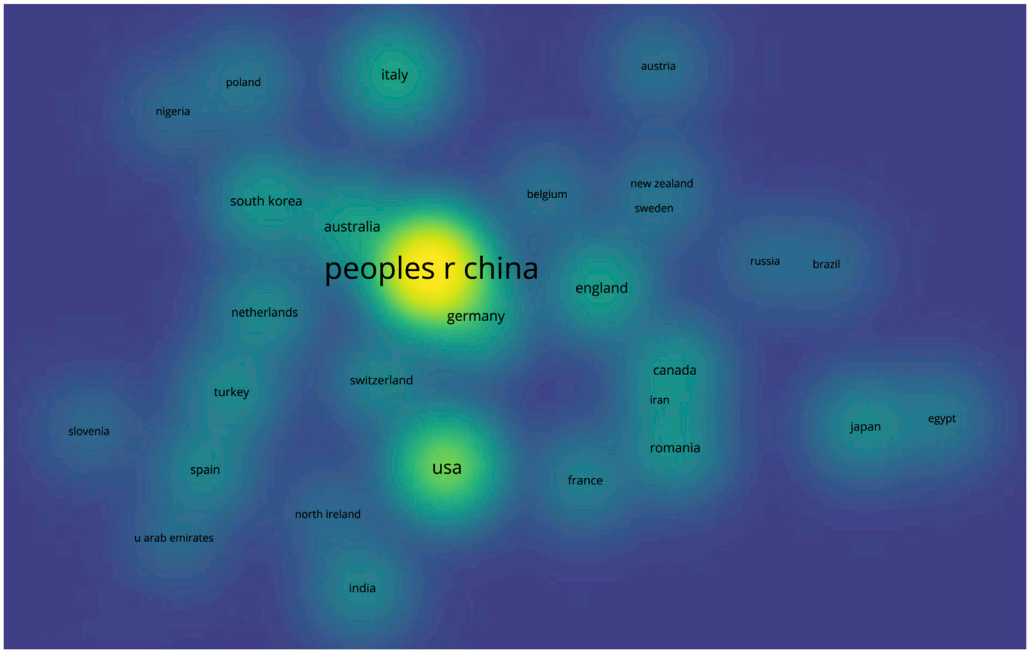

FIGURE 2
Density visualization of the distribution of all publications across countries. (Larger and brighter bubbles indicate the greatest number of publications in the field of additive manufacturing technology in pelvic surgery from a specific country, while closer bubbles in space indicate closer national collaborations.).

TABLE 3 The top 5 most productive institutions in the field of additive manufacturing technology in pelvic surgery.

Rank	institutions	Publications	Percentage	Average citation
1	Southern Medical University	17	5.8	15
2	Shanghai Jiao Tong University	16	5.4	16.1
3	Peking University	9	3.1	28.1
4	Huazhong University of Science and Technology	7	2.4	11.3
5	Sichuan University	7	2.4	4

Journal of Orthopaedic Surgery and Research (10 articles, 6.8%), Orthopaedic Surgery (9 articles, 6.1%), BMC Musculoskeletal Disorders (8 articles, 5.4%), and the Indian Journal of Orthopaedics (7 articles, 4.7%) (Table 4). To help authors easily and precisely submit their manuscripts, a visualization of cluster density was used to analyze the co-cited journals. As shown in Figure 4, these articles can be classified into three groups. The most cited blue cluster journals primarily published articles on joint surgery, while the green cluster journals often explored articles focused on fracture, and the red cluster journals were mainly interested in articles related to biological materials (Figure 4). Readers can retrieve and read periodicals from this range, which helps them improve their knowledge in this field.

Analysis of authors

1,506 authors contributed to the selected 291 publications. The top 10 high-yield authors are listed in Table 5. T. Ji (139 citations) is the most cited of the aforementioned authors, while L. Wang (17 citations) is the least cited. The majority of the high-yield authors in this field are from Shanghai Jiao Tong University School of Medicine, and all the authors are Chinese. The network of author collaborations is shown in Figure 5. The lines between the bubbles on the network visualization signify collaboration relationships, while the authors are represented by the bubbles, whose areas indicate the number of published papers.

Analysis of keywords

Keywords summarized the main points of a research. It is possible to describe the research hotspots and trends in this field using keyword co-occurrence analysis. As illustrated in Figure 6, high-frequency keywords such as 3D printing, reconstruction, surgery, additive manufacturing, arthroplasty, and so on constitute this field's research topic. Furthermore, the network visualization of keyword co-occurrence analysis revealed that the keywords are mainly divided into 3 clusters. Cluster 1 focuses on

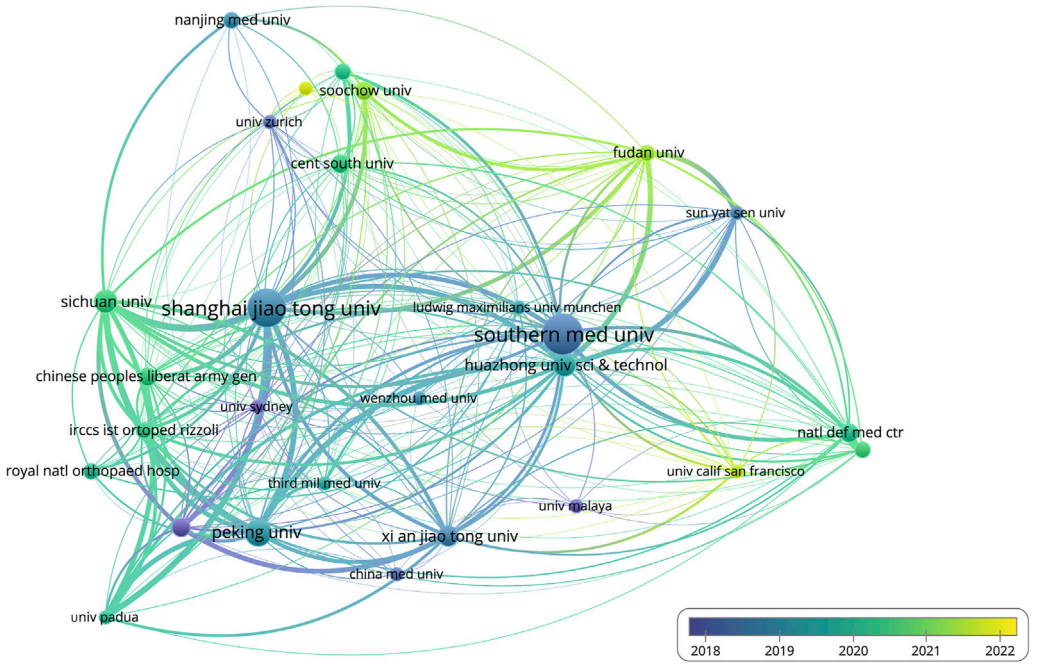

FIGURE 3
Visualization of institutional cooperation and publication period. (The size of the bubble represents the amount of paper issued by the institutions. The larger the bubble, the more paper is issued. In terms of time, the brighter the bubbles, the more recent research the organization has completed. Furthermore, the more connections there are between different bubbles, the closer the collaboration between different institutions will become.).

TABLE 4 Top 5 productive journals in the field of additive manufacturing technology in pelvic surgery.

Rank	Journal	Number	Percentage
1	international orthopaedics	15	10.1
2	journal of orthopaedic surgery and research	10	6.8
3	orthopaedic surgery	9	6.1
4	bmc musculoskeletal disorders	8	5.4
5	indian journal of orthopaedics	7	4.7

pelvic fractures, and its keywords include 3D printing, surgery, fixation, acetabular fractures, and so on; Cluster 2 focuses on total hip arthroplasty, and its keywords include additive manufacturing, arthroplasty, hip, total hip arthroplasty, and so on; Cluster 3 focuses on pelvic tumors, with the keywords reconstruction, pelvic, resection, tumors, implant, and so on. According to the findings, the use of additive manufacturing technology in pelvic surgery is primarily focused on pelvic fractures, pelvic tumors, and hip diseases.

Discussion

The current study presents the findings of a bibliometric analysis of 291 articles on additive manufacturing technology in pelvic surgery conducted between January 2009 and November 2022 using the WoSCC database and VOSviewer software. The volume of publications shows that the development path from 2009 to the present is divided into two phases: 2009–2015, the early phase of slow development, and 2016-present, the era of rapid development. Furthermore, the year 2021 saw the most single-year publications in the field of additive manufacturing technology in pelvic surgery until November 2022. The overall trends suggest that more scholars will be engaged in this area in the future, contributing new scientific discoveries.

The analysis of countries, institutions, and authors enables the investigation of collaboration between various research topics. Based on the number of publications and average citations, China is the most productive and influential country for additive manufacturing technology in pelvic surgery. It is noteworthy that the top 5 most productive institutions and the top 10 authors are all from China. Moreover, the top 10 authors, K.R. Dai (Rank 2), Y.Q. Hao (Rank 3), and H.W. Li (Rank 9) are all from Shanghai Jiao Tong University School of Medicine. According to the three authors' article

FIGURE 4
Density visualization of the co-cited journals. (A wider range of circles indicates that the journal has been cited more frequently. Different colors represent different clusters, so the co-cited journals can be seen to be divided into three clusters.).

TABLE 5 The 10 high-yield authors in the field of additive manufacturing technology in pelvic surgery.

Rank	Author	Publications	Percentage	Affiliation
1	M.X. Lu	6	2.1	Sichuan University, China
2	K.R. Dai	6	2.1	Shanghai Jiao Tong University School of Medicine, China
3	Y.Q. Hao	6	2.1	Shanghai Jiao Tong University School of Medicine, China
4	J. Fu	6	2.1	Sun Yat-sen University, China
5	W.H. Huang	6	2.1	Southern Medical University, China
6	J. Wang	5	1.7	Southeast University, China
7	L. Wang	5	1.7	The Affiliated People's Hospital of Jiangsu University, China
8	C.C. Hung	5	1.7	Tri-Service General Hospital and National Defense Medical Center, China
9	H.W. Li	5	1.7	Shanghai Jiao Tong University School of Medicine, China
10	T. Ji	5	1.7	Beijing Jishuitan Hospital, China

(Hao et al., 2021; Wu et al., 2021; Kong et al., 2022), they have more and better collaboration, and they mostly publish articles on additive manufacturing technology in pelvic tumors, pelvic implants, pelvic fractures, and the disease of the hip joint. These results offer a very great prospect for additive manufacturing technology in pelvic surgery. Of course, the analysis of the above information reveals that the development of additive manufacturing technology in the field of pelvic surgery may be unbalanced, as the current state of research, primarily by Chinese scholars, may bring some geographical differences, implying that the study's results may not be applicable to all humans. Furthermore, the visualization map shows weak connections, indicating a lack of coordination among countries, organizations, and authors. Therefore, global academic collaboration between countries/regions and institutions needs to be expanded.

In terms of journal information, we discovered that International Orthopaedic is the most productive journal in the field of additive manufacturing technology in pelvis surgery, as well as having the better results (Rank 4) in co-cited journals. Journal analysis can assist researchers in locating relevant publications for which to search and submit manuscripts. Keywords represent not only current research hotspots, but also future research trends.

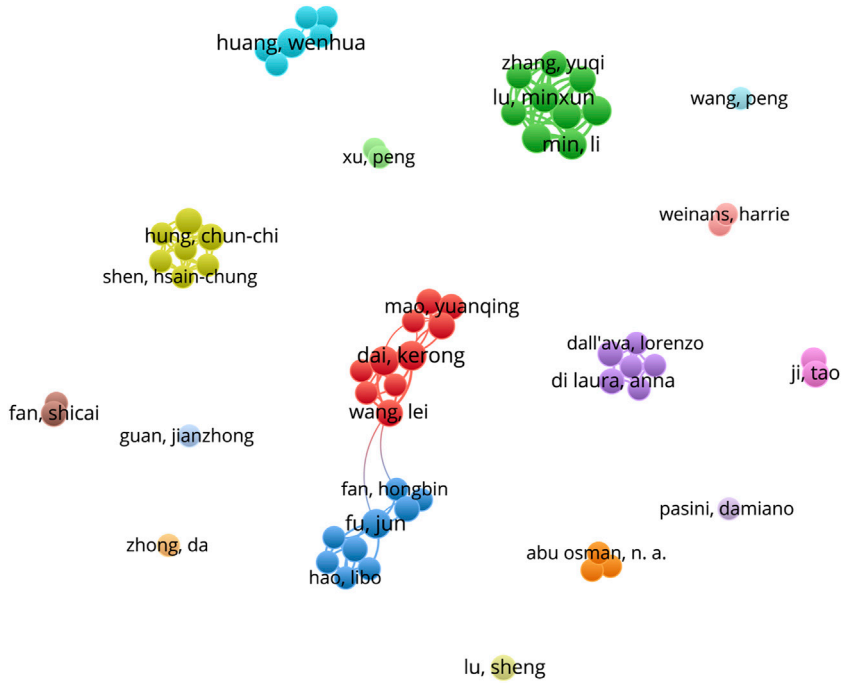

FIGURE 5
Cooperation network of productive authors. (The map's bubbles represent authors, and the lines connecting the bubbles represent collaborative relationships. The larger the bubble area, the greater the number of publications.).

Through visual analysis of keywords, we identified the research hotspots in the field since the last decade. The most common keywords in the field of additive manufacturing technology in the pelvis surgery are "3D printing", "reconstruction", "surgery", "additive manufacturing", "arthroplasty", "accuracy", "hip", "pelvis", "fixation", "resection", "acetabular fracture". In order to better grasp the current research hotspots, we thoroughly read and evaluated all retrieved articles and selected the top 10 most cited publications (Arabnejad Khanoki and Pasini, 2012; Cartiaux et al., 2014; Wong et al., 2015; Wu et al., 2015; Zeng et al., 2016; Arabnejad et al., 2017; Kim et al., 2017; Liang et al., 2017; Upex et al., 2017; Wei et al., 2017), carefully evaluating them in terms of Title, Purpose, Results, Limitations, Journal, and Citation (Table 6). According to current research, the application of additive manufacturing technology in pelvic surgery primarily addresses the following diseases: pelvic tumor, pelvic fracture, and hip joint disease (mainly total hip arthroplasty).

Pelvic tumor

The third most typical site for metastatic bone cancers is the pelvis, which frequently displays pain and limited movement clinically (Han et al., 2019). Tumor resection and pelvic reconstruction are common steps in pelvic tumor surgery. Due to the irregularity of pelvic anatomy, the proximity of important blood vessels and nerves, and the limited surgical access, pelvic tumor surgery is significantly more challenging. The success of pelvic tumor surgery depends on the complete removal of the tumor and a successful pelvic reconstruction. Additive manufacturing technology has demonstrated unparalleled superiority in pelvic tumor surgery due to its personalization, high-precision, and rapidly accessible manufacturing (Chen et al., 2016). Preoperative surgical planning, intraoperative guides for precise osteotomy planes, and implant reconstruction with 3D printed prostheses have led to the increasing application of additive manufacturing technology in pelvic tumor surgery (Biscaccianti et al., 2022).

A 3D printing workflow for pelvic tumor surgery was described by Wong et al. (2015). The full scope of the tumor was firstly outlined, and its volume was extracted from computed tomography (CT) or magnetic resonance imaging (MRI) images, followed by the creation of a 3D bone tumor model and the design of tumor resection margins. Then, the shape of the virtual resected bone defect was reconstructed by overlapping mirrors in the unaffected relative pelvic region, and a patient-specific pelvic implant was designed while taking surgical access and surrounding soft tissues into account. After that, to complete the biomechanical evaluation, the designed implant is subjected to finite element analysis using dedicated engineering software. During the procedure, the tumor was removed using a Patient-specific instrument (PSI) according to a predetermined plan, and the bone defect area was well adapted with a patient-specific computer-aided design (CAD) implant, which was subsequently fixed. The results of this study also imply that tumor PSI may facilitate more challenging multiplanar osteotomies in the complex anatomical pelvic region. This enables the surgeon to remove the bone tumor with sufficient margins and to preserve the most normal bone possible for improved functional restoration. To investigate the accuracy of patient-specific

TABLE 6 Top 10 cited articles in the field of additive manufacturing technology in pelvic surgery.

Study	Title	Purpose	Results	Limitations	Journal	Citation
Arabnejad et al. (2017)	Fully Porous 3D Printed Titanium Femoral Stem to Reduce Stress-Shielding Following Total Hip Arthroplasty	Tuning material architecture of Total Hip Arthroplasty to achieve a substantial reduction of bone resorption secondary to stress shielding	A high strength fully porous material with tunable mechanical properties is introduced for use in hip replacement design	The study is still in the preliminary stages of research	Journal of Orthopaedic Research	203
Wong et al. (2015)	One-step reconstruction with a 3D-printed, biomechanically evaluated custom implant after complex pelvic tumor resection	Describing a novel workflow of performing a partial acetabular resection in a patient with pelvic chondrosarcoma and reconstruction with a custom pelvic implant in a one-step operation	The patient could walk unaided with a good hip function. No tumor recurrence and implant loosening were noted at 11 months after surgery	Further study in a larger population is needed to assess the clinical efficacy of the workflow in complex bone tumor surgery	Computer Aided Surgery	125
Arabnejad Khanoki and Pasini, (2012)	Multiscale design and multiobjective optimization of orthopedic hip implants with functionally graded cellular material	To solve the problems of bone-implant interface instability and bone resorption during total hip rarthroplasty	In this paper proposing a novel type of implant that can minimize concurrently bone résorption and implant interface failure	There are 5 optimizations available to improve this design	Journal of Biomechanical Engineering	107
Liang et al. (2017)	Reconstruction with 3D-printed pelvic endoprostheses after resection of a pelvic tumour	To report the feasibility of using 3D-printing technology for patients with a pelvic tumour who underwent reconstruction	The use of 3D-printed pelvic prostheses for reconstruction of the bony defect after resection of a pelvic tumour was safe, without additional complications, and gave good short-term functional results	The main limitation of this study is the relatively short follow-up	Bone & Joint Journal	100
Zeng et al. (2016)	A combination of three-dimensional printing and computer-assisted virtual surgical procedure for preoperative planning of acetabular fracture reduction	To evaluate the feasibility, accuracy and effectiveness of performing 3D printing technology and computer-assisted virtual surgical procedures for preoperative planning in acetabular fractures	The 3D printing technology combined with virtual surgery for acetabular fractures is feasible, accurate, and effective leading to improved patient-specific preoperative planning and outcome of real surgery	long-term outcomes are not known, and need to be followed up	Injury	88
Cartiaux et al. (2014)	Improved Accuracy with 3D Planning and Patient-Specific Instruments During Simulated Pelvic Bone Tumor Surgery	The study investigated accuracy of patient-specific instru-mentation (PSI) for bone-cutting during simulated tumor surgery within the pelvis	Using PSI technology during simulated bone cuts of the pelvis can provide good cutting accuracy	The strudy does not exactly represent actual pelvic surgery	Annals of Biomedical Engineering	84
Wu et al. (2015)	Printed Three dimensional Anatomic Templates for Virtual Preoperative Planning Before Reconstruction of Old Pelvic Injuries: Initial Results	To assess the use of three-dimensional (3D) printing techniques for surgical management of old pelvic fractures	Preoperative planning using the 3D printed models was feasible in all cases	the small number of patients and the absence of long-term follow-up data	Chinese Medical Journal	66
Upex et al. (2017)	Application of 3D printing for treating fractures of both columns of the acetabulum: Benefit of pre-contouring plates on the mirrored healthy pelvis	The purpose of this technical note is to describe how we used 3D printing as an aid to treat acetabular fractures	3D printing is a highly relevant and an easy-to-use technology from a clinical point of view for treating complex fractures	For now, the limiting factor is the time needed to print a full-size (1:1 model) of the hemipelvis	Orthopaedics & Traumatology: Surgery & Research	65
Wei et al. (2017)	One-step reconstruction with a 3D-printed, custom-made prosthesis after total *en bloc* sacrectomy: a technical note	To describe the design of a 3D-printed custom-made prosthesis for reconstruction after total *en bloc* sacrectomy, the surgical technique, and the clinical and functional outcome of a patient	The patient received one-stage total *en bloc* sacrectomy through posterior approach followed by reconstruction with the 3D-printed sacral prosthesis	The report is of only one case	European Spine Journal	63

(Continued on following page)

TABLE 6 (*Continued*) Top 10 cited articles in the field of additive manufacturing technology in pelvic surgery.

Study	Title	Purpose	Results	Limitations	Journal	Citation
Kim et al. (2017)	Sacral Reconstruction with a 3D-Printed Implant after Hemisacrectomy in a Patient with Sacral Osteosarcoma: 1-Year Follow-Up Result	Hemisacrectomy and sacral reconstruction using a 3D-printed implant	This is the first report of a case of hemisacral reconstruction using a custom-made 3D-printed implant	Distinct from conventional implants, the strength of 3D-printed im-plants may not be guaranteed	Yonsei Medical Journal	57

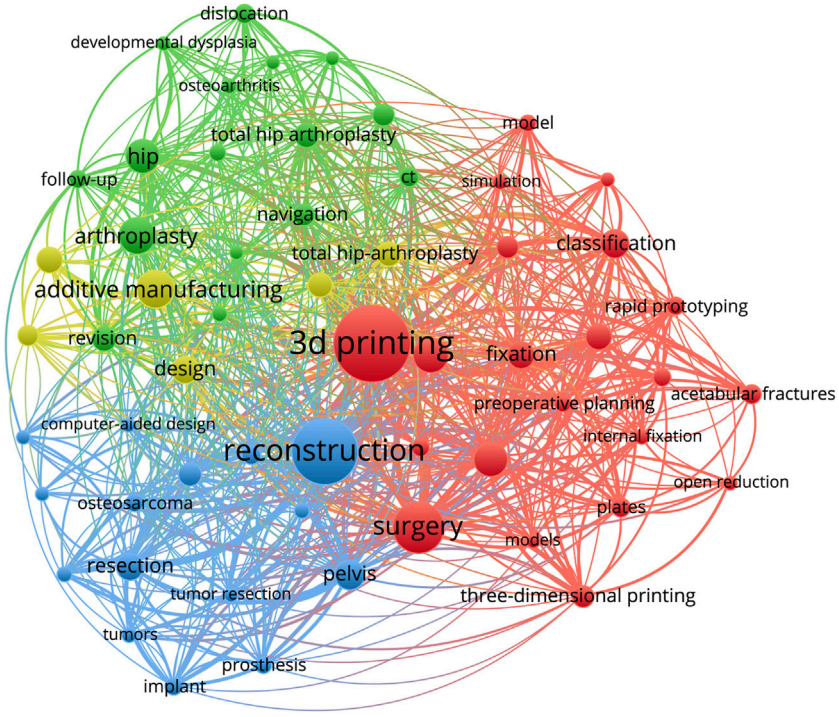

FIGURE 6
Network visualization of keywords. (The larger the bubbles are, the higher the probability of the keyword appearing. Then the more connections there are between the two bubbles, the more publications they appear in together, and the stronger the correlation will become. Furthermore, the different colors of the bubbles represent different clusters, implying that the keyword represented by the same color of bubble has a stronger correlation.).

instrument (PSI) for bone cutting during pelvic tumor simulation, 24 surgeons (10 senior and 14 junior) were asked to perform tumor resection, and the results revealed no significant differences in terms of the position of the cutting plane and the surgical margins obtained between senior and junior surgeons (Cartiaux et al., 2014).

A study found that using 3D-printed pelvic prostheses to reconstruct defects after pelvic tumor resection is feasible and safe, with good short-term functional outcomes (Liang et al., 2017). When it comes to the long-term outcomes of reconstructive surgery, rigid fusion between bone and implant has been a major issue. 3D-printed prostheses, as compared to other implants, can be contoured to fit the bone defect more precisely and machined with a porous bone contact surface to guide bone growth and improve long-term stability (Shah et al., 2016). The results of a 1-year follow-up of sacral reconstruction with 3D-printed implants after hemisacrectomy in patients with sacral osteosarcoma show that good bone connections can be achieved on both densely structured strut surfaces and loosely structured porous meshes (Kim et al., 2017). All the evidence suggests that additive manufacturing technology is already playing an important role in the field of pelvic oncology surgery and will become even more indispensable in the future.

Pelvic fracture

Pelvic fractures are a common type of fracture in clinical practice, mostly caused by high-energy injuries such as traffic accidents, industrial accidents, and falls from height. Complex pelvic and acetabular anatomy makes clinical diagnosis and therapy rather challenging. Researchers have never stopped looking into pelvic fractures since they are frequently accompanied by severe shock and pelvic organ injury, which has a high mortality and disability rate (Tachibana et al., 2009). The

major objectives of pelvic fracture surgery are to restore the symmetry and integrity of the pelvic ring, pay attention to handling soft tissues carefully, hasten postoperative healing and early rehabilitation, and improve long-term hip joint function (Halvorson et al., 2014). Additive manufacturing technology, which is widely used in preoperative diagnosis and planning of pelvic fractures, intraoperative navigation, and prosthetic endoprostheses, among other things, can assist clinicians in diagnosis and treatment by realizing a panoramic simulation of pelvic structures. The first polyethylene pelvic model was reportedly used in orthopedic surgery in 1979, with excellent results (Tonner and Engelbrecht, 1979).

There are several aspects to the use of additive manufacturing technology in the surgical treatment of pelvic fractures. To start, it can print a 1:1 3D model to assist orthopedic surgeons in understanding the extent and type of fracture as well as the displacement of the fracture mass. This will enable them to make a precise preoperative diagnosis, weigh potential intraoperative risks, and develop the best surgical plan. Second, additive manufacturing technology can "tailor" personalized implants to match the patient's bones more precisely when used in conjunction with intraoperative navigation technology, effectively shortening the operation time, significantly reducing the incidence of postoperative infections and other complications, and restoring function of the affected limb more quickly. Furthermore, the 3D-printed navigation template aids in determining the precise location of the bone plate and screws, and the combination of the navigation template and pre-curved fixation can accurately and effectively repair the pelvic fracture (Chen et al., 2017). Cimerman and Kristan (2007) described a surgical planning software for pelvic and acetabular fractures with a mouse-based CAD-style interface that produced personalized, precise surgical plans that greatly increased the success rate of surgery. And in other studies, 3D printed models applied to pelvic fracture surgery significantly reduced operative time, surgeon fatigue, and blood loss (Starosolski et al., 2014).

Hip joint disease

With the aging trend, the number of patients requiring total hip arthroplasty grows each year. Total hip arthroplasty (THA) has emerged as one of the most effective treatments for advanced hip disease (femoral head necrosis, hip dysplasia, femoral neck fracture, degenerative hip arthritis, rheumatoid arthritis, ankylosing spondylitis, etc.). For patients with hip dysplasia and total hip revision, the emergence of additive manufacturing technology undoubtedly opens a whole new path of personalized and precise medical treatment.

Hip dysplasia is typically imaged by showing diminished acetabular coverage of the femoral head, a shallow and thin acetabular wall, acetabular bone abnormalities, and osteosclerosis (Du et al., 2020). Clinical management of severe hip dysplasia is frequently difficult due to the severity of the acetabular defect and significant femoral head dislocation. Using additive manufacturing technology to design a 1:1 pelvic model, which can clearly demonstrate the anatomical morphology of the patient's hip joint and help the surgeon understand the true and false socket positions in relation to the acetabular wall defect condition. In turn, it can successfully benefit the surgeon by enhancing preoperative planning, obtaining the accurate hip joint's center of rotation, and enhancing surgical accuracy and safety (Won et al., 2013). An personalized titanium tricompartmental cup, first proposed by Christie et al. (2001) is a custom-made acetabular prosthesis with three winged projections attached to the outer edge of the cup that can be screwed to the ilium, pubic bone, and sciatic bone, respectively, when the acetabular defect is very large. It allows for the precise and stable restoration of acetabular anatomy, as well as the restoration of strong bone contact and hip biomechanics. However, it is crucial to note that fitting a custom triple wing socket cup necessitates significant iliac bone exposure, which increases the risk of nerve and vascular injury (Christie et al., 2001).

Furthermore, additive manufacturing technology is becoming more widely used in total hip revision. Despite technological advancements that have resulted in the success of current total hip arthroplasties, more than 13% of hip prostheses still require revision surgery due to bone resorption and aseptic implant loosening (Kurtz et al., 2007). In 2017, Hughes et al. conducted a study of 3D printed pelvic models in hip revision patients, using a pelvic model for surgical rehearsal prior to revision surgery, grinding layer by layer and anticipating the size of the socket cup. Depending on the size of the bone defect, structural bone grafting or tantalum metal pads were used for simulation, with screw positions and trajectories determined to ensure prosthetic stability while avoiding screw damage to blood vessels or nerves (Hughes et al., 2017). As a result, there was better preoperative planning, less operative time, and excellent outcomes. Further research has shown promising early results in hip revision using 3D printed titanium trabecular lattice structures to fill and reconstruct extensive acetabular bone defects (Colen et al., 2013). It is worth noting that Arabnejad et al. (2017) worked on new fully porous 3D printed titanium femoral stems to reduce stress shielding after total hip arthroplasty and to lower the incidence of total hip revision.

The field of medical education has also been revolutionized by additive manufacturing technology today. For many years, the teaching methods for medical students and physicians have remained at the level of flat images. Traditional teaching methods have significant drawbacks for orthopedic clinical education with complicated spatial structure and demanding a lot of spatial concept capacity. As a result of the development of additive manufacturing technology, two-dimensional elements are transformed into three-dimensional conformations and presented as interactive software or printed models, enabling students to fully comprehend the spatial structure of real objects without the use of any material objects (Abdulcadir et al., 2020). Taking into account the complicated anatomy of the pelvis, 3D printed models can guide newcomers in understanding the borders of pelvic tumors, the typology of complex pelvic fractures, etc (Lee et al., 2022; Wu et al., 2022). Moreover, physicians can also quickly develop their operating skills while learning *via* surgical training based on 3D printed models. Overall, additive manufacturing technology is regarded as the best educational tool among the ones that are now on the field.

In general, the outcomes of additive manufacturing technology in pelvic surgery are promising. However, its application in this field has some limitations. First, some researchers have revealed that creating 3D models typically requires a lot of time, rendering them unsuitable for application in emergency medical circumstances (Lopez et al., 2021). Second, no 3D printed product is capable of fully replicating and displaying bone, muscle, skin, and other tissues.

Third, the cost of establishing 3D printing facilities (hardware and software) is prohibitively expensive for most of the medical institutions, and as a result, the treatment fee is also expensive for patients. Meanwhile, in this study, as with prior bibliometric assessments, it is inevitable that it will be difficult to fully collect all the literature related to this field in the WoSCC database due to the differences in literature search algorithms and the speed of literature updates. Nevertheless, this study can still be used to illustrate the general states and trends of research topics.

Conclusion

In this study, bibliometric analysis was employed for comprehensively and systematically reviewing of publications related to additive manufacturing technology in pelvic surgery. In addition, the relevant research results were presented and discussed in detail using visualization tools, revealing that 3D printing technology is the hottest field of pelvic surgery and will continue to play an important role in the future of pelvic surgery.

Data availability statement

The original contributions presented in the study are included in the article/Supplementary Material, further inquiries can be directed to the corresponding author

Author contributions

JLi and JW searched the literature and drafted the initial manuscript. JLv and JB worked on the images and table. SM and JxL revised the manuscript and edited the language. HW reviewed the final manuscript. All authors contributed to the article and approved the submitted version.

Funding

This work was supported by the National Natural Science Foundation of China (Grant Number 81902273).

Conflict of interest

The authors declare that the research was conducted in the absence of any commercial or financial relationships that could be construed as a potential conflict of interest.

Publisher's note

All claims expressed in this article are solely those of the authors and do not necessarily represent those of their affiliated organizations, or those of the publisher, the editors and the reviewers. Any product that may be evaluated in this article, or claim that may be made by its manufacturer, is not guaranteed or endorsed by the publisher.

Supplementary material

The Supplementary Material for this article can be found online at: https://www.frontiersin.org/articles/10.3389/fbioe.2023.1123459/full#supplementary-material

References

Abdulcadir, J., Dewaele, R., Firmenich, N., Remuinan, J., Petignat, P., Botsikas, D., et al. (2020). *In vivo* imaging-based 3-dimensional pelvic prototype models to improve education regarding sexual anatomy and physiology. *J. Sex. Med.* 17 (9), 1590–1602. doi:10.1016/j.jsxm.2020.05.025

Arabnejad Khanoki, S., and Pasini, D. (2012). Multiscale design and multiobjective optimization of orthopedic hip implants with functionally graded cellular material. *J. Biomech. Eng.* 134 (3), 031004. doi:10.1115/1.4006115

Arabnejad, S., Johnston, B., Tanzer, M., and Pasini, D. (2017). Fully porous 3D printed titanium femoral stem to reduce stress-shielding following total hip arthroplasty. *J. Orthop. Res.* 35 (8), 1774–1783. doi:10.1002/jor.23445

Biscaccianti, V., Fragnaud, H., Hascoët, J., Crenn, V., and Vidal, L. (2022). Digital chain for pelvic tumor resection with 3D-printed surgical cutting guides. *Front. Bioeng. Biotechnol.* 10, 991676. doi:10.3389/fbioe.2022.991676

Cartiaux, O., Paul, L., Francq, B. G., Banse, X., and Docquier, P. L. (2014). Improved accuracy with 3D planning and patient-specific instruments during simulated pelvic bone tumor surgery. *Ann. Biomed. Eng.* 42 (1), 205–213. doi:10.1007/s10439-013-0890-7

Chen, X., Chen, X., Zhang, G., Lin, H., Yu, Z., Wu, C., et al. (2017). Accurate fixation of plates and screws for the treatment of acetabular fractures using 3D-printed guiding templates: An experimental study. *Injury* 48 (6), 1147–1154. doi:10.1016/j.injury.2017.03.009

Chen, X., Xu, L., Wang, Y., Hao, Y., and Wang, L. (2016). Image-guided installation of 3D-printed patient-specific implant and its application in pelvic tumor resection and reconstruction surgery. *Comput. Methods Programs Biomed.* 125, 66–78. doi:10.1016/j.cmpb.2015.10.020

Christie, M. J., Barrington, S. A., Brinson, M. F., Ruhling, M. E., and DeBoer, D. K. (2001). Bridging massive acetabular defects with the triflange cup: 2- to 9-year results. *Clin. Orthop. Relat. Res.* 393, 216–227. doi:10.1097/00003086-200112000-00024

Cimerman, M., and Kristan, A. (2007). Preoperative planning in pelvic and acetabular surgery: The value of advanced computerised planning modules. *Injury* 38 (4), 442–449. doi:10.1016/j.injury.2007.01.033

Coccolini, F., Stahel, P. F., Montori, G., Biffl, W., Horer, T. M., Catena, F., et al. (2017). Pelvic trauma: WSES classification and guidelines. *World J. Emerg. Surg.* 12, 5. doi:10.1186/s13017-017-0117-6

Colen, S., Harake, R., De Haan, J., and Mulier, M. (2013). A modified custom-made triflanged acetabular reconstruction ring (MCTARR) for revision hip arthroplasty with severe acetabular defects. *Acta Orthop. Belg* 79 (1), 71–75.

Du, Y., Fu, J., Sun, J., Zhang, G., Chen, J., Ni, M., et al. (2020). Acetabular bone defect in total hip arthroplasty for crowe II or III developmental dysplasia of the hip: A finite element study. *Biomed. Res. Int.* 2020, 1–12. doi:10.1155/2020/4809013

Fuhrmann, R., Feifel, H., Schnappauf, A., and Diedrich, P. (1996). Integration of three-dimensional cephalometry and 3D-skull models in combined orthodontic/surgical treatment planning. *J. Orofac. Orthop.* 57 (1), 32–45. doi:10.1007/bf02189047

Halvorson, J. J., Lamothe, J., Martin, C. R., Grose, A., Asprinio, D. E., Wellman, D., et al. (2014). Combined acetabulum and pelvic ring injuries. *J. Am. Acad. Orthop. Surg.* 22 (5), 304–314. doi:10.5435/jaaos-22-05-304

Han, Q., Zhang, K., Zhang, Y., Wang, C., Yang, K., Zou, Y., et al. (2019). Individual resection and reconstruction of pelvic tumor with three-dimensional printed customized hemi-pelvic prosthesis: A case report. *Med. Baltim.* 98 (36), e16658. doi:10.1097/md.0000000000016658

Hao, Y., Luo, D., Wu, J., Wang, L., Xie, K., Yan, M., et al. (2021). A novel revision system for complex pelvic defects utilizing 3D-printed custom prosthesis. *J. Orthop. Transl.* 31, 102–109. doi:10.1016/j.jot.2021.09.006

Hughes, A. J., DeBuitleir, C., Soden, P., O'Donnchadha, B., Tansey, A., Abdulkarim, A., et al. (2017). 3D printing aids acetabular reconstruction in complex revision hip arthroplasty. *Adv. Orthop.* 2017, 1–7. doi:10.1155/2017/8925050

Kim, D., Lim, J. Y., Shim, K. W., Han, J. W., Yi, S., Yoon, D. H., et al. (2017). Sacral reconstruction with a 3D-printed implant after hemisacrectomy in a patient with sacral osteosarcoma: 1-Year follow-up result. *Yonsei Med. J.* 58 (2), 453–457. doi:10.3349/ymj.2017.58.2.453

Kong, K., Zhao, C., Chang, Y., Qiao, H., Hu, Y., Li, H., et al. (2022). Use of customized 3D-printed titanium augment with tantalum trabecular cup for large acetabular bone defects in revision total hip arthroplasty: A midterm follow-up study. *Front. Bioeng. Biotechnol.* 10, 900905. doi:10.3389/fbioe.2022.900905

Kurtz, S., Ong, K., Lau, E., Mowat, F., and Halpern, M. (2007). Projections of primary and revision hip and knee arthroplasty in the United States from 2005 to 2030. *J. Bone Jt. Surg. Am.* 89 (4), 780–785. doi:10.2106/jbjs.F.00222

Lee, A. K., Lin, T. L., Hsu, C. J., Fong, Y. C., Chen, H. T., and Tsai, C. H. (2022). Three-dimensional printing and fracture mapping in pelvic and acetabular fractures: A systematic review and meta-analysis. *J. Clin. Med.* 11 (18), 5258. doi:10.3390/jcm11185258

Liang, H., Ji, T., Zhang, Y., Wang, Y., and Guo, W. (2017). Reconstruction with 3D-printed pelvic endoprostheses after resection of a pelvic tumour. *Bone Jt. J.* 99 (2), 267–275. doi:10.1302/0301-620x.99b2.Bjj-2016-0654.R1

Lopez, C. D., Boddapati, V., Lee, N. J., Dyrszka, M. D., Sardar, Z. M., Lehman, R. A., et al. (2021). Three-dimensional printing for preoperative planning and pedicle screw placement in adult spinal deformity: A systematic review. *Glob. Spine J.* 11 (6), 936–949. doi:10.1177/2192568220944170

Moss, J. P., Coombes, A. M., Linney, A. D., and Campos, J. (1991). Methods of three dimensional analysis of patients with asymmetry of the face. *Proc. Finn. Dent. Soc.* 87 (1), 139–149.

Peng, C., Kuang, L., Zhao, J., Ross, A. E., Wang, Z., and Ciolino, J. B. (2022). Bibliometric and visualized analysis of ocular drug delivery from 2001 to 2020. *J. Control Release* 345, 625–645. doi:10.1016/j.jconrel.2022.03.031

Shah, F., Snis, A., Matic, A., Thomsen, P., and Palmquist, A. (2016). 3D printed Ti6Al4V implant surface promotes bone maturation and retains a higher density of less aged osteocytes at the bone-implant interface. *Acta biomater.* 30, 357–367. doi:10.1016/j.actbio.2015.11.013

Starosolski, Z. A., Kan, J. H., Rosenfeld, S. D., Krishnamurthy, R., and Annapragada, A. (2014). Application of 3-D printing (rapid prototyping) for creating physical models of pediatric orthopedic disorders. *Pediatr. Radiol.* 44 (2), 216–221. doi:10.1007/s00247-013-2788-9

Tachibana, T., Yokoi, H., Kirita, M., Marukawa, S., and Yoshiya, S. (2009). Instability of the pelvic ring and injury severity can be predictors of death in patients with pelvic ring fractures: A retrospective study. *J. Orthop. Traumatol.* 10 (2), 79–82. doi:10.1007/s10195-009-0050-x

Tonner, H. D., and Engelbrecht, H. (1979). A new method for the preparation of special alloplastic implants for partial replacement of the pelvis. *Fortschr Med.* 97 (16), 781–783.

Upex, P., Jouffroy, P., and Riouallon, G. (2017). Application of 3D printing for treating fractures of both columns of the acetabulum: Benefit of pre-contouring plates on the mirrored healthy pelvis. *Orthop. Traumatol. Surg. Res.* 103 (3), 331–334. doi:10.1016/j.otsr.2016.11.021

Wei, R., Guo, W., Ji, T., Zhang, Y., and Liang, H. (2017). One-step reconstruction with a 3D-printed, custom-made prosthesis after total *en bloc* sacrectomy: A technical note. *Eur. Spine J.* 26 (7), 1902–1909. doi:10.1007/s00586-016-4871-z

Won, S. H., Lee, Y. K., Ha, Y. C., Suh, Y. S., and Koo, K. H. (2013). Improving pre-operative planning for complex total hip replacement with a Rapid Prototype model enabling surgical simulation. *Bone Jt. J.* 95-b (11), 1458–1463. doi:10.1302/0301-620x.95b11.31878

Wong, K. C., Kumta, S. M., Geel, N. V., and Demol, J. (2015). One-step reconstruction with a 3D-printed, biomechanically evaluated custom implant after complex pelvic tumor resection. *Comput. Aided Surg.* 20 (1), 14–23. doi:10.3109/10929088.2015.1076039

Wu, J., Xie, K., Luo, D., Wang, L., Wu, W., Yan, M., et al. (2021). Three-dimensional printing-based personalized limb salvage and reconstruction treatment of pelvic tumors. *J. Surg. Oncol.* 124 (3), 420–430. doi:10.1002/jso.26516

Wu, W., Liu, S., Wang, L., Wu, B., Zhao, L., Jiang, W., et al. (2022). Application of 3D printing individualized guide plates in percutaneous needle biopsy of acetabular tumors. *Front. Genet.* 13, 955643. doi:10.3389/fgene.2022.955643

Wu, X. B., Wang, J. Q., Zhao, C. P., Sun, X., Shi, Y., Zhang, Z. A., et al. (2015). Printed three-dimensional anatomic templates for virtual preoperative planning before reconstruction of old pelvic injuries: Initial results. *Chin. Med. J. Engl.* 128 (4), 477–482. doi:10.4103/0366-6999.151088

Yeung, A. W. K., Tzvetkov, N. T., Georgieva, M. G., Ognyanov, I. V., Kordos, K., Jóźwik, A., et al. (2021). Reactive oxygen species and their impact in neurodegenerative diseases: Literature landscape analysis. *Antioxid. Redox Signal* 34 (5), 402–420. doi:10.1089/ars.2019.7952

Zeng, C., Xing, W., Wu, Z., Huang, H., and Huang, W. (2016). A combination of three-dimensional printing and computer-assisted virtual surgical procedure for preoperative planning of acetabular fracture reduction. *Injury* 47 (10), 2223–2227. doi:10.1016/j.injury.2016.03.015

Zhao, M., Zhang, H., and Li, Z. (2022). A bibliometric and visual analysis of nanocomposite hydrogels based on VOSviewer from 2010 to 2022. *Front. Bioeng. Biotechnol.* 10, 914253. doi:10.3389/fbioe.2022.914253

Zhu, S., Liu, Y., Gu, Z., and Zhao, Y. (2021). A bibliometric analysis of advanced healthcare materials: Research trends of biomaterials in healthcare application. *Adv. Healthc. Mater* 10 (10), e2002222. doi:10.1002/adhm.202002222

Frontiers in
Bioengineering and Biotechnology

Accelerates the development of therapies, devices, and technologies to improve our lives

A multidisciplinary journal that accelerates the development of biological therapies, devices, processes and technologies to improve our lives by bridging the gap between discoveries and their application.

Discover the latest Research Topics

See more →

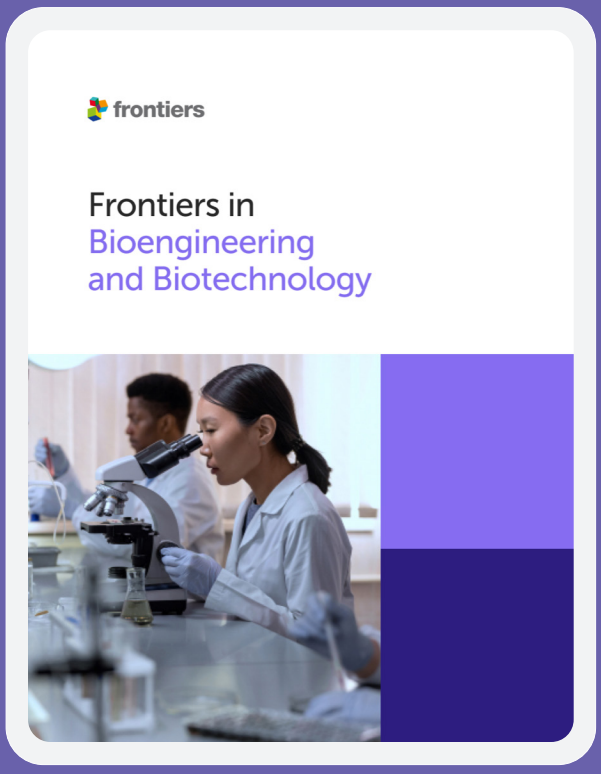

Frontiers

Avenue du Tribunal-Fédéral 34
1005 Lausanne, Switzerland
frontiersin.org

Contact us

+41 (0)21 510 17 00
frontiersin.org/about/contact